MECHANICS of MARINE VEHICLES

B.R. Clayton and R.E.D. Bishop

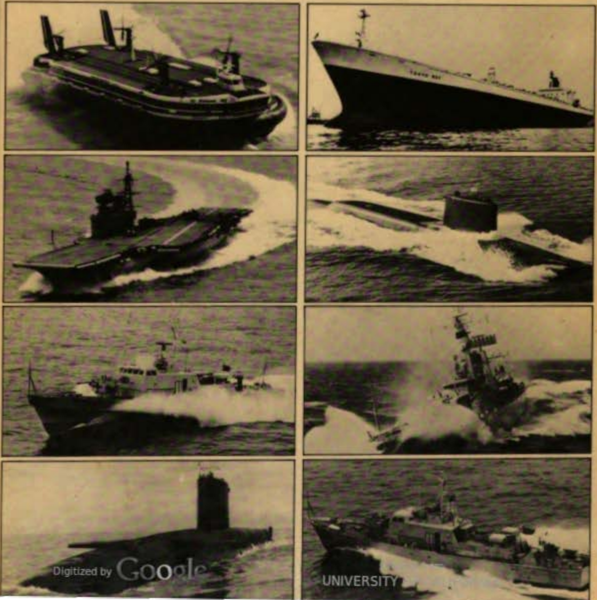

Mechanics of Marine Vehicles

Marine vehicles must be capable of operating and surviving in extreme conditions. These dramatic photographs on the following two pages show:

(a) the bows of a submarine, USS Birmingham, clear of the water following an emergency surfacing manoeuvre (courtesy of Fairplay International);

(b) a frigate travelling at speed in a rough sea which forces the bows to rise clear of the water and subsequently fall back in a 'slamming' motion (courtesy of the Admiralty Marine Technology Establishment, UK);

(c) a fully-laden supertanker with little freeboard which results in substantial deck-wetting in heavy seas (courtesy of Fairplay International).

Mechanics of

Marine Vehicles

B. R. Clayton

Lecturer, Department of Mechanical Engineering, University College London

R. E. D. Bishop

Vice-Chancellor and Principal, Brunel University; formerly Kennedy Professor, Department of Mechanical Engineering, University College London

GULF PUBLISHING COMPANY

HOUSTON, LONDON, PARIS, TOKYO

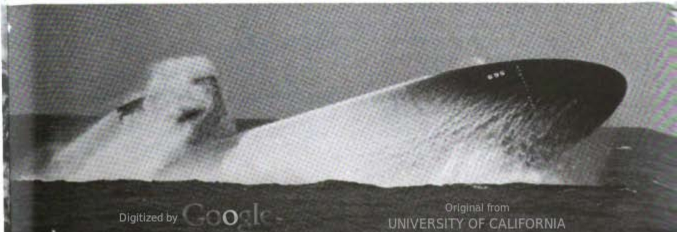

First published 1982 by
E. & F. N. Spon Ltd
11 New Fetter Lane, London EC4P 4EE
This edition published by
Gulf Publishing Company
P.O. Box 2608
Houston, TX 77001

Printed in Great Britain by
J. W. Arrowsmith Ltd, Bristol

ISBN 0-87201-897-0
Library of Congress Catalog Card No. 82-81291

Contents

PREFACE	xiii
ACKNOWLEDGEMENTS	xiv
1 INTRODUCTION	1
1.1 The Design Process	1
1.2 Naval Architecture and Related Fields	2
1.3 Mechanics of Marine Vehicles	4
1.4 A Note on Units	7
2 THE OCEAN ENVIRONMENT	9
2.1 Introduction	9
2.2 Topography of the Oceans	9
2.3 Life on the Earth	12
2.3.1 The Energy Balance	12
2.3.2 Plant and Animal Life	15
2.4 Characteristics of the Stationary Model	15
2.4.1 The Water Molecule	16
2.4.2 Sea Water	16
2.4.3 Ice in the Sea	17
2.4.4 Heat Budget of the Oceans	19
2.4.5 Distribution of Physical Properties	20
2.4.6 Stratification	31
2.5 Characteristics of the Dynamic Model	31
2.5.1 Motion of the Atmosphere	32
2.5.2 Motion of the Hydrosphere	42
2.6 The Hostile Environment	54
References	55
3 THE MARINE VEHICLE AT REST	57
3.1 Introduction	57
3.2 Marine Vehicle at Rest in a Stationary Fluid	57
3.3 Weight of a Vehicle	58
3.3.1 Weight Distribution	60
3.3.2 Centre of Gravity	60

3.4 Buoyancy Force on a Vehicle	61
3.4.1 Centre of Buoyancy	63
3.4.2 Surface of Buoyancy	63
3.4.3 Buoyancy Calculations	68
3.4.4 Cross Curves of Buoyancy	70
3.4.5 Curve of Buoyancy	71
3.4.6 Evolute of the Curve of Buoyancy	74
3.5 Equilibrium and Stability of Weight and Buoyancy	75
3.5.1 Totally Immersed Rigid Vehicle	77
3.5.2 Partially Immersed Vehicles	78
3.5.3 Stability of Surface Ships	80
3.5.4 Effect of Liquid with a Free Surface on Ship Stability	82
3.5.5 Curves of Buoyancy in Ship Calculations	84
3.5.6 Cross Curves of Righting Moments in Ship Calculations	88
3.6 Equilibrium of Weight, Buoyancy and Direct Thrust Acting Simultaneously	89
3.7 Equilibrium and Stability of Ships: Some Practical Considerations	91
3.7.1 Flotation and Trim	91
3.7.2 Stability of Ships and Floating Bodies	95
3.8 Vehicle at Rest in a Non-stationary Fluid	102
3.8.1 Aerostatic Force	102
3.8.2 Thrust Force of a Fluid	105
3.8.3 Stability Considerations	105
3.9 The Structure and its Loading	107
3.9.1 Deterministic and Probabilistic Analysis	109
3.10 External Loading by Gravity and Buoyancy	111
3.10.1 Gravity and Buoyancy Loading of Conventional Surface Ships	114
3.11 External Loading by Inertia and Hydrodynamic Forces	124
3.12 External Loading by Hydrostatic Pressure	126
3.13 External Loading of Some Unconventional Vehicles	129
3.14 Unit Analysis in General	130
3.15 Recent Developments in Quasi-static Structural Analysis	130
References	132
4 MODELLING MARINE SYSTEMS	133
4.1 Introduction	133
4.2 Dimensional Formulae	134
4.2.1 Types of Magnitudes	136
4.3 Dimensional Analysis	139
4.3.1 Rayleigh's Method	139
4.3.2 The 'Pi' Theorem	141
4.4 Physical Similarity	145
4.4.1 Geometric Similarity	146
4.4.2 Kinematic Similarity	147

4.4.3 Dynamic Similarity 150
4.5 Modelling Marine Vehicles 154
4.5.1 The Model System 156
4.5.2 The Marine-vehicle System 157
4.5.3 Homologous Series of Models 161
4.5.4 Model Requirements 162
4.5.5 Departures from the Basic System 164
4.6 Model Testing 167
4.6.1 Towing Tank 167
4.6.2 Water Tunnel 171
4.6.3 Manoeuvring Tank 172
4.6.4 Circulating Water Channel 179
4.6.5 Models 181
References 183

5 STEADY MOTION AT LOW SPEEDS 184

5.1 Introduction 184
5.2 Fluid Forces 185
5.3 Zones of Operation 187
5.4 Field of Flow 188
5.4.1 Flow in the Boundary Layer 189
5.4.2 Flow in the Main Stream 192
5.4.3 Distortion of the Air–Water Interface; Waves 196
5.5 Resistance (Drag) with No Lift or Side Force 199
5.6 Fluid Forces from Momentum Considerations 201
5.6.1 Resistance of a Deeply Submerged Vehicle 201
5.6.2 Resistance of a Ship at the Interface 204
5.7 Resistance of Deeply Submerged Vehicles 208
5.7.1 Benefits of a Streamlined Submarine 212
5.8 Resistance of Interface Vehicles 214
5.8.1 Components of Resistance 215
5.8.2 Interaction Effects 222
5.8.3 Estimation of Ship Resistance 223
5.8.4 Full-scale Ship Tests 232
5.8.5 Other Sources of Resistance 235
References 240

6 STEADY MOTION AT HIGH SPEEDS 244

6.1 Introduction 244
6.2 Planing Craft 245
6.2.1 Generation of Hydrodynamic Forces 245
6.2.2 Hull Geometry 250
6.2.3 Forces on a Planing Craft 253

6.2.4 Estimation of Forces on a Planing Craft 257
6.2.5 Behaviour of a Planing Craft 264
6.2.6 Definition of Fully-planing Operation 266
6.3 Hydrofoil Craft 267
6.3.1 Generation of Lift Forces 268
6.3.2 Geometry of Hydrofoil Sections 273
6.3.3 Data for Hydrofoil Sections 274
6.3.4 Hydrofoils of Finite Span 276
6.3.5 Hydrofoils Close to a Free Surface 281
6.3.6 Forces on a Foil-borne Vehicle in Steady Motion 287
6.3.7 Hydrofoil Vehicle at 'Take-off' 295
6.3.8 Drag Force on a Hydrofoil Vehicle 296
6.4 Air Cushion Vehicles (ACV) 298
6.4.1 Hovering Flight: Cushion Pressure 301
6.4.2 Hovering Flight: Cushion Flow 305
6.4.3 Hovering Flight: Performance 307
6.4.4 Forward Flight over Land 310
6.4.5 Forward Flight over Water 313
6.4.6 Flexible Skirts 314
6.4.7 Forces on Amphibious ACV 317
6.4.8 Forces on Non-amphibious ACV 320
6.5 Comparative Performances of High-speed Marine Vehicles 322
Appendix: Design Equations for Planing Craft 333
References 334

7 **PROPULSION** 338

7.1 Introduction 338
7.2 A Review of Propulsors 339
7.2.1 Oars, Paddles and Paddle Wheels 341
7.2.2 Wind-generated Thrust 342
7.2.3 Jet Propulsion 345
7.2.4 Screw Propeller 349
7.3 Thrust and Efficiency of an Actuator Disc 353
7.3.1 Axial Acceleration Without Downstream Rotation 353
7.3.2 Effect of Rotation in the Slipstream 360
7.4 Flow Through a Screw Propeller 362
7.4.1 Vortex System of a Propeller 363
7.4.2 Blade Element Theory 365
7.5 Propeller–Hull Interaction 366
7.6 Propulsive Efficiency 370
7.7 Propeller Tests 371
7.7.1 Open-water Performance 371
7.7.2 Self-propulsion Tests 375
7.8 Estimation of Propeller Efficiency 376

7.9 Cavitation 380
7.9.1 Development of Cavitation on Propeller Blades 381
7.10 Propeller Design 386
7.11 Propulsion for High-speed Craft 389
References 392

8 CONTROL IN STEADY PLANAR MOTION 396

8.1 Introduction 396
8.2 Steady Two-dimensional Parasitic Motion of a Symmetric Body 397
8.2.1 Parasitic Motion of Translation 400
8.2.2 Parasitic Motion of Rotation 402
8.2.3 Combined Translation and Rotation 404
8.3 Steady Motion of Control Surfaces 406
8.3.1 Forces and Moment Applied to the Hull 407
8.3.2 Lift and Drag Forces 410
8.3.3 Some Practical Considerations 412
8.4 Control of Steady Motion in the Horizontal Plane 413
8.4.1 Directional Stability of a Hull 414
8.4.2 Hull–Rudder Combination 415
8.4.3 Position of the Rudder 416
8.4.4 Some Comments on Rudder Design 418
8.5 Control of Steady Motion in the Vertical Plane 421
8.5.1 Hydroplanes 422
8.5.2 Hull–Hydroplane Combination 424
8.5.3 Some Practical Notes on Hydroplanes 429
8.6 Performance of Control Surfaces 431
8.6.1 Approximate Formulae for Rudders 433
8.6.2 All-movable Control Surfaces 434
References 439

9 STRUCTURAL DYNAMICS 440

9.1 Introduction 440
9.2 General Linear Theory 441
9.2.1 Use of Lagrange's Equations 444
9.3 'Dry Land' and 'Wet Sea' Problems 448
9.3.1 Practical 'Dry Land' Problems 448
9.3.2 Practical 'Wet Sea' Problems 450
9.4 Hull Vibration 450
9.4.1 Excitation of Periodic Vibration by a Propeller 451
9.4.2 Excitation of Periodic Vibration by Waves 454
9.5 Structural Dynamics of a Uniform Beam in Symmetric Motion 454
9.5.1 Free Vibration 455
9.5.2 Forced Vibration 459

9.6 Application of Beam Analysis to Ship Hulls in Steady Motion 466
9.6.1 Rigid Ship Approximation for Behaviour in Waves 468
9.6.2 Response in the Two-node and Higher Modes 469
9.6.3 Numerical Methods for Hull-girder Vibrations 470
9.6.4 Section Properties 476
9.7 Structural Dynamics of Ship Hulls in Antisymmetric Motion 479
9.7.1 Free Vibration 479
9.8 Marine Shafting Vibrations 486
9.8.1 Torsional Vibration 486
9.8.2 Longitudinal Vibration 489
9.8.3 Flexural Vibration 490
9.9 Concluding Note 490
Appendix I: Theoretical Basis of 'Transient Resonance Testing' 490
Appendix II: Some Mathematical Results Used in the Theory of Propeller Excitation 492
References 493

10 (*with A. G. Parkinson*) DIRECTIONAL STABILITY AND CONTROL 495

10.1 Introduction 495
10.2 Unsteady Motions in General 495
10.3 Axes Fixed to a Rigid Body 497
10.3.1 Position and Orientation of the Vehicle 498
10.3.2 Equations of Motion 503
10.3.3 Uses of the General Equations 509
10.4 'Linearized' Equations of Motion 510
10.4.1 Theory of Small Disturbances 510
10.4.2 Symmetric and Antisymmetric Disturbances from a Steady Symmetric Reference Motion 513
10.4.3 Nature of the Deviations $\Delta X, \ldots, \Delta N$ for a Totally Immersed Vehicle 515
10.4.4 Nature of the Deviations $\Delta X, \ldots, \Delta N$ for an Interface Vehicle 524
10.4.5 Uses of the Linear Equations of Motion 527
10.5 Measurement of the Deviations $\Delta X, \ldots, \Delta N$ with Models 528
10.5.1 Measurement of Slow Motion Derivatives 530
10.5.2 Oscillatory Model Testing 533
10.6 Control Surfaces 542
10.6.1 Elementary Analysis of Control-surface Motion 543
10.6.2 Control-surface Derivatives 545
10.6.3 'Horizontal Motion' of a Surface Ship 547
10.6.4 Steering Indices 552
10.6.5 Dimensionless Linear Equations of Motion 553
10.7 Manoeuvring Trials 555
10.7.1 The Pull-out Manoeuvre 556
10.7.2 The Spiral Manoeuvre 557

10.7.3 The Circle Manoeuvre 560
10.7.4 The Zig-zag Manoeuvre 561
10.8 Final Remarks 562
Appendix: Equations of Motion of a Rigid Vehicle with Body Axes whose Origin is not at the Centre of Mass 563
References 564

Notation 566

Index 590

Preface

Towards the end of the 1960s a postgraduate course on naval architecture was started in the Department of Mechanical Engineering in University College London. The subject was to be developed from first principles to an advanced level and the course would therefore be particularly demanding. It was imperative that those who embarked upon it should possess an adequate background in applied mechanics. Inevitably, while some would be products of the Department's own undergraduate courses in mechanical engineering, others would come from other universities and, indeed, other disciplines. If mass slaughter were to be avoided, therefore, some preparation would be needed. But what form should it take?

In the event several members of the Department wrote sets of notes, not on naval architecture, but on the underlying applied mechanics. Originally, these notes were produced in the form of papers under the collective title 'The Mechanics of Fluid-borne Vehicles'. Naturally, as time went on, the material was altered, sometimes drastically; new needs were perceived, and corrections and improvements were made. In particular, a major change resulted in the exclusion of aeronautical topics, so that 'Fluid-borne Vehicles' became 'Marine Vehicles'. There was also a continuing need to bring the references up to date in a field that has been, and still is, developing rapidly. This book is based on the papers as they now stand, some of them having been modified more than once by more than one colleague. Here and there, additions have been made by practitioners among our colleagues (e.g. in Section 3.7) and, although we were responsible for the original text we have not seen fit to edit these additions and modifications out again.

The purpose of this book is to provide its readers with a dependable base from which to move into more advanced studies of vehicles associated with maritime technology. It is not aimed solely at the would-be ship designer, although that is one of its main objectives.

It is a pleasure to acknowledge the assistance given by several of the authors' colleagues, some of whom have now left the Department. In particular, Dr W. K. Allen wrote the first versions of various notes. Professor A. G. Parkinson was much concerned with directional stability and control and revised the material which now comprises Chapter 10. Dr Eatock Taylor's work on structural dynamics is also much appreciated.

Finally, we are grateful to Sonia Clayton who not only took on the task of converting an often hideously scrappy manuscript into typescript but also maintained, at the same time, a happy ship at home.

University College London B.R.C.
May 1981 R.E.D.B.

Acknowledgments

Permission to publish photographs supplied by the following establishments is gratefully acknowledged.

National Maritime Institute: Figures 4.10–4.13, 4.18, 4.20, 4.21, 7.22, 7.24.

Admiralty Marine Technology Establishment (Haslar): Figures 4.14–4.17(a) and (b), 4.19, 4.22–4.24, 7.28, 7.29, 8.22.

British Hovercraft Corporation: Figures 6.47(b), 6.65.

1
Introduction

1.1 The Design Process

Like any other type of design, that of marine vehicles (that is, of ships, submarines, buoys, waterwings, etc.) is a form of art. This does not mean that it is something vaguely connected with 'the arts': rather, the process of design demands a skill which may even extend to a form of cunning, for design cannot be done (at least not realistically, imaginatively or comprehensively) just by following rules.

The reason why design cannot logically be called 'a science' lies at the very root of science. The object of science is to gain knowledge by observing, describing and interpreting various phenomena; it does so often by reference to simpler phenomena. Science does not seek to go further than this, although it would certainly have to do so if it were to be capable of giving positive guidance to the designer.

In effect the design process creates trial solutions which need to be tested analytically against requirements. Thus a preliminary design is analysed and then modified in the light of new information and insight obtained from this analysis. The modified design is then similarly evaluated, and so the process gradually continues towards a design that is suitable for development in detail. The alternation between synthesis and analysis is characteristic of all design, even though the alternatives may have to be examined at any stage.

Until a basic approach has been developed a number of preliminary designs may have to be examined in parallel, in accordance with general engineering practice. Thus a mechanical engineer might have to decide whether a power-actuated control system should be driven by hydraulic, electric or pneumatic means. Until a decision is reached all these possibilities must be kept in mind.

A proposal for a particular kind of marine vehicle will be the result of an examination of some conceptual need governed by economic or other constraints. Concept design such as this will not be considered further other than to note that the results of a technical design may have to be fed back into that framework for reappraisal. It is important, however, to determine exactly the system which is of interest and to state the objectives plainly. The following questions are commonplace in the early design stage. Is the objective to create a marine vehicle which is technically excellent? Or should it have a minimum procurement cost or a minimum life cost? Or is it to achieve a stated level of readiness or safety or maintenance or performance? Just what compromise *is* required?

Having defined the system which will be analysed and stated the objective(s), it is often convenient to construct a model of the problem. This is usually mathematical in character and represents the response of the proposed design to its environment. Physical laws derived by Newton, Bernoulli, Lanchester, Euler and many of their successors often provide suitable models and so, at little expense, the design may be examined theoretically – and modified if necessary – without the need to build and test a physical model, or even a prototype.

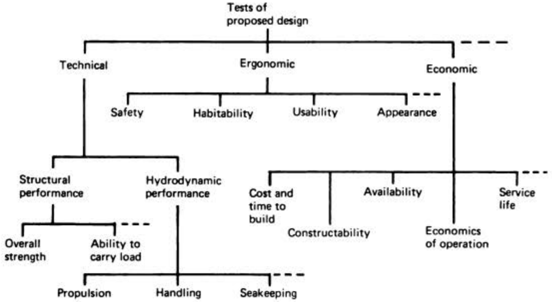

Fig. 1.1

Briefly, and rather crudely, the lines of thought suggested in Fig. 1.1 could form the basis of a sound approach to design. Note that the 'tree' is only partly complete; it can be continued, depending on where the system boundary is drawn. It is not our present purpose, however, to examine the philosophy or techniques of the design process. We merely note that the design process is one of formulation, evaluation and modification.

The factors which need evaluation often, perhaps usually, have to meet conflicting requirements. Consequently, compromise is an important factor in design. And an important function of the analytical side of the design process is to give guidance on the making of compromises, for it is often necessary to know the consequences of the acceptance of a compromise.

Of course, rules can be – and frequently are – framed to help the designer avoid pitfalls when making trial designs. This is the value of experience. But experience is an equivocal asset: used intelligently (i.e. questioningly) it can save a great deal of unproductive effort; used unintelligently (i.e. unquestioningly) it can still save effort, but it can also be stultifying.

1.2 Naval Architecture and Related Fields

In the required operation of marine vehicles, lives are often at stake and huge sums of money at risk. In addition, the problems confronting the designer are essentially *difficult* ones, particularly on the technical side, as we shall see. The decision to proceed with a new design is thus not to be taken lightly.

In the past these difficulties have forced engineers to specialize in particular types of marine vehicles. Naval architects, for instance, have designed ships, amassing in the process considerable knowledge over the years. The reader who intends eventually to design ships would be foolish to disregard this accumulated knowledge and experience.

The problem here is not that of mastering naval architecture, however. We are concerned with marine vehicles *in general*, and there are many types of craft quite distinct from conventional surface ships. For example

bathyscaphes	paravanes
dracones	planing craft
hovercraft	sea-bed crawler vehicles
hydrofoil craft	submarines
inflatable craft	submersibles (manned or unmanned)
multi-hull craft	surf boards
oil and gas drilling rigs	torpedoes.

Obviously we cannot study all of these (and others not mentioned) as the naval architect studies ships. In fact, our aim will be to provide a discussion of the mechanical problems that any or all of these types may raise.

By the very nature of the subject consideration must be given to solid mechanics (i.e. the mechanics of the vehicle) and to fluid mechanics (the mechanics of its environment). Now for the purpose of analysis it is almost invariably best to identify either (a) the vehicle or a part thereof, or (b) the fluid or a part thereof. That is to say, it is usually better never to contemplate a composite system comprising solid and fluid. Accordingly it is necessary to consider the forces that act across the fluid–solid boundary.

The fluid forces exerted by the environment on an isolated vehicle may be constant or time dependent. The régime will in fact be one of the three types indicated in Fig. 1.2. The adjectives 'hydrostatic', 'steady' and 'unsteady' will sometimes be employed to describe the loading of the vehicle by the fluid. (Note that approximations may be made by treating unsteady loading as steady, or steady loading as hydrostatic, thus rendering otherwise intractable problems amenable to analysis.) Here, then, is one way in which an analysis can be broken into parts.

A second way of conveniently forming a boundary within which an analysis may be confined is suggested by the relevant properties of the vehicles themselves. Whether or not a vehicle is assumed to be 'rigid' depends on what the analyst hopes to achieve. Thus, although the rigid dynamics of a submarine is acceptable in discussion of its handling characteristics, it is nonsense in a discussion of submarine vibration. The assumption of rigidity is made in studying handling characteristics because it is suspected that the effect of a submarine's flexibility will be negligible.

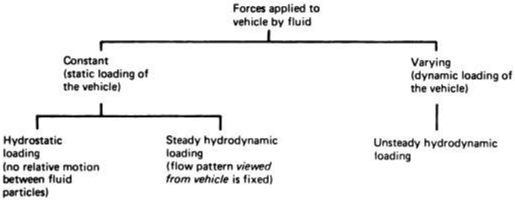

Fig. 1.2

Within the framework outlined in Table 1.1 it is possible to introduce most of the significant techniques of contemporary analysis of marine vehicles. Note, however, that this framework covers only a part of the designer's task. Many areas of speculation must be left untouched, although some of them, notably economics, ergonomics, material properties and prime movers, are vitally important.

Table 1.1 Topics in the mechanics of marine vehicles.

Topic	Vehicle		Fluid forces applied to vehicle		
	Rigid	Deformable	Hydrostatic	Steady	Unsteady
The ocean environment	Some relevant physical and oceanographic properties of the sea				
Structural analysis		X	X	X	
Vehicles at rest	X		X		
Models	X		X	X	X
Vehicles in steady motion	X			X	
Propulsion	X			X	
Control of steady planar motion	X			X	
Directional stability and control	X				X
Structural dynamics		X			X

1.3 Mechanics of Marine Vehicles

Obviously, a firm grasp of the principles of mechanics and their relevance and application is crucial for the success of any design project concerned with marine vehicles, which may often be extremely complex. The finally adopted vehicle system consists of a combination of many inter-related sub-systems, for example, communications, air-conditioning, navigation, control, catering, etc. Consequently, design teams are formed of specialists in different fields together with others able to coordinate the separate and sometimes conflicting interests to a final result which will provide the optimum amalgam. The importance associated with the various sub-systems depends, of course, on the type of vehicle under consideration. Clearly, the operating characteristics of a fishery patrol vessel will differ considerably from those pertaining to a coastal ferry running a regular commercial service. Nevertheless, detailed studies can be carried out in common areas such as environmental conditions, stability, power and speed, control and the like. Many of these items can be investigated with physical models, and again these take on a wide variety.

In the following chapters the preceding points are developed on a broad basis but with emphasis always placed on principles rather than empiricism. Nevertheless, detailed answers to most questions relating to the mechanics of marine vehicles are generally impossible to formulate without some reliance being placed on past experience. As stated earlier, it would be quite wrong to ignore or scorn accumulated knowledge – and it would be equally wrong to accept it without question. Empiricism is therefore included in those places where it contributes fruitfully to the analysis. At the same time attention is drawn to the appropriateness and accuracy of experimental data and to the assumptions required by an analysis before the data may be used.

The ocean environment in which a vehicle operates naturally has a strong influence on design and the duties to which the vehicle, and its sub-systems, are put. Perhaps the most dramatic effects of the environment occur at the air–water interface as a result of the interaction between the two viscous fluids. Strong winds, waves of various lengths, heights and steepnesses, spray, etc., limit the progress of ships and may cause discomfort to the crew and passengers, substantial structural damage, or even cause the vehicle to capsize. Communications (radio and radar) become impaired under certain environmental conditions and changes in the properties of sea water limit the performance of sonar devices used by submarines and anti-submarine craft. Ice in the sea is also a substantial hazard and inhibits movement in many coastal waters, inland seas and rivers. These matters are discussed in Chapter 2.

Clearly, any marine vehicle must remain in stable equilibrium when being launched and must maintain this condition when floating stationary or tied up to a jetty. (Even a hovercraft must float stably if, for example, the cushion lift fans fail and the skirts cannot be inflated.) Furthermore, the attitude of the vehicle when stationary must be consistent with bottom clearance, ease of loading cargo, crew comfort, safety and so on. The vehicle must also continue to have an acceptably stable attitude as stores are consumed or cargo taken aboard. These topics are investigated in Chapter 3 along with an introduction to structural analysis. The vehicle must have a structure compatible with the loading and its distribution. Once more, the details of the main structural design vary from one vehicle to another depending upon the application, and so we could anticipate a quite different structure being used for a submarine as compared to a cargo carrier or a hovercraft. The purpose of the sections devoted to structural analysis is to show how the subjects covered in, say, courses on structures, stress analysis, plasticity, etc., may be brought to bear on problems related to marine vehicles. It is shown that reference to the 'ship girder' can produce techniques suitable for a 'static' analysis which may be linked to extreme loadings and steady motion.

In general, when vehicles are underway statics no longer yields answers of acceptable accuracy. Whereas straightforward, albeit tedious, arithmetic is called for in the solution of statics problems of the type considered in Chapter 3, things become rather more complicated when hydrodynamics is involved. Indeed, equations of motion can only be solved with the aid of experimentally determined coefficients. As prototype vehicles are large, relative to the required test facilities, smaller models are necessary, and the background to modelling and the rules by which model results are projected to full-scale performances are examined in Chapter 4 . The extent and importance of test facilities are illustrated by means of photographs and a table of principal dimensions.

Chapters 5–8 are concerned with the aspects of steady motion of marine vehicles on the assumption that in many instances perturbations on steady states are negligible when the overall behaviour of a given vehicle is being considered.

Chapter 5 discusses the equilibrium conditions required for the steady motion of ships and other displacement vehicles, such as deeply submerged submarines, operating at low speeds, say at less than 17.5 m s^{-1} ($\cong$ 35 knots). The dilemma facing designers in transferring model data to full-scale predictions is discussed and contemporary techniques to combat the difficulties are described. Components of resistance are analysed and special attention is paid to the problems of encountering ice in the sea.

There is a tendency nowadays for some navies and commercial operators to adopt high-speed craft which, because of power limitations, are smaller than conventional displacement vehicles. Different principles are then required and these are given in Chapter 6 in relation to planing craft, hydrofoil craft and hovercraft. An overall appraisal of high- and low-speed craft is given along with data showing the best operating régimes.

The resistance to motion of a marine vehicle must be overcome by a suitable propulsor and the means by which this is achieved are presented in Chapter 7. Here the complexity of hydrodynamic interactions between the hull and, for example, a propeller is so great as to defy any kind of rigorous theoretical description. Although analyses are being developed which will gradually reduce the necessity for extensive experimental work much effort is still devoted to physical scaling of interaction processes. A brief appraisal of various types of propulsor is given, but it is concluded that for most purposes the screw propeller, open or shrouded, is still the best type by far. A method of determining the overall dimensions of a propeller is described along with present-day developments on the initial stages of propeller design within the limitations of a steady flow analysis.

Having designed a marine vehicle which suits specified environmental limitations, remains stable and which is provided with a propulsor that matches the resistance of the vehicle some means of controlling and manoeuvring the craft is needed. Control surfaces are invariably in close proximity to a hull or propulsor and so hydrodynamic, and thus structural, interactions are again called into play. A straightforward approach to the analysis of control surfaces is outlined in Chapter 8 and is based upon a first-order, small-perturbation theory. It is then possible to describe the principal features of some steady manoeuvres related to ships and submarines. Data are also given for the estimation of forces on rudders and hydroplanes when uniform flow is again assumed.

Whereas the 'steady-motion' approach to the design of marine vehicles allows the overall features of the vehicle to be assessed, there are numerous detailed matters which call for more refined theories. If these are ignored then important non-linearities, fluctuating forces, resonances, etc., are missed. And these, in turn, could produce catastrophic failure of components, overshoot manoeuvres and instabilities. However, greater accuracy cannot be achieved without more complex and often more elegant analyses, and Chapters 9 and 10 are concerned with an introduction to a 'dynamic' or 'unsteady-motion' approach. Thus, Chapter 9 is devoted to structural dynamics and differentiates between 'dry land' and 'wet sea' problems. The theory of beam vibrations is developed and its application to ship hulls is described in some detail. The underlying theory of the structural dynamics of ship hulls in antisymmetric motion is given along with a brief appraisal of 'added' mass. This chapter concludes with a summary of the structural problems likely to be encountered with marine shafting.

The directional stability and control of marine vehicles are covered in Chapter 10. The general equations of motion are developed and subsequently linearized (the vastly simplified forms of these equations are examined in Chapter 8). The nature of the deviations from steady motion are described and the slow motion coefficients or derivatives in the equations of motion for ships and submarines are examined. More general predictions of the performances of control surfaces are presented and a number of model and full-scale experiments used to assess performance are described.

To conclude this section, we should perhaps stress the importance of mechanics to the potential naval architect, who would probably prefer to become better acquainted with ships! In the very first technical paper read before the Institution of Naval Architects, the Rev. Dr Joseph Woolley laid great stress on the importance of scientific fundamentals – of mechanics – to those who design and build ships [1]. That importance has not declined in any way. Indeed, it provides the *raison d'être*, in a modern context, for the material that follows.

1.4 A Note on Units

In this book SI units (Système International d'Unités) are preferred. Approximate British units are given in parentheses although this practice is sometimes omitted if confusion might result owing to congestion of data; the main exception occurs in Chapter 2 which deals with topics in oceanography, meteorology and climatology, for in these subjects modern practice generally favours the widespread use of metric and better still SI units.

A number of useful conversion factors (discussed in Chapter 4) are given in the following list although some rounding-off has taken place in the presentation of subsequent data. Exact equivalences are given in bold type.

Length

$$1 \equiv \frac{\mathbf{25.4}\ \text{mm}}{1\ \text{in}} \equiv \frac{\mathbf{304.8}\ \text{mm}}{1\ \text{ft}} \equiv \frac{\mathbf{6080}\ \text{ft}}{1\ \text{British nautical mile}}$$

Area

$$1 \equiv \frac{0.0929\ \text{m}^2}{1\ \text{ft}^2} \equiv \frac{645\ \text{mm}^2}{1\ \text{in}^2} \equiv \frac{0.836\ \text{m}^2}{1\ \text{yd}^2}$$

Velocity

$$1 \equiv \frac{\mathbf{0.3048}\ \text{m s}^{-1}}{1\ \text{ft s}^{-1}} \equiv \frac{0.515\ \text{m s}^{-1}}{1\ \text{British knot}} \equiv \frac{0.447\ \text{m s}^{-1}}{1\ \text{m.p.h.}}$$

Second moment of area

$$1 \equiv \frac{8.63 \times 10^{-3}\ \text{m}^4}{1\ \text{ft}^4} \equiv \frac{4.162 \times 10^{-7}\ \text{m}^4}{1\ \text{in}^4}$$

Volume

$$1 \equiv \frac{2.832 \times 10^{-2}\ \text{m}^3}{1\ \text{ft}^3} \equiv \frac{1.639 \times 10^{-5}\ \text{m}^3}{1\ \text{in}^3} \equiv \frac{0.7646\ \text{m}^3}{1\ \text{yd}^3}$$

Mass

$$1 \equiv \frac{0.4536\ \text{kg}}{1\ \text{lbm}} \equiv \frac{1016\ \text{kg}}{1\ \text{tonm}} \equiv \frac{\mathbf{1000}\ \text{kg}}{1\ \text{tonnem}}$$

Volume flow rate

$$1 \equiv \frac{2.832 \times 10^{-2}\ \mathrm{m^3\ s^{-1}}}{1\ \mathrm{ft^3\ s^{-1}}}$$

Density

$$1 \equiv \frac{16.02\ \mathrm{kg\ m^{-3}}}{1\ \mathrm{lbm\ ft^{-3}}} \equiv \frac{62.4\ \mathrm{lbm\ ft^{-3}}}{\mathbf{1000}\ \mathrm{kg\ m^{-3}}}$$

Moment of inertia (second moment of mass)

$$1 \equiv \frac{0.042\,14\ \mathrm{kg\ m^2}}{1\ \mathrm{lbm\ ft^2}} \equiv \frac{2.926 \times 10^{-4}\ \mathrm{kg\ m^2}}{1\ \mathrm{lbm\ in^2}}$$

Force

$$1 \equiv \frac{4.448\ \mathrm{N}}{1\ \mathrm{lbf}} \equiv \frac{9964\ \mathrm{N}}{1\ \mathrm{tonf}}$$

Moment of force, or Torque

$$1 \equiv \frac{1.356\ \mathrm{N\ m}}{1\ \mathrm{lbf\ ft}} \equiv \frac{3037\ \mathrm{N\ m}}{1\ \mathrm{tonf\ ft}}$$

Pressure; Stress

$$1 \equiv \frac{6895\ \mathrm{N\ m^{-2}}\dagger}{1\ \mathrm{lbf\ in^{-2}}} \equiv \frac{1.544 \times 10^{7}\ \mathrm{N\ m^{-2}}}{1\ \mathrm{tonf\ in^{-2}}} \equiv \frac{1.013 \times 10^{5}\ \mathrm{N\ m^{-2}}}{1\ \mathrm{atmosphere}} \equiv \frac{\mathbf{10^5}\ \mathrm{N\ m^{-2}}}{1\ \mathrm{bar}}$$

Work; Energy

$$1 \equiv \frac{1.356\ \mathrm{J}}{1\ \mathrm{ft\ lbf}} \equiv \frac{3.766 \times 10^{-7}\ \mathrm{kW\ h}}{1\ \mathrm{ft\ lbf}} \equiv \frac{\mathbf{3.6 \times 10^6\ J}}{\mathbf{1\ kW\ h}}$$

Power

$$1 \equiv \frac{1.356\ \mathrm{W}}{1\ \mathrm{ft\ lbf\ s^{-1}}} \equiv \frac{\mathbf{550}\ \mathrm{ft\ lbf\ s^{-1}}}{1\ \mathrm{hp}} \equiv \frac{746\ \mathrm{W}}{1\ \mathrm{hp}}$$

(Absolute or dynamic) viscosity

$$1 \equiv \frac{47.9\ \mathrm{N\ s\ m^{-2}}}{1\ \mathrm{lbf\ s\ ft^{-2}}} \equiv \frac{\mathbf{0.1}\ \mathrm{N\ s\ m^{-2}}}{1\ \mathrm{poise}}$$

Kinematic viscosity

$$1 \equiv \frac{0.0929\ \mathrm{m^2\ s^{-1}}}{1\ \mathrm{ft^2\ s^{-1}}} \equiv \frac{\mathbf{10^{-4}}\ \mathrm{m^2\ s^{-1}}}{1\ \mathrm{stokes}}.$$

Reference

1. Woolley, J. (1860), On the present state of the mathematical theory of naval architecture. *Trans. Inst. Nav. Archit.*, 1, 10–38.

† The unit N m^{-2} is given the name pascal (Pa).

2
The Ocean Environment

2.1 Introduction

To specify realistic operational requirements the designer of a marine vehicle must have some understanding of oceanography and meteorology, for he must consider the operation of the vehicle and the conditions within it. In the following sections a number of relevant topics from these disciplines are introduced in order to provide understanding of the marine-vehicle environment.

The oceans have been in existence for at least 3 billion years – more than half the age of the Earth – according to the analysis of rounded, well worn pebbles embedded in specimens of sedimentary rocks. The origin of the oceans is still in doubt, however [1]. The topographical features of the planet are changing continuously, albeit slowly relative to the human lifespan. Shore lines distort, continents rise, fall and drift, and the mean sea level changes. During the main ice ages the seas were 100–200 m below their present level owing to the presence of large volumes of frozen water; the land masses were consequently larger. At present, the Earth is emerging from an ice age. If the Antarctic and Greenland ice sheets were to melt the seas would rise about 50 m and therefore flood large areas of low-lying coastal plains.

One might expect that the chemical composition and therefore the physical characteristics of the seas are changing. In fact, experiments have shown that the composition of the salts dissolved in sea water is nearly always the same regardless of location, although the total concentration varies from place to place. This implies that since the formation of the oceans the water has been well mixed and a steady equilibrium state obtained except for brief, local disturbances, such as near to coastlines and estuaries. However, we shall not examine these regions in any great detail.

In the design of marine vehicles one may be interested in the properties of the ocean floor, the water itself or the atmosphere above. Usually, of course, one is concerned with the interfaces between these zones – principally that at the sea surface – and the transition from one zone to another takes place abruptly. (The mean density of the sea bottom is around 2.5 Mg m^{-3}, that of sea water is approximately 1.03 Mg m^{-3} and the mean density of air at sea level is 1.23 kg m^{-3}.)

2.2 Topography of the Oceans

A rather simple, idealized model of the Earth can be obtained by assuming the planet possesses geometric symmetry. Essentially, the Earth would then consist of three major regions: solid material of variable (but generally large) density; liquid of moderate density; and gases of low density. These regions would be held together by gravitational attraction and the substances stratified into a central core of very heavy metal surrounded by successive smooth, spherical shells of heavy rock, light rock, water and, finally, gas layers. The Earth may thus be compared with a wet football, the hydrosphere being a relatively thin film of water on the surface of a large solid sphere. This model of the Earth is illustrated in Fig. 2.1.

In reality land masses protrude through the surface of the hydrosphere, so that water only covers about 71 per cent of the total surface area. Furthermore, the ratio of water to land in the southern hemisphere is considerably greater (4:1) than in the northern hemisphere (1.5:1). The average depth of the oceans is close to 4 km. (A sea is a smaller body of water often surrounded by land or island chains and possesses local distinguishing characteristics.) The maximum depth of the hydrosphere is about 11 km (at Challenger Deep in the Marianas Trench). There the water is perpetually near freezing point yet forms of life are still to be found, as confirmed by the United States bathyscaphe *Trieste* which touched bottom in 1960.

Essentially, there is but one ocean and all the land masses are islands. For convenience, however, the ocean is divided into five principal regions each displaying important differences of detail in their characteristics. These may be described briefly as follows.

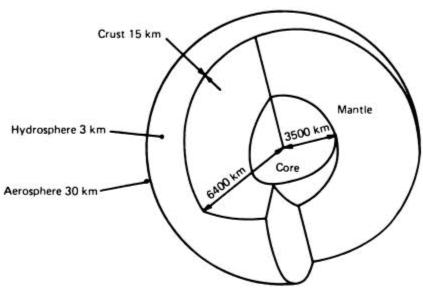

Fig. 2.1 Model of the Earth.

The Pacific Ocean. This ocean contains more than half the water in the hydrosphere and averages about 3.9 km in depth. Few rivers flow into the Pacific Ocean and as its surface area is about ten times the area of the land draining into it the fresh-water content near to the surface is quite small. Conditions in the South-East and South-West Pacific Basins resemble more closely than elsewhere those which might be anticipated on the idealized model described earlier. A particularly distinctive feature of the Pacific Ocean is the presence of many trenches and islands which define areas of earthquakes and active volcanoes. Indeed, the greatest continuous slope on the Earth is the Hawaiian volcano Mauna Kea, which rises sheer from the sea bed to about 9.5 km of which about 4.2 km is above sea level. (The height of Mount Everest is 8.84 km.) Another impressive slope rises from the depths of the Peru–Chile trench to the crest of the Andes, a height of about 5 km.

The Atlantic Ocean. This is a narrow twisted body of water averaging 3.3 km in depth and is adjacent to many shallow seas such as the Caribbean, Mediterranean, Baltic and North Seas, the Gulf of Mexico and so on. Many rivers flow into the Atlantic Ocean including such great ones as the Congo and the Amazon. The surface area of the ocean is only 1.6 times the land area drained into it and so the surface water contains a greater proportion of fresh water than that of the Pacific Ocean. Within the Atlantic Ocean is the so-called Mid-Atlantic Ridge, which extends along the middle of the ocean from north to south and then continues somewhat less definitively through the Indian and South Pacific Oceans. In the Atlantic Ocean it separates the bottom waters which consequently have different properties on the east and west sides of the Ridge. Moreover, it forms the biggest *continuous* 'mountain' range on Earth being 16 000 km long and 800 km wide. The total Mid-Ocean Ridge is probably the most extensive single feature of the Earth's topography. The complete length of the ridge is over 48 000 km, its width often over 1000 km and the height relative to the adjacent sea floor varies between 1 km and 3 km. The origin and structure of the Mid-Atlantic Ridge is still in doubt, but many geologists believe it to be the result of upwelling of the mantle material.

The Indian Ocean. This averages 3.8 km in depth and receives fresh water from large rivers such as the Ganges and the Brahmaputra. The surface area of the ocean is 4.3 times that of the land drained into it and is thus intermediate between the Pacific and Atlantic Oceans. An important influence on the Indian Ocean is its susceptibility to radical seasonal variations of atmospheric conditions which are due to the proximity of the large land masses of Africa to the West and India to the North.

The Antarctic Ocean. The three preceding major bodies of water are connected to form this continuous ocean belt known also as the Southern Ocean. This ocean surrounds the frozen Antarctic land mass and, as we shall see later, induces a deep-ocean circulation.

The Arctic Ocean. Although it is often considered an extension of the Atlantic Ocean, quite recent investigations have shown that the Arctic Ocean is divided into two basins, the Canadian and the Eurasian on either side of the so-called Lomonosov Ridge. The Arctic Ocean surrounds the northern polar ice cap which permanently covers about 70 per cent of this ocean's surface.

Typically, an ocean may be about a thousand times as wide as it is deep and a cross section might be similar to that illustrated in Fig. 2.2. The main régimes, in relation to distance from the land, are the shore, the continental shelf, the continental slope and the deep-sea bottom, which is sometimes called the 'benthic' boundary.

The *shore* may be defined as that part of the land mass which is closest to the sea and which has been modified by the action of the sea. The beach is the seaward limit of the shore and extends roughly from the highest to the lowest tide levels. Sandy beaches are usually in a state of slow continuous change as material is removed and deposited by waves and water currents near the shore line.

The *continental shelf* extends seawards below the water surface at an average gradient of 1 in 500. The shelf has an average width of 65 km but may vary from a few kilometres to 700 km as in the Bering Sea, for example. The bottom material is usually sand and less commonly mud or rock. At a depth of about 130 m but some-

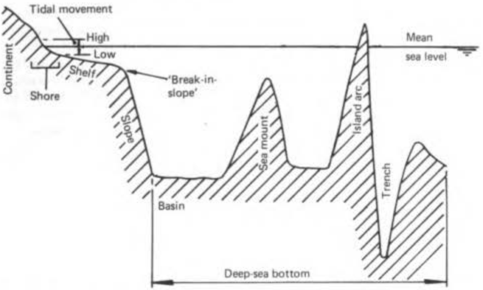

Fig. 2.2 Typical sea-bed topography.

times as much as 500 m the so-called 'break-in-slope' occurs where the gradient increases rapidly to approximately 1 in 20. This rapid increase marks the start of the continental slope which then extends to the deep-sea bottom to mark the edge of the continental land mass. Not surprisingly, the shelves contain many of the raw materials found in the adjacent land. Consequently, undersea mine shafts and, recently, drilling platforms have been constructed in these areas to obtain oil, gas, sulphur and limestone commercially [2].

The *continental slope* averages about 4 km vertically from the shelf to the deep-sea bottom but increases in places to 9 km in a relatively short horizontal distance. In general, the continental slope is considerably steeper than the slopes on land. The material on the continental slope is primarily mud with outcrops of rock. Submarine canyons are usually found there, either V-shaped or with vertical sides; they occur most often off coasts with rivers, but never, it seems, off desert areas.

The *deep-sea bottom* is the most extensive area and depths of 3–6 km occur over 76 per cent of the ocean basins and a further 1 per cent is deeper. It was only with the advent of the laying of cables that the original view of a totally flat sea bottom had to be discarded and replaced by one showing mountains, valleys and plains. The valleys may often extend as circular arcs in planform to great depths forming the well known trenches in the Pacific Ocean.

Similarly, individual mountains called *sea mounts* may project above the water surface to form islands, while the tops of others are below the surface and become ridges when found in a range. In some of the large basins, however, the sea floor is very smooth and stretches of the abyssal plain in the western North Atlantic Ocean have been measured to be smooth within 2 m over distances of 100 km.

2.3 Life on the Earth

2.3.1 *The Energy Balance*

The Earth receives energy by solar radiation which reaches the surface of the planet in the form of:

(i) infrared radiation at long wavelengths (greater than 1 μm) which we sense as heat;
(ii) visible light at intermediate wavelengths (0.35–0.7 μm, mainly centred around 0.5 μm) corresponding to the blue and blue-green parts of the visible spectrum;
(iii) ultraviolet radiation (short wavelengths less than 0.1 μm) which burns the human skin.

A typical breakdown of the incident solar radiation is shown in Fig. 2.3, and the heat-transfer process from the surface of the Earth is depicted in Fig. 2.4. Clearly,

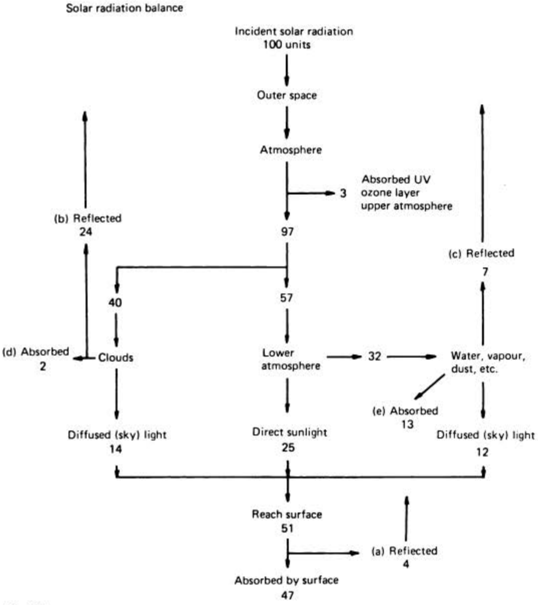

Fig. 2.3

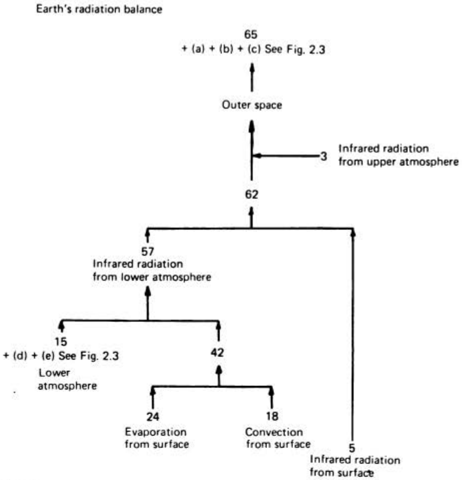

Fig. 2.4

for steady-state equilibrium the 47 units of energy received by the Earth from the Sun must be dissipated to avoid large-scale changes in temperature, other than local and seasonal variations. The relatively low temperature of the Earth's surface allows only 5 units of energy to be radiated to outer space. The remaining 42 units are transferred to the atmosphere by a combination of convection and evaporation (which accounts for more than half this total). If the planet were dry, 97 per cent of the incident solar radiation would reach the Earth's surface and heat transfer from it could only occur by convection and radiation. Thus to achieve thermal equilibrium the temperature of the Earth would need to be far higher than it is now. Evaporation from the oceans therefore provides both a heat shield and a highly effective method of heat transfer. Apart from providing an equable mean temperature both daily and seasonal variations are moderated in contrast to, say, a dry planet such as the Moon. Indeed, we only have to compare the temperature records for desert areas with those for oceanic regions on the Earth to appreciate this point.

A further result of the evaporation of water from the ocean surfaces is the hydrocycle. Water vapour entering the atmosphere undergoes upward convection and is then conveyed by winds over the land masses. As the moist air is forced upwards either by high land or by a low, cold (and therefore heavier) belt of air, the vapour

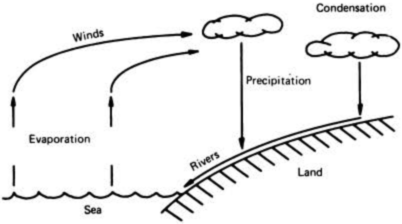

Fig. 2.5 The hydrocycle.

condenses as cloud, fog, rain, or snow. Latent heat is released to the atmosphere and water is precipitated onto the land before returning to the oceans from rivers (see Fig. 2.5). The oceans therefore provide water to sustain life on land.

2.3.2 *Plant and Animal Life*

There is no large-scale vertical mixing in the oceans and a stratified state of hydrostatic equilibrium exists. Hence a warm surface layer of water is isolated from the cooler, deeper waters. Within this layer 90 per cent of the incident solar radiant energy is absorbed in a depth of 40 m. Since plant life requires sunlight for survival we find that most plants occur in the upper 100 m of water and this region therefore supports the major quantity of marine animal life. However, in contrast to plant life, marine animals can and do survive without sunlight. They are therefore found in great variety throughout the depths of the oceans.

Numerically, the most abundant creatures are insects and small marine organisms and the quantity increases in the warmer regions of the Earth. Their effect on engineering systems can lead to results that are at best frustrating and at worst disastrous. The presence of organic growth at sea can, for example, completely invalidate the data from corrosion tests made under laboratory conditions. Biological activity produced by the lower organisms which attach themselves to and bore through man-made structures may lead to fouling, corrosion and fatigue failures. The larger animals bite through and often completely sever underwater cables and mooring ropes. Ship resistance may double during time out of dock as a result of barnacles and marine growth on the immersed hull. Finally, the noises made by animal life, such as the snapping of shrimps and the echo-sounding clicks and whistles of dolphins, affect the performance of acoustic devices and communication systems.

2.4 Characteristics of the Stationary Model

A logical discussion of the oceans can be formulated by considering first those characteristics which appear to be unaffected by the motion of the water. We have observed already that the great age of the oceans suggest that they must be well mixed chemically. Oceanographers often use this important concept to determine the salinity of water from the more readily measurable chlorinity or, alternatively, by the measurement of electrical conductivity.

Pure water and, to a similar extent, sea water exhibit some unusual properties for liquids. Water has high values of specific heat capacity, latent heat of fusion and evaporation, surface tension, heat conduction, dielectric constant and transparency as well as the ability to dissolve impurities, and these factors have a considerable effect on the external environment. To explain these matters we must turn our attention to the chemistry of the oceans and the physical properties of sea water.

2.4.1 *The Water Molecule*

As suggested by the chemical formula, H_2O, the water molecule consists of two hydrogen atoms bonded to one oxygen atom. However, the properties of water are so dissimilar from other substances having similar molecular weights, such as ammonia, methane or hydrogen fluoride, that we must look to a more adequate representation of the water molecule. Let us continue with the notion that bonding occurs in such a way that the hydrogen atoms, which are positively charged, are situated on one side of the oxygen atom. The result is a so-called polar molecule which is negatively charged on one side and positively charged on the other. Probably, then, simple molecules of water bond together by way of their hydrogen atoms to form clusters of molecules. This process is called polymerization and results in a substance behaving as one with an effective molecular weight considerably greater than 18. If polymerization did not take place water would exist as a gas at the temperatures and pressures found on the Earth; it would melt at -100°C and boil at -80°C. Instead, water exists on the Earth's surface as a gas, a liquid and a solid (ice).

At the surface temperatures found on the Earth the structure of water is not static; internal bonds break and reform rapidly so that clustered and simple molecules co-exist. This continual interchange enables liquid water to exhibit fluidity because at any instant unbound molecules, which are free to rotate and move, surround the clusters and assist the flow. When ice is melted to liquid water not all intermolecular bonds are broken, but when water vapour is formed no bonds remain and so individual molecules move and rotate freely filling any bounded space.

As water is cooled from, say, 10°C its density will be influenced by two opposing effects:

(i) reduced molecular or atomic vibration tending to increase density, and
(ii) the formation of bulky molecular clusters tending to reduce density.

Initially, the density of water increases as its temperature is reduced, but as the number of clusters increases the density reaches a maximum, at about 4°C, and thereafter decreases. This unusual property allows fresh-water fish to survive in the deep waters where the temperature remains at about 4°C even though colder water and ice occur near the surface.

2.4.2 *Sea Water*

On average sea water contains some 35‰ (parts per thousand) of dissolved salts, and so, in small quantities, the remaining 965‰ determine the physical properties. However, the dissolved salts have a profound effect on the structure of the oceans.

The principal salts, given as a ratio of the total salt content, are shown in Table 2.1 and may be considered representative of all the oceans.

Note that sodium chloride, for example, exists as sodium cations and chloride anions which retain their charges in water. The ions in crystalline substances are held together, whereas in water the ions first attract, and then become surrounded by, the charged water molecules so that the salt crystals dissolve. This is why water is such a good solvent. Gases are also dissolved in sea water and it may be assumed that at one time or another all the water of the oceans was at or near the surface. Surface water in contact with the atmosphere would have become saturated with air and by the processes of diffusion and advection (stirring by wind and currents) the gases would have been distributed throughout the entire body of water. The most abundant gases found dissolved in sea water are nitrogen, oxygen (including that in carbon dioxide) and argon with traces of the other inert gases. The amounts of the gases that actually dissolve in the surface waters depend on the solubility coefficients which in turn are functions of temperature and salinity. The quantity of gas in the surface waters is greatest in the colder, less saline regions. With the exception of oxygen, all the gases tend to be retained in a saturated state by the water as it sinks from the surface. Measurements have shown that the gas concentrations then change little with location.

Table 2.1 *Proportions of dissolved salts in sea water (adapted from [2]).*

Ions	% by mass
Cl^-	55.0
Na^+	30.9
SO_4^{--}	7.8
Mg^{++}	3.7
Ca^{++}	1.2
K^+	1.1
Sr^{++}	
Br^-	0.3
C(as HCO_3^- or CO_3^{--})	

The concentration of oxygen in the surface water is between 5 and 10 ml/litre compared with a concentration of about 210 ml/litre in air. Marine organisms must, therefore, have either highly efficient methods of extracting oxygen or lower metabolic (energy) requirements, or both, to survive. On the other hand, the concentration of carbon dioxide in the ocean waters is about 50 ml/litre while in the atmosphere it is 0.3 ml/litre. (This contrast accounts for the differences between the methods of photosynthesis adopted by marine and land plants.) Thus, one litre of surface water contains about 55 ml of gaseous oxygen and about 600 litres (860 g) of oxygen combined chemically with hydrogen. If some practical method of extraction could be devised then divers, for example, could obtain 1 litre of oxygen from less than 2 ml of sea water.

2.4.3 *Ice in the Sea*

Ice in the sea comes mainly from the freezing of sea water and is thus called 'sea ice'. When sea water freezes, crystals of pure ice form first and increase the salinity of the remaining liquid. However, some of the concentrated salt solution ('brine') becomes trapped within the open structure of the crystals. New sea ice, in bulk, cannot be regarded as pure water – it has a salinity of 5–15‰, and the faster ice forms the more saline it becomes. When ice thickens or when rafting occurs the brine gradually trickles down from the elevated ice to the water level and eventually leaves almost saltless, clear, old ice. This ice, if more than about one year old, can be melted and used as drinking water, whereas new ice is not potable. Sea ice must therefore be considered as a material of variable composition with properties which depend significantly on its previous history.

Whereas pure water freezes at 0°C the freezing point of sea water with a salinity of 35‰ is −1.91°C. Unlike pure water, the maximum density of sea water (when the salinity is 24.7‰) occurs at a temperature of −1.33°C, which also corresponds to the freezing point. (The frequently quoted temperatures of maximum water density at higher salinities are therefore below the freezing point and so are meaningless.)

Incipient freezing in the sea is indicated by a 'greasy' appearance on the surface arising from the presence of flat ice crystals. As freezing continues, individual plates or spicules of ice develop in quantity ('frazil' ice) and these tend to aggregate into 'slush' ice. Further aggregation results in rounded sheets of 'pancake' ice which then freeze together to form 'flow' or 'sheet' ice. The rate of ice formation increases with low salinity, lack of water and air movement, shallow water and the presence of old ice which keeps the water calm. At an air temperature of −30°C some 30 mm of ice can form in one hour and 300 mm in three days, the rate decreasing with thickness because ice is a poor conductor of heat.

Ice at the polar cap is very hummocky and on average several years old. After some melting in summer the average thickness of the ice decreases to about 2.5 m and open water spaces, called 'polynyas', may form. In the autumn these freeze over and the ice in them is squeezed into ridges, or pushed so that one piece slides up over another – a process known as 'rafting'. The average thickness in winter increases to about 3.5 m, but hummocks may cause the height locally to be around 10 m above sea level with increases in depth to as much as 50 m below sea level. Although the polar cap is always present it does not consist of the same ice. Some is carried away in the East Greenland Current while replacement occurs from the rafting of pack ice. The pack ice is outside the polar cap, and whereas the former can be penetrated by ice-breakers the latter is quite impenetrable. About 25 per cent of the Arctic area is covered with pack ice, this area being least in September and greatest in May. Finally, fast ice forms from the shore (to which it is held fast) and moves out towards the pack. In the winter fast ice has a thickness of 1–2 m but melts completely in the summer. The ice which prevents or impedes navigation off the northern coasts of Canada, the east coast of Greenland, the Bering sea and so on is the pack ice which is several metres thick in those regions. Separate pieces are called 'floes' and should not be confused with 'icebergs'.

Icebergs, which are a danger to shipping in the North Atlantic and the Antarctic, originate as pieces 'calving-off' glaciers. When icebergs are calved-off the Greenland glaciers they often extend to 70 m above sea level, but this height decreases rapidly thereafter. The height of icebergs carried by the Labrador Current into the North Atlantic is generally about 30 m; the largest recorded was 80 m high and 500 m long. The density of an iceberg is about 900 kg m^{-3}, which is a little less than that of pure ice as a result of the gas-bubble content. The ratio of submerged volume to the volume above sea level is close to 7. Icebergs also occur in the Southern (Antarctic) Ocean and on present evidence they seem to be found between 50 and 40°S while pack ice extends only to 65 or 60°S. This zonal distribution probably arises from the character of the ocean currents in the Southern Ocean, and these will be discussed later. More details on the formation, movement and distribution of sea ice are given in [3].

2.4.4 *Heat Budget of the Oceans*

Variations of temperature with location and time are indications of the rate of heat transfer to or from the oceans by means of currents, absorption of solar energy, loss by evaporation, etc. Assuming a steady thermal state exists and considering the world ocean as a whole (for which there will be no advective heat transfer because all the ocean currents are 'internal' and must add to zero) the equation for thermal equilibrium is

$$Q_s = Q_h + Q_e + Q_b$$

where Q refers to the rate of heat transfer per unit area of the sea surface. The subscript s refers to solar radiation transferred to the ocean, and the subscripts h, e and b refer respectively to heat transfer by convection, evaporation and back radiation from the surface of the sea to the atmosphere.

Calculations have shown that the average magnitudes of the heat fluxes are:

$$Q_s = 150\ \mathrm{W\,m^{-2}} \quad Q_h = 10\ \mathrm{W\,m^{-2}} \quad Q_e = 80\ \mathrm{W\,m^{-2}} \quad Q_b = 60\ \mathrm{W\,m^{-2}}$$

although precise values vary considerably with location. For example, Q_s changes dramatically from winter to summer at high latitudes but is virtually unchanged in equatorial areas throughout the year. The quantities Q_h and Q_e often change sign with the seasons whereas Q_b remains substantially constant, although it is affected by the presence of clouds as a result of modifications to Q_s (see Fig. 2.3).

The average heat fluxes in the northern hemisphere are shown in Fig. 2.6(a). Values of Q_s (direct) have been adjusted to allow for cloud cover and it is the major flux to a latitude of 50°N beyond which direct light and diffused (sky) light contribute equal proportions. Back radiation and convection vary little, although evaporation is large at equatorial and tropical latitudes and reduces to almost zero in the polar region. The net gain and loss of heat flux are shown in Fig. 2.6(b) where, of course, the values of Q must be multiplied by the surface area of the sea to calculate the total rate of heat transfer. When this is done it is found that equilibrium prevails.

We have merely hinted here at some of the important features of heat transfer in the oceans and more details can be found, for example, in [4].

Any thermal energy gained by the surface water from solar radiation is not retained solely in the surface region but is mixed vertically downwards. The upper few millimetres of water may thus share heat with a water column some one hundred metres deep. Hence, the average temperature rise in the sea surface is about 10^{-4} K min^{-1} whereas the corresponding figure for rock might be 1 K min^{-1}, assuming solar radiation to be absorbed at the same rate on land and sea. From this we can conclude that the oceans are warmed very slowly in comparison with the land and can store a large amount of heat at a given surface temperature. Similarly, warm waters cool far more slowly than land.

Human survival at sea is also limited by the thermal properties of water. The oceans are invariably cooler than the human body and because the sea is a good

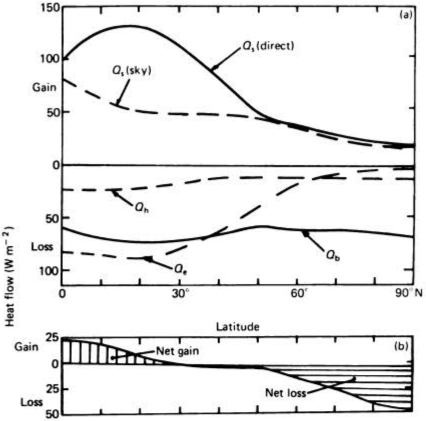

Fig. 2.6 Heat fluxes in the northern hemisphere.

heat sink there is a rapid and large heat transfer to the sea water. Such a transfer does not occur to the same extent in air, which has a specific heat capacity of about one-quarter and a thermal conductivity of about one-twentieth that of water.

2.4.5 *Distribution of Physical Properties*

Before discussing the distribution of the more important properties of the ocean it is worth listing and comparing some mean values with their counterparts in the atmosphere. Table 2.2 shows the magnitudes of the physical properties of particular importance to the study of marine vehicles. Apart from salinity, both the aerosphere and the hydrosphere have the same properties, but it is the difference between the corresponding magnitudes that has such a profound effect on vehicle behaviour. Conditions in the standard atmosphere to an altitude of 11 km are computed with the assumption that the air is in adiabatic thermal equilibrium. Temperature then decreases at a constant rate (the 'adiabatic lapse rate' is approximately 9.75 K km^{-1} although a mean practical value is about 6 K km^{-1}), pressure falls rapidly and therefore density decreases with altitude. Generally speaking, surface tension is not regarded to be of primary importance in the present context. However, if the air–water interface possessed the surface tension of an air–oil interface movement there would be a rather messy business. Water does not stick to surfaces but runs off leaving them comparatively dry.

Table 2.2 Physical properties of the aero–hydrospheres.

Property	Symbol	Unit	Aerosphere			Hydrosphere
			Sea level	3.5 km	15 km	
Pressure	p	10^5 Pa	1.013	0.657	0.120	1.013 + 0.1/m depth
Temperature	θ	°C	15.0	−7.8	−56.5	+ 30 to −2
Density	ρ	kg m^{-3}	1.226	0.864	0.194	1028 at 0°C 1023 at 30°C
Salinity	s	‰	–	–	–	35
Kinematic viscosity	υ	10^{-6} m^2 s^{-1}	13.3 at 0°C 16.0 at 30°C			1.826 at 0°C 0.849 at 30°C
Speed of sound waves	a	m s^{-1}	331.5 at 0°C			1445 at 0°C and s = 35‰
Specific heat capacities	c_p c_v	kJ kg^{-1} K^{-1}	1.0 0.715			4.217 at 0° 4.178 at 30°C
Thermal conductivity	k	W m^{-1} K^{-1}	0.024 at 0°C 0.026 at 30°C			0.570 at 0°C 0.607 at 30°C

The spatial distribution of the properties in the surface and the upper waters tends to be 'zonal', that is, a particular property varies little along given lines of latitude (east–west direction) but shows significant variations along a line of longitude (north–south direction). Some surface properties averaged over all lines of longitude are shown by the typical curves in Fig. 2.7. Note that there will, of course, be seasonal and daily ('diurnal') modifications locally.

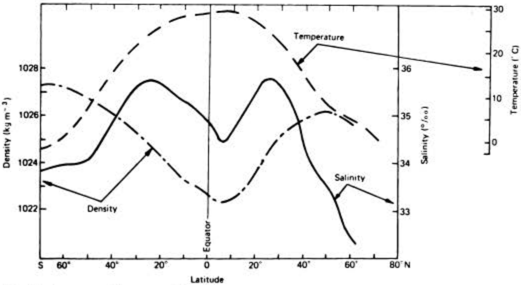

Fig. 2.7 Average surface properties of the oceans.

The density of the surface waters has a single minimum at the equator corresponding to the maximum temperature there but shows only a slight dependence on salinity. Cooling, evaporation and ice formation all tend to increase density. There is a significant correlation between the salinity of surface waters and the rates of evaporation and precipitation. The zonal influence showing mean longitudinal variations is shown in Fig. 2.8. The maxima at 30°N and 30°S are located near regions of high pressure in the aerosphere where clear skies and the trade winds increase salinity as a result of heating and evaporation.

The variation of physical properties with ocean depth is extremely important to the designer of marine vehicles and ocean structures, and so we shall now examine these in some detail.

(a) *Pressure*

The pressure at a point in a stationary fluid results from the weight (a gravitational force) of the overlying material and depends, therefore, on the fluid density and the height of the column of fluid (or fluids) above the location considered. Suppose we

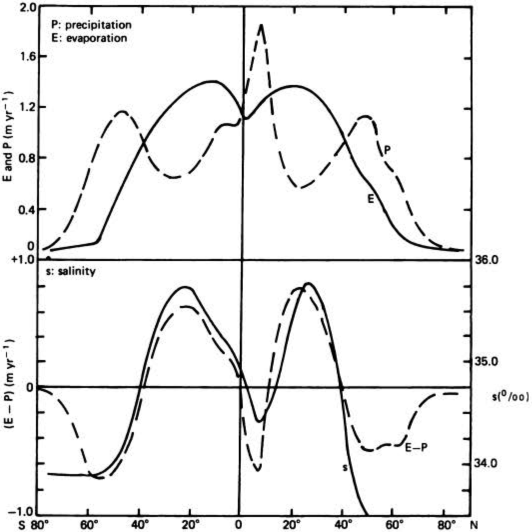

Fig. 2.8 Mean variations of evaporation and precipitation.

take the air–water interface as a datum for pressure. The pressure there, arising from a column of air extending radially outwards from the interface to outer space, is about 10^5 Pa. Pressure will thus decrease from this value with altitude but increases with depth in the hydrosphere. The pressure gradients are quite different, however, due to the large and virtually constant density of water. We can say with reasonable accuracy that pressure increases with depth in water at the rate of 10^5 Pa (about one atmosphere) for every increase of 10 m. Thus, at a depth of 10 m the pressure is 2×10^5 Pa, at 100 m the pressure is 11×10^5 Pa = 1.1 MPa and at the bottom of Challenger Deep (about 11 km) the pressure is approximately 110 MPa or 1100 atmospheres!

In addition to the effects of solar radiation on the temperature and density of the oceans, adiabatic compression or expansion takes place if a sample of water is moved away from or towards the interface. Both the temperature and density of the water change, the extent depending on the salinity. A valid comparison between the various properties of the ocean which may initiate motion must take account of adiabatic processes and this raises the concept of a *potential* magnitude to complement the corresponding *in situ* magnitude. For example, if water of salinity 35‰ at an *in situ* temperature of 4°C were raised adiabatically to the surface from a depth of 4 km its *potential* temperature would become 3.59°C. The temperature change with depth resulting from an adiabatic process is approximately 0.1 K km^{-1}, although in practice the effect is nonlinear [3]. Similar comments apply to changes of density with pressure. For sea water of constant temperature 0°C and uniform salinity 35‰ the *in situ* density is about 1046 kg m^{-3} at a depth of 4 km, whereas the *potential* density (at the interface) is about 1028 kg m^{-3}.

(b) *Temperature*

Below the surface the ocean can be divided into three zones according to the vertical distribution of temperature as shown in Fig. 2.9. There is an upper zone of depth 50–200 m with a temperature similar to the surface value as a result of continuous advection. Below this, extending to depths of 500–1000 m, is a region of rapidly

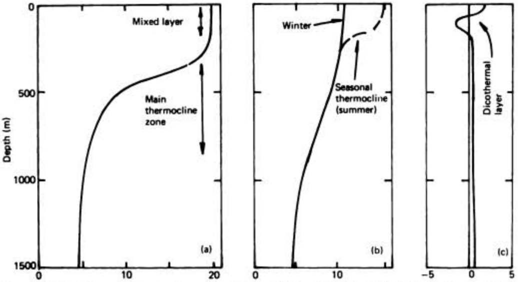

Fig. 2.9 Variations of temperature with depth; (a) low latitudes; (b) middle latitudes; (c) high latitudes.

decreasing temperature called the *thermocline zone* (the depth at which the temperature gradient is a maximum is called the *thermocline*. Finally, a deep zone exists where the temperature is practically independent of depth.

Although the depth limits of the thermocline zone are often difficult to determine accurately it is accepted that a thermocline is always present at depths between 200 and 1000 m in the low and middle latitudes. In high northern latitudes there is often a *dicothermal* layer of very cold water, possibly at a temperature as low as

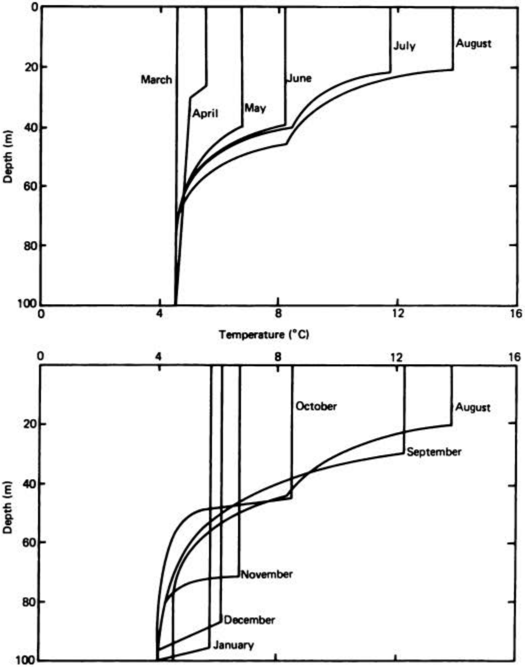

Fig. 2.10 Typical seasonal variation of temperature with depth in North Pacific Ocean.

−1.6°C, sandwiched between the warmer surface water and the deep waters at 50–100 m below the interface (Fig. 2.9). The thermocline zones are highly stable and outweigh the effect of salinity in the determination of sea-water density. These zones thus separate the surface waters from the deep waters.

A typical seasonal distribution of temperature for a location in the eastern North Pacific Océan is shown in Fig. 2.10. From March to August the temperature increases gradually owing to the large absorption of solar radiation and hence a constant-temperature layer is always in evidence down to about 30 m. After August there is a net loss of heat from the sea and the effect of continuous winds is to reduce the seasonal thermocline until the constant temperature condition of March is approached. Note that the overall variation of temperature is about 9°C, whereas a typical variation on a continental land mass is commonly 20°C or more.

(c) *Salinity*

The variation of salinity with depth cannot be explained as easily as the temperature distribution. In the upper waters of the open oceans the major factor determining the vertical stability of a body of sea water is the density, which is influenced primarily by temperature (except in the polar regions). Hence, water of higher temperature (lower density) is found in the upper layers and water of lower temperature (higher density) is present in the deeper layers. The variations of salinity are not sufficient to overcome the effect of temperature on density and it is thus quite possible for the upper, warmer layers to have high or low salinity.

Typical distributions of salinity are shown in Fig. 2.11 for the Atlantic and Pacific Oceans. The region of rapid change in salinity is called the ***halocline zone***.

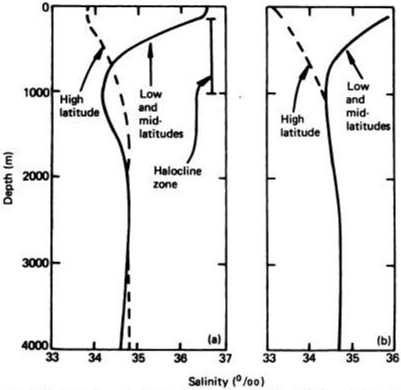

Fig. 2.11 Variations of salinity with depth: (a) Atlantic Ocean; (b) Pacific Ocean.

In the tropics a salinity maximum is often detected below the constant-salinity top layers owing to the intrusion of a thin layer of the highly saline and slightly denser water in the subtropical areas (Fig. 2.7) which flows towards the equator.

(d) *Density*

Natural systems seek an equilibrium state of minimum energy and accordingly it is found that the waters of greatest density occur at the greatest depths. The density of a fluid depends on its pressure, temperature and, in the case of sea water, slightly on salinity. To date it has not proved possible to make direct measurements of density *in situ* with the necessary precision; instead they are calculated from the equation of state of sea water (although even this cannot be formulated precisely). However, *in situ* measurements of density may give a misleading explanation of the dynamic behaviour of the oceans.

Noting that the ocean density always lies between 1020 and 1055 kg m^{-3}, let

$$\sigma_{s,t,p} = (\text{relative density} - 1) \times 1000$$

The subscripts s, t, p refer to corresponding values of salinity, temperature and pressure to yield the *in situ* density. Thus, for a density of 1028 kg m^{-3} we have

$$\sigma_{s,t,p} = \left(\frac{1028.0}{1000.0} - 1\right) \times 1000 = 28.0.$$

The potential density will be represented by $\sigma_{s,t,0}$ because the surface pressure can be considered as zero gauge. Provided we are concerned with bodies of water which do not change depth too greatly, the adiabatic change of temperature can be neglected and the temperature and salinity can be taken as those *in situ*. For most applications $\sigma_{s,t,0}$ is used and this is generally abbreviated to σ_t.

Figure 2.12 shows that σ_t is nearly uniform in the shallow surface layers of the equatorial and tropical regions. There is then a rapid increase in density and depth (the *pycnocline zone*) to about 2 km and thereafter σ_t increases very slowly to a value of about 27.9 irrespective of latitude. At high latitudes, where σ_t is 27.0 or more at the surface, the pycnocline is less evident and is, in fact, absent in the polar oceans. The temperature-controlled pycnocline represents a stable layer which offers an efficient barrier to the passage of water, salts and gases in a vertical direction. Any spatial variation of density takes place only in the presence of currents. The cold, high-density surface water at high latitudes sinks gradually along constant-density surfaces called *isopleths* inclined at some (small) angle to the air–water interface. Deep ocean currents are thus formed which move towards the equator.

(e) *Light Transmission*

The optical properties of sea water influence the colour, the visual conditions and the biological activity of the oceans. When sunlight reaches the surface of the water some is reflected, the amount depending on the proportion of direct sunlight to diffuse skylight. For a calm surface the fraction of the reflected direct light varies from about 2 to 40 per cent of the total as the sun moves from overhead to low on the horizon. On the other hand, about 8 per cent of the diffuse light is reflected throughout the day. All of these quantities are to some extent affected by surface waves but little quantitative data are available on this aspect.

When short-wavelength (0.4–0.7 μm) solar radiation, that is, light, passes through the surface of the sea it is either *dispersed* or *absorbed*. Dispersion (or scattering)

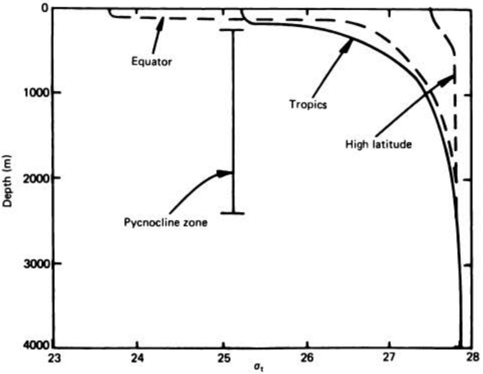

Fig. 2.12 Variations of density with depth using σ_t variable.

simply involves an alteration of the direction of the light, whereas absorption results in the conversion of radiant energy to internal energy with a consequent rise in water temperature. The reduction in intensity which the light experiences on passing through the water is called *extinction*. The rate at which light is absorbed in water depends on the wavelength, as shown in Fig. 2.13, and the degree of extinction varies with both depth and turbidity, as illustrated in Fig. 2.14.

The non-visual energy contained in the long-wavelength part of the spectrum, say above 4 μm, which accounts for about 1 per cent of the total energy, is absorbed within one millimetre of the surface due to the very high absorption coefficient of water at these wavelengths. Indeed, some 50 per cent of the solar radiation entering the oceans is absorbed in the upper centimetre and 90 per cent in the upper 40 m of water. The least absorption occurs in the blue-green part of the spectrum and thus light of this colour penetrates further. This is why the clear oceans, free of organic and plant matter, are predominantly blue-green in colour (see Fig. 2.13).

Figure 2.14 shows that in the clearest oceans most of the solar radiation is absorbed and thus extinction is complete at depths greater than about 100 m, whereas a depth of 10 m is more applicable to turbid coastal waters. Evidently, the work of frogmen and divers is severely restricted by the limited visibility even when powerful artificial light sources are available. Nevertheless, in clear ocean water there is usually enough light at 50–100 m to permit a diver to work effectively.

(f) *Sound Transmission*

Whereas electromagnetic (light) energy in the visible spectrum is attenuated less than mechanical (sound) energy in the atmosphere, the reverse is true in the sea.

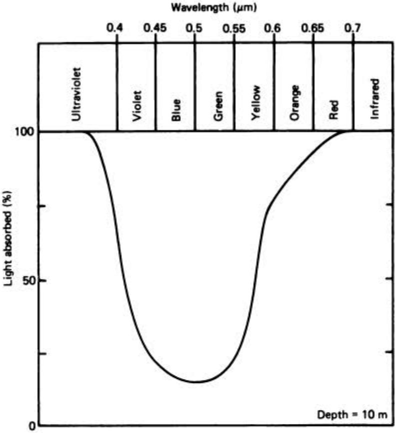

Fig. 2.13 Light absorption in water.

Indeed, water is a very efficient medium for the transmission of sound and the velocity of propagation of sound waves is about 4.5 times that in air (see Table 2.2). As a result of this disparity between the propagation velocities only a small amount of sound energy starting in air, for example, will penetrate the interface into water, in contrast to the relatively easy passage of light across the interface. It is thus not possible for conversations to take place directly between, say, a submerged diver and the crew of a support ship. However, submerged transducers contained in hydrophones, or echo-sounders, are used both to receive and transmit sound energy, and it is these devices that are used extensively to determine the depth of the oceans. At smaller ranges of depth echo-sounders can be used to detect submarines and shoals of fish.

Submarines carry a number of sonar (*so*und *n*avigation *a*nd *r*anging) devices each of which may comprise many transducers in the form of an array. In order to avoid detection by other submarines, ships, sonobuoys and so on, the submarine usually adopts a passive, listening role. On-board computers record on magnetic tape and process the signals resulting from the conversion of mechanical vibration to electrical output by the piezoceramic material forming the body of the transducer. Detection and classification of the source of the noise may then be carried out. If the source is of interest and needs to be investigated its range may be obtained by measuring the time taken for an echo to be received from the source following the emission of an active short pulse of sound energy. The direction of the source

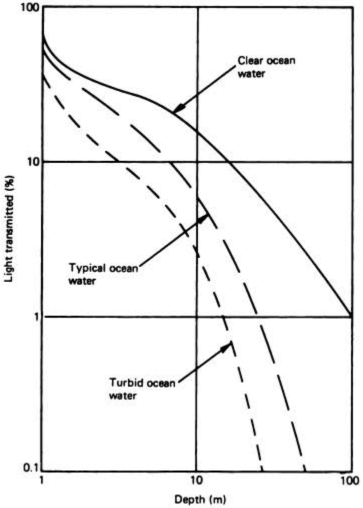

Fig. 2.14 Extinction of light in water.

relative to a listening submarine may be found from a sonar array by arranging for the transducer to have (electrically) a variable sensitivity. It is possible to 'sweep' a wide area using a time-delay circuit and the maximum response from the beam formed by the array corresponds to the direction of the source. The subjects of sonar design and signal processing have become exceedingly sophisticated in recent years and are quite beyond our scope here. However, a comprehensive introduction to underwater noise in relation to ships and submarines is given in [6].

The propagation velocity of longitudinal waves in an elastic liquid is given by $a = (K/\rho)^{1/2}$, where K represents the bulk modulus of elasticity and ρ the density of water. As both K and ρ depend upon temperature, salinity and pressure then so does a. The value of a for sea water increases by approximately 4 m s^{-1} per degree Kelvin rise in temperature, by 1.5 m s^{-1} per 1‰ increase in salinity and by 18 m s^{-1} per 1 km increase in depth. Taking into consideration the variations of temperature and salinity with depth it is not surprising to find a pronounced minimum value of a at some depth. This depth of minimum velocity varies from about 1 km in low and middle latitudes to practically zero in polar regions. Figure 2.15

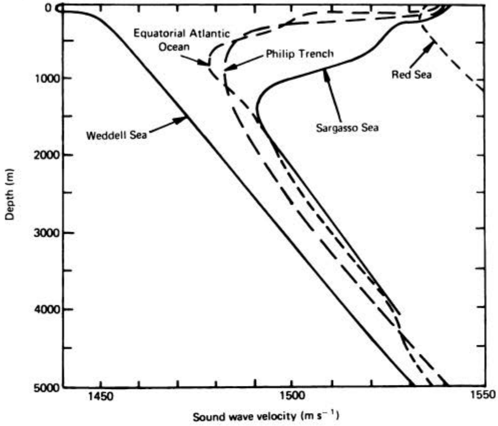

Fig. 2.15 Sound-wave velocity variations with depth.

shows some typical vertical distributions of lateral sound wave propagation velocity for different seas of the world oceans [5].

Owing to the dependence of physical properties on depth, refraction of sound waves will occur. This is why it is difficult to form sound images in the oceans – a situation analogous to the blurred view seen through hot air rising from a radiator or though the exhaust from a jet engine. However, sound waves transmitted at the depth of minimum velocity of propagation tend to stay at that depth because refraction takes place from above and below. This property is referred to as a *sound channel* (see Fig. 2.16) and use is made of it by the sofar (*so*und *f*ixing *a*nd *r*anging) technique. Low-frequency sound waves from an underwater explosion, for example,

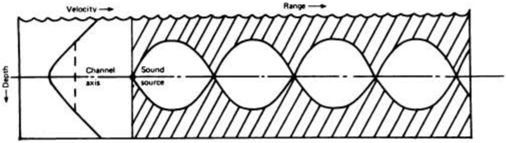

Fig. 2.16 Formation of a deep sound channel.

may then be detected after travelling many thousands of kilometres. A 'fix' on the source of the explosion may then be obtained by triangulation using records from, say, three receiving stations at known locations. Similarly, sound waves produced by a submarine may be refracted downwards so that a listener at the surface some horizontal distance away will hear nothing. This is one reason why submarines dive deeply into the sound channel when attempting to avoid detection. But as a result they are surrounded by shadow zones which reduce the effectiveness of their own receivers and transmitters. High frequencies are rarely used for underwater sound propagation because, as with light energy, low wavelengths are readily absorbed. Nevertheless, it is sometimes necessary to use frequencies of 100–200 kHz to improve resolution and reduce the effects of scattering, but this often entails a reduction in the penetration produced by echo-sounders. It is interesting to note that the ambient noise present in the oceans is predominantly at low frequencies, that is, below about 1 kHz [7].

2.4.6 *Stratification*

The variation of physical properties with depth in the oceans has been represented by smooth curves fitted to experimental points. In fact the sea has been found to exist in a strongly stratified state consisting of horizontal layers of water of uniform properties. For example, temperature and salinity may change abruptly from one layer to the next in increments of about 0.01°C and 0.1‰ respectively, but remain constant within the accuracy of measurement inside each layer. This situation arises from the stratification of a vertical water column into a stable state of increasing density with depth combined with the dependence of density on temperature and salinity.

The oceans may, however, be conveniently divided into three regions which result from the rapid extinction of solar radiation together with wind-induced mixing (advection)

(i) the surface zone: saturated, warm, well-lighted, less dense, more saline water;
(ii) the pycnocline: the density gradient is such that a very stable layer of water is formed and acts as a barrier to vertical movements of water and organisms; and
(iii) the deep zone: dark, cold and independent of local events occurring at the surface.

2.5 Characteristics of the Dynamic Model

We have mentioned already that equilibrium conditions throughout the oceans do not prevail and that movement can occur even at great depths. The main disturbing forces are:

(i) external forces acting at or near the boundaries arising from thermal and mechanical actions; and
(ii) internal forces developed by the gravitational fields of the Sun and Moon which produce tidal motions.

From these influences we can identify two, more or less independent phenomena, namely currents and deep-ocean circulation. Through ease of observation most data have been accumulated from the surface currents, and as these are brought about by the interaction of wind and water at the interface we must examine motions in both the atmosphere and hydrosphere.

2.5.1 *Motion of the Atmosphere*

The atmosphere absorbs solar radiation in small amounts over large distances and in doing so the rate of heat generation is slight. However, the rate of absorption by land and sea is rapid and consequently these surfaces are heated. The temperature of the air in close proximity to the Earth is then increased which results in a reduction of density. Buoyancy forces induce the low-density air to rise into the atmosphere and a convective circulation current is produced. From these observations it would be natural to conclude that near the equator, where the Earth is at its highest temperature, air would rise, while at the poles the cool air would approach the surface. Large circulation cells, one in each hemisphere and moving in the opposite sense, could be anticipated, and indeed were described in 1735 by George Hadley (see Fig. 2.17). The north–south circulation provides the energy to induce winds; easterlies and westerlies result from the deflection of the basic motion by the Earth's rotation.

However, recent measurements of wind direction at ground level and at high altitude have shown that this model is too simple. Certainly in the lower atmosphere (troposphere) the general circulation of air takes on a pattern similar to that shown in Fig. 2.18. Also shown in this figure are the principal areas of high and low atmospheric pressure at the Earth's surface, although, as we shall see later, these areas are broken up into slowly traversing regions. The nature of the air flow outside the edge (tropopause) of the troposphere, that is in the stratosphere, has

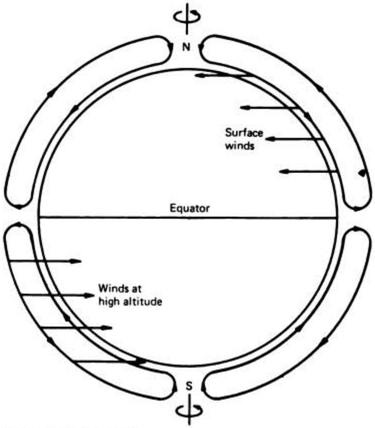

Fig. 2.17 Hadley model.

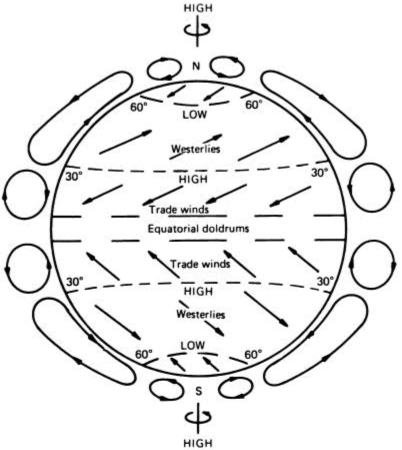

Fig. 2.18 Modern model of aerosphere.

not yet been fully investigated or explained. It is known that large, so-called *jet streams* occur there, or just inside the tropopause, which comprise belts of air travelling at speeds often approaching 150 m s^{-1}. There is little doubt that eddies from these jet streams often initiate storms which influence weather conditions close to the surface of the Earth. High-flying aircraft have sometimes used the jet streams effectively to gain a tail wind and thus reduce flying time and fuel consumption.

There are three main circulation cells in each hemisphere: the two smaller ones, at high and low latitudes, conform with Hadley's suggested directions of motion, whereas the large circulation cell in the middle latitudes moves in the opposite sense. Rotation of the Earth causes the air in the cells to be deflected from the north–south direction. The relative effect increases as the poles are approached but is zero at the equator. This is known as the Coriolis effect, and to an observer on the Earth any object moving at the surface experiences an acceleration perpendicular to its direction of motion. Deflection to the right occurs in the northern hemisphere and to the left in the southern hemisphere, as shown in Fig. 2.19. Furthermore, a body moving in a curved path will experience a centripetal acceleration towards the instantaneous centre of curvature of the path and, for real fluids, a shear stress owing to the relative motion between adjacent layers. These additional factors modify the Coriolis effect but the sense of the deflection remains.

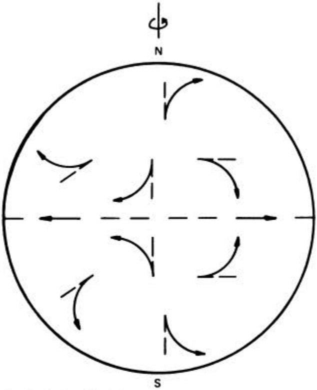

Fig. 2.19 Coriolis effect.

Combining the Coriolis effect with the circulation cells in Fig. 2.18 shows that surface wind directions conform to the observed easterly winds at 5–25° latitude, westerly winds at 35–55° and polar easterly winds at 60–85°. In the equatorial region of 5°N to 5°S there is a belt of low pressure; air streams converge and rise and the surface winds are light and variable, often inducing cloudiness with a heavy rainfall. This region is often referred to as the *doldrums*, although a better description would be *intertropical front* or *convergence zone*. The *trade winds* (so named by early mariners for their reliability in trading ventures) blow from the south-east in the southern hemisphere and from the north-east in the northern hemisphere and both converge onto the equatorial belt. The origin of the trade winds is in the *horse latitudes* where high pressure prevails as cool air descends from the upper troposphere. This is another surface region of calms or variable winds accompanied by clear skies. (In the days of sailing ships it was in these latitudes that horses were thrown overboard to lighten a ship if it were becalmed too long!) The cells into which the high pressure is divided are generally quite well defined over the oceans. At the poles air is cooled and becomes denser thus causing an inflow of air at high altitude. Near the surface there is a migration of air from the high pressure at the poles to the low-pressure subpolar front where it again warms and rises to complete the polar cells. Coriolis effects result in the surface winds being north-easterly in the northern hemisphere and south-easterly in the southern hemisphere although these are generally called *polar easterlies*. The subpolar, high- and subtropical, low-pressure belts induce motion in the mid-latitude cell which deflect the surface winds to form the *prevailing westerlies.* The surface winds for January and July are shown in Figs. 2.20(a) and (b) together with the main regions of high and low pressure.

The westerlies and polar easterlies converge at the polar fronts and the great difference between the temperatures of these air streams gives rise to cyclonic storms or lows. The prevailing direction of these cyclonic zones is westerly, although the strong winds within the storms may blow in any direction. Land masses disrupt the westerlies in the northern hemisphere and so, for example, the British Isles and the north European coast experience a continuous sequence of cyclones throughout most of the year. In the southern hemisphere there are few land masses to affect the progress of the westerlies and this fact, combined with the large longitudinal pressure gradient, gives rise to strong and persistent winds. According to latitude these were, and still are, referred to as the 'roaring forties', the 'howling fifties' and even the 'screeching sixties'.

The triple-cell configuration illustrated in Fig. 2.18 requires an input of kinetic energy to support the east-west winds. It has been suggested [8] that this energy is supplied to the wind systems by large rotating masses of air in the form of either cyclones or anticyclones.† The generation of a cyclone in the northern hemisphere is depicted in Fig. 2.21(a) which shows the view looking towards the surface of the Earth. The polar easterlies often thrust down into the mid-latitudes in a fairly irregular manner and an interface between cold and warm air forms, for instance over the Atlantic Ocean, between the easterlies and the warm westerlies. The interface is unstable as a result of the effects of friction and the differences in density of the two air streams and a wave-like flow pattern is created. Low pressure develops at the crest of the wave front because the warm, humid, low-density air rides over and is replaced by the cold, dry, dense air. The warm, moist air rises to form progressively heavier cloud until saturation is reached and intense precipitation occurs (see Fig. 2.21(b)) accompanied by strong winds. The winds blow into the low-pressure centre and so in the northern hemisphere the Coriolis effect causes an anticlockwise motion. There is thus developed a 'low', or storm centre – a *cyclone* – which may be *occluded* from the frontal system. Examples are seen on most weather maps of the mid-latitudes.‡

The colder air masses have lower vapour content and will thus exhibit well defined areas of high pressure usually referred to as *anticyclones.* An anticyclone is essentially the opposite of a cyclone; at the centre is a region of high-pressure, descending air which gives rise to an outward velocity. Again the Coriolis effect alters the direction to form a mass of air rotating clockwise in the northern hemisphere. In the mid-latitudes, therefore, the continuous progression of wet 'lows' is accompanied by a series of adjacent dry 'highs'. Anticyclones translate quite slowly and are generally oval-shaped and large in area, whereas cyclones are normally smaller and often circular. The rate of progression of a cyclone varies, but on average it is about 10–15 $m\,s^{-1}$ and provided that the discontinuity in temperature and moisture content is maintained along its fronts the cyclone will persist. If the cyclonic area is broad and shallow it is called a *trough* of low pressure.

In addition to the preceding 'extratropical' cyclones a further series of 'tropical' cyclones are found along the region of the intertropical front. Owing to the lack of

† These, it seems, are influenced significantly by the jet streams progressing towards the equator.
‡ A warm front is indicated by a line joining semicircular symbols (often coloured red) and a cold front by a line joining triangular symbols (often coloured blue).

(a)

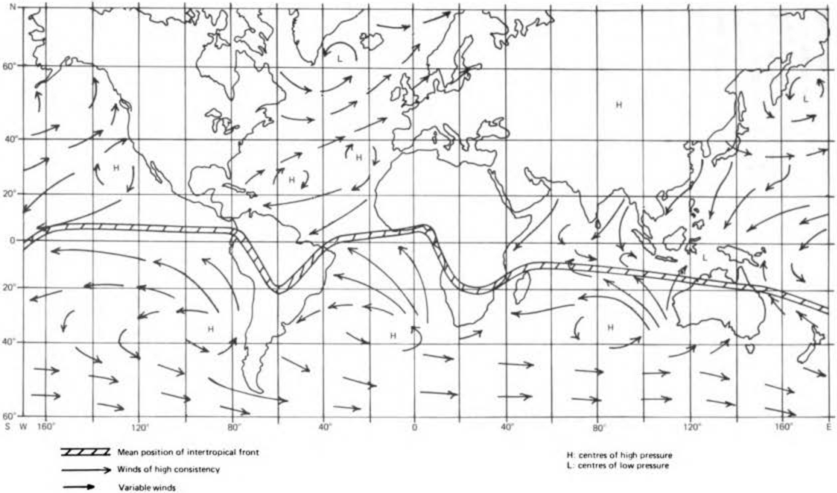
N
60°
40°
20°
0
20°
40°
60°
S
W
160°
120°
80°
40°
0
40°
80°
120°
160°
E
H
L
Mean position of intertropical front
Winds of high consistency
Variable winds
H: centres of high pressure
L: centres of low pressure

(b)

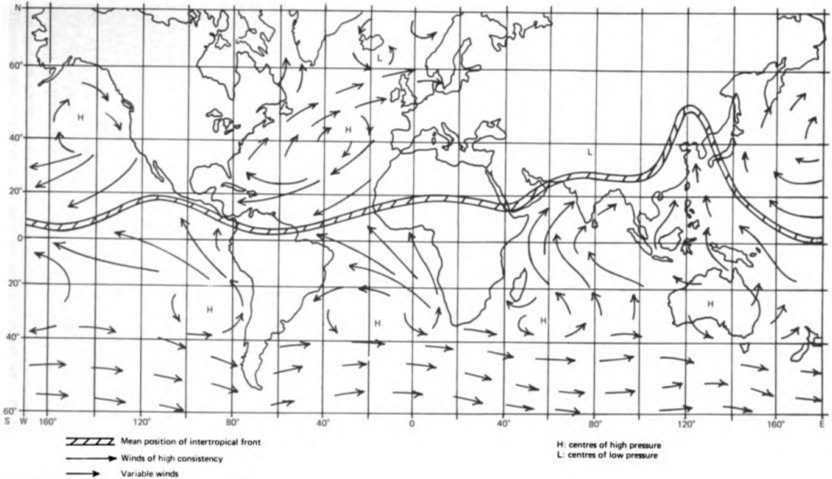

Fig. 2.20 Mean surface winds: (a) January; (b) July.

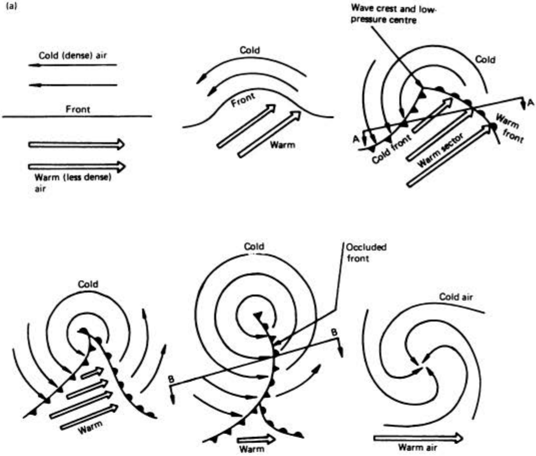

Fig. 2.21 Development of a cyclone in northern hemisphere: (a) radial view.

great contrasts in temperature the tropical cyclone tends to be less specific in size, shape and wind system. Nevertheless, over tropical oceans relatively small, and consequently extremely intense, cyclones do develop. These are variously called hurricanes, typhoons or cyclones (not to be confused with the normal, low-pressure cyclones) and do not occur in the South Atlantic as the intertropical front does not extend far enough south.

The energy of a hurricane increases with the abundance of moisture in the air which releases its latent heat on entering the low-pressure 'eye' before rising and causing torrential rain. The diameter of a typical hurricane is 150–1000 km and increases as movement away from the low latitudes takes place. It is difficult to record accurately wind speeds in a hurricane but certainly values in excess of $65\ \mathrm{m\,s^{-1}}$ (150 m.p.h.) occur and gusts have been estimated to be as high as $110\ \mathrm{m\,s^{-1}}$ (250 m.p.h.). The relatively calm 'eye' at the centre of the storm may be 10–50 km in diameter and at a pressure as low as possibly 90 kPa and exceptionally 85 kPa compared with normal pressures of about 101 ± 1 kPa.† Consequently, ocean water

† Meteorologists tend to use a unit of pressure called the bar (b) ($\equiv 10^5$ Pa) although it is not an approved SI unit. Thus, 90 kPa $\equiv$ 900 mb and so on.

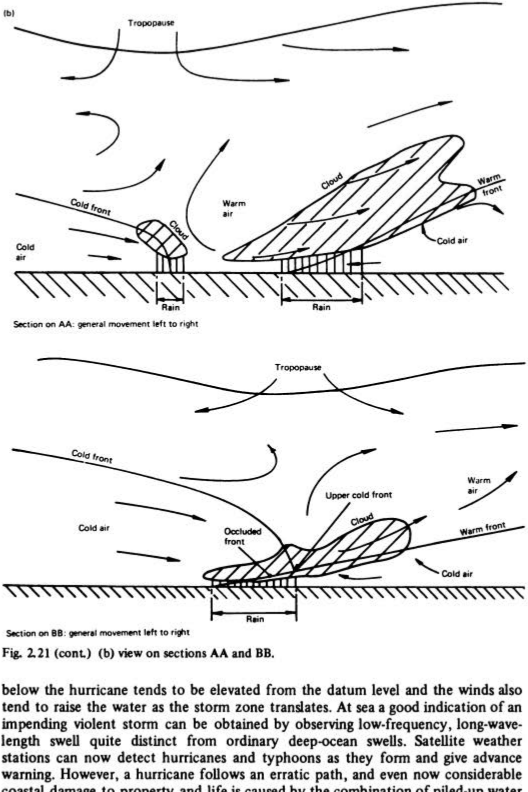

Fig. 2.21 (cont.) (b) view on sections AA and BB.

below the hurricane tends to be elevated from the datum level and the winds also tend to raise the water as the storm zone translates. At sea a good indication of an impending violent storm can be obtained by observing low-frequency, long-wavelength swell quite distinct from ordinary deep-ocean swells. Satellite weather stations can now detect hurricanes and typhoons as they form and give advance warning. However, a hurricane follows an erratic path, and even now considerable coastal damage to property and life is caused by the combination of piled-up water in the form of a 'storm tide' and the strong winds.

The most violent storms in the mid-latitudes are *tornadoes* or *twisters* [9]. The tornado is a tight cyclonic whirl a few hundred metres in diameter at the ground with a centre of extremely low pressure (e.g. 80 kPa or even as low as 75 kPa) in which speeds of 90–150 m s^{-1} are quite common. Tornadoes are formed in the warm sector of cyclonic systems just ahead of the cold front where cold air is over-running aloft. They usually travel parallel to the cold front towards the centre of low pressure at a velocity of some 25 m s^{-1} with periodic short intervals at rest. Over the sea, tornadoes form *water spouts* and these occur most frequently where cold continental air pushes over warm water, such as that off the east coasts of the United States, China and Japan and occasionally off the coast of Britain. When in contact with the surface a water spout picks up some spray, but its funnel is composed primarily of condensed water vapour in the low-pressure core.

Apart from local, and sometimes severe, perturbations of the basic pattern of the atmospheric circulation there are other large-scale seasonal effects such as the monsoons of India and China. A full discussion of monsoons and other seasonal factors may be found in [10].

When a wind blows, particles in contact with a surface have no velocity relative to that surface as a result of friction. However, above the surface the wind velocity increases asymptotically to the prevailing mainstream value. The velocity profile within this rather thin region is shown in Fig. 2.22 and is similar to that for a turbulent boundary layer over a flat plate set parallel to the oncoming flow. Wind speeds are usually measured at a standard altitude of 10 m above the local land or sea surface and are often quoted in terms of the Beaufort Scale, which is shown in Table 2.3. The scale is not accurate enough for detailed work but it provides a

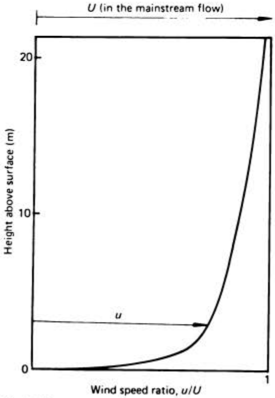

Fig. 2.22

Table 2.3 The Beaufort Scale.

Number	Wind speed at 10 m ($km\ h^{-1}$)	Wind description	Mean wave height (m)	Noticeable effect of wind on land	At sea
0	< 2	calm	none	smoke vertical; flags still	surface mirror smooth
1	2–5	light air	< 0.5	smoke drifts; vanes static	ripples; no foam crests
2	5–11	light breeze	0.5	wind felt on face; leaves, flags rustle; vanes move	waves are short and more pronounced
3	11–19	gentle breeze	1	leaves and twigs in motion; light flags extended	crests begin to break
4	19–30	moderate breeze	1.5	raises dust; moves small branches	longer waves; many white caps
5	30–40	fresh breeze	2	small trees sway	pronounced waves; white caps everywhere
6	40–50	strong breeze	3	large branches move; telephone wires 'sing'	large waves; extensive foam crests
7	50–60	moderate gale	4	whole trees in motion	sea heaps up; foam blows
8	60–75	fresh gale	5	twigs break off; progress impeded	waves increase; dense foam streaks
9	75–85	strong gale	6	chimney pots removed	higher waves; foam clouds
10	85–100	whole gale	7.5	trees uprooted; structural damage	long hanging crests; great foam patches
11	100–120	storm	8.5	widespread damage	ships hidden in troughs; air filled with spray; sea covered with foam
12	120	hurricane	> 8.5	countryside devastated	ships swamped; sea a maelstrom

dramatic description of the winds and is sufficient for many purposes. When the scale was proposed by Admiral Beaufort in 1806 no ship was considered capable of withstanding hurricanes. However, such limitations now have less significance as efforts are made to explore the nature, and predict the behaviour, of such extreme weather conditions. Present practice by the designers and operators of marine vehicles favours the use of sea states to describe the prevailing conditions.

The dynamic description of the atmosphere is seen to be one of rapid and extensive movement which is influenced by the interaction between the land and the sea. Disturbances of the mean circulatory motions are thus frequent and often severe.

2.5.2 *Motion of the Hydrosphere*

The hydrosphere differs from the atmosphere in two major respects. First, apart from the exceedingly small amount of heat conduction from the bottom, the oceans are surface-heated whereas the atmosphere is bottom-heated. As a result, large-scale convection currents arising solely from temperature differences do not take place in the hydrosphere. Secondly, the greater density of sea water (about 850 times that of air) implies the need for larger forces to induce motion while the greater viscosity of water (about 100 times that of air) requires large forces to maintain the motion. Consequently, movements in the hydrosphere are more sluggish than those in the atmosphere. Nevertheless, just as high-speed jet streams in the upper atmosphere influence conditions close to the Earth's surface so do the slow, but extensive, deep-ocean (abyssal) currents. The interaction between surface and deep layers and the general fluid dynamics of the oceans require an analysis too complicated to be dealt with here [11]. We shall therefore be content to give a simple description of the major characteristics.

(a) *Flow in the Upper Waters of the Oceans*

A description of the surface currents of the oceans can be divided into the overall, average features, which are taken over a long period of time and are part of the *climatic* circulation, and random, short-term variations, which form a *synoptic* picture of day-to-day conditions. Precisely the same division can be made for the aerosphere, but in this case synoptic features can change dramatically within a few hours whereas alterations in surface currents will not be noticed for several days or weeks. A climatic map of some part of the oceans would indicate the average path of a particular current but on any particular day the flow path may be as much as 150 km off this course.

Figure 2.23 shows the principal surface currents which are induced primarily by wind-induced shear forces at the surface. When allowance is made for the influence of the land masses and the Coriolis force, the permanent surface-water currents generally coincide with the permanent wind pattern (shown in Figs. 2.20(a), (b)). This climatic map is of value in a study of long-term effects such as erosion, transport of particulate matter, organisms and animal life, and the effect on overall climate, but a synoptic map is of more value to navigation. An example of a synoptic variation in the direction of a surface current is provided by the Kuroshio which flows along the west coast of Japan. Careful monitoring of velocity and position every three months showed that on several occasions part of the current deviated from the ocean path by as much as 3° of latitude over a two-year period. No fully acceptable explanation has yet been put forward for this odd behaviour.

The absence of land masses causes the westerlies in the lower latitudes of the southern hemisphere to induce east-bound currents known as the West Wind Drift. Similarly, the trade winds induce west-bound equatorial currents but these are obstructed by the main continents. There is no circumpolar westerly drift in the northern hemisphere but instead very large circulation currents (or 'gyres') are maintained in the North Atlantic and North Pacific Oceans. Currents such as the Gulf Stream, generated at the western boundary of the North Atlantic Ocean, and the Kuroshio (Japan Current), along the western boundary of the North Pacific Ocean, are the limits of two major gyres. Table 2.4 shows the estimated average volume transport of water and the average surface velocity in the core of the stream for some of the principal surface currents of the oceans. The mean velocity in the

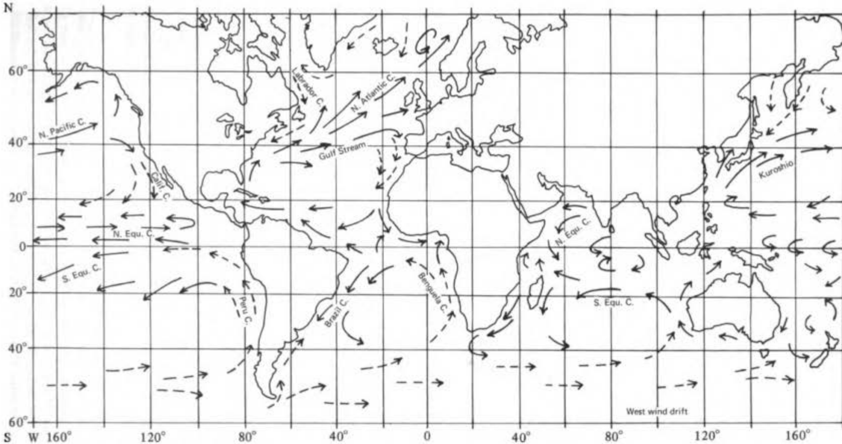

Fig. 2.23 Major surface ocean currents: ——→ warm currents; – – → cool currents.

Table 2.4 The main ocean currents.

Current	Volume transport (10^6 m^3 s^{-1})†	Velocity (m s^{-1})
Gulf Stream	38–55	1.2–1.4 exceptionally 2.5
North Atlantic Drift	10–14	0.1
Labrador	5.6	0.1
South Equatorial (flowing along the Guiana Coast into the Gulf Stream)	6	0.5–1.0
Brazil and Benguela	35	0.3–0.5
West Wind Drift	125–175	0.1–0.3
(Near Drake Passage)	75	0.1–0.5
Peru (Humboldt)	10–15	0.3–0.5
South Pacific Equatorial	20–30	0.3–0.7
Pacific Equatorial Counter	40	1.0
Cromwell	40	1.5
North Pacific Equatorial	45	0.2–0.3
Kuroshio (Japan)	35–70	0.7–1.1
North Pacific Drift	15–20	0.1–0.2
California	10	0.1

† The unit 10^6 m^3 s^{-1} is often called, in the present context, the Sverdrup (Sv) after the oceanographer H. U. Sverdrup.

clockwise gyre of the North Atlantic Ocean is about 0.2–0.3 m s^{-1} and so water in it takes approximately 3 years to complete one circuit.

Below the South Equatorial Current at the equator there flows an equatorial undercurrent known as the Cromwell Current which remained undetected until 1952 [12]. It consists of a thin ribbon of water some 200 m thick and about 300–400 km wide and is believed to flow easterly from off the New Guinea coast to Ecuador, a distance of 12 000 km or more. The core has been found to lie between depths of 10–100 m and may even break surface at times in the eastern Pacific. It is remarkable that a current with a thickness-to-width ratio of less than 1/1500 should persist for such great distances. Although this may be considered the largest equatorial undercurrent others have been found in the eastern Atlantic and Indian Oceans. Furthermore, at a depth of about 500 m another undercurrent, flowing westwards, has been discovered below the Cromwell Current. Clearly the vertical structure of water movement in the upper layers of the Pacific equatorial region – and probably elsewhere – is rather complex. Much is still not understood about the generation of surface currents, counter currents and undercurrents, or the interaction between them.

There are several interesting mechanisms by which currents and circulations can be generated in the upper layers of the oceans [13] and we now consider some of them.

(i) *Ekman Spiral.* When a wind blows over the sea a force on the surface results from the combination of frictional shear stress there and any surface pressure gradient in the atmosphere. The force is in the direction of the wind but the surface water will be deflected to the right in the northern hemisphere (to the left in the southern hemisphere) by rotation of the Earth. The 'horizontal' momentum of the surface waters is transmitted downwards by the presence of viscous stresses. The development of this circulation system was first investigated by V. W. Ekman in 1905 for flow in a homogeneous ocean of infinite extent and constant eddy viscosity. Regardless of wind strength his theory predicted the surface current and the net movement of the mass of water to be at 45° and 90° respectively to the wind direction. Observations suggest a surface deflection of 20 –50° and this applies also to the drift of polar pack ice.

For the sake of definiteness suppose a wind is blowing due north in the northern hemisphere over an ocean which may be thought to consist of a vertical stack of thin horizontal layers. The surface water will experience a frictional force to the north and a Coriolis force to the east giving a resultant force, and thus motion, in a direction 45° east of north, say. This layer will thus exert a frictional force 45° east of north on the layer of water below it, but again the Coriolis force will cause a further easterly shift of this layer. Moreover, the velocity of the top layer will be less than that of the wind and the second layer will have a velocity lower than the top layer, and so on. Indeed, it can be shown that in a real fluid the velocity of the layers will decrease exponentially with depth and thus the angular shift in the direction of each layer will also decrease. Using a vector representation for the velocity of each layer it can be seen, in Fig. 2.24, that the projection of the vectors on a

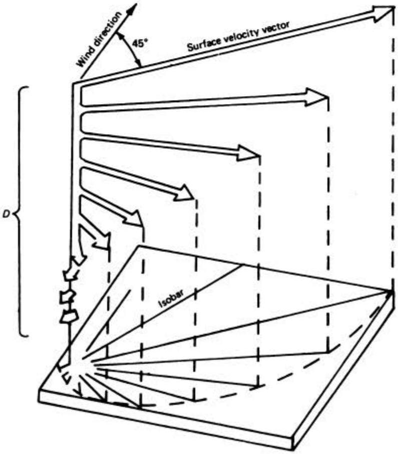

Fig. 2.24 Ekman spiral.

horizontal plane produces the so-called *Ekman Spiral*. According to this theory a depth D should be reached where the wind-induced velocity is reduced to near zero in a direction 180° from the surface current. This is known as the 'depth of frictional resistance' and for a wind of $7\ \mathrm{m\ s^{-1}}$ it is about 180 m at a latitude of 5° and, because the Coriolis force is greater, 60 m at a latitude of 50°.

(ii) *Upwelling*. A wind blowing northwards, for example, along a western coast in the southern hemisphere would cause, on the basis of the Ekman motion, a net movement of water offshore. This must be replaced by an inshore upward movement of water from below the Ekman Spiral inducing a local vertical circulation cell. Similar considerations can be given to the equatorial currents. The upwelled water is usually cooler than the surface water, an effect which leads to a reduction of local land and air temperatures which encourages the formation of fog.

(iii) *Geostrophic Currents*. These surface currents are induced by a combination of wind and gravitational effects. The prevailing winds in the North Atlantic Ocean, for example, form a virtually closed system. The resulting Ekman layers transport water towards the Sargasso Sea where it 'piles up' into a low hill about one metre high. Gravitational forces then tend to induce a flow 'down the hill', but again a Coriolis acceleration influences the motion. In the absence of friction these two accelerations must cancel for steady motion. Equilibrium prevails only if the water flows around the elevation in the sea's surface, the velocity of motion being greater on that part of the surface with the steeper slope. Similar circulations at constant height will occur if the surface of the ocean is depressed. Friction reduces the circulatory velocities and produces a downward drift of water towards the lower levels thus tending to eliminate the surface rise or depression.

(b) *Deep-ocean Circulation*

The preceding explanation of wind-driven (advective) currents does not fit with the observed vertical distribution of water properties along the surface route. To account for this and other objections to the existence of surface currents only we require an explanation of deep-ocean circulation. This circulation is a convective (*thermohaline*) circulation arising primarily from the effects of temperature and salinity on density. The density of sea water increases with cooling and so sinkage may occur which results in the displacement of the deeper water. The thermohaline circulation can develop either directly from this cause or indirectly when ice is formed and the salinity of the remaining water increases. In the North Atlantic Ocean cooling is the dominant effect, whereas freezing takes precedence in the Antarctic Ocean. In each case the sinking water flows slowly along the continental shelf, down the continental slope and then becomes an abyssal current close to the ocean floor. The 'Antarctic Bottom Waters' flow round the polar continent to mix with adjacent water masses before flowing northwards, to the east of Australasia, Asia and Africa, to fill the deep basins of the Pacific, Indian and South Atlantic Oceans. This water is typically at a temperature of −0.4°C and a salinity of 34.66‰. Antarctic waters are somewhat more dense than the southerly flowing Arctic waters and when these meet the northern water flows over the top of the southern water. A large-scale mixing process takes place in the South Atlantic Ocean off the east coast of South America. A comparison [14] between the surface and deep-ocean circulations for the Atlantic Ocean is shown in Fig. 2.25. After sinking below the surface, the bottom waters are isolated from the atmosphere and solar radiation for possibly 500 to 2000 years.

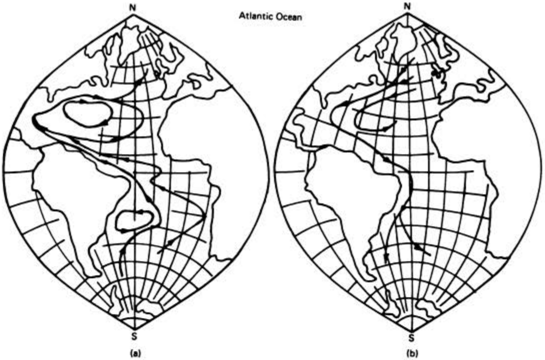

Fig. 2.25 Ocean circulations: (a) surface water; (b) deep water.

(c) *Ocean Waves*
The distortion of the air–ocean interface into both regular and irregular waves is a matter of common observation. Waves induce a mixing action near to the interface and this encourages evaporation and increased gas solubility. Winds and changes in barometric pressure in the atmosphere provide the source, while the waves provide the means of energy transfer to the surface layers of the oceans. The regular tidal rise and fall of the still-water level of the sea is commonly seen on most coastlines. We will now examine these wave systems.

(i) *Wind-generated Waves*. The precise mechanism of wave generation by wind forces is not fully understood but it is thought that the initial *capillary* waves play an important rôle. These waves first develop as ripples less than 10 mm high and are produced when a wind blows over a still-water surface. They tend to move with the wind and are very numerous but short-lived. The size of the larger *gravity* waves depends on the wind speed, its duration and its travel (or *fetch*).

Let us consider first a simple, idealized train of waves in the open ocean such as that portrayed in Fig. 2.26. The wave train is seen to consist of a regular succession of consecutive crests and troughs; no resultant bulk transport of water takes place, only the disturbance is propagated. The velocity of propagation c of a wave train is the ratio of the wavelength λ to the wave period t, where the latter is the time required for two consecutive crests (or troughs) to pass a point fixed in the Earth.

Observation of a small, freely floating body (not necessarily at the surface) reveals that it moves forward with the oncoming crest and then backward into the following trough until it returns to its original position. In deep water the motion is almost circular and the distance travelled by the body in the wave period is πH, where H is the wave height. As $c = \lambda/t$ and the average speed of the body at the water surface is $v = \pi H/t$ then the ratio $v/c = \pi H/\lambda$. There is no specific relationship

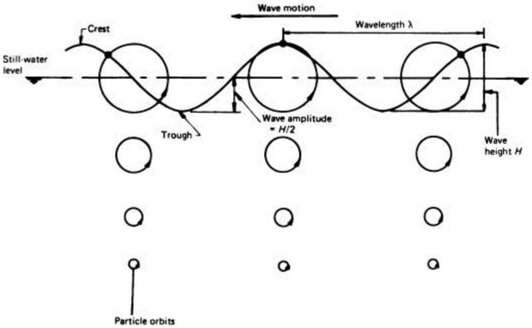

Fig. 2.26 Deep-water waves.

between H and λ although invariably wave heights are much smaller than wave lengths. When waves are too high they become unstable and the crests begin to break. A theory, put forward by Stokes [15], suggests that instability occurs when $H/\lambda > 1/7$, a prediction reasonably upheld in practice. An average wave in the seas with, say, a height of 3 m and a length of 180 m has a mean velocity of water particles of only about one-twentieth of the wave velocity. Thus for most conventional displacement ships the orbital velocities have a small effect on performance and are usually ignored, but this is not necessarily true of hydrofoil craft. Fig. 2.26 shows that the orbit diameters decrease (in theory exponentially) towards the bottom. At depths greater than about one-half the wavelength the motion of the water particles is negligible compared with, say, the cruise speed of a deeply submerged submarine. Under these circumstances the passage of waves is of little importance. However, even the small velocities at depth can be great enough to alter the topography of the sea bottom and so could be an important factor in the siting of harbours and jetties.

In our simple wave system suppose that the surface distortion is sinusoidal and that the pressure over the interface is constant. It may be shown [15,16] that the wave velocity is given by

$$c = \left\{ g\left(\frac{\lambda}{2\pi}\right) \tanh\left(\frac{2\pi h}{\lambda}\right) \right\}^{1/2} \tag{2.1}$$

where h is the water depth measured from the still-water level. We now distinguish between various depths of water and see how Equation (2.1) is modified. When h/λ_d (the subscript d implies deep water) is large, $\tanh(2\pi h/\lambda_d) \to 1$ and thus

$$c_d^2 = g\lambda_d/2\pi \tag{2.2}$$

or, since $c_d = \lambda_d/t$, we may write

$$c_d = g\frac{t}{2\pi} = \frac{g}{f} \tag{2.3}$$

where f is the wave frequency. Bearing in mind that $\tanh \pi = 0.9963$ corresponds to $h/\lambda_d = \frac{1}{2}$ we can say that Equations (2.2) and (2.3) represent, with sufficient accuracy, the propagation velocity for *deep-water waves* when $h/\lambda_d \geqslant \frac{1}{2}$. The velocity of deep-water waves is thus proportional to the square root of the wavelength. In a real 'sea state', wind-induced waves of different wavelengths move at different velocities to form a 'fully roused' sea.

If we focus attention on a small area of sea we may observe the passing of a wave, but if an attempt is made to follow it with the eye we soon find that it vanishes. This is the result of the initial addition of a series of waves to form the crest, but as each wave is, in general, of a different wavelength the consequent difference of velocity will cause these same components of the series to run out from the crest. Hence, sea waves often form a dispersive system.

We have seen that climatic conditions in the atmosphere generate regions of high and low pressure which give rise to storms. Within the storms the sea is fully roused and is largely a random process of propagating crests and troughs. However, on travelling out of the storm (the velocity of the longer waves is usually greater than the speed of translation of the storm) waves extend and become more regular to form a *swell*. Unlike currents, waves suffer no effect from the Coriolis acceleration as negligible net movement of water occurs. Waves therefore move in the direction of the generating wind (which may be reasonably steady outside the storm area). Long swell suffers little attenuation in deep water, even when a sustaining wind is not blowing, provided that only light headwinds are encountered. Consequently, the effect of a storm off the coast of New Zealand (or Florida) may be detected in Alaska (or Cornwall). The energy of the waves is finally dissipated in turbulence as the waves run ashore and break on a beach, this process giving rise to *surf*.

When h/λ_d is small the surface waves run into shallow water and so $\tanh(2\pi h/\lambda_d) \rightarrow 2\pi h/\lambda_d$. Thus,

$$c_s^2 = gh \tag{2.4}$$

where the subscript s implies shallow water. We now see that the wave velocity depends only on water depth. Whereas deep-water gravity waves constitute a dispersive system, that is, the velocity for a given depth depends on the wavelength, the shallow-water waves do not: instead all the waves propagate at a given velocity irrespective of their individual wavelengths. The question now arises, 'when can water be regarded as shallow?' To obtain an accuracy consistent with that adopted for deep water the shallow-water depth must be defined by $h/\lambda_d < 1/200$. But as the accuracy of wave measurements is no better than 5 per cent, a practical limit for shallow water is $h/\lambda_d < 1/20$. Between this value and the deep-water limit lies the region of intermediate depth and here the full equations defining the velocity and other wave characteristics must be used. These points are discussed in detail in [15]. The orbital path of a water particle in shallow water (and in intermediate water) is elliptical, as shown in Fig. 2.27. The ratio of the minor-to-major axis tends to unity (circular orbit) near the surface but becomes zero adjacent to the sea bottom where the particle simply oscillates parallel to the wave path.

As waves travel onto a beach or into shoal water the wave height, relative to the

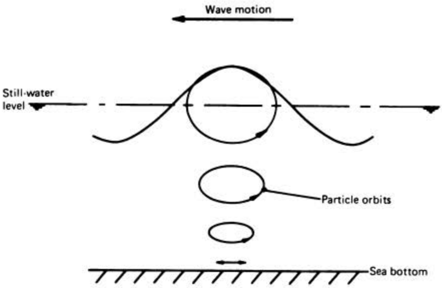

Fig. 2.27 Shallow-water waves.

deep-water value, first decreases somewhat and then increases quite markedly. In so doing the waves slow down, but as the period remains unchanged the wavelength is therefore reduced. Just before a wave breaks it is much steeper than it was offshore and this often makes the launching of small craft difficult. Indeed, not only an excessive wave height, but also the steepness of a wave can cause damage to ships in the oceans and may even cause them to capsize. High-speed ocean currents, such as the Gulf Stream and the Kuroshio, are notorious for producing steep confused seas whenever the waves are against the current.

In deep water the simple wave system considered here contains kinetic and potential energy in equal proportions. The total energy of a wave front can be enormous, and using a simple theory it can be shown that a wave 3 m high and 150 m long possesses a total energy of about 1.6 MJ per metre-length of crest. The effect of shallow water on wave speed results in wave refraction and much of the total wave energy is concentrated above the still-water level. This energy is then dissipated by surf as it breaks on a beach and can be the cause of extensive destruction on coastal features such as points, headlands and breakwaters [17]. For example, at Wick in Scotland the end of a breakwater was capped by a block of concrete of mass 8×10^5 kg and secured to the foundation by iron rods of about 90 mm diameter. In 1872 both the capping and the foundation (a total mass of 13.5×10^5 kg) were removed by waves. The structure was rebuilt and a larger cap of 26×10^5 kg was added. In due course this too was removed by wave action.

The simple harmonic wave form discussed so far has the advantage that combinations of such waves, displaying different heights and lengths, can be superimposed to form an analytical description of the real sea. (In fact the surface waves at sea form a random process as discussed in [18].) Observations of deep-ocean waves, however, have shown that the surface distortion displays a sharper crest and a flatter trough than a harmonic wave of the same height and length. A useful geometric construction producing the required features takes the form of a trochoid. A trochoidal curve is the locus of a point on a circular disc which is traced out when the disc is perpendicular to and rolls along the underside of a horizontal plane. The wavelength is proportional to the radius of the disc, R, and the wave height is proportional to the radial distance, r, of the point from the centre of the disc. The trochoid is not symmetric about the horizontal locus of the centre of the disc and consequently the still-water level is somewhat below this locus (it may be shown to be $r^2/2R$). As with harmonic waves particle orbits below trochoidal waves in deep water are circular with the radius decreasing exponentially with depth. This concept of a trochoidal wave has been frequently used to assess extreme hydrostatic loadings on ships as discussed in Chapter 3.

(ii) *Tides*. The tidal movement relative to the still-water level is usually between 0.5 and 2.0 m. Local geographical features can often produce larger variations whereas a land-locked sea has virtually no tidal movement. Although the tides are periodic they do not occur at the same time each day. In addition seasonal changes occur, but even so tidal behaviour can nowadays be computed and predicted accurately.

Sir Isaac Newton deduced that the gravitational attraction between two bodies is proportional to the product of their masses and inversely proportional to the square of the distance between them. All bodies in the universe exert forces on the waters of the Earth but only two bodies are of major importance: the Moon, because of its proximity, and the Sun, because of its large mass. However, the Sun is also a great distance from the Earth in comparison with the Moon and as a result its tide-raising forces are about 0.46 times those of the Moon. The Earth has a mass about 81 times that of the Moon and the distance between their centres is approximately 60 Earth diameters. This two-body system can be considered to rotate about a point C (see Fig. 2.28) located within the Earth some 4700 km from its centre and along the common line of centres. Let us assume for the moment that the Earth does not rotate about its own axis – we can introduce the motion later. Figure 2.29 shows the direction of motion of the particular point P on the surface of the Earth. The 'centrifugal' force on the particle at P is directed towards the centre of rotation C′ and PC′ is parallel to the line joining the centres of the Earth and the Moon, that is, ECO produced. Thus the direction of the force F will be the same for all particles. Even though the Moon is 384 000 km from the Earth a line drawn from a point on the surface of the Earth to the centre of the Moon can subtend an angle of 1° to the common centre line. Furthermore, a point on the near side of the Earth is closer by 3 per cent of the separation than a point on the far side. The lunar gravitational force L will, in general, be inclined to F (except when P is at O or O′) and the

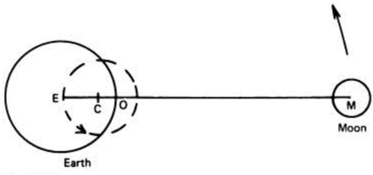

Fig. 2.28

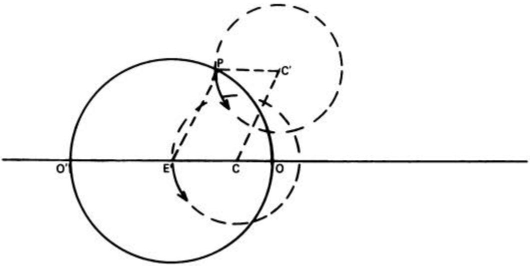

Fig. 2.29

resultant T must be the tide-raising force on that part of the Earth covered by the (non-rigid) oceans. Since it is the gravitational force which produces the initial circular motions of the Earth and Moon then L is the vector sum of F and T as shown in Fig. 2.30. A particle at the centre of the Earth experiences a gravitational force equal to F and so if P is to the right of WZ (in Fig. 2.30) we must have $L > F$ but $L < F$ when P is to the left of WZ. When P is on WZ, L and F are very nearly equal but inclined slightly to each other; the system of the tide-raising forces is then similar to that shown in Fig. 2.31. The component of the tidal force normal to the surface of the Earth is very small compared with the weight of a given particle and is therefore of little significance. It is the tangential components of T which produce tides, and these are shown in Fig. 2.32 where the lengths of the arrows indicate the relative magnitude of the force. These tangential forces give rise to the so-called *equilibrium tide* and two high-waters develop, one directly under the Moon and the other on the opposite side of the Earth.

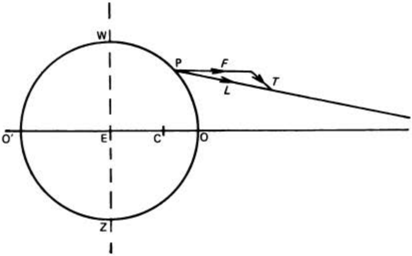

Fig. 2.30

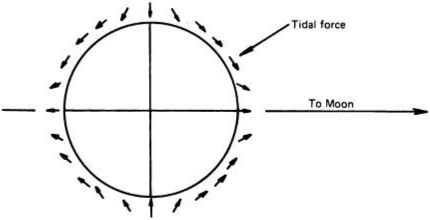

Fig. 2.31

Now the Earth rotates about its own axis in one solar day. The given point P will then have occupied two high-tide positions relative to the Moon in 24 hours. The high tides do not in fact occur at intervals of 12 hours because the Moon itself moves relative to the Sun. The lunar day is 24 hours and 50 minutes long and thus the lunar tide has a period of 12 hours and 25 minutes and a wavelength equal to one-half the circumference of the Earth.

The resonant frequency of oscillations in some gulfs and channels is about 12 hours, so that excessively high tides may be expected such as those in the Bristol Channel (up to 15 m) and the Bay of Fundy (up to 21 m). Rotation of the Earth about its own axis results in a Coriolis force being applied to the tidal oscillation of the oceans. As a result the path of a particle, projected onto a tangential plane, is elliptical with a clockwise motion when viewed from above in the northern hemisphere. Near coasts the interruption of the path often leads to a substantial pressure gradient in the water normal to the coastline and to the development of abnormally high tides known as 'Kelvin edge waves'. This simple picture is complicated by the variation in distance between the Earth and Moon as each moves in its own orbit around the Sun. The effectiveness of the Moon in raising tides is greatest when it is nearest to the Earth (perigee) and least when furthest away (apogee). Furthermore,

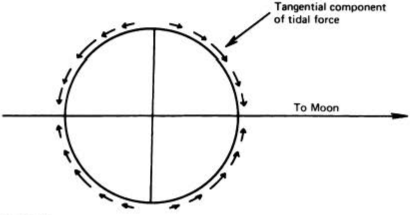

Fig. 2.32

when the tide-raising effects of the Sun and Moon reinforce each other, *spring* tides occur whereas *neap* tides when they oppose each other; the ratio of these forces is $(1+0.46)/(1-0.46) \cong 8/3$. Finally, when a spring tide occurs at perigee the highest spring tides will occur and correspond to a new and full Moon. However, all these processes are modified by the rotation of the axes of the planet, the inertia of water, friction and the local topography of the coastline and sea bottom [19].

2.6 The Hostile Environment

The preceding sections clearly show that to a human and the equipment he uses the oceans present a hostile environment. Danger arises on the surface of the sea from adverse weather and sea states which may result in a loss of stability from icing, holing from a collision with floating ice or rocks, or impact damage from enormous waves generated by gale-force winds, and so on. Table 2.5 lists some of the environmental hazards which must be taken into account by the designer of a marine vehicle.

Table 2.5 Environmental hazards.

Cause	All equipment/personnel	Additional for exposed equipment/personnel
Climatic	salt-laden atmosphere	wind
	condensation	water on deck
	dust, fluff	salt spray
	temperature extremes	hail
	humidity extremes	rain
	odour, aerosols	blown snow
	ship motion	ice accretion
	vibration, slamming	sea ice
	noise	total immersion
	ice at sea	sunlight
		funnel smoke
		sand abrasion
Others	corrosive conditions	fish
	oil contamination	crustaceans
	animal life	sea weed
	mould	flotsam
		sea bottom

Should a vessel capsize and the occupants become immersed in sea water for any length of time there is a distinct probability that death will follow. For the efficient operation of various body systems, the internal temperature of the human body must be maintained within the range $37 \pm 2°C$. In the atmospheric environment adequate temperature control is obtained from various combinations of perspiration and evaporative cooling, internal heating from inefficient work transfer (running, rubbing of hands and the like) and enveloping the body in heat-insulating clothing.

Temperature control of the human body in water is a far more serious problem. As sea water is invariably cooler than the body heat is transferred to the water. The instinct to generate internal heat by increasing activity such as the use of muscles in swimming merely assists the heat transfer process by forced convection and also increases the rate at which the body temperature falls. Below about 35°C the blood flow to the brain becomes impeded, resulting in delirium and unconsciousness. If this does not cause drowning then further heat loss leads to heart failure. The condition of low body temperature is known as hyperthermia. When the cruise liner *Laconia* became engulfed in flames, 200 passengers took to the water and 120 died from hyperthermia despite a water temperature of 18°C. Following this disaster passengers and crew forced to abandon ship are now required to wear plenty of clothing to improve insulation and to help them float until rescued rather than swim about unnecessarily.

The hostility of the external environment must be eliminated from the internal environment within the marine vehicle if the crew and equipment are to operate reliably and efficiently. In practice, we can go only some way towards this ideal. For example, unpleasant rolling motions can be reduced by incorporating active or passive stabilizers in a ship. Now that nuclear submarines patrol deeply submerged on missions lasting several months ergonomic, physiological and psychiatric matters have gained great importance. Undoubtedly, experiences with manned space flights have helped to improve the design of crew-operated equipment, relaxation areas, recreational facilities and so on. Air-conditioning and ventilation can be used to avoid extremes of temperature and particularly of humidity. It is possible to define the limits of temperature and humidity consistent with the reliability of equipment but it is far more difficult to specify quantitatively the meaning of human comfort. The ranges of external temperature and relative humidity met by a ship cruising for long periods could be 45°C and 50 per cent respectively. These limits demand the installation of air-conditioning and ventilating systems in various compartments of the marine vehicles. To proceed further would be out of context here, but a full treatment of air-conditioning in general is given in [20] and useful information for ships is presented in [21].

References

1. Bullard, E. (1969), The origin of the oceans. *Sci. Am.*, 221, 3, 66–75. (Note: The September 1969 issue of *Scientific American* is devoted to 'The Ocean'.)
2. Brahtz, J. F. (ed.) (1968), *Ocean Engineering*, John Wiley and Sons, New York.
3. Defant, A. (1961), *Physical Oceanography*, Vol. 1, Clarendon Press, Oxford.
4. Pickard, G. L. (1966), *Descriptive Physical Oceanography*, Pergamon, Oxford.
5. Dietrich, G. and Kalle, K. (1963), *General Oceanography*, Wiley Interscience, New York.
6. Clayton, B. R. (1977), *An Introduction to Underwater Noise*, Ministry of Defence, Foxhill, Bath.
7. Wenz, G. M. (1962), Acoustic ambient noise in the ocean; spectra and sounds. *J. Acoust. Soc. Am.*, 34, 1936–56.
8. Starr, V. P. (1956), The general circulation of the atmosphere. *Sci. Am.*, 195, 6, 40–5.
9. Hindley, K. (1977), Learning to live with twisters. *New Scientist*, 4 August, 280–2.
10. Lamb, H. H. (1972), *Climate: Past, Present and Future*, Methuen, London.
11. Veronis, G. (1973), Large scale ocean circulation. *Adv. Appl. Mech.*, 13, 1–92.
12. Cromwell, T., Montgomery, P. B. and Stroup, E. D. (1954), Equatorial undercurrent in Pacific revealed by new methods. *Science*, 119, 648–9.
13. Stewart, R. W. (1969), The atmosphere and the ocean. *Sci. Am.*, 221, 3, 76–86.
14. Stommel, H. (1957), A survey of ocean current theory. *Deep Sea Res.*, 4, 149–84.
15. Kinsman, B. (1965), *Wind Waves; Their Generation and Propagation on the Ocean Surface*, Prentice Hall, New Jersey.
16. Milne-Thomson, L. M. (1968), *Theoretical Hydrodynamics*, 5th Edn, Macmillan, London.

17. Bascom, W. (1959), Ocean waves. *Sci. Am.*, 201, 2, 74.
18. Price, W. G. and Bishop, R. E. D. (1974), *Probabilistic Theory of Ship Dynamics*, Chapman and Hall, London.
19. Tricker, R. A. R. (1964), *Bores, Breakers, Waves and Wakes*, Mills and Boon, London.
20. Jones, W. P. (1973), *Air Conditioning Engineering*, 2nd Edn, Edward Arnold, London.
21. Jones, S. J. and Macvicar, J. K. W. (1959), The development of air conditioning in ships. *Trans. Inst. Nav. Archit.*, 101, 241–64.

3
The Marine Vehicle at Rest

3.1 Introduction

To determine whether or not a marine vehicle will be capable of maintaining a stationary and upright condition (usually essential requirements) it is necessary to examine the forces which act on the vehicle in the vertical direction, that is, along an extended radius of the Earth. The equilibrium relationships that these forces must satisfy then require investigation. For a ship the principles of hydrostatics are used to assess launching and docking procedures, initial stability tests, flooding calculations, grounding and tethering forces at docks and jetties, the effects of loading and carrying cargo, and so on.

It is now our purpose to introduce the basic relations used for these investigations although details of the many empirical techniques available are left for the reader to consult in the cited references. Attention is drawn to the limitations of a number of derived formulae which are often used well beyond their supposed limit of validity. The following discussion will be restricted to statics even though the operational environment of marine vehicles is generally dynamic. The motion response of a marine vehicle undergoing a dynamic excitation is examined in Chapter 10.

The vehicle at rest must not only remain in stable equilibrium with the system of external forces acting upon it but also have the strength to sustain these forces. Consequently, a (static) structural analysis must be undertaken. However, as with the general case of a motion response to dynamic excitations, the questions raised by problems of structural dynamics are also left until later (see Chapter 9). The structural strength and integrity of marine vehicles are obviously matters of great importance and there are a number of ways that marine vehicles can be put to the test, for example, by the application of forces; by biological attack; by chemical attack; and by changes of temperature.

In this chapter we shall examine a number of structural (as distinct from properties of materials) problems and confine our attention to purely mechanical effects. This means that we shall consider the application of forces, namely 'loading actions'. Temperature changes also give rise to a form of loading action which could produce important mechanical effects, but these will not be examined here. Again our concern is with the basic principles and how these may be applied to marine vehicles.

3.2 Marine Vehicle at Rest in a Stationary Fluid

Many fluid-borne vehicles are capable of remaining stationary in a stationary fluid, while others such as gliders, hydrofoil craft, submarines, aeroplanes and parachutes depend on their motion for supporting forces. Vertical forces may be applied by ground reaction, by attached cables, by aerostatic means, as in an air-cushion vehicle (ACV), or by the conveyance of fluid downwards as in a helicopter. There are, however, two forces of overwhelming importance which are always present (except in space or in a vacuum), namely weight W and buoyancy F_B. The buoyancy force is, by Archimedes' Principle, equal and opposite to the weight of fluid displaced by a vehicle in the fluid. In the case of a helicopter, shown in Fig. 3.1, the buoyancy force is small compared with the weight of the craft and must be supplemented by the thrust F_T exerted by the air on the rotor. The purpose of the rotor is to increase the linear momentum of the air perpendicular to the plane of rotation of the rotor so that F_T may be varied over a wide range about the equilibrium value by adjusting the blade pitch.

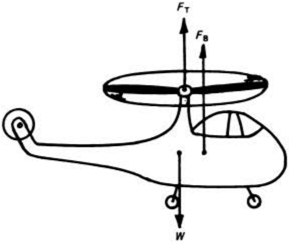

Fig. 3.1

When, for example, a uniform, wooden, rectangular block floats in water it is clear that

$$W = F_B. \tag{3.1}$$

Furthermore, equilibrium demands that these two forces must be colinear. As we shall see later, the block floats with its *largest* flat face parallel to the surface provided its relative density is not too close to unity or zero. The other two possible configurations in which flat faces are parallel to the surface are not realized because they are unstable. Plainly, then, we must not only study the equilibrium of forces, but also the stability of that equilibrium.

It is interesting to note that the American research ship *Flip* is designed to float not only like a conventional surface vessel with its keel horizontal but also (after suitable flooding) with its keel vertical. Like a slowly submerging submarine, the slowly tilting ship raises not one stability problem but, in theory, an infinity of them. Similar considerations arise when oil rigs are upturned at their chosen sites after being towed out in another attitude.

3.3 Weight of a Vehicle

When a 'system' is isolated for the purpose of analysis, its mass, and hence its weight, is determined. There is, of course, an element of choice in defining the system. For instance, we might wish to include, or exclude, consideration of the gas in the bags of a dirigible or the ballast water in the external tanks of a submarine. The calculations for a damaged and partially flooded ship provide a choice of this sort. If the water admitted by the hull is included as part of the ship, the 'added weight' method of analysis is used. If, on the other hand, the damage is regarded as not altering the weight but, rather, as changing the external configuration presented to the sea, then the 'lost buoyancy' approach is employed.

Once a system is chosen, weight (or gravity force) is inevitably a factor, and it is plain to see that generally speaking large weight is usually inconvenient. Difficulty is experienced in lifting an excessive weight into the atmosphere in an aircraft or an ACV, and excessive weight will require deeper immersion of a surface ship and hence produce greater resistance to motion through the water.

For the purpose of discussion it is sometimes convenient to consider the weight of a chosen system to be the sum of several components. We may say, for instance, that

$$W = W_h + W_m + W_f + W_p + W_o \tag{3.2}$$

where W_h is the weight of the bare hull, fuselage or structure; W_m the weight of the power plant; W_f the weight of the fuel carried; W_p the weight of the payload (i.e. passengers, their personal effects and cargo); and W_o is all other weight (such as crew, stores, water, ballast auxiliary plant, etc.). The maximum permitted value of W is sometimes called the 'gross weight', or 'all-up weight', W_g. In marine practice, the quantity $W_g - (W_h + W_m)$ is called the 'deadweight'; although W_m is then considered to include the weight of all fittings (such as auxiliary plant, navigation equipment, the galley stove, etc.). The deadweight is obviously a measure of the usefulness of a cargo ship and in some vehicles it is by far the major part of W_g. Lifebelts, water wings and rubber dinghies are particularly splendid in this respect.

Measurements typical of the orders of magnitude but nevertheless approximate, for the components of weight of some vehicles are shown in Table 3.1.

Table 3.1 Components of weight of some marine vehicles. Units are MN with tonf in parentheses.

Vehicle	W_h	W_m	W_f	W_p	W_o	W_g
Super VC-10 airliner at take-off	0.361 (36)	0.132 (13)	0.561 (56)	0.224 (23)	0.212 (22)	1.490 (150)
R-101 dirigible at take-off on its last fatal flight	1.006 (101)	0.169 (17)	0.249 (25)	– 0.239 – (24)		1.663 (167)
Frigate	6.83 (685)	4.43 (445)	4.86 (488)	2.72 (273)	9.06 (909)	27.90 (2800)
Destroyer	17.32 (1738)	9.36 (940)	7.82 (784)	7.91 (794)	19.36 (1944)	61.77 (6200)
Very large cargo carrier (VLCC)	448 (45 000)	29.8 (3000)	29.8 (3000)	2470 (248 000)	9.96 (1000)	29.90 (300 000)
Air-cushion vehicle	0.518 (52)	0.229 (23)	0.149 (15)	0.637 (64)	0.209 (21)	1.742 (175)

3.3.1 *Weight Distribution*

For some purposes, particularly the estimation of stresses in ship structures, the distribution of weight is important. (The corresponding distribution of mass is required in an analysis based on dynamics.) Detailed determination of weight distribution is generally a tedious business and relevant data are often stored in a computer on the basis of a form of book-keeping. Where the vehicle is of an essentially 'prismatic' form, however, a simple and common approximation may be adopted. In this approach the idea of a 'gravity force/unit run'; q_g, is used, so that for a vehicle of length L

$$W = \int_0^L q_g(x)\mathrm{d}x \tag{3.3}$$

where x is the distance from the stern, say, measured in the vehicle parallel to the water surface. A typical approximation to the distribution of $q_g(x)$ is shown in Fig. 3.2. As the curves in the figure are usually obtained by a 'piecewise' process of calculation, they are often 'stepped'.

3.3.2 *Centre of Gravity*

In the design of a fluid-borne vehicle it is usually necessary to ascertain the position of its centre of gravity G (as well as its weight) at an early stage. The fore-and-aft position of G (determined by the coordinate X_G), for a ship whose q_g curve has been found, may be obtained by taking moments at a section $x = 0$ about an axis

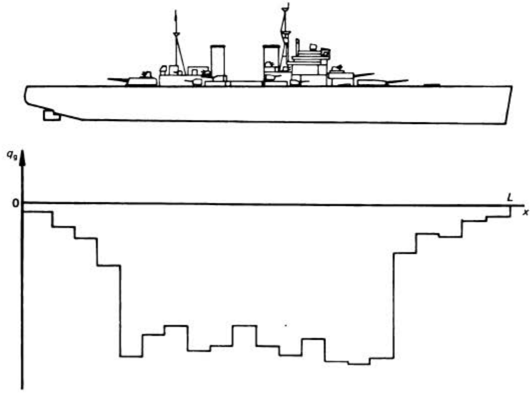

Fig. 3.2 Typical weight distribution for a large warship.

in a plane parallel to the water plane and in a direction perpendicular to the direction of x, so that

$$X_G = \frac{\int_0^L q_g x \, dx}{\int_0^L q_g \, dx}. \tag{3.4}$$

By a similar process the other coordinates of G may be found by integration, although one might not think in terms of q_g curves to do so. In ship calculations, G is commonly found by taking moments about the mid-section (usually referred to by the symbol ⨷) for the longitudinal position, about the lower surface of the keel K for the height and about the fore-and-aft plane of geometric symmetry of the hull for the transverse position.

In general, such calculations as these are reasonably accurate and can be checked later when the vehicle has been built. For a vessel that floats on the surface, this is done by means of an 'inclining experiment'. From the observed results of the experiment and the known position of the centre of buoyancy B (which can be calculated accurately since it depends only on geometry) the position of G can be located. Within limits, it may be possible to adjust the position of G if necessary, by ballasting. However, a vehicle generally has a preferred upright configuration in which it is designed to operate. This 'intended attitude' is usually associated with a fore-and-aft plane of symmetry of external form, and this plane is approximately vertical when the vehicle is at rest in the stationary fluid. The centre of gravity G will normally lie in this plane of symmetry or very close to it. For a surface ship, G will normally lie at or just above the water plane and slightly abaft amidships. It may be interesting to note that the possession of an intended attitude and of 'starboard-and-port symmetry' is not only a feature of the vast majority of fluid-borne vehicles but also of animals (including humans).

3.4 Buoyancy Force on a Vehicle

Suppose that a set of axes $OXYZ$ is fixed with respect to the Earth with the plane OXY horizontal and with OZ pointing vertically downwards. Let us now consider a rectangular element of fluid whose sides are of length δx, δy, δz parallel to OX, OY, OZ respectively, as shown in Fig. 3.3. If the subscripts 1 and 2 refer respectively to the lower and upper faces of the element and z represents the distance from the plane OXY to the element measured downwards parallel to OZ then

$$z_1 - z_2 = \delta z.$$

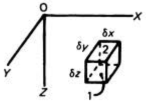

Fig. 3.3

The element is considered small enough to assume that the fluid pressures p_1 and p_2 each act uniformly over the lower and upper faces respectively. Thus the upward fluid force on the lower face of the element is $p_1 \delta x \delta y$ which is equal to the sum of the pressure force on face 2 and the weight of the fluid contained in the element, that is, $p_2 \delta x \delta y + \rho g \delta x \delta y \delta z$, where ρ is the density of the fluid and g is weight per unit mass. For equilibrium to prevail there must be no net force in the OZ direction, so that

$$p_1 \delta x \delta y = p_2 \delta x \delta y + \rho g \delta x \delta y \delta z$$

whence

$$\frac{p_1 - p_2}{\delta z} = \rho g.$$

In the limit, as $z \to 0$ and $p_1 \to p_2$, we may write

$$\frac{\mathrm{d}p}{\mathrm{d}z} = \rho g. \tag{3.5}$$

Integration of this equation for a constant-density fluid yields

$$p = \rho g z \tag{3.6}$$

where the plane OXY is assumed to lie in the 'free' surface, that is the air–water interface, and the pressure p is measured relative to the surface value. As the latter is considered to be at 'atmospheric' pressure then p is a gauge pressure. The assumption of a constant density for water is generally acceptable in hydrostatics, but the very small changes which occur in large volumes of water, especially in the oceans, have a significant effect on other relevant factors in the operation of marine vehicles, such as sound-wave propagation, as discussed briefly in Chapter 2.

Now suppose that the rectangular element of fluid is replaced by an equal-sized element of a different material. The latter may be said to 'displace' fluid from the space it occupies. The fluid which remains (and in which the element is placed) behaves in a similar manner and still exerts its upthrust. This upthrust is a 'buoyancy force' of amount

$$\begin{aligned}\delta F_B &= \left(\frac{\mathrm{d}p}{\mathrm{d}z}\delta z\right)\delta x \delta y \\ &= \rho g \delta x \delta y \delta z\end{aligned}$$

or

$$\delta F_B = \rho g \delta \nabla$$

where $\delta \nabla$ is the volume of the rectangular element. We may regard δF_B as a contribution to the buoyancy force exerted upon an immersed body of finite volume. If the sum of all these contributions is taken over the finite immersed volume ∇ of which the element forms a small part we find that

$$F_B = \rho g \nabla = \Delta^*. \tag{3.7}$$

In other words, the total buoyancy force is equal to the weight Δ^* of fluid displaced.

(Archimedes' Principle is thus deducible by simple reasoning from Newton's hypotheses.)

The presence of the buoyancy force F_B is a consequence of gravity, because an identifiable volume of fluid has weight. The buoyancy force always acts in the opposite direction to OZ – upwards – in order to support the weight of displaced fluid. It follows that F_B acts through the centre of gravity of the displaced fluid and consequently for a fluid of constant density it must act through the geometric centre (or 'centroid') B of the volume ∇.

The discussion above is intended as a very brief revision of certain elementary results in the theory of hydrostatics. These results will be important in the discussion which follows and the reader who wishes to undertake a more thorough revision of the topic can do so by consulting, for example, [1] or [2].

3.4.1 *Centre of Buoyancy*

When a vehicle such as a submarine is totally immersed its centre of buoyancy is located at a fixed point within it. As already pointed out, we can choose the system of interest to consider the vehicle with or without its ballast water, or we may even deal with some portion of the vehicle. The position of B does not move within the system as the position and orientation of the vehicle is changed; only a change in the external geometry of the submerged vehicle can alter the location of B. In this respect a surface vehicle is quite different. If the immersed portion of a ship is changed (e.g. when the vessel assumes an angle of inclination or when the draught is adjusted) the position of B moves relative to the ship. The way in which B moves is vitally important, as we shall see when we examine the stability of floating bodies. Accordingly, we shall now study in more detail how B migrates when a body is inclined, and to do this we need to define the terms used to describe angles of inclination of floating bodies. (By a floating body we usually mean a body in equilibrium at the interface between air and a liquid such as water. These considerations, however, apply to any interface separating fluids of differing densities. For example, the migration of B would be affected by a layer of oil on water.)

Suppose that a floating body such as a ship is at rest in its intended upright attitude so that the axis OX (illustrated in Fig. 3.3) is identified with the fore-and-aft direction and OY points to starboard. An inclination obtained by rotating the ship about an axis parallel to OX is called a 'heel'; a similar inclination about OY is called a 'trim'. Conventionally, positive values of heel and trim are associated with clockwise angles of rotation as seen looking along the fixed axes away from the origin O. It is necessary to stress two important points about these definitions. First, as can be easily verified, a given oblique inclination cannot be specified unambiguously merely as a combination of a heel and a trim; the order in which these latter inclinations are applied is significant. Second, the word 'trim' is used in a quite different sense when it is applied to totally immersed bodies such as submarines.

3.4.2 *Surface of Buoyancy*

Let us now consider the general case of a floating body which is not prismatic and which does not possess an axis or a plane of symmetry. Figure 3.4 shows a body that is partly immersed in water, the displacement volume being ∇. The buoyancy force F_B acts at B, the centroid of the immersed volume. That section of the body which lies in the horizontal plane of the water surface is called the 'water-plane section'. A set of rectangular axes $Oxyz$ is fixed to the body with Oxy in the water-

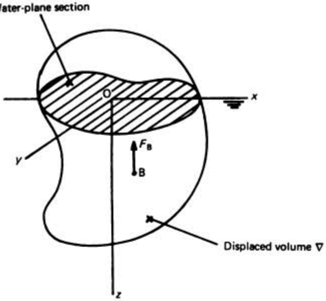

Fig. 3.4

plane section and Oz pointing downwards. The buoyancy force F_B therefore acts in the direction $-Oz$. The problem here is to discover how B migrates relative to the body as the position of the body is altered. (We do not consider here how equilibrium is to be maintained or what forces must be applied to move the body.) It is convenient to examine any movement, in terms of the axes we have chosen, as a combination of translation and rotation. Three translations and three rotations are therefore possible.

Clearly a bodily translation along any line in the water-plane section will not change the immersed portion of the body, so B remains fixed. A translation of the body parallel to Oz, on the other hand, changes ∇ and shifts B relative to the body. The increase in buoyancy force δF_B, resulting from an increase in depth of immersion δz, is given by

$$\delta F_B = (A\rho g)\delta z \tag{3.8}$$

where A is the water-plane area. In the limit $\delta z \to 0$, Equation (3.8) may be written as

$$\frac{dF_B}{dz} = A\rho g \tag{3.9}$$

and this measure is used to determine the parallel sinkage or rise which results from the addition or subtraction of a small mass (and therefore weight). For rule-of-thumb purposes sinkage is often expressed as TPI, that is, tonne force ($\cong 10^4$ N) or ton force parallel immersion, which indicates the mass, tonne or ton, that must be placed evenly on the body to cause a sinkage of one metre or one inch respectively. The preceding arguments are reversed if mass is removed to produce a parallel rise. Because the addition of mass is small, the centre of buoyancy resulting from its even distribution is at half-depth below the new water plane. If h is the vertical distance between this point and the original centre of buoyancy B the rise of the centre of buoyancy to B′ for the new condition will be given by

$$\overline{\mathrm{BB}}' = \frac{h\delta F_{\mathrm{B}}}{\Delta^* + \delta F_{\mathrm{B}}} = \frac{hA\delta z}{\nabla + A\delta z}. \tag{3.10}$$

A similar expression may be obtained for the change in location of the centre of gravity, except h now refers to the distance between the initial centre of gravity and that of the added mass.

Let us now turn our attention to the rotation of a floating body and assume, for the sake of simplicity, that displacement is unchanged. We shall first show how the orientation of the body can be altered so that this requirement is met. Suppose that the floating body shown in Fig. 3.4 rotates through a small angle β about the axis Oy (as shown in Fig. 3.5). For the immersed volume to remain unchanged it is necessary that

$$\int z\mathrm{d}A = \int (z - x\beta)\mathrm{d}A, \tag{3.11}$$

where z is the mean depth of an element, of small cross-sectional area δA, in the body measured from the Oxy plane in the water plane before β is applied as indicated in Fig. 3.5. The integration is performed over the water-plane section and related to positive values of the coordinate z. As β is small and nonzero, it follows that

$$\int x\mathrm{d}A = 0. \tag{3.12}$$

The small rotation that concerns us, therefore, can be made about an axis in the water plane, provided that the axis passes through the centroid of the section. This point is usually referred to as the 'centre of flotation'.

If the body is rotated through various angles β about various axes in the water plane (all of which pass through the centroid), B moves over a surface that is fixed in the body. Thus, suppose that we rotate the body through the small angle β and

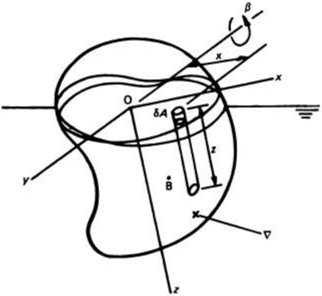

Fig. 3.5

that Oy is a centroidal axis in the water plane. The initial coordinates of B (the geometric centre of ∇) are $\bar{x}, \bar{y}, \bar{z}$ where

$$\bar{x} = \frac{1}{\nabla}\int xz\mathrm{d}A; \quad \bar{y} = \frac{1}{\nabla}\int yz\mathrm{d}A; \quad \bar{z} = \frac{1}{\nabla}\int \tfrac{1}{2}zz\mathrm{d}A \tag{3.13}$$

from the definition of B. During the small rotation the centre of buoyancy moves to B′, which has coordinates $\bar{x}', \bar{y}', \bar{z}'$, so that

$$x' = \frac{1}{\nabla}\int x(z - x\beta)\,\mathrm{d}A \tag{3.14a}$$

$$y' = \frac{1}{\nabla}\int y(z - x\beta)\,\mathrm{d}A \tag{3.14b}$$

$$z' = \frac{1}{\nabla}\int \left\{\tfrac{1}{2}(z - x\beta) + x\beta\right\}(z - x\beta)\,\mathrm{d}A = \frac{1}{\nabla}\int \tfrac{1}{2}(z^2 - x^2\beta^2)\,\mathrm{d}A. \tag{3.14c}$$

We are now in a position to examine the movement of the centre of buoyancy from $\mathrm{B}(\bar{x}, \bar{y}, \bar{z})$ to $\mathrm{B}'(\bar{x}', \bar{y}', \bar{z}')$.

Consider first the movement of the centre of buoyancy parallel to Oz. The rise is

$$z - z' = \frac{\beta^2}{2\nabla}\int x^2\mathrm{d}A \tag{3.15}$$

which is positive and becomes exceedingly small for small values of β. Now B and B′ are neighbouring points on a surface and so that surface is concave upwards at B′ and horizontal at B.

We note next that a rotation about the axis Oy does not necessarily move B to B′ in the same plane perpendicular to Oy. Nevertheless, if B and B′ *are* to lie in a common plane perpendicular to Oy, then it is necessary that

$$\bar{y}' = \bar{y}$$

so that

$$\int xy\mathrm{d}A = 0. \tag{3.16}$$

Hence Ox and Oy are the *principal* axes of the water-plane section.

Let us assume that the small rotation β is made about a principal centroidal axis in the water plane. If the axis Oy is taken perpendicular to the plane of the paper, the initial and final positions of B and B′ will be as shown in Figs. 3.6(a) and (b) respectively. The vertical plane containing these two points intersects the axis Oy at right angles. The initial, vertical line which passes through B intersects the vertical line through B′ at the point M′, which is known as a 'pro-metacentre'. Now, since $\bar{z} - \bar{z}'$ is very small according to Equation (3.15), the distance $\overline{\mathrm{BB}}'$ is, to first order, given by

$$\overline{\mathrm{BB}}' = \bar{x} - \bar{x}' = \frac{\beta}{\nabla}\int x^2\mathrm{d}A. \tag{3.17}$$

The integral is the second moment of area of the water-plane section about the principal axis Oy, and is best represented algebraically by $(Ak^2)_{\mathrm{O}y}$ where k is the

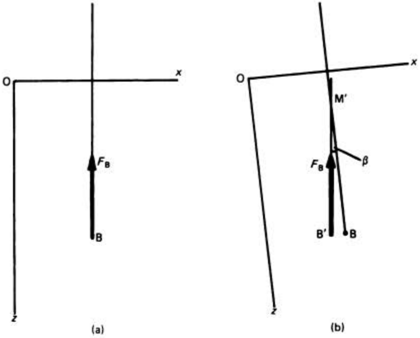

Fig. 3.6

radius of gyration of the water-plane area A about Oy. It is a matter of convention that the symbol I is used for the second moment of area in the present context (the algebraic expressions are also rather neater) and so it follows that

$$\overline{\mathrm{BM}}' = \frac{\overline{\mathrm{BB}}'}{\beta} = \frac{I}{\nabla}. \tag{3.18}$$

Equation (3.18) is of profound importance and we will return to it later.

Whatever axis (aa, bb, . . . ; see Fig. 3.7) through the centroid O of the water-

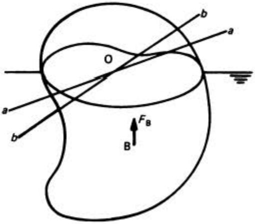

Fig. 3.7

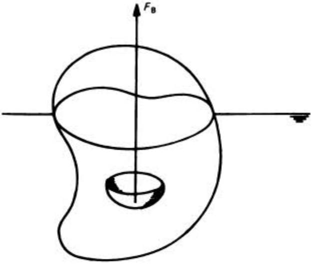

Fig. 3.8

plane section is used during a small rotation, **B** moves parallel to the water surface. Furthermore, **B** moves relative to the vehicle on a surface known as the 'surface of buoyancy', which is concave upwards and fixed in the vehicle (Fig. 3.8). These findings relate to a fixed volume of immersion ∇ and hence to a definite buoyancy force. The tangential plane at any point on the surface of buoyancy is parallel to the corresponding water plane. Therefore, the normal at any point on the surface of buoyancy is vertical when **B** is at that point. The more deeply immersed a body is, the smaller is its surface of buoyancy, and if the body is totally immersed the surface contracts to a point that is fixed at the centroid of the body, that is, at the volumetric centre.

It may be that the geometry of the body at any given position in space is always associated with the same immersed volume. This is obviously so for a convex solid such as an ellipsoid or a cube; the surface of buoyancy is then convex and closed.

While each displacement has a unique surface of buoyancy, the body may admit water by flooding if its orientation is altered sufficiently. If it is then returned to a series of orientations that it had before flooding, **B** migrates over a different surface of buoyancy. In practical calculations for a ship, however, it is conventional to assume that there is no ingress of water even when the vessel is turned right over, as might be the case with a self-righting lifeboat. Ingress of water is then considered separately.

3.4.3 *Buoyancy Calculations*

The concept of a surface of buoyancy features in theoretical hydrostatics but such a surface is not normally calculated in practice. Nevertheless, the idea is a useful one and it is of interest to interpret what can be achieved in practice in terms of it. Suppose that a set of axes $A\xi\eta\zeta$ is attached to our general body as shown in Fig. 3.9, with the plane $A\xi\eta$ parallel to the water-plane section. Once the ζ coordinate of the water-plane section has been specified, the position of the centre of buoyancy **B** may be calculated and specified in terms of the coordinates ξ, η, ζ. The value of the immersed volume ∇ can also be found.

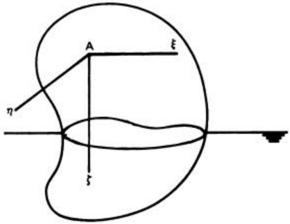

Fig. 3.9

If the body is now rotated in steps of 5°, say, about the axis $A\eta$ similar calculations may be made at each stage. If desired the process could be repeated for rotation through a full 360°. Equally, the location of B and the immersed volume may be computed for every stage during a rotation about the axis $A\xi$. Again, for each 5° position of the rotation about $A\eta$ a complete rotation (in steps) can be made about $A\xi$, and for each 5° position of the rotation about $A\xi$ a complete rotation (in steps) can be made about $A\eta$. Note that no restriction is placed on the size of the rotation; we are not concerned here with small departures from some reference configuration. Furthermore, these last two cases do not give the body the same sets of orientations, as can be easily verified by first imagining the body rotated through 90° about $A\eta$ and then 90° about $A\xi$ and then reversing the order.

Using the preceding technique sets of results could be found, each giving (i) the coordinates ξ, η, ζ of B, and (ii) the corresponding immersed volume ∇. By adopting a suitable process of interpolation all the positions of B for some chosen value of ∇ could be found and the appropriate surface of buoyancy determined. A group of surfaces could then be deduced so that each member corresponded to a particular value of ∇. Each would be a closed convex surface with the property that when B lies at any point on it the corresponding upward buoyancy force is directed along the inward normal.

Several approaches can be realized for the problem of determining a surface of buoyancy, although eventually all reduce to that illustrated in Fig. 3.10. A series of planes is found, all of which cut off the same volume ∇ from the body. The centroids B of the various cut-off pieces lie on the surface of buoyancy corresponding to ∇.

Inevitably we must turn our attention to prismatic bodies (e.g. to ship hulls) and consider heel and trim rather than generalized rotations. Should the body have a vertical fore-and-aft plane of symmetry, then the surface of buoyancy might have an egg-like shape with a longitudinal fore-and-aft axis so that the plane of hull symmetry divides the surface into two symmetric halves. If the prismatic body also has a transverse plane of symmetry (as occurs in a kayak, for instance) then that plane will also divide the surface of buoyancy into two symmetric halves.

It is not suggested that the method described above for calculating a surface of buoyancy should be followed in practice, or even that the surfaces be normally

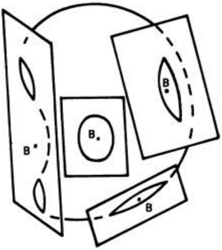

Fig. 3.10

determined. Indeed, modern literature on naval architecture seems to contain few references to the geometry of surfaces of buoyancy. It is perhaps interesting to note that books on differential geometry refer to the significant results first obtained by Dupin, for Dupin was also a pioneer of the theory of hydrostatics and developed in considerable detail the concept of the surface of buoyancy [3].

3.4.4 *Cross Curves of Buoyancy*

Suppose that a series of surfaces of buoyancy have been calculated, each surface for some particular volume ∇. Let these surfaces intersect a plane $A\xi\zeta$, fixed in a body, as indicated in Fig. 3.11(a). All the (closed) curves shown are considered to be fixed to the body. Now let the body be rotated through an angle β about $A\eta$, as shown in Fig. 3.11(b). For each volume ∇_1, ∇_2, ∇_3, . . . the buoyancy force acts vertically

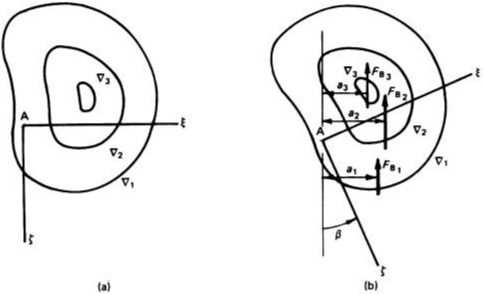

Fig. 3.11

upwards perpendicular to the corresponding surface of buoyancy (although not, in general, in the A$\xi\zeta$ plane). Let these forces be $F_{B_1}, F_{B_2}, F_{B_3}, \ldots$ corresponding to the surfaces for ∇_1, ∇_2, ∇_3, ... Bearing in mind that these forces do not in general act in the plane of the paper, that is in the plane A$\xi\zeta$, but are parallel to it, we now consider the distances a_1, a_2, a_3, . . . of $F_{B_1}, F_{B_2}, F_{B_3}, \ldots$ from that vertical plane through A which contains Aη. These distances may be plotted against the displacement ∇ for a chosen value of β as shown in Fig. 3.12. A family of these curves, plotted for a series of β, is known as a set of 'cross curves of buoyancy'.

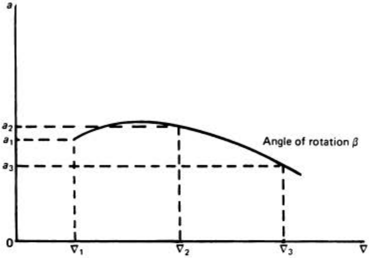

Fig. 3.12 Cross curve of buoyancy.

3.4.5 *Curve of Buoyancy*

The prismatic shape of most marine vehicles – notably ships – suggests a simple approximation in the analysis of buoyancy. The surfaces of buoyancy for all the possible immersed volumes of such a body are elongated. Moreover, the port-and-starboard symmetry that marine vehicles usually possess ensures that each surface is symmetric about the fore-and-aft plane of symmetry.

Figure 3.13(a) shows the side view of a typical ship in its intended (upright) attitude together with a side elevation of its surface of buoyancy. (The geometry of the illustrated surface of buoyancy is not meant to be representative of any particular kind of ship.) The centre of buoyancy is at B_1, the lowermost point on the surface. Suppose that the ship is heeled through a right angle by rotation about a fore-and-aft axis parallel to the water plane and that it is then raised or lowered (keeping the axis parallel to the water plane) so that ∇ is unchanged and the same surface of buoyancy is relevant. This surface can now be seen in plan view and may take the form illustrated in Fig. 3.13(b). The centre of buoyancy is at B_2, which is well aft of B_1. The explanation for this migration aft may be deduced from our previous discussion. The change of attitude may be considered as being the sum of a large number of small rotations, each about a suitable centroidal axis in the prevailing water-plane section. Although this centroidal axis is initially a *principal* axis of the water-plane section, it does not remain one. Therefore the centre of buoyancy starts to move parallel to the axis of rotation.

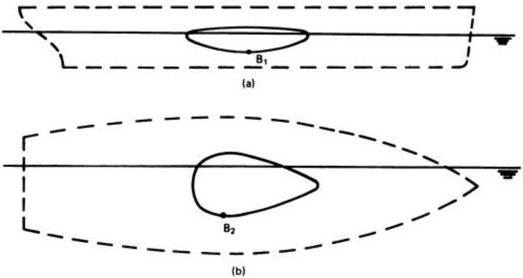

Fig. 3.13

This is an important point and worthy of some further discussion. Suppose that this imaginary experiment were performed on a scow. The water-plane section would at first have the shape depicted in Fig. 3.14(a) and would finally be of the form shown in Fig. 3.14(b). In both diagrams, Oy is the prevailing centroidal axis of rotation (O being the centroid of the water-plane section), but whereas Oy begins as a principal axis it does not remain one, so that the principal centroidal axes at the last small rotation would be Ox' and Oy' (see Fig. 3.14(b)).

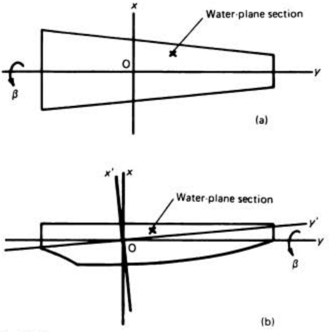

Fig. 3.14

It is interesting to consider a vessel with fore-and-aft and port-and-starboard symmetry, such as a lifeboat, a kayak or a 'double-ender' yacht. If a *transverse* axis in the water-plane section of such a craft remains an axis of symmetry of the water-plane section, then the centre of buoyancy remains in the transverse plane of symmetry if a heel is executed.

The effect illustrated in Fig. 3.13 has been exaggerated for the purpose of explanation. In reality, a ship's surfaces of buoyancy must be elongated and nearly ellipsoidal to correspond with the usual geometry of the immersed volume. At least for initial calculations it is usually assumed that heel and trim may be treated independently. That is to say, if the ship is given an angle of heel only with a constant immersed volume, the centre of buoyancy follows a curve which lies wholly in a single transverse plane; if it is given an angle of trim only, B moves always in the fore-and-aft plane of symmetry. As a result it is implicitly assumed that if an angle of heel is applied, the principal axes in the water-plane section remain in the transverse and fore-and-aft directions. The importance of this assumption is that the heeling of a ship must be considered even more carefully than trimming, for reasons that will become clear. It is indeed fortunate that this assumption is quite accurate for moderate angles of heel, since it simplifies analyses considerably.

Figure 3.15(a) shows a vessel in its intended attitude with B at the lowermost point of that surface of buoyancy which is relevant to its displacement. Figure 3.15(b) shows a cross section of the vessel in which B lies on the closed curve of intersection with the surface of buoyancy. Under the terms of the previous assumption, B moves on this curve when the ship is heeled. Thus if the angle of heel is ϕ, as indicated in Fig. 3.15(c), the centre of buoyancy lies at B′, the lowermost point of the 'curve of buoyancy'.

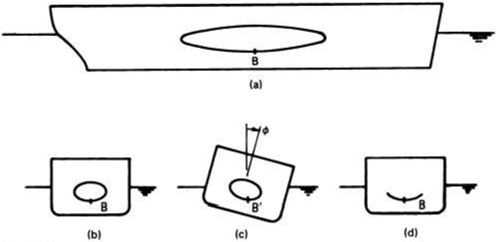

Fig. 3.15

For a conventional ship it would be unreasonable to invoke the idea of a curve of buoyancy if the angle of heel were more than, say, 40 degrees, which is a large angle for any normal ship. In other words, it would be more sensible to depict the curves of buoyancy shown in Fig. 3.15(b) not as a closed curve but rather as a limited portion such as that drawn in Fig. 3.15(d).

3.4.6 *Evolute of the Curve of Buoyancy*

It was indicated earlier that the curvature of the curve of buoyancy is of some importance and that the radius of curvature is given by $\overline{BM'} = I/\nabla$. The pro-metacentre M′ is the centre of curvature of a corresponding point on the curve of buoyancy and the locus of M′ is the 'evolute' of the curve of buoyancy.

The transverse curve of buoyancy of a ship, or similar marine vehicle, has port-and-starboard symmetry about the fore-and-aft plane of symmetry. The evolute of the curve of buoyancy must be likewise symmetric. If we consider a small change of heel angle $\delta\phi$ corresponding to a small increase in the distance from B to M′, given by $\delta(\overline{BM'})$, then the radius of curvature of the evolute of buoyancy is given by $r = \delta(\overline{BM'})/\delta\phi$. In the limit $\delta\phi \to 0$, $r = d(\overline{BM'})/d\phi = (1/\nabla)(dI/d\phi)$ assuming that the displaced volume is unchanged during the small change of heel. This result shows that the radius of curvature of the evolute, and therefore of the curve of buoyancy, must change sign when I is a maximum or minimum at particular values of r. If r changes sign, the evolute has a cusp and clearly this occurs in the upright condition, around deck-edge immersion and at a heel angle of 90°. Two possible arrangements are shown in Fig. 3.16. However, for conventional ships, the curves of B and M′

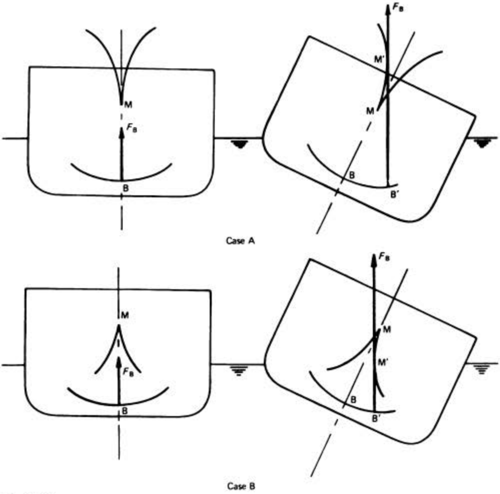

Fig. 3.16

are of little value beyond a heel angle of 90°. For this reason only the bottom portion of the curve of buoyancy, and its corresponding evolute, are shown in Fig. 3.16. Indeed, unless a vehicle is substantially symmetric about a mid-ship transverse plane a two-dimensional analysis beyond a heel angle of 40° is suspect because trim is ignored. On the other hand, for self-righting lifeboats and righting oil rigs the matter is of great interest, and when longitudinal symmetry does not prevail three-dimensional analyses must be used. Nevertheless, it is useful to examine a case for which the closed curve may be legitimately drawn. An ellipsoid that is rotated in incremental steps, with a constant partial immersion so that some chosen minor axis is always kept horizontal, satisfies the necessary conditions of symmetry as shown in Fig. 3.17. The evolute of the curve of buoyancy is then closed and may take the shape portrayed.

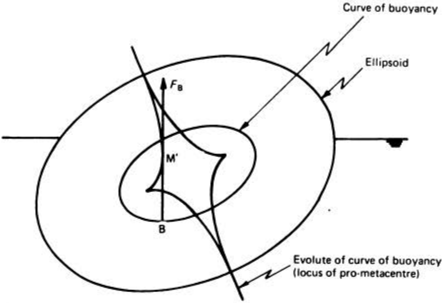

Fig. 3.17

If the difference between the major and minor semi-axes shown in Fig. 3.17 is diminished (without changing the magnitude of that semi-axis perpendicular to the plane of the paper) then the curve of buoyancy becomes more and more circular. The evolute collapses to a point at the centre of a body of circular cross section as shown in Fig. 3.18.

3.5 Equilibrium and Stability of Weight and Buoyancy

It is now necessary to examine the condition of equilibrium that exists when the weight and buoyancy force act simultaneously because the attitude of a floating body depends on these two forces. The body settles until the buoyancy force is equal to the weight and rotates until the centres of buoyancy and gravity, B and G respectively, lie on the same vertical line; the configuration then is one of stable equilibrium. At least one position of stable equilibrium must exist otherwise the body would continue to rotate indefinitely. There is often more than one equili-

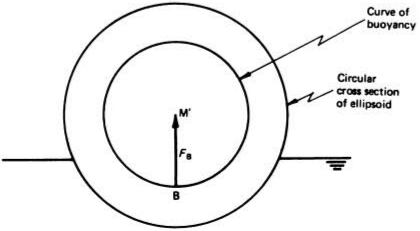

Fig. 3.18

brium position, however, and G may lie above or below B. (A degenerate case arises with bodies of revolution in which the centre of gravity lies exactly on the axis. Thus a ball, for example, will float in neutral, rather than stable, equilibrium since B is *always* directly beneath G and so cannot provide a righting moment, as shown in Fig. 3.19.)

The equilibrium condition of a floating body may be expressed in the following way: (i) the weight Δ^* of the displacement volume ∇ of water must be equal to the weight W of the body, so determining the relevant surface of buoyancy; and (ii) the lowermost point of the surface of buoyancy B must lie on a vertical line through G and either above or below it. This concept is much easier to grasp than that which remains, namely, whether or not the equilibrium configuration will be restored if a very small disturbance of that configuration occurs. In other words, is the equilibrium stable or unstable? In addressing ourselves to this question, we must remember that the small disturbance may be of *any* realizable sort. We have, in effect, to apply 'tests' to the equilibrium to see what happens when the small disturbances occur. With one exception all the disturbances that we shall consider relate to a *rigid* vehicle, although there is no reason in mechanics why distortions should be excluded.

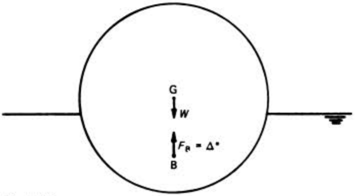

Fig. 3.19

3.5.1 *Totally Immersed Rigid Vehicle*

The equilibrium condition for submarines, submersibles, balloons, dirigibles and similar vehicles is simply $W = F_B(= \rho g \nabla = \Delta^*)$, where the forces W and F_B must act in the same vertical line. The centre of gravity G and the centre of buoyancy B are both fixed in the vehicle which takes up a definite attitude in its equilibrium configuration. Thus B must lie either vertically below or vertically above G if W and F_B are the only external forces acting when the vehicle is at rest in its intended attitude. It is the stability of these equilibrium configurations that must now be examined.

Small disturbances of translation in a horizontal direction do not change the condition of equilibrium. So far as they are concerned the stability is neutral.

To study the effect of small angles of rotation we can conveniently rotate the vehicle about two horizontal axes at right angles to each other. (Rotation about the vertical axis clearly does not affect the condition of equilibrium.) For example, consider the submerged submarine represented in Fig. 3.20. It is evident that if B is above G a small inclination of heel or trim produces a righting couple, and so the arrangement in Fig. 3.20(a) is associated with hydrostatic stability. By contrast, the arrangement in Fig. 3.20(b) shows that if G lies above B there is a tendency for any small inclination to be increased, and so the equilibrium is unstable. The distance $\overline{GB}$ thus represents a measure of a submarine's hydrostatic stability for heel and trim.

In practice B cannot lie far from the central axis of a submarine, and so for stability G must lie below the centre line. Typical values for $\overline{GB}$ lie in the range

$$0.3 \text{ m} < \overline{GB} < 0.6 \text{ m (i.e. } 1 \text{ ft} < \overline{GB} < 2 \text{ ft).}$$

It is implicitly assumed in the foregoing discussion that the submarine in question has a rigid and incompressible structure. But this is not strictly true and consequently we must consider a stability problem of a rather different sort which relates to the submarine's ability to maintain a specified depth of operation.

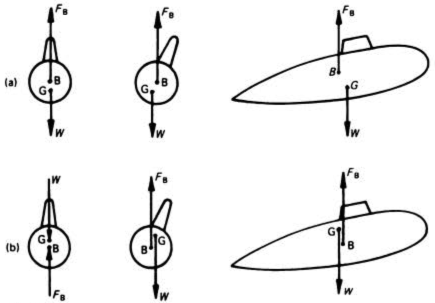

Fig. 3.20

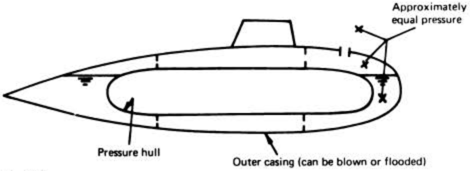

Fig. 3.21

Figure 3.21 shows a greatly simplified form of a submarine. At depth, the pressure hull withstands the full local pressure. Now it is a convention of military submarine practice to include the water in the main ballast tanks in calculations of both weight and buoyancy. Let us, however, examine the situation in another way. When the submarine is submerged, ∇ is the volume of the pressure hull and of all water-excluding parts such as the propeller. (It is worth remarking that for every 8 kN ($\cong$ 0.8 tonf) of solid steel in a marine vehicle about 1 kN ($\cong$ 0.1 tonf) of buoyancy force is available, since the relative density of steel is approximately 7.8.) The buoyancy force which acts on the pressure hull alone, F_B^* say, corresponds to a given depth of operation. If ∇^* is the volume of the pressure hull at that depth,

$$F_B^* = \rho g \nabla^* \tag{3.19}$$

where ρ is the corresponding density of the water. With an increase of depth the pressure p increases and

$$\left(\frac{1}{g}\right)\frac{\partial F_B^*}{\partial p} = \nabla^* \frac{\partial \rho}{\partial p} + \rho \frac{\partial \nabla^*}{\partial p} = \rho \nabla^* \left(\frac{1}{\rho}\frac{\partial \rho}{\partial p} + \frac{1}{\nabla^*}\frac{\partial \nabla^*}{\partial p}\right). \tag{3.20}$$

The partial derivative is used in Equation (3.20) to emphasize that pressure alone may not be entirely responsible for changes in F_B^*. As we saw in Chapter 2 both temperature and salinity vary with depth, but for the present purpose these are likely to be associated with second-order effects. Now $\partial\rho/\partial p$ is positive because of the slight compressibility of water, and $\partial\nabla^*/\partial p$ is negative because of the compressibility of the pressure hull. It follows that $\partial F_B^*/\partial p$ may be positive or negative according to which of these two compressibility effects is the greater. As the weight of the submarine is constant, the condition $\partial F_B^*/\partial p > 0$ is one of stability in depth, while that of $\partial F_B^*/\partial p < 0$ is one of instability. In steel structures the compressibility effects are small and to all intents and purposes the stability in depth can generally be taken as neutral.

3.5.2 *Partially Immersed Vehicles*

Let us suppose that the configuration shown in Fig. 3.4 is one of equilibrium with G lying somewhere on the vertical line through B and $F_B = W$. The body has six degrees of freedom and so may be given (i) displacements in the directions Ox, Oy; (ii) displacements in the direction Oz; (iii) rotations about Ox, Oy; and (iv) rotation about Oz. These then are possible tests that may be applied in checking the stability. Now the relative positions of B and G will not be altered by small disturbances of types (i) and (iv). Furthermore, stability certainly prevails were (ii) is concerned. We are left to apply tests of type (iii) which, as we have already shown, do not affect the magnitude of F_B provided that O lies at the centroid of the water-plane section.

Suppose that Ox, Oy are *principal* axes of the water-plane section and that we rotate the body slightly about Oy to check the stability of an equilibrium configuration in which G lies below B, as in Fig. 3.22. The rotation moves the centre of buoyancy from B to B′, producing a righting couple. The same is true if the rotation is performed about Ox. Hence the equilibrium must be stable if G lies below B. It does not follow, however, that if G is above B the vehicle is unstable, as we shall now show.

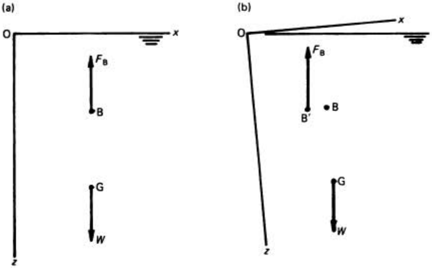

Fig. 3.22

It would appear that the designer has merely to ensure that G lies below B in the intended attitude of a surface craft to guarantee stability. The reasons why this rule is not normally followed are (i) it would be difficult to contrive, and (ii) the vessel concerned would be uncomfortably 'stiff' and would sustain large inertial forces in its upper works as a consequence. Normally G lies above B in the intended attitude, a fact which at first sight may seem surprising.

Let us consider a small angular displacement β about the principal axis Oy, as before, but this time let G lie above B. The initial and final positions of G and the centre of buoyancy are as shown in Fig. 3.23. As G, B and B′ all lie in the same vertical plane, the vertical through B′ intersects $\overline{\text{GB}}$ extended at M. Note that the smaller is β the more closely does $\overline{\text{BB}}'$ become parallel to the water surface and perpendicular to both $\overline{\text{BM}}$ and $\overline{\text{B'M}}$. It follows that M is the centre of curvature of the curve (or, rather, cross section of the surface of buoyancy) on which B and B′ lie. We previously called a point like M a 'pro-metacentre' denoted by the symbol M′; but in this single context, where the equilibrium configuration is referred to the upright condition, M′ becomes a 'metacentre' denoted by M. Equation (3.18) can then be written as

$$\overline{\text{BM}} = \frac{I}{\nabla}. \qquad (3.21)$$

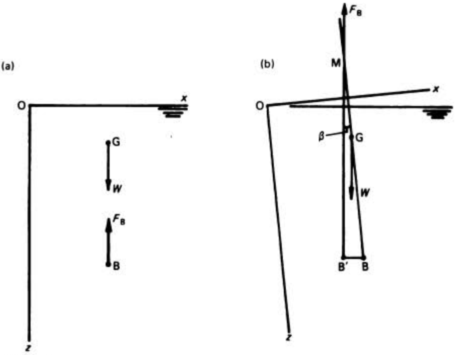

Fig. 3.23

It will be seen from Fig. 3.23(b) that if M lies above G the position of equilibrium is stable, while if M lies below G the equilibrium is unstable. It is theoretically possible for M and G to coincide, in which case neutral stability prevails.

Having checked the stability with a small rotation about Oy, we should now apply a small rotation about Ox to find a second metacentre. It is an elementary property of all plane areas that one can find two perpendicular axes through the centroid for which the products of the areas vanish. These are the principal axes of the area. If a *small* rotation is performed about any oblique axis in the water-plane section it can be resolved as a vector into two component rotations about the two principal axes, each associated with a metacentre M. The required condition of stability is that neither of the two points M shall lie below G. The distance $\overline{GM}$, which represents a measure of a surface ship's initial stability, is usually called the 'metacentric height' and for rotations about the principal axes is often given subscripts L (longitudinal) and T (transverse).

It must be understood that a general treatment of the hydrostatic stability of an irregular body gives rise to some complicated problems. These can be vastly simplified, however, if the idea of a 'curve of buoyancy' can be invoked. We shall therefore turn our attention to that particular case, making special reference to surface ships.

3.5.3 *Stability of Surface Ships*

As we have already noted, the conventional displacement ship requires special considerations of its own. These arise from its prismatic form and its longitudinal plane of symmetry, a feature which it shares with other types of vehicle such as pontoons, floating docks, etc. The possession of this form and symmetry implies that plane transverse curves of buoyancy may usefully be assumed to exist.

Suppose that the ship is placed in water and that its immersion and attitude are such that $\overline{BG}$ is vertical with both G and B lying in the plane of symmetry. In this configuration axes $Oxyz$ may be fixed in the hull with Oxy in the water-plane section, O being the centroid and with Ox pointing forward, as shown in Fig. 3.24. The axes Ox, Oy will be the principal centroidal axes because Oxz (which contains the vertical line $\overline{BG}$) is the plane of symmetry and Oy is perpendicular to that plane. If the ship is now rotated through a small angle of heel ϕ, about Ox, a metacentre associated with 'transverse stability', M_T, may be defined. Similarly, if the ship is trimmed through a small angle θ about a transverse axis a second metacentre associated with 'longitudinal stability', M_L, is identified. For each of these two metacentres the distance $\overline{BM} = I/\nabla$ can be calculated. The calculation is one of some accuracy as it involves geometric quantities only.

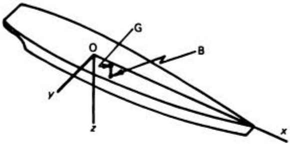

Fig. 3.24

Having found $\overline{BM}$ we can go on to find the metacentric height $\overline{GM}$, which is a measure of the stability. This requires prior knowledge of $\overline{BG}$, that is, of the position of the centre of gravity relative to B. As we have already mentioned the position of G can be calculated with reasonable accuracy, although the calculation is rather tedious and time consuming.

Because the hydrostatic stability of a ship is of cardinal importance to the naval architect, it is necessary that the calculations of the position of G should be checked. This is done by means of an 'inclining experiment' which can be regarded as an independent determination of the centre of gravity G. The experiment is normally performed only for heel since transverse inclinations are easier to arrange and for most ship shapes $\overline{GM}_T < \overline{GM}_L$.

In its most rudimentary form the test entails moving a body of weight w across the deck of a ship and noting the small inclination produced, as indicated in Fig. 3.25. The movement of the centre of gravity $\overline{GG'}$ is given by

$$wd = W\overline{GG'}$$

where W includes the weight of the movable body. But

$$\overline{GG'} = \overline{GM}\,\phi$$

and so

$$\overline{GM} = \frac{wd}{W\phi}. \tag{3.22}$$

The values of w, d and ϕ are noted and W is found by calculation or measurement.

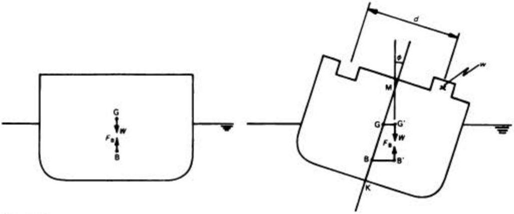

Fig. 3.25

As stability depends on the small difference between two often large distances ($\overline{GM} = \overline{KM} - \overline{KG}$), the inclining experiment must be performed with very great care and accuracy as described in, for example, [4].

Some idea of how B, G and M may be placed in a ship can be obtained from Table 3.2, which shows some approximate values and in which K is the lowermost point (i.e. keel), M_T is the metacentre for heel about a longitudinal axis, and M_L is the metacentre for trim about a transverse axis.

Table 3.2 *Some typical locations of* B, G, M_T *and* M_L *measured relative to the keel. Units are metres with feet in parentheses.*

	Distance			
Vehicle	$\overline{KB}$	$\overline{KG}$	$\overline{KM_T}$	$\overline{KM_L}$
Frigate	2.56 (8.40)	4.94 (16.21)	5.92 (19.42)	250 (820)
Destroyer	2.95 (9.68)	6.95 (22.80)	7.80 (25.59)	396 (1300)
Container Ship	5.6 (18.37)	17.0 (55.77)	17.3 (56.76)	280 (917)

3.5.4 *Effect of Liquid with a Free Surface on Ship Stability*

When a partially filled tank is tilted the centre of gravity of a liquid contained in it moves relative to the sides of the tank.† It follows, therefore, that when the stability of a ship is examined account must be taken of the displacement of the centre of gravity resulting from the movement of tanks containing liquids with a free surface. To take a simple, but important case consider the result of a small angle of heel ϕ about the Ox axis in the water-plane section as shown in Fig. 3.26. If ϕ is assumed

† Many different liquids are carried in ships. For example, fresh water for drinking and for the boilers; salt water for ballast, baths, bilge water; and oil for fuel and lubrication, etc.

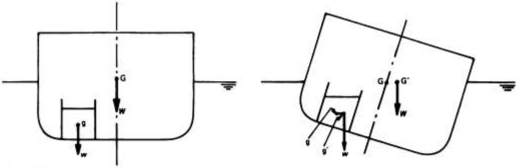

Fig. 3.26

to be so small that G moves horizontally to G′ then

$$W.\overline{GG'} = w.\overline{gg'}. \tag{3.23}$$

Now the horizontal movement of the centre of gravity of the liquid, $\overline{gg'}$, is the same as the horizontal movement of the tank's centre of buoyancy if the tank were floating with the volume of liquid ∇_1 as the immersed volume. (In both cases one would be concerned with the movement of the centroid of ∇_1.) Therefore, from Equation (3.23),

$$W.\overline{GG'} = w\frac{I_1}{\nabla_1}\phi \tag{3.24}$$

where I_1 is the second moment of area of the surface of liquid in the tank about an axis through the centroid of the free surface parallel to the axis of rotation of the ship. That is

$$\overline{GG'} = \frac{\phi}{W}\frac{w}{\nabla_1}I_1 = \frac{\phi}{W}\rho_1 g I_1 \tag{3.25}$$

where ρ_1 is the density of the liquid. If there are several tanks, then

$$\overline{GG'} = \frac{\phi g}{W}\sum \rho_1 I_1.$$

Consider now the application of a small angle of heel in a test for stability. As G will move to G′ as a result of the movement of liquid, there is an apparent loss of metacentric height which amounts to

$$\overline{GG''} = \frac{\overline{GG'}}{\phi} = \frac{g}{W}\sum \rho_1 I_1 \tag{3.26}$$

as shown in Fig. 3.27. The liquid in the tanks thus has a destabilizing effect. Moreover, this effect is independent of both the position of the tanks and the amount of liquid contained in them.

A similar phenomenon occurs with the weights of suspended masses which are free to swing (e.g. a boat just about to be lowered into the water from davits, or a load being lifted by a floating crane). It will be readily seen that the centre of

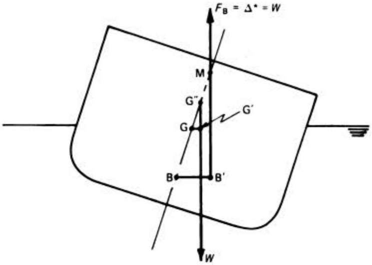

Fig. 3.27

gravity of a freely suspended mass must be regarded as lying at its point of suspension when the stability of the vehicle is being investigated. Standing passengers may also be treated as if their centres of gravity were in their feet, if they are not otherwise deemed to be in contact with the ship.

3.5.5 *Curves of Buoyancy in Ship Calculations*

As already explained in Section 3.4.5, it is reasonable to assume that for moderate angles of heel a curve of buoyancy lies in the transverse plane containing $\overline{BG}$ (as well as a second one in the plane of hull symmetry). In this case it is possible to examine such angles of heel and yet still monitor the movement of the centre of buoyancy since it is confined to the one transverse plane. Determination of 'curves of righting moments' then becomes possible.

Figure 3.28 shows the curves of buoyancy and evolutes that were previously drawn in Fig. 3.16. Since we have assumed that the centre of gravity lies in the plane of the curve of buoyancy and its evolute, G may be represented in the diagrams. It is drawn in Fig. 3.28 in the plane of hull symmetry so that $\overline{BG}$ lies in the plane in the equilibrium configuration. Two possible cases are shown with the evolute of the curve of buoyancy pointing downwards (case A) and upwards (case B).

For any angle of heel Φ the normal to the curve of buoyancy is vertical. If the perpendicular is drawn from G to the line of action of the buoyancy force F_B (i.e. to the point Z) then the righting moment is $W.\overline{GZ}$, corresponding to the angle Φ.

It will be seen that as Φ is increased in case A, $\overline{GZ}$ increases monotonically, as indicated in Fig. 3.29. In case B, however, $\overline{GZ}$ increases and then decreases until it becomes zero when $\Phi = \Phi_0$. This condition corresponds to that illustrated by the broken line in Fig. 3.28 and represents a state of unstable equilibrium. Any slight further increase in Φ would evidently produce a capsizing moment. The curve of $\overline{GZ}$ against Φ is thus of the form shown (for case B) in Fig. 3.29 where usually $40° < \Phi_0 < 70°$. A typical example for a large naval ship, such as that in Fig. 3.2, is shown in Fig. 3.30. In the limiting case $\Phi \to 0$, $M' \to M$ and $\overline{GZ} \to \overline{GM}\Phi$. Thus for fixed G and M, $d\overline{GZ}/d\Phi = \overline{GM}$, and the slope of the $\overline{GZ}$ curve at the origin is a

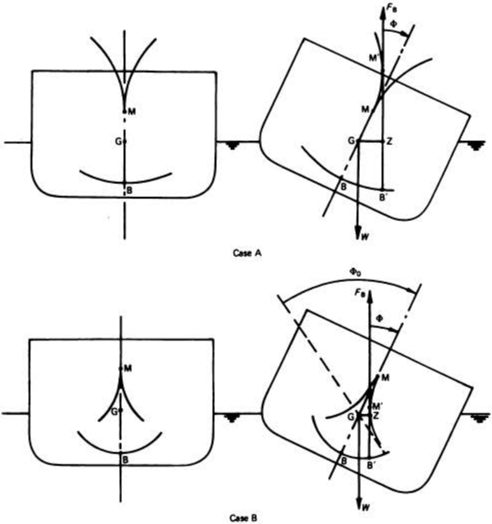

Fig. 3.28

measure of the metacentric height and may be read off the $\overline{GZ}$ scale as indicated in Fig. 3.30.

A ship may sometimes be initially unstable transversely in the upright condition because of free-surface effects which disappear at small angles of heel. On each side of the upright the ship becomes stable at an angle known as the 'angle of loll', Φ_L,

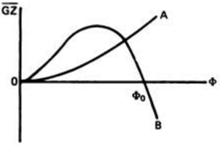

Fig. 3.29

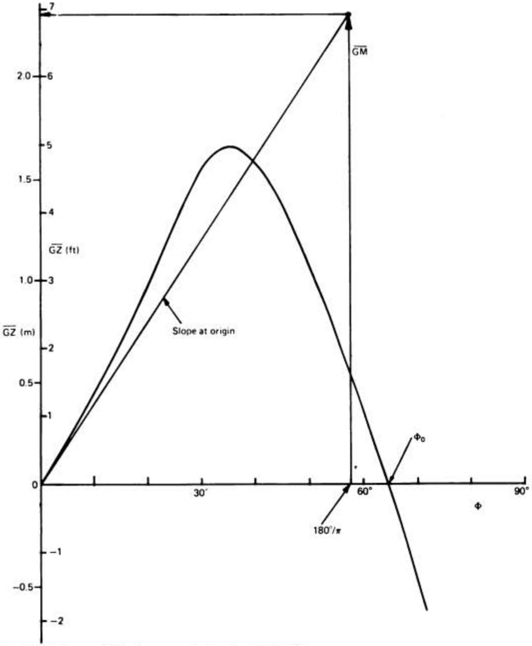

Fig. 3.30 Curve of righting moments for a large warship.

and this is illustrated by the $\overline{GZ}$ curve in Fig. 3.31. If this loll condition is not recognized as such and weights are introduced in an attempt to bring the ship back to the upright, the effects could well be to move the ship's centre of gravity laterally from its original location G to a new location G′ so that $\overline{GZ}$ is reduced by an amount $\overline{GG'}\cos\Phi$, as shown in Fig. 3.31, so worsening the angle of loll to Φ'_L. It may be seen from Fig. 3.31 that one indication of a possible loll condition is that the slope of the $\overline{GZ}$ curve at the origin is negative and thus $\overline{GM}$ is negative, that is, M is below G.

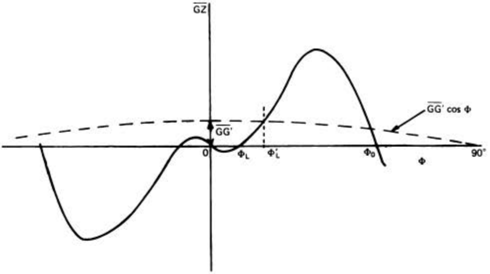

Fig. 3.31

A curve of righting moments does not possess great intrinsic value for the following reasons:

(i) It is impossible for a ship *at rest* to have an angle of heel in water *at rest* (assuming of course that the upright position is associated with stable equilibrium).
(ii) The possibility that equipment, cargo and fittings will shift is ignored.
(iii) Since a ship is not normally symmetric about a transverse plane the principal axes of the water-plane section depart increasingly from fore-and-aft and athwartships as heel is increased. In other words, because the ship is not symmetric about the transverse plane containing G, B moves out of that plane so that the ship assumes a trim (as well as the heel).

These shortcomings notwithstanding, it would clearly be prudent to obtain some idea of how the righting moment varies, even if it is only by comparing the curves obtained with those of previous 'successful' designs. Hawkey [5] describes the loss of a controversial experimental ship through insufficient grasp by its amateur designer of this very point. Further examples are discussed in [6].

As we shall discover elsewhere in naval architecture, there is a considerable temptation to refine calculations that are known to depend on gross assumptions even if, as here, the results can only provide rough guidance to the designer. The traditional $\overline{GZ}$ curve is known to be vastly inaccurate on the last of the above three accounts at heel angles of more than about 45°. Indeed, for some hull forms neglect of trim fails to reveal important phenomena, such as the reduction in righting moment in ships with a break of fo'c'sle that occurs when the after end of the weather deck is immersed as a result of the trim by the stern that develops as heel is increased. The designer would certainly wish to have some guidance on such behaviour as this, so that suitable action could be taken if necessary. Accordingly, now that buoyancy calculations are carried out using digital computers, allowance for trim may be made in estimating curves of righting moments. The exact nature of the allowance will not be dealt with here, however. Practical details of ship stability are discussed in [7] and a comparable analysis of partially flooded ships is given in [8].

In Fig. 3.28 we chose to assume that G was positioned in the fore-and-aft plane of hull symmetry. It may not be so, however, and in this case the idea of a curve of buoyancy is very useful. The shapes (and existence) of the curve and its evolute are dependent on the geometry of the hull. If the position of G is offset, as in Fig. 3.32, then the curve of buoyancy shows what the equilibrium configuration will be. Moreover, if the angle of heel is varied, the variation of $\overline{GZ}$ (and hence of righting moment) with Φ may be determined, as shown for the loll condition in Fig. 3.31.

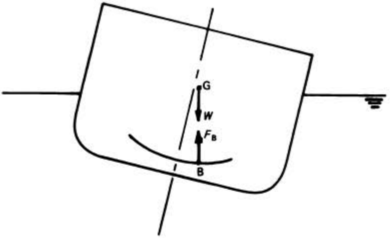

Fig. 3.32

3.5.6 *Cross Curves of Righting Moments in Ship Calculations*

During its life a ship has to float with various volumes of displacement ∇. Therefore the designer cannot confine his attention to a single surface of buoyancy; strictly speaking he should consider a number of such surfaces. Where conventional displacement ships are concerned, this effectively means that a number of curves of righting moments must be considered. Thus the $\overline{GZ}$ curve shown in Fig. 3.30 is merely one of a set, each member of which corresponds to some selected condition of the ship.

Now the cross curves of righting moments could be found if the appropriate cross curves of buoyancy described earlier were calculated as a preliminary step. In fact, computations are usually made by direct numerical integration using a digital computer, thus bypassing the task of finding the curves of buoyancy.

The cross curves of righting moments are of value in design: they relate solely to the geometry of the ship and permit curves of righting moments (or $\overline{GZ}$) to be drawn once the centre of gravity has been located in the plane of the transverse curve of buoyancy. The cross curves of righting moments shown in Fig. 3.33 relate to the ship in Fig. 3.2. The point S, about which moments were taken, was arbitrarily fixed at some 8.4 m (28 ft) above the underside of the keel in the fore-and-aft plane of hull symmetry at the cross section containing G and B. This choice of an arbitrary point S arises because G is not necessarily a fixed point in the ship when changes of displacement occur. Only when S is fixed relative to, say, the keel can

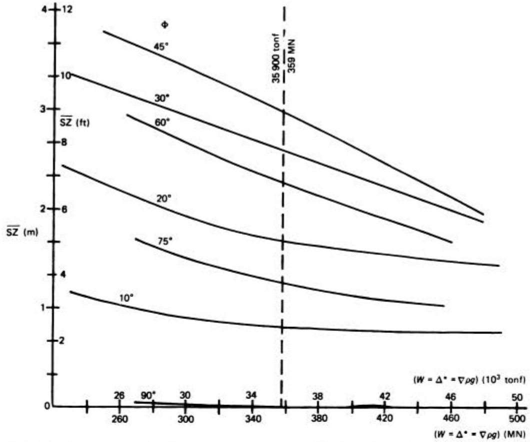

Fig. 3.33 Cross curves of righting moments (curves of stability) for the ship of Fig. 3.2.

the cross curves of righting moments giving $\overline{SZ}$ be considered to depend on geometry alone.

In naval architecture the cross curves of righting moments are usually plotted in the manner of Fig. 3.33 and described as 'curves of stability'. However, the use of the word 'stability' in this context (where large angles of heel are referred to) is rather inappropriate.

3.6 Equilibrium of Weight, Buoyancy and Direct Thrust Acting Simultaneously

So far we have examined W and F_B and considered the stability of the equilibrium that exists between them. It is by no means uncommon for significant problems to arise with a more complex loading involving the application of direct forces. In particular, cases arise in the docking and grounding of ships. While no new principles are introduced by these problems, one or two general points need to be examined.

An important practical problem arises when a ship is taken into dry-dock. To understand it fully it is necessary to know that ships are often 'trimmed by the stern'; that is, the straight portion of the keel is tilted downwards at the rear. The reasons for doing this are (i) it may decrease the resistance of the hull to forward motion, (ii) it increases the immersion of large propellers, (iii) it usually improves directional stability, and (iv) it localizes docking stresses to an area where the hull is suitably strengthened. It is this last point with which we will be concerned.

Suppose that a ship is trimmed by the stern and made to rest on dock blocks at its after cut-up (ACU). Before the ACU touches the blocks the ship is as shown in Fig. 3.34, where O is the centroid of the water-plane section and, for the sake of clarity, the trim angle is shown exaggerated. As the level of water is lowered, contact is made at the ACU. Thenceforth θ is reduced as the reaction force at the ACU increases until the ship is about to settle down all along the keel. During the process of settling, *until just short of coming finally to rest*, there is a problem of stability in heel. This is because shores can only be used at the ACU, and if there are no shores the question arises as to whether or not the system is stable. Thus the ship might not remain upright as shown in Fig. 3.35(a) but heel as indicated in Fig. 3.35(b). Here we show W as the weight of the vehicle and do not refer to the displacement Δ^* (the weight of water displaced by the freely floating ship) owing to the presence of the force P applied at K.

The force P applied at the ACU is greatest just before complete settlement. The worst condition is therefore as shown in Fig. 3.36 with ∇' as the new immersed volume. It is necessary for this condition that a check on the stability in heel must be made by finding P and the height $\overline{KM}_T$, where M_T is the transverse metacentre for the lowered water plane at which complete settlement just occurs (as in Fig. 3.35).

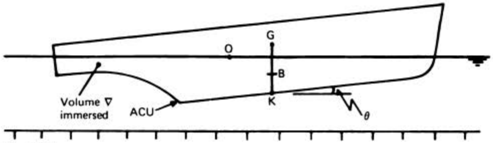

Fig. 3.34

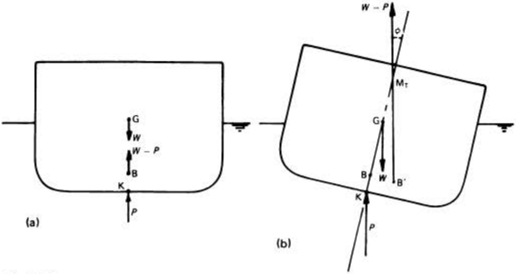

Fig. 3.35

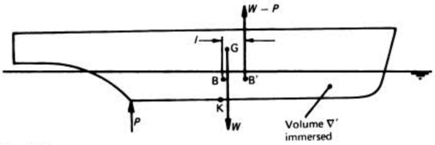

Fig. 3.36

The transition from the initial to the final (critical) configuration can be thought of as occurring in two stages:

(i) reduction of ∇ to ∇' by the application of P at such a point that θ is unchanged at the point O in Fig. 3.34 for small changes in ∇'; and
(ii) reduction of θ to zero without change of ∇' by a couple which, when added to the force P, has the effect of shifting P to the ACU.

In other words, it is helpful to consider an intermediate stage between the initial and final ones already described.

The advantage of breaking down the determination of P into these two steps is that, if θ is sufficiently small, both may be analysed in terms of the simple theory of Sections 3.5.3–3.5.6.

3.7 Equilibrium and Stability of Ships: Some Practical Considerations

In the preceding sections the approach to questions of equilibrium and stability of floating bodies has been quite general, the main purpose being to draw to the reader's attention the various problems associated with the hydrostatics of such bodies. (Many other problems arise when the hydrodynamics of marine vehicles are considered, as we shall find later, but clearly a ship must be stable when alongside a jetty or hove-too in a channel otherwise an examination of the more complete dynamic problems is largely a fruitless exercise.) To carry out a full analysis of launching, docking, flotation, trim and static stability is a time-consuming numerical task and beyond our scope here. The various techniques are outlined, for example, in [4]. However, a note of caution must be issued because in many instances calculations have been undertaken using concepts which are inappropriate. Some cases have been alluded to earlier, and in practice answers which admittedly predict the hydrostatic behaviour of a *given* ship with acceptable accuracy have often relied on questionable empiricism. Nevertheless, provided that account is always taken of the limitations of the theory, the following developments are important in the static analysis of ships.

3.7.1 *Flotation and Trim*

The trim of a surface ship is the difference between the draught aft T_A and the draught forward T_F measured at some specified locations a distance L apart in the fore-and-aft plane of symmetry, that is, the Oxz plane in Fig. 3.24. The locations usually chosen for measurement are the fore perpendicular, namely the perpendicular at the intersection of the stem with the water line at design load, and the aft perpendicular, namely the perpendicular (often) through the rudder stock or some other significant point near the stem. Thus L is referred to as the length between perpendiculars and is usually written L_{PP}. Consequently, we may refer to 'trim by the stern' $T_A - T_F$, or 'trim by the bow' $T_F - T_A$. Taking the former case as an example we may then write for the angle of trim

$$\tan\theta = (T_A - T_F)/L_{PP} \cong \theta \tag{3.27}$$

when the angle of the trim is small, as it often is of course. As shown earlier, if a floating body undergoes an angular displacement without a change of volume displacement the rotation must take place about an axis passing through the centroid of the water-plane section – in other words, at the centre of flotation. To avoid a change of trim, therefore, the centre of gravity of any small mass added to the ship must lie on the vertical containing the centre of flotation. Any other location of additional mass will change both draught and angle of trim which may be thought of as a combination of parallel immersion and change of trim angle.

For parallel immersion (or rise) use is made of TPI in practical calculations as described in Section 3.4.2. The phrase 'tonne force parallel immersion' is largely historical and a natural development of the original 'ton force parallel immersion'. The unit tonne force, equivalent to 1000 kg x 9.81 N kg^{-1}, is not itself an SI unit of force. Furthermore, the distance of immersion in SI units is taken to be one metre, whereas that corresponding to ton force has been taken as one inch. In short, there seems little point in adopting a change from the abbreviation TPI provided that 'force per unit parallel depth of immersion' is understood and that the units of measurement are clearly stated. Some typical values of TPI using preferential SI units are: frigate, 10 MN m^{-1} ($\cong$ 25 tonf in^{-1}); destroyer, 19 MN m^{-1} ($\cong$ 48 tonf in^{-1}); cargo vessel of 200 MN ($\cong$ 20 000 tonf) displacement, 27 MN m^{-1} ($\cong$ 67 tonf in^{-1}); VLCC, 120 MN m^{-1} ($\cong$ 300 tonf in^{-1}).

In analogy with TPI we may introduce a practical measure of the moment required to produce a standard change of trim. It was found in Section 3.4.2 that for rotation about the centre of flotation the centre of curvature of the curve of buoyancy was the pro-metacentre M$'$ on the evolute. If we restrict our attention to small angles of trim then the point M$'$ becomes nearly the fixed point M, the metacentre. Moreover, for rotations in the fore-and-aft plane of symmetry the distance from the centre of buoyancy to the longitudinal metacentre M_L, given by $\overline{BM}_L$, is very large for most ships. This is illustrated in Table 3.2, and for many purposes we can assume that $\overline{BM}_L$ and $\overline{GM}_L$ are essentially the same, especially for naval ships.

Let us apply a moment C at the centre of flotation O so that the ship suffers a trim by the stern. This is indicated in Fig. 3.37 in which the ship is kept stationary but the water level is rotated from the reference condition WL to the trimmed condition W_1L_1. A wedge of water is immersed aft and a corresponding wedge emerges forward so that the centre of buoyancy moves from B to B_1. The buoyancy force F_{B_1} (= Δ^*) acts in a direction perpendicular to W_1L_1 and its line of action meets the original direction of F_B (= Δ^* for constant displacement) perpendicular to WL at M_L. The weight displacement W(= Δ^*) of the ship acts through G and is perpendicular to WL before trim and to W_1L_1 after trim, so that the moment C must give rise to the couple $\Delta^*.\overline{GZ}$, where GA is the perpendicular distance between the parallel lines of action of F_{B_1} and W. Whence

$$C = \Delta^*.\overline{GZ} = \Delta^*.\overline{GM}_L \sin\theta.$$

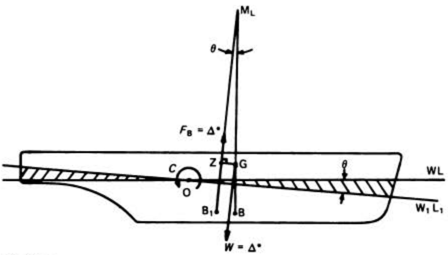

Fig. 3.37

For small trim angles $\sin \theta \cong \theta$ and therefore

$$C = \Delta^*.\overline{GM}_L \theta. \tag{3.28}$$

Now if the trim in Equation (3.27) is written as t we may rearrange Equation (3.28) to give

$$C = \Delta^*.\overline{GM}_L \frac{t}{L_{PP}},$$

or

$$\frac{C}{t} = \frac{\Delta^*.\overline{GM}_L}{L_{PP}}. \tag{3.29}$$

The moment to cause trim MCT (applied at the centre of flotation) is C and the moment to cause unit trim is C/t. Thus the left-hand side of Equation (3.29) is referred to as MCT 1 metre or MCT 1 inch. Provided that the *trim is small* the change of trim caused by an application of moment C at the centre of flotation is C divided by the MCT (for the appropriate unit distance). Confusingly, a mixed set of units is often used, but it is strongly recommended that consistent units be taken for all calculations and any conversion to other units left as a final stage.

As $\overline{GM}_L$ and $\overline{BM}_L$ are both large and nearly equal for most ships, 'MCT unit trim change' may be written as

$$\text{MCT(utc)} = \frac{\Delta^*.\overline{BM}_L}{L_{PP}} = \frac{\Delta^*}{L_{PP}} \frac{I_L}{\nabla} = \frac{\rho g I_L}{L_{PP}} \tag{3.30}$$

where I_L is the second moment of area of the water-plane section about a transverse axis (Oy) through the centre of flotation. Typical values of MCT are: frigate, 61 MNm m^{-1} ($\cong$ 500 tonf ft in^{-1}); destroyer, 168 MNm m^{-1} ($\cong$ 1400 tonf ft in^{-1}); cargo vessel of 200 MN ($\cong$ 20 000 tonf) displacement, 207 MNm m^{-1} ($\cong$ 1725 tonf ft in^{-1}); VLCC, 1900 MNm m^{-1} ($\cong$ 16 000 tonf ft in^{-1}). It may be noted from Equation (3.30) that MCT depends on the *geometry* of the water-plane section *and* on the *density* of the water in which the vessel floats. However, although the concept of MCT unit trim change is useful, any calculation of the metacentric height $\overline{GM}_L$ from it is only approximate. Present practice now favours the greater use of cross curves of righting moment, but both TPI and MCT are contained in the quoted hydrostatic data for most ships.

As an example of the use of TPI and MCT we can consider the small changes of draught and trim which occur as a ship moves from water of density ρ_1 to that of a slightly different density ρ_2. Assuming that the weight displacement of the ship, Δ^*, does not change then

$$\Delta^* = \rho_1 g \nabla_1 = \rho_2 g \nabla_2$$

and so

$$\delta\nabla = \nabla_2 - \nabla_1 = \nabla_1 \left(\frac{\rho_1 - \rho_2}{\rho_2}\right). \tag{3.31}$$

Buoyancy from this additional water layer occurs not at the centre of buoyancy B_1 in water of density ρ_1 but, approximately, at the centre of flotation O at a horizontal distance a away from it, as shown in Fig. 3.38, as a result of near parallel sinkage.

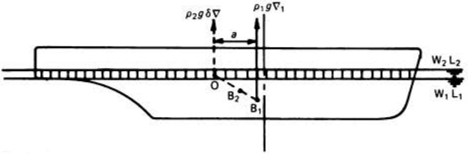

Fig. 3.38

Thus B_1 moves to B_2 corresponding to $W_2 L_2$ so that the horizontal component of $\overline{B_1 B_2}$ equals

$$\frac{a\rho_2 g\delta\nabla}{\rho_2 g\nabla_2} = \frac{a\delta\nabla}{\nabla_2} = \frac{a\nabla_1}{\nabla_2}\left(\frac{\rho_1 - \rho_2}{\rho_2}\right) = \frac{a(\rho_1 - \rho_2)}{\rho_1}.$$

But B_2 and G must be in a vertical line so the ship trims a small angle θ about O to make the horizontal component of $\overline{B_1 B_2}$ equal to $\overline{B_2 M}\,\theta$. Hence

$$\theta = \frac{a}{\overline{B_2 M}}\left(\frac{\rho_1 - \rho_2}{\rho_1}\right) \simeq a\left(1 - \frac{\rho_2}{\rho_1}\right)\frac{\Delta^*}{I_{L2}\rho_2 g} = a\left(1 - \frac{\rho_2}{\rho_1}\right)\frac{\Delta^*}{L_{PP}(\mathrm{MCT})} \tag{3.32}$$

where I_{L2} corresponds to water of density ρ_2. In addition, the parallel sinkage causes an even change of draught δT given by

$$\delta T = \frac{\delta\nabla}{A_{WL}} = \frac{\nabla_1}{A_{WL}}\left(\frac{\rho_1 - \rho_2}{\rho_2}\right) = \frac{\rho_2 g\delta\nabla}{(\mathrm{TPI})} \tag{3.33}$$

where A_{WL} is the water-plane area of the hull.

3.7.2 *Stability of Ships and Floating Bodies*

We shall consider first the problem of initial stability, which corresponds to very small departures from an assumed equilibrium condition. We can therefore think in terms of an identifiable fixed metacentre M. Angular displacements take place about the principal centroidal axes defined in Fig. 3.24. Of particular concern to us is the question of stability about the Ox axis, and consequently we apply a small angle of heel ϕ to the ship. As in Fig. 3.25, for example, there are three locations of importance in problems of initial stability, namely, the centre of gravity G, the centre of buoyancy B and the metacentre M.

(a) *Effect on Stability of Small Changes to the Dimensions of an Immersed Hull*
A measure of the streamlined shape of a ship may be obtained from the 'fineness coefficient' defined as the water-plane area of the hull divided by the product of the water-line length L_{WL} and the maximum breadth (beam) B_{WL}, at the water line when floating at the operating displacement. Clearly, $B_{WL} \times L_{WL}$ is the area of the circumscribing rectangle at the water line. When, in an initial design, a ship is required to operate under conditions somewhat different from those originally intended small modifications to the hull form may be necessary and which may have a significant effect on stability. For example, when operation in confined waters requires small changes to draught and beam it is useful if these changes can be made without an alteration to the fineness of the ship. For this to hold, all dimensions in a given orthogonal direction must be changed in the same ratio although the ratio need not be the same for each direction.

Adopting generally B, L, T to indicate wetted beam, length and draught we may write for the displacement

$$\Delta^* \propto B \times L \times T = k_1 BLT \tag{3.34}$$

where k_1 is a constant. Let us now suppose that B, L and T are each increased by a small amounts δB, δL and δT respectively so that Δ^* experiences a concomitant small increase $\delta\Delta^*$. Then

$$\begin{aligned}\Delta^* + \delta\Delta^* &= k_1(B + \delta B)(L + \delta L)(T + \delta T)\\ &= k_1(BLT + BT\delta L + LT\delta B + BL\delta T)\end{aligned}$$

when products of small terms are neglected. Use of Equation (3.34) finally yields

$$\frac{\delta\Delta^*}{\Delta^*} = \frac{\delta B}{B} + \frac{\delta L}{L} + \frac{\delta T}{T} \tag{3.35}$$

which indicates that the sum of the fractional changes in the main dimensions gives the fractional change in the displacement.

Equation (3.21) for $\overline{\mathrm{BM}}$ can be written as

$$\overline{\mathrm{BM}} = \frac{I}{\nabla} = k_2 \frac{LB^3}{BLT} = k_2 \frac{B^2}{T} \tag{3.36}$$

where k_2 is another constant. We here consider M as the transverse metacentre, since stability in heel is likely to be the most critical problem. Using a similar process as before we find that a small increase in $\overline{\mathrm{BM}}$, arising from small increases in B and

T, is given by

$$\frac{\delta(\overline{\mathrm{BM}})}{\overline{\mathrm{BM}}} = \frac{2\delta B}{B} - \frac{\delta T}{T} = \frac{\delta(\overline{\mathrm{BG}}) + \delta(\overline{\mathrm{GM}})}{\overline{\mathrm{BG}} + \overline{\mathrm{GM}}}. \tag{3.37}$$

Several interesting cases arise from Equations (3.35) and (3.37) depending on the changes which take place. For example, if L and T are constant then the increase in displacement is

$$\delta\Delta^* = \Delta^* \frac{\delta B}{B}$$

and also if G remains fixed in the ship then for small angles of heel about principal centroidal axes in the water plane the distance $\overline{\mathrm{BG}}$ remains unchanged. Thus, Equation (3.37) gives

$$\frac{\delta(\overline{\mathrm{GM}})}{\overline{\mathrm{GM}}} = 2\left(\frac{\overline{\mathrm{BM}}}{\overline{\mathrm{GM}}}\right)\frac{\delta B}{B} \tag{3.38}$$

and as $\overline{\mathrm{BM}} > \overline{\mathrm{GM}}$ for most ships the fractional increase in $\overline{\mathrm{GM}}$ is more than twice the fractional increase in B. An increase in beam can therefore be seen as a good device for increasing the righting moment for transverse angular displacements, other factors remaining unchanged (which they seldom do).

If Δ^* and T remain constant and the height of G above the keel $\overline{\mathrm{KG}}$ is again constant, Equation (3.38) holds. Furthermore, L must be reduced in the same proportion as B is increased. When Δ^* and L are kept constant

$$\frac{\delta T}{T} = -\frac{\delta B}{B}$$

and the possibility of a variation in $\overline{\mathrm{KG}}$ arises. One may easily show that if $\overline{\mathrm{KG}} \propto T$,

$$\frac{\delta(\overline{\mathrm{GM}})}{\overline{\mathrm{GM}}} = \left(3 + 4\frac{\overline{\mathrm{BG}}}{\overline{\mathrm{GM}}}\right)\frac{\delta B}{B}; \tag{3.39}$$

and if $\overline{\mathrm{KG}}$ is constant

$$\frac{\delta(\overline{\mathrm{GM}})}{\overline{\mathrm{GM}}} = \left(3 + 4\frac{\overline{\mathrm{BG}}}{\overline{\mathrm{GM}}} - \frac{\overline{\mathrm{KG}}}{\overline{\mathrm{GM}}}\right)\frac{\delta B}{B}. \tag{3.40}$$

(b) *Stability of a Uniform Rectangular Block*

The material making up the rectangular block must have a density less than that of the liquid in which it is immersed otherwise the block will not float. Thus, the density of the block relative to that of the liquid, $\bar{\rho}$, must be less than unity. Let us suppose that the block of length L, breadth B and height H floats to a draught T as shown in Fig. 3.39(a). Note that a *uniform* rectangular block floating in static equilibrium, the line joining the centres of gravity G, and buoyancy B, to the metacentre M, is not only vertical but parallel to one edge of the block. We will not examine the orientation of the block when initial stability prevails.

The weight of the block must equal the upward buoyancy force, and so

$$\bar{\rho}BLH = BLT,$$

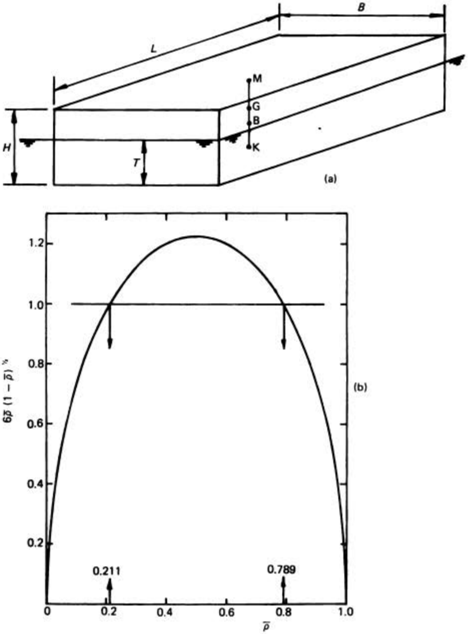

Fig. 3.39

that is,

$$\bar{\rho} = \frac{T}{H}. \tag{3.41}$$

If we identify K with a point on the bottom surface of the block at the intersection with $\overline{BG}$ produced we can write

$$\overline{KB} = \frac{T}{2}; \quad \overline{BM} = \frac{I}{\nabla} = \frac{LB^3}{12BLT} = \frac{B^2}{12T}; \quad \overline{KG} = \frac{H}{2}.$$

Here we have chosen to examine the initial stability of the block undergoing a small angular displacement about a centroidal axis in the water plane and parallel to the longest side of length L. The metacentric height is therefore given by

$$\overline{\mathrm{GM}} = \overline{\mathrm{KB}} + \overline{\mathrm{BM}} - \overline{\mathrm{KG}} = \frac{T}{2} + \frac{B^2}{12T} - \frac{H}{2},$$

or, using the result in Equation (3.41),

$$\overline{\mathrm{GM}} = \frac{B^2 - 6H^2\bar{\rho}(1-\bar{\rho})}{12\bar{\rho}H}. \qquad (3.42)$$

The condition for initial stability is that $\overline{\mathrm{GM}} > 0$, and for this to be true Equation (3.42) shows that

$$\frac{B}{H} > \{6\bar{\rho}(1-\bar{\rho})\}^{1/2}. \qquad (3.43)$$

We see that for the block to float in stable equilibrium restrictions are placed on both geometry and relative density.

The variation of the right-hand side of the inequality (3.43) is shown in Fig. 3.39(b) and is seen to exceed unity when $\bar{\rho}$ lies between 0.211 and 0.789. In other words,

$$B > H \text{ when } 0.211 < \bar{\rho} < 0.789, \qquad (3.44)$$

a condition which ensures that the block will float with its largest surface parallel to the water plane as we have taken $L > B$. Similar arguments apply for stability about a centroidal water-plane axis parallel to the side B.

When $\bar{\rho}$ lies outside the range given in condition (3.44) the condition (3.43) can be satisfied for values of B which may or may not be greater than H. The block may then float in stable equilibrium with any face uppermost.

The preceding discussion also applies to a rectangular pontoon provided that the wall thickness is uniform. In this case $\bar{\rho}$ is not the relative density of the material comprising the walls of the pontoon but the ratio of its total mass to the total volume enclosed by its external dimensions.

(c) *The Wall-sided Formula*

In Section 3.4.2 the angular displacement of a floating body was considered to be small and it was concluded that the rise of the centre of buoyancy was negligible compared with the corresponding horizontal translation. Angular displacements are also considered small for the assessment of initial stability, but in this case it is useful to determine relationships for second-order effects as these may, in some circumstances, be significant.

For stability calculations many ships may be considered to be 'wall-sided', that is, the part of the outer hull which emerges or submerges, following an angular displacement, is perpendicular to the water plane when the ship is upright. The hulls of most ships away from the bow and stern tend to be wall-sided, at least for small angles of heel of less than 10°, say. Container ships and very large crude-oil carriers (VLCC) are quite obviously consistent with the wall-sided assumption owing to their box-like form, that is, they have a high 'block coefficient' defined as ∇/BTL_{PP}.

In Fig. 3.40 an elemental length δL, perpendicular to the plane of the diagram, of a ship with a wall-sided cross section is given a small angle of heel ϕ. We again

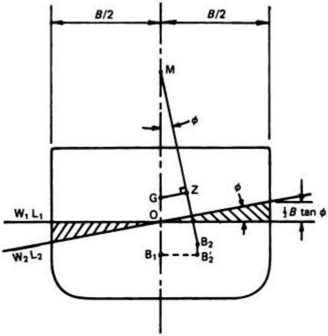

Fig. 3.40

adopt the notion that the ship remains stationary with a rotation of the water line from W_1L_1 to W_2L_2 through angle ϕ about the centre of flotation O so that the volume of water displaced by the ship remains unchanged. If O is not the origin of the principal centroidal axes then the points shown in Fig. 3.40 must be regarded as projections on to the chosen transverse plane of the actual points in the ship. Because ϕ is small we may invoke the concept of a metacentre M, which can be considered a stationary point and, in the upright position of the ship, lies on the vertical centre line along with the centre of gravity G and the centre of buoyancy B_1. After the application of the angular displacement ϕ, B_1 moves to B_2 and the buoyancy force lies on a line perpendicular to the new water line W_2L_2 and intersects $\overline{B_1G}$ produced at M. The point Z lies at the foot of the perpendicular drawn from G to $\overline{B_2M}$. As the general derivation of the coordinates of the centre of buoyancy given in Section 3.4.2 applies here, the procedure may be used for a wall-sided cross section with a vertical plane of symmetry.

Because ϕ is small the water-plane area of the ship is little changed and hence the moment of the volume of the elemental wedge (shaded in Fig. 3.40) transferred from the emerged side (on the left) to the immersed side (on the right) is given by

$$\frac{1}{2} \times \frac{B}{2} \times \frac{B}{2} \tan\phi \times \delta L \times 2 \times \frac{2}{3} \times \frac{B}{2}.$$

In the limit $\delta L \to 0$, and the total moment of transfer of volume is thus

$$\int_0^L \frac{B^3}{12} \tan\phi \, dL = \frac{LB^3}{12} \tan\phi = I \tan\phi$$

where I is the second moment of area intercepted in the water plane W_1L_1. Thus the shift of B_1 to B_2' in a direction parallel to W_1L_1 is given by

$$\overline{B_1B_2'} = \frac{I \tan\phi}{\nabla} = \overline{B_1M} \tan\phi \tag{3.45}$$

from Equation (3.21).

The shift of B_2' to the final position B_2 in a direction perpendicular to W_1L_1 is obtained in a similar manner from Equation (3.21):

$$\begin{aligned}\overline{B_2'B_2} &= \frac{1}{\nabla}\int_0^L \frac{1}{2}\times\frac{B}{2}\times\frac{B}{2}\tan\phi\times 2\times\frac{1}{3}\times\frac{B}{2}\tan\phi \,\mathrm{d}L \\ &= \frac{1}{\nabla}\int_0^L \frac{B^3}{24}\tan^2\phi \,\mathrm{d}L \\ &= \frac{I}{2\nabla}\tan^2\phi = \frac{1}{2}\overline{B_1M}\tan^2\phi.\end{aligned} \tag{3.46}$$

Before proceeding further it is worth examining Equations (3.45) and (3.46) in relation to Fig. 3.40. It may be noted that Equation (3.45) is inconsistent with the geometry of Fig. 3.40 because B_2' and B_2 are two different points. Furthermore, M is the limiting position of the pro-metacentre M′ (see Fig. 3.16) when $\phi \to 0$ and $\overline{B_1M}$ is *not* equal to $\overline{B_2M'}$. The distance $\overline{B_2M'}$ is related to the second moment of area of the instantaneous water plane W_2L_2 where the beam then is $B\sec\phi$. A measure of the error in the approximation is in fact the distance $\overline{B_2'B_2}$, but again Equation (3.46) is in error because I is related to the water plane W_1L_1.

With these limitations in mind let us obtain a useful relationship for the righting level $\overline{GZ}$. From the geometry of Fig. 3.40 we find that

$$\begin{aligned}\overline{GZ} &= \overline{B_1B_2'}\cos\phi + \overline{B_2'B_2}\sin\phi - \overline{B_1G}\sin\phi \\ &= \left(\overline{B_1M} - \overline{B_1G} + \frac{\overline{B_1M}}{2}\tan^2\phi\right)\sin\phi,\end{aligned}$$

that is,

$$\overline{GZ} = \left(\overline{GM} + \frac{\overline{B_1M}}{2}\tan^2\phi\right)\sin\phi \tag{3.47}$$

after using Equations (3.45) and (3.46). Equation (3.47) is referred to as the 'wall-sided formula'. Since $\overline{GM}$ and $\overline{B_1M}$ can be calculated for a given condition of ship $\overline{GZ}$ may be readily obtained. Nevertheless, even though an additional term is contained in Equation (3.47) compared with the first-order expression

$$\overline{GZ} = \overline{GM}\sin\phi, \tag{3.48}$$

the small-angle assumption is implicit in the use of both Equations (3.47) and (3.48).

But how small is this amount? To some extent this is at the discretion of the analyst. Suppose that the second term in parentheses in Equation (3.47) can be considered small (and therefore B_2 and B_2' are separated by a negligible distance) if it is no more than 10 per cent of the metacentric height $\overline{GM}$, that is

$$\tan^2 \phi \leqslant \frac{1}{5} \frac{\overline{GM}}{\overline{B_1M}}.$$

For ships $\overline{B_1M}$ may typically be five times as large as $\overline{GM}$ and so

$$\tan \phi \leqslant \frac{1}{5}$$

or $\phi < 12°$. Certainly substantial, but unknown, errors arise if Equation (3.47) is used for angles of heel greater than 15°. For higher angles reference must be made to estimates of $\overline{GZ}$ based, usually indirectly, on complete surfaces of buoyancy or on cross curves of stability (see, for example, Fig. 3.33) knowing the location of G relative to the fixed point S.

Should the wall-sided ship contain an off-centre, vertical-sided tank partially filled with a liquid then the righting lever $\overline{GZ}$ is reduced. To first order, the destabilizing effect is given by Equation (3.27) so that

$$\overline{GZ} = \left(\overline{GM} - \frac{g}{W}\,\Sigma\rho_l I_1\right) \sin \phi. \tag{3.49}$$

To second order an analysis similar to that leading to Equation (3.47) produces the equivalent form for the effects of a liquid free surface within the hull:

$$\overline{GZ} = \left\{\overline{GM} - \frac{g}{W}\,\Sigma\rho_l I_1 + \frac{1}{2}\left(\overline{BM} - \frac{g}{W}\,\Sigma\rho_l I_1\right) \tan^2 \phi\right\} \sin \phi. \tag{3.50}$$

The preceding restriction on the magnitude of ϕ is also placed on Equation (3.50).

(d) *Complete Stability*

An examination of complete stability requires the removal of the restriction to small angular displacements and inevitably invalidates the wall-sided assumption. We have seen that different loading conditions cause the centre of gravity of a ship to move, and consequently cross curves of stability are based on a righting lever measured relative to an arbitrary fixed point S in the ship. Even if the displacement remains constant, so that the volumes of the emerged and submerged parts of the ship are equal, the centre of flotation moves out of the longitudinal, vertical centre plane. Simple equations relating the righting lever to the angular displacement can no longer be derived in a straightforward way.

Nowadays it is usual to derive the data for plotting cross curves of stability from computer programs describing the hull shape. Nevertheless, there are still occasions where the use of manual techniques is valuable, especially as these techniques illustrate principles and levels of accuracy more clearly. Numerous techniques are outlined in [4] but they will not be pursued further here.

A recent approach to transverse stability is given in [9] where it is recognized that ships in service may suffer significant changes in weight displacement from the original design values. These changes may cause sufficient deterioration in the transverse stability of a ship to necessitate ballasting, or limiting the use of fuel, or some other type of variable loading. The procedure is to adopt constant stability criteria and then to calculate ship hull shapes to satisfy the derived specifications. A number of criteria may be contemplated. For example, a constant transverse righting moment $\Delta^*.\overline{GZ}$ shows that the change in second moment of area of the water plane is equal to the product of the added buoyancy volume – equivalent to the added weight displacement – and the height of the added weight above the initial water surface. This result may be reduced to simple geometric terms by imposing restrictions on the slope of the hull cross section at the water line along the length of the ship.

Another possibility is to keep the metacentric height constant with changing displacement. The result is a purely geometric relation for small changes, namely

$$\frac{dB}{dT} = \frac{\overline{KM} - T}{B},$$

which avoids assumptions concerning the height of added weight. Furthermore, changes of trim may also be incorporated quite simply in this second criterion in addition to the parallel sinkage. The results of the hydrostatic analyses, when translated in terms of flare of the hull, tend to agree with the naval architects' empirical results obtained through experience.

The principles can be extended to non-hydrostatic conditions and used as a preliminary to studying the dynamic roll behaviour of a ship in waves. For such a treatment it is necessary to take into account the distribution of pressure forces on the hull rather than integral values of ship form such as centres of volume, second moments of area of the water plane, etc. Both large and small angles of heel can be examined as well as changes in vertical pressure gradient in the water arising from the presence of waves. However, since quasistatic conditions are assumed it is likely that hydrodynamic effects such as wave making, viscous shear stresses on the hull and so on could lead to different results. Nevertheless, the addition of flare and reduction of $\overline{GZ}$ do seem reasonable stability criteria for most ship operations and designs.

3.8 Vehicle at Rest in a Non-stationary Fluid

Certain types of fluid-borne vehicle are capable of remaining at rest while supported by fluid forces other than buoyancy. This is evidently true of hovercraft and helicopters, but the fluid which supports these vehicles does not remain at rest. We shall examine briefly the nature of the supporting forces involved and refer in passing to the stability problems associated with them.

3.8.1 *Aerostatic Force*

The air-cushion vehicle (ACV) or hovercraft is one form of ground effect machine (GEM). GEMs are vehicles that are supported either wholly or in part by air pressure below, or by suction above, through operating close to the ground. As a hovercraft generates its supporting force without requiring forward speed to generate pressure differences, it is an 'aerostatic' GEM.

An aerostatic supporting force may be developed in two principal ways: by the use of (i) a plenum chamber or (ii) a peripheral jet, both of which are shown schematically in Fig. 3.41. There are several variants of each type, incorporating skirts and side walls, and most of them arise from the wish to improve cushion performance by reducing the air leakage gap. These matters and the performance of hovercraft generally will be taken up in more detail in Chapter 6. We are concerned

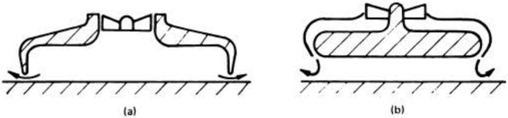

Fig. 3.41 Schematics of air-cushion vehicles: (a) plenum chamber; (b) peripheral jet.

here only with a simple representation of the hovercraft at rest but supported clear of the ground by a cushion of air at a pressure in excess of the ambient value.

It is not easy to calculate the aerostatic force generated in a hovercraft with any great accuracy. Some practical methods of estimation that have been used will now be outlined in a rudimentary fashion. The basic difference between plenum chamber and peripheral jet systems is made clear from the theory used.

(a) *Plenum Chamber Craft*

Figure 3.42 shows a half section of the plenum chamber of a hovercraft. The atmospheric pressure is p_a and the gauge pressure (relative to atmospheric pressure) within the chamber is p_c. Let us examine the steady flow of unit mass of air from a point within the chamber where the air is assumed to be stationary to a point in the side jet. We consider the air to be inviscid and of constant density ρ. The application of Bernoulli's equation to a given streamline passing through a point in the cushion to a point in the constant-thickness jet gives

$$p_a + p_c = p_a + \frac{1}{2}\rho V_j^2,$$

where V_j is the (uniform) velocity of the jet and the effects of changes in elevation are considered negligible. It follows that

$$V_j = \sqrt{(2p_c/\rho)}.$$

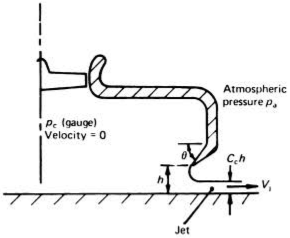

Fig. 3.42

In practice, V_j is somewhat lower than this owing to the presence of viscous shear stresses at the perimeter of the orifice (which has a length l and height h). These shear stresses acting at the ground and on the edge of the craft give rise to a coefficient of velocity C_v which is slightly less than unity. It is thus found that the actual jet velocity is given by

$$V_j = C_v\sqrt{(2p_c/\rho)}. \tag{3.51}$$

The mass of air entering and escaping from the chamber in a time interval δt is

$$\delta m = \rho l C_c h V_j \delta t$$

where C_c is a coefficient that is a measure of the contraction of the jet after leaving the orifice. In the limit $\delta t \to 0$, and using Equation (3.51), we may write

$$\frac{dm}{dt} = \dot{m} = \rho l C_c h V_j = C_d l h\sqrt{(2\rho p_c)} \tag{3.52}$$

where $C_d = C_v \times C_c$ is the discharge coefficient for the peripheral orifice surrounding the air chamber. It is found that C_d depends on the angle θ (shown in Fig. 3.42).

The aerostatic force, F_A is now

$$F_A = p_c S = \frac{\dot{m}^2 S}{2\rho C_d^2 l^2 h^2} \tag{3.53}$$

where S is the planform area of the chamber measured to the lower edge of the chamber wall.

Provided that the surface on which the vehicle is supported is horizontal and the gap h is constant round the cavity, F_A acts vertically upwards. In addition, F_A acts through the centroid of the planform area.

The pressure p_c will not in fact be constant throughout the chamber. As a result of the acceleration of the air, there will be a gradual reduction in pressure as the periphery is approached; therefore F_A is over-estimated. Moreover F_A acts through the centroid of the planform area only if conditions are symmetric about a vertical centre line.

This theory can be regarded only as a very crude approximation for a hovercraft at rest (or at low speed) over water because the air gap changes significantly from what the free surface would indicate it should be. Considerable distortion of the water surface occurs, as would be expected. The theory is thought to be fairly useful for a hovercraft travelling over land and at high speeds over water.

(b) *Peripheral Jet Craft*

Any one of a number of theories can be used to estimate F_A for peripheral jet craft. We shall consider a very simple (and not wholly convincing) one here. The idea of the peripheral jet is that the jet is deflected by the high-pressure air trapped under the vehicle as shown in Fig. 3.43.

If the fluid is assumed to be of constant density we may choose a control volume with end sections 1 and 2 of equal area $a \times \delta l$, the distance δl being measured perpendicular to the plane of the diagram. The assumed uniform velocity of air through these two sections will be the same, V_j say. We shall equate the impulse to the increase of momentum in the direction of outflow for the time δt. This impulse, which is applied at the inner surface of the control volume by the entrapped air is

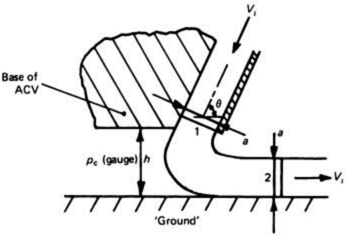

Fig. 3.43

$p_c h\delta l\delta t$. The increase of momentum is the momentum of the emerging element of air at end section 2 minus the component of the momentum of the entering air at end section 1 in the same direction. That is,

$$\{(V_j a\delta l\delta t\rho)V_j \; - \; V_j a\delta l\delta t\rho(-V_j \cos\theta)\} = p_c h\delta l\delta t$$

whence

$$p_c h = V_j^2 a\rho(1 + \cos\theta) \tag{3.54}$$

The aerostatic force is then

$$F_A = p_c S = \frac{V_j^2 Sa\rho(1 + \cos\theta)}{h} \tag{3.55}$$

where S is again the planform area of the lower surface of the base of the craft. As might be expected, there are many improvements on this theory in the literature (see Chapter 6).

3.8.2 *Thrust Force of a Fluid*

The only common air-borne vehicle that uses a rotating propeller to produce a vertical thrust is the helicopter; VTOL aircraft mostly use vectored jet thrust for vertical support. In both cases the thrust is obtained by accelerating air downwards. For our present purposes it is sufficient to note that the thrust acts along the axis of the rotor or the jet. Consequently, if the vehicle tilts the line of action of the thrust will tilt with it. The magnitude of the thrust, F_T, will change only if the operating conditions are varied. In other words, the controls of the prime mover must be adjusted. In particular, F_T is independent of the attitude of the vehicle.

3.8.3 *Stability Considerations*

In the equilibrium configuration of an ACV, $W = F_A$, and we shall do little more here than indicate in a decidedly rough-and-ready way that the equilibrium can be inherently stable.

An ACV clearly has neutral stability for a small lateral translation and positive stability for a small vertical translation. This is because a small downward motion reduces the clearance h which increases the aerostatic force F_A. On the other hand, a small upward motion increases h and so reduces the upward force.

It remains for us to examine what happens if the vehicle experiences a small tilt. For simplicity we assume that the small angular displacement ϕ is one of heel about a line drawn in a fore-and-aft plane of symmetry, as in Fig. 3.44. (To maintain the equality of W and F_A it is necessary to heel the vehicle about a particular axis in the plane of symmetry.) The line of action of F_A moves towards the point of least skirt clearance, through a distance y, say. This movement raises some questions as to the cross flow athwartships under the vehicle. (Sometimes a longitudinal partition is placed in the cushion to impede such flow.) The righting moment about the centre of gravity G is yF_A, which is essentially a positive quantity. Any attempt to estimate y is unlikely to yield reliable results, however.

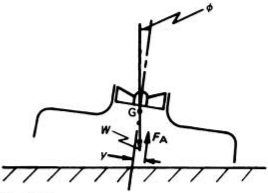

Fig. 3.44

We turn, finally, to vehicles that are supported by fluid thrust forces. The magnitude of F_T will normally be independent of small vertical, or horizontal, motions, because its magnitude is under the direct control of a driver. The vehicle is thus in a state of neutral stability as far as displacements are concerned.

Consider now a small rotation as shown in Fig. 3.45. As the direction of F_T rotates with the vehicle and thus always acts along a line fixed to the vehicle, the rotation makes no significant difference to the equilibrium. The vehicle is therefore in a state of neutral stability in rotation also.

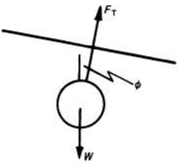

Fig. 3.45

This discussion is of course a highly idealized one. It is unsatisfactory for a helicopter with its flexible, hinged rotor blades, but for conceivable underwater application (in manoeuvring for instance) it is probably fairly reliable.

3.9 The Structure and its Loading

To continue our study of statics, it is convenient to isolate the vehicle structure as a mechanical 'system'. Such a system experiences both internal and external forces. Let us begin by considering the *external* forces, that is, those forces which act across the boundary surface of the system. Some idea of the complexity of external loading can be obtained by examining Fig. 3.46. It will be readily understood that the study of loading actions forms a complete, and very difficult, subject in its own right.

The loading actions from external forces give rise to *internal* forces, which produce stresses and hence strains and deflections. (These may be augmented by strains from thermal effects.) Total strains and deflections may be sufficiently large to be associated with 'failure' in some sense. Some examples of failure are:

(i) gross plastic collapse, involving ductile failure;
(ii) cracking by 'brittle fracture';
(iii) fatigue – note that some stress cycling can be of *very* low frequency, as with docking stresses or the submergence of submarines;
(iv) structural instability, for example, wrinkling of plating or buckling of bottom grillages;
(v) excessive static deflection, causing the misalignment of a shaft for instance;
(vi) excessive vibration or noise;
(vii) tearing, for example, of the skirt of an ACV;
(viii) other deteriorations of material, for example separation of the laminates of a dracone or of fibre glass.

The complex area of general structural analysis is conventionally divided into (i) *structural statics*, in which time-dependent forces are excluded, and (ii) *structural dynamics*, in which time-dependent forces do appear. Our purpose is to introduce here the first of these types of analysis and to discuss structural dynamics in Chapter 9. Structural statics (or, less accurately but more commonly, 'structural analysis') is mainly concerned with the strength and ability of structures to withstand loading actions without unacceptable distortions – and to continue to do so for a stipulated life-time.

In order to apply criteria of failure it is usually necessary to investigate stresses, strains and deflections. We have therefore to examine *internal* forces, and to find these internal forces, given the external ones, is the classic problem of structures. The technique is, of course, to consider the behaviour of *parts* of the system, as indicated in Fig. 3.47. The approach is to invoke the three principles upon which the whole of structural analysis (both static and dynamic) is based. These principles relate to: (i) force and moment equilibrium of systems and sub-systems; (ii) geometric compatibility of sub-systems with each other; and (iii) a physical law governing the relevant properties of the material concerned as regards stress, strain, temperature, etc. (It will be recalled that there is an important special case of structures in which equilibrium may be examined without reference to the physical law relating to stress and strain, namely, that of 'static determinacy'.)

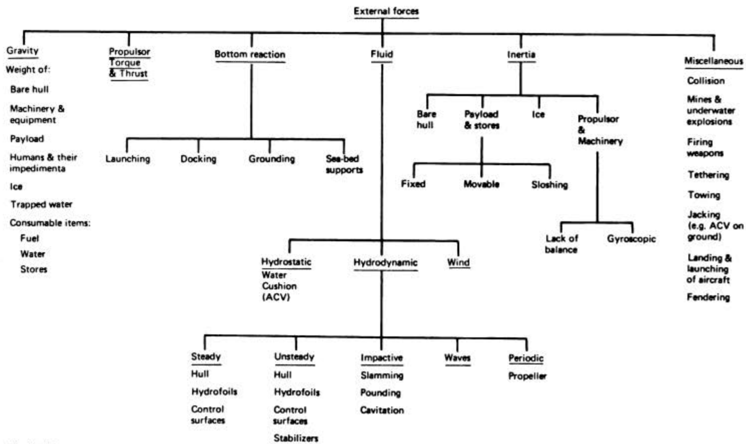
External forces
Gravity
Weight of:
Bare hull
Machinery & equipment
Payload
Humans & their impedimenta
Ice
Trapped water
Consumable items:
Fuel
Water
Stores
Propulsor Torque & Thrust
Bottom reaction
Launching
Docking
Grounding
Sea-bed supports
Fluid
Hydrostatic Water Cushion (ACV)
Hydrodynamic
Wind
Steady
Hull
Hydrofoils
Control surfaces
Unsteady
Hull
Hydrofoils
Control surfaces
Stabilizers
Impactive
Slamming
Pounding
Cavitation
Waves
Periodic
Propeller
Inertia
Bare hull
Payload & stores
Fixed
Movable
Sloshing
Ice
Propulsor & Machinery
Lack of balance
Gyroscopic
Miscellaneous
Collision
Mines & underwater explosions
Firing weapons
Tethering
Towing
Jacking (e.g. ACV on ground)
Landing & launching of aircraft
Fendering

Fig. 3.46

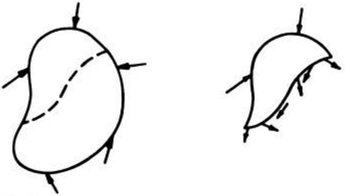

Fig. 3.47

Over the years a tremendous volume of work has been done in the study of the classic problem of structures; and, as this type of analysis readily admits the use of automatic computation, great strides have been made recently, especially with ships. Nevertheless, serious uncertainties remain and much more work needs to be done. But this is not the only, and indeed perhaps not the principal, area where research is badly needed. With the sole (and important) exception of deeply submerged vehicles, the study and specification of loading actions remain a serious source of difficulty. In other words, what are external forces and how important are their dynamic effects?

3.9.1 *Deterministic and Probabilistic Analysis*

It is impossible to assign definite values to real phenomena, but we can usually at least consider the probability that specified values will be exceeded. The behaviour of engineering systems under the influence of the forces of nature has this probabilistic character. Thus random analysis must generally be used to describe phenomena adequately. Random analysis, because it accepts and takes uncertainties into account, obviously has enormous attractions [10]. It is a relatively new development which is steadily gaining ground in aeronautics and naval architecture, amongst other fields, but although it may well come to be used exclusively in marine work in the future it is at present only at the development stage. Furthermore, our knowledge of loading actions and material behaviour is still inadequate.

For the present it is usually necessary to continue to accept the deterministic approach. In this traditional technique definite values are assigned to those parameters that are selected to describe the 'input' of an engineering system. In assigning definite values to the input the analyst may have views on how likely they are, but these views are not expressed explicitly in his calculations. Definite values are then sought for those parameters that are chosen to describe the 'output'. The analysis is performed using a prescribed and agreed mathematical model of the system. In structural analysis the 'input' is the loading, the 'model' is the idealized form of the structure adopted for the purpose of analysis, while the mechanical parameters of interest (usually stresses, strains, deflection or collapse load) constitute the 'output'.

Provided that the analytical methods of calculation are not at fault, deterministic analysis does not give the wrong answers; it may simply not pose the right questions. Even so, deterministic analysis can be said to represent a useful framework and it would be foolish to deny that it has had great success up to now. The following examples are typical deterministic problems from the field of ship structures:

What stresses and deflections will a main transverse bulkhead experience if an adjacent compartment is flooded?

What stress occurs at the base of a mast when the ship rolls in simple harmonic motion with an amplitude of 25°?

In contrast, typical probabilistic problems raise such questions as:

What is the probability that the stress at the base of the mast will ever exceed 60 per cent of the yield point of the steel?

What is the probability that fatigue cracking will occur in the fore-end plating of a frigate?

Not surprisingly, problems of the latter sort are very much more difficult to solve than those of the former.

Deterministic analysis at first sight appears to have some merit in yielding a definite set of values on which to base decisions; a random analysis yields only probabilities of the occurrence of various sets of values. But the certainty of the deterministic approach may be unreal; it is also potentially dangerous if it conceals ignorance. Nevertheless, in this chapter we will deal with deterministic structural analysis. The analyst selects 'design cases' to provide a basis on which to choose the sizes of structural members. In so doing he has to decide:

(i) which structural members justify his attention; time and effort will preclude an examination of everything, so that experience has to be called into play;
(ii) what forms of loading to take into account;
(iii) how the structural component under consideration can be isolated from its surroundings for the purpose of analysis, and then itself idealized; and
(iv) what types of 'failure' to take into account (unstable collapse, fatigue cracking, deflection, etc.).

Note that the analysis raises a question of 'scale'. Some problems of structural analysis are essentially general. For example,

How thick should the shell of a submarine's pressure hull be?

In contrast, some problems can be regarded as essentially local, a 'unit analysis', so to speak. For example,

What reinforcement should be provided around a hatch in a submarine's pressure hull?

It will be appreciated that it is impossible to draw up a list of all the potential design cases that can arise. Indeed it would be misleading here to attempt to put into spurious order what may seem a chaotic subject. Part of the structural analyst's skill lies in seeing what may or may not be important, and this can vary enormously from vehicle to vehicle and with operating conditions. For example, the structure of a ship's side is determined by considerations of loading by gravity and buoyancy forces, but in a nuclear-powered ship a quite different design case must be considered. It arises from the need to protect the reactor in a collision by using the plastic deformation of the hull to absorb energy.

3.10 External Loading by Gravity and Buoyancy

Perhaps the most basic problem of structural analysis in the marine field is that of a prismatic body floating on the surface of still water. In general, such a body is stressed because the gravity force per unit length q_g is not everywhere balanced by the buoyancy force per unit length q_B. To illustrate this point let us consider a rudimentary, long, thin barge floating on the water surface, as shown in Fig. 3.48.

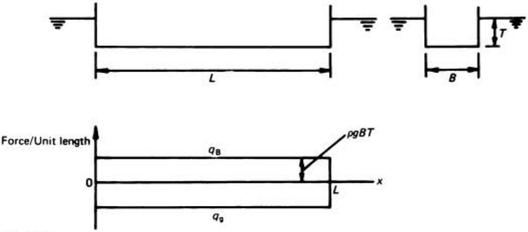

Fig. 3.48

The uniform barge is rectangular and we shall neglect the weight of the ends, so that q_g is constant. For equilibrium to prevail it is necessary that the net upward force and the net moment of forces about an axis perpendicular to the plane of the paper are both zero. These conditions give, respectively,

$$\int_0^L q_g \mathrm{d}x + \int_0^L q_B \mathrm{d}x = 0 \tag{3.56}$$

$$\int_0^L q_g x \mathrm{d}x + \int_0^L q_B x \mathrm{d}x = 0. \tag{3.57}$$

For this case,

$$q_g = -q_B$$

so that the net load per unit length is

$$q = q_g + q_B = 0$$

for all values of x. Hence there is no bending moment at any section of the body.

Suppose that an additional uniformly distributed load per unit length, a, is placed on the middle half of the barge. The curves obtained for q_g, q_B and q are those shown in Fig. 3.49. However, the net loading q is now associated with shear forces and bending moments.

Let us consider an element of the barge at a distance x from the origin O and of

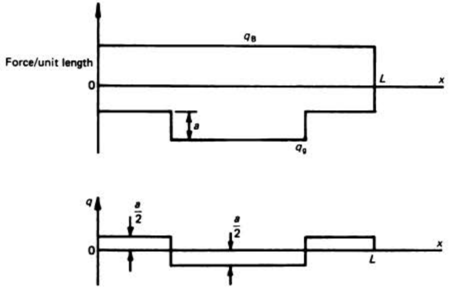

Fig. 3.49

length δx in the x direction, as shown in Fig. 3.50. The element is shown perpendicular to the x axis because deflections (and therefore slopes) of a load-bearing structure are invariably small. The sign convention adopted here is to regard forces as positive upwards (i.e. in the Oz direction) and moments as positive when clockwise. The magnitudes of the shear force and bending moment on face 1 of the element are, respectively, S and M with the corresponding magnitudes $S + \delta S$ and $M + \delta M$ on face 2. Thus, for equilibrium of the element, the net force and net moment on it must both be zero. That is

$$S + \delta S + q\delta x - S = 0$$

and

$$M + \delta M - (S + S + \delta S)\frac{\delta x}{2} - M = 0.$$

Taking δx to be small, retaining first-order terms and then proceeding to the

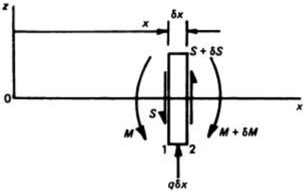

Fig. 3.50

limit $\delta x \to 0$ gives

$$\frac{dS}{dx} = -q; \qquad \frac{dM}{dx} = S. \tag{3.58}$$

The curves of shear force and bending moment for the barge are therefore as shown in Fig. 3.51. Note in this figure that $|S|$ is a maximum when $q = 0$ and $|M|$ is a maximum when $S = 0$, in keeping with expressions (3.58).

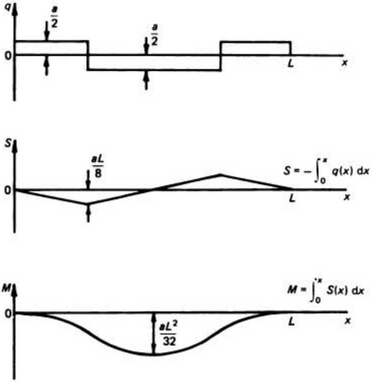

Fig. 3.51

If the uniformly distributed load per unit length, a, is shifted to one end (so as to extend over the range $0 \leqslant x \leqslant L/2$), the loading curve is as shown in Fig. 3.52. The variation of q_B shown here may be deduced by combining parallel immersion for the load $aL/2$ spread evenly, and the trim change on application of the moment $aL^2/8$ about mid-span caused by point loads distant $L/4$ (downward) and $3L/4$ (upward) from the origin. Thus, at distance L from O,

$$q_B = b + \frac{a}{2} - \frac{3a}{4} = b - \frac{a}{4}$$

and at O,

$$q_B = b + \frac{a}{2} + \frac{3a}{4} = b + \frac{5a}{4}.$$

From these expressions we should be able to find new curves of S and M. Further-

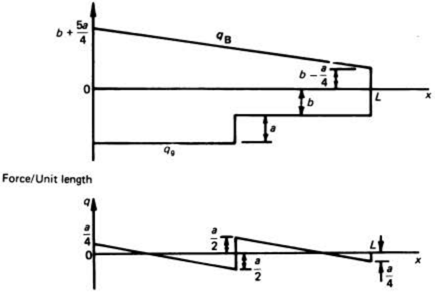

Fig. 3.52

more, if the assumptions implicit in beam theory are accepted as tenable, it is possible to calculate stresses, strains and deflections.

This simple approach has ignored the question of how the loading is accepted by the structure. The creation of internal forces by the application of external loads will depend upon how these loads are applied. Loading applied to the deck would give rise to local internal forces quite different from those that would be obtained if the same loading were applied to the hold or the side. In other words, to avoid complications, we allocate gravity and buoyancy forces to those specific discrete lengths of ship in which they act and assume that they are evenly spread within that length.

The barge which we have examined has been static. Static analysis may also be applied to bodies which are moving but have achieved a steady state, such as a motor car moving along a road at constant speed in still air. A marine vehicle, however, moves at the interface of two fluids and creates a pressure field in each fluid which causes the interface to distort. The resulting self-generated wave system changes the static load distribution and may well exacerbate the original condition. While it is not common practice to do so, the bending moment so caused might perhaps be superimposed on that discussed in the next section.

3.10.1 *Gravity and Buoyancy Loading of Conventional Surface Ships*

Although the foregoing remarks relate to a highly idealized vehicle – a rectangular barge with weightless ends in still water – they are of direct relevance to conventional surface ships. Let us therefore pause briefly to consider a practical surface ship in still water. The loading curves resulting from a step-by-step weight analysis are similar to those shown in Fig. 3.53. Note, however, that the q_g curve can be significantly affected by the placing of cargo and that calm water will not provide the greatest variation of q_B.

More severe loading will occur when a ship is running into, or before, relatively long waves at sea. In the past, structural analysts, working long before the days of

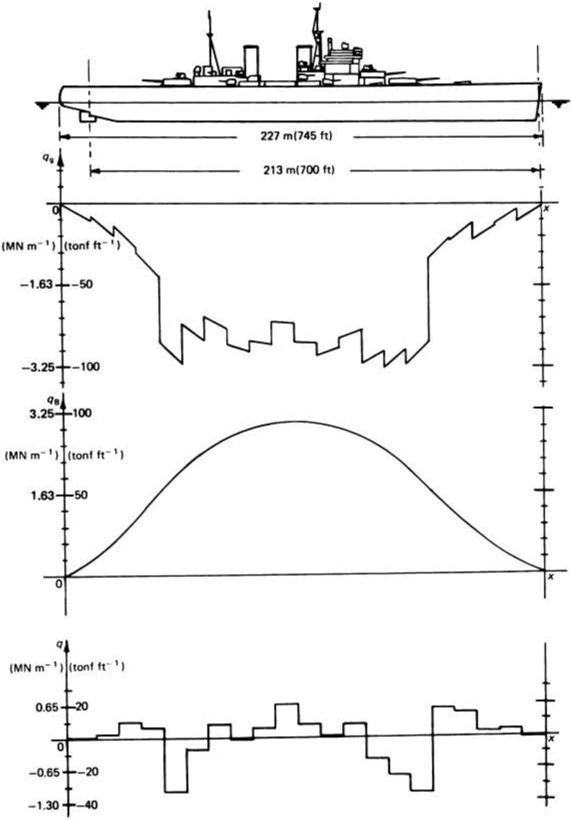

Fig. 3.53 Loading curves for the ship of Fig. 3.2.

random analysis (with its ability to take account of the random character of seaways), tackled this problem by simplifying it drastically. Two 'worst cases' were derived for the q_g and q_B curves, as indicated in Fig. 3.54. The main assumptions underlying these 'worst cases' are:

(i) All dynamic effects are negligible†.
(ii) The ship is statically balanced on a single wave equal in length to the ship so that (a) the buoyancy force due to simple hydrostatic pressure and the weight are equal, and (b) the centres of buoyancy and gravity lie at the same longitudinal position.
(iii) The wave is trochoidal and with a height, from trough to crest, equal to one-twentieth of its length.
(iv) In the 'hogging worst case' (with wave crest amidships) specified disposable weight is removed from amidships. In the 'sagging worst case' (with wave trough amidships) all disposable weight is removed from the ends.
(v) Direct stresses and strains in the 'ship beam' – or 'ship girder', as it is sometimes referred to – can be found by applying simple beam theory with S and M found by integrating $q(x)$.

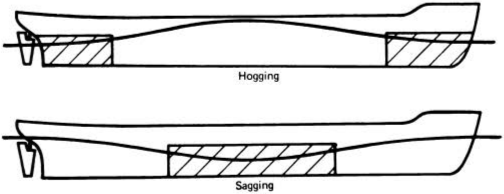

Fig. 3.54

From the last assumption it follows that the greatest direct stresses occur at points furthest from the neutral axis, as the direct stress $\sigma = My/I$. (Here y is the distance of the point in question from the neutral axis about which the second moment of area of the cross section, in which the point lies, is I.) In the hogging worst case the greatest tensile stress occurs in the deck and in the sagging worst case in the keel. This is because the heavy keel structure tends to produce a neutral axis *aa* slightly below mid-depth of the cross section, as illustrated in Fig. 3.55.

The fact that a ship design is examined in this way does not mean, simply, that a ship is likely to fail under direct stress. (A ship *could* do so, of course, and ships have broken in two in a seaway, possibly as a result of failure in tension.) Indeed, too high a bending moment could produce failure by buckling of plating near the keel when the ship is hogging or in the deck when the ship is sagging. The point is that the longitudinal strength calculation, as it is commonly called, does give the

† More recent analyses of very large ships [11] have shown that this assumption is no longer tenable for those cases.

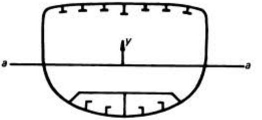

Fig. 3.55

analyst a 'feel' for a design. Estimated tensile stresses for successful designs of the past are shown in Table 3.3. Note in this table that the differences between the two sets of stresses arise from the difference between the hogging and sagging bending moments and the heaviness of the keel structure which tends to give a low neutral axis (as already mentioned).

Table 3.3 *Estimated direct stresses for ships (from [4]). Units are metre for length and $MN\ m^{-2}$ for stress, with ft and tonf in^{-2} respectively in parentheses.*

Ship	Length	Direct stress σ	
		Deck (hogging)	Keel (sagging)
Frigate	100 (328)	110 (7.122)	90 (5.825)
Destroyer	150 (492)	125 (8.094)	110 (7.122)
Cargo vessel	200 (656)	110 (7.122)	90 (5.825)
Aircraft carrier	250 (820)	140 (9.065)	125 (8.094)
Oil tanker	300 (984)	140 (9.065)	125 (8.094)

Figures 3.56, 3.57 and 3.58 show shear force and bending moment curves for the ship to which Fig. 3.53 refers. They relate to the still-water case, the hogging worst case and the sagging worst case respectively.

It is customary in mercantile practice to separate the still-water bending moment from the total. The remainder is the augmentation of the still-water bending moment by a wave and is called the wave bending moment. There is a good reason for this. The wave bending moment is due wholly to the geometry of the wave and the ship. It is, therefore, often considered to be proportional to $B_{WL}L_{WL}^{n}$ where n lies between 2.3 and 2.5. This relationship has been based upon the assumption of long sea waves having a trochoidal contour as described in Chapter 2. The constant of proportionality is a function of the type of ship and the block coefficient of the underwater form. The still-water bending moment, however, is substantially under the control of the ship's master, who must closely follow the directives of the Owners and Classification Societies if his method of working his holds is not to cause unacceptable still-water bending moment, or even fracture.

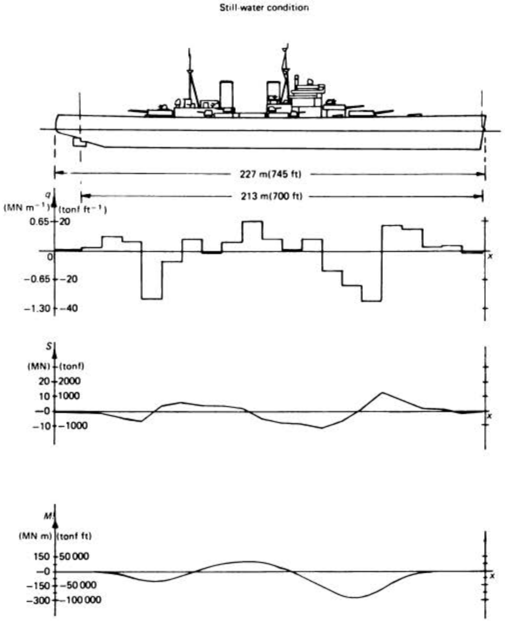

Fig. 3.56 Still-water loading, shear force and bending moment curves for the ship of Fig. 3.2.

The 'ship girder' can also be examined in terms of the distribution of shear stresses τ in response to the shear force S. Use may be made of an elementary result of beam theory, namely,

$$\tau = \frac{S(A\bar{y})}{Ib}. \tag{3.59}$$

In this equation, $A\bar{y}$ is the first moment, about the neutral axis of a given transverse cross section of the hull, of that part of the cross section beyond the location at which τ is required. The second moment of area of the whole cross section about

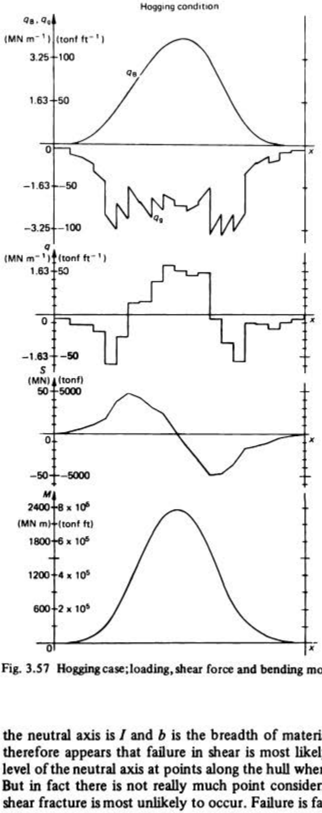

Fig. 3.57 Hogging case; loading, shear force and bending moment curves for the ship of Fig. 3.2.

the neutral axis is I and b is the breadth of material at the location of interest. It therefore appears that failure in shear is most likely to occur in the sides near the level of the neutral axis at points along the hull where the shear force is a maximum. But in fact there is not really much point considering acceptable values of τ since shear fracture is most unlikely to occur. Failure is far more likely to consist of panel wrinkling, as indicated in Fig. 3.59. Liability to wrinkle depends on panel thickness,

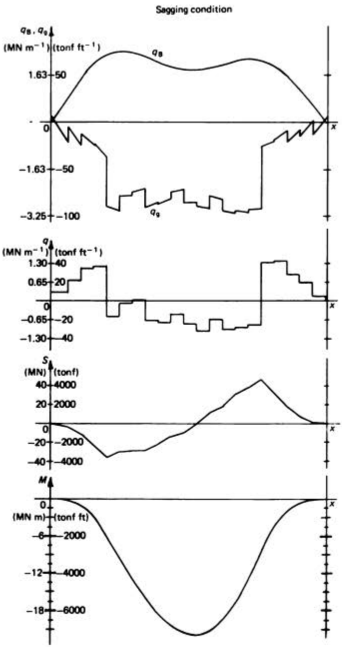

Fig. 3.58 Sagging case; loading, shear force and bending moment curves for the ship of Fig. 3.2.

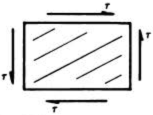

Fig. 3.59

stiffener spacing and size of plate, as well as on the ship's cross section. In short, this is a problem of unit analysis.

Understandably, early analysts regarded the direct stresses determined in the longitudinal strength calculation, as having some standing in their own right. It was soon recognized that because of the unrealistic calculations the computed stresses were meaningful only in a more limited sense. As already mentioned, they provide a basis for comparison between a new design and previous successful practice. Because of this comparative nature it does seem that the many refinements in the calculation are rather misguided.

Perhaps the most sensible refinement is that which takes account of the observation that waves are less steep the longer they are. This fact led naval architects to use the empirical relationship,

$$\begin{pmatrix}\text{height from}\\ \text{trough to crest}\end{pmatrix} = 1.1\sqrt{\begin{pmatrix}\text{length from}\\ \text{crest to crest}\end{pmatrix}},$$

and to identify the length of the wave, again, with the length of the ship, a postulate which is a less demanding one for long ships.

One of the undoubted advantages of the deterministic ship girder approach is that it provides a simple (if somewhat unrealistic) assessment of field stresses. This can reasonably be used as a sort of background against which particular problems can be investigated. Thus, in the hope, that the significance of the results will be masked by extraneous complications, one can examine:

(i) the effects of stress concentration (as at hatchways, abrupt changes of section, etc.);
(ii) the possibilities of local collapse or yield (i.e., the longitudinal strength calculation makes a convenient basis for unit analysis);
(iii) the effects of 'built-in' stresses (but these are very difficult to analyse and the additional complications of rolling and welding of plates do not help);
(iv) application of more refined theories of beam analysis (e.g. 'shear flow' theory);
(v) thermal effects (e.g. from solar radiation), and particularly with refrigerated cargoes;
(vi) the magnitude of the wholesale deflection of a ship in a seaway (assuming that the problem *is* one of statics). The beam equation may be written

$$q = -\frac{dS}{dx} = -\frac{d^2M}{dx^2} = -\frac{d^2}{dx^2}\left(-EI\frac{d^2\nu}{dx^2}\right) = \frac{d^2}{dx^2}\left(EI\frac{d^2\nu}{dx^2}\right), \tag{3.60}$$

where E is Young's modulus, and integrated to give estimates of hull deflections ν which may be needed for sensor calculations, for instance;
(viii) some effects of ship motion (e.g. when a ship rolls violently and extra stress analysis may be needed in which S and M are resolved for the principal directions).

It has been suggested that the longitudinal strength calculation leads quite naturally to considerations of unit analysis. That is to say, the calculation allows the analyst to look more closely at local effects in a ship's hull. In general there are three basic types of sub-structure relevant to the ship girder under gravity and buoyancy loadings which may be conveniently isolated and which are described below.

(a) *Stiffened Plates* (Fig. 3.60)
Such units as these may be flat or curved and may have odd shapes. The loading to which they are subjected arises from predictions of longitudinal strength calculations, (possibly) hydrostatic pressure and (possibly) other loading actions such as localized weight of equipment.

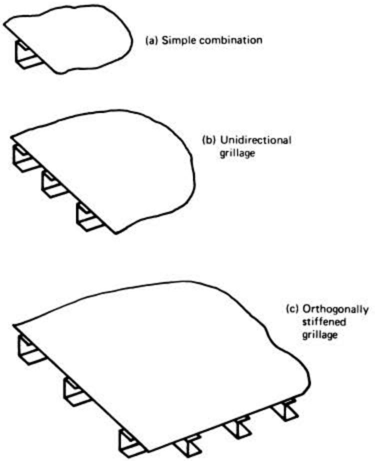

Fig. 3.60

(b) *Single Panels*
These are usually rectangular, being supported on longitudinal and transverse frames. They may be flat (requiring analysis by plate theory) or curved (demanding shell theory). The membrane, or 'in-plane', loading will be that suggested by the longitudinal strength calculation. There may be additional loads (usually normal loads) arising from hydrostatic pressure or from some other cause, such as fendering for example.

The naval architect's preoccupation with flat plates is naturally one of long standing. As a result, one of the most interesting practical results in the mathematical theory of elasticity was published in that context by the Institution of Naval Architects in 1913 [12]. It relates to the stresses around an ellipse cut out of a uniformly loaded plate. (When the ratio of the semi-axes is large, the conditions of a plate with a crack in it is approached. When the semi-axes are equal, the theory relates to a panel with a circular hole. With suitable manipulation of the results information can be obtained on cut-outs such as hatchways in deck plating.)

(c) *Frames* (Fig. 3.61)
Frames are used in many ways in the construction of ships and it is often convenient to identify them and analyse their stresses as such. A ship's hull can be regarded as an elongated box, and this box has to be strengthened. If the internal strengthening is predominantly in a fore-and-aft direction, the ship is said to be 'longitudinally framed' (Fig. 3.61(c)), and when the stiffening is at right angles to the fore-and-aft direction the ship is said to be 'transversely framed' (Fig. 3.61(b)). There are, of course, many possibilities for isolating frames that may have significance. The loading of these frames is that suggested by the longitudinal strength calculation plus additional loads of a localized nature. Alternatively, an investigation of the effects of stressing by gravity and buoyancy in 'worst cases' of *transverse* loading of a hull (as when the different tanks of a tanker ship are filled) may be undertaken.

It is now clear that the various structural units of a surface ship raise all the classic problems in the theory of structures. Inevitably it is necessary to contemplate beams and frames, plates and shells, and grillages. In general, the loading of these units is only part of the problem to which the longitudinal strength calculation refers. Twisting of a hull may occur in a seaway and thus torsional distortions have sometimes to be investigated. Exactly how a stress analysis would be carried out for particular selected units is best seen through examples. There can be no cut-and-dried procedure; nor can a comprehensive list be drawn up of all the problems which will be encountered because new designs raise new problems.

In the last decade, large advances have been made in the application of random analysis to the prediction of stresses in ships in a seaway. Nevertheless, the deterministic approach of the longitudinal strength calculation, now carried out by computer, continues to be used. It is interesting to note that random analysis and full-scale measurements suggest that stresses greater than those given by the longitudinal strength calculation rarely occur. Either as a consequence of good design or of undue conservatism, most ship hulls appear to possess adequate strength. For example, the active life of a warship is about 20 years, and normally it is not because the hull has 'worn out' that the ship is scrapped, but rather that the weaponry or propulsion systems are obsolete or that combat tactics have changed. Provided that proper maintenance procedures are observed, hull strength is usually preserved. It is sometimes found, however, especially for ferries, that the hull in the region of the water

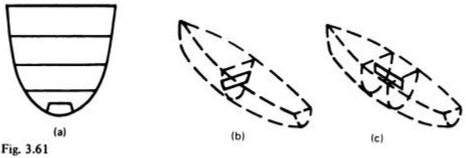

Fig. 3.61

line needs most care and attention because of its wet-and-dry existence, the bumping of debris, fendering and so on. Nevertheless, it would be a serious oversimplification to imply that the object of research is really to find out by how much the requirements of the gravity and buoyancy loading strength calculations can be safely relaxed; it is by no means rare that a tanker has to be strengthened after her acceptance trails.

In practice the beam theory of longitudinal strength calculations raises a large number of questions. As one would expect, there is an enormous literature covering the subject. No complete bibliography could possibly be given here; nor would it be particularly helpful if it were. But the reader's attention is drawn to one particular paper [13] which describes tests on a ship's hull – tests that included loading to the point where major structural failure occurred.

3.11 External Loading by Inertia and Hydrodynamic Forces

Despite its shortcomings, the idea behind gravity and buoyancy loading of the ship girder is certainly useful (and ingenious), but it is based upon the implicit assumption that the ship ploughs straight through the sea without significant vertical accelerations. Now, when a high-speed ship moves at speeds which may well be over 25 m s^{-1} ($\cong$ 50 knots), it is obvious that dynamic effects cannot be ignored. The ride is 'hard' and the question naturally arises as to what sort of loading this implies.

On the basis of experience with past craft, the Brave Class of fast patrol boats was assumed in [14] to be subject to a instantaneous worst condition of the form shown in Fig. 3.62. The acceleration was much greater than that under free-fall conditions. We must now consider a vertical inertia force and the hydrodynamic force needed to provide it. In all its generality this is a problem of structural dynamics as both the inertial and hydrodynamic forces are time dependent. But if the instantaneous worst acceleration (and, hence, inertia loading) is as shown in Fig. 3.62, it is arguable that allowance must be made for it under the assumption that it is maintained. In the design of the Brave Class boats it was therefore assumed that a steady *inertia* force per unit length q_i, was applied as shown in Fig. 3.63. As indicated in Fig. 3.64 this corresponded to a resultant vertical force of about 4.35 MN (4.37 tonf) whose line of action could easily be found as it passed through the centre of area of the total load curve.

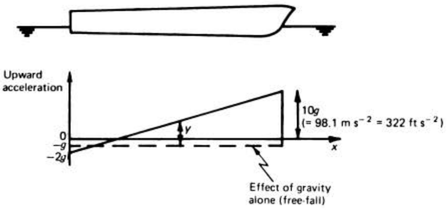

Fig. 3.62

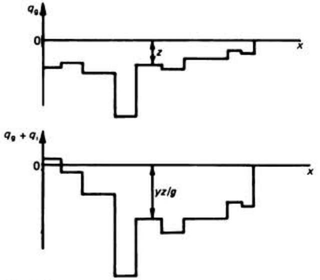

Fig. 3.63

The curve of $q_g + q_i$ gives the worst vertical downwards force applied to the hull and is therefore supported by hydrodynamic forces – but how? We know that for equilibrium under steady load conditions

$$\int_0^L (q_g + q_i)\mathrm{d}x + \int_0^L q_h \mathrm{d}x = 0$$

$$\int_0^L (q_g + q_i)x\mathrm{d}x + \int_0^L q_h x\mathrm{d}x = 0$$

where q_h is the vertical component of the hydrodynamic force per unit length of hull. But these equations do not provide a specification of q_h. The technique adopted was to satisfy the first of the fore-going requirements and to approximate the second in the following manner.

The curve of q_h was assumed to be an isosceles triangle with maximum pressure corresponding to 138 kN m^{-2} (20 lbf in^{-2}) acting vertically upwards. (The under-

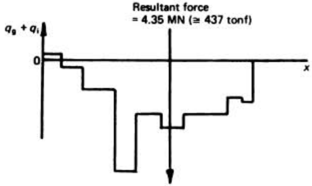

Fig. 3.64

lying theory of this assumption is discussed in Section 6.2.1.) At the point along the length of the boat at which the resultant hydrodynamic force must act, the beam is 6.05 m (19.83 ft). Therefore

$$138(\text{kN m}^{-2}) \times 6.05(\text{m}) \times \Delta x = (q_{\text{h}})_{\text{max}} \times \Delta x$$

so that

$$(q_{\text{h}})_{\text{max}} = 835 \text{ kN m}^{-1} \ (25.5 \text{ tonf ft}^{-1}).$$

If the q_{h} curve is now represented by the triangle shown in Fig. 3.65, the length a shown is given by

$$\frac{2a \times 835(\text{kN m}^{-1})}{2} = 4350 \text{ kN } (\cong 437 \text{ tonf})$$

whence $a = 5.21$ m ($\cong 17.09$ ft), a not unreasonable value for a boat that is about 28 m ($\cong 92$ ft) long.

By this means we can obtain curves of

$$q \quad \{= (q_{\text{g}} + q_{\text{i}}) + q_{\text{h}}\}$$

$$\left.\begin{matrix} S \\ M \end{matrix}\right\} \quad \text{by successive integrations.}$$

If it is then assumed that simple beam theory may be applied, we may proceed with a stress analysis. It must be pointed out, however, that in a craft like a fast patrol boat we are very much concerned with unit analysis because local effects, particularly in the hull bottom, are vital.

The approach used with the Brave Class fast patrol bqats illustrates the kind of drastic assumptions the structural analyst may be forced to make.

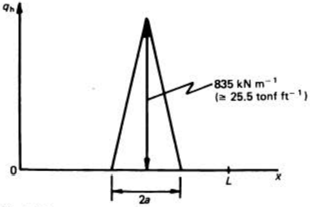

Fig. 3.65

3.12 External Loading by Hydrostatic Pressure

When a submarine, or other underwater vehicle, floats on the surface it undergoes the same sorts of loading action as other surface craft; but when it is submerged the far more exacting conditions of loading by hydrostatic pressure must be examined.

Note, however, that for once there is no difficulty in prescribing the 'loading action'. The analyses to be developed by the designer are those which describe the hydrostatic compression of a shell (either elastic or plastic). They raise problems of stability, such that the question is not so much 'Is this loading safely withstood?' as 'Is this loading realizable?' The Euler strut gives a simple illustration of structural instability.

Submarines and submersibles normally operate in a state of approximately neutral buoyancy, which means that gravity and buoyancy forces more or less cancel (although there will be a residual distribution of shear force and bending moment as the net $q(x)$ is not everywhere zero). The stresses of the submerged 'ship girder' are, however, relatively small compared with those resulting from hydrostatic loading. The latter are therefore commonly examined in isolation. The problem is essentially one of external hydrostatic loading of a thin shell, that is, of the 'pressure hull'. The pressure hull of a deep-diving vehicle – a bathyscaphe or a submersible – is usually of a fairly 'pure' form: it may be spherical or shaped like a dumb-bell, as indicated in Fig. 3.66. The pressure hull of a typical military submarine is more complex, being roughly as illustrated in Fig. 3.67. This is a shell stiffened with:

(i) stiffening rings (inside and outside);
(ii) main transverse bulkheads (inside the pressure hull);
(iii) wing bulkheads (outside the pressure hull, and between the pressure hull and the outer hull);
(iv) deep frames (large stiffening rings inside the pressure hull); and
(v) miscellaneous decks, flats, floors, minor bulkheads, etc.

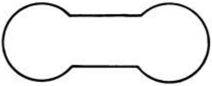

Fig. 3.66

A detailed introduction to the field of stability is given in [15] and the problem relating to submarines is discussed in [16]. Although it is not our purpose here to examine these matters it is worth noting in general terms the sort of problems which need to be tackled. Failure can be thought of as taking any of five possible forms:

(i) general instability of the shell, when the stiffening is of rather light construction;
(ii) local elastic instability of the shell between stiff rings;
(iii) local yield of the shell between stiff rings;
(iv) local elastic instability of a stiffener plus associated plating (although this is more readily avoided than (ii) and (iii)); and
(v) local instability of the domed bulkhead.

There are several sources of difficulty which may be encountered when seeking that type of failure most likely to occur, even from a purely analytical point of view.

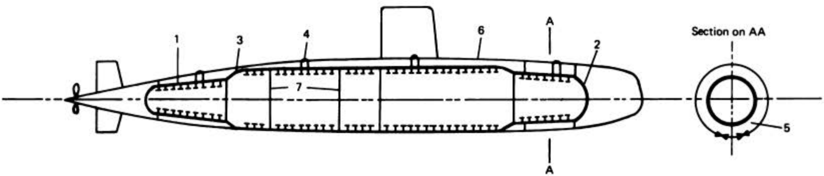

Fig. 3.67 Structural features of a submarine. 1. Pressure-hull plating and framing; 2. Domed bulkhead; 3. Curved transition; 4. Hatch; 5. External ballast tank; 6. Hull plating; 7. Main transverse bulkheads.

These are notably:

(i) gross out-of-roundness, that is, designed departure from a cylindrical form;
(ii) small out-of-roundness owing to small errors of manufacture (which causes unwanted circumferential bending of the rings);
(iii) major discontinuities (such as the main transverse bulkheads or intersections of cones and cylinders) which cause unwanted longitudinal bending of the shell; and
(iv) minor discontinuities (such as pressure hull hatches, manufacturing cracks in the material or lack of homogeneity) which cause stress concentrations in the shell that can be very significant in relation to fatigue.

Unlike most surface ships, deep-diving submarines tend to be governed by weight in their design with a small difference between weight and buoyancy. The designer is consequently obliged to work to lower factors of safety than is the practice in surface ships. This, in its turn, requires the acceptance of higher stress levels, and with them the risk of fatigue. Indeed, to a large extent the fatigue problem is the *result* of possible structural instability, as it is the latter that demands structural stiffening, and it is this stiffening that introduces stress concentrations. Fatigue has in fact become a greater problem than instability in submarine design.

3.13 External Loading of Some Unconventional Vehicles

So far we have discussed: (i) combined gravity and buoyancy loading (and have noted its relevance to naval architecture); (ii) combined gravity, inertia and hydrodynamic loading; and (iii) hydrostatic loading. (All of these cases are of a 'general' nature, and in every case the calculations would be supplemented with suitable unit analysis.) These general cases do not by any means exhaust the possibilities and, although it is not possible to list all the particular cases that may arise with a novel design, some comments are in order; these comments are in fact no more than statements of engineering common sense.

Hydrofoil Craft. A longitudinal strength calculation would be performed in the normal way for a hydrofoil craft at rest, but design cases are likely to arise when the vessel is 'foil-borne'. Here again consideration would be allowed for hull acceleration, perhaps along the lines discussed for the fast patrol boat [17]. But the 'hull inertia and gravity loading' ($q_i + q_g$) is balanced by more or less concentrated forces when the hull is foil-borne. Particular attention would also be paid to unit analysis of the foils and foil structure.

Dracones. The ship girder analysis is quite irrelevant here because the flexural rigidity is almost zero. In fact the q_g and q_B curves are approximately as shown in Fig. 3.68. Attention is much more likely to be focused on unit analysis, that is on the strength of seams and attachments and on the behaviour when kinking of the fabric occurs.

Hovercraft. The structural analysis of hovercraft is a rather specialized field as illustrated in [18]. It must be remembered that a hovercraft may function in one of several distinct modes, for example, cushion-borne (with or without wave impact), floating, supported by the ground or on jacks, towing or being towed. Particular care has to be taken over the possibility of fatigue failure, and in certain vital areas – especially in the design of skirts – emphasis remains very much on experience.

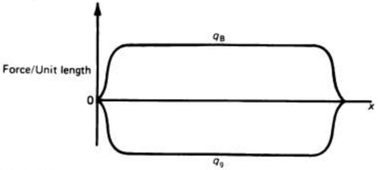

Fig. 3.68

No régime of over-riding importance in design (comparable with 'gravity and buoyancy loading' of the ship girder) has emerged for hovercraft. Particular care has to be taken, however, with (i) 'gravity and buoyancy analysis' when floating, (ii) wave impact at speed, and (iii) skirt strength. Some effort is placed on 'progressive strengthening' (or 'fail safe'), so that as failure of a component occurs a stronger alternative becomes exposed to the loading.

3.14 Unit Analysis in General

We have only indicated how to proceed from general considerations of external loading to more detailed unit analysis. In practice, many facets of the structural analysis of a surface ship have little to do with the longitudinal strength calculation and analyses are often completed on an *ad hoc* basis. This is evident by considering the following examples:

(i) Propeller shafting; this is principally loaded in torque and thrust (but it might be necessary to include bending also, possibly by the inclusion of inertia forces in a vibration analysis).
(ii) Rudder stock; the main concern here will be with hydrodynamic forces and the forces exerted by the actuating mechanism.
(iii) Masts; apart from gravity loading, it would be necessary to investigate wind forces and inertia forces.
(iv) Davits; these would require investigation of gravity forces and operating forces, while it might also be desirable to include inertia forces.
(v) Bulkheads; the flooding of compartments raises questions about the strength of bulkheads and watertight doors, and here the loading is hydrostatic.

3.15 Recent Developments in Quasi-static Structural Analysis

The advent of large capacity, fast, digital computers has led to the development of two powerful mathematical tools which are now in common use. These tools are generally described under the headings of 'Strip Theory' and 'Finite Element Techniques'. The former allows the analyst to assess hydrodynamic forces on the hull and, with these prescribed, the latter may be introduced to determine the load, stress and bending moment distribution in a structure.

Classical hydrodynamic theory describes the shape of the streamlines in a perfect (inviscid) fluid flowing in some constrained manner, for instance, past a solid surface. A potential function is used to represent an energy source or sink and the flow is often referred to as a 'potential flow'. The mathematical representation of the potential function then leads to the derivation of streamlines across which there is no flow. A closed streamline may thus be replaced by a thin solid wall which could represent a hull, rudder, hydroplane, stabilizer and so on. It is then possible to determine velocities and pressures in the flow or on a streamline. No effects of viscosity can be considered since the presence of shear stresses in the fluid are automatically precluded in the definition of the velocity potential. The fundamentals of potential flow theory are fully discussed in, for example, [19, 20]. For motion in a seaway, forces and therefore the potential function become time dependent, and, furthermore, the wave systems created at the ends of the ship cause interference with each other and the imposed wave system.

When applied to a ship the potential-flow analysis centres about the flow past many transverse, finite strips into which the hull is imagined to be cut. The strips are all joined together by compatible boundary conditions, and wave loading, being regarded as an inviscid process, can also be taken into account. Two-dimensional flow is considered so that the problem of heave and pitch of a ship may be examined on the assumption that surge has a negligible effect on hull loadings. The complexity of interference between the bow and stern wave systems is avoided if the length of the wave is small compared with the length of the ship. Although this may seem to be a severe restriction strip theory has been found in many cases to give quite good agreement with experiment. The technique described also provides the means for tackling the more realistic problem related to random seas. We shall not pursue the subject further here, but the reader can find details in [21, 22] and in [23] the development is summarized in terms of fluid velocities and accelerations.

The fluid loadings, deduced by strip theory or developments of it, may be added to gravity loadings to give the total load distribution on the hull. The assessment of longitudinal (and in fact many local) strength problems may be performed in one exercise by representing the ship (or a particular unit of the ship) as a massive collection of inter-related problems which describe the loading on each finite element of the structure under investigation. The structure is divided by many imaginary cuts which meet at nodes, thus forming finite elements which may be of a rectangular or triangular shape and sometimes irregular or three-dimensional. The displacements at the nodes are related to the displacement at any point within a given element by a displacement function. Strains can be found from the displacements and the stresses determined. Nodal forces are made equivalent to boundary forces and displacements of elements obey compatibility rules. Finally, the whole array of applied forces and internal forces satisfies equilibrium relations. The result requires the solution of a large number of simultaneous equations which are conveniently represented in matrix form. Reference [24] may be consulted for details on the use of finite element techniques in structural analysis.

There is now a considerable number of computer programs available to solve both strip theory problems and finite element problems for whole ship structures. Nevertheless, the analyses are far from perfect at present and in no way remove the responsibility of the designer to understand – and question – the premises upon which they are built. For the problems are in reality of *dynamic* origin.

References

1. Ramsey, A. S. (1961), *Hydrostatics*, Cambridge University Press, Cambridge.
2. Lamb, Sir H. (1949), *Statics*, 3rd Edn, Cambridge University Press, Cambridge.
3. Weatherburn, C. E. (1947), *Differential Geometry in Three Dimensions*, Cambridge University Press, Cambridge.
4. Rawson, K. J. and Tupper, E. C. (1976), *Basic Ship Theory*, 2nd Edn, Vol. 1, Longmans, London.
5. Hawkey, A. (1963), *H.M.S. Captain*, Bell, London.
6. Barnaby, K. C. (1968), *Some Ship Disasters and Their Causes*, Hutchinson, London.
7. Moore, C. S. (1967), *Intact Stability, Chapter 2 of Principles of Naval Architecture* (ed. J. P. Comstock), Society of Naval Architects and Marine Engineers, New York.
8. Robertson, J. B. (1967), *Subdivision and Stability in Damaged Condition, Chapter 3 of Principles of Naval Architecture* (ed. J. P. Comstock), Society of Naval Architects and Marine Engineers, New York.
9. Burcher, R. K. (1980), The influence of hull shape on transverse stability. *Trans. R. Inst. Nav. Archit.*, 122, 111–28.
10. Price, W. G. and Bishop, R. E. D. (1974), *Probabilistic Theory of Ship Dynamics*, Chapman and Hall, London.
11. Goodman, R. A. (1971), Wave excited hull vibration in large tankers and bulk carriers. *Trans. R. Inst. Nav. Archit.* 113, 167–84.
12. Inglis, C. E. (1913), Stresses in a plate due to the presence of cracks and sharp corners. *Trans. Inst. Nav. Archit.*, 55, Part 1, 219–30. See also: Timoshenko, S. P. and Goodier, J. N. (1951), *Theory of Elasticity*, 2nd Edn, McGraw-Hill, New York.
13. Lang, D. W. and Warren, W. G. (1952), Structural strength investigations on destroyer *Albuera. Trans. Inst. Nav. Archit.*, 94, 243–86.
14. Revans, J. T. and Gentry, A. A. C. (1960), The Brave Class patrol boats. *Trans. R. Inst. Nav. Archit.*, 102, 367–89.
15. Evans, J. H. and Adamchak, J. C. (1969), *Ocean Engineering Structures*, MIT Press, Cambridge, Mass, pp. 97–138.
16. Kendrick, S. (1965), The buckling under external pressure of ring stiffened circular cylinders. *Trans. R. Inst. Nav. Archit.*, 107, 139–56.
17. Crewe, P. R. (1958), The hydrofoil boat: its history and future prospects. *Trans. Inst. Nav. Archit.*, 100, 329–73.
18. Elsley, G. H. and Devereux, A. J. (1968), *Hovercraft Design and Construction*, David and Charles, Newton Abbot.
19. Lamb, Sir H. (1945), *Hydrodynamics*, Cambridge University Press, Cambridge.
20. Milne-Thomson, L. M. (1968), *Theoretical Hydrodynamics*, 5th Edn, Macmillan, London.
21. Korvin-Kroukovsky, B. W. (1961), *Theory of Seakeeping*, Society of Naval Architects and Marine Engineers, New York.
22. Gerritsma, J. and Beukelman, W. (1967), Analysis of the modified strip theory for the calculation of ship motions and wave bending moments. *Int. Shipbuild. Prog.*, 14, 319–37.
23. Lewis, E. V. (1967), *The Motions of Ships in Waves, Chapter 9 of Principles of Naval Architecture* (ed. J. P. Comstock), Society of Naval Architects and Marine Engineers, New York.
24. Zienkiewicz, O. C. (1971), *The Finite Element Method in Engineering Science*, McGraw-Hill, London.

4
Modelling Marine Systems

4.1 Introduction

In any discussion of the mechanics of marine vehicles continual reference will be made to systems of one sort or another. Great care must be taken in all investigations to define accurately not only a system – that is, an unvarying collection of matter – but also the boundaries within which a system is contained. Furthermore, we must pay due regard to the environment outside the system boundaries because activity within this environment may well influence the behaviour of the system. For example, suppose the resistance to motion of a ship is to be estimated. The system boundaries may be the hull of the ship, the air–water interface and an imaginary surface in the water at some distance from the hull. However, in confined waters this imaginary surface may no longer be arbitrary but might necessarily include the banks of a canal or the bottom of a channel. The presence of these constraints in the environment will clearly influence the system behaviour.

Systems involving the natural phenomena of the oceans, the atmosphere, geographical features and so on are notoriously difficult to investigate in detail. Thus, for the purpose of analysis and from the point of view of economics, we are compelled to make use of models of the full-scale (often called the 'prototype') system. It is possible, with laboratory models, to ensure some control over the many variables of influence so that those of particular interest can be isolated for special study. A theoretical analysis of the problem commences with a mathematical model, which is generally a simplified and idealized description in order to be soluble. These two descriptions are not mutually exclusive but are used together to predict the characteristics of the prototype system. We shall be concerned here with the conditions necessary to satisfy physical similarity between a model and a prototype system and the best ways of achieving this.

Let us consider steady flow of a fluid of constant density through a circular orifice. If the effects of viscosity are neglected, hydrodynamic theory predicts that the volume flow rate Q_v is given by

$$Q_v = \frac{A_o(2\Delta p^*/\rho)^{1/2}}{\{1 - (A_o/A_1)^2\}^{1/2}} \tag{4.1}$$

where A_o is the area of the orifice, A_1 the flow area some distance upstream from the orifice, Δp^* the drop in piezometric pressure† across the orifice and ρ the density of the fluid. If the orifice is situated in the vertical side of a large tank containing liquid then $A_1 \gg A_o$ and we can put $\Delta p^* = \rho g h$, where h is the drop in

† Piezometric pressure $p^* = p + \rho g z$, where p is the fluid pressure at a point in the fluid and z is the vertical height above a horizontal datum line. For a vertical orifice the datum is usually chosen to be the horizontal centre line.

pressure head over the orifice and is constant for steady flow. Thus, Equation (4.1) becomes

$$Q_v = A_o(2gh)^{1/2}. \tag{4.2}$$

A simple mathematical model such as this is found to overestimate the flow rate for a real fluid by some 50 per cent. Unfortunately, with this theory the complex effects of friction cannot be accounted for completely. It is only on the basis of experiments that we can write Equation (4.2) as, for example,

$$Q_v = C_d A_o(2gh)^{1/2}. \tag{4.3}$$

and subsequently determine the coefficient of discharge C_d.

The prototype may be a part of a more complex system, and tests on scale models are then invariably necessary to provide confidence in the predicted behaviour of real systems. Often the lack of space in a laboratory leads to the construction of model systems smaller in size than the corresponding prototype. This is usually true for the experimental assessment of the main structures of marine vehicles, but there are occasions when models larger than the prototype are called for. Fluidic devices, fuel injection systems and flow in capillary networks are just a few examples. Modelling the ocean environment is a particularly difficult problem especially if the investigation is concerned with the influence of the bottom topography or coastal outline on, say, the behaviour of waves and currents. Suppose we consider an undistorted model of a section of the sea bed on a line from Lands End to Boston. If a model were constructed so that horizontal distances were scaled in the ratio $1{:}5 \times 10^6$ the length of the model would be about 1 m ($\cong$ 40 in). However, if the same ratio were applied to vertical distances, the average depth of the ocean would be about 0.6 mm ($\cong$ 0.024 in) on the model. Clearly, such a thin film of water is unlikely to make for accurate test work. The ratio of vertical distances on the model to the corresponding distances in the prototype must be increased to produce compatibility with experimental facilities, but then a distorted model results. Note that the problem here is very much more difficult than simply enlarging a small part of the model as perhaps a photographer would. Should a local enlargement be possible the environment about the system boundary must be known, and that requires full knowledge of the interaction effects throughout the environment (i.e. the ocean in the foregoing example).

While maps, drawings, plans, statues and the like delineate the outward features of a system we must also find some way of describing its characteristics. This is an essential requirement of engineering models because relative motion often exists within or around the system and brings into play a distribution of forces. However, before we examine the essential properties of such models we need to identify the physical variables which would influence our real system and, if truly representative, our model of it. This calls for a discussion of both dimensional formulae and dimensional analysis. The discussion will be necessarily brief and only the most important aspects will be emphasized. More details and other related items are given, for example, in [1].

4.2 Dimensional Formulae

The measurement of any physical quantity consists essentially of a comparison with a standard amount of that quantity, and that standard amount is called the unit.

For example, the length of a marine vehicle is obtained by stating the number of times a standard unit of length must be used successively to complete the measurement. The 'unit length' may be one of a number available and the method of expressing the result is of greatest value if it has been approved by the scientific community. The result of measuring the physical quantity is termed the magnitude of the quantity. Thus the length, say, of a marine vehicle may be quoted as 100 metres, 328.1 feet, or 0.1 kilometre for example, but whichever unit of length is used the actual length of the vehicle is unaltered. We thus see that the magnitude Q of any measured quantity is expressed in the form

$$Q = nU \tag{4.4}$$

where n represents the numeric (that is, the number of times the unit must be used successively to complete the measurement) and U is the unit. Furthermore, the magnitude Q can be expressed as

$$Q = n_a U_a = n_b U_b = n_c U_c = \ldots \tag{4.5}$$

where the subscripts imply that a different unit has been used which requires a corresponding change in the numeric.

Equations (4.4) and (4.5) illustrate the essential difference between *physical algebra*, which is used to express relations between the magnitudes of physical quantities, and *ordinary algebra*, which is essentially the expression of relations among numbers. In physical algebra certain restrictions have to be placed on processes such as addition, subtraction and equating. These processes have intelligible meaning only when related to the magnitudes of physical quantities of the same kind, for then their magnitudes can be expressed in terms of the same unit. When this condition is met the equation relating several magnitudes is said to be *dimensionally homogeneous*. Consider the process of adding the magnitudes of physical quantities of the same kind. In the equation

$$Q_1 = Q_2 + Q_3 \tag{4.6}$$

the magnitude of Q_1 is the sum of the magnitudes of Q_2 and Q_3. Rewriting Equation (4.6) in analogy with Equation (4.4) leads to the result

$$n_1 U_1 = n_2 U_2 + n_3 U_3, \tag{4.7}$$

which is dimensionally homogeneous.

We can now arrange for the magnitudes on the right-hand side of Equation (4.7) to have the same units as the magnitude on the left-hand side. Equation (4.5) shows that

$$\frac{n_a U_a}{n_b U_b} = 1 = \frac{n_b U_b}{n_c U_c} = \ldots \tag{4.8}$$

and each of these ratios, equal to unity, is called a *conversion factor*. As unity may be introduced as a factor into an expression without altering the value of the expression, a change of units cannot affect an equation in physical algebra. With the aid of Equation (4.8) we can write Equation (4.7) as

$$n_1 = n_2 \left(\frac{n_a}{n_b}\right) + n_3 \left(\frac{n_a}{n_c}\right) = \text{a numeric.} \tag{4.9}$$

Thus, if we consider the addition of two magnitudes of length to obtain a third magnitude of length, we would write

$$l_1 = l_2 + l_3 \tag{4.10}$$

which might take the particular form,

$$n_1(\text{mm}) = 5(\text{cm}) + 1(\text{ft}). \tag{4.11}$$

With the aid of Equation (4.8) we have,

$$\frac{1(\text{cm})}{10(\text{mm})} = 1 = \frac{1(\text{ft})}{304.8(\text{mm})} \tag{4.12}$$

whence Equation (4.11) becomes

$$\begin{aligned} n_1 &= \frac{5(\text{cm})}{1(\text{mm})} + \frac{1(\text{ft})}{1(\text{mm})} \\ &= 50 + 304.8 = 354.8. \end{aligned} \tag{4.13}$$

The need to compare one magnitude with another of the same kind is of fundamental importance and requires the process of division. For example, we may need to form the ratio

$$\frac{Q_1}{Q_2} = \frac{n_1 U_1}{n_2 U_2}. \tag{4.14}$$

Because the units U_1 and U_2 are of like kind, the results of Equation (4.8) can be used to give

$$\frac{Q_1}{Q_2} = \frac{n_1 n_b}{n_2 n_a} = n_3 = \text{a numeric}. \tag{4.15}$$

4.2.1 *Types of Magnitudes*

Magnitudes of physical quantities may be regarded as *fundamental* or *derived*. Fundamental magnitudes are those which are not defined in terms of the magnitude of any other physical quantity, for example the measurement of length by comparison with a calibrated rule. The method of measurement and size of units used for other quantities have no effect on the expressions for the magnitude of length. On the other hand, a derived magnitude *is* defined in terms of other quantities and, in general, the expression for a derived magnitude is altered by changes in the units of other quantities.

For our purposes we shall take the fundamental magnitudes to be:

(i) Length ≡ the distance between two points along a defined curve in space;
(ii) Mass ≡ the amount of matter contained in a specified body; and
(iii) Time interval ≡ the period that elapses between the occurrence of particular events.

The system of measurement in which the magnitudes of length, mass and time interval are regarded as fundamental is often termed the *gravitational system*. When thermodynamic effects are considered it is necessary to include some other physical quantity – usually temperature – as a fundamental magnitude.

Essentially, it is the unit which distinguishes one magnitude from another. We now adopt the symbol [X] which, for the moment, is defined as 'a unit of X' where X is some physical quantity. Thus [L] represents a unit of length, [M] a unit of mass and [T] a unit of time interval. Note that the symbol [L] refers only to a possible unit of length and is not restricted to one particular unit; a similar proviso applies to [M] and [T]. Several sets of units are in common use, such as the British ft–lbm–sec system, the CGS and the MKS systems. However, we shall use preferentially SI units.

If the magnitudes of length and time interval are regarded as fundamental, the magnitude of velocity, say, may be regarded as derived. The magnitude of the velocity, V, of a body may be defined by the equation

$$V = l/t \tag{4.16}$$

where l is the magnitude of the length travelled by the body during a time interval t (short enough to ensure that V is constant during that time interval). For a particular example, the magnitude of length $l = n_1\,[\mathrm{L}]$ and the magnitude of time interval $t = n_2\,[\mathrm{T}]$, where n_1 and n_2 are numerics. The magnitude of velocity is therefore given by,

$$V = \frac{n_1\,[\mathrm{L}]}{n_2\,[\mathrm{T}]} = n_3\,\frac{[\mathrm{L}]}{[\mathrm{T}]} \tag{4.17}$$

where $n_3 = n_1/n_2$ is, of course, another numeric. The magnitude of velocity is necessarily expressed in Equation (4.17) as the product of a numeric and a unit and thus the ratio $[\mathrm{L}]/[\mathrm{T}]$ represents a possible unit of velocity. That is, the *dimensional formula* for velocity is given by $[\mathrm{L}]/[\mathrm{T}]$ which may be expressed as

$$[\mathrm{V}] \equiv [\mathrm{L}]/[\mathrm{T}] \tag{4.18}$$

where the brackets denote the dimensional formula of the magnitude contained within them. The power to which the fundamental unit is raised in the dimensional formula of any magnitude is said to be the *dimension* in respect to that fundamental magnitude in the formula.

The dimensional formula for acceleration can be derived with the aid of Equation (4.18) if we accept the equation for the magnitude of acceleration to be

$$a = \frac{\mathrm{d}V}{\mathrm{d}t}. \tag{4.19}$$

The increase of velocity can be written as $n_4\,[\mathrm{V}]$ and the (short) interval of time as $n_5\,[\mathrm{T}]$. Thus

$$a = \frac{n_4\,[\mathrm{V}]}{n_5\,[\mathrm{T}]} = n_6\,\frac{[\mathrm{V}]}{[\mathrm{T}]} = n_6\,\frac{[\mathrm{L}]}{[\mathrm{T}]^2}. \tag{4.20}$$

The dimensional formula for the derived magnitude of acceleration is therefore given by,

$$[\mathrm{a}] \equiv [\mathrm{L}]\,[\mathrm{T}]^{-2}. \tag{4.21}$$

The dimensional formula for force follows from Equation (4.21). As the magnitude of force is, by convention, defined by the equation $F = ma$ where m is the magnitude of mass, then,

$$[F] \equiv [M][L][T]^{-2} \equiv [MLT^{-2}].\dagger \tag{4.22}$$

Other dimensional formulae can be deduced by similar reasoning from those of the fundamental magnitudes. The defining equation relating the magnitudes of force, mass and acceleration is

$$n_7[F] = n_8[M] \times n_9[a]. \tag{4.23}$$

Thus a force which induces an acceleration of 1 m s^{-2} when acting upon a mass of 1 kg would have a magnitude of 1 kg m s^{-2}. In SI units the name 'newton', often abbreviated to 'N', is given to the unit kg m s^{-2}, although in either form the connection with fundamental units is not clearly apparent.

A most important point must now be made: a dimensional formula is characteristic not of, say, velocity itself but of the units with which the magnitude is expressed. It is quite wrong to suppose that dimensional formulae offer information about the intrinsic nature of the physical quantities with which they are associated – these details must come from the definition of the quantity. We may cite here the examples of work and torque, each of which has the dimensional formula

$$[\text{force}] \times [\text{distance}] \equiv [ML^2T^{-2}]$$

but an essentially different definition. For work the distance is measured along the line of action of the force, whereas for torque the distance is perpendicular to the line of action of the force (and so a rotation may be produced). Another regularly quoted magnitude in this context is the so-called friction velocity. This arises in turbulent boundary-layer theory, by virtue of the ratio $\sqrt{(\tau/\rho)}$ (where τ is the local shear stress) which has the dimensional formula

$$[\sqrt{(\tau/\rho)}] \equiv [(ML^{-1}T^{-2}M^{-1}L^3)^{1/2}] \equiv [LT^{-1}],$$

that is, of velocity. Clearly, it is quite misleading to consider that friction possesses velocity. It may also be shown that kinematic viscosity (a fluid property) and circulation (related to the lift force on a body in a flowing fluid) have the same dimensional formula $[L^2T^{-1}]$.

A dimensional formula is not unique because it depends on which magnitudes are regarded as fundamental and on how the derived magnitudes are defined; in other words, it defines the way in which the unit is related to those of the chosen fundamental magnitudes. It therefore follows that any magnitude which may be expressed as a numeric only has no dimensions and is therefore *dimensionless* (or non-dimensional). The ratio of magnitudes of like kind must, therefore, be dimensionless (see Equation (4.15)). For example, plane angle may be defined as the ratio which the length of a circular arc subtended by the angle bears to the radius of the arc and is thus a derived magnitude. When these two lengths are equal the magnitude of angle is unity in so-called 'radian measure'. (Note also that the magnitude of angle measured by a scale of degrees, that is, by a proportion of a complete rotation and sometimes called 'protractor measure', is a fundamental one [2, 11].)

† The single pair of brackets here is a useful abbreviation and will be used, where appropriate, henceforth.

4.3 Dimensional Analysis

In general, a relation can be dimensionally homogeneous only if the individual magnitudes enter it in certain definite combinations. Knowledge of the form of a particular relation is valuable both in interpreting the results of experiments and also in suggesting the most profitable arrangement which a series of experiments should take. The search for the most informative relation is called *dimensional analysis*. It has its greatest use in complex problems and in those which involve a large number of variables. Often, on the basis of dimensional analysis experiments can be simplified, and provided that the effects of some variables are known the effect of other particular variables may be readily determined. However, dimensional analysis alone can *never* give the complete solution to a problem.

To proceed we must pose a question: How does the magnitude Q_1, of especial interest, depend on the other magnitudes $Q_2, Q_3, Q_4, \ldots$, which may affect its value?' The problem may be set by seeking a relation of the form

$$Q_1 = \phi(Q_2, Q_3, Q_4, \ldots) \tag{4.24}$$

where ϕ means 'some function of' and we attempt to obtain some, but not of course complete, information about the detailed nature of the function. We can use the well known Weierstrass' Approximation Theorem to express Equation (4.24) as the series

$$Q_1 = k_1 Q_2^{a_1} Q_3^{b_1} Q_4^{c_1} + k_2 Q_2^{a_2} Q_3^{b_2} Q_4^{c_2} + k_3 Q_2^{a_3} Q_3^{b_3} Q_4^{c_3} + \ldots \tag{4.25}$$

where $k_1, k_2, k_3, \ldots$ are numerics and are therefore dimensionless; the relationships between the (dimensionless) exponents may be found by invoking dimensional homogeneity. The principle of dimensional homogeneity requires the dimensional formula of Q_1 to be the same as the dimensional formula for each of the other terms in the series of Equation (4.25) and so, taking as an example four magnitudes, we may write

$$[Q_1] \equiv [Q_2^{a_1} Q_3^{b_1} Q_4^{c_1}] \equiv [Q_2^{a_2} Q_3^{b_2} Q_4^{c_2}] \equiv \ldots \equiv [Q_2^{a} Q_3^{b} Q_4^{c}]. \tag{4.26}$$

The numerics do not, of course, enter into a dimensional formula.

The analysis cannot be started until the physical variables whose magnitudes $Q_2, Q_3, Q_4, \ldots$ enter the problem have been determined. It is vitally important to include all the relevant variables otherwise serious errors will result. On some occasions it is necessary to include a 'variable' which may not in fact change in magnitude. Weight per unit mass, g, is an example which is clearly a significant parameter in problems concerned with gravitational forces. Although it is important not to exclude from account any variable which is likely to have a bearing on the problem, there is little virtue in including irrelevant variables. These simply clutter the analysis and obscure the interpretation of experimental results. The logical and optimum choice of the magnitudes used in a dimensional analysis requires a proper understanding of their nature. For example, the viscosity of a fluid would be included in problems concerned with fluid motions but excluded from those in which the fluid is at rest.

4.3.1 *Rayleigh's Method*

To illustrate the use of dimensional analysis let us return to the problem of flow though a simple orifice in the side of a tank containing fluid at constant pressure and discharging to the atmosphere. This system has been discussed earlier and leads to the solution

$$Q_v = A_o(2\Delta p^*/\rho)^{1/2} \tag{4.27}$$

which we know overestimates the volume flow rate Q_v. For the flow of a real fluid what physical variables would we expect to exert an influence on Q_v? Certainly the piezometric pressure drop across the orifice Δp^* should be included together with the size of the orifice represented by a length l, the density of the fluid ρ and, because the fluid is in motion, the dynamic viscosity μ. The list is now complete since the effects of compressibility of the fluid will not be considered and the orifice will be assumed large enough for surface tension to be irrelevant. We can now write

$$Q_v = \phi(\Delta p^*, l, \rho, \mu) \tag{4.28}$$

where again ϕ means 'some function of'. In Equation (4.28) Q_v occurs on only one side of the equation and is thus called the *dependent* variable as its value depends on the remaining *independent* variables on the other side of the expression. Evidently, a change in, say, l will not affect μ but will change Q_v. However, the words dependent and independent refer only to the mathematical arrangement and do not carry any implication of physical cause and effect.

Using the development leading to Equation (4.26) we find that the dimensional formula for a typical term in the series expansion of the function on the right-hand side of Equation (4.28) is

$$[Q_v] \equiv [(\Delta p^*)^a l^b \rho^c \mu^d]. \tag{4.29}$$

For this problem, the magnitudes of length, mass and time interval can be regarded as fundamental with the dimensional formulae [L], [M] and [T] respectively. The relation connecting the dimensional formulae now becomes

$$[\mathrm{L}^3\mathrm{T}^{-1}] \equiv [(\mathrm{ML}^{-1}\mathrm{T}^{-2})^a \mathrm{L}^b (\mathrm{ML}^{-3})^c (\mathrm{ML}^{-1}\mathrm{T}^{-1})^d]. \tag{4.30}$$

Dimensional homogeneity is achieved if we equate the exponents of [L], [M] and [T] on each side of Equation (4.30). That is,

$$\left.\begin{aligned} [\mathrm{L}]: &\quad 3 = -a + b - 3c - d \\ [\mathrm{M}]: &\quad 0 = a + c + d \\ [\mathrm{T}]: &\quad -1 = -2a - d \end{aligned}\right\} \tag{4.31}$$

from which it is found that

$$b = 2a + 1; \qquad c = a - 1; \qquad d = 1 - 2a.$$

No further information can be found about the exponents because the three expressions in (4.31) contain four unknowns. Nevertheless, we can say that Q_v may be expressed as a series of terms in the form $k_n(\Delta p^*)^a l^b \rho^c \mu^d$, that is

$$k_n \left\{\frac{l\mu}{\rho}\right\} \left\{\frac{\Delta p^* l^2 \rho}{\mu^2}\right\}^a.$$

Hence

$$Q_v = \left\{\frac{l\mu}{\rho}\right\} \left\{k_1 \left[\frac{\Delta p^* l^2 \rho}{\mu^2}\right]^{a_1} + k_2 \left[\frac{\Delta p^* l^2 \rho}{\mu^2}\right]^{a_2} + \ldots\right\} \tag{4.32}$$

or, using the approximation theorem 'in reverse',

$$Q_v = \left\{\frac{l\mu}{\rho}\right\} \phi_1 \left\{\frac{\Delta p^* l^2 \rho}{\mu^2}\right\} \tag{4.33}$$

where ϕ_1 is a different function from that in Equation (4.28). The use of the appropriate dimensional formulae shows that in Equation (4.33) both $Q_v\rho/l\mu$ and $\Delta p^* l^2 \rho/\mu^2$ are dimensionless. The dimensional homogeneity of the equation is thus unaffected by the values of a_1, a_2, etc., and it is for this reason that we cannot obtain further information about these exponents.

Several examples of the Rayleigh method (sometimes referred to as the 'indicial' method) are given in [1], but we shall not take the analysis any further here. Instead, we turn our attention to another powerful and logical procedure and subsequently reconsider the flow through the orifice.

4.3.2 *The 'Pi' Theorem*

The object of the so-called 'Pi' theorem, first stated explicitly by Buckingham, is to assemble all the magnitudes entering the problem considered into a number of dimensionless products, or Π's, and thence to derive an algebraic expression connecting the Π's.

Suppose that the magnitude Q_1 of a physical variable depends on other, independent magnitudes $Q_2, Q_3, \ldots, Q_n$ and on no others. Then we can write

$$Q_1 = \phi(Q_2, Q_3, \ldots, Q_n), \tag{4.34}$$

or

$$\phi(Q_1, Q_2, Q_3, \ldots, Q_n) = 0.$$

The Pi theorem now states that if q is the number of distinct† fundamental magnitudes required to express the dimensional formulae of all the n magnitudes then these n magnitudes may be grouped into $n - q$ independent dimensionless Π's such that

$$\phi(\Pi_1, \Pi_2, \Pi_3, \ldots, \Pi_{n-q}) = 0. \tag{4.35}$$

We see that the number of terms is reduced to $n - q$; that is, there are q less terms in Equation (4.35) than in the original expression (4.34). In some cases this reduction can present a major simplification of experimental procedures, as we shall see later.

The simplest way of ensuring that the Π's are independent (i.e. not merely multiples of each other) was devised by Buckingham and is as follows. From among the n original variables a number of them q are selected to form what is often called a 'recurring set'. The choice of the variables in the recurring set is not entirely arbitrary. Apart from not forming a dimensionless group among themselves the variables must also contain all the fundamental magnitudes for the problem. When the recurring set has been chosen each of the remaining $n - q$ magnitudes is in turn combined with those of the recurring set in such a way as to form a dimensionless Π group. Quite often there is more than one choice for the recurring set and the arrangement of the groups is then dictated by the purpose to which the analysis is put.

† The implications of the word distinct in this context are discussed later.

To illustrate the use of Buckingham's Pi theorem let us return to the problem of flow through an orifice. We shall start with Equation (4.28), namely

$$Q_v = \phi(\Delta p^*, l, \rho, \mu).$$

There are five physical variables here which may be expressed in terms of three fundamental magnitudes ($n = 5$, $q = 3$) leading us to expect $5 - 3 = 2$ dimensionless products. There is in fact more than one recurring set which satisfies the necessary conditions, but we shall choose l, ρ and μ. The dimensional formulae of these magnitudes are

$$[l] \equiv [\mathrm{L}]; \quad [\rho] \equiv [\mathrm{ML}^{-3}]; \quad [\mu] \equiv [\mathrm{ML}^{-1}\mathrm{T}^{-1}]. \tag{4.36}$$

It is clear that a dimensionless group cannot be derived from these as only μ contains time interval in its dimensional formula.

With each of the remaining variables, Q_v and Δp^*, we express the recurring set l, ρ and μ in such a way that a Π group is formed. For example

$$\Pi_1 = Q_v l^{a_1} \rho^{b_1} \mu^{c_1}; \quad \Pi_2 = \Delta p^* l^{a_2} \rho^{b_2} \mu^{c_2} \tag{4.37}$$

where the exponents of Q_v and Δp^* have been put arbitrarily to unity. (Any exponent in a Π group can be made equal to unity by taking the appropriate root of the product – a dimensional group remains.) We can now write the respective dimensional formulae;

$$[\Pi_1] \equiv [\mathrm{M}^0\mathrm{L}^0\mathrm{T}^0] \equiv [\mathrm{L}^3\mathrm{T}^{-1}][\mathrm{L}]^{a_1}[\mathrm{ML}^{-3}]^{b_1}[\mathrm{ML}^{-1}\mathrm{T}^{-1}]^{c_1}. \tag{4.38}$$

Equating the exponents of [L], [M] and [T] yields the following set of simultaneous equations:

$$3 + a_1 - 3b_1 - c_1 = 0$$
$$b_1 + c_1 = 0$$
$$-1 - c_1 = 0$$

and so

$$a_1 = -1; \qquad b_1 = -1; \qquad c_1 = -1$$

whence

$$\Pi_1 = \frac{Q_v \rho}{l\mu}. \tag{4.39}$$

Similarly,

$$[\Pi_2] \equiv [\mathrm{M}^0\mathrm{L}^0\mathrm{T}^0] \equiv [\mathrm{ML}^{-1}\mathrm{T}^{-2}][\mathrm{L}]^{a_2}[\mathrm{ML}^{-3}]^{b_2}[\mathrm{ML}^{-1}\mathrm{T}^{-1}]^{c_2} \tag{4.40}$$

from which

$$a_2 = 2; \qquad b_2 = 1; \qquad c_2 = -2$$

whence

$$\Pi_2 = \frac{\Delta p^* l^2 \rho}{\mu^2}. \tag{4.41}$$

Equation (4.28) can now be replaced by the Π representation, namely

$$\phi(\Pi_1, \Pi_2) = 0 = \phi\left\{\frac{Q_v\rho}{l\mu}, \frac{\Delta p^* l^2 \rho}{\mu^2}\right\} \tag{4.42}$$

or,

$$\frac{Q_v\rho}{l\mu} = \phi_1\left\{\frac{\Delta p^* l^2 \rho}{\mu^2}\right\}. \tag{4.43}$$

Another, sometimes quicker, method of forming the Π groups involves expressing the fundamental magnitudes in terms of the dimensional formulae of the members of the recurring set. Thus, from Equation (4.36), we can write

$$\begin{aligned} &[\mathrm{L}] \equiv [l]; \quad [\mathrm{M}] \equiv [\rho \mathrm{L}^3] \equiv [\rho l^3] \\ &[\mathrm{T}] \equiv [\mu^{-1}\mathrm{ML}^{-1}] \equiv [\mu^{-1}\rho l^2]. \end{aligned} \tag{4.44}$$

Using the results of Equations (4.44) in the dimensional formulae for Q_v and Δp^* we obtain

$$[Q_v] \equiv [\mathrm{L}^3\mathrm{T}^{-1}] \equiv [l^3\mu\rho^{-1}l^{-2}] \equiv [l\mu\rho^{-1}].$$

As Q_v has the same dimensional formula as $l\mu\rho^{-1}$, the ratio $Q_v\rho/l\mu$ is dimensionless and corresponds to Π_1 of Equation (4.39). Similarly,

$$[\Delta p^*] \equiv [\mathrm{ML}^{-1}\mathrm{T}^{-2}] \equiv [\rho l^3 l^{-1}\mu^2\rho^{-2}l^{-4}] \equiv [\rho^{-1}l^{-2}\mu^2],$$

and so the ratio $\Delta p^*\rho l^2/\mu^2$ corresponds to Π_2 in Equation (4.41).

Because the Π groups are dimensionless we are at liberty to rearrange the functional relationship between them by the processes of division, multiplication or by raising to any power, provided that the total number of Π's is contained in the resulting groups. Such manoeuvres often lead to a more convenient expression between the magnitudes and indicate which of them can be changed most conveniently during an experiment. As an example, the following functional relationship between six Π's,

$$\psi(\Pi_1, \Pi_2, \Pi_3, \Pi_4, \Pi_5, \Pi_6) = 0$$

could be rewritten, for the sake of convenience, as

$$\psi_1\left\{\frac{\Pi_1\Pi_2^2}{\Pi_5}, \Pi_2^{2/3}, \frac{\Pi_3}{\Pi_4}, \frac{\Pi_4^{1/2}}{\Pi_5}, \frac{\Pi_5\Pi_6}{\Pi_2^5}, \Pi_6\right\} = 0.$$

where ψ_1 is another unknown function

For the orifice flow it is more useful to rewrite Equation (4.42) as

$$\text{function}\left\{\frac{\Pi_1}{\Pi_2^{1/2}}, \Pi_2^{1/2}\right\} = 0 = \text{function}\left\{\frac{Q_v}{l^2}\left(\frac{\Delta p^*}{\rho}\right)^{-1/2}, \frac{\rho l}{\mu}\left(\frac{\Delta p^*}{\rho}\right)^{1/2}\right\}$$

that is,

$$Q_v = l^2\left(\frac{\Delta p^*}{\rho}\right)^{1/2} \text{function}\left\{\frac{l\rho}{\mu}\left(\frac{\Delta p^*}{\rho}\right)^{1/2}\right\} \tag{4.45}$$

which would have been obtained directly had we chosen l, ρ and Δp^* as our recurring set of variables.

It was stated earlier that q represents the number of distinct fundamental magnitudes and we must now consider briefly what we mean by the word distinct. There are some problems in which the condition of homogeneity in respect of one of the fundamental magnitudes is the same as that for another. Alternatively, it may happen that the homogeneity condition for one fundamental magnitude is the same as that obtained by adding or subtracting the equations for the homogeneity of two other fundamental magnitudes. In the application of the Pi theorem to the above problem, for which one more dimensionless product than expected is obtained, it is found that either a recurring set cannot be formed or it is impossible to determine completely the exponents of the magnitudes forming the Π's. The most common example occurs in the analysis of static systems, where the only quantities involved are forces, lengths, areas and volumes; thus only two fundamental magnitudes, those of force and length, are required. To summarise, the number of Π's is equal to the number of magnitudes entering the problem minus the ***maximum*** number whose magnitudes will not by themselves form a Π group (and are therefore available for use as a recurring set).

Suppose now we consider the flow of a liquid discharging to atmosphere through a simple, circular orifice in the side of an open-topped, constant-head tank. We may take the head across the orifice, h, to be the height of the free surface of the water in the tank above the horizontal centre line of the orifice. Furthermore, l^2 is proportional to a typical area, for example the area of the orifice A_o. We can now replace $\Delta p^*/\rho$ by gh and Equation (4.45) becomes

$$Q_v = A_o(gh)^{1/2} \text{ function } \left\{\frac{l\rho(gh)^{1/2}}{\mu}\right\}. \tag{4.46}$$

A comparison of Equation (4.46) with Equation (4.3) shows that the coefficient of discharge, which is introduced to correct the theoretical result and provide agreement with measurements, is given by

$$C_d = \frac{Q_v}{A_o(2gh)^{1/2}} = \frac{1}{\sqrt{2}} \text{ function } \left\{\frac{l\rho(gh)^{1/2}}{\mu}\right\}. \tag{4.47}$$

The relationship (4.47) tells us nothing about the behaviour of C_d other than the likelihood that it depends in some unknown way on the dimensionless group $l\rho(gh)^{1/2}/\mu$. The form that the function takes can be found only from experiment and at this stage we cannot even be sure that C_d may prove to be constant.

Figure 4.1 shows typical experimental data for an orifice of the type discussed above. Textbooks of fluid mechanics, for example [3], show that the velocity of the liquid on the centre line of the *vena contracta*† is given by $(gh)^{1/2}$. The group $l\rho(gh)^{1/2}/\mu$ is therefore proportional to the ratio of inertia forces to viscous shear forces and is called the orifice Reynolds number Re_o. The discharge coefficient given by Equation (4.47) can thus be represented by the single curve of Fig. 4.1 for a given orifice. To produce such a correlation curve we need only measure Q_v, by collecting a known volume (or mass) of liquid in a given time interval, use Equation

† The *vena contracta* is that part of the jet which has the minimum cross sectional area and a somewhat smaller value than the orifice area. Provided that h is considerably greater than the diameter of the orifice the effects of gravity on the free jet can be ignored and the boundary of the jet at the *vena contracta* is horizontal.

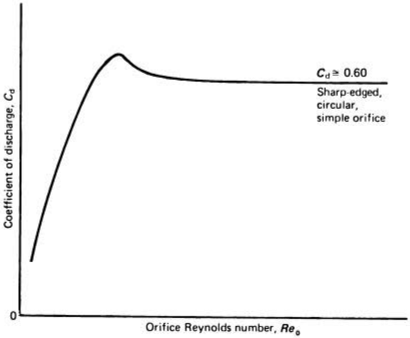

Fig. 4.1 Variation of discharge coefficient for a simple orifice.

(4.47) and calculate a series of values of Re_o. The orifice Reynolds number can be changed most easily by adjusting the head across the orifice h and the typical length l can be taken as the orifice diameter. The correlation curve has even wider generality because it will apply to any one of a family of geometrically similar orifices, each of which will have the same C_d for a given Re_o regardless of what liquid is used. It is this feature which allows us to predict the performance of a prototype from that deduced for a model. Similarity, however, involves rather more than just similar geometries: to categorize the nature of the system to be modelled we need to discuss the topic of physical similarity.

4.4 Physical Similarity

Physical similarity has wide relevance and with the aid of dimensional analysis it becomes a powerful concept in the interpretation of experimental data obtained from tests on model and prototype systems. In general, two (or more) systems are said to be physically similar in respect to certain specified physical quantities when the ratio of corresponding magnitudes of these quantities between the systems is everywhere the same. Not only must this proposition be satisfied by the contents of the system but also by the system boundary, inputs and outputs. Nevertheless, depending on the information sought it is not always necessary to use the same materials for the construction of the model and prototype nor, in the case of fluid flow problems, need the same fluid be used.

Suppose we are concerned with the possible material failure of a rudder mechanism. It would be somewhat reckless to test the appropriate model system to destruction owing to the risk of damage to the test equipment. However, it is possible to establish the distribution of fluid forces over the immersed surface of the model, assuming that the deformation of the model is similar to that of the prototype. Provided that the systems appropriate to the flows about the model and the prototype are similar we may invoke the laws of physical similarity to establish the force distribution over the prototype. The model and prototype materials need not be the same. We may now safely load the prototype (or a model of it) when placed in a materials testing machine so that any failure which might occur will not be hazardous.

The most important problems in the mechanics of marine vehicles require an investigation of geometric, kinematic and dynamic similarity. Although the effects of heat transfer, chemical and nuclear reactions, and magnetic fields may enter some specialized analyses they will not be considered here.

4.4.1 *Geometric Similarity*

If the specified physical quantities are lengths, then similarity between systems is called geometric similarity, that is, similarity of shape. Whether the boundaries of solid bodies or patterns of movement are considered, the characteristic property of geometric similarity is that the ratio of any length in one system to the corresponding length in the other system is the same throughout. This ratio is usually called the *scale factor*. Thus a 10 mm diameter sphere in a circular wind tunnel of 100 mm diameter is a one-tenth scale model of a 100 mm diameter sphere in a circular duct of 1 m diameter provided that the roughness of the corresponding surfaces is similar. Note that all the solid boundaries must be geometrically similar, so that the preceding systems are not geometric models of a 100 m diameter smooth sphere in a volume of infinite extent, such as a spherical meteorite in space. This difficulty is always encountered when models of aircraft in flight or ships at sea are considered, because laboratory tests are carried out in enclosed wind tunnels or water channels and tanks. It must be ensured that the confining boundaries of the model experiment (which are absent from the prototype system) do not have any significant influence on the behaviour of the model system; if they do then account must be taken of the effects in the subsequent analysis of the model results.

Another, very important, departure from true geometric similarity in models of flow systems arises from the failure to scale the inevitable roughness of the solid boundaries. Accurate representation of surface roughness entails not only scaling of the heights of individual protuberances but also their distribution over the surface, which is usually determined by the process used to manufacture the prototype. In submarines, for example, there are many protuberances and excrescences distributed over the surface (apart from the actual roughness of the main surface of the hull), but these are rarely modelled accurately as their effect on performance is either assumed negligible or accounted for empirically. Although great care may be taken in the manufacture of the model some roughness will remain. Provided that the roughness height is everywhere small compared with the characteristic length of the model (e.g. overall length, diameter, etc.) the surfaces of both the model and the prototype can be considered 'hydraulically smooth'. Perfect geometric similarity in respect to surface roughness is then not essential. However, should this not be the case, serious error may result from the interpretation of model data. As we shall see later, the behaviour of flow in a region close to a solid boundary, that is in the boundary layer, changes radically if the roughness height reaches a certain critical value.

4.4.2 *Kinematic Similarity*

Kinematic similarity is similarity of motion, which implies both geometric similarity and similarity of time intervals. Thus, in two (or more) systems, as the corresponding lengths and corresponding time intervals are in a fixed ratio the velocities of corresponding objects must also be in a fixed ratio of magnitude at corresponding times. Furthermore, the accelerations of corresponding objects must be similar. An example of kinematic similarity is found in a planetarium, where parts of the universe are reproduced to a given length scale factor and planetary motions are copied in a fixed ratio of time intervals. If the system involves a fluid, then visualization of the flow is assisted by the concept of a fluid particle.

Let us consider an isolated volume of fluid contained in a box of arbitrary shape with impermeable walls. A pressure-detecting instrument can be connected to the box so that it covers a small part of the surface area. Suppose now the box to be so small that it contains just one molecule of fluid (Fig. 4.2). The instrument will detect an occasional pressure peak each time the molecule collides with the measurement surface as it follows an erratic path within the box. The pressure on the surface, as recorded by the instrument, is then discontinuous and the concept of a time-average pressure would be of little use. A statistical analysis would be needed to estimate the chances of the molecule striking the area considered and hence to deduce a probable upper and lower limit of the pressure. As the box is increased in size, it will contain more and more molecules of fluid and the chance of an impact with the measurement area will clearly increase. Pressure peaks become more frequent and the range of probable values decreases, giving rise to a more meaningful idea of an average pressure as indicated in Fig. 4.3. It is on reasoning such as this that a simple approach to a kinetic theory for gases can be based to determine the magnitude of pressure. When the box is large enough to contain many molecules there will be a continual bombardment of the surface, but each bombardment will not be of equal magnitude, so that we would expect an irregular fluctuation of pressure with a well defined average (detected on a manometer or Bourdon gauge) as shown in Fig. 4.4. This average pressure will then be useful in describing one feature of the state of the fluid contained in the space of a system.

A fluid particle is defined as the smallest quantity of matter of fixed identity

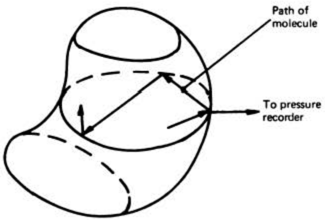

Fig. 4.2

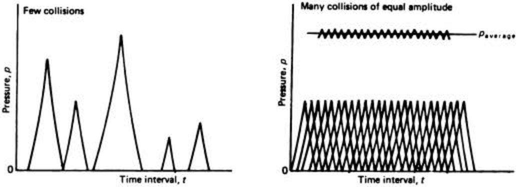

Fig. 4.3

which can be considered to possess continuous properties. Observation of the behaviour of fluid particles is described in macroscopic terms, whereas the treatment of molecular behaviour is sub-microscopic. In normal engineering analyses we can regard the fluid as a continuum. That is, instead of considering a conglomeration of molecules we assume there to be a continuous distribution of matter with no voids. The conditions we consider are those pertaining to average values of a property, so our view is invariably on a macroscopic scale.

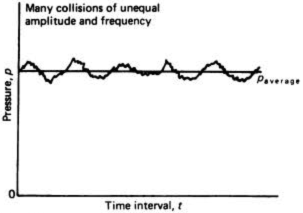

Fig. 4.4

Although the properties of a fluid are molecular in origin we can assume the fluid particle, even though it may be small, to contain a very large number of molecules. In particular, the motion of a fluid can be described by:

pathlines, which are the trajectories of individual particles;
streaklines, which are the loci of instantaneous positions of fluid particles which have passed through the same point in space at some previous time;
streamlines, which, at any instant of time, are tangential to the velocity vectors of the particles located on them.

These lines are illustrated in Fig. 4.5. When the flow is steady the velocity of the fluid particle instantaneously occupying each point in the field of flow is independent of time. All these lines then coincide. For unsteady flow the situation is rather more complicated, and in all but a few very simple cases the shape and location of

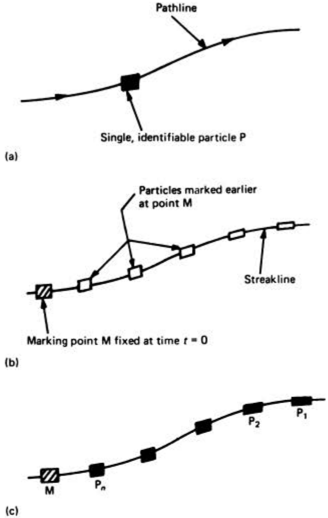

Fig. 4.5 Definitions: (a) pathline; (b) streakline; (c) pathline, streakline and streamline for steady flow.

the three lines differ markedly. Figure 4.6 shows one instantaneous position of the lines which all pass through a particular reference point in the unsteady flow past an oscillating plate.

Most of the fluid motions we meet in practice are unsteady, for example, winds, sea states, etc. However, the unsteady perturbation about a mean (time independent) condition is often small and for the sake of simplicity steady flows are often assumed in first-order analyses. The results so obtained are often not far removed from reality which is rather gratifying because the construction of both theories and experiments related to unsteady flows presents great difficulties.

The 'picture' of the motion of the fluid offered by the instantaneous pathlines, streamlines and streaklines is referred to as the flow pattern. In addition to calculating the coordinates of the lines there are many methods by which flow visualization techniques can be used to depict a continuous pattern of flow whether it be steady or unsteady. A review of these techniques for use in water is given in [4] and additional techniques for air flows along with some excellent photographs of flow patterns and stall phenomena are summarized in [5] and [6].

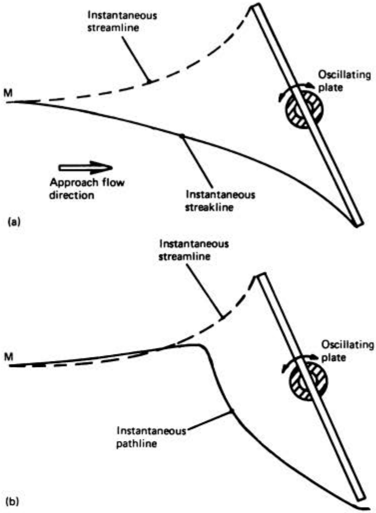

Fig. 4.6 Flow past on oscillating plate: (a) streakline and streamline; (b) pathline and streamline. (Particle leaves M at time streamline drawn.)

When the flow pattern in a model system is geometrically similar to that in the prototype system then these two systems are said to possess kinematic similarity. Since the solid (impermeable) boundaries of a flow system themselves consist of streamlines (no velocity normal to them exists), then kinematic similarity must require geometrically similar models. In practice, prototypes often possess local excrescences below the water line – this is particularly true of submarines – but their effect is usually considered to be local and not to develop widespread effects over the hull. To model these disturbances exactly would be extremely complex and is rarely, if ever, done. The assumption that local disturbances do not modify significantly the smooth hull performance is perhaps rather dangerous and may account, in part, for the frequent disparity between model predictions and prototype performance of submarines.

4.4.3 *Dynamic Similarity*

Two systems will be dynamically similar when the magnitudes of forces at similarly located points in each system are in a fixed ratio at corresponding times. Thus, the magnitude ratio of any two forces in one system must be the same as the magnitude ratio of the corresponding forces in the other system. The forces which may act upon a fluid particle or on a solid boundary of the flow can be classified as follows:

(i) Body forces. These result from gravitation and are proportional to the mass of the body (we shall ignore those induced by electromagnetic or electrostatic fields);
(ii) Surface forces. These are components normal to a given element of the surface (pressure forces) and tangential to a given element of the surface (shear forces);
(iii) Line forces such as surface tension. These arise from molecular attraction and induce capillary effects;
(iv) Elastic forces. These arise from the compressibility of the fluid; and
(v) Inertia force. This is not an independent force but represents the force resisting acceleration of the particle.

Fortunately, not all these forces are present, or have a significant effect, in many of the major problems to be studied. We can concentrate on the similarity of the most important forces, but even this is not straightforward.

Let us consider a fluid particle located at some point in the flow system and suppose that electromagnetic and electrostatic forces are absent. The principal forces acting instantaneously on the particle may be, for example, gravity forces (F_g), forces arising from difference of pressure (F_p), shear forces (F_s), surface tension forces (F_{st}) and elastic forces (F_e) in the directions shown in Fig. 4.7. These forces, not necessarily coplanar, can be added vectorially by means of a force polygon. The force equal in magnitude, but opposite in direction, to the resultant is the

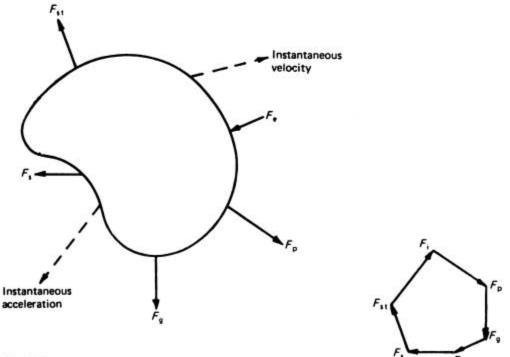

Fig. 4.7

inertia force (F_i) shown in Fig. 4.7. Algebraically, we may write the force equation as the vector sum

$$F_g + F_p + F_s + F_{st} + F_e + F_i = 0. \tag{4.48}$$

The forces which act upon the fluid particles and solid boundaries are an essential part of the 'character' of the flow system. If a model system is to reproduce this character the model forces must be represented to an appropriate scale to ensure dynamic similarity. Thus, the force polygon for a fluid particle in the model system must be geometrically similar to the corresponding one in the prototype system, as shown in Fig. 4.8. Furthermore, if any force vector has a preferred direction, for example gravity forces are directed towards the centre of the Earth, then the force polygons will have the same orientation relative to corresponding datum points in the systems. In analogy with Equation (4.48), the force equation for the model

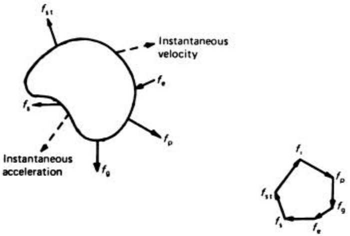

Fig. 4.8

system is

$$f_g + f_p + f_s + f_{st} + f_e + f_i = 0 \tag{4.49}$$

and for similarity of force polygons

$$\begin{aligned} f_g &= \lambda F_g; \quad f_p = \lambda F_p; \quad f_s = \lambda F_s; \\ f_{st} &= \lambda F_{st}; \quad f_e = \lambda F_e; \quad f_i = \lambda F_i \end{aligned} \tag{4.50}$$

where λ is a scale factor. We can eliminate λ by considering the ratios of forces, each ratio by convention being constructed from the inertia force (because it is usually the most important force) and from one other kind of force. Equation (4.50) then yields for the ratios of the magnitudes of forces,

$$\frac{f_i}{f_g} = \frac{F_i}{F_g}; \quad \frac{f_p}{f_i} = \frac{F_p}{F_i}; \quad \frac{f_i}{f_s} = \frac{F_i}{F_s}; \quad \frac{f_i}{f_{st}} = \frac{F_i}{F_{st}}; \quad \frac{f_i}{f_e} = \frac{F_i}{F_e} \tag{4.51}$$

where, again by convention, f_i (and F_i) is the denominator for the ratio of pressure force to inertia force, but is the numerator for the remaining force ratios.

Let us look more closely at the force ratios represented in Equation (4.51) and see how these forces may be related to the physical variables describing the model and prototype systems. The magnitude of the inertia force acting on a particle of fluid is equal to the mass of the particle multiplied by its instantaneous acceleration. Suppose the particle is a rectangular parallelepiped of fluid of sides δx, δy and δz referred to a rectilinear coordinate system. The instantaneous velocity of the particle V increases to $V + \delta V$ over a small time interval δt so that its acceleration will be $\delta V/\delta t$, that is, $V\delta V/\delta x$ in the x direction. The mass of the parallelepiped of fluid is $\rho\delta x\delta y\delta z$, and hence the magnitude of the inertia force in the prototype system, say, is given by

$$F_i = \rho V\left(\frac{\partial V}{\partial x}\right)\delta x\delta y\delta z \tag{4.52}$$

in the limit $\delta V \to 0$ and $\delta x \to 0$. The partial derivative $\partial V/\partial x$ is used in Equation (4.52) because V may depend on variables other than x.

The magnitude of the gravity force on the particle (i.e. weight) is simply mass multiplied by weight per unit mass g:

$$F_g = \rho g\delta x\delta y\delta z. \tag{4.53}$$

A pressure force will arise from the difference in pressure Δp across two opposite faces of the parallelepiped and so, taking the end faces as a typical example, we have

$$F_p = \Delta p\delta y\delta z. \tag{4.54}$$

A shear force will occur on both of the side faces of the parallelepiped as well as on the top and bottom surfaces. However, only one face of the parallelepiped needs to be considered to determine the form of the expression for shear force. Thus, with a side face as typical, we can write

$$F_s = \mu\left(\frac{\partial V}{\partial y}\right)\delta x\delta z. \tag{4.55}$$

The line force, arising from surface tension γ, along one edge of the parallelepiped (δx, say) is expressed as

$$F_{st} = \gamma\delta x. \tag{4.56}$$

It is sometimes necessary to consider the compressibility of the fluid, in which case elastic forces become important. For a given degree of compression the increase in pressure is proportional to the bulk modulus of elasticity, K. Furthermore, if we assume also that the flow under consideration is isentropic† it can be shown (e.g. in [3]) that the velocity with which a sound wave is propagated through the fluid is $c = \sqrt{(K/\rho)}$. Thus the elastic force on a side face of the parallelepiped, say, is given by

$$F_e = K\,\delta x\delta z = \rho c^2\delta x\delta z. \tag{4.57}$$

If it is assumed now that we are seeking dynamic similarity between the model and prototype systems, we require geometric and thus kinematic similarity as well.‡

† A frictionless adiabatic process (no heat transfer to or from the surroundings, i.e. across the system boundary).

‡ In addition to geometric similarities of the force polygons and the system boundaries, dynamic similarity presupposes kinematic similarity owing to the presence of the inertia forces in the systems.

All lengths and velocities are then scaled uniformly and related to arbitrarily selected reference values l and V in the flow systems. With the prototype system as an example velocity gradients, such as $\partial V/\partial x$, are proportional to V/l and accelerations, such as $V\partial V/\partial x$, are proportional to V^2/l. Therefore

$$\begin{aligned} &F_i \propto \rho V^2 l^2; \qquad F_g \propto \rho g l^3; \qquad F_p \propto \Delta p\, l^2; \\ &F_s \propto \mu V l; \qquad F_{st} \propto \gamma l; \qquad F_e \propto \rho c^2 l^2. \end{aligned} \tag{4.58}$$

The force ratios may now be expressed in the forms

$$\begin{aligned} &\frac{F_i}{F_g} \propto \frac{V^2}{gl}; \qquad \frac{F_p}{F_i} \propto \frac{\Delta p}{\rho V^2}; \qquad \frac{F_i}{F_s} \propto \frac{\rho V l}{\mu}; \\ &\frac{F_i}{F_{st}} \propto \frac{\rho V^2 l}{\gamma}; \qquad \frac{F_i}{F_e} \propto \frac{V^2}{c^2} \left(= \frac{\rho V^2}{K} \text{ for isentropic flow} \right). \end{aligned} \tag{4.59}$$

Force ratios corresponding to those in expressions (4.59) can be deduced for the model system in a similar manner. By taking the ratio for inertia force to gravity force as typical, dynamic similarity requires

$$\left(\frac{V^2}{lg}\right)_M = \left(\frac{V^2}{lg}\right)_P \tag{4.60}$$

where the subscripts M and P correspond to the model and prototype systems respectively. Usually, for experiments on marine vehicles g is the same throughout, but corresponding values of V and l are usually different.

4.5 Modelling Marine Vehicles

The flow of a fluid in a pipe can be used as a classic example of the value of dimensional analysis. (As we shall see later, the basis for the estimation of skin-friction forces on the hulls of marine vehicles developed as an extension of the analysis of pipe flows.) Early in the nineteenth century Darcy conducted experiments with the flow of water, under turbulent conditions, in long, unobstructed, straight pipes of uniform diameter. His results suggested that the head 'lost to friction', h_f, in the region of fully developed flow could be represented by the formula

$$h_f = \frac{4fl}{d}\frac{\bar{V}^2}{2g} \tag{4.61}$$

where h_f corresponds to a drop Δp^* of piezometric pressure over length l of pipe in which the mean velocity (flow rate divided by cross sectional area) is $\bar{V}$, f is a coefficient and d is the diameter of the pipe. Values of h_f were then presented in tabular form for various lengths, diameters and types of pipe, different flow rates and for a range of fluids.

Osborne Reynolds reported in 1883 that for geometrically similar pipes $\bar{V}_c d/\nu$ was constant, where $\bar{V}_c$ is a critical mean velocity and $\nu = \mu/\rho$ is the kinematic viscosity of the fluid. He discovered that 'at the critical velocity the flow changed abruptly from a streamline (lamellar) flow to an eddying (sinuous) flow'. Furthermore, Reynolds showed that for pipe flows the functional relationship

$$\left(\frac{\rho d^3}{\mu^2}\right)\frac{dp}{dx} = \phi\left(\frac{\bar{V}d}{\nu}\right) \tag{4.62}$$

held, where dp/dx is the pressure gradient along the pipe. In 1911, Lord Rayleigh used the 'Principle of Dynamical Similarity' (which he developed in 1909) to show that Equation (4.62) could be generalized to

$$R' = \rho \bar{V}^2 \phi_1 \left(\frac{\bar{V}d}{\nu} \right) \tag{4.63}$$

where R' is the resistance per unit surface area of the pipe and ϕ_1 is some other function. He also pointed out that similarity of motion in fluids at constant values of $\bar{V}d/\nu$ will exist when the pipe walls for different experiments are geometrically similar, and that this similarity extends to those irregularities in the surfaces which constitute roughness.

The form of Equation (4.63) suggested to Stanton and Pannell, in 1914, that a given pipe should yield a unique curve when $R'/\rho\bar{V}^2$ was plotted against $\bar{V}d/\nu$, and this they found to be true. The result is now well known: at small values of $\bar{V}d/\nu$ the flow is laminar and as $\bar{V}d/\nu$ increases there is a sudden but rather ill-defined change to a transition region in which $R'/\rho\bar{V}^2$ increases. Then, for higher values of $\bar{V}d/\nu$, a gradual decrease in $R'/\rho\bar{V}^2$ is evident. Stanton and Pannell produced further curves for air and water flows which applied to pipes made of material different from their own, but they put no quantitative value to the pipe roughness.

Equation (4.61) can be used to determine a functional relationship for the friction factor, f, as follows. The piezometric pressure drop over a length l of the pipe is

$$\Delta p^* = \rho g h_f = \frac{4\rho f l}{d} \frac{\bar{V}^2}{2}$$

and

$$R' = \Delta p^* \left(\frac{\pi d^2/4}{\pi d l} \right) = \Delta p^* \left(\frac{d}{4l} \right) = \frac{4\rho f l}{d} \left(\frac{\bar{V}^2}{2} \right) \left(\frac{d}{4l} \right),$$

whence

$$R' = \frac{f}{2} \rho \bar{V}^2.$$

Equation (4.63) then shows that

$$\frac{f}{2} = \phi_1 \left(\frac{\bar{V}d}{\nu} \right). \tag{4.64}$$

Following the publication of Stanton and Pannell's work there came a spate of papers which attempted to find the algebraic form of the functions ϕ and ϕ_1. For example, Lees in 1915 suggested that, within the accuracy of experimental measurements, the pressure loss over a length l of the pipe was given by

$$\Delta p^* = \left(\frac{l\rho\bar{V}^2}{d} \right) \left\{ K_1 + K_2 \left(\frac{\bar{V}d}{\nu} \right)^{K_3} \right\}$$

where $K_1 = 0.0018$, $K_2 = 0.153$ and $K_3 = -0.35$. But this result applies to smooth pipes, such as those made from drawn brass or lead. It was Nikuradse in 1933 who made the significant step towards identifying roughness quantitatively; he artificially roughened the inner surface of pipes by evenly distributing sand grains of known size over the prepared surface. The application of dimensional analysis to such a system yields the functional relationship

$$\frac{f}{2} = \phi_2\left(\frac{\bar{V}d}{\nu}, \frac{\bar{k}}{d}\right) \tag{4.65}$$

where $\bar{k}$ is the mean height (in this case the diameter) of the sand grains. The result is too well known [3] to require further discussion here, but it is important to realize that the dimensionless group $\bar{k}/d$ does not take into account the roughness shape nor the distribution of roughness. Both these parameters influence the flow to some considerable extent. Nikuradse found that f became independent of $\bar{V}d/\nu$ when the latter parameter reached high values. Under these conditions the values of f can be compared with those for commercial pipes, which exhibit a similar behaviour at high $\bar{V}d/\nu$, to enable an equivalent uniform grain size to be specified for the pipes. Moody did this in 1944, and his modified diagram together with the earlier results of Colebrook are in use to day.

Although we have expended some effort in discussing the historical development of the analysis of pipe flows it is not at all out of context here. Many workers, including William and R. E. Froude, used the methods propounded by those concerned specifically with flow in pipes to develop an equivalent assessment of the effects of roughness on the skin friction of flat plates. However, some difficulties arise owing to the absence of fully developed turbulent flow on a plate. Furthermore, the radically different behaviour between laminar and turbulent flows requires careful examination otherwise model data may become erroneous. These matters are dealt with in more detail where they arise in Chapter 5. Our main purpose now is to establish the relevance of dimensional analysis and physical similarity to the modelling of marine vehicles.

4.5.1 *The Model System*

Ideally the model system should consist of a scaled representation, true in every detail, of the prototype system although the systems may not consist of the complete vehicle. Only that part of the vehicle important to the problem under investigation needs to satisfy all the requirements of physical similarity. We have indicated already that if an investigation is concerned only with the flow of water around the immersed portion of the hull of a floating vessel, then an accurate reproduction of the superstructure of the prototype is unnecessary. This is not, of course, true of fully submerged vehicles. We may also decide that models of the bare hull, free of appendages such as sonar domes, shaft brackets, bilge keels and so on, are quite satisfactory for some tests (the effect of the appendages could be determined separately). Geometric features of our model may therefore be different in some known respect from the prototype. Surface roughness is, unfortunately, a departure from our requirements and one about which we can do relatively little in a controllable manner. Isolated, artificial roughness, such as a set of studs, a trip wire, a strip of sand paper, or a similar device, may be attached to the underwater forepart of the model surface in order to encourage transition from laminar to turbulent flow. By doing this it is hoped that the boundary-layer flow on the (usually larger) prototype is accurately developed on the model. In detail this is unlikely to be the case, but often the overall measure of ship resistance can be obtained with surprisingly little error when the special techniques of analysis described in Chapter 5 are used.

The distribution of forces on the wetted surface of a floating vehicle in motion differs from that around a stationary vehicle; consequently, the attitude of the vessel may vary with speed. The wetted surface will also change in area and shape particularly for some craft designed for high-speed operation. The planing craft operates as a conventional displacement boat at low speeds and settles well into the water. With an appropriate design of hull, hydrodynamic forces in an upward direction are developed on the under surface so that the craft rides high in the water to reduce the wetted area. If this behaviour were not to take place a quite unacceptable expenditure of energy would be required to propel the craft at speeds in excess of 10 m s^{-1} (or 20 knots). The effect of dynamic forces on a planing hull is shown in Fig. 4.9. A similar effect, albeit by fundamentally different mechanisms, occurs in the operation of hydrofoil craft and air-cushion vehicles and is experienced to some extent by all floating vehicles when in motion. The model system must therefore be capable of reproducing a variation in attitude and depth of immersion. For steady motion the weight of the model must be adjusted, by the addition of ballast or some other form of loading, so that the correct draught is taken up when the model is stationary. During the subsequent motion the support or suspension systems must allow unhindered changes of attitude and draught. Matters are somewhat more complicated during unsteady motion, for then the inertia of the craft (in addition to the inertia of the fluid particles) must be modelled. This entails an accurate *distribution* of mass within the hull otherwise corrections to experimental data must be introduced to allow for the differences in mass distribution. An alternative procedure is to allow the model to run at a series of different fixed attitudes and draughts to cover the range expected from the prototype in operation.

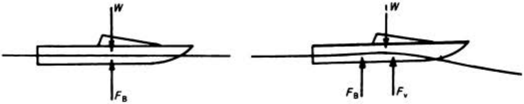

(a) Stationary or low speed
$F_B - W = 0$;
F_B = buoyancy force
W = all-up weight

(b) Higher speeds
$F_B + F_v - W = 0$;
F_v = hydrodynamic vertical supporting force

Fig. 4.9

Finally, it is essential in all cases to ensure that the outer boundaries of the prototype flow system are modelled correctly. If the prototype operates in an environment free of boundary influence, then the same must be true of the model tests, although some form of correction may be required when test facilities have limited space.

4.5.2 *The Marine-vehicle System*

The basic system to be examined consists of the outside form of the hull of a floating vehicle in an expanse of water large enough to exclude effects from the outer boundaries. At this stage we shall omit a consideration of the method of propulsion, including that part outside the hull. This is not because the matter is unimportant – rather, it is so important that we shall devote a separate chapter to it. Suppose also that the only motion of the water arises from the passage of the vehicle. Usually, the effects of air and water are considered separately, but as the main source of fluid forces arises from contact with water we shall concentrate our attention on that medium. For steady motion we should expect the local hydrodynamic force δF to depend on:

(i) the size of the vehicle, represented by a typical length, l;
(ii) the speed of the vehicle V;
(iii) the properties of water, for example, dynamic viscosity μ, density ρ, bulk modulus K, local absolute vapour pressure p_v and surface tension γ; and
(iv) weight per unit mass g, because the possibility of deformation of the air–water interface is included.

During the passage of the vehicle through the water those fluid particles in the vicinity of the hull will accelerate from rest to (possibly) a high velocity. As a result, regions of low pressure are formed in which the water may boil locally to form bubbles of vapour. The presence of small solid particles and dissolved air assist the process as these act as nuclei for bubble formation. The vapour bubbles may then be swept onward by the main flow towards the regions of high pressure whereupon they collapse. The subsequent onrush of water filling the cavities results in high impact loads on adjacent solid surfaces with a real possibility of severe structural damage and the generation of a great deal of noise. Evaporation of the water can occur only if the local absolute static pressure, p, is reduced to the local absolute vapour pressure, which depends among other things on the local temperature. The likelihood of this process, called *cavitation*, will be indicated by the difference between the static and the vapour pressures, that is, by $p - p_v = \Delta p_v$, say.

The magnitude of the hydrodynamic force can now be written as a functional relationship between the magnitudes of the other physical variables. That is,

$$\text{function}\,(\delta F, l, V, \mu, \rho, K, \Delta p_v, \gamma, g) = 0. \tag{4.66}$$

The dimensional formulae of these variables are as follows:

$$[\delta F] \equiv [\mathrm{ML\,T^{-2}}]; \quad [l] \equiv [\mathrm{L}]; \quad [V] \equiv [\mathrm{LT^{-1}}];$$
$$[\mu] \equiv [\mathrm{ML^{-1}\,T^{-1}}]; \quad [\rho] \equiv [\mathrm{ML^{-3}}]; \quad [K] \equiv [\mathrm{ML^{-1}\,T^{-2}}];$$
$$[\Delta p_v] \equiv [\mathrm{ML^{-1}\,T^{-2}}]; \quad [\gamma] \equiv [\mathrm{MT^{-2}}]; \quad [g] \equiv [\mathrm{LT^{-2}}].$$

We have used $q = 3$ fundamental magnitudes – mass, length and time interval – and thus, with $n = 9$ independent variables, we should expect $n - q = 9 - 3 = 6$ dimensionless Π groups. Let us take the variables ρ, l and V as the recurring set since these satisfy the necessary requirements described in Section 4.3.2. It is a straightforward matter now to use the rules of the Pi theorem to determine the dimensionless groups. These are:

$$\Pi_1 = \frac{\delta F}{\rho V^2 l^2}; \quad \Pi_2 = \frac{\rho V l}{\mu}; \quad \Pi_3 = \frac{V^2}{gl}$$

$$\Pi_4 = \frac{\rho V^2}{K}; \quad \Pi_5 = \frac{\Delta p_v}{\rho V^2}; \quad \Pi_6 = \frac{\rho V^2 l}{\gamma}$$

and so,

$$\text{function}\left(\frac{\delta F}{\rho V^2 l^2}, \frac{\rho V l}{\mu}, \frac{V^2}{gl}, \frac{\rho V^2}{K}, \frac{\Delta p_v}{\rho V^2}, \frac{\rho V^2 l}{\gamma}\right) = 0. \tag{4.67}$$

The hydrodynamic force δF can be regarded as the resultant of a force normal to an elemental area of the surface and two shear forces mutually perpendicular to each other tangential to the surface. The normal force arises from a difference in pressure Δp and is therefore proportional to $(\Delta p)l^2$. Similarly, the shear forces are proportional to $\tau_s l^2$ where τ_s is the local shear stress. Therefore, we have,

$$\begin{aligned}\frac{\Delta p}{\rho V^2} &= \phi_1\left[\frac{\rho V l}{\mu}, \frac{V^2}{gl}, \frac{\rho V^2}{K}, \frac{\Delta p_v}{\rho V^2}, \frac{\rho V^2 l}{\gamma}\right] \\ \frac{\tau_s}{\rho V^2} &= \phi_2\left[\frac{\rho V l}{\mu}, \frac{V^2}{gl}, \frac{\rho V^2}{K}, \frac{\Delta p_v}{\rho V^2}, \frac{\rho V^2 l}{\gamma}\right].\end{aligned} \tag{4.68}$$

The groups within the brackets of Equations (4.68) are seen to be identical with those contained in expressions (4.59). It is quite legitimate and more convenient to modify the various groups to the form

$$\begin{aligned}c_p &= \phi_3(Re, Fr, Ca, \sigma, We) \\ c_f &= \phi_4(Re, Fr, Ca, \sigma, We)\end{aligned} \tag{4.69}$$

where

$$c_p = \frac{\Delta p}{\frac{1}{2}\rho V^2} = \text{pressure coefficient}$$

$$c_f = \frac{\tau_s}{\frac{1}{2}\rho V^2} = \text{local skin-friction coefficient}$$

$$Re = \frac{\rho V l}{\mu} = \frac{V l}{\nu} = \text{Reynolds number} \propto \left(\frac{\text{inertia force}}{\text{viscous force}}\right)$$

$$Fr = \frac{V}{\sqrt{(gl)}} = \text{Froude number} \propto \left(\frac{\text{inertia force}}{\text{gravity force}}\right)^{1/2}$$

$$Ca = \frac{\rho V^2}{K} = \text{Cauchy number} \propto \left(\frac{\text{inertia force}}{\text{elastic force}}\right)$$

$$\sigma = \frac{p - p_v}{\frac{1}{2}\rho V^2} = \text{cavitation number}$$

$$We = V\left(\frac{\rho l}{\gamma}\right)^{1/2} = \text{Weber number} \propto \left(\frac{\text{inertia force}}{\text{surface tension force}}\right)^{1/2}.$$

Often ρV^2 is replaced by $\frac{1}{2}\rho V^2$ since the latter has a useful physical interpretation as the dynamic pressure of a fluid stream. Furthermore, if K is the isentropic bulk modulus,

$$Ca = \frac{\rho V^2}{K} = \frac{V^2}{c^2} = (Ma)^2,$$

where Ma is the Mach number and may be used to replace Ca in Equation (4.69).

The vector sum of the local forces acting on the wetted surface of the vehicle will be $F = \Sigma\delta F$, and this force will also depend on the dimensionless groups in parentheses on the right-hand side of Equation (4.69). The resultant hydrodynamic force can be resolved into three orthogonal components which might be, for example, resistance (or drag force) in the direction opposite to that of V and lift and side forces both in directions perpendicular to that of V. Dimensionless groups can be formed from these forces: for example, the resistance R can be used to obtain the group $R/\rho V^2 l^2$. Again we can replace ρV^2 by $\frac{1}{2}\rho V^2$ and l^2 is proportional to a typical area A of the vehicle, which could be the wetted surface area or a cross sectional area of the wetted hull. In any case, we can write

$$C_R = \frac{R}{\frac{1}{2}\rho V^2 A} = \phi_5(Re, Fr, Ma, \sigma, We). \tag{4.70}$$

A designer of a marine vehicle will undoubtedly be concerned with the power P required to propel the vehicle at a steady velocity V against a resistance R. The power required is thus RV and a power coefficient can be defined so that

$$C_P = \frac{P}{\rho V^3 A} = \phi_6(Re, Fr, Ma, \sigma, We). \tag{4.71}$$

We must now qualify the definition of the 'typical' length l used in the discussion so far. If the model system is in every respect a true geometric representation of the prototype system, then literally any length can be employed to indicate the size of the vehicle. We could use the height of the funnel or the diameter of a porthole, but clearly there would be little value in doing so as it is often unnecessary to model the entire prototype. Were we to examine the distribution of wind forces on the superstructure then the funnel would require accurate modelling, but, as stated already, our chief concern is with hydrodynamic forces. It is more sensible to adopt a typical length which is more directly related to the magnitude of that part of the vehicle with which we are concerned. The length l is most commonly defined as the length of a straight line joining the intersections of the bow and stern with the water plane for a stationary ship; the maximum longitudinal length of a submarine; the mean chord length of a stabilizer or hydroplane; and so on. There are instances when it is useful to define l as the cube root of the displacement volume ∇, that is

$$l^3 = \nabla = \frac{\Delta^*}{\rho g}$$

whence

$$l = \left(\frac{\Delta^*}{\rho g}\right)^{1/3}$$

where Δ^* is the weight displacement. The group $P/\rho V^3 l^2$ can be combined with $(Fr)^2$ to obtain an alternative to Equation (4.71):

$$\left(\frac{P}{\rho V^3 l^2}\right) \times \left(\frac{V^2}{gl}\right) = \frac{P}{V\Delta^*} = \phi_7(Re, Fr, Ma, \sigma, We). \tag{4.72}$$

When the Weber number, We, is large the surface-tension forces will be small compared with the inertia forces and the effects of surface tension can thus be ignored. This will be so when large models which move at moderate or high speeds are used. On the other hand, surface tension plays an important part in the behaviour of small models operating at low speeds. Difficulties from this source will be encountered when small models are used to examine docking procedures or replenishment at sea and the motion of water droplets (spray) and bubbles.

If in a given flow system the value of the Mach number at each point in the fluid is small, the speed of propagation of sound waves, $c = (K/\rho)^{1/2}$, is large and so changes in pressure produce only small variations in density. Under these conditions the fluid may be considered to be of constant density (i.e. incompressible) without serious error. The speed of propagation of sound waves in sea water near the surface is approximately 1500 m s^{-1} ($\cong$ 5000 ft s^{-1}) and thus the arbitrary limit for constant density flow (when *Ma* is less than about 0.3) is likely to apply in most cases (except, perhaps, for propellers rotating at high speed). The motion of a body in air is more likely to be affected by changes in density because the sonic velocity is approximately 350 m s^{-1} ($\cong$ 1150 ft s^{-1}) at normal temperature and pressure, and speeds in excess of 120 m s^{-1} ($\cong$ 400 ft s^{-1}) are quite common especially in propulsion units. Nevertheless, we shall exclude further discussion of the effects of compressibility in our treatment of the mechanics of marine vehicles.

Finally, it is unlikely that cavitation would be present near the hull as a result solely of motion of the hull. Although particles of fluid adjacent to the hull are accelerated their velocity is not so large as to reduce the local pressure to that approaching the fluid vapour pressure. An exception may arise from motion about stabilizers, fins and hydroplanes, and, of course, near to propeller blades, bosses and rudders. These are, however, discussed separately, and we can consider from now on that our basic model system for steady motion is described by the resistance equation

$$C_R = \text{function}\ (Re, Fr). \tag{4.73}$$

It is true that cavitation, for example, occurring locally at some part of the complete hull–propeller system may well modify the flow over a considerable region. However, the analysis of these interactions is exceedingly complex and more often than not the effects are accounted for empirically by the adoption of correlation factors. For the present purposes these complications may be set aside, although their possible presence should always be borne in mind.

4.5.3 *Homologous Series of Models*

A number of models which are geometrically similar in every respect comprise a homologous series. In practice, a departure from this occurs particularly in respect of the size, shape and distribution of the surface roughness. Furthermore, complete dynamic similarity may not be possible as a result of limitations imposed by laboratory test facilities. The departure from geometric and dynamic similarity on these counts is often referred to as *scale effect*. Small 'corrections' to the model performance are applied by adopting correlation allowances, obtained empirically from similar, previous tests, in order to predict the prototype performance with greater accuracy.

Occasionally, however, deliberate geometric changes to a member of a homologous series are required to satisfy some special application, such as operation in waters of confined depth or width, or to accommodate special cargoes. A new design may not be warranted, and it is therefore desirable to investigate a series of geometrically related bodies to find either an optimum shape or deduce the loss in performance when small departures from this optimum are made. For example, a series of wetted hull shapes may be generated by varying the ratio of beam to length (a *fineness ratio* – there are numerous other definitions).

Specification of the geometry of the hull of a ship is essentially an exercise in surveying. Sets of curves (called 'Bonjean' curves) are employed at various locations along the hull to describe transverse vertical and horizontal sections and longitudinal vertical sections. The coordinates of these curves become dimensionless when divided respectively by the draught T, the beam B, and the length l of the ship. The form of the hull is then reduced to a basic shape. The length l may be used to indicate the size of the hull and the ratio B/l can then be used to observe the effects of the changes in the fineness ratio whereas changes in T/l indicate the effect of *section coefficient* (related to draught – again there are other definitions for this).

For completeness, let us denote the mean height of surface roughness by $\bar{k}$ and assume the roughness distribution is the same for all models and the prototype. The additional dimensionless groups B/l, T/l and $\bar{k}/l$ can now be incorporated into the resistance equation (4.73) to yield

$$C_R = \text{function}\,(Re, Fr, B/l, T/l, \bar{k}/l) \tag{4.73a}$$

and used to investigate the effects of geometric changes on the behaviour of the basic model.

4.5.4 *Model Requirements*

For the present, we return to the basic case described by Equation (4.73), namely

$$C_R = \text{function}\,(Re, Fr).$$

Reference to the definitions following Equations (4.69) shows that, to achieve dynamic similarity between a prototype system and its geometrically similar model system, restrictions are placed on the values of the Reynolds number and the Froude number. In short, at corresponding times we require the values of Re and Fr to be the same for each system. That is,

$$(Re)_M = (Re)_P \quad \textit{and} \quad (Fr)_M = (Fr)_P \tag{4.74}$$

where, again, the subscripts M and P denote respectively the values in the model system and in the prototype system. Thus, when dynamic similarity exists between the two systems we have, from Equation (4.73),

$$(C_R)_M = (C_R)_P \tag{4.75}$$

and so

$$(R)_P = (\tfrac{1}{2}\rho V^2 A)_P (C_R)_M = \frac{(\rho V^2 A)_P}{(\rho V^2 A)_M}(R)_M. \tag{4.76}$$

The resistance of the model can thus be measured and then 'scaled' to deduce the resistance of the prototype vehicle.

In Equation (4.76) the typical area is usually the wetted surface area, but since

$A \propto l^2$ we can write

$$\frac{A_P}{A_M} = \left(\frac{l_P}{l_M}\right)^2 = S^{-2}$$

where S is the length scale factor and is equal to l_M/l_P.

It now remains to find the *corresponding speed* of the vehicle to satisfy the conditions imposed by dynamic similarity. There are two such conditions from Equations (4.74), namely,

$$\left.\begin{array}{ll}\text{(i)} & V_M = \left(\dfrac{l_P}{l_M}\dfrac{\nu_M}{\nu_P}\right)V_P = \left(\dfrac{\nu_M}{\nu_P}\right)S^{-1}V_P \\ \text{and} & \\ \text{(ii)} & V_M = \left(\dfrac{l_M}{l_P}\right)^{1/2}V_P = S^{1/2}V_P,\end{array}\right\} \tag{4.77}$$

from which

$$\frac{\nu_M}{\nu_P} = S^{3/2}. \tag{4.78}$$

When the prototype is small it is sometimes possible to use a full-scale model, and then $S = 1$. Tests on such a model should be both accurate and valuable since laboratory conditions can be controlled easily. On the other hand, the prototype vehicle may have a length of 400 m ($\cong$ 1310 ft) or more for a surface ship, whereas the size of the model is governed by the extent of the test facilities and instrumentation and the cost of building models. The largest ship models in use at present are about 13 m ($\cong$ 45 ft) long and so $S \cong 0.033$. Equation (4.78) shows that the ratio ν_M/ν_P would need to vary between unity and 0.006 according to the scale factor. For the model tests at full scale, $\nu_M = \nu_P$, and obviously sea water or a 3.5 per cent brine solution would be used. For the model tests at the smallest scale, however, we need a liquid having a kinematic viscosity of $2.5\text{–}5.5 \times 10^{-9}$ m^2 s^{-1} ($\cong 27\text{–}59 \times 10^{-9}$ ft^2 s^{-1}) depending on temperature. Other physical and chemical properties of the liquid must also be acceptable.

Unfortunately, there is no known liquid which satisfies these conditions. Indeed, liquids of any practical use have kinetic viscosities remarkably similar to that of water. We may therefore conclude that dynamic similarity between the model and prototype systems is impossible when inertia, viscous and gravity forces are important. The interpretation of test data raises considerable difficulties and the subject will be discussed more fully later.

Gravity forces are only called into play when distortion of the free surface, that is the air–water interface, occurs. When the prototype and thus the model are sufficiently deeply submerged this disturbance is no longer significant and Fr can be omitted from consideration. Only the equality of Re is required, but to achieve this is often far from easy. Dynamic similarity between deeply submerged vehicles is established when

$$\left(\frac{Vl}{\nu}\right)_M = \left(\frac{Vl}{\nu}\right)_P. \tag{4.79}$$

If the kinematic viscosity of the liquid in the model system is little different from that in the prototype system we have, from (i) of Equation (4.77),

$$V_M = S^{-1} V_P. \tag{4.80}$$

For a scale model of one-fortieth of the prototype size Equation (4.80) yields

$$V_M = \left(\frac{1}{40}\right)^{-1} V_P = 40 V_P.$$

Hence, for a prototype speed of 10 m s^{-1} ($\cong$ 20 knots) the model speed required is 400 m s^{-1} ($\cong$ 800 knots), which is quite impracticable. In any case, at such speeds and beyond, the effects of compressibility of the liquid (and air surrounding the model) would drastically alter the flow characteristics to prevent the achievement of dynamic similarity. The best that can be hoped for is that V_M is great enough to ensure that $(Re)_M$ is well in excess of the critical value. A turbulent boundary layer can then be assumed to cover most of the model, but since $(Re)_M$ is less than $(Re)_P$ the transition from laminar to turbulent flow will be correspondingly further aft for the model. However, the relative surface roughness of the model is likely to be greater than that of the prototype, and the individual bumps will doubtless encourage a transition point further forward on the model than would be obtained from a hydraulically smooth surface. Nevertheless, the experience of experimenters has shown that in some cases the laminar layer on the model can be quite extensive and result in misleading predictions of the prototype resistance. Here, then, is another reason why turbulence stimulators are fixed near the bows of both submerged and interface models in an effort to obtain dynamic similarity with the prototypes. Although the technique is simple and relatively successful it is doubtful if dynamic similarity is actually achieved.

Provided that a free surface does not affect the motion of a prototype and a model, tests can be carried out with the aid of a pressurized wind tunnel. By increasing air pressure at constant temperature it is often possible to reduce ν_M sufficiently to satisfy the requirements expressed by Equation (4.79).

4.5.5 *Departures from the Basic System*

So far we have dealt with the basic model system described, for example, by Equation (4.73). Apart from the effects of the compressibility of air on the performance of fans and propellers on hovercraft there are no further instances in which *Ma* need be retained in expressions describing the performance of prototypes and their models.

When there is a real possibility of cavitation near the appendages attached to the hull of a model ship then tests must take account of this especially if high-speed operation is contemplated. The condition for dynamic similarity in respect of the cavitation number, σ, is

$$(\sigma)_M = (\sigma)_P$$

that is,

$$\left(\frac{\Delta p_v}{\frac{1}{2}\rho V^2}\right)_M = \left(\frac{\Delta p_v}{\frac{1}{2}\rho V^2}\right)_P. \tag{4.81}$$

It is only when the possibility of cavitation is absent, that is when $\Delta p_v > 0$ (and usually taken as some pressure difference rather greater than zero depending on the purity of the water), that we have no need to consider *absolute* pressures. Since there are no voids in the water the reference pressure may be taken as that at the free surface. The local pressure relative to the reference pressure is then proportional to the corresponding depth below the free surface and, for geometric similarity, that distance is proportional to l. Thus the dimensionless pressure difference analogous to the parameters in Equation (4.81) is

$$\Delta p/\tfrac{1}{2}\rho V^2 \propto l/\tfrac{1}{2}\rho V^2.$$

Consequently, for dynamic similarity and a given liquid we see that

$$V_M = S^{1/2} V_P, \tag{4.82}$$

which is the same criterion as that based on the equality of Froude numbers given by (ii) of Equation (4.77). Under these conditions, however, the model does not give an acceptable indication of cavitation inception in the prototype system.

Remembering that the vapour pressure p_v is an absolute pressure, we can write Equation (4.81) in the form

$$\frac{p_M + (p_a)_M - (p_v)_M}{\rho_M V_M^2} = \frac{p_P + (p_a)_P - (p_v)_P}{\rho_P V_P^2}$$

where p_a is the ambient pressure at the air–water interface. At a depth z_M below the interface in the model system the gauge pressure $p_M = \rho_M g z_M = \rho_M g S z_P = S(\rho_M/\rho_P)p_P$, where z_P is the corresponding depth in the prototype system. Let us assume now that the liquid used in both cases has the same density, so that $\rho_M = \rho_P = \rho$, but different vapour pressures. We then find that,

$$\frac{Sp_P + (p_a)_M - S(p_v)_M}{S} = p_P + (p_a)_P - (p_v)_P$$

which reduces to

$$\frac{(p_a)_M}{(p_a)_P} = S + \frac{(p_v)_M - S(p_v)_P}{(p_a)_P}. \tag{4.83}$$

Equation (4.83) shows that $(p_a)_M$ is less than $(p_a)_P$ because $S < 1$, for tests with ship model hulls, and both $(p_v)_M$ and $(p_v)_P$ are less than $(p_a)_P$. The value of p_v for pure water at 15°C is 1725 Pa ($\cong$ 0.25 lbf in^{-2}), although for sea water a 'safe' value to adopt might be ten times as great as this. Atmospheric pressure for the prototype is not usually far removed from 1 atmosphere (101.3 kPa $\cong$ 14.7 lbf in^{-2}). Thus, for a model to full-size scale ratio $S = 0.05$ and with $(p_v)_P = 10(p_v)_M$ Equation (4.83) shows that $(p_a)_P \cong 17(p_a)_M$, and when the vapour pressures of laboratory water and sea water are taken to be the same then $(p_a)_P \cong 15(p_a)_M$. In other words, the ratio of the model free-surface pressure to the prototype free-surface pressure is not too different from the scale factor S. This imposes severe restrictions on most laboratory equipment although a number of cavitation tunnels and circulating water channels can be depressurized. A recently developed installation in The Netherlands allows the complete building which houses a towing tank to be evacuated. The ambient pressure at the surface of the water in the tank can be reduced to about 5 kPa (about one-twentieth of an atmosphere) so that cavitation experiments can be scaled accurately.

High speed craft such as planing and hydrofoil boats generate a considerable quantity of spray from struts and that part of the hull in contact with the water. The spray, often under the influence of the wind, is thrown rearward relative to the hull and may impact upon the elevated hull, the foredeck or the upper structure. The result is an increment of spray resistance, the magnitude of which depends on both Froude number (controlling the initially propelled sheet of water) and the Weber number (controlling the break up of the sheet into droplets). Undoubtedly, viscosity also influences the initial instability of the sheet of liquid before the formation of the droplets. It is evident from the definition of *We* that the modelling of spray formation requires the additional criterion

$$V_M = S^{-1/2}/V_P \tag{4.84}$$

if the same fluid properties are taken for both systems. Equation (4.84) provides yet another relationship between V_M and V_P different from those in Equations (4.80) and (4.82). Even if different liquids are used problems still remain, because the same physical restrictions apply to γ/ρ as to μ/ρ ($= \nu$). The precise behaviour of spray is still not clear and an empirical increment of resistance is usually included in the total.

Finally, although we have been concerned with the steady motion of a vehicle through a large expanse of water at rest, we must consider the surface waves invariably present during the prototype motion. The assessment of hydrodynamic forces and moments on a ship's hull in a random seaway is complex. Many investigations are therefore based on a simple harmonic disturbance propagated at the interface with a velocity C relative to the Earth. It is a straightforward exercise to show that if the model wave system is geometrically similar to that of the prototype an additional, dimensionless group V/C must be added to the right-hand side of the functional relationship (4.73), for example. The wavelength, that is the distance between successive wave crests (or troughs), is proportional to the 'typical' length l and so

$$\frac{V}{C} \propto \frac{V}{Nl}$$

where N is the wave frequency.† In order to satisfy the conditions of similarity between the model and prototype systems we must have

$$\left(\frac{V}{Nl}\right)_M = \left(\frac{V}{Nl}\right)_P, \tag{4.85}$$

and therefore

$$V_M = S\left(\frac{N_M}{N_P}\right)V_P.$$

If the model scaling is consistent with equality of Froude number then $V_M = S^{1/2} V_P$ and

$$N_M = S^{-1/2} N_P. \tag{4.86}$$

† The group Nl/V is sometimes called the Strouhal number.

As S is usually less than unity for ship model tests it can be seen that the wave frequency of the model is greater than that of the prototype.

4.6 Model Testing

There is no intention here to produce an exhaustive list of those facilities available for model tests; instead, the chief attributes of different types of equipment which affect the mechanics of marine vehicles will be summarized. Nevertheless, it is instructive to put these installations into perspective by quoting some overall sizes where applicable. Many establishments have developed their own specialized techniques of testing models depending on the extent of the available instrumentation and data processing apparatus. Essentially, the facilities can be collected into two groups. Members of the first group have a free surface present and are represented by the towing tank, the manoeuvring tank and the circulating water channel. The second group, represented principally by the water tunnel (the hydraulic analogue of a wind tunnel), has a totally enclosed test section and no free surface. The models are sometimes free-running and remotely controlled, or the motion of the model may be controlled by a mechanical linkage fixed to a moving platform. Waves are generated at the free surface by wave-makers which can take the form of oscillating plates, wedge-shaped plungers or cylinders transmitting pneumatic oscillations.

Some of the main features of a range of test facilities are summarized in Table 4.1 and are now discussed briefly. References [7–10] may be consulted for additional information.

4.6.1 *Towing Tank*

This is probably the most widely used of all the test facilities owing to its value in estimating the resistance to motion of marine vehicles. Essentially, the equipment consists of a long, open-topped tank of rectangular cross section containing water. In large tanks a rail runs along the top of each side wall for the total length of the tank. (An alternative, when the installation is smaller, consists of an elevated monorail supporting a light carriage lying in the longitudinal centre plane.) A carriage usually spans the water and is supported by wheels running on the side rails. The size of the carriage is a compromise between lightness to allow rapid acceleration to the steady test speed and stiffness to avoid deformation when carrying observers and recording equipment. The carriage can be driven either by motors situated 'on-board' driving the wheels, or by a motor located 'on-shore' driving an endless cable fixed to the carriage. Fig. 4.10 shows a view of the 400 m ($\cong$ 1310 ft) long Number 3 towing tank at the National Maritime Institute and illustrates the principal features of this type of facility.

A resistance dynamometer connects the model to the carriage. Although a simple spring-balance system could be used it is not sufficiently accurate. A purely mechanical system usually entails measuring the displacement of one end of a suitably damped pivoted arm, the other end of which is connected by linkages and springs to the model. More recently strain-gauge dynamometers have been adopted as these are compact and require little displacement to yield a good frequency response. In addition, therefore, to their value in recording steady forces they can detect fluctuating loads and, moreover, be housed inside the model if necessary. This allows direct measurement of, for example, the thrust and torque on the propeller shaft of a

Table 4.1 *Characteristics of some test facilities.*

	Towing tank				Cavitation tunnel		Manoeuvring/ seakeeping tank			Circulating water channel		
	Length	Depth	Width	Maximum speed	Test section	Operating speed	Length	Depth	Width	Test section width	Test section depth	Operating speed
	m (ft)	m (ft)	m (ft)	$m\ s^{-1}$ ($ft\ s^{-1}$)	m (ft)	$m\ s^{-1}$ ($ft\ s^{-1}$)	m (ft)	m (ft)	m (ft)	m (ft)	m (ft)	$m\ s^{-1}$ ($ft\ s^{-1}$)
NMI[1]	400 (1312) 152 (500)	7.6 (24.9) 3.7 (12.1)	14.6 (47.9) 9.1 (29.9)	15 (49.2) 3.7 (12.1)	1.12 dia. (3.67) 0.46 square (1.51)	15 max. (49.2) 9 max. (29.5)	30.5 (100) 60 (197)	2.3 (7.5) 1.0 (3.3)	30.5 (100) 60 (197)	3.7 (12.1)	1.1–2.5 (3.6–8.2)	0.3–3.0 (1.0–9.8)
AMTE (H)[2]	164 (538) 270 (886)	2.4 (7.9) 5.5 (18.0)	6.1 (20.0) 12 (39.4)	7.5 (24.6) 12 (39.4)	0.65 square (2.13) 2.63 × 1.30 (8.63 × 4.27)	6–12 (19.7–39.4) 4.5–8 (14.8–26.2)	122 (400)	5.5 (18.0)	61+ (200)	1.4 (4.6)	0.2–0.84 (0.66–2.76)	5.5 max. (18.0)
EEL/BHC[3]	188 (167) 76 (249) 197 (646)	1.3 (4.3) 0–1.7 (0–5.6) 1.7 (5.6)	2.4 (7.9) 3.7 (12.1) 4.6 (15.1)	13.1 (43.0) 9.1 (30.0) 15.2 (50.0)	0.25 × 0.33 (0.82 × 1.08)	5.2 max.* (17.1)	54.8 (180) 24 (80)	0.6 (2.0) 1.7 (5.6)	14.6 (47.9) 3.7† (12.1)	0.25 (0.82)	0.33 (1.08)	5.2 max.* (17.1)
NSRDC[4]	845 (2772) 905 (2970)	6.7 (22.0) 3.0–4.8 (9.8–15.7)	15.6 (51.2) 6.4 (21.0)	10 (32.8) 30 (98.4)	0.9 dia. (2.95)	25 max. (82.0)	110 (361)	6.1 (20.0)	73.2 (240)	6.6 (21.7)	2.7 (8.9)	5.0 max. (16.4)
NRC[5]	137 (449)	3.0 (9.8)	7.6 (24.9)	8 (26.2)			122 (400)	5.1 (16.7)	60.9 (200)			
NSMB[6]	216 (709) 252 (827) 220 (722) 240 (787) 100 (328)	0–1.25 (0–4.1) 5.5 (18.0) 4.0 (13.1) 8.0 (26.2) 2.5 (8.2)	15.7 (51.5) 10.5 (34.4) 4.0 (13.1) 18.0 (59.0) 24.5 (80.4)	5 (16.4) 9 (29.5) 15/30 (50/100) 4†† (13.1) 4.5 (14.8)	0.9 × 0.9 (2.95 × 2.95) octagonal cross section	11 max. (36.1)	60 (197)	0–1.2 (0–4.0)	40 (131)			
DSRL[7]	240 (787)	6.0 (19.7)	12.0 (39.4)	14 (45.9)	0.8 square (2.62)	11 max. (36.1)						
NSFI[8]	27 (89) 175 (574)	1.0 (3.3) 5.5 (18.0)	2.5 (8.2) 10.5 (34.4)	2.6 (8.5) 8 (26.2)	1.2 dia. (3.94)							

SSPA[9]	260	5.0	10.0	14								
	(853)	(16.4)	(32.8)	(45.9)								
BEC[10]	155	2.0	8.0	5	0.6 square	1.8–6.0	30	2.4	7	1.0	1.0	6.3 max.
	(509)	(6.6)	(26.2)	(16.4)	(2.0)	(5.9–19.7)	(98)	(7.9)	(23.0)	(3.3)	(3.3)	(20.7)
	220	4.0	13.0	10**	0.6 × 0.15	18 max	20	1.3	2.7			
	(722)	(13.1)	(42.7)	(32.8)	(2.0 × 0.5)	(59.1)	(66)	(4.3)	(8.9)			
VWS[11]	250	4.8	8.0	20	0.42 square					11.8	<1.2	6–9 max.
	(820)	(15.7)	(26.2)	(65.6)	(1.38)					(38.7)	(3.9)	(20–30)
	120	1.1	8.0	4.2	0.30 square							
	(394)	(3.6)	(26.2)	(13.8)	(0.98)							
HSV[12]	80	0.7	4.0	3.6			25 dia.	3.0‹	–			
	(262)	(2.3)	(13.1)	(11.8)			(82)	(9.8)				
	80	3.0	5.0	3.6								
	(262)	(9.8)	(16.4)	(11.8)								
	300	6.0	18.0	8.0								
	(984)	(19.7)	(59.1)	(26.2)								
	30	1.2	6.0	0.0023 min.†								
	(98)	(3.9)	(19.7)	(0.0075) to								
				1.9 max.								
				(6.2)								
BIZ[13]	37.5	2.5	3.0	3			32 dia.	2.5‹	–			
	(123)	(8.2)	(9.8)	(9.8)			(105)	(8.2)				
	238	6.2	12.5	8								
	(781)	(20.3)	(41.0)	(26.2)								
	293	3.5	5.0	12								
	(961)	(11.5)	(16.4)	(39.4)								
MMB[14]	235	7.25	12.5	10								
	(771)	(23.8)	(41.0)	(32.8)								
	98	2.25	3.5	7								
	(322)	(7.4)	(11.5)	(23.0)								
	340	3.0	6.0	20								
	(1115)	(9.8)	(19.7)	(65.6)								
SRIM[15]	375	8.5	18.0	15	0.60 × 0.45	0.4–2.0	80	4.5	80			
	(1230)	(27.9)	(59.1)	(49.2)	(1.97 × 1.48)	(1.3–6.6)	(262)	(14.8)	(262)			
	140	0–3.5	7.5	6			12 dia.	0–0.9‹				
	(459)	(0–11.5)	(24.6)	(19.7)			(39)	(0–3.0)				
	29	0–1.5	8.0	2								
	(95)	(0–4.9)	(26.2)	(6.6)								
	50	4.5	8.0	2.5								
	(164)	(14.8)	(26.2)	(8.2)								

Notes

* Can be used as closed- or free-surface facility. † For ice-breaking and ice resistance experiments. ** Connected by lock to basin 65 m (213 ft) diameter, 5 m (16.4 ft) deep with rotating arm. ‹ Facility with rotating arm. †† Facility can be depressurized.

1. National Maritime Institute; formerly National Physical Laboratory – Ship Division (UK). 2. Admiralty Marine Technology Establishment (Haslar); formerly Admiralty Experiment Works (UK). 3. Experimental and Electronic Laboratories, British Hovercraft Corporation (UK). 4. Naval Ship Research and Development Centre (USA). 5. National Research Council, Marine Dynamics and Ship Laboratory (Canada). 6. Netherlands Ship Model Basin. 7. Danish Ship Research Laboratory. 8. Ship Research Institute of Norway. 9. Swedish State Ship Building Experimental Tank. 10. Bassin d'Essais des Carènes (France). 11. Versuchsanstalt fur Wasserbau und Schiffbau (West Germany). 12. Hamburgische Schiffbau Versuchsanstalt (West Germany). 13. Brodarski Institut Zagreb (Yugoslavia). 14. Meguro Model Basin (Japan). 15. Ship Research Institute Mitaka (Japan).

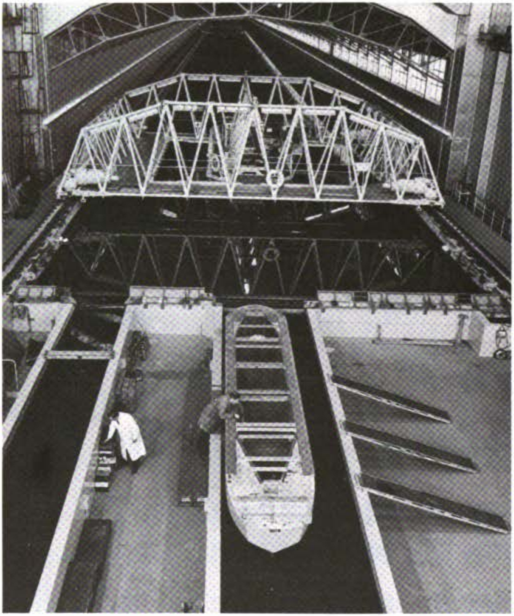

Fig. 4.10 NMI No. 3 towing tank.

self-propelled model. Furthermore, a multi-component balance can be constructed to allow the simultaneous measurement of force of components in various directions.

The size of the towing tank depends on the size of models to be used, and these are strongly influenced by the limits of financial investment. For acceptably accurate data the steady 'on-run' time for the model is about 5–7 seconds. Time must be allowed for the accelerating run-up phase and deceleration at the end of the run with a further emergency stopping distance. Once the maximum steady speed and the carriage size are determined the appropriate drive motors can be designed. These motors decide the acceleration of the carriage and an overall length of the tank can then be estimated. The maximum model size also determines the cross sectional area of the tank necessary to avoid measurable side-wall and bottom interference with the flow pattern. At one time it was considered that if the maximum immersed cross sectional area of the model did not exceed 1 per cent of the cross sectional area of the tank then boundary interference would be negligible. Later, extensive tests with a model of the *Lucy Ashton* indicated that a value of 0.4 per cent should be adopted. For the sake of ease in construction a rectangular cross section is used for the tank, and the depth is about one-half the breadth since the model is towed along the longitudinal centre line of the water surface.

The first towing tank was built by William Froude in 1871 and installed on a site at Torquay. Although Froude died in 1879 the value of the tank and the results from it were appreciated during its use for about 13 years. The tank was then moved to the Admiralty Marine Technology Establishment, Haslar†, where some of the original equipment from the modified tank built in 1886 still remains. Froude's early models were about 3 m (≅ 10 ft) long, but now the AMTE models are on average about 5 m (≅ 16 ft) long for use in the more recently constructed tanks.

The length of most towing tanks is in the range 120–250 m (≅ 400–850 ft) which accommodates models 3 m (≅ 10 ft) long running at maximum speeds of 5–15 m s^{-1} (≅ 10–30 knots). For those tanks containing wave-making facilities beaches are installed at each end of the tank (one just behind the wave-maker) to dissipate the propagated wave pattern. This eliminates the possibility of end-reflected waves interfering with those generated by the model during the test run and also prevents the setting-up of a standing-wave pattern. The maximum height of waves that can be continuously generated is usually about 0.5 m (≅ 20 in) with wave-lengths between 1 and 12 m (≅ 3–40 ft). In the NSRDC high-speed tank it is often found that the *model* resistance is as high as that of a 90 m (≅ 300 ft) long cargo ship with a displacement of 60 MN (≅ 6000 tonf) travelling at, say, 5 m s^{-1} (≅ 10 knots)! This tank is especially valuable for testing models of high-speed craft such as planing and hydrofoil boats and hovercraft. Several facilities exist which have been purpose-built for use with these craft and special methods of rapid recording and storage of data have been developed in this context.

4.6.2 *Water Tunnel*

The principal purpose of the water tunnel is to simulate on a model cavitation conditions similar to those on the prototype. We saw from Equation (4.83) that, for ship models with $S < 1$, this simulation leads to $(p_a)_M < (p_a)_P$; that is, the water pressure must be lower than the normal atmospheric pressure. A vacuum pump is used to achieve this while a second pump circulates the remaining water, which completely fills the tunnel, round the closed circuit. The main regions giving rise to cavitation are adjacent to the backs of the propeller blades and the propeller bosses, stabilizers, hydroplanes and rudders, all of which operate fully submerged.

Bubbles generated by cavitation and air coming out of solution would interfere with the flow pattern about the model as well as hindering observation through windows in the tunnel wall. For these reasons a resorber cylinder is built into the circuit to increase temporarily the water pressure as it passes through, thereby

† Known previously as the Naval Experiment Works and subsequently the Admiralty Experiment Works (AEW).

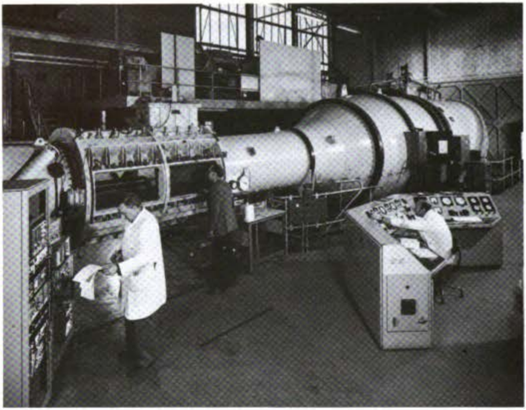

Fig. 4.11 NMI No. 2 cavitation tunnel.

restoring clarity and the original quantity of absorbed gas. The NMI Number 2 cavitation tunnel, shown in Fig. 4.11, is interesting in that it extends no less than 55 m ($\cong$ 180 ft) below ground level in order to remove bubbles and to reduce the unsteadiness and non-uniformity of the flow to a minimum. The range of working pressures is 10–600 kPa ($\cong$ 0.1–6 atmospheres). Comprehensive instrumentation at the propeller shaft consists of strain-gauge transducers for the measurement of thrust and torque. Both mean and fluctuating components are taken and these, along with the outputs from flush-mounted pressure transducers on the model stern, are fed to multi-channel data loggers, with variable integration periods, for subsequent analysis.

In order to model the prototype system more closely cavitation tests on a ship propeller are often conducted behind part of the stern of a model fixed to the horizontal roof of the test section (Fig. 4.12).

4.6.3 *Manoeuvring Tank*

It is essential to know if a prototype ship can keep to a given course and to determine the manoeuvrability of the ship when the rudder is applied. The torque required to turn the rudder must be ascertained and, in some cases, the extent to which the ship is controllable at low speeds and in confined waters when docking is valuable information. Furthermore, the behaviour of surface ships in waves of any heading is clearly important and the best way to examine this is by using a manoeuvring

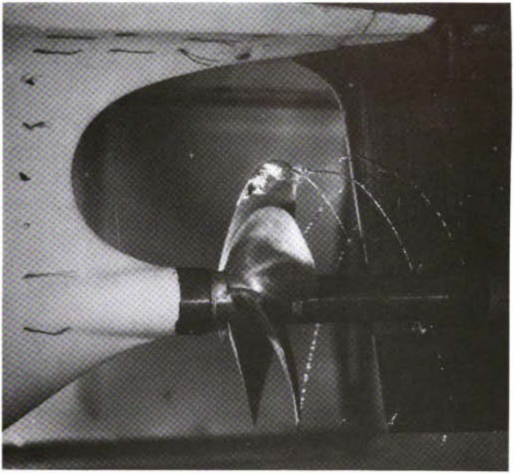

Fig. 4.12 Stern–propeller combination.

tank containing free-running models complete with rudder(s) and propeller(s). Figure 4.13 shows a typical, self-propelled model heading obliquely through a unidirectional series of waves generated at one end of the manoeuvring tank.

Strain-gauge dynamometers in the models are used to assess the propeller torque and thrust and gyroscopes measure angular displacements. In a seaway a ship may experience very large hydrodynamic loadings at the bow and along the keel when travelling at high speeds. Momentarily the local upward dynamic force exerted by the waves exceeds the corresponding buoyancy force so that the ship may rise out of the water. As the ship subsequently 'falls back' into the sea there is a sudden change in vertical acceleration and very severe impact loads occur as it re-enters the water. The process is called *slamming*, and the installation of accelerometers on board models can be used to assess the problem (in both free-running models and in those attached to towing carriages). An example of the full-scale behaviour in rough seas and a model reproduction of the motions is shown in Fig. 4.14 (the model is mounted in a towing tank).

The direction of the models and therefore rudder adjustment is activated by radio signals at high frequency. Waves are generated by wave-makers which can operate

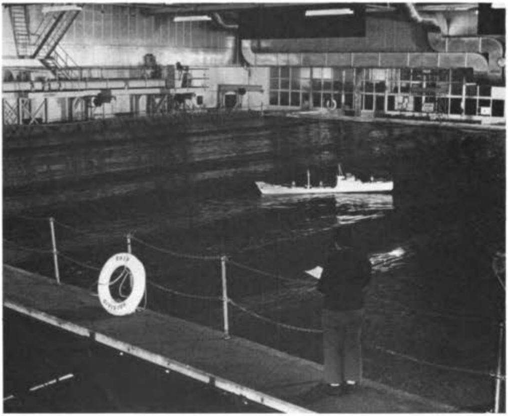

Fig. 4.13 Model ship in NMI No. 4A manoeuvring tank.

along two of the walls surrounding the square or rectangular tank and so either a unidirectional or a confused wave system can be simulated at the interface. The usual procedure, however, is to adopt a unidirectional wave pattern, with a beach at the opposite end of the tank in order to dissipate the wave energy and thus avoid reflection. The model is then driven straight into the oncoming waves followed by a 90° turn to obtain a beam sea and finally a second 90° turn gives the following-sea condition. Control and stability tests are carried out in calm water so that estimates can be made of both the ease with which the ship can turn in a circle manoeuvre and the rapidity of response to full rudder to achieve a straight-line motion following the circle trajectory. The analysis of the results obtained from models approaching a unidirectional wave system at different angles is rather simpler than attempting to reproduce the conditions of a confused sea state, even though this is the more usual case for the prototype in a seaway.

The heading and velocity of the model may be obtained from the traces, on an intermittently exposed film, of small lights fixed to known stations on the model. The camera may be located above the tank and the position of the model relative to a fixed point in the tank may be deduced from a grid reference painted on the tank floor. Data are usually recorded from a telemetry system onto magnetic tape for subsequent computer analysis, although traces are often taken on a multi-channel ultraviolet recorder.

The sizes of some manoeuvring tanks are shown in Table 4.1. Situated towards one end of the AMTE tank is a concrete pillar on which is mounted a pivoted,

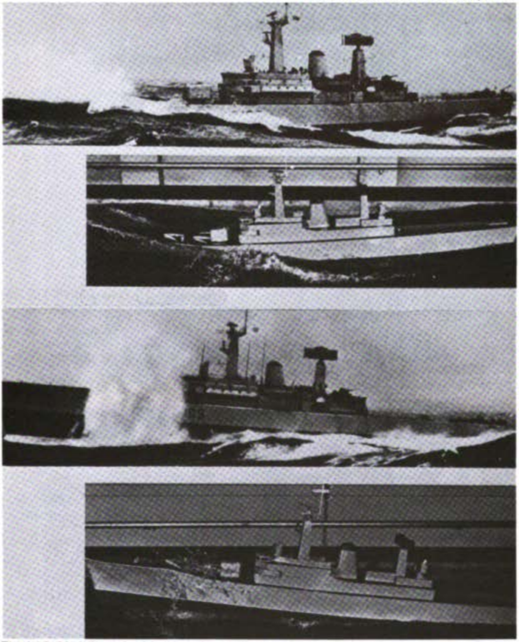

Fig. 4.14 Modelling of a ship in rough seas. (Lower picture in each case taken in towing tank.)

horizontal, rotating arm. The arm can be operated at speeds up to 35 degrees per second and models can be attached at various radii up to 27.5 m ($\cong$ 90 ft). The main purpose of the rotating arm is to obtain experimental values of some of the angular velocity derivatives contained in the general equations of motion for a rigid vehicle (which are derived and examined in Chapter 10). Both surface ship and submarine models can be attached to the arm (see Figs 4.15 and 4.16) and the results supplement those derived from experiments with the Planar Motion Mechanism, discussed in Chapter 10, used in conjunction with a towing carriage over a towing tank or a fixed installation over a circulating water channel. Fig. 4.17 shows Planar Motion Mechanisms (PMM).

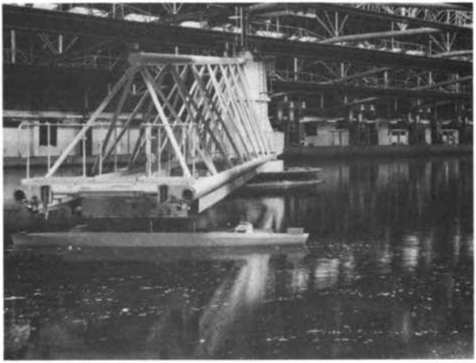

Fig. 4.15 AMTE rotating arm with a ship model attached.

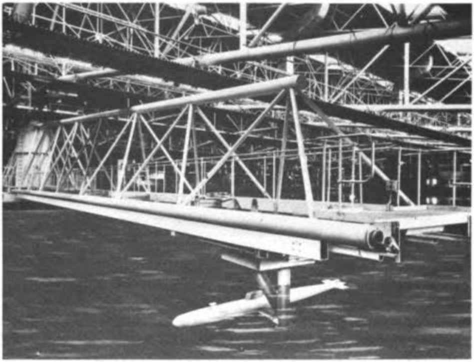

Fig. 4.16 AMTE rotating arm with a submarine model attached.

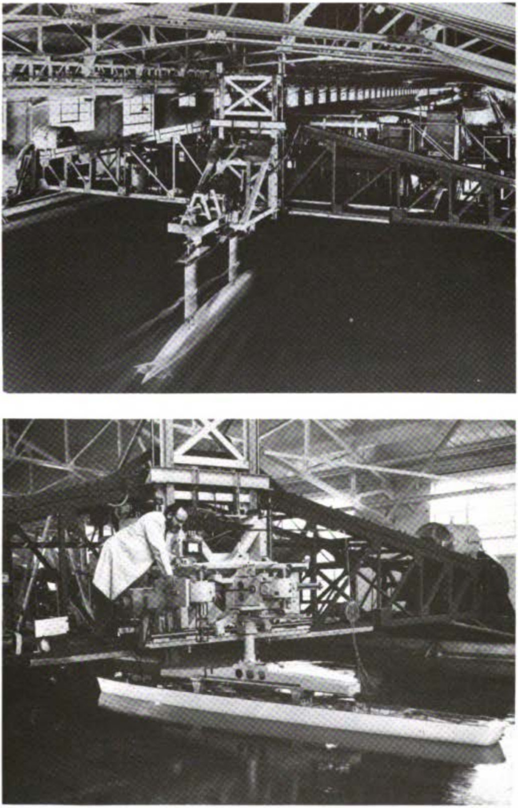

Fig. 4.17 AMTE towing tank with planar motion mechanism attached to carriage: (a) vertical motion; (b) horizontal motion.

One of the manoeuvring tanks at the NSRDC has a channel near one wall 15.25 m ($\cong$ 50 ft) wide and a depth somewhat greater than 10.5 m ($\cong$ 35 ft) so that free-running submarine models can be tested. It was in this tank that the optimum shape was found for high-speed nuclear submarines which could exhibit good control when fully submerged.

A large open-air tank at the National Maritime Institute can be used for manoeuvring tests on large models in shallow water (Fig. 4.18). The models can be radio-controlled or operated by a crew. The tank is particularly useful for interaction experiments and for modelling sections of canals, docks, harbours and so on. Figure 4.18 shows a self-propelled model being steered against a current along a curved length of a shallow canal. Recording instruments and cameras in the model log the movements of the rudder and the path followed relative to the banks. Beam wind forces, which can be important in canal navigation, are reproduced, when needed, by sideways-facing air propellers mounted on the deck of the model.

At first sight, these large tanks containing free-running models appear to be ideal as they avoid interference of the flow by supports attached to the model. Unfortunately, many problems face the experimenter, not the least being the necessity to incorporate a great deal of instrumentation in the hull of small models. Some idea of the complexity of a fully instrumented, remotely controlled model for use in seakeeping experiments can be had from Fig. 4.19. Moreover, the model must be

Fig. 4.18 NMI No. 7 open-air manoeuvring tank with self-propelled model.

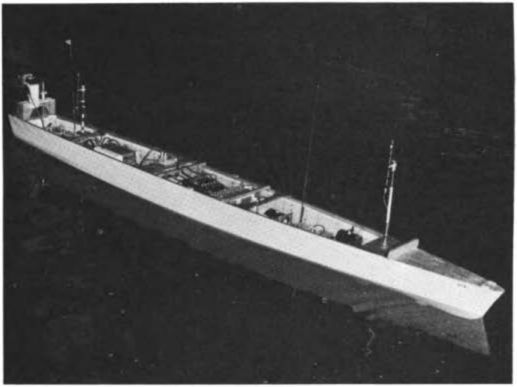

Fig. 4.19 Fully instrumented, free-running model ship.

ballasted correctly to simulate the stability characteristics of the prototype as well as having the correct distribution of mass to scale the inertia forces of the dynamic system accurately. So, even after theoretical analyses are verified by model tests, the final proof of the design comes with ship trials; but by then errors are extremely costly and consequently methods of improving the accuracy and reliability of model testing are still pursued with enthusiasm.

4.6.4 *Circulating Water Channel*

This device is in many ways similar to the water tunnel except that the working section has a free surface (see Fig. 4.20). Windows surround the complete test section to assist lighting and photography and thus provide easily assessed evidence of flows round novel forms or modifications to existing hulls. It is then possible to investigate phenomena associated with the deformation of the interface arising from the relative motion of vehicles only just submerged. Hydrofoils can be treated similarly, and the nature of air entrainment by draw-down from the surface (ventilation) can be likewise investigated. Although a drag balance or PMM can be fixed above the test surface the measurements so recorded are often not accurate enough for design calculations. Instead, the channel is used primarily for flow visualization, the measurement of free-surface deformation and for measuring pressure and shear stress on the surface of models (see Fig. 4.21). In some cases a false floor can be adjusted so that shallow-water experiments can be conducted.

Cavitation conditions on submerged foils can be encouraged by adding a roof above the test section so that the air pressure can be reduced by a vacuum pump.

Fig. 4.20 NMI circulating water channel.

Fig. 4.21 Surface pressure measurements on a model in the NMI circulating water channel.

Fig. 4.22 AMTE circulating water channel with removable roof.

This facility forms part of the AMTE channel and a minimum pressure at the water surface of 40 kPa (≅ 0.4 atmospheres) can be achieved. Figure 4.22 shows a view of the AMTE channel, with the test section roof removed, but with the drag balance fitted and attached to a model frigate. The flow direction is from the bottom-left to the top-right position in the figure. To provide a uniform velocity distribution near to the surface the effects of shear flows close to the inlet nozzle walls need to be removed. This may be done by injecting high-velocity water near to the roof traversing the inlet region of the test section. The pipe and control valve towards the bottom-left position of Fig. 4.22 are used for this technique.

The limitations of water channels are rather similar to those of tunnels in respect of the lack of flow steadiness and uniformity, but careful design of the entry to the working section and its walls helps to alleviate these problems.

4.6.5 *Models*

Models are manufactured to a suitable scale from the prototype ship's lines. Originally, varnished wooden models were used, but it was difficult to maintain dimensional tolerances over long periods, alternating between immersion and storage under changeable atmospheric conditions. Most models are now manufactured from wax by methods essentially the same as those put forward by William Froude in 1873. The material is 95 per cent paraffin wax with small additions of beeswax and a substance called ceresin, both of which have the effect of hardening the wax, thus increasing rigidity and reducing porosity. The wax produces a good uniform surface, but nowadays just as good, if not better, results are obtained with models made from glass-reinforced plastic or expanded polystyrene coated with a waterproof layer of plastic.

The wax model is cast roughly to the hollow-shaped hull and then placed upside down on a table above which are two mechanical cutting tools (see Fig. 4.23). These tools are carried on arms which move horizontally and vertically to remove simultaneously the surplus wax from each side of the longitudinal, vertical centre plane of the model. The position of the cutters is controlled by a pointer which follows a plan of the ship's lines. A series of steps are cut into the outer surface of the hull and these are then faired-in to the final shape (see Fig. 4.24). Before testing and during storage the model is submerged in water to ensure a uniform temperature throughout before tests begin, for otherwise the model might become distorted. The plastic models are generally made by hand lay-up techniques using finely chopped, strand-matt reinforcement fibres and a wax former.

The type of model depends on the tests. Clearly, for calm-water resistance it is necessary only to model the underwater part of the hull, and the material above the water line is kept to a minimum. On the other hand, for models used in waves and in tests for sea-worthiness, there must be complete modelling of freeboard and shape of topsides. In most cases the models are used with turbulence stimulators near the bows. Many laboratories find that the most reliable results are obtained by employing studs but, as mentioned already, no discrete roughness simulation can be expected to produce complete dynamic similarity between the model and the prototype. To ease the interpretation of test data the size, spacing, shape and location of the studs are now standardized and used by the major laboratories of the world.

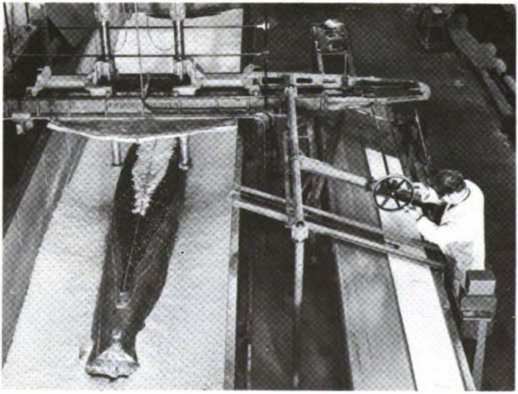

Fig. 4.23 Cutting a wax model.

Fig. 4.24 Fairing the surface of a wax model.

References

1. Massey, B. S. (1971), *Units, Dimensional Analysis and Physical Similarity*, Van Nostrand Reinhold, London.
2. Massey, B. S. (1976), The compleat angle. *Int. J. Mech. Engng Ed.*, 4, 2, 156–8.
3. Massey, B. S. (1979), *Mechanics of Fluids*, 4th Edn, Van Nostrand Reinhold, London.
4. Clayton, B. R. and Massey, B. S. (1967), Flow visualisation in water: A review of techniques. *J. Sci. Instrum.*, 14, 2–11.
5. Werlé, H. (1973), Hydrodynamic flow visualisation. *Ann. Rev. Fluid Mech.*, 5, 361–82.
6. Merzkirch, W. (1974), *Flow Visualisation*, Academic Press, New York.
7. Silverleaf, A. (1965), Development of experimental techniques for ship model work. *Ship Rep. NPL*, No. 73.
8. Comstock, J. P. (ed.), (1967), *Principles of Naval Architecture*, Society of Naval Architects and Marine Engineers, New York.
9. Phillips-Burt, D. (1970), *Ship Model Testing*, International Textbook Company Ltd, London.
10. Du Cane, P. (1974), *High-speed Small Craft*, David and Charles, Newton Abbot.
11. Clayton, B. R. (1982), 2π or not 2π? *Chartered Mech. Engr*, 29, 2, 30.

5
Steady Motion at Low Speeds

5.1 Introduction

Before discussing in detail the steady motion of marine vehicles, it is necessary to examine, at least qualitatively, just what is meant in this context by 'steady'. For example, a surface ship moving in a seaway will, in general, encounter and generate waves at the air–water interface. Neither the surface area exposed to air nor to water will remain a constant proportion of the total surface area of the vehicle. It is thus reasonable to expect the resistance to motion to vary also. (In most cases we shall concentrate on that component of resistance arising from submersion of the hull in water since this will give rise to the major resisting force.) A propulsor, such as a propeller, operates at a constant speed of rotation for long periods and provides a nominally constant thrust to maintain the forward motion of the vehicle. The combination of a variable resistance and constant thrust will evidently result in a continual change of forward speed, that is, the vehicle will 'surge'.

Suppose now we consider all the waves at the interface to be absent or, alternatively, let the vehicle be deeply submerged and approach completely still water. Surely then we can have steady motion of the vehicle? Strictly speaking, the answer is no. Even if the fluid were considered inviscid it can be demonstrated that any propulsor imparting angular momentum to fluid particles by means of a rotor containing blades must produce an unsteady (i.e. time dependent) forward thrust [1]. It is therefore clear that absolutely steady motion is an ideal which cannot be achieved in practice. However, owing to the immensely complex behaviour of the flow about marine vehicles, some simplification of our system must be made. We shall assume that steady motion *can* exist for surface ships, submarines, air-cushion vehicles, planing craft and hydrofoil craft. For example, the expression for forward velocity V is assumed to take the form

$$V = \bar{V} + V',$$

where $\bar{V}$ is the time average value and V' the fluctuating component. We then require $|\bar{V}'| \ll |\bar{V}|$ for an acceptable definition of steady motion.

Whether or not the vehicle can proceed at a steady velocity in a given, straight reference direction requires an investigation of directional stability and is considered later. For the present, we shall assume that a steady, horizontal reference motion can exist in the fore-and-aft direction, that is, parallel to a vertical plane of symmetry. Once relative motion takes place between the vehicle and the surrounding fluid the laws of hydrostatics no longer hold because particles of fluid are displaced from their positions at rest during the passage of the vehicle. Furthermore, the particle motions are unsteady and the unsteadiness is augmented by surface waves and wake flows. Hydrodynamic forces are therefore applied by the fluid to the vehicle in addition to the hydrostatic buoyancy force, which may also be modified by the motion.

In order to obtain and maintain steady motion it is necessary to develop a thrust, T, from a propulsor device. When steady motion has been attained the forces and moments acting on the vehicle are in equilibrium. The conditions to achieve this will now be our main concern.

5.2 Fluid Forces

Let us examine the essential difference between the fluid forces applied to a vehicle at rest and those forces applied to a vehicle when relative motion exists. Consider first a stationary, substantially axisymmetric vehicle, with the longitudinal section shown in Fig. 5.1, immersed in a fluid of infinite extent which is at rest. (The body can be likened to the bare hull of a submarine or airship.) The upward buoyancy force, F_B, exterted by the fluid on the vehicle results from the distribution of static pressure over the surface of the vehicle. For equilibrium the buoyancy force must be equal to the weight displacement of the vehicle, that is

$$F_B = \Delta^* = W = \rho g \nabla$$

and, as we have seen in Chapter 3, this equation remains true for *any* orientation of a floating body. The vehicle will remain in a state of stable equilibrium only if the centre of buoyancy B lies above the centre of gravity G.

Suppose now the vehicle (an airship, say) moves forward in the direction of its longitudinal axis with a steady velocity V by the application of a constant propulsive thrust T, as shown in Fig. 5.2. The flow pattern about the vehicle can be assumed

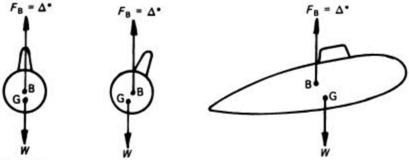

Fig. 5.1

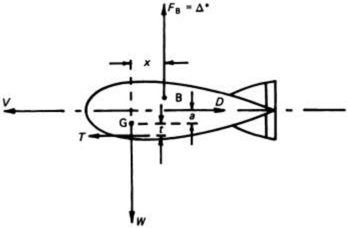

Fig. 5.2

to be axisymmetric, so that forces normal to the direction of V resulting from any modification of the pressure distribution will cancel out. The fluid dynamic force in an upward direction, namely the lift L, is therefore zero and only F_B remains. A drag force D, parallel to the direction of V, results from the distribution of shear stress over the surface and from the dissipation of energy in the wake. For equilibrium we must have

$$\Delta^* = F_B = W$$

$$T = D$$

$$tT + aD - xF_B = 0.$$

Data for the airship R–101 suggests that $\Delta^* = 1.67$ MN ($\cong$ 167 tonf), $T = 50.25$ kN ($\cong$ 11 300 lbf), $a + t = 8.84$ m ($\cong$ 29 ft), and thus we find that $x = 0.266$ m ($\cong$ 0.88 ft). In other words, adjustment of the position of G (by moving ballast, for example) so that x has this value would enable the airship to fly 'straight and level'.

If, as is shown in Fig. 5.3, the vehicle moves forward at an angle of trim (i.e. the angle between the velocity vector and the longitudinal axis is no longer zero) the axial symmetry of the flow is destroyed. In addition to the buoyancy force there is usually a dynamic force F, and the question arises as to how these forces can be identified separately. When the fluid is set in motion by the passage of a vehicle, then (i) the fluid gains kinetic energy at the expense of its pressure and potential energy, and (ii) the curvature of the streamlines alters the pressure gradients in the fluid so that static equilibrium no longer prevails. The pressure distribution over the body is therefore modified and, as a result, the integrated pressure force exerted on the body changes in magnitude and direction. Note also that the shear stresses on the surface of the body will also contribute to the total force.

It is convenient to take F_B as the buoyancy force on a *stationary* vehicle; F is then defined as the vector difference between the actual fluid force and that which would prevail in the static case. The total fluid force (excluding the reaction to the thrust) is therefore the resultant of F and F_B, say F_T. In other words, F_T is the vector sum of F and F_B. Thus for steady motion of the vehicle the forces F, F_B, W and T or, alternatively, F_T, W and T must be in equilibrium to form a closed force polygon. Because of port-and-starboard symmetry no side forces are present and all

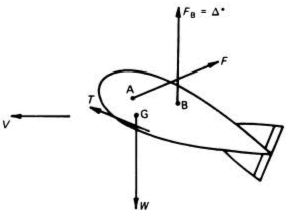

Fig. 5.3

the forces must therefore lie in the vertical centre plane. It is often useful under these circumstances to resolve F into lift and drag force components.

Similar arguments to those above can be applied to vehicles in motion at the interface. However, distortion of the interface modifies the magnitudes of F_B, F and T. Furthermore, the earlier concept of steady flow must be introduced. For interface vehicles it is usual to think in terms of vertical and horizontal forces such as those shown in Table 5.1. The force P_T is a towing force and since the lift force L is invariably associated with fully submerged bodies the symbol F_v has been preferred to imply a vertical dynamic force. When F_v is absent the resistance R is usually associated with the total force on the vehicle in a rearward direction parallel to the direction of motion. The resistance then consists of drag components developed on various parts of the vehicle, some of which may be fully or partially immersed in either air or water.

Table 5.1 Force notation.

	Vertical forces		Horizontal forces	
Vehicle	Upward	Downward	Forward	Aft
Conventional ship	F_B	W	T	R
Planing craft	F_B, F_v	W	T	D
Dracone	F_B	W	P_T	R
Hydrofoil	F_B, L	W	T	D

In Table 5.1 it has been assumed that steady motion occurs in the fore-and-aft plane of symmetry. Obviously, the relative magnitudes of F, F_B, W and T can vary enormously from one vehicle to another and, for a given vehicle, from one operating condition to another. For example, owing to the very low relative density of air the contribution of F_B to the total vertical force supporting an aircraft is negligible. In contrast, the buoyancy forces on bodies moving in, or on the surface of, water can be extremely large. As we shall see there are some vehicles, for example hydrofoil craft and planing craft, for which F_B may become a relatively small proportion of F_T as V increases. Aerodynamic as well as hydrodynamic forces may be significant for some interface vehicles (e.g. sailing craft which rely on wind forces to produce the propulsive thrust on a sail). Although it is reasonable to expect some interdependence between aerodynamic and hydrodynamic forces they are generally considered separately in most analyses.

5.3 Zones of Operation

There are three principal zones in which we may expect significant differences in the behaviour of a marine vehicle. These zones are shown in Fig. 5.4:

I is a region in which the vehicle can be considered immersed in a fluid of infinite extent in all directions;

II represents a region in which the flows round, and therefore the fluid forces on, a vehicle are modified by the proximity of a solid boundary; and

III is where the behaviour of the vehicle is affected by the proximity of an interface between two fluids.

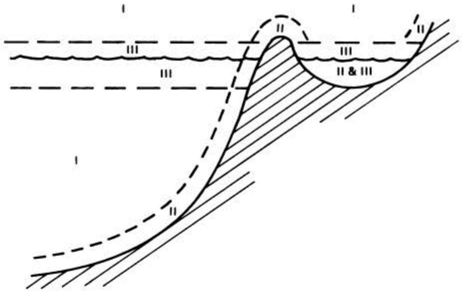

Fig. 5.4 Zones of operation for marine vehicles.

The boundaries of these zones are imprecise as they depend on the geometry of the vehicle and on the properties of the fluid concerned. Sometimes the sea bed cannot be assumed rigid or solid and then the operation of a vehicle near to it would be more like that in a zone of type III rather than type II. However, vehicles in a zone of type II will not be investigated here and neither will the following, rather important problems: (i) shallow running of submarines and torpedoes; (ii) operation of ships in shallow and/or restricted waters; and (iii) ships running close together during refuelling. Instead, attention is focused on vehicles in zone I applied to the sea and zone III *at* the interface in deep water. In both cases the upstream flow relative to the vehicle is considered to be uniform and steady, the water density is assumed constant throughout and the only waves at the interface are those generated by the passage of the vehicle.

5.4 Field of Flow

When relative motion occurs between a fluid and a marine vehicle the forces exerted by the fluid on the vehicle are of two main types:

(i) those distributed over the complete wetted surface of the vehicle including that of rudders, stabilizers, hydroplanes, etc.; and

(ii) propulsion forces which are localized near some form of propulsor such as the blades of a propeller.

Forces of type (i) are discussed in this chapter and those of type (ii) are dealt with in Chapter 7. The usual assumption will be made that the two types of forces can be examined separately although subsequently some effort is made to 'allow' for any error that arises from the effects of interaction.

The relative motion between the main flow of fluid and the vehicle will be regarded as steady throughout. The standpoint adopted is that of an observer stationed on the vehicle; he thinks he is on a stationary vehicle in a fluid moving with a steady approach velocity. Three flow régimes require special consideration: (i) flow very close to the surface of the vehicle; (ii) flow at some distance from the vehicle; and (iii) flow at and close to an air–water interface including distortion of that interface.

5.4.1 *Flow in the Boundary Layer*

It is characteristic of all real fluids that whenever relative motion exists between the fluid and a solid surface no 'slip' takes place at the surface. No matter how smooth the solid boundary or how small the viscosity may be, the particles adjacent to the boundary do not move (provided that we omit gases at very low pressure). The relative velocity of the fluid must therefore increase from zero at the boundary to that corresponding to the velocity in the main stream. The region in which this increase takes place is called the *boundary layer* and it may be very thin indeed, although the velocity increases continuously – there is no abrupt step change. Outside the boundary layer conditions in the main stream prevail and as a result of the absence of large velocity gradients there the effects of viscosity are found to be negligible.

The rapid change of tangential velocity with distance normal to the boundary implies the presence of large shear stresses. It was Prandtl who, in 1904, suggested that the flow of a real fluid past a solid boundary could be considered in two parts:

(i) a *thin* boundary layer in which shear stresses are of prime importance; and
(ii) the flow beyond the boundary layer which may be regarded as that of an ideal (inviscid) fluid.

The concept of a thin boundary layer requires a definition of thickness, but unfortunately this lacks precision because the conditions in the main stream are approached asymptotically. Nevertheless, a meaningful definition may be based on the accuracy with which measurements can be made of, say, velocity. By accounting for changes in flow rate, momentum and energy, more precise measures of thickness can be deduced mathematically, but at some loss of physical reality.

Figure 5.5 shows the longitudinal section of a stationary body deeply immersed in a fluid of infinite extent. For our purposes the body may be assumed to be either axisymmetric or two-dimensional of infinite length normal to the plane of the paper. The uniform upstream flow moves steadily towards the body in a direction parallel to its centre line. The boundary layer extends downstream beyond the body to form a wake containing relatively slow-moving eddies which translate at a lower velocity than that of the main stream. Note that the boundary-layer thickness increases towards the rear of the body so that, by virtue of continuity of mass flow, some fluid must pass into the boundary layer. The line defining (loosely) the 'outer edge' of the layer (shown as a broken line in Fig. 5.5) is not, therefore, a streamline. The extent of the retarded flow in a direction normal to the surface of the body may sometimes become so great towards the rear of the body that the concept of a 'thin' boundary layer is no longer tenable. Under these conditions any simplification of the equations describing the flow in such a region would undoubtedly lead to misleading results.

The complete equations describing the motion of a viscous fluid are extremely complex and defy complete solution even for the steady flow of a constant-density fluid. The Prandtl assumption goes a long way towards simplifying the analyses but the resulting 'boundary-layer equations' are still too complicated to allow a general

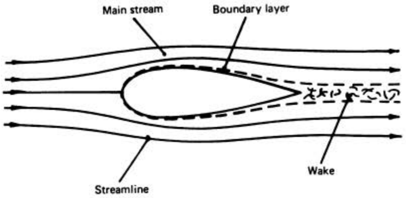

(a) Body axis parallel to approach flow

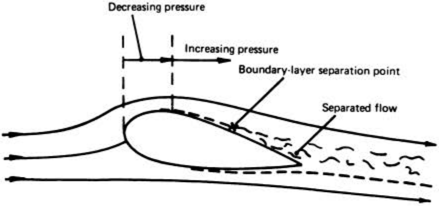

(b) Body axis inclined to approach flow

Fig. 5.5

solution. However, many particular solutions do exist, especially for two-dimensional flow. Approximate analyses use these accurate, but often impractical, solutions to assist the formulation of more general methods of determining the main boundary-layer characteristics. Of major importance is the estimation of the local shear stress on a body in order to calculate the total skin-friction force. The component of this force in the direction of the approach flow constitutes the skin-friction drag.

The boundary layer on an immersed vehicle consists, in general, of three identifiable regions. These are shown (not to scale) in Fig. 5.6(a) for a uniform flow approaching a flat plate at a steady velocity U_∞. In the forward region the flow is laminar, and viscous shear stresses alone resist fluid motion. With increasing thickness downstream the boundary layer becomes unstable and the flow within it becomes irregular and turbulence exists. Although the transition region can be identified as that in which the behaviour of fluid particles is different from what might be found elsewhere in the boundary layer, we can go little further with a precise description. In most cases the unstable, randomly fluctuating, transition region extends over a very small length of the body. Attention is drawn to these facts in Fig. 5.6(a). Downstream from the transition region most of the flow in the boundary layer is entirely turbulent and thickness increases further. However, turbulence must die out adjacent to the surface, and so below the turbulent layer is an even thinner, laminar sub-layer. The existence of the laminar sub-layer is hard to justify in the

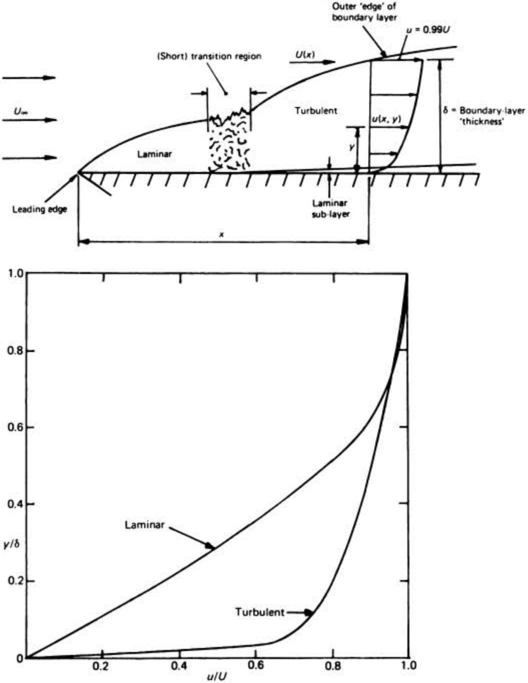

Fig. 5.6 Formation of a boundary layer: (a) principal characteristics; (b) typical variations of tangential velocity *u*.

transition region (and even harder to detect experimentally!) and consequently has been omitted from Fig. 5.6(a).

In a turbulent layer the continuous momentum changes between fluid particles result in a velocity distribution more nearly uniform than in a laminar layer (Fig. 5.6(b)). However, the velocity gradient in the sub-layer is considerably greater than in a wholly laminar layer and therefore the shear stress at the solid boundary for a turbulent layer is also greater.

Since the flow in the boundary layer is retarded by the action of shear stresses the energy of the fluid is relatively low. When the pressure at the outer edge of the boundary layer increases in the direction of flow in the main stream the kinetic energy of the boundary-layer flow decreases rapidly. Eventually, this kinetic energy is insufficient to overcome the retardation imposed by the 'adverse' pressure gradient so that the boundary layer separates from the body. A large, slow-moving eddy region develops downstream from the 'separation point' (or rather 'line' for a three-dimensional body) which supplements the flow in the wake as shown in Fig. 5.5(b). If separation of a laminar boundary layer occurs it is possible, in theory, to identify a separation streamline which emanates from the separation point and marks the division between the forward flow in the main stream and the reverse eddy flow. However, the separation region is unsteady and causes the separation point to oscillate back and forth. Further details on the general behaviour and properties of boundary layers are given in [2] and more advanced topics are examined in [3].

For the sake of definiteness we have discussed the boundary-layer flow over a fully immersed body, but it is often assumed that the preceding remarks apply equally to vehicles which travel at the air–water interface.

The actual distribution of the local shear stress on the hull of a moving displacement ship is exceedingly difficult to predict owing to the complexity of turbulent boundary-layer theory applied to three-dimensional bodies. An approximate method of calculation is given in [4] and a comparison is made in [5] with experimental data from both model and full-scale tests. Although the equations which attempt to describe the boundary layer are difficult to solve (but the development of large-capacity computers is easing that problem) it is the formulation of an adequately general tubulent-flow model that presents the analyst with the major barrier to progress.

The designer of a marine vehicle may be required to assess the extent of the laminar and turbulent boundary layers and thus to predict the transition zone. On a given vehicle these regions will depend on the turbulence intensity of the flow in the main stream, the speed of the vehicle and the surface roughness of the vehicle. While the laminar and turbulent régimes can be predicted with some accuracy the transition flow cannot. Furthermore, models for test work are often so small that the laminar and transition flows extend over a substantial part of the hull and most of the appendages, whereas the major proportion of the prototype hull would be covered by a turbulent boundary layer. Any extrapolation of the boundary-layer parameters through the transition region to the turbulent flow is thus likely to be suspect. In an attempt at a more accurate representation of the prototype flow a model is often equipped with turbulence stimulators to encourage the early onset of transition. This is achieved by fixing a row of studs (and sometimes pins or trip wires) close to the bow in order to precipitate an intense local disturbance, and experimental results seem to confirm the usefulness of these devices in the prediction of ship resistance.

5.4.2 *Flow in the Main Stream*

In the main stream the variation of tangential velocity along a normal to the body is negligible and thus viscous (shear) stresses must also be negligible. Relative to the vehicle the local velocity in the main stream is usually far smaller than the local sonic velocity so that the compressibility of the fluid can be ignored. (An exception could be the local velocity relative to the tips of large propellers used on hovercraft.) Thus we have no need to consider the local Mach number and we can assume that the flow in the main stream approaches that of an inviscid, constant-density fluid. The equations of motion for such a fluid may be linearized by the introduction of a potential function (or velocity potential) and the consequent assumption of irrotational flow in which *no* element of the moving fluid undergoes a net rotation [2]. As a result, there has been extensive mathematical treatment of the problem, especially for steady flow.

Suppose the flow were inviscid and steady throughout. The streamlines about a stationary body of revolution, remote from solid boundaries and interfaces, might then look like those shown in Fig. 5.7(a). The points labelled St are stagnation

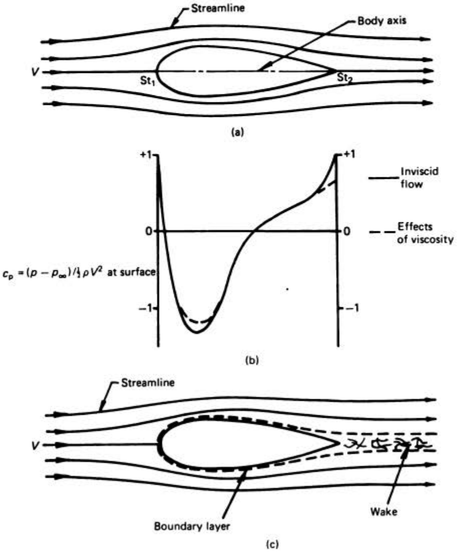

Fig. 5.7

points at which the body brings the fluid to rest. Provided that the geometry of the body is known, techniques are available [6] for calculating the surface velocities and the Bernoulli equation then yields the corresponding surface pressures. (The 'tailoring' of shapes to represent practical hull forms, e.g. airships, torpedoes and submarines is discussed in [7].) Thus, we can write

$$\frac{p - p_\infty}{\frac{1}{2}\rho V^2} = 1 - \left(\frac{q}{V}\right)^2 = c_p, \tag{5.1}$$

where p and q are the local pressure and velocity at any point on the surface of the body and p_∞ is a reference static pressure well upstream from the body. The dimensionless coefficient c_p is referred to as the 'pressure coefficient', and it can be seen that at a stagnation point, where $q = 0, c_p = 1$ and the corresponding stagnation pressure p_0 is given by

$$p_0 = p_\infty + \tfrac{1}{2}\rho V^2. \tag{5.2}$$

At other points on the body the values of c_p might conform with the distribution shown by the full line in Fig. 5.7(b). Resolution of the forces $p\delta S_w$, where δS_w is a small element of the (wetted) surface area, in the axial direction and subsequent summation of these forces over the surface show that the resultant axial force arising from differences of pressure is zero.

Now in viscous flow the boundary layer distorts the streamlines as shown in Fig. 5.7 (c). The location of the stagnation point St_1, closest to the leading edge of the body, is little affected by the boundary layer, but the rear stagnation point St_2 no longer exists owing to the presence of a wake. Provided that the boundary layer can be considered thin, Prandtl's theory suggests that the pressure at the outer edge of the layer is impressed on the surface of the body. In other words, inertia forces within the boundary layer acting in a direction normal to the surface of the body are negligible and thus the normal pressure gradient is considered to be insignificant. However, a second limitation of the Prandtl hypothesis is the assumption that the surface curvature of the body is small compared with the boundary-layer thickness. This is often the case, but not if an adverse longitudinal pressure gradient is sufficiently great to cause a rapid thickening, and thence separation, of the boundary layer near to the leading edge where the radius of curvature of the body surface is small. We may well find that although the pressure distribution over the body can be deduced for inviscid flow it is just at those locations where boundary-layer theory breaks down that a substantial departure from the measured distribution occurs. This is shown in Fig. 5.7 (b) where the broken line represents the actual variation of c_p. It is now clear from the modified distribution that the pressure drag can no longer be zero. On the other hand, assuming that the flow field still remains axisymmetric there will be no resultant force perpendicular to the axis of the body.

Much of what has been said in the context of deeply immersed vehicles applies also the mainstream flow about the submerged hull of a ship. It is reasonable to expect that the pressure distribution over the hull depends largely on the flow in the main stream and, in addition, pressure recovery is incomplete owing to the formation of a wake at the stern. Unfortunately, a considerable complication now arises from the presence and generation of gravity waves at the interface.

The steady mainstream flow (and also the boundary-layer flow) has a wave system superimposed upon it. In practice, the two flows are treated separately under the assumption that they co-exist without mutual interaction. This is reasonably accurate when the waves are *small* and we can then refer to a 'flow pattern' and a 'wave pattern'. Here small waves are considered to be those having a ratio of amplitude† to wavelength† of less than, say, one-fiftieth. The flow pattern may be thought of as a half of the flow about a special craft so constructed that the wetted part of the hull is reflected at the interface to form a double craft as shown in Fig. 5.8. The double craft is then totally immersed in the flow to form the basis of a useful technique for model testing in addition to offering a good opportunity for visualization of the flow pattern [8].

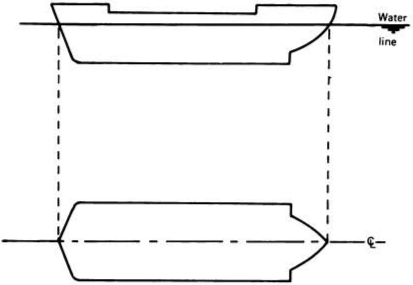

Fig. 5.8 The double-hull model.

The fine forms of naval hulls generate a substantially irrotational flow pattern in the main stream despite significant viscous effects in the boundary layer and the wake. In fact, the presence of the boundary layer must induce some rotational flow into the approaching irrotational flow in the main stream. Modern tanker forms with high *block coefficients*‡ and bluff bows have been found [9] to induce twin counter-rotating vortices which extend from the forward bilges into the downstream flow. The vortices emanate from the boundary layer and are generated by the viscous shear stresses there. The original vortices are thus wholly rotational, but as they trail downstream only the core remains so the outer portion tends to irrotational flow. Similar vortices are found at the tips of an aerofoil section wing of finite span and in a mathematical model these are superimposed on the main flow. An adequate description of the flow field is thus obtained except close to the points of origin and near the cores of the vortices. The mainstream flow around the hull may therefore be compared with flow close to the tip of a wing or around a lifting body but with the added complication of interface distortion.

† See Chapter 2 for definitions of these quantities.

‡ That is, the ratio (immersed volume)/(volume of a rectangular block whose length is the waterline length, breadth is the beam and depth is the draught). This ratio may be over 0.9 for a tanker whereas a frigate or destroyer might have a value of about 0.6.

5.4.3 *Distortion of the Air–Water Interface; Waves*

Surface waves are generated when a vehicle moves at or near the interface. (Generally, wind-induced gravity waves are encountered but, at this stage, we shall refrain from discussing any *unsteady* motion in a seaway.) The fluid forces acting on the hull of a vehicle moving steadily in calm water are influenced by the generated wave system. Nevertheless, it is reasonable to suppose that a theory based on the flow of an inviscid, constant-density fluid describes the mainstream conditions remote from the hull boundary layer. Indeed, it is conventional to suppose that the wave system is produced by the hull *plus* its boundary layer as the vehicle moves through the otherwise calm water.

Some analyses of the fluid motion combine the flow and wave patterns by adopting a suitable choice of a single parameter, namely, the potential function ϕ, the flow being assumed irrotational. The problem has been examined in [10] and we shall not elaborate on it further but simply point out the conditions which ϕ must satisfy. Assuming that ϕ is constructed for a distribution of sources and sinks in a uniform flow, then:

(i) the boundary conditions must be satisfied for the free surface;

(ii) to satisfy the distinction between the flow pattern and the wave pattern the mathematical form of ϕ requires an 'image' distribution of sources and sinks to prevent flow across the interface plane of symmetry (Fig. 5.8), and the latter must not violate this condition of no flow; and

(iii) unless some simple shape is to be used for the craft shown in Fig. 5.8, such as an ellipsoid or Rankine body, an assembly of sources and sinks must be 'tailored' to suit the hull form, which must itself be a stream surface.

The preceding mathematical technique is an extremely complicated application of standard hydrodynamic theory and solutions have only recently become available with the aid of large-capacity digital computers. Pressure distribution over the hull can be found from the stipulated form of ϕ and thus the wave-making resistance can be deduced.

Alternatively, to avoid this complication and yet retain a surprisingly accurate physical picture of the wave pattern we might proceed as follows. Considering the wave pattern only let us assume that:

(i) waves are initiated in the uniform flow by a disturbance at the bows of the ship;

(ii) the approximately uniform beam of a conventional ship will prevent the generation of waves as the water (assumed inviscid) slides past the hull; and

(iii) waves are initiated at abrupt changes of section – in particular at the start of the run (at the after cut-up†) – but these waves will be the 'opposite' of those generated at the bows.

Thus, using the idea of a localized disturbance at the bows and another of opposite sense near the stern, both superimposed on the steady uniform flow, it is possible to predict strikingly realistic wave patterns.

In 1887, Lord Kelvin developed a theory [11] to describe the wave patterns

† Usually abbreviated to ACU.

behind a moving pressure point at the interface (or, alternatively, a stationary disturbance in a uniform flow). He published [12] the first sketch of the wave system for a point of small area, but arbitrary shape moving uniformly in a straight line. This is shown in Fig. 5.9 and closely resembles the drawings of the wave pattern emanating from the bows of long, largely parallel-sided, model ships given earlier by William Froude [13]. Further work by Lord Kelvin appeared in 1904 [14] after which the method of analysis was known as 'Kelvin's method of stationary phase'. Essentially, the integration of a mathematical function is required which consists of a highly oscillatory, and largely self-cancelling, component and another component that varies only slightly over the range of integration, that is, the stationary phase. More details of the Kelvin wave pattern are given by Havelock [15].

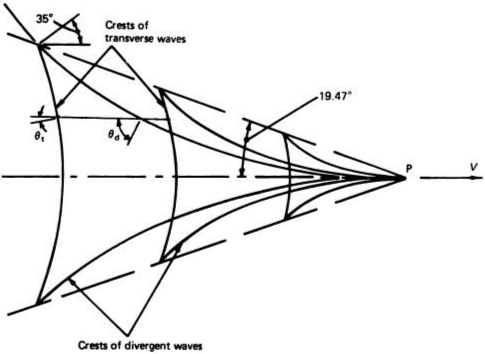

Fig. 5.9 Wave crests for surface pressure pulse moving in a straight line.

For the motion of a pressure point P in a straight line (see Fig. 5.9) let θ be the angle which defines the direction of the normal to a crest relative to the direction of steady forward velocity V. The wave pattern will, of course, move with P, that is, the pattern is stationary relative to P. It can be shown that two ranges of θ exist, namely θ_t and θ_d, given by

$$0 < \theta_t < 35° \quad \text{corresponding to transverse waves;}$$

$$35° < \theta_d < 90° \quad \text{corresponding to divergent waves.}$$

The two sets of waves intersect at a cusp when $\theta = \theta_t = \theta_d = 35°$ and the bounding 'cusp line' makes an angle arcsin $(1/3) = 19.47°$ with the direction of motion. At the cusp line both wave crests add to form the highest waves of the system. The theory has been reworked [16] to show that it can be extended to cover motion in a circular path, and the results are indicated in Fig. 5.10.

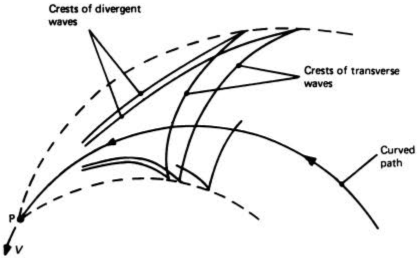

Fig. 5.10 Wave crests for surface pressure pulse moving along a curve.

We can assume for a ship that the bow and the stern act as a positive and negative pressure point respectively. The resulting combined wave pattern is somewhat like that of Fig. 5.11, and photographs presented in [16] confirm that the actual wave pattern is very similar to this. In practice, the transverse crests are observed most

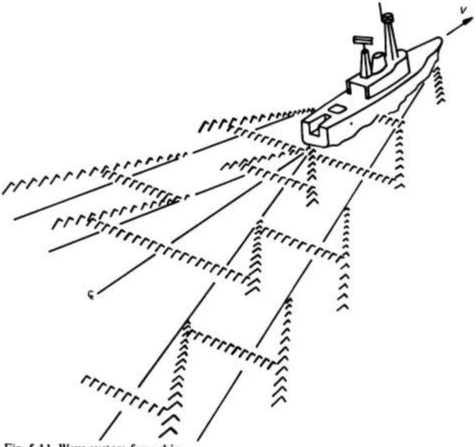

Fig. 5.11 Wave system for a ship.

readily close to the mid-section of a conventional ship or just aft of the stern for a ship at high speed. The stern waves are often more difficult to identify owing to the general disturbance produced by the wake. Furthermore, the divergent waves are discernible some way from the hull where they take the form of an echelon. This is because the height of the combined transverse–divergent crests decreases less rapidly than the separate transverse waves bounded by the cusp lines.

5.5 Resistance (Drag) with No Lift or Side Force

As we are concerned here with the steady motion of marine vehicles at low speeds the main supporting force arises from buoyancy. It is most unlikely that a deeply submerged vehicle could be designed so that precise equality between weight and buoyancy existed as there would undoubtedly be some redistribution of fluid forces over the vehicle as soon as motion commenced. A small, net hydrodynamic force, either upwards or downwards, would be generated which had, in general, a moment about the centre of mass of the vehicle. By the adjustment of, say, hydroplanes on a submarine it would be possible to approach a condition of zero, net, vertical hydrodynamic force on the hull. Similarly, once motion of a surface ship takes place the inevitable redistribution of pressure on the wetted hull modifies the fluid forces there. Regions of low pressure develop in the vicinity of, for example, a bluff bow or a square transom. In the first case a 'bows-down' attitude may result whereas the second case produces a 'sinkage by the stern' and is typical of high-speed craft when moving at low speeds. The wetted surface area changes, therefore, and we cannot really regard the separation of lift force from buoyancy force as a purely arbitrary matter.

Nevertheless, let us examine the forces on a vehicle with a fore-and-aft vertical plane of symmetry in the absence of both vertical and sideways dynamic forces. Weight and buoyancy force can be considered separately by means of hydrostatics. The only fluid force remaining is the drag, or, since this *is* the only force, we can use the conventional terminology 'resistance'. In general, of course, the total drag consists of a summation of forces associated with pressure *and* shear stress distributions over the wetted surface of the hull. Similarly, the total resistance can be considered to comprise two components:

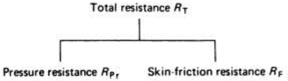

If the vehicle is deeply submerged then, owing to the presence of shear stresses at the surface of the body, a component of resistance arises from skin friction, that is, R_F. In addition, the presence of a boundary layer prevents pressure recovery as shown in Figs. 5.7 (b) and (c), and so another component, the viscous pressure resistance†, R_{PV}, also contributes to the total R_T and is the only component of

† In aerodynamics this component is usually called form drag. However, the word 'form' has other (mainly geometric) connotations in naval architecture and we shall therefore refrain from using it in the present context.

pressure resistance. Hence

$$R_T = R_{PV} + R_F = R_V \tag{5.3}$$

where R_V is called the viscous resistance.

A vehicle moving at the air–water interface raises extremely complicated analytical problems. To simplify the analysis it is necessary to make some crude assumptions about the behaviour of the flow. The main difficulty lies in the matter of wave formation as a result of ship motion. Waves generated by the moving ship significantly modify the hull pressure distribution compared with that which would be obtained if the waves were absent. We might, therefore, usefully break down the total resistance into components as follows:

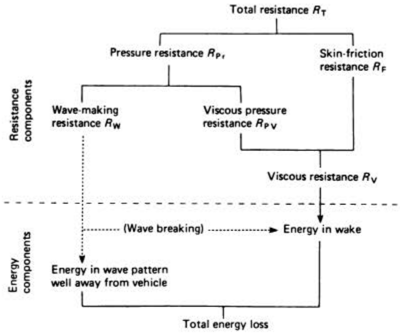

In this breakdown of resistance no interaction effects between the components are assumed to occur and the wave energy is related directly to the wave-making resistance experienced by the vehicle. Waves in a viscous fluid do not always have a continuous profile but sometimes break near the peaks. When this happens some energy is transferred from the wave pattern to the downstream viscous wake. Observation of the flow round tankers with bluff bows has shown that wave breaking occurs close to the bow. We would therefore expect a significant modification of the flow pattern near to the surface of the ship which would in turn affect the viscous resistance. This interaction should not be considered a direct source of resistance, however, because interaction between the wave formation and the boundary-layer growth occurs whether wave breaking is present or not. The energy of a wave system can be detected at large distances from the vehicle causing the disturbance. Eventually, the energy in the wake is finally dissipated by large-scale turbulence into thermal energy.

From the preceding component form of the total resistance we can write, for the interface vehicle,

$$R_T = R_W + R_{PV} + R_F. \tag{5.4}$$

This method of apportioning components of the total resistance is by no means rigorous nor is it adopted universally. Certainly the separation of R_T into numerous components independently identified can lead to additional difficulties of assessment. Some analysts do not, therefore, split R_{Pr} into separate contributions.

5.6 Fluid Forces from Momentum Considerations

5.6.1 *Resistance of a Deeply Submerged Vehicle*

The resistance to motion of a marine vehicle may be deduced by applying the steady-flow momentum equation to the fluid passing through a specified control volume of which the vehicle is an integral part. We shall assume that the fluid which flows past a deeply submerged, fixed, impermeable, axisymmetric vehicle is homogeneous and possesses uniform properties. The upstream flow approaches the body at a uniform, steady velocity V relative to the body in a direction parallel to its axis of symmetry as shown in Fig. 5.12. Fixed in the body are rectangular coordinate axes Oxyz centred at O on the axis of symmetry with Ox positive in the direction of V, Oy positive to port and Oz positive downwards. We shall concentrate on the fluid passing through a control volume whose outer surface, entirely within the

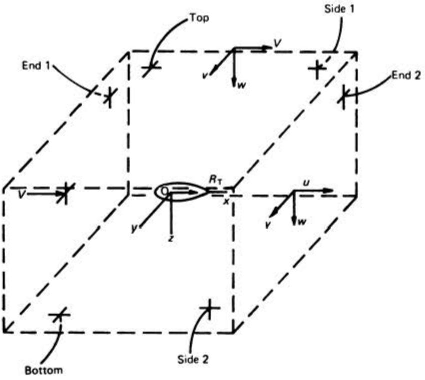

Fig. 5.12

fluid, forms a rectangular parallelepiped surrounding the vehicle. The vehicle itself forms the inner surface of the control volume. End planes 1 and 2 of the outer surface are, respectively, well upstream and well downstream from the body and each is parallel to the Oyz plane. The side planes and the top and bottom planes are located in the main stream far from the body and so shear stresses and flow disturbances on these planes are negligible. These four planes are parallel to V and the local velocities on them are V, v and w in the Ox, Oy and Oz planes respectively. At end plane 2 the local velocity components are u, v and w relative to the body with u in the Ox direction. The velocity V is constant over the whole of end plane 1, the side planes and the top and bottom planes. However, the velocities u, v and w may vary over any given plane and from one plane to another. We shall use the symbol A to denote area generally and is here referred to any of the planes associated with the control volume.

No mass of fluid is assumed to accumulate inside the control volume and so continuity requires that

$$\int_{\text{end 1}} \rho V \mathrm{d}A + \int_{\text{top}} \rho w \mathrm{d}A + \int_{\text{side 1}} \rho v \mathrm{d}A = \int_{\text{end 2}} \rho u \mathrm{d}A + \int_{\text{bottom}} \rho w \mathrm{d}A + \int_{\text{side 2}} \rho v \mathrm{d}A,$$

that is,

$$\int_{\text{bottom}} \rho w \mathrm{d}A + \int_{\text{side 2}} \rho v \mathrm{d}A - \int_{\text{top}} \rho w \mathrm{d}A - \int_{\text{side 1}} \rho v \mathrm{d}A = \int_{\text{end 2}} \rho(V - u)\mathrm{d}A \tag{5.5}$$

since V is constant over the upstream end plane 1 and an element of area δA of a plane tends to $\mathrm{d}A$ in the limit $\delta A \to 0$.

Suppose now that all body forces (magnetic, electric, gravitational, etc.) are absent and that end plane 2 is sufficiently far from the body to ensure that the pressure p_2 is constant over the plane and equal to the pressure p_1 over end plane 1. At a given depth z, along Oz, the hydrostatic forces on the end planes are of course equal and opposite. The only force exerted by the control volume is that arising directly from contact between the body and the viscous fluid. This force is R_{T} in the Ox direction and is the total resistance of the vehicle. Using Newton's Second Law of Motion we can equate the force exerted by the fluid on the vehicle to the decrease of momentum flux along Ox within the control volume. Thus,

$$\begin{aligned} R_{\mathrm{T}} &= \left(\int_{\text{end 1}} \rho V^2 \mathrm{d}A + \int_{\text{top}} \rho w V \mathrm{d}A + \int_{\text{side 1}} \rho v V \mathrm{d}A \right) - \left(\int_{\text{end 2}} \rho u^2 \mathrm{d}A + \int_{\text{top}} \rho w V \mathrm{d}A + \int_{\text{side 1}} \rho v V \mathrm{d}A \right) \\ &= \int_{\text{end 2}} \rho(V^2 - u^2)\mathrm{d}A - V \left(\int_{\text{bottom}} \rho w \mathrm{d}A + \int_{\text{side 2}} \rho v \mathrm{d}A - \int_{\text{top}} \rho w \mathrm{d}A - \int_{\text{side 1}} \rho v \mathrm{d}A \right) \end{aligned}$$

since V is constant. By virtue of Equation (5.5) we can write, for constant ρ,

$$R_{\mathrm{T}} = \rho \int_{\text{end 2}} (V^2 - u^2)\mathrm{d}A - \rho V \int_{\text{end 2}} (V - u)\mathrm{d}A$$

which reduces to

$$R_{\mathrm{T}} = \rho \int_{\text{end 2}} (V - u)u\mathrm{d}A. \tag{5.6}$$

The flow through end plane 2 may be divided into a viscous region containing the wake trailing downstream from the body and the main stream where viscous effects are negligible. In the main stream Bernoulli's equation applies to any streamline between end planes 1 and 2; (remember that our earlier assumptions satisfy the necessary conditions to make the application valid). Because we have taken $p_1 = p_2$ the velocity of the fluid in the main stream at end plane 2 must be V. Thus, outside the wake $V - u = 0$ and inside the wake $u < V$. Hence,

$$R_\mathrm{T} = \rho \int_{\text{wake}} (V - u) u \, \mathrm{d}A. \tag{5.7}$$

Equation (5.7) implies that the results obtained by traversing a pitot-static tube across the far wake should yield values of u from which R_T could be calculated. However, the flow in the wake is unsteady and this raises problems in the interpretation of measurements. In practice we cannot extend the planes forming the control volume too far. Even in the absence of the confining walls of a towing tank or wind tunnel, etc., it is not usually possible to obtain data from traverses far enough downstream for the pressure in the fluid to have returned to a constant value. Consequently, wake traverses must be made in a plane normal to V at some location nearer to the stern of the body than plane 2, say at plane 3.

Let us assume that the flow between plane 3 and the far downstream plane 2 acts as though it were steady and inviscid. Using the subscript 2 and 3 to indicate conditions at planes 2 and 3 respectively we may write, from continuity,

$$u_2 \delta A_2 = u_3 \delta A_3$$

for constant-density flow. Under our specified conditions Bernoulli's equation may be applied between planes 2 and 3 so that, neglecting changes of elevation,

$$p_2 + \tfrac{1}{2}\rho u_2^2 = p_3 + \tfrac{1}{2}\rho u_3^2$$

for a given streamline.

The stagnation, or total, pressure at plane 3 is defined as

$$p_\mathrm{st} = p_3 + \tfrac{1}{2}\rho u_3^2$$

and so

$$\tfrac{1}{2}\rho u_3^2 = (p_\mathrm{st} - p_2) - (p_3 - p_2)$$

to give finally

$$\frac{u_3^2}{V^2} = \frac{p_\mathrm{st} - p_2}{\tfrac{1}{2}\rho V^2} - \frac{p_3 - p_2}{\tfrac{1}{2}\rho V^2} = t - c_\mathrm{p}$$

where

$$c_\mathrm{p} = \frac{p_3 - p_2}{\tfrac{1}{2}\rho V^2} = \frac{p_3 - p_1}{\tfrac{1}{2}\rho V^2}$$

is the local pressure coefficient (compare Equation (5.1)). From the definition of t we see that, at plane 2,

$$t = u_2^2 / V^2.$$

Thus, the wholly viscous, total resistance of the deeply submerged body is now

$$R_{\mathrm{T}} = \rho \int_{\text{wake at plane 2}} (V - u_2) u_2 \, \mathrm{d}A_2 = \rho \int_{\text{wake at plane 3}} (V - u_2) u_3 \, \mathrm{d}A_3 .$$

With the appropriate substitutions we then find that

$$R_{\mathrm{T}} = \rho V^2 \int_{\text{wake at plane 3}} (1 - t^{\frac{1}{2}})(t - c_{\mathrm{p}})^{\frac{1}{2}} \mathrm{d}A_3 \tag{5.7a}$$

which may be evaluated from a traverse recording stagnation and static pressures.

Another problem arises when the body is a model enclosed in the test section of a wind or water tunnel of constant cross section. Should this be the case then shear stresses will act at the boundaries of the control volume owing to the boundary layer there. The streamline pattern about the body will be altered significantly by the plane walls of the tunnel which are themselves streamline surfaces. Finally, since the velocities of fluid particles in the wake are less than those in the main stream continuity across the end planes of the constant-area test section demands that the velocity in the main stream at end plane 2 must exceed V. Hence $p_2 < p_1$ and an additional force, arising from this difference of pressure, will act in the Ox direction. Assuming that p_1 and p_2 are uniform over end planes 1 and 2 respectively, and that the area of each plane is A, then

$$R_{\mathrm{T}} = (p_1 - p_2)A + \rho \int^{A} (V - u) u \, \mathrm{d}A . \tag{5.8}$$

Some of these problems may be overcome if the cross sectional area of the test section can be changed. However, this facility is difficult to construct and operate reliably, and it is generally more rewarding to use the numerous correction factors available to deduce the actual resistance R_{T} from the pitot results. Alternatively, the resistance can be measured directly on a mechanical balance or some variant of it. Obviously, for inviscid flow there is no wake and $p_1 = p_2$, showing therefore that $R_{\mathrm{T}} = 0$, as we should expect.

Equations (5.7), (5.7a) and (5.8) apply equally to vehicles moving in any fluid provided that the effects of compressibility can be neglected. This theory forms the basis of an indirect method of measuring the drag experienced by wings, aerofoils, hydrofoils, struts, fuselages and so on.

5.6.2 *Resistance of a Ship at the Interface*

The procedure used for the fully submerged vehicle can be applied to an interface vehicle, but the presence of the interface calls into play additional boundary conditions. Let us consider a vehicle which, for the sake of definiteness, can be a ship held stationary at the air–water interface by an external force equal to R_{T} but in the opposite direction. The approach flow is a liquid of constant properties moving at a uniform velocity V relative to the ship, as shown in Fig. 5.13.

Rectangular coordinate axes Oxyz are fixed in the ship with Ox in the fore-and-aft vertical plane of symmetry which is parallel to the direction of V. Distances x, y, z are measured respectively along Ox, Oy and Oz. The surface of the fixed control

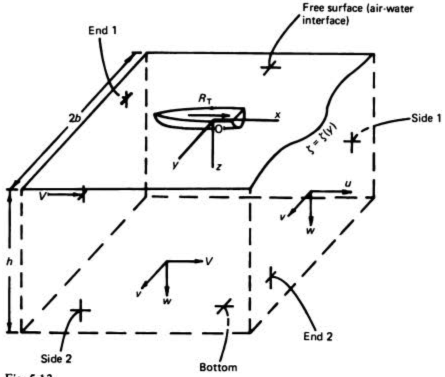

Fig. 5.13

volume surrounding the ship is made up as follows:

(i) End planes 1 and 2 well upstream and well downstream from the ship respectively. These planes are both perpendicular to Ox.

(ii) Side planes 1 (starboard) and 2 (port) which are vertical and parallel to the Oxz plane. Each side plane is at a distance b from Ox.

(iii) The air–water interface (usually referred to as the 'free' surface) forms the top surface along with the wetted hull of the ship. When the flow is undisturbed by the presence of the ship the free surface coincides with the Oxy plane

(iv) The bottom plane is parallel to the Oxy plane and at a depth h measured along Oz.

Any local disturbance of the flow arising from the presence of the body is taken to be small on both side planes and the bottom plane; the local velocities on these planes then have components, V, v, w parallel to Ox, Oy, Oz respectively. Shear stresses are also assumed to be absent on these planes.

On end plane 1 the only velocity is V and this is constant. At end plane 2 the free surface is distorted owing to wave generation, and the vertical displacement of the surface is described by $z = \zeta$ = function (y) at a given x. The depth of the bottom plane at end plane 2 is therefore $h - \zeta$ below the free surface. The local velocity components relative to the ship on end plane 2 are u, v, w parallel to Ox, Oy, Oz respectively. These velocities are considered steady but are functions of y and z; only V is steady *and* constant. No flow crosses the top surface of the control volume and therefore the continuity requirement can be expressed as

$$\int_{\text{side 1}} \rho v \mathrm{d}A - \int_{\text{bottom}} \rho w \mathrm{d}A - \int_{\text{side 2}} \rho v \mathrm{d}A = \int_{-b}^{+b} \int_{\zeta}^{h} \rho u \mathrm{d}z \mathrm{d}y - \int_{-b}^{+b} \int_{0}^{h} \rho V \mathrm{d}z \mathrm{d}y \qquad (5.9)$$

where again $\mathrm{d}A$ represents the limit of an element of plane area δA.

In the Ox direction the decrease of momentum flux of the liquid passing through the control volume is given by

$$V\left(\int_{\text{side 1}} \rho v \mathrm{d}A - \int_{\text{bottom}} \rho w \mathrm{d}A - \int_{\text{side 2}} \rho v \mathrm{d}A\right) + \int_{-b}^{+b}\int_{0}^{h} \rho V^2 \,\mathrm{d}z\,\mathrm{d}y - \int_{-b}^{+b}\int_{\zeta}^{h} \rho u^2 \,\mathrm{d}z\,\mathrm{d}y$$

since V is constant. This expression, after substitution from Equation (5.9), reduces to

$$\rho \int_{-b}^{+b}\int_{\zeta}^{h} (V-u)u\,\mathrm{d}z\,\mathrm{d}y. \tag{5.10}$$

Note the similarity between expression (5.10) and the right-hand side of Equation (5.6). However, since ζ is not everywhere zero at end plane 2 and no flow takes place across the interface we cannot now put $V = u$ outside the wake. The integration in (5.10) must therefore be carried out over the whole area of end plane 2.

Now the fluid force exerted on the vehicle by the fluid, given by expression (5.10), represents only a part of the total force on the vehicle. Additional steady forces, having components inclined to the Oxy plane, may occur on the top surface of the control volume owing to the ambient pressure over the distorted region downstream from the vehicle. The projected area of the distortion in the Oyz plane is equal to

$$\int_{-b}^{+b} \zeta \,\mathrm{d}y$$

at end plane 2. Assuming uniform atmospheric pressure p_a over the interface, the net force exerted by the top plane on the atmosphere in the Ox direction is

$$p_\mathrm{a} \int_{-b}^{+b} \zeta \,\mathrm{d}y.$$

The pressure distribution on the end planes also gives rise to forces on the control volume in the Ox direction. The resultant 'pressure' force exerted *by* the end planes on the fluid *outside* the control volume in the Ox direction is

$$\int_{-b}^{+b}\int_{\zeta}^{h} p_2 \,\mathrm{d}z\,\mathrm{d}y - \int_{-b}^{+b}\int_{0}^{h} p_1 \,\mathrm{d}z\,\mathrm{d}y$$

where p_1 and p_2 are the local pressures on end planes 1 and 2 respectively. It cannot be assumed that p_1 and p_2 are equal and constants as they were for the fully submerged vehicle because the free surface is distorted and there is no flow across it.

We now apply Newton's Second Law of Motion in the Ox direction to the fluid passing through the control volume. Thus, the total force exerted by the fluid on its surroundings must equal the decrease of momentum flux of the fluid and so for the Ox direction

$$R_\mathrm{T} + \int_{-b}^{+b}\int_{\zeta}^{h} p_2 \,\mathrm{d}z\,\mathrm{d}y - \int_{-b}^{+b}\int_{0}^{h} p_1 \,\mathrm{d}z\,\mathrm{d}y + p_\mathrm{a}\int_{-b}^{+b} \zeta \,\mathrm{d}y = \rho \int_{-b}^{+b}\int_{\zeta}^{h} (V-u)u\,\mathrm{d}z\,\mathrm{d}y. \tag{5.11}$$

The terms in Equation (5.11) which involve pressure can be related to each other by the use of the steady-flow energy equation [2]. Shaft work and heat transfer (to or from the surroundings) are absent from our problem, so that for flow in a stream filament connecting the end planes we can write, noting that z is measured downwards from the undisturbed free surface,

$$\frac{p_1}{\rho g} + \frac{V^2}{2g} - z_1 = H = \frac{p_2}{\rho g} + \frac{1}{2g}(u^2 + v^2 + w^2) - (z_2 - \zeta) + e \tag{5.12}$$

where H is the total energy of the fluid per unit weight and e represents the loss of energy per unit weight† between the end planes. At the interface $p_1 = p_a$ and $z_1 = 0$, therefore,

$$\frac{p_a}{\rho g} + \frac{V^2}{2g} = H \tag{5.13}$$

because V is constant over the upstream end plane. Substitution for p_1 and p_2 from Equation (5.12) into Equation (5.11) and rearrangement of the limits of integration leads to the expression

$$\begin{aligned} R_T = {} & \rho \int_{-b}^{+b}\int_{\zeta}^{h} (V - u)u\,dz\,dy + \rho g H \int_{-b}^{+b} \zeta\,dy - \tfrac{1}{2}\rho V^2 \int_{-b}^{+b}\int_{0}^{h} dz\,dy \\ & + \tfrac{1}{2}\rho \int_{-b}^{+b}\int_{\zeta}^{h} (u^2 + v^2 + w^2)\,dz\,dy + \tfrac{1}{2}\rho g \int_{-b}^{+b} \zeta^2\,dy \\ & + \rho g \int_{-b}^{+b}\int_{\zeta}^{h} e\,dz\,dy - p_a \int_{-b}^{+b} \zeta\,dy. \end{aligned} \tag{5.14}$$

The first, third and fourth terms on the right-hand side of Equation (5.14) can now be written as

$$\tfrac{1}{2}\rho \int_{-b}^{+b}\int_{\zeta}^{h} \{v^2 + w^2 - (u - V)^2\}\,dz\,dy - \tfrac{1}{2}\rho V^2 \int_{-b}^{+b} \zeta\,dy.$$

With the aid of this expression and Equation (5.13) the resistance equation (5.14) is seen to be

$$\begin{aligned} R_T = {} & \tfrac{1}{2}\rho \int_{-b}^{+b}\int_{\zeta}^{h} \{v^2 + w^2 - u_{abs}^2\}\,dz\,dy + \tfrac{1}{2}\rho g \int_{-b}^{+b} \zeta^2\,dy \\ & + \rho g \int_{-b}^{+b}\int_{\zeta}^{h} e\,dz\,dy \end{aligned} \tag{5.15}$$

where $u_{abs} = (u - V)$ is the absolute velocity component of the fluid along Ox at end plane 2 which would be seen by an observer moving with the stream at a velocity V.

The first double integral on the right-hand side of Equation (5.15) represents the contribution to resistance arising from local changes in the kinetic energy and momentum of the fluid. These changes result from orbital velocities associated with

† Grouped in e are the increase of internal energy per unit weight and the unrecovered energy per unit weight 'lost' to friction.

wave formation *and* shear stresses in the viscous wake. (In a seaway formed by wind-induced waves orbital velocities already exist, as we saw in Chapter 2, and we are thus more properly concerned with changes of orbital velocity.) The second integral on the right-hand side of Equation (5.15) represents the change of potential energy as a result of wave formation, and the final double integral represents the change of internal energy due to friction. It is sometimes assumed that the wave-making resistance R_W is given by the sum of the first two terms on the right-hand side of Equation (5.15) and that the viscous resistance R_V is given by the final term. Interaction between these two sources invalidates the generality of such a break-down, although an acceptable accuracy may well be obtained when $R_W \gg R_V$, that is, when the downstream velocities of fluid particles resulting from wave formation greatly exceed those induced by friction forces. Nevertheless, if we consider again the motion of a deeply submerged vehicle for which free-surface effects are negligible, the development of Equation (5.8) leads to Equation (5.15) but with the second integral on the right-hand side omitted. Thus for the deeply submerged vehicle

$$R_T = \tfrac{1}{2}\rho\int^A (v^2 + w^2 - u_{abs}^2)\mathrm{d}A + \rho g\int^A e\mathrm{d}A, \tag{5.16}$$

and clearly the first integral here plays a part in the now wholly viscous resistance as it does in the assessment of wave resistance for surface ships.

5.7 Resistance of Deeply Submerged Vehicles

The total resistance to the steady motion of a deeply submerged vehicle is given by

$$R_T = R_{PV} + R_F = R_V, \tag{5.3}$$

the viscous resistance. A dimensionless total resistance coefficient can be defi

$$C_T = \frac{R_T}{\frac{1}{2}\rho V^2 A} \tag{5.17a}$$

where $\frac{1}{2}\rho V^2$ is the dynamic pressure of the flow in the approaching main stream and A is a characteristic area of the body. Thus, in dimensionless terms, Equation (5.3) becomes

$$C_T = C_{PV} + C_F \tag{5.18}$$

where the viscous pressure resistance coefficient is given by

$$C_{PV} = \frac{R_{PV}}{\frac{1}{2}\rho V^2 A} \tag{5.17b}$$

and the skin-friction resistance coefficient is given by

$$C_F = \frac{R_F}{\frac{1}{2}\rho V^2 A}. \tag{5.17c}$$

It is useful at this stage to associate the relative magnitudes of the resistance components in Equation (5.18) with the shape of the body. We regard a 'bluff' body as one for which $C_{PV} \gg C_F$ since then boundary-layer separation produces a large wake. A sphere, cylinder or disc set across the main flow are examples of bluff bodies. On the other hand, a streamlined body is so shaped that it does not experience large, adverse pressure gradients. The boundary layer thickens slowly and so separation occurs towards the rear of the body or may even be avoided. The wake is small and skin friction now predominates so that we may anticipate a considerable decrease in C_T. To emphasize the benefit of streamlining a body it is worth noting that for a given Reynolds number the resistance per unit span of a smooth cylinder with the cross section of a low-speed aerofoil may be no more than that of a smooth circular-section cylinder having a diameter of 0.005 of the length between the front and rear points of the aerofoil.†

When systems to be compared are dynamically similar to each other the corresponding coefficients in Equation (5.18) are equal. Since geometric similarity then prevails, the area A can be related to any component of the vehicle, for example, the area of the fin, rudder, sonar dome, etc. However, it is rather more logical to take A as the wetted surface area of the hull, S_W, or the square of the length overall, because it is the hull that is principally responsible for R_T. Dimensional analysis suggests that all the resistance coefficients in Equation (5.18) are functions only of Reynolds number when the effects of compressibility, surface tension and cavitation are neglected. Experiments have confirmed this dependence for both laminar and turbulent flows in the boundary layer. It was pointed out in Section 4.5.4 that difficulty is experienced in obtaining equality of Reynolds numbers between the bare hulls of a model and prototype of a deeply submerged vehicle. However, provided the model speed is not too low and turbulence stimulators are used in the bow region satisfactory results may be obtained. This is not so when model appendages are considered because these have small dimensions compared with the hull and yet experience the same forward velocity. The corresponding Reynolds number, based on the fore-and-aft length of the appendage (e.g. the chord length of an aerofoil if the appendage has that cross section), may be lower than the critical value so that the boundary-layer flow could be substantially laminar compared with predominantly turbulent flow on the prototype appendage. It is, therefore, difficult to ensure that the flow patterns about the model and prototype appendages are similar. In a practical analysis, attention is given first to the assessment of C_T for the bare hull to which is added the total appendage resistance estimated separately. But this procedure ignores the interaction between the flows about the appendages and the hull.

Instead of a bare hull of the model suppose we consider a deeply submerged, thin, smooth, rectangular flat plank of the same length and wetted area which is towed at a constant speed through still water in a direction parallel to its length. Further, let us assume (i) that wave resistance is negligible and (ii) that $C_{PV} = 0$ since the cross sectional area of the plank is exceedingly small. The resistance to motion arises entirely from skin friction, and comprehensive tabulated data for the resistance of planks such as this are readily available.

Using the subscripts M and P for the model and the prototype respectively, we might now reason as follows. First, assume that $(C_F)_M$ is given by the plank resistance corresponding to the model Reynolds number $(Re)_M$. Next, measure $(C_T)_M$ by one of the various methods discussed in Section 4.6. Now $(C_{PV})_M$ can be found

† This length is associated with the chord length of an aerofoil and is defined more precisely in Chapter 6.

from Equation (5.18), that is

$$(C_{PV})_M = (C_T)_M - (C_F)_M \,. \tag{5.19}$$

The model results must now be related to those of the prototype. As we have seen, dynamic similarity cannot be achieved between the model and prototype owing to the geometric scale that must be used. The range of $(Re)_M$ is thus substantially lower than the range of $(Re)_P$ at practical operating speeds. As a rough guide the range of $(Re)_M$ is about $6 \times 10^5 - 8 \times 10^6$ whereas $(Re)_P$ can be as high as 2×10^9.

Nevertheless, let us continue by assuming that $(C_{PV})_M$ for the model range of Re is constant and that it remains unchanged in the range of Re for the prototype. There is certainly experimental evidence to support this contention, at least over the range of $(Re)_M$ shown in Fig. 5.14†. The total resistance coefficient for the prototype now follows from

$$(C_T)_P = (C_{PV})_M + (C_F)_P \tag{5.20}$$

where $(C_F)_P$ is obtained from plank data for the value of $(Re)_P$.

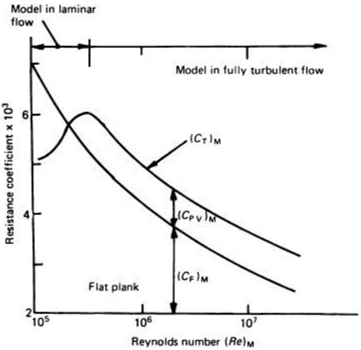

Fig. 5.14 Typical resistance coefficients for a deeply submerged model hull.

The total resistance of a model is often measured by transducers carried below the interface and mounted between the model and its support so as to minimize the effects from wave making by the travelling supports. Use is made also of 'idle runs' in which the model is left off its supports. Care must be taken to account for,

† The shape of the C_F curve for the smooth, thin, flat plank is what we would expect from turbulent boundary-layer theory. That is, $C_F \propto (Re)^{-1/5}$, where Re is based on the length of the plank and use is made of the empirical one-seventh power variation of velocity with distance through the boundary layer measured from the solid surface.

or eliminate, the interference of the flow by the proximity of the walls and the bottom of the various types of water tank used for the tests. Although this procedure may form the basis of a practical analysis of the resistance of submarines we must now look critically at the assumptions involved. The plank data that have been formulated in the past were obtained on nominally smooth planks. Any significant surface roughness was removed by applying a varnished coating to the surface. Unlike flow in pipes, there is no question of a fully developed flow for flat planks; the boundary layer continues to grow with distance from the leading edge. Thus a particular roughness height and distribution will have a profound influence on the boundary-layer flow near to the leading edge of the plank, but the effects decrease downstream as the thickness of the boundary layer increases. Consequently, the skin-friction resistance coefficient of a rough plank will depend on its length as well as the geometry of the roughness. Furthermore, we have indicated already the immense difficulty of modelling roughness even though it is known that roughness plays an important part, especially near the leading edge, in the determination of skin-friction resistance for streamlined vehicles. Even if it were possible to provide geometric similarity of roughness the question arises as to which model-roughness Reynolds number to adopt: that corresponding to $(Re)_M$ or to $(Re)_P$, since equality of Reynolds number cannot usually be achieved. The most reliable data for C_F are therefore obtained from smooth bodies – in this case planks – and some correlation factor is thus required to transfer these data to model and prototype hulls.

A second, and important, difference between flat planks and submarine hulls concerns the surface shape. It is clear that the lengths of streamlines about a curved surface between two fixed points on the axis of symmetry are greater than those between the same two points on a flat plank of the same length. For a given approach velocity the average velocity of a fluid particle close to a curved surface must therefore be larger than that of a particle flowing past the equivalent plank. For the flow of a viscous fluid these remarks apply equally to the flow in the main stream outside the boundary layer. Since particles in contact with the submarine are at rest, this must mean that the local rate of change of tangential velocity with respect to distance normal to the surface of the submarine must be greater than that for the plank. Consequently, the corresponding mean shear stress at the surface of the submarine exceeds that for the plank. The surface areas of the plank and the corresponding submarine are equal, so that C_F for the model is somewhat larger than C_F for the plank (theory suggests, however, that this difference may not be excessive). Equation (5.19) shows that the 'curvature' effect and separation resistance, should separation occur, are included in $(C_{PV})_M$.

The problem of assessing the resistance of appendages has been raised already. Although tests on a bare hull remove the difficulty of low Reynolds-number flows about the hydroplanes, fin and rudder on the model we must again adopt a correlation factor to take account of the interference effects.

As a result of these difficulties a correlation allowance C_A is defined as

$$C_A = \begin{pmatrix} (C_T)_P \\ \text{from full-} \\ \text{scale tests} \end{pmatrix} - \begin{pmatrix} (C_T)_P \\ \text{from Equation} \\ (5.20) \end{pmatrix}. \tag{5.21}$$

Here C_A will include the effects of differences in roughness, curvature and corner interaction. Experience has shown that a range of values of C_A, applicable to different types of vehicle, can be adopted with some measure of confidence. Nevertheless, should an unusual form of vehicle be required the appropriate value of C_A could be far removed from known values for other vehicles. Values of C_A for submarines might be as great as 1.2×10^{-3} as a result of the large number of excrescences and protuberances on the full-scale hull which are not simulated in the model tests. The significance of C_A in this case can now be appreciated since a typical value of $(C_T)_P$ calculated from Equation (5.20) may be 2.5×10^{-3}.

So far we have discussed a method of predicting the resistance of a new prototype submarine. The surface roughness arising from the painted hull, say, can be predicted (and measured) with considerable accuracy. However, in service C_T will increase as a result of both fouling and corrosion. Fouling is caused by animal and vegetable growth, and these can be controlled effectively by anti-fouling paints containing some toxic material. Corrosion can occur if the paint coating is broken and, furthermore, the subsequent erosion of the hull serves to increase roughness and thus resistance. These points will be considered again later in the context of surface ships.

5.7.1 *Benefits of a Streamlined Submarine*

Two geometric parameters are required to specify the extent to which a submarine is streamlined: the elongation of the hull may be described by the *slenderness ratio* defined as L_{ov}/d_{max}, where L_{ov} is the overall length of the bare hull and d_{max} is the corresponding maximum diameter, or the equivalent diameter of a non-circular cross section; and the *prismatic coefficient* defined as $\nabla/L_{ov}A_{max}$, where ∇ is the immersed volume of the hull and A_{max} is the corresponding maximum cross sectional area, which indicates the departure of the hull from a uniform prism of volume $L_{ov}A_{max}$. If the submarine has circular frames the prismatic coefficient is $4\nabla/\pi L_{ov}d^2_{max}$. The effects of these parameters on the resistance components of several submarine designs led eventually to the present form for the nuclear-powered boats.

The *USS Nautilus* was designed in 1948 to test a pressurized nuclear power plant at sea with good performance at the air–water interface as a primary consideration. The hull configuration was, therefore, not unlike those of earlier designs, as shown in Fig. 5.15. On the other hand, *USS Albacore* was developed simultaneously, but separately, to demonstrate the improvement in submerged performance obtained by using a single, large, efficient screw and a body-of-revolution hull form. The shape of the hull was that of an elongated tear drop (Fig. 5.16) and little account was taken of the performance at the interface. This is a reasonable approach for nuclear submarines which operate deeply submerged over long periods and often at high speeds.

Figure 5.17 shows the resistance of deeply submerged, steadily moving submarines, each with a volume displacement of about 2800 m^3 ($\cong 10^5$ ft^3) deduced from model tests on bare hulls [17]. The appendages were not considered for this comparative analysis. As the slenderness ratio increases for a body of revolution,

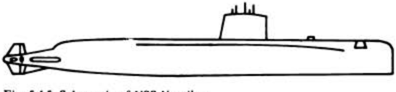

Fig. 5.15 Schematic of *USS Nautilus*.

Fig. 5.16 Schematic of *USS Albacore*.

of constant immersed volume, the surface area also increases and therefore the skin-friction resistance increases. In contrast, the adverse pressure gradient over the rear of the body decreases, as does the size of the wake, and the viscous pressure resistance also becomes smaller. Alternatively, a reduction in the slenderness ratio increases both the size of the wake and the viscous pressure resistance. Between these two extremes is a minimum value of total resistance which occurs when the slenderness ratio is about 6. Point 1 on Fig. 5.17 corresponds to the *Albacore*. The geometry of this boat is seen to be near the optimum, which accounts for its success when

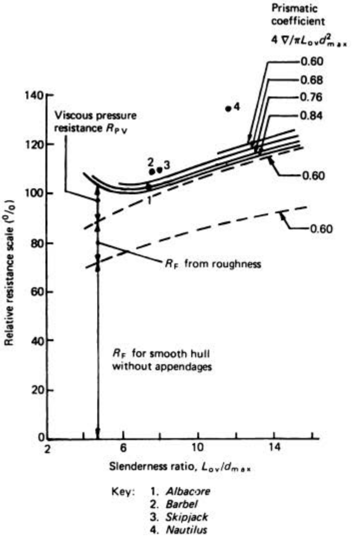

Fig. 5.17 The benefits of streamlining.

operating fully submerged. *USS Nautilus*, shown in point 4, is badly designed from the point of view of submerged performance owing to the large contribution of R_{PV}. Subsequently, the best features of both these submarine hulls were incorporated into *USS Barbel* and *USS Skipjack* whose relative positions are also shown in Fig. 5.17.

The major component of bare-hull resistance arises from skin friction and this is significantly affected by surface roughness. (In Fig. 5.17 an arbitrary allowance for roughness was made.) Apart from roughness, the effect of appendages on the total resistance of the boat is to increase C_{PV} because C_F for the appendages is small. Although much effort is made to keep the appendage resistance low it often affects C_T for a submarine more than major changes in hull design. For example, the bridge fin may account for 15–30 per cent of the bare-hull resistance, while the additional contribution from hydroplanes, rudder, shaft, struts, etc. may raise the proportion to 50 or 60 per cent.

Proposals for constructing commercial submarines have been much discussed from time to time [18]. The chief advantages of such vessels would be elimination of wave resistance and the independence from weather conditions. For a given volume displacement the submarine has a greater wetted surface area than a surface ship and therefore a larger value of R_F for a given speed. Only when high cruising speeds are contemplated, say above 12 ms^{-1} ($\cong$ 24 knots), is this hydrodynamic disadvantage overcome to yield a value of R_T for the submarine smaller than that for the ship. However, problems of construction, docking and operation, and the public's probable aversion to underwater travel over long distances, are the most likely reasons preventing the adoption of very large (super) submarines.

5.8 Resistance of Interface Vehicles

The following discussion will be confined to the low-speed steady motion of ships at the air–water interface which is disturbed only by the passage of the ship. As with submarines it is unlikely that an accurate calculation or measurement could be achieved of both the pressure distribution over the wetted hull and the aerodynamic pressure distribution on the above-water profile (including the superstructure). Instead, use is made of overall measures and estimates of the contributions to the total resistance in a way similar to that for the deeply submerged vehicle examined earlier. Separate attention is given to the aerodynamic and the hydrodynamic contributions to the overall resistance of the complete ship, although the hydrodynamic forces are generally the most important. (Some exceptions to this might be ships with propulsion failures adrift in gales or trawlers with heavy icing on the superstructure.)

As a starting point Equation (5.4) is adopted as a reasonable, if not necessarily the best, way of representing the components of resistance, that is,

$$R_T = R_W + R_{PV} + R_F\,. \tag{5.4}$$

Dimensionless coefficients of resistance can be formed by dividing this equation throughout by $\frac{1}{2}\rho V^2 S_w$, $\frac{1}{2}\rho V^2 L_{WL}^2$ or $\frac{1}{2}\rho V^2 \nabla^{2/3}$ according to convenience. Here the water-line length is L_{WL}, that is the length of the intersection of the vertical middle plane of the ship and the water plane, and ∇ is the volume displacement. These quantities are taken at a specified condition of ship loading and in calm water.

The preceding equation now becomes

$$C_T = C_W + C_{PV} + C_F \,. \tag{5.22}$$

The nature of these components will now be examined.

5.8.1 *Components of Resistance*

Suppose that a model of the prototype ship is towed along the water surface of a tank and that the total resistance to motion is measured at different, but constant, forward speeds. Values of C_T can be calculated and the dependence of this coefficient on V for a series of geometrically similar models will be of the type (a) shown in Fig. 5.18. If a deeply submerged, double-hull model, discussed earlier, is now towed through the water the variation with V of half of the 'double-model' resistance takes the form depicted by curve (b) in Fig. 5.18. This latter curve is similar to the C_T curve for, say, a model submarine (as shown in Fig. 5.14) for which $C_T = C_{PV} + C_F$. However, the C_T curve for the ship is quite different from that of the submerged vehicle. It is reasonable to assume that for a given V the difference between curves (a) and (b), that is $\overline{AC} - \overline{BC} = \overline{AB}$ in Fig. 5.14, accounts for the coefficient of wave-making resistance C_W.

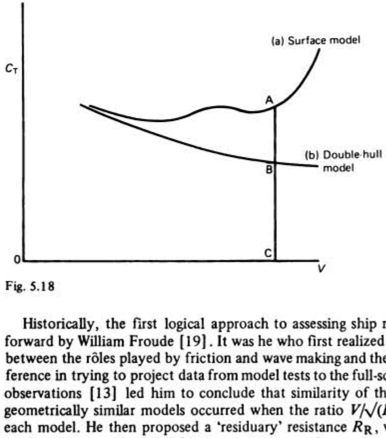

Fig. 5.18

Historically, the first logical approach to assessing ship resistance was that put forward by William Froude [19]. It was he who first realized the essential difference between the rôles played by friction and wave making and the significance of this difference in trying to project data from model tests to the full-scale ship [20]. Froude's observations [13] led him to conclude that similarity of the wave patterns about geometrically similar models occurred when the ratio $V/\sqrt{(L_{WL})}$ was the same for each model. He then proposed a 'residuary' resistance R_R, which was given by the total resistance minus the friction resistance and considered to be a function of $V/\sqrt{(L_{WL})}$ only. In algebraic terms

$$R_R = R_T - R_F = R_{PV} + R_W,$$

or, in coefficient form

$$C_R = C_T - C_F = C_{PV} + C_W \tag{5.23}$$

where C_R is assumed to be a function of $V/\sqrt{(L_{WL})}$ (which is, of course, proportional to Froude number Fr). The values of R_F, and hence C_F, were assumed to correspond to those deduced from data on planks towed fully submerged through a tank of water. It was also found that C_F depended on the product VL_{WL}. The viscosity and density of water were taken to be constant, despite known temperature changes, so that C_F became a function of Reynolds number Re. (We must remember here that William Froude developed his ideas before the advent of dimensional analysis.) The difference between the criteria for C_R and C_F is often known as the 'ship-model tester's dilemma'! Froude overcame this difficulty by testing the model at the prototype value of $V/\sqrt{(L_{WL})}$ and then making the bold assertion that C_R was the same for the model and the prototype. For ships of fairly fine form, as considered by Froude, we can therefore assume C_W to be a function of Fr only, and since C_{PV} is then small this means that C_R is a function of Fr only. Note, however, that this assumption is far less likely to be true for bluff ships such as tankers and container ships which have high block coefficients.

Let us consider a ship moving forward at a steady velocity V and suppose we can identify (ideally) a bow- and a stern-wave pattern of the Kelvin type. Relative to the ship, both the tranverse and divergent sine-wave patterns are stationary and so the velocity of propagation of the transverse waves must also be V. The wavelength, λ, of the transverse wave system is equal to that of free-surface progressive waves also with a velocity of propagation V. Hence, from Equation (2.2)

$$\lambda = 2\pi V^2/g. \tag{5.24}$$

Owing, no doubt, to the effects of viscosity it is found that those waves in the immediate vicinity of a ship are somewhat shorter than the wavelength deduced from Equation (5.24). If a line normal to the crest of a divergent wave makes an angle θ with the direction of motion of the ship, the wave velocity in that direction is $V\cos\theta$ and the corresponding wavelength is given by

$$\lambda' = \frac{2\pi V^2}{g}\cos^2\theta. \tag{5.25}$$

Equations (5.24) and (5.25) indicate that as V increases the wavelength increases and, for a given shape of hull, so will the wave amplitude. A concomitant increase in wave energy therefore results in an increase of the wave-making resistance of ships.

The curve describing the variation of C_W with Fr for a given homologous series of hull shapes is not monotonic but consists of a number of humps and hollows. Wigley [21] determined the variation of C_W by considering it to be the sum of two separate components identified by the transverse and divergent wave systems. The result for a hull shape defined algebraically and for the wave system depicted in Fig. 5.19 is shown in Fig. 5.20. The behaviour of C_W can be explained, at least partially, in the following manner.

Divergent waves from the bow and the stern regions will interfere only weakly with each other, but the transverse waves can show strong interference. Thus, if the bow and stern transverse waves are in phase mutual reinforcement occurs at the stern and large waves are formed there. As a crest is formed first at the bow and a trough is formed at the stern reinforcement will occur for the typical example

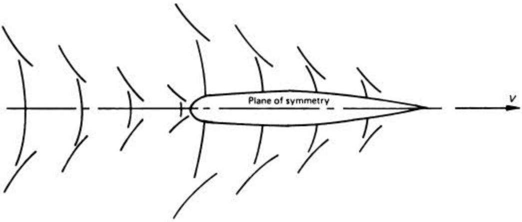

Fig. 5.19

shown in Fig. 5.21(a). (It has been observed that the first crest of the bow-wave system develops not exactly at the bow but at a distance of about $\lambda/4$ aft of the bow.) On the other hand, as shown by the example in Fig. 5.21(b), considerable cancellation takes place when the two wave systems are in anti-phase. There is not, of course, a complete absence of waves in this instance since the amplitudes of the bow and stern waves are unequal.

Reinforcement takes place when $L_{\mathrm{WL}} - \lambda/4$ is an odd number of half wavelengths. Hence

$$L_{\mathrm{WL}} - \frac{\lambda}{4} = (2n - 1)\frac{\lambda}{2}$$

that is,

$$\frac{\lambda}{L_{\mathrm{WL}}} = \frac{4}{4n - 1} \tag{5.26}$$

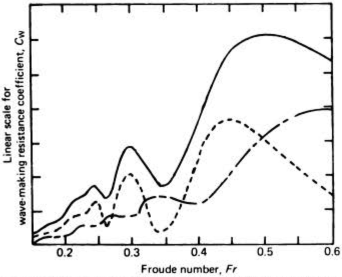

Fig. 5.20 Components of wave-making resistance coefficient C_W. —, total C_W; – – –, C_W from transverse waves; – - – -, C_W from divergent waves.

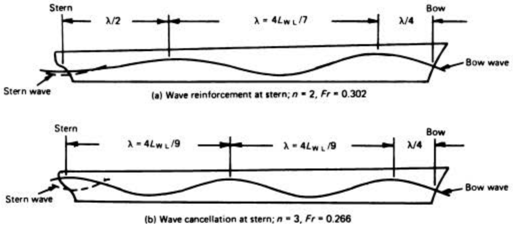

Fig. 5.21

where $n = 1, 2, 3, \ldots$, and is the number of crests accruing over the length L_{WL}. Equation (5.24) can be written as

$$\frac{\lambda}{L_{WL}} = 2\pi\frac{V^2}{gL_{WL}} = 2\pi(Fr)^2. \tag{5.27}$$

When λ and V mutually satisfy Equations (5.26) and (5.27) the C_W curve for the transverse waves will exhibit a 'hump'.

Now if the wave systems are in anti-phase at the stern $L_{WL} - \lambda/4$ must be an even number of half wavelengths. Hence

$$L_{WL} - \frac{\lambda}{4} = (2n-2)\frac{\lambda}{2}$$

that is,

$$\frac{\lambda}{L_{WL}} = \frac{4}{4n-3} \tag{5.28}$$

where n = 1, 2, 3, . . . , as before. Therefore, when λ and V mutually satisfy Equations (5.27) and (5.28) the C_W curve for transverse waves will depict a 'hollow' at the appropriate Froude number. The results are shown in Table 5.2.

The variation of wave-making resistance with forward velocity of the ship V may be assessed using, for example, energy relationships for the transverse and divergent wave systems. It is found that the total wave resistance is the sum of two principal

Table 5.2 Prediction of humps and hollows.

Humps (Equations (5.26) and (5.27))			Hollows (Equations (5.28) and (5.27))		
n	λ/L_{WL}	Fr	n	λ/L_{WL}	Fr
1	4/3	0.46	1	4/1	0.80
2	4/7	0.30	2	4/5	0.36
3	4/11	0.24	3	4/9	0.27
4	4/15	0.21	4	4/13	0.22

components. The first is proportional to V^6 and represents the resistance which would be obtained if bow- and stern-wave interference did not occur. The second component, which represents the interference effects, is proportional to the product of V^6 and a series of harmonic terms in V^2 and is therefore oscillatory. As a result, the total variation of C_W oscillates above a mean curve proportional to $(Fr)^4$ with increasing amplitude up to the hump corresponding to $n = 1$. For Froude numbers higher than 0.46 (see Table 5.2) the oscillatory components largely cancel both themselves and the steady component resulting in a continuous decrease of wave-making resistance with increasing forward speed.

Figure 5.20 shows that, for $n \geqslant 2$, all the humps and hollows predicted by the transverse system alone occur at very nearly the same Froude numbers, as do the corresponding humps and hollows of the total C_W curve. However, when Fr is greater than about 0.4 the effect of the divergent waves on the total wave-making resistance becomes increasingly dominant and the hump corresponding to $n = 1$ appears at $Fr \cong 0.5$. As the Froude number is increased Equation (5.27) indicates that the wavelength increases rapidly until eventually it becomes very much greater than L_{WL}. The first crest of the two transverse wave systems is then well aft of the stern and as the divergent waves are not usually visible close to the hull the water about the vehicle appears nearly horizontal. The pressure distribution about a high-speed vehicle is therefore quite similar to that about a vehicle progressing at a very low speed when $\lambda \ll L_{WL}$. This means that the wave-making resistance of high-speed vehicles ($Fr \geqslant 1.5$, say) is small as it is for vehicles operating at very low speeds ($Fr \leqslant 0.15$, say). Although the wave-making resistance of a conventional displacement ship may decrease with rising forward speeds this advantage is more than outweighed by a rapid increase in the viscous resistance; the total resistance and therefore the propulsive power then become extremely large.

A ship may be required to maintain a constant operational speed for long periods and it is clearly desirable that it should not do so at a hump on the C_W curve. Even with the elementary theory presented here it is possible to locate quite accurately the relative operating positions of different types of ship as shown in Fig. 5.22. The Froude numbers correspond to maximum speeds and these may be quite different from the cruising speed. This fact is rather more pertinent to the operation of naval ships where high speeds are often required for short duration but at the expense of high power consumption. It is important to recognize that Fig. 5.22 is not meant to imply the existence of a unique C_W curve for all ships, but merely to locate the ships according to the series of humps and hollows. The hump for $n = 1$ is called the 'main' or 'primary' hump, whereas that for $n = 2$ is referred to as the 'prismatic' hump. The latter is so named because C_W in that range of Froude number is sensitive to changes in the prismatic coefficient†.

We have assumed hitherto that the distance between the bow and stern pressure points is L_{WL} and that the first transverse crest occurs at $\lambda/4$ aft of the bow. It has in fact been found that, at least for warships, the distance between the first crest at the bow and the first trough at the sterm is about $0.9L_{WL}$ and this is taken also to be the spacing between the bow and stern pressure points. Substituting $0.9L_{WL}$ for $L_{WL} - \lambda/4$ into the equations preceding Equations (5.26) and (5.28) leads to

† The prismatic coefficient is $\nabla/L_{PP}A_m$ where L_{PP} is the length between perpendiculars (i.e. the length between two arbitrary marks on the hull, one near the bow and the other near the stern) and A_m is the cross sectional area of the hull at the midship transverse plane.

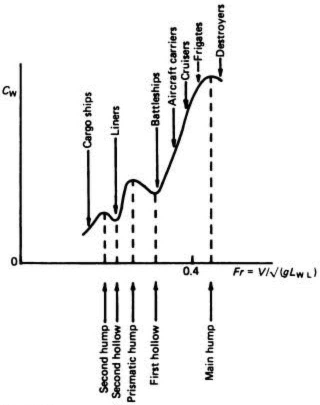

Fig. 5.22

expressions acceptable for warships, namely,

$$\left.\begin{aligned} \text{Humps:}\quad & \frac{\lambda}{L_{WL}} = \frac{1.8}{2n-1} \\ \text{Hollows:}\quad & \frac{\lambda}{L_{WL}} = \frac{0.9}{n-1} \end{aligned}\right\} \tag{5.29}$$

Table 5.3 Predicted and measured Froude numbers for warships.

	Predicted and measured Froude numbers				
	Main hump	First hollow	Prismatic hump	Second hollow	Third hump
Predicted for all vessels	0.54	0.38	0.31	0.27	0.24
Destroyer	0.51	0.36	0.30	0.25	–
Submarine on surface	–	0.35	0.30	0.26	0.23
Cruiser	0.52	0.32	0.30	–	–
Depot ship	–	0.33	0.31	0.27	0.24

The combination of Equations (5.29) and (5.27) allows theoretical predictions of Froude numbers corresponding to humps and hollows. The results appear in Table 5.3 together with some measured values which are seen to be in close agreement.

The discussion so far implies that some control might be exercised over the magnitude of the wave-making resistance by specifying appropriate Froude numbers. However, this could impose unacceptable limits on the operation of a ship, and so a better approach would be perhaps to design a hull shape consistent with minimum wave-making resistance. This has been attempted (e.g. [10]) but the mathematical boundary conditions placed on the theory which is developed from the Kelvin wave-making source (representing a solution for a source-type flow in the presence of a free surface) are rather difficult to satisfy accurately. A distribution of 'sources' and 'sinks' [2] can be used to represent a ship hull but it is far from straightforward to decide which parts of the hull should be modelled most closely. Waves are largest at the ends of the ship, where the hull is generally wedge-shaped so that the hull profile is quite close to the longitudinal vertical plane of symmetry. This plane is therefore chosen as that on which the source-sink system can be distributed in order to produce the best results for ships operating at low speeds. It has been shown in [10] that if the perturbation velocities u, v, w (of Fig. 5.13) are small, that is, a 'thin-ship' assumption, the wave-making resistance may be deduced either by means of the downstream wave pattern or by calculating the surface pressures on the hull. The latter method is preferable because the approximation adopted for the free-surface condition are more likely to affect the downstream wave system than the pressure on the hull. In some cases the theory matches experimental data rather well, but as we might expect agreement is poor for bluffer forms.

Suggestions concerning 'wavy' hulls have been put forward but these ideas are adequate for small ranges of speed only. A flexible body analogous to a dolphin is obviously impossible for ships. Rather more success has been achieved with the 'bulbous bow', a device first introduced at the beginning of the twentieth century. Indeed, the effectiveness of bulbous bows was discovered, apparently by accident, after the reintroduction of ram bows on ships of the United States at the end of the nineteenth century. It was found that by increasing the submergence of the ram and generally rounding-off the profile bow waves were partially neutralized and wave-making resistance was reduced. A bulb of this type fitted to the battleship *USS Delaware* resulted in a substantial speed advantage over comparable ships.

The earliest theoretical calculations on the effectiveness of bulbous bows were developed by Wigley [22]. The bulb should be nearly spherical in shape and fitted to the hull just ahead of the fore foot (i.e. close to where the nominally longitudinal keel turns upwards to form the underwater stem leading to the bow of the ship). When in this position, the accelerating flow over the surface of the bulb generates a low-pressure region which may extend to the water surface. The high-pressure region developed in the water by the passage of the bow is therefore largely cancelled by the 'bulb wave' interference and the resultant wave then has a reduced amplitude. Turbulent-flow conditions near to the bow are also reduced and so, therefore, is the loss of energy through wave breaking (see Section 5.5). For high Froude numbers (e.g. up to 0.57) the reduction of wave-making resistance outweighs the inevitable increase of both skin-friction and viscous pressure resistance. However, at low Froude numbers (e.g. less than 0.24), there is little benefit from a bulbous bow and in some cases an overall increase of resistance has been found. For the bulbous bow to offer significant advantages Wigley suggested the following design criteria should be used:

(i) The useful speed range of a bulb corresponds approximately to $0.24 \leqslant Fr \leqslant 0.57$.

(ii) The best position of the bulb is with its centre at the bow, that is, with its nose forward of the hull.

(iii) The bulb should extend as low as possible in the water and be as short and wide as possible consistent with fairness in the lines of the hull. This will prevent excessive spray and avoid a 'wet' ship.

(iv) The top of the bulb must be well below the surface of the water.

The limitation to a maximum Froude number is due to the onset of cavitation around the bulb and stem and large skin-friction resistance.

A great deal of work on the design of bulbous bows, and wave resistance generally, has been carried out in Japan, notably by Inui [23]. In the subsequent analysis the bow and stern waves are kept separate and then cancelled by waves produced from local distributions of 'sources' and 'sinks' in the fluid. The latter distributions define an additional body shape, namely the bulb, and it is seen that the possibility of both bow and stern bulbs are permitted. This procedure was shown to be beneficial in reducing the size of the wave pattern generated in calm water even though only a bulb at the bow was used. The optimum shape of a bulb on a given hull form depends on Froude number, and the designs then operate best over a narrow range of ship speeds. Consequently, the installation of Inui and other bulbous bow shapes is usually to be found on fast cargo ships, bulk carriers, ferries, crude-oil carriers, and some ocean-going tugs which have a well defined operating speed for long periods of time. Naval ships, other than replenishment vessels, have quite different operating criteria and rarely incorporate bulbous bows. Another factor contributing to this situation is the uncertainty of the response in heavy seas of a fine-form ship with a bulbous bow. More recent work, showing a comparison between theory and experiment, is given in [24].

Further details of the design and performance of bulbous bows are given in [25]. The reader's attention is also drawn to an excellent review of the wave-making resistance of ships by Wehausen [26].

5.8.2 Interaction Effects

The interaction between viscosity and wave effects can be assessed by considering the total resistance coefficient C_T to comprise the following contributions:

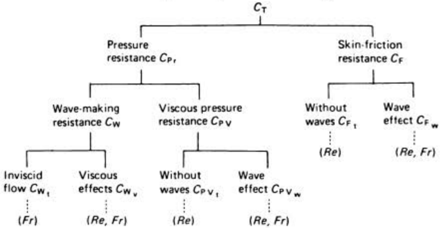

The subscript t refers to a theoretical value and C_{W_t} is therefore the coefficient of wave resistance that would be obtained if the fluid were inviscid. The boundary layer on the hull and separation near the stern (both viscous effects) undoubtedly modify the distortion of the interface and therefore C_{W_t} must be augmented by C_{W_v} to yield C_W. Although C_{W_t} is a function of Fr only, it is clear that C_{W_v} must depend on both Fr and Re. The theoretical viscous resistance C_{V_t} is given by the sum $C_{F_t} + C_{PV_t}$, and each component depends on Re only, provided that the interface is not distorted. As we have seen C_{V_t} can be determined from experiments with a deeply submerged, double-hull model. Wave formation alters the pressure and stress distributions over the wetted hull, and it is thus necessary to include in our analysis the interaction components C_{F_w} and C_{PV_w} which are both functions of Fr and Re. These interaction effects must occur in principle, but their significance is the subject of debate [27].

It was pointed out in Section 5.5 that once in motion a ship may take on a pure sinkage or rise or a change of attitude (trim). For many ships operating at low speeds sinkage by the bow exceeds that by the stern, so that a trim by the bow is observed. As the speed increases the bow rises, and for $Fr > 0.3$, say, there is a gradual increase in trim by the stern. A resistance contribution C_{att} is added to C_T to allow empirically for changes in attitude from that at rest.

We have always assumed the ship to proceed along a straight path with the vertical plane of symmetry parallel to the direction of the resultant velocity V. Should this condition not be so, for instance, as a result of cross currents, unequal thrust from the propulsors, asymmetry of the hull, etc. a small drift velocity occurs. The ship can then be regarded as equivalent to a large body of small span set at a small angle of incidence to the flow. The pressure on one side of the hull exceeds that on the other and this pressure difference causes a flow under the keel from the high- to the low-pressure side. This motion will augment further the total resistance of the ship because the 'leakage' flow develops into downstream 'tip vortices', which eventually dissipate in the viscous fluid and which therefore represent a source of energy loss. (The generation of tip vortices is discussed in more detail in Chapter 6.)

5.8.3 *Estimation of Ship Resistance*

The difficulties of estimating R_T have been described already. Essentially, problems arise because there is no known general form for the relationship between C_T, Re and Fr. We therefore have to split C_T into various components and consider the following points: (i) different components obey different scaling laws; (ii) C_T can be split into more than one system; and (iii) there are more ways than one of dealing with some components.

Froude's method of deriving a bare-hull resistance is not only interesting but has remained useful for nearly a century. However, the method relies heavily on empiricism and experiment and is now being gradually superceded by analytical methods. The basic procedure is as follows:

(1) Measure the value of R_T for the model with $(Fr)_M = (Fr)_P$.

(2) Calculate or measure the value of R_F for the model from data for submerged planks of the same length, surface area, finish and Reynolds number as the model.

(3) From (1) and (2) evaluate the residuary resistance,

$$(R_R)_M = (R_T)_M - (R_F)_M$$

and hence deduce $(C_R)_M$. Now C_R is assumed to be a function of *Fr* only so that $(C_R)_M = (C_R)_P$.

(4) Calculate or measure the value of R_F for the plank corresponding to $(Re)_P$ and hence deduce $(C_F)_P$.

(5) The prototype resistance can now be obtained from the equation

$$(C_T)_P = (C_F)_P + (C_R)_M.$$

The assumption that C_R is a function of *Fr* is seen to be erroneous because

$$C_R = C_W + C_{PV}$$

and we know that C_{PV} is primarily a function of *Re*. Nevertheless, for fine hull forms operating at high Froude numbers, say greater than 0.35, C_{PV} is small and the wave-making resistance is a large part of the whole. Then

$$C_R \cong C_W(Fr)$$

and the Froude method gives a good estimate of the total resistance.

On the basis of the resistance equation (5.22) we can write, to a first order of accuracy,

$$C_T(Re,Fr) = C_W(Fr) + C_{PV}(Re) + C_F(Re) \tag{5.30}$$

and the components may be examined separately or in some combination.

(i) C_T: This is obtained from towing tests on a model, but difficulties are encountered in scaling to the prototype.

(ii) C_F: This may be found for the model and the prototype as follows:

(a) Use (simplified) boundary-layer theory.

(b) Use plank data as in the Froude method.

(c) Integrate the shear-stress distribution over the hull as measured by Preston tubes, Stanton tubes, hot-film probes, etc., which rely on a known relationship between the local shear stress in the boundary layer and some characteristic of the adjacent fluid velocity. An example of the use of Preston tubes to deduce the skin-friction resistance of a model liner is given in [28].

(iii) C_{PV}: There is no known way of determining this directly.

(iv) C_W: This can be found by the following means:

(a) Calculate the pressure resistance of the body in an *inviscid* fluid for which $C_{PV} = 0$.

(b) Calculate the wave resistance using the relationship

$$R_W = \tfrac{1}{2}\rho\int_{-b}^{+b}\int_{\zeta}^{h}(v^2 + w^2 - u_{abs}^2)\,dz\,dy + \tfrac{1}{2}\rho g\int_{-b}^{+b}\zeta^2\,dy, \tag{5.31}$$

as derived from Equation (5.15), by employing measured or calculated functions of $\zeta(y)$ and using measured or assumed distributions of u, v and w downstream from the ship [29, 30].

(v) $C_{PV} + C_F$: This combination may be deduced for the prototype by taking measurements on the model at the same Reynolds number. Often equality of *Re* is impossible to achieve and extrapolation of the model results to those for the prototype is required. Experimental procedures are:

(a) Tow a submerged double-hull model so that $(Re)_M = (Re)_P$ and then, because of the double hull,

$$(C_{PV} + C_F)_M = 2(C_{PV} + C_F)_P.$$

(b) Perform a velocity traverse across the wake of a submerged double-hull model and assume the wake is 'double' that of the ship.

(c) Conduct a velocity traverse across the wake of an interface model. However, this will entail further assumptions and include the added effect of energy transfer by wave breaking (e.g. see [31]).

Attention has been drawn to the defects of the Froude method, and it is natural to ask if there are any improvements of the basic technique. It is argued in [32] that Equation (5.30) should at least be modified to the form

$$C_T(Re, Fr) = C_W(Fr) + C_{PV}(Re, Fr) + C_F(Re) \tag{5.30a}$$

and that techniques should be developed in order to measure separately each component on the right-hand side of the above equation. Even then questions of interaction are largely ignored so that greater refinement may be necessary. Separate scaling of the components should then follow and eventually, perhaps, a full theoretical analysis may be developed. This final goal, however, is undoubtedly some way off, although the importance of the three-component analysis is clearly evident in the case of present-day, full-form ships. For the latter, another difficult problem arises from the large difference between $(Re)_M$ and $(Re)_P$. Substantial regions of separated flow which may occur adjacent to the model are often absent from the full-scale prototype when running at the same Froude number. Consequently, $(C_{PV})_M$ is greater than it would be if the flow had remained attached and the boundary layer had grown naturally. Under these conditions scaling laws for viscous resistance become quite unreliable. The matter is discussed in [8] in relation to a double-hull model mounted in a compressed-air wind tunnel. A revealing series of flow visualization pictures and measurements indicates that serious deficiencies in prediction techniques may occur if the model length is less than 6 m or so.

In the past a great deal of work was done on plank tests and an immense quantity of data was accumulated. Account was taken of surface roughness but any application of the results always introduced the same inconsistency, namely that of adopting data from flat surfaces for the curved surfaces of ships. The development of boundary-layer theory allowed Blasius, in 1904, to deduce an expression for the skin-friction coefficient $C_F(= R_F/\frac{1}{2}\rho SV^2)$ of a thin, flat plate of surface area S placed parallel to the oncoming flow. The boundary layer was assumed to be laminar, two-dimensional and steady with the result that

$$C_F = 1.327(Re)^{-1/2} \tag{5.32}$$

where Re is based on the overall length of the plate L. In 1921, Prandtl and von Karman derived independently the corresponding expression for turbulent flow over the whole of a flat plate, namely

$$C_F = 0.072(Re)^{-1/5}. \tag{5.32}$$

The relationships (5.32) and (5.33) are depicted in Fig. 5.23. Generally, three boundary-layer régimes will occur on the plate: laminar, transition and turbulent. Transition commences when the local Reynolds number, based on distance from

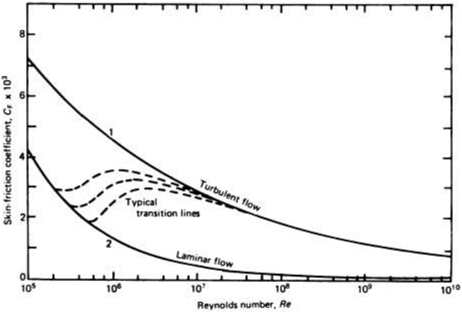

Fig. 5.23 Skin-friction coefficient for a semi-infinite flat plate. Curve 1: Prandtl–von Karman $C_F = 0.072(VL/\nu)^{-1/5}$; curve 2: Blasius $C_F = 1.327(VL/\nu)^{-1/2}$.

the leading edge of the plate, is about 4×10^5, but this value is somewhat longer for very smooth plates.

In 1932, Schoenherr [33] collected William Froude's plank data together with results from other tests and plotted C_F as a function of Re. Although transition no doubt occurred on many of the planks, Schoenherr examined his results in the light of the Prandtl–von Karman theory. By so doing he found the equation for a skin-friction line;

$$0.242(C_F)^{-1/2} = \log\{(Re) \times C_F\} \tag{5.34}$$

applicable to smooth surfaces. This equation was adopted by the American Towing Tank Conference (ATTC) in 1947, and it was decided that an allowance of +0.0004 should be added to the resulting values of $(C_T)_P$ to account for the roughness of new ships. The subsequent values of $(C_T)_P$ then produced a good correlation with full-scale, ship resistance tests. For a submarine the preceding allowance, given the symbol C_A, accounts not only for roughness, but also for other factors.

Widespread use of the ATTC 1947 line showed it to be unreliable in correlating the results from small and large models. The advent of fully welded, and therefore smoother, ship hulls showed that C_A could be zero or even negative. Furthermore, Schoenherr used data from planks of different homologous series which therefore possessed a wide range of aspect ratios†. Finally, the transcendental equation (5.34) for C_F makes its use somewhat awkward in the design process.

At the International Towing Tank Conference (ITTC) in 1957 the weaknesses of the ATTC 1947 friction line were recognized and as a result an alternative was

† The aspect ratio $\mathcal{R}$ is defined as the square of the span divided by the plan area, which for a rectangular plank reduces to the breadth divided by the length measured in the direction of the flow in the main stream.

proposed and accepted. This is the ITTC 1957 model-ship correlation line given by

$$C_F = \frac{0.075}{\{\log(Re) - 2\}^2} \tag{5.35}$$

and now in common use in most model-ship tanks. The results obtained for C_F from either Equation (5.34) or (5.35) may be used with the Froude analysis to estimate the total resistance of a prototype. However, the value of C_F obtained from friction lines must not be regarded as the value corresponding precisely to the model or ship hull but rather as a component in the resistance analysis. Accordingly we shall refer to C_A as the 'model-ship correlation allowance' given by

$$C_A = (C_T)_P \text{ measured} - (C_T)_P \text{ estimated.} \tag{5.36}$$

In order to improve on earlier work Hughes [34, 35] carried out further resistance tests on planks and pontoons up to $Re = 3 \times 10^8$ and found that C_F increased as AR decreased as a result of side-edge effects. The data were correlated by means of a unique curve, independent of Reynolds number, which related the reciprocal of AR to the ratio C_F/C_{F_0}, where C_{F_0} is the value of C_F at $AR = \infty$ and corresponds to truly two-dimensional flow over a flat surface set parallel to the oncoming main stream. Extrapolation to the two-dimensional case was therefore made as shown in Fig. 5.24. This allowed Hughes to construct his 'basic', turbulent, skin-friction curve for plane, smooth surfaces which was described by the equation

$$C_{F_0} = \frac{0.066}{\{\log(Re) - 2.03\}^2} \tag{5.37}$$

When plotted on a logarithmic scale the curves of C_F for given values of AR are then displaced from the basic C_F curve by a constant ordinate, independent of Re, as indicated in Fig. 5.25. Although Equations (5.35) and (5.37) are similar they yield different curves, the Hughes line being below the ITTC and ATTC lines as shown in Fig. 5.26. The Hughes line is, of course, for truly two-dimensional flows whereas the other curves are not.

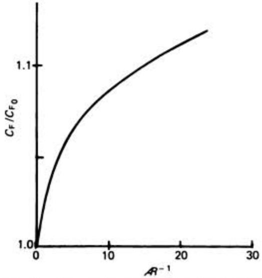

Fig. 5.24 The variation of C_F with AR for flat planks.

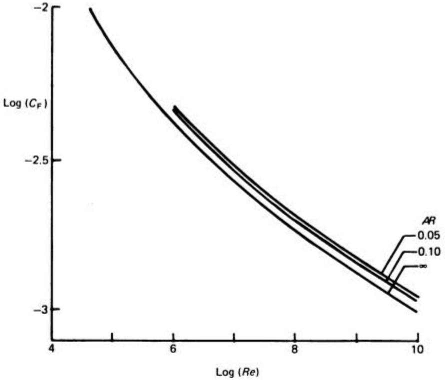

Fig. 5.25 Hughes' basic skin-friction curve.

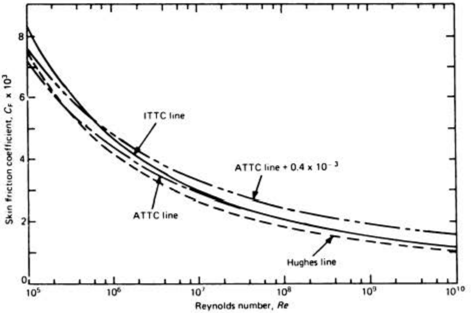

Fig. 5.26 Skin-friction coefficient correlation lines. ITTC line, $C_F = 0.075/\{\log(Re) - 2\}^2$; ATTC line, $0.242/\sqrt{C_F} = \log\{(Re) \times C_F\}$; Hughes line, $C_{F_0} = 0.066/\{\log(Re) - 2.03\}^2$.

To calculate the total resistance coefficient of a smooth hull Hughes proposed the relation

$$C_T = C_{F_0} + C_{FORM} + C_W = C_V + C_W, \tag{5.38}$$

where C_{FORM} is the coefficient of 'form' resistance. The so-called 'form effect' accounts for the three-dimensional flows over a real hull and includes pressure resistance arising from curvature of the hull and thus from the streamlines in the flow.

The procedure for calculating ship resistance using Hughes' proposals is to determine first the basic skin-friction curve from Equation (5.37). At very low speeds the value of C_W is approximately zero. Let us suppose that the point K_M in Fig. 5.27 represents the upper speed limit for which this approximation is acceptable. This point on the $(C_T)_M$ curve is usually referred to as the 'run in' point. Based on theoretical reasoning and experimental evidence Hughes considered that

$$\frac{\overline{G_M K_M}}{\overline{G_M H_M}} = \frac{\overline{G_M H_M} + \overline{H_M K_M}}{\overline{G_M H_M}} = 1 + \frac{(C_{FORM})_M}{(C_{F_0})_M} = 1 + k = r = \frac{(C_V)_M}{(C_{F_0})_M}, \tag{5.39}$$

where the parameter

$$k = \frac{(C_{FORM})_M}{(C_{F_0})_M} = \frac{(C_V)_M - (C_{F_0})_M}{(C_{F_0})_M}. \tag{5.39a}$$

Both k and the 'form factor' r are taken to be independent of Reynolds number. Furthermore, it is assumed that r is the same for all models and ships in a given homologous series. Hence we can write, for example,

$$\log(\overline{G_M K_M}) - \log(\overline{G_M H_M}) = \text{constant}. \tag{5.40}$$

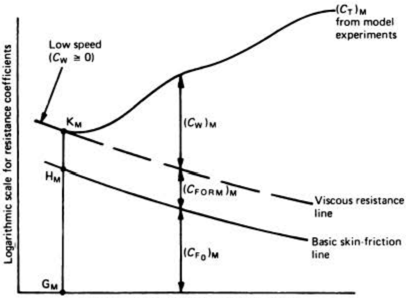

Fig. 5.27 Hughes' resistance components.

Thus, for logarithmic scales, a line can be drawn through K_M to be a constant ordinate above the C_{F_0} line for all Reynolds numbers so as to indicate the form effect. The difference between the $(C_T)_M$ curve and the three-dimensional friction line must correspond to the wave-making component and is taken to be the same as that for the prototype ship since the model tests are run with $(Fr)_M = (Fr)_P$. By virtue of Equations (5.37) and (5.39) the friction lines can be extended to the prototype range of Reynolds numbers. The curve of $(C_T)_P$ is then obtained by adding $(C_W)_M = (C_W)_P$ to $(C_{F_0} + C_{FORM})_P = (C_V)_P$ starting at a 'run in' point K_P corresponding to the same Froude number as the model point K_M. A typical extrapolation process is shown in Fig. 5.28, but note here that, in keeping with practice, a linear and not a logarithmic scale has been used for the ordinate.

Now in the Froude method the whole of the model residuary resistance coefficient

$$
\begin{aligned}
(C_R)_M = (C_T)_M - (C_{F_0})_M &= (C_T)_M - (C_V)_M + (C_{FORM})_M \\
&= (C_W)_M + (C_{FORM})_M
\end{aligned}
\tag{5.41}
$$

is transferred unchanged to the prototype as indicated in Fig. 5.28. However, in the Hughes technique C_{FORM} decreases as *Re* increases (as we might expect from Equations (5.37) and (5.39)) and consequently the transfer to the prototype *Re* results in a value of $(C_T)_P$ lower than that predicted by the Froude method. As before, a model-ship correlation allowance is required to bring the estimated results into line with full-scale test measurements.

In [25] the ATTC 1947, ITTC 1957 and Hughes correlations together with Froude's method have been used to estimate the resistance of a given ship. These predictions give a range of resistance which varies by as much as 17 per cent. However, by the judicious use of correlation allowances recommended by the various towing tank committees the final values can be brought to within 2 per cent or so of each other. This simply highlights the need for more accurate and generally

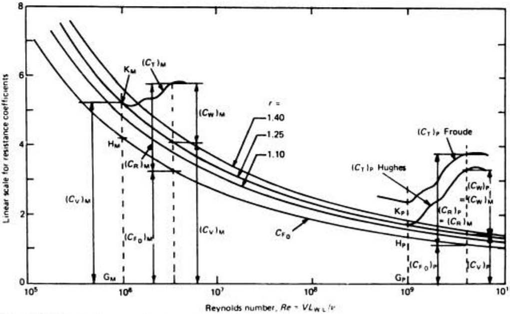

Fig. 5.28 Hughes' extrapolation technique.

applicable theories and scaling techniques since values of C_A for ships radically different in form from earlier types are unlikely to be known with much confidence. Nevertheless, it has been found that in conventional displacement ships without excessively high block coefficients the use of the ITTC 1957 friction line along with the Froude breakdown of resistance gives good results, with the conventional Froude method giving high values of $(C_T)_P$ and the Hughes method giving low values of $(C_T)_P$.

Telfer [36, 37] suggested that a number of geometrically similar models, which he called geosims, of different scale could be tested to obtain curves of $(C_T)_M$ as a function of Reynolds number for each model. These curves are shown in Fig. 5.29. The function of *Re* for the linear scale of the abscissa in this figure is chosen so that the line for the viscous resistance coefficient (C_V) is straight when plotted with C_V as ordinate on a linear scale. It has been found experimentally that curves of constant Froude number joining the geosims can be drawn both parallel to each other and to the C_V curve. These *Fr* curves may then be extended to the prototype *Re* to construct the C_T curve for the prototype. As Scott [38] has shown the straight line for C_V which passes through the 'run in' points of the geosims applies only for a limited range of *Re*. For example, it was found that for one particular hull shape (that of the *Lucy Ashton*, described in the following section) estimates of C_V could be made accurately from the relation

$$10^3 C_V = \frac{9.5}{\log(Re) - 4}$$

so that an extrapolated straight line could be plotted using a linear scale of $\{\log(Re)–4\}^{-1}$ for the abscissa. The range of *Re* for the model was 4×10^6 to 2×10^7 and for the smoothest ship about 2×10^8 for good accuracy. Furthermore, an accurate approximation of Gadd's assessment [39] of Hughes' pontoon data [34, 35] gave a skin-friction-coefficient relationship for the preceding range of *Re* as

$$10^3 C_{F_0} = \frac{8.6}{\log(Re) - 4},$$

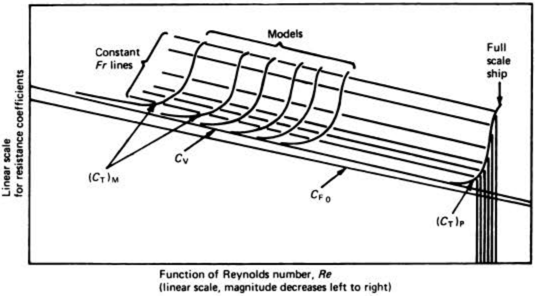

Fig. 5.29 Telfer's geosims.

which indicates a value of $r \cong 1.105$. It should be noted that for Scott's extrapolation and for the slopes of the straight lines shown in Fig. 5.29, the magnitude of the function of Reynolds number on the abscissa decreases from left to right.

Unfortunately, this ingenious method suffers from several important disadvantages:

(i) numerous models and tests are required and are expensive;
(ii) small models exhibit extensive laminar boundary layers; and
(iii) models are limited in size by the test facilities, so that the range of $(Re)_M$ is small and may result in a rather inaccurate extrapolation to $(Re)_P$.

It is clear from the few techniques discussed here that the estimation of the resistance to motion of a ship proceeding steadily through calm water is by no means finalized [40]. The 'ship-tester's dilemma' remains; yet with improvements in mathematical analysis, supported by more accurate test data, we may eventually arrive at a reliable prediction of resistance for hull forms of arbitrary shape.

5.8.4 *Full-scale Ship Tests*

Compared with the vast quantity of model data those determined from full-scale ship trials are quite sparce. There are a number of reasons for this disparity. For example, it is difficult to measure the 'tow-rope' resistance owing to the problem of maintaining a given speed and heading for an acceptable period. It is indeed rare to obtain flat-calm sea conditions in deep, sheltered waters for comparison with model experiments at the corresponding values of displacement and draught. Furthermore, the reaction to the towing force may cause the towed ship under test to alter trim from the nominal value associated with normal running at the same speed. The cost of running a series of resistance tests is usually high, and to conduct these tests a ship may have to be taken out of its intended operation for an unacceptably long period. This limitation applies to naval ships (data from which are often necessarily classified) and particularly to commercial ships. Capital cost represents a huge financial investment and, perhaps understandably, operators require new vessels to earn revenue as soon as possible after the commissioning trials which are concerned specifically with contractual obligations on speed, fuel consumption and handling. Nevertheless, there have been a number of valuable full-scale tests which have attempted to identify ship resistance components and to validate (or otherwise) predictions from models and theory. Some of these are now discussed briefly.

William Froude conducted resistance tests [41] on *HMS Greyhound*, a copper-sheathed, wooden-hull corvette of length 52.58 m ($\cong$ 172.5 ft) towed by *HMS Active*. The tow rope was attached to a dynamometer on the fo'c'sle of *Greyhound* and to a boom rigged to starboard on *Active* so that the stern of the latter was nearly 60 m ($\cong$ 200 ft) ahead and displaced laterally nearly 14 m ($\cong$ 45 ft) relative to the bows of *Greyhound*. The trials were carried out in good weather at speeds up to 6.5 m s^{-1} ($\cong$ 13 knots) and for *Greyhound* at several displacement (and therefore draught) conditions. After separate account was taken of wind resistance it was deemed that satisfactory agreement occurred between model predictions and full-scale measurements. However, this vindication of Froude's hypothesis depended on assumptions about the relative roughness of the copper sheathing on *Greyhound* compared with the artificial roughening of the smooth model surfaces.

A comprehensive set of data was obtained from experiments on the *Lucy Ashton* under the direction of the British Ship Research Association [42–45]. The *Lucy*

Ashton was an old River Clyde paddle steamer of length 58.06 m (≅ 190.5 ft) near the end of its useful life. The paddles were removed, the wetted hull cleaned and smoothed, and four jet-aircraft engines used for propulsion. The latter were displaced well outside the beam of the ship on a gantry so that interference from the jet efflux was avoided. The total thrust from the jet engines thus equalled the ship resistance. With this arrangement the effect on resistance from adding appendages to the bare hull could be assessed without causing a modification to the structure of the flow approaching the propulsors. The speed range covered was approximately 3–7 m s^{-1} (6–14 knots). A series of model tests was also conducted on six geosims of linear scale 1:21.2–1:6.35 and predictions made on the basis of Telfer's method [37].

A number of important conclusions were deduced from the *Lucy Ashton* tests:

(i) The effects of a smooth hull in reducing the total resistance were appreciated after a 3 per cent improvement was obtained as a result of the fairing of seams and the application of smooth paint. Increased resistance from hull fouling during service amounted to as much as 30 per cent of the clean-hull value at the higher speeds.

(ii) Resistance predictions using Froude's residuary resistance method were somewhat sensitive to ship speed and tended to overestimate full-scale resistance at lower speeds. Provided that a correlation allowance was included the Schoenherr ship-model friction line, Equation (5.34), gave good results. Telfer's prediction technique using geosims was also good and confirmed the accuracy of scaling wave-making resistance.

(iii) Tests showed that at corresponding speeds the scaled model, appendage resistance increment (twin shaft, bosses and brackets) was about twice that obtained for the ship. This indicated the difficulty of accurately modelling hull flows *and* appendage flows at the same time.

Another series of tests using jet-aircraft engines has been performed with the German research vessel *SS Meteor* [46]. This vessel has a length of 72.8 m (≅ 239 ft) and was run up to 6 m s^{-1} (≅ 12 knots) with ship-model correlations based on three geosims of linear scales 1:25, 1:19 and 1:13.75. Full-scale tests were conducted on naked-hull resistance and subsequently self-propulsion with the ship propeller installed. The ITTC 1957 model-ship correlation line was used to extrapolate skin-friction resistance with $\{\log(Re) - 2\}^{-2}$ as the abscissa. Good predictions of resistance were reported for both *Meteor* and for geosim extrapolations of a tanker.

Some idea of the orders of magnitude of the resistance components, as a percentage of the total resistance at cruising speed, can be appreciated from the following data:

Resistance component	Frigate	Tanker
Frictional R_F	60	60
Viscous pressure R_{PV}	10	30
Wave-making R_W	30	10

It is seen that the viscous resistance R_V accounts for 70 per cent of the total resistance of the frigate and no less than 90 per cent of the tanker resistance.

Comparable results have been given [47, 48] for the resistance of two Cross Channel ships, the *Koningin Elisabeth* and her sister ship the *Reine Astrid*, at a

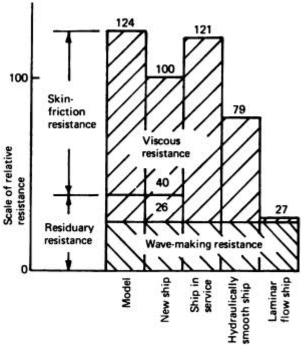

Fig. 5.30 Relative resistance for a Cross Channel ship.

cruise speed of 11 m s^{-1} ($\cong$ 22 knots) as shown in Fig. 5.30. The trials data have been detailed in [49] along with trials data for a cargo liner and a tanker. Attempts have then been made to calculate wave resistance theoretically based on the techniques developed in [50] and to deduce viscous resistance from wind-tunnel tests on model hulls (single and double). The appropriate form factor was deduced using the ITTC 1957 friction line. The purpose of the work was to ascertain the accuracy of breaking down the total resistance into just two components, namely wave resistance and viscous resistance, and then to predict the results from model and full-scale tests. The predictions showed errors up to 8 per cent in the model tank results and up to 15 per cent for the ship trials. Although a refinement of the techniques may be called for (and this is debatable if one is concerned only with the effects of parameter modifications at an early design stage), programmes such as this provide much needed information for the design data base.

Results from full-scale resistance trials on naval ships and submarines are rather scarce, no doubt as a result of security restrictions, especially in the case of the latter. However, some results of full-scale towing trials on *HMS Penelope* have been reported in [51]. This frigate, of length 109.73 m ($\cong$ 360 ft) between perpendiculars, was towed by *HMS Scylla* of the same class using a tow rope some 1830 m ($\cong$ 6000 ft) long. The tow-rope pull was measured by a dynamometer on the fo'c'sle of *Penelope* at speeds between approximately 6 and 11.5 m s^{-1} (12 and 23 knots). Estimates of resistance and power coefficient (using *Scylla*) could be made, as well as pitot-tube surveys in the wake of the towed ship. Briefly, the ITTC 1957 correlation line with C_A = 0.0004 produced good agreement with the measured resistance of *Penelope* after removal of the propellers. It was found, however, that the surface roughness of the frigate was substantially greater than that of the new ship and resulted in a resistance 14 per cent greater than that predicted from model tests. The full value of these results has yet to be determined, but doubtless they will assist in the refinement of the techniques for resistance estimation.

The importance of R_V is its size, and errors in estimation can lead to serious difficulties in the selection of the propulsive machinery. Apart from reducing the surface roughness little can be done to reduce R_V for a streamline form. Although R_W is relatively small (e.g. about 15 per cent of the total resistance in the examples considered in [49]) it can, at least, be modified at the design stage so that some worthwhile changes in R_T are possible.

5.8.5 *Other Sources of Resistance*

So far we have concentrated on the predictions of total resistance of the bare wetted hull, but there are other sources of resistance which need to be estimated to give the overall resistance under full-scale operating conditions. Mention has been made (in Section 5.8.2) of an increment to C_T arising from a change in attitude (or trim) of a ship of given displacement from that when stationary to that when underway. The change originates from the redistribution of pressure on the hull during the commencement of motion, and for most conventional ships, especially those of full form, trim is by the bow. The effect is accentuated by the presence of a bulb and this departure from hydrostatic conditions is often represented by an attitude resistance coefficient C_{att}. It might be expected that, if towing tests are carried out on a freely suspended model, the attitude taken up by the model should be the same as that of the ship provided that the weight distribution is modelled accurately. This, however, is not at all straightforward as measuring equipment has to be installed in an already congested model. In addition, it is not entirely clear to what extent the values of Froude number and Reynolds number affect the attitude, and therefore some degree of empiricism must be introduced.

An interesting problem has arisen from changes of trim when full-form ships, particularly VLCC, are underway. The very large draught of these ships now invalidates the assumption of deep-water conditions as fully laden vessels approach harbours or progress along channel routes. Let us assume that, by virtue of its forward motion, the ship has a trim by the bow indicating significant suction pressures on the hull in that region and high mainstream water velocities realtive to the hull. As the ship travels into a region in which the water depth decreases the keel approaches the sea bottom nearest to the bow. The water flow relative to the hull is therefore similar to that through a Venturi meter [2] in which the lowest pressures at the throat correspond to the conditions below the bow of the ship. Several factors are now called into play. The ship will settle lower in the water, a behaviour often referred to as *squat*, which in turn causes a further increase in C_{att}. Since the clearance under the keel has been reduced there is a danger of collision with obstructions. Erosion of the sea bed, if it consists mainly of mud or sand, may also take place. Although this can be, in effect, a means of dredging clear a channel the deposition of the bed material elsewhere may cause further problems by silting up banks and reducing the breadth of the channel. In order to reduce squat the speed of the ship may be reduced, but then manoeuvrability becomes more difficult. The various mechanisms of the phenomenon are discussed in [52].

The overall resistance coefficient of a ship may contain additional sources represented by the coefficients of (a) appendage resistance C_{app}, (b) aerodynamic resistance of the above-water profile C_{aero}, (c) the propeller–hull interaction resistance increment $C_{p/h}$, and (d) ice resistance C_{ice}, if operation takes place in arctic waters. Let us consider these in turn.

(a) C_{app}

The flow over model appendages such as shaft(s), bilge keels, stern tube(s), brackets, bosses, etc. will be substantially laminar owing to low values of Re. Extrapolation to the prototype is thus likely to produce errors in appendage resistance. Several rough-and-ready correlation rules exist [25], but much work still needs to be done before these become reliable. For example, the addition of appendages can increase the model resistance by as much as 15 per cent of the bare-hull value, whereas only half this increment is likely to occur for the full-scale ship.

The effect of appendages on resistance has been investigated more recently by Holtrop [53]. It was noted that by simply adding the wetted surface area of the appendages S_{app} to the wetted surface area of the bare hull S_w gave a total wetted surface area S_{tot} which, when introduced into Equation (5.39a), say, to obtain k from R_V (at 'run in'), underestimated the appendage resistance. It was suggested that the form factor for the bare hull $r_1 = 1 + k_1$ should be increased by an amount $(k_2 - k_1)S_{app}/S_{tot}$, where the 'appendage form factor' is $1 + k_2$. The increase was small when the appendage length was of the same order as the ship length as in the case of bilge keels. On the other hand, the increase can be substantial when the appendages are small in length, for example, shaft bossings in a twin-screw ship where the effect of aft appendages on resistance is known to be considerable. This behaviour no doubt owes much to the effect of wake flows from short, bluff appendages on both viscous pressure resistance of the appendages themselves and subsequent interference on the flow past the hull within the region of the appendages. A series of experiments by Holtrop led to a graphical relationship between $1 + k_2$ and a 'virtual' appendage length L_{app} expressed as a proportion of the ship length. This technique of representing the form factor of the bare hull plus appendages as $1 + k$ where

$$1 + k = 1 + k_1 + (k_2 - k_1)S_{app}/S_{tot}$$

was used in [49] with some success for the ships examined there.

(b) C_{aero}

Aerodynamic resistance arises from the relative velocity between the above-water profile of the ship and the atmosphere. This relative velocity is not, in general, equal to V nor is it in the same direction. The superstructure can rarely be thought of as streamlined, even for forward motion of the ship in still air. For operation at normal speeds into a head wind, the aerodynamic force (resistance) is given by Hughes [54] as

$$F_{aero} = R_{aero} = C_{aero} \times \tfrac{1}{2}\rho_a V_a^2 S_T, \tag{5.42}$$

where ρ_a represents the density of the air, V_a represents the velocity of the air relative to the ship (= V in still air), and S_T represents the transverse projected surface area of the above-water profile (account being taken of the streamlining effect of the hull).

Hughes found that C_{aero} varied between 1.0 and 2.0 for different ships and also that Equation (5.42) could be used for wind directions other than ahead. For a given above-water profile he showed that the maximum resistance to motion occurred when the wind was about 30° off the bow. Considerable reductions in R_{aero} can be achieved with quite simple streamlining which will also cause an increase in ship speed for the same propulsive power. However, as we saw in Chapter 2, when a wind blows there is a substantial velocity gradient normal to the water surface up to a height of 20 m (≅ 70 ft) or so. Recent work in wind tunnels which has taken this into account suggests that Hughes' values of C_{aero} would be some 30–50 per cent too great.

Measurements and calculations using tankers and their models show considerable differences from Hughes' early work owing to the substantially different geometries of the above-water profile of the ships examined. In [55] the wind coefficients affecting resistance and therefore loss of speed of tankers have been investigated. It was pointed out that the aerodynamic resistance to be added to the hydrodynamic resistance consists essentially of three parts:

(i) Direct wind resistance acting in the fore-and-aft direction;

(ii) Steering resistance arising from the transverse force and yawing moment of the above-water parts of the ship in a steady wind. To compensate for this force and moment the ship assumes a drift angle on the hull and a rudder deflection (these latter topics are discussed in Chapter 8).

(iii) Steering resistance produced by an unsteady wind. Under unsteady wind conditions the ship will yaw (see Chapter 8) and thus develop a further contribution to wind resistance.

Model tests were carried out on a 2.2 m (≅ 7.2 ft) long model in a wind tunnel and several modifications were made to the deckhouse configuration to determine its influence on the total wind resistance. An important feature of the model work was the simulation of an atmospheric boundary layer over the ground board to which the hull was fixed at the assumed water line. However, under these circumstances the question arises as to which velocity should be used in forming the dimensionless aerodynamic resistance coefficient. One possibility is to weight V_a with respect to height in the absence of the ship and at, say, the mid-section location. Taking horizontal strips of height δh across the projected above-water area in the vertical plane, of height h_s, allows V_a^2 at infinity to be replaced by

$$\frac{1}{h_s}\int_0^{h_s} V_a^2 \, \mathrm{d}h.$$

Although corrections such as this may lead to adjustments of up to 20 per cent for the coefficients, it was decided in [55] to adopt the mainstream velocity for the model tests as the reference value. In addition, the square of the water-line length was used instead of projected area, together with additional data provided on both transverse and longitudinal projected areas since these were deemed to be the main parameters affecting the wind resistance coefficients along with the relative wind direction. Deckhouse geometry, trim and so on were found to be of secondary importance. The model results were compared with those given in [56] and others and with calculations [57]. Although the magnitudes of the resistance coefficient varied for a given wind direction there was a general similarity in shape of the curves which covered a wide range of above-water profiles.

Following full-scale tests on a tanker with a length of over 300 m (≅ 1000 ft) and with a deadweight of 2.82 GN (≅ 282 000 tonf) it was concluded that the main contribution to added resistance comes from direct wind resistance. Even with improved design of the above-water parts it was found that R_{aero} amounted to 2 per cent of R_T for a ship travelling through still air. Results for a typical tanker profile with the relative wind on the bow showed that R_{aero}/R_T increased to 7.5 per cent when $V_a/V = 2$ and to 17 per cent when $V_a/V = 3$, which is equivalent to a ship travelling at 6 m s^{-1} ($\cong$ 12 knots) into a wind of 12 m s^{-1} ($\cong$ 24 knots). Clearly then, wind speed plays a significant part in the power estimation of tankers and fast cargo ships; wind resistance may result in speed reductions of five to ten per cent. The operation of the rudder to correct for yaw and drift produces further increments. However, it is still not clear if a general approach to air resistance can be made or whether the separate treatments of aerodynamic and hydrodynamic resistance components conceal some important interaction effects.

(c) $C_{p/h}$

Assuming that $(C_T)_P$ has been found we must now allow for the effect of the propeller on the ship resistance. The coefficient of resistance of the ship–propeller combination $(C_T)_{s/p}$ is usually found empirically by the addition of a suitable value of $C_{p/h}$ obtained from towing tests on the propeller–hull combination. Thus

$$(C_T)_{s/p} = C_T + C_{p/h}. \tag{5.43}$$

The correction may be negative as the propeller could improve the flow conditions at the stern to reduce C_{PV}.

The determination of any augmentation to the resistance which results from the addition of a propeller to a hull with appendages is rather complicated and depends, in no small degree, on experimentation and empiricism. The effects of geometric scale on Reynolds number are again important owing to the small size of model propellers used for the propulsion of hulls in towing and manoeuvring tanks. The various techniques used to predict the overall thrust requirement from propulsors are discussed in Chapter 7.

The overall resistance of the full-scale prototype ship is given by

$$(R_{ov})_P = [\tfrac{1}{2}\rho_w S_w V^2 \{(C_T)_{s/p} + C_{att} + C_{app}\} + \tfrac{1}{2}\rho_a S_T V_a^2 C_{aero}]_P \tag{5.44}$$

where ρ_w is the density of water and S_w is the wetted surface area of the hull. However, throughout the preceding discussion resistance to motion has been estimated on the assumption that the hull is clean; that is, we have allowed roughness as the result of manufacture, but not as that which arises from fouling and corrosion. Clearly, as the underwater surface of the hull becomes dirty with time spent at sea the resistance to motion increases. Account of this is usually taken by modifying the skin-friction resistance coefficient for the clean ship. A usual assumption supposes C_F to increase by 0.25 per cent per day spent at sea and the deep-and-dirty (i.e. normal displacement) state is reached after six months. Thus the increase of C_F which must be added to the clean C_F to give the deep-and-dirty friction coefficient is

$$\left(\frac{365}{2} \times \frac{0.25}{100}\right) C_F = 0.456 C_F$$

and so

$$\left(\underset{\text{deep-and-dirty}}{C_F}\right) = 1.456C_F = C_{F_{d/d}}.$$

This value of $C_{F_{d/d}}$ is therefore incorporated into C_T of Equation (5.43).

(d) C_{ice}.

Arctic marine technology has long been associated with the running of the industrial and commercial enterprises of northern Europe and the USSR. Everyday life must be sustained against the harshness of long winters which can disrupt transport and communications systems. The promise of extensive oil, gas and mineral deposits in Alaska and northern Canada, along with advanced warning and defensive networks, has given rise to intensive programmes of technological development albeit based on the same basic principles. The successful erection and operation of oil and gas platforms in the North Sea has led to the widespread investigation of further sources fringing on arctic waters. The policing of existing and proposed platforms requires, therefore, the operation of marine vehicles in regions where substantial ice coverage of the sea surface may occur for considerable periods of the year. The passage of ice past fixed structures gives rise to similar problems of resistance augmentation. Some ships are of course designed for ice-breaking duties, either as specialist craft opening channels in areas of sea ice up to the pack-ice regions or as cargo vessels with specially strengthened bows to make single transits.

The resistance to motion of a ship through ice may be as much as fifty times that of the open-water resistance at corresponding speeds. The first attempts at resistance estimation concentrated on the depth and penetration of an ice cover which could be broken by a vessel when ramming. Nowadays, resistance is studied in the context of continuous steady state motion, and this has suggested that ice resistance is a complex function of ice geometry and physical properties, weight per unit mass g, ship geometry and speed, and various form parameters. The ice resistance is then added to the hydrodynamic resistance R_T of the underwater hull which at the low speeds appropriate to movement through ice comprises mainly the viscous component R_V.

One form of the ice resistance equation now in common use [58] is

$$R_{ice} = C_1 \sigma_i B h_i + C_2 \rho_i g B h_i^2 + C_3 \rho_i B h_i V^2 \tag{5.45}$$

where C_1, C_2 and C_3 are coefficients, σ_i is the flexural yield stress of ice, ρ_i is the density of ice, h_i is the thickness of the surface ice, B is the beam of the ship and V is the forward speed of the ship. For various homologous series of hull shapes the coefficients become rather complicated functions and difficult to predict consistently.

The three terms on the right-hand side of Equation (5.45) may be interpreted as follows:

First term: the resistance arising from both cutting and bending forces imposed by the bow of the ship;

Second term: the resistance arising from the submergence and subsequent overturning of pieces of broken ice as the channel is cleared;

Third term: the resistance resulting from moving aside pieces of ice from the side of the ship during passage along the cleared channel; this component is a function of the speed of the ship.

Since the speed of ships is low when negotiating ice floes, it is found [59] that of the various equations for R_{ice} now in use the differences stem from the third term on the right-hand side of Equation (5.45). The exponent of V may vary between 1 and 2, but if we retain the form of Equation (5.45) then the coefficient of ice resistance may be represented as

$$C_{ice} = \frac{R_{ice}}{\rho_i g B h_i^2} = C_1 \frac{\sigma_i}{\rho_i g h_i} + C_2 + C_3 \left(\frac{V}{\sqrt{(gh_i)}}\right)^2. \tag{5.46}$$

The quantity $\sigma_i/\rho_i g h_i$ is referred to as the ice strength parameter and is the ratio of the flexural yield stress to gravity loading of the floating ice per unit surface area, and $V/\sqrt{(gh_i)}$ is the ice-thickness Froude number. It is seen in Equation (5.46) that no effect of skin friction is included owing to the absence of Reynolds number, but since inertia forces associated with ice movements are very large this is hardly surprising.

To date the development of reliable and general techniques for predicting the coefficients C_1, C_2 and C_3 has defied theoretical analysis. The most reliable data come from model tests in tanks using saline or synthetic ice, but even then disagreement occurs [60]. Usually, the model ice density and ice–hull friction factor are kept equal to the corresponding values at full scale. It is then straightforward to show that the model ice thickness, flexural yield stress and elastic modulus are smaller than the corresponding ship values by the linear scale factor. These conditions are best satisfied by using low-salinity ice near its melting point and by giving careful attention to the model surface. Tests have confirmed the form of Equation (5.46), but the results of experiments with a variety of model and ship forms [61] show that the resistance coefficients vary widely: C_1, 0.000 to 0.0483; C_2, 13.32 to 132.09; C_3, 0.0495 to 0.322.

The preceding discussion has been restricted to steady forward speeds through ice floes of uniform thickness. Such conditions seldom exist, however, because ice floes are discontinuous, have variable thicknesses and properties as a result of different ages and are ridged with hummocks to produce hard spots. The treatment of ship motions through non-uniform ice is beyond the scope of this book, but a summary can be found in [59] and a theoretical analysis of ship resistance to continuous motion in ice is given in [62]. Some full-scale trials data are given in [63] and correlations between full-scale and model tests are presented in [64].

References

1. Dean, R. C. (1959), On the necessity of unsteady flow in fluid machines. *J. Basic Engng, (Trans. Am. Soc. Mech. Engrs)*, 81, 24–8.
2. Massey, B. S. (1979), *Mechanics of Fluids*, 4th Edn, Van Nostrand Reinhold, London.
3. Schlichting, H. (1979), *Boundary Layer Theory*, 7th Edn, McGraw-Hill, New York.
4. Gadd, G. E. (1971), The approximate calculation of turbulent boundary layer development on ship hulls. *Trans. R. Inst. Nav. Archit.*, 113, 59–71.
5. Gadd, G. E. (1973–4), A comparison of some model and full scale hull boundary layer measurements. *Trans. North-East Coast Inst. Engrs Shipbuilders*, 90, 51–8. (See also: *Ship Rep. NPL*, No. 179, April 1974.)
6. Milne-Thomson, L. M. (1968), *Theoretical Hydrodynamics*, 5th Edn, Macmillan, London.
7. Thwaites, B. (ed.) (1960), *Incompressible Aerodynamics*, Clarendon Press, Oxford.

8. Gadd, G. E. (1977), Scale effect on stern separation and resistance of a full hull form. *Trans. R. Inst. Nav. Archit.*, 119, 391–403.
9. Shearer, J. R. and Steele, B. N. (1970), Some aspects of the resistance of full form ships. *Trans. R. Inst. Nav. Archit.*, 112, 465–86.
10. Gadd, G. E. (1968), On understanding ship resistance mathematically. *J. Inst. Math. Applic.*, 4, 43–57.
11. Kelvin, Lord (then Sir W. Thomson) (1887), On the waves produced by a single impulse in water of any depth, or in a dispersive medium. *Proc. R. Soc.*, 42, 80–3.
12. Kelvin, Lord (then Sir W. Thomson) (1887), On ship waves. *Proc. Inst. Mech. Engrs*, 3, 409–34.
13. Froude, W. (1877), Experiments upon the effect produced on the wave making resistance of ships by length of parallel middle body. *Trans. Inst. Nav. Archit.*, 18, 77–97. (See also: *The Papers of William Froude*, (1955), 311–19, Institution of Naval Architects, London.)
14. Kelvin, Lord (1904), (a) On deep water two-dimensional waves produced by any given initiating disturbance, (b) On the front and rear of a free procession of waves in deep water, (c) Deep water ship waves. *Proc. R. Soc. (Edinb.)*, 25, (a) 185–96, (b) 311–27, (c) 562–87.
15. Havelock, T. H. (1934), Wave patterns and wave resistance. *Trans. Inst. Nav. Archit.*, 76, 430–46.
16. Stoker, J. J. (1957), *Water Waves*, Wiley Interscience, New York.
17. Arentzen, E. S. and Mandel, P. (1960), Naval architectural aspects of submarine design. *Trans. Soc. Nav. Archit. Mar. Engrs*, 68, 622–92.
18. Russo, V. L., Turner, H. and Wood, E. N. (1960), Submarine tankers. *Trans. Soc. Nav. Archit. Mar. Engrs*, 68, 693–742.
19. Froude, W. (1868), Observations and suggestions on the subject of determining by experiment the resistance of ships. *Memorandum* to Mr E. J. Reed, Chief Constructor of the Navy. (See also: *The Papers of William Froude*, (1955), 120–7, Institution of Naval Architects, London.)
20. Froude, W. (1876), The fundamental principles of the resistance of ships. *Proc. R. Inst. Gt Br.*, 8, 188–213, (See also: *The Papers of William Froude*, (1955), 298–310, Institution of Naval Architects, London.)
21. Wigley, W. C. S. (1942), Calculated and measured wave resistance of a series of forms defined algebraically, the prismatic coefficient and angle of entrance being varied independently. *Trans. Inst. Nav. Archit.*, 84, 52–74.
22. Wigley, W. C. S. (1936), The theory of the bulbous bow and its practical application. *Trans. North-East Coast Inst. Engrs Shipbuild.*, 52, 65–83.
23. Inui, T. (1962), Wavemaking resistance of ships. *Trans. Soc. Nav. Archit. Mar. Engrs*, 70, 283–353.
24. Yim, B. (1974), A simple design theory and method for bulbous bows of ships. *J. Ship Res.*, 18, 141–52.
25. Todd, F. H. (1967), *Resistance and Propulsion*, Chapter 7 of *Principles of Naval Architecture*, (ed. J. P. Comstock), Society of Naval Architects and Marine Engineers, New York.
26. Wehausen, J. V. (1973), The wave resistance of ships. *Adv. Appl. Mech.*, 13, 93–245.
27. Amfilokhiev, W. B. and Conn, J. F. C. (1971), Note on the interaction between the viscous and wavemaking component resistances. *Trans. R. Inst. Nav. Archit.*, 113, 43–57.
28. Steele, B. N. and Pearce, G. B. (1968), Experimental determination of the distribution of skin friction on a model of a high speed liner. *Trans. R. Inst. Nav. Archit.*, 110, 79–100.
29. Gadd, G. E. and Hogben, N. (1965), The determination of wave resistance from measurements of the wave pattern. *Ship Rep. NPL*, No. 70.
30. Shearer, J. R. and Cross, J. J. (1965), The experimental determination of the components of ship resistance for a mathematical model. *Trans. R. Inst. Nav. Archit.*, 107, 459–73.
31. Townsin, R. L. (1971), The viscous drag of a 'Victory' model. Results from wake and wave pattern measurements. *Trans. R. Inst. Nav. Archit.*, 113, 307–21.
32. Paffett, J. A. H. (1972), Resistance Components: Report of Resistance Committee, Appendix 2, *Proc. 13th ITTC*, Berlin/Hamburg, 1, 53–60.
33. Schoenherr, K. E. (1932), Resistance of flat surfaces moving through a fluid. *Trans. Soc. Nav. Archit. Mar. Engrs*, 40, 279–313.
34. Hughes, G. (1952), Frictional resistance of smooth plane surfaces in turbulent flow. *Trans. Inst. Nav. Archit.*, 94, 287–322.

35. Hughes, G. (1954), Friction and form resistance in turbulent flow and a proposed formulation for use in model and ship correlation. *Trans. Inst. Nav. Archit.*, 96, 314–76.
36. Telfer, E. V. (1927), Ship resistance similarity. *Trans. Inst. Nav. Archit.*, 69, 174–90.
37. Telfer, E. V. See further work on geosims in *Trans. Inst. Nav. Archit.*, e.g. 92, 1–29, 1950; 93, 205–34, 1951; 95, 135–56, 1953.
38. Scott, J. R. (1969), On estimation of smooth ship resistance for model tests. *Trans. R. Inst. Nav. Archit.*, 111, 203–16.
39. Gadd, G. E. (1967), A new turbulent friction formulation based on a reappraisal of Hughes' results. *Trans. R. Inst. Nav. Archit.*, 109, 511–29.
40. Conn, J. F. C. (1975), Ship resistance – retrospect and prospect, *Trans. North-East Coast Inst. Engrs Shipbuild.*, 91, 67–84.
41. Froude, W. (1874), Experiments with *HMS Greyhound. Trans. Inst. Nav. Archit.*, 15, 36–73.
42. Denny, M. E. (1951), BSRA resistance experiments on the *Lucy Ashton*, part I: Full scale measurements. *Trans. Inst. Nav. Archit.*, 93, 40–57.
43. Conn, J. F. C., Lackenby, H. and Walker, W. P. (1953), BSRA resistance experiments on the *Lucy Ashton*, part II: The ship-model correlation for the naked hull condition. *Trans. Inst. Nav. Archit.*, 95, 350–436.
44. Lackenby, H. (1955), BSRA resistance experiments on the *Lucy Ashton*, part III: The ship-model correlation for the shaft appendage condition. *Trans. Inst. Nav. Archit.*, 97, 109–66.
45. Livingston-Smith, S. (1955), BSRA resistance experiments on the *Lucy Ashton*, part IV: Miscellaneous investigations and general appraisal. *Trans. Inst. Nav. Archit.*, 97, 525–61.
46. Grothues-Spork, H. (1965), On geosim tests for the research vessel *Meteor* and a tanker. *Trans. Inst. Mar. Engrs*, 77, 259–78.
47. Aertssen, G. (1961), Sea trails on two cross channel twin-screw motorships. *Trans. R. Inst. Nav. Archit.*, 103, 181–218.
48. Lackenby, H. (1962), The resistance of ships with special reference to skin friction and hull surface condition. *Proc. Inst. Mech. Engrs*, 176, 981–1014.
49. Aertssen, G., Gadd, G. E. and Colin, P. E. (1980), A method of ship resistance prediction: wave resistance and viscous resistance, *Trans. R. Inst. Nav. Archit.*, 122, 407–26.
50. Gadd, G. E. (1976), A method of computing the flow and surface wave pattern around full forms. *Trans. R. Inst. Nav. Archit.*, 118, 207–19.
51. Canham, H. J. S. (1975), Resistance, propulsion and wake tests with *HMS Penelope*. *Trans. R. Inst. Nav. Archit.*, 117, 61–94.
52. Dand, I. W. and Furguson, A. M. (1973), The squat of full ships in shallow water. *Trans. R. Inst. Nav. Archit.*, 115, 237–55.
53. Holtrop, T. (1977), A statistical analysis of performance test results. *Int. Shipbuild. Prog.*, 24, 23–8.
54. Hughes, G. (1930), Model experiments on the wind resistance of ships. *Trans. Inst. Nav. Archit.*, 72, 310–30.
55. van Berlekom, W. B., Trägårdh, P, and Dellhag, A. (1975), Large tankers – wind coefficients and speed loss due to wind and sea. *Trans. R. Inst. Nav. Archit.*, 117, 41–58.
56. Shearer, K. D. A. and Lynn, W. M. (1960), Wind tunnel tests on models of merchant ships. *Trans. North-East Coast Inst. Engrs Shipbuild.*, 76, 229–66.
57. Isherwood, R. M. (1973), Wind resistance of merchant ships. *Trans. R. Inst. Nav. Archit.*, 115, 327–38.
58. Lewis J. W. and Edwards, R. Y. (1970), Methods for predicting icebreaking and ice resistance characteristics of icebreakers. *Trans. Soc. Nav. Archit. Mar. Engrs*, 78, 213–49.
59. Peirce, T. H. (1979), Arctic marine technology: a review of ship resistance in ice. *Trans. R. Inst. Nav. Archit.*, 121, 219–35.
60. Crago, W. A., Dix, P. J. and German, J. G. (1971), Model icebreaking experiments and their correlation with full scale data. *Trans. R. Inst. Nav. Archit.*, 113, 83–108.
61. Vance, G. P. (1975), A scaling system for vessels modelled in ice. *Ice Tech. Symp.*, Society of Naval Architects and Marine Engineers, New York.

62. Milano, V. R. (1973), Ship resistance to continuous motion in ice. *Trans. Soc. Nav. Archit. Mar. Engrs*, 81, 274–306.
63. Noble, P. G., Allan, R. J., Dunne, M. A. and Johnson, B. (1978), Ice effect trials in arctic waters on *CCGS Louis S. St Laurant. Trans. Soc. Nav. Archit. Mar. Engrs*, 86, 277–303.
64. Edwards, R. Y., Lewis, J. W., Wheaton, J. W. and Coburn, J. (1972), Full-scale and model tests of a Great Lakes icebreaker. *Trans. Soc. Nav. Archit. Mar. Engrs*, 80, 170–207.

6
Steady Motion at High Speeds

6.1 Introduction

The search for effective high-speed vehicles has a long history, but it is only over the past 25 years or so that intense activity has taken place. Design requirements such as high speed, reliability, passenger comfort, manoeuvrability over the speed range, good seakeeping qualities (i.e. minimum response to waves) and so on have now been joined by considerations of fuel economy, ferry demands, launching platforms for missiles and helicopters in naval applications, endurance for fishery protection duties and many others. As a result a number of well known concepts have been further developed and refined and a variety of other craft and surface effect ships (SES) are under evaluation. Recent discussions of many fast craft and their proposed duties can be found, for example, in [1, 2] and we shall later make specific reference to some particular work therein. However, we shall confine our attention here to the principal forms of high-speed craft, namely, planing craft, hydrofoil craft and hovercraft, the latter as a particular case of an air-cushion vehicle (ACV). Nevertheless, brief mention is made of new ideas in the belief that future scenarios may incorporate them in important military and commercial rôles.

For an examination of the steady motion of high-speed vehicles the main parameters of interest are the total resistance and its components as functions of forward speed. It is convenient to think both in terms of resistance coefficients as well as actual resistances. It was shown in Chapter 5 that the coefficient of wave-making resistance C_W for conventional displacement ships increases with Froude number *Fr* until *Fr*, based on water-line length L_{WL}, is about 0.5, whereupon C_W declines steadily for higher values of *Fr*. When $Fr \geqslant 1.5$ the wave-making resistance R_W is a relatively small component of the total resistance R_T because C_W is exceedingly small. Although for conventional displacement ships the coefficient of viscous resistance C_V $(= C_F + C_{PV})$ decreases as *Fr* increases, the viscous resistance R_V $(= R_F + R_{PV})$ increases rapidly for a constant wetted area owing to its dependence on V^2. For speeds greater than, say, 20 m s^{-1} ($\cong$ 40 knots) the conventional displacement vehicle is uneconomic because of the enormous power installation and fuel tanks required. We must now examine, therefore, the means by which the *rate* of increase of resistance with increasing forward speed can be limited.

Briefly, this may be done as follows:

(i) Raise the hull in the water, by the application of a dynamic supporting force, to reduce the wetted surface area of the hull.

(ii) Raise the hull clear of the water and support the vehicle by dynamic forces applied to appendages fixed to the vehicle.

(iii) Raise the hull clear of the water and support the craft by means of aerostatic jet reaction forces.

The vehicles typical of these three modes of support are, respectively, (i) the planing craft, (ii) the hydrofoil craft, and (iii) the air-cushion vehicle (the hovercraft). In type (iii) there is a whole range of so-called ground-effect machines (GEM) including the operation of air bearings, but we shall take a simple form of hovercraft to demonstrate the principle of generating aerostatic forces.

It will be assumed that for all these craft forward motion takes place at a steady velocity V along the line of longitudinal symmetry of each vehicle and in a direction parallel to the air–water interface, that is, horizontal.

6.2 Planing Craft

The pressure distribution over the wetted hull of a displacement vehicle in motion changes from that which prevails under hydrostatic conditions. As a result the attitude (trim) of the vehicle adjusts to the new equilibrium requirements, although generally the displacement volume is little changed. However, if the hull is suitably shaped, the hydrodynamic forces developed during forward motion can be sufficient to support the craft with a substantial proportion of the hull out of the water. The wetted area is thus less than at low speed, and so for a given speed R_V is also reduced. However, the aerodynamic resistance of the above-water profile is increased somewhat. The wave-making resistance becomes small at high speeds and even though R_T is then large it is considerably less than the resistance of a conventional displacement ship moving at the same speed.

When at rest the planing craft resorts to buoyancy for support, whereas at low forward speeds a combination of hydrostatic and hydrodynamic supporting forces exists. We shall examine the means of generating the hydrodynamic supporting forces on an immersed hull and consider subsequently the craft in 'full flight' when these forces predominate.

6.2.1 *Generation of Hydrodynamic Forces*

When a fixed, flat plate is held normal to and symmetrically across an inviscid, homogeneous, steady, free jet of water the jet divides evenly about the stagnation streamline on approaching the plate and then escapes along the surface as shown in Fig. 6.1. It is supposed that, for the sake of simplicity, the ambient pressure p_a surrounding the jet and the rear of the plate is constant. The momentum of the jet

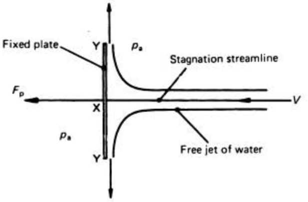

Fig. 6.1

in the direction of the approach velocity V is destroyed and a force F_p must therefore be exerted on the jet by the plate in a direction opposite to that of V. Clearly, the plate itself experiences an equal and opposite reaction. Alternatively, F_p can be considered to result from the distribution of pressure on the wetted surface. The pressure on the wetted surface of the plate reduces from a stagnation value at X to p_a at the edges Y, and this 'favourable' pressure gradient sustains the flow. It must be admitted that for real (viscous) fluids the behaviour of a jet impinging normally onto a plate is far more complicated than described here owing to the formation of a large eddy region at X and shear stresses at the surface of the plate.

Suppose the plate is rotated to some fixed inclination relative to the direction of the jet. The previous symmetry is now lost, a larger proportion of the jet being directed downwards as shown in Fig. 6.2. The stagnation streamline is neither completely straight nor coincident with the axis of the jet. Consequently, the net reaction F_p does not act at the stagnation point St but at the centre of pressure X, which is some distance aft of St. For an ideal fluid shear stresses are absent and F_p then results only from the pressure distribution on the wetted plate and is thus normal to the surface. If the jet approaches the plate horizontally F_p must have an upward (vertical) component F_v opposing the weight of the plate. In addition, there is a component of F_p parallel to the jet, in the direction of V, which can be interpreted as a drag force (resistance). An equivalent force system could be obtained if the jet were a stationary, horizontal column (an impossibility, of course!) and if the plate were propelled forward with a velocity V. The nearest practical equivalent to this, which would correspond to the mode of operation of a planing craft, is an inclined plate moving at an air–water interface. Obviously, the plate cannot extend across the whole of the upstream water, and the disturbance caused by the vehicle would then be restricted to a region near to and including the interface. Figure 6.3 illustrates the two-dimensional flow pattern relative to a flat plate which is of infinite extent normal to the plane of the paper and which is moving over the surface of a stationary body of water of infinite depth at a steady velocity V. Provided that the inclination of the plate is small the amount of water thrown forward is also small and is assumed, in theory, to travel to infinity (but in practice it degenerates to spray).

Of particular interest are the variations of local velocity q and local pressure p on the wetted surface of the plate. Results may be generalized by considering the velocity ratio q/V and the pressure coefficient $c_p = (p - p_a)/\frac{1}{2}\rho_w V^2$, where ρ_w is the density of the water. Typical results are shown in Fig. 6.4. The pressure distribution is sharply peaked near the stagnation point and theory indicates that this characteristic becomes more pronounced as the inclination decreases. It is also evident that because c_p is always positive the local pressure p is greater than p_a.

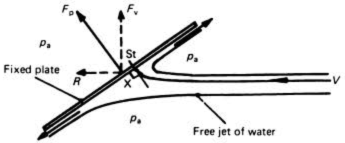

Fig. 6.2

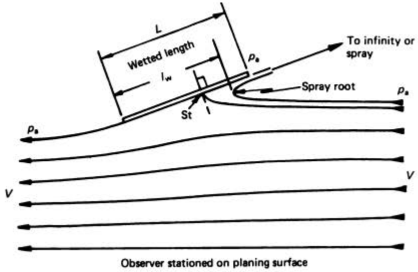

Fig. 6.3

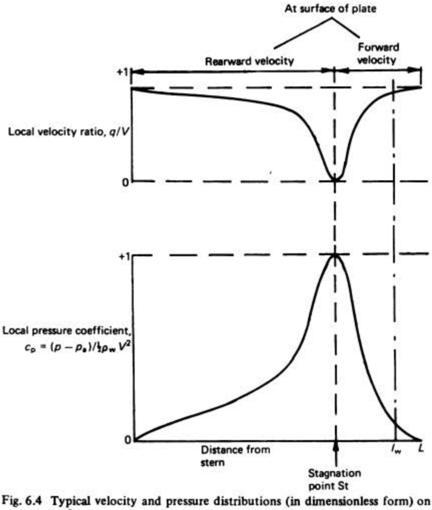

Fig. 6.4 Typical velocity and pressure distributions (in dimensionless form) on wetted planing surface.

Furthermore, pressure always decreases in the direction of the flow of water relative to the plate. The maximum pressure on a planing surface can be extremely high: for example, with $c_p = +1$, $V = 30\ \mathrm{m\ s^{-1}}$ ($\cong$ 60 knots) and $\rho_w = 1000\ \mathrm{kg\ m^{-3}}$ ($\cong$ 62.4 lbm ft^{-3}) the surface pressure relative to ambient, that is the gauge pressure, $p - p_a = \frac{1}{2}\rho_w V^2 = \frac{1}{2} \times 10^3 \times 900\ \mathrm{Pa} = 4.5 \times 10^5\ \mathrm{Pa}$ ($\cong$65.3 lbf in^{-2}) or about 4.5 atmospheres.

The normal force F_p and the location of the centre of pressure can be ascertained from the pressure distribution over the wetted surface. Alternatively, F_p can be deduced from a consideration of changes in either momentum flux or energy flux of the water in the vicinity of the plate. Details of both approaches are given by Du Cane [3] and the energy analysis is selected here for discussion. Let us suppose that a flat planing surface, inclined at an angle α to the air–water interface, moves forward horizontally at a steady velocity V through still water as shown in Fig. 6.5. The flow over the planing surface is two-dimensional and we take the view of a stationary observer placed outside the flow system. It is assumed that the main bulk of water over which the plate passes is stationary far upstream, far downstream and far below the interface. The only energy imparted to the water is, therefore, that 'thrown forward' off the underside of the plate. A simple application of Bernoulli's equation to the free-surface streamline shows that V is constant along that streamline if the ambient pressure is constant and the elevation of the leading edge of the plate above the interface is small enough to be neglected. The effect of the boundary layer on the wetted surface of the plate is neglected in the following analysis so that the water thrown forward must have a uniform velocity V relative to the plate. The absolute velocity of this water is thus the vector sum of the plate velocity V and the relative velocity of the water tangential to the plate, that is, $2V\cos(\alpha/2)$. The mass flow rate of the water thrown forward is $\rho_w V\delta$ per unit width, where δ is the depth of the water at the leading edge of the plate. By continuity, δ must equal the depth of the stagnation streamline below the interface well upstream from the plate. Hence, the energy flux supplied to the water by unit width of the plate must be

$$\tfrac{1}{2}(\rho_w V\delta)\,\{2V\cos(\alpha/2)\}^2$$

and this equals the rate at which work is done *on* the water by unit width of the plate. That is,

$$F_p' V \sin\alpha = \tfrac{1}{2}(\rho_w V\delta)\,\{2V\cos(\alpha/2)\}^2$$

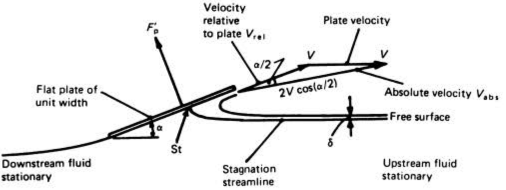

Fig. 6.5

since p_a has been assumed constant throughout. Whence,

$$F'_p = \rho_w V^2 \delta \left(\frac{2\cos^2(\alpha/2)}{\sin\alpha} \right)$$

that is,

$$F'_p = \rho_w V^2 \delta \cot(\alpha/2). \tag{6.1}$$

Equation (6.1) shows that a dynamic force is developed only if $\delta \neq 0$; in other words, water must be thrown forward and a sprayless planing craft is therefore impossible. Under some conditions the spray may fall back onto the hull and create an extra source of resistance to motion.

Since α has been assumed small the vertical (upward) dynamic force can be written as

$$F'_v = F'_p \cos\alpha = \rho_w V^2 \delta \cos\alpha \cot(\alpha/2) \cong \frac{2\rho_w V^2 \delta}{\alpha}. \tag{6.2}$$

Equation (6.2) may be divided throughout by $\frac{1}{2}\rho_w V^2 l$, where l is a characteristic length, to give

$$\frac{F'_v}{\frac{1}{2}\rho_w V^2 l} = C_{F'_v} = \frac{4}{\alpha}\left(\frac{\delta}{l}\right). \tag{6.3}$$

$C_{F'_v}$ can be considered to be a vertical force coefficient and is analogous to the section lift coefficient for fully submerged bodies. It is important to note that the analogy is not a strong one and that the generation of a lift force on a fully submerged body is fundamentally different from the derivation of F'_v. (The point is reconsidered in more detail in Section 6.3.1.) For small values of α we can use the approximation

$$C_{F'_v} \cong \alpha \left\{ \frac{\partial}{\partial\alpha}\left(C_{F'_v}\right) \right\}_{\alpha=0} \tag{6.4}$$

with the result that

$$\frac{\delta}{l} = \frac{\alpha^2}{4} \left\{ \frac{\partial}{\partial\alpha}\left(C_{F'_v}\right) \right\}_{\alpha=0} \tag{6.5}$$

In practice, the approximation defined by Equation (6.4) loses accuracy for flat plates of finite width owing to side-edge effects which disturb the two-dimensional nature of the flow. At $\alpha = 0$ both $C_{F'_v}$ and $\partial(C_{F'_v})/\partial\alpha$ are zero, but the latter is virtually constant at values of α slightly greater than zero. Thus Equation (6.5) should strictly read

$$\frac{\delta}{l} = \frac{\alpha(\alpha - \epsilon)}{4} \left\{ \frac{\partial}{\partial\alpha}\left(C_{F'_v}\right) \right\}_{\alpha=\epsilon}$$

where

$$C_{F'_v} = (\alpha - \epsilon) \left\{ \frac{\partial}{\partial\alpha}\left(C_{F'_v}\right) \right\}_{\alpha=\epsilon}$$

and ϵ might be of the order of 0.1 degrees.

6.2.2 *Hull Geometry*

While the flat plate under consideration is likely to satisfy hydrodynamic requirements at high speeds it is hardly a practical geometry. Local surface pressures on the wetted surface are very high and give rise to an uncomfortable ride. Furthermore, as the plate offers little resistance to drift the control of lateral motions is poor. These problems are overcome by the round-bottom hull (or round-bilge) form illustrated in Fig. 6.6. Once forward motion commences the boat sinks by the stern and a flat region of the hull is required to limit the sinkage and therefore the trim. As high speeds are approached a fine entry to the water is necessary, particularly in a seaway (i.e. in the presence of waves). The fore-body of rounded hulls thus becomes very narrow and little use can be made of the internal space. Instead, better results are obtained at high speed if the original flat plate remains as such near the stern but the under surface of the plate is transformed into an increasingly pronounced 'V' as the leading edge is approached with that edge sharpened, as shown in Fig. 6.7. To achieve good planing results and preserve the flat-plate characteristics the sides of the craft meet the under-surface 'V' at hard angles, that is, there is no rounding-off at the abrupt junction. Craft exhibiting this type of geometry are thus said to possess a 'hard-chine, V-bottom hull' and many of the present high-speed boats are of this kind.

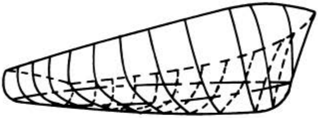

Fig. 6.6 Round-bilge hull form.

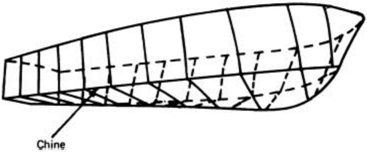

Fig. 6.7 Hard-chine, 'V' bottom hull form.

The angle which a 'V' hull makes with the horizontal is called the deadrise angle β, as indicated in Fig. 6.8. Contrary to our theoretical models the wetted beam is not, of course, infinite. The parameter used to account for this difference is the aspect ratio AR, which was introduced in Chapter 5. However, the definition of aspect ratio for the planing craft is not so straightforward to formulate as it was for the rectangular plank. For example, the chine line is not usually straight for practical craft and so the arithmetic average or mean wetted beam $\bar{b}_w$ must be used. We may

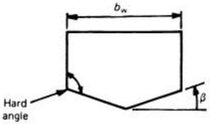

Fig. 6.8 Cross section of 'V' bottom of deadrise angle β.

now adopt the definition

$$\mathcal{R} = \frac{\overline{b_w^2}}{S} \tag{6.6}$$

where S is the plan area of the wetted surface. Similarly, the length of the wetted plan profile of the planing hull varies across the breadth and we therefore adopt a mean wetted length $\bar{l}_w$ defined as $S/\bar{b}_w$ so that

$$\mathcal{R} = \frac{\bar{b}_w}{\bar{l}_w}. \tag{6.7}$$

Once departure is made from the flat to the 'V' bottom the spray produced by the planing craft is no longer thrown wholly forward. The velocity of the spray is still V but it is directed transversely (with perhaps a rearward component) relative to the hull as illustrated in Fig. 6.9. Evidently, the more sternwards the relative velocity of the spray the lower become its absolute velocity and therefore its kinetic energy with the result that hydrodynamic forces on the hull are reduced. The resulting smoother ride thus improves passenger comfort and navigational control. For hulls with a small deadrise angle the spray emerges more or less at right angles to

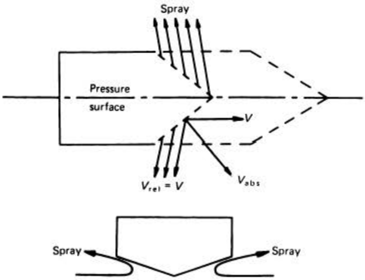

Fig. 6.9 Spray direction.

the forward direction, which gives rise to large hydrodynamic forces on the wetted hull and a hard ride. This behaviour is typical of power boats used for racing. Precautions are taken to protect individual crew members (not always with success) in an effort to minimize the wetted surface of the hull and maximize speed and endurance. Excessive wetting of round-bottom boats is avoided by fitting spray rails along the hull which form the same abrupt discontinuity of shape as the chine line and thus encourage a sharp detachment of water flow.

The total (all-up) weight W of the craft for cruise conditions includes the weight of the crew, stores, fuel, passengers, weapons and the like. (Note that we have abandoned the term weight displacement used for conventional ships because a planing craft cannot be regarded as a wholly displacement vehicle.) If R_T is the total resistance of the craft at a particular operating condition then a figure of merit, often called efficiency, can be deduced from the ratio W/R_T. The approximate effect of deadrise angle on maximum values of W/R_T is shown in Table 6.1, which was deduced from the results in [4] and presented in [3]. A compromise between hardness of ride, impact loading on the hull and high planing efficiency leads to a mean deadrise angle $\bar{\beta}$ of between 10 and 15 degrees. Consistent with this range of $\bar{\beta}$ and the corresponding range of $(W/R_T)_{max}$ it is found that $\mathcal{R}$ obtained from Equation (6.7) is of the order of 1.5 and the trim angle α is about 5 to 5.5 degrees. Various practical reasons often limit the trim angle to values rather less than this and 4 degrees is rarely exceeded when steady planing motion at the cruise speed has been reached.

Table 6.1 The variation of deadrise angle with maximum weight-to-resistance ratio.

$\bar{\beta}$(deg)	0	10	20	30
$(W/R_T)_{max}$	9.6	8.5	6.3	5.0

An operational craft with an aspect ratio of 1.5 would possess poor longitudinal stability. In practice values of $\mathcal{R} \leqslant 0.5$ are adopted, but a sacrifice in W/R_T must be made if the trim angle is to remain small. At the risk of sustaining very high bottom loadings and a hard ride the value of the mean wetted length $\bar{l}_w$ can be reduced significantly at high speeds by introducing a step in the hull (see Fig. 6.10) extending from the transom to about midships [5]. Sometimes a multiple step is incorporated to allow the bottom loading to be shared at two or more locations, but the added complication of the design, and relatively large resistance at low speeds, militate against this procedure. It is thus more usual to have stepless craft except in power boats and sporting craft. The addition of a small flap, trim tab or wedge at the transom provides a simple method of limiting both $\bar{l}_w$ and α at high speeds. With this device in operation the boat rises with forward speed but α is kept small and virtually unchanged. As the finer fore-body of the hull then continues to be submerged the viscous resistance of the hull decreases and may more than compensate for the additional resistance of the flap.

The availability of large digital computers and the development of complex programs have allowed a more detailed analysis of bottom loadings resulting from the pressure distribution on the wetted surface of planing craft to be undertaken.

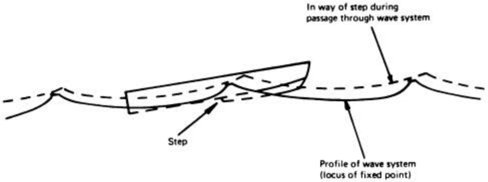

Fig. 6.10 Stepped hull.

In particular, the surface may be divided into a matrix of finite surface elements (often rectangular) for any given wetted planform. Hydrodynamic equilibrium and compatibility conditions must be satisfied at each element. An example of this approach is given in [6] where inviscid flow theory is used for calm-water planing and the equations of motion linearized to first-order magnitudes. The method compares well with some previous results and empirical data related to hard-chine craft. Furthermore, symmetry of the craft about the fore-and-aft axis is not an essential analytical requirement. Some calculations are also presented of the loadings on a stepped hull and of the effects of adding a wedge at the after end of the planing surface. The benefits of both these devices are shown in terms of a reduced power requirement for speeds above that corresponding to the lowest speed at which the transom stern runs dry.

6.2.3 *Forces on a Planing Craft*

Although it has been suggested that a planing craft moving at its cruise speed is supported by dynamic forces, it follows that if the resultant hydrodynamic force is applied to the under surface of the hull some part of the hull must be submerged. Thus for the semi-displacement craft it is necessary, as it was for the conventional displacement vessel, to adopt some means of identifying a buoyancy force when motion takes place. By this means we should be able to define the 'fully-planing régime', but as we shall see later this is not so evident as might be expected. Generally, the hard (chine) angle is nearly 90 degrees and $\bar{\beta}$ is so small that at a given speed we can assume that the boat is a rectangular box with a wetted beam $\bar{b}_w$, a wetted length $\bar{l}_w$, and at a trim angle α. The transom of the boat is usually unwetted, since the water cannot follow the rapid change of contour at the stern. The ideal hydrostatic system of forces is that shown in Fig. 6.11.

At some depth z below the free surface the (gauge) pressure on the wetted hull is $p = \rho_w g z$. The hydrostatic force on an elemental area of the surface $\bar{b}_w(\delta z/\sin\alpha)$ is, therefore,

$$\delta F_h = p\bar{b}_w\left(\frac{\delta z}{\sin\alpha}\right) = \left(\frac{\rho_w g \bar{b}_w}{\sin\alpha}\right) z\delta z.$$

In the limit $\delta z \to 0$ integration with respect to z between $z = 0$ at the surface and $z = \bar{l}_w \sin\alpha$ at the transom gives the net hydrostatic force acting at the centre of

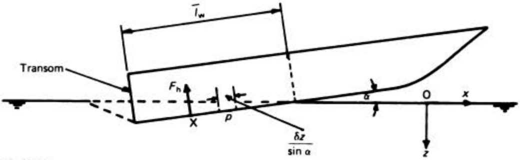

Fig. 6.11

pressure X, whence

$$F_h = \tfrac{1}{2}\rho_w g \bar{b}_w \bar{l}_w^2 \sin\alpha. \tag{6.8}$$

The upward (vertical) component of F_h is given by

$$F_h \cos\alpha = \tfrac{1}{2}\rho_w g \bar{b}_w \bar{l}_w^2 \sin\alpha \cos\alpha = \frac{\rho_w g \bar{b}_w \bar{l}_w^2}{4} \sin 2\alpha. \tag{6.9}$$

Note that because the transom is not submerged F_h has a rearward horizontal component given by

$$F_h \sin\alpha = \tfrac{1}{2}\rho_w g \bar{b}_w \bar{l}_w^2 \sin^2\alpha.$$

Furthermore, the vertical component of F_h does not act through a centre of buoyancy – it acts at X – and perhaps ought to be called a vertical hydrostatic force. The force is certainly not the buoyancy force applicable to displacement vehicles.

The system of forces acting on a planing craft in steady forward motion is shown in Fig. 6.12(a). Assuming geometric symmetry about the fore-and-aft vertical plane, the net forces acting on the craft may be taken to lie in that plane. The system thus comprises the following components:

F_h: the hydrostatic force, given by Equation (6.8), acting at the centre of pressure X on the bottom of the hull;

F_p: the net hydrodynamic force resulting from the variation of pressure over the wetted hull and acting at the hydrodynamic centre H on the bottom of the hull;

F_s: the net skin-friction force on the wetted hull;

T: the thrust produced by a propulsor to maintain the steady forward speed V; and

W: the all-up weight of the craft.

In order to reduce resistance at low forward speeds it is usual to provide some longitudinal curvature of the hull, especially near the bow. So, although the local pressure and shear stress are normal to each other on the wetted hull, the corresponding net integrated forces acting through the hydrodynamic centre need not be, the relative inclination depending on the shape of the hull. This has been taken into account by directing F_p and F_h at angles $\alpha + \phi$ and $\alpha + \psi$ to the vertical respectively. However, to avoid subsequent complication F_s has not been generalized in this way. In any case, when the craft is travelling at a high cruise speed the wetted hull has negligible longitudinal curvature.

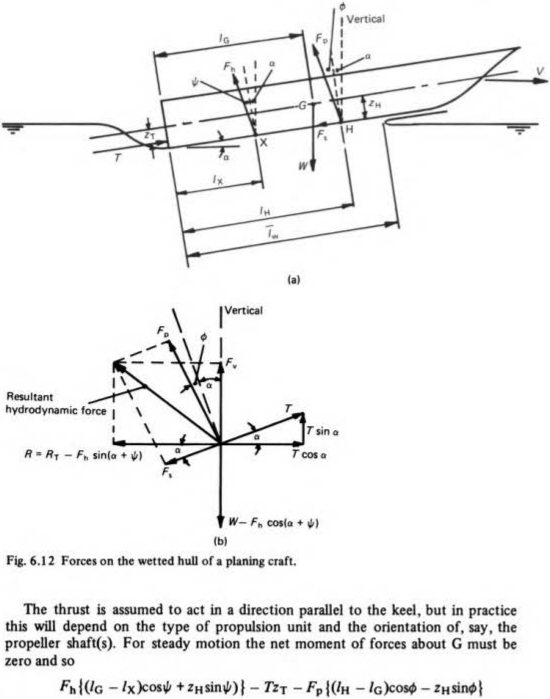

Fig. 6.12 Forces on the wetted hull of a planing craft.

The thrust is assumed to act in a direction parallel to the keel, but in practice this will depend on the type of propulsion unit and the orientation of, say, the propeller shaft(s). For steady motion the net moment of forces about G must be zero and so

$$F_h\{(l_G - l_X)\cos\psi + z_H\sin\psi)\} - Tz_T - F_p\{(l_H - l_G)\cos\phi - z_H\sin\phi\} + F_s z_H = 0. \tag{6.10}$$

Figure 6.12(b) shows the force diagram in which F_v is the vertically upward (supporting) dynamic force and R is the horizontal dynamic force (resistance). The resultant dynamic force on the hull can be considered to be the vector sum of either the components F_v and R or F_p and F_s. Thus, for the equilibrium of forces

$$W - F_h \cos(\alpha + \psi) - F_p \cos(\alpha + \phi) + F_s \sin\alpha - T \sin\alpha = 0,$$

that is

$$W - F_h \cos(\alpha + \psi) = F_v + T \sin\alpha \tag{6.11}$$

and

$$T \cos\alpha - F_h \sin(\alpha + \psi) - F_p \sin(\alpha + \phi) - F_s \cos\alpha = 0,$$

that is

$$T \cos\alpha = R + F_h \sin(\alpha + \psi) = R_T \tag{6.12}$$

where R_T is the total resistance equal to the horizontal component of the propulsive thrust.

At low forward speeds the equations of motion for a conventional displacement vehicle can be derived from Equations (6.10)–(6.12). The stern can then be assumed fully wetted so that the horizontal components of F_h must cancel. Hence, the resultant hydrostatic force is directed vertically upwards and is, therefore, the buoyancy force F_B which acts through the centroid of the immersed volume, that is, at the centre of buoyancy B. We know that at low speeds when $\alpha \to 0$ and $F_v \to 0$, $\phi \to \pi/2$. Assuming further that $T \sin\alpha \cong T\alpha \ll W$, Equations (6.11) and (6.12) reduce to

$$W = F_B \tag{6.13}$$

$$R = F_p + F_s = T = R_T \tag{6.14}$$

where F_p is the viscous pressure resistance which is small at low speeds. Since F_p and F_s are now parallel the hydrodynamic centre has no meaning and z_H must be interpreted as z_p and z_s, the distances below G of the lines of action of F_p and F_s respectively. The moment equation (6.10) reduces to

$$F_B(l_G - l_B) - Tz_T + F_p z_p + F_s z_s = 0 \tag{6.15}$$

where $l_X = l_B$, the distance from the stern to the centre of buoyancy.

When the forward speed is very high and significant planing action takes place $F_h \ll F_p$. For efficient planing α is small, $F_s \ll F_p$ and ϕ is small because β varies little over the wetted length. Furthermore, $T \sin\alpha \cong T\alpha \ll F_p$, and the force equations (6.11) and (6.12) can be simplified to

$$W = F_p \cos(\alpha + \phi) = F_v \tag{6.16}$$

$$\begin{aligned} R_T &= T \cos\alpha \cong T \\ &= F_p \sin(\alpha + \phi) + F_s \cos\alpha \\ &= W \tan(\alpha + \phi) + F_s. \end{aligned}$$

Then, as α and ϕ are very small

$$R_T = W\alpha + W\phi + F_s. \tag{6.17}$$

Equation (6.17) shows that the total resistance consists of three components which may be identified as follows:

(i) The component $W\alpha = \alpha F_v$ is called the induced resistance, or drag, and results from the inclination of F_p from the vertical owing to the trim angle of the craft.

(ii) The component $W\phi$ may be identified with wave-making and viscous pressure resistance. At high speed and small immersion the wave-making resistance is small.

(iii) F_s is the skin-friction resistance.

This breakdown of the total resistance illustrates a general principle associated with high-speed vehicles. At the (high) design speed the wave-making resistance is negligible, but the craft experiences induced drag in contrast to the reverse situation for conventional displacement vehicles at normal operating speeds.

Finally, at high speeds the moment equation (6.10) can be simplified to

$$F_p\{(l_H - l_G)\cos\phi - z_H\sin\phi\} = F_s z_H - T z_T$$
$$= F_s z_H - \left(\frac{F_p\sin(\alpha+\phi)}{\cos\alpha} + F_s\right) z_T,$$

which gives, on rearrangement,

$$(l_H - l_G) = (z_H - z_T)\left(\frac{F_s}{F_p}\sec\phi + \tan\phi\right) - z_T\tan\alpha. \tag{6.18}$$

As ϕ and α are both small it is reasonable to assume that z_H and z_T are both small and nearly equal. Equation (6.18) then shows that for 'fully-planing' conditions which correspond to the presence of dynamic supporting forces only

$$l_H \cong l_G, \tag{6.19}$$

that is, the hydrodynamic centre is located on the hull very closely below the centre of gravity. This result is incorporated in a design method for planing craft which is discussed in more detail later.

6.2.4 *Estimation of Forces on a Planing Craft*

In the following discussion it will be assumed that the longitudinal plane of symmetry of the craft is vertical and that fully-planing conditions apply so that $F_h \ll F_p$ and $T\alpha \ll F_p$.

For a hard-chine hull the independent variables which affect the values of F_v (or F_p), F_s and l_H are:

V, which is determined primarily by the propulsive thrust;

α, which is determined by the geometry of the wetted hull;

β, which determines the geometry of the wetted hull;

$\bar{l}_w$, which depends on the depth of immersion and the orientation of the hull;

$\bar{b}_w$, the mean wetted beam, which is determined by the geometry of the hull and is consistent with low drag;

g, the weight per unit mass, which is associated with distortion of the interface; and

ρ_w, μ_w, the density and dynamic viscosity respectively, which are properties of the water.

Note that $\bar{b}_w$ has been included in the list of independent variables for hard-chine hulls. If the deadrise were formed by two intersecting plates extending a large distance transversely then the wetted beam would vary with F_p and would not then be regarded as an independent variable. The wetted beam is also an independent variable for the case of a planing flat plate of finite aspect ratio since it affects the extent of side-edge effects. In reality, β varies with distance from the transom from, say, 3 degrees at the transom to 17 degrees at the mid-length. Generally, an average value of deadrise angle is used in analysis and in this given case we might take $\bar{\beta} = 10$ degrees. Experiments have shown, however, that for planing surfaces consisting of intersecting flat plates changes of β affect the dependent variables nonlinearly, so that some error will be involved in adopting $\bar{\beta}$.

For the hard-chine craft we can write the functional relationship

$$F_v = \text{function}\,(V, \alpha, \bar{\beta}, \bar{l}_w, \bar{b}_w, g, \rho_w, \mu_w) \tag{6.20}$$

and similarly for F_s and l_H. The application of dimensional analysis leads to

$$\frac{F_v}{\frac{1}{2}\rho_w V^2 \bar{l}_w^2} = \text{function}\left\{\alpha, \bar{\beta}, \frac{\bar{b}_w}{\bar{l}_w}, \frac{V}{\sqrt{(g\bar{l}_w)}}, \frac{\rho_w V \bar{l}_w}{\mu_w}\right\} \tag{6.21}$$

and similarly for $F_s/\frac{1}{2}\rho_w V^2 \bar{l}_w^2$ and $l_H/\bar{l}_w$. It must be remembered that Equation (6.21) applies to high-speed cruise operation, but attention must also be given to motion at low speeds.

Other, mainly geometric, variables need consideration, such as fore-body shape, chine shape, longitudinal curvature of the hull and so on. In principle, these are generally decided upon with regard to cargo, fuel, operating rôle, propulsion system, etc. When the designer has chosen a hull shape he must then determine values of F_s and l_H to calculate R_T and thus T for given values of $W(= F_v), \bar{\beta}, \bar{b}_w, g, \rho_w$ and μ_w at a steady cruise speed V. Because the flow about a practical hull is extremely complicated reliance is placed on accurate experimental data. Unfortunately, the form in which the functional relationship (6.21) is expressed contains the unknown wetted length $\bar{l}_w$ on both sides of the expression. However, as Murray [7] and others have argued it is the wetted beam that is the important parameter (because it varies little with speed) and not the wetted length. Thus, Equation (6.21) can be rearranged, according to the rules of dimensional analysis (discussed in Chapter 4), as follows

$$\frac{F_v}{\frac{1}{2}\rho_w V^2 \bar{b}_w^2} = \frac{W}{\frac{1}{2}\rho_w V^2 \bar{b}_w^2} = C_v = \text{function}\left\{\alpha, \bar{\beta}, \frac{\bar{b}_w}{\bar{l}_w}, \frac{V}{\sqrt{(g\bar{b}_w)}}\right\}. \tag{6.22}$$

The Reynolds number $Re = \rho_w V \bar{l}_w/\mu_w$ is not included in Equation (6.22) as experiments have shown it to have a negligible effect on the vertical force coefficient C_v. Since $\bar{\beta}$ and $V/\sqrt{(g\bar{b}_w)}$ are both known at the beginning of the design stage, Equation (6.22) shows C_v to depend on the two unknowns α and $\bar{b}_w/\bar{l}_w$.

To calculate the skin-friction coefficient C_F, and thence F_s, use is made of plank data such as those offered by the Schoenherr or the ITTC lines described in Chapter 5. In other words, C_{F_s} is assumed equal to C_F for the corresponding flat plank at a given Re and an additional allowance of 0.0004 is then included as for displacement ships. However, as the method of calculating C_F is the same as that for ships it must be open to the same criticisms raised earlier. The inclusion of a correlation allowance for the accurate use of model data is undoubtedly necessary but there seems to be no clear justification for its magnitude. It is thus implied that

$$C_F = \frac{F_s}{\frac{1}{2}\rho_w V^2 S_w} = \text{function}\left(\frac{\rho_w V \bar{l}_w}{\mu_w}\right) \tag{6.23}$$

$$\left(= \frac{0.075}{\{\log(Re) - 2\}^2}, \text{ for example}\right),$$

where S_w ($= \bar{l}_w \bar{b}_w \sec\bar{\beta}$) is the wetted surface area of the hull and $\bar{l}_w$ is again unknown. The form of C_F in Equation (6.23) is different from that suggested earlier, following Equation (6.21), but is in a more convenient form and obeys the rules of dimensional analysis.

In an effort to improve the prediction of the skin-friction force on a planing hull, miniature Preston tubes were used in [8] to provide a measure of the local shear stress. Owing to the small size of the model hull, that is length 0.9 m ($\cong$ 3 ft), beam 0.2 m ($\cong$ 8 in), the use of Preston tubes, about one-quarter of the usual length of 51 mm ($\cong$ 2 in), was first justified. An array of tubes was then set into the wetted hull of the model which had zero deadrise, vertical sides and a rectangular planform. Transom wedges of 2 and 5 degrees were included with the basic case and the tests carried out in a recirculating water channel. Following corrections to the Preston tube readings owing to the effects of pressure gradients in the hull boundary layer it was found that the integrated skin-friction coefficient for the model tested was about 2 per cent higher than the basic Hughes line (see Chapter 5) at a given Reynolds number. However, when account was taken of the aspect ratio $\bar{b}_w/\bar{l}_w = 0.2$ m/0.8 m = 0.25 for the model, it was found that the experimental C_{F_s} curve fell about 4 per cent below the Hughes and Schoenherr predictions. It may be concluded, therefore, that this difference arises from side-edge effects of planing hulls which are absent from fully submerged flat plates and planks. The result could be an over-estimation of the skin-friction force on a planing hull if the standard procedure for displacement vessels is used.

The analysis of experimental data has shown that the location of the hydrodynamic centre H is independent of both *Re* and *Fr* ($= V/\sqrt{(g\bar{b}_w)}$). Whence,

$$\frac{l_H}{\bar{b}_w} = \text{function } (\alpha, \bar{\beta}, \bar{b}_w/\bar{l}_w) \tag{6.24}$$

in which α and $\bar{l}_w$ are unknown.

The data in [9] can be used to develop a design method from empirical relations between the independent variables. Summaries of this development [7, 10–12] illustrate the technique with examples and charts are used to reduce the amount of algebraic manipulation of transcendental equations. For the reader's convenience and ease of reference the relationships are collected and discussed in the Appendix at the end of this chapter. The results of a typical calculation using the preceding data are shown in Fig. 6.13. In this case $W = 450$ kN ($\cong$ 45 tonf), $V = 21$ m s^{-1} ($\cong$ 42 knots), $\bar{\beta} = 8.25$ degrees, $\bar{b}_w = 3.76$ m ($\cong$ 12.3 ft), $l_G = 8.63$ m ($\cong$ 28.3 ft) and the overall length of the boat was 20.55 m ($\cong$ 67.4 ft) at the still-water line. As it happens, the location of the centre of gravity leads to an operating trim angle of just over 4 degrees and a resistance value just about the minimum. More usually, the $l_H = l_G$ condition is satisfied for rather smaller values of α (as shown in [7]) and this will not produce minimum resistance operation. It is pointed out that too large an angle of trim might result in porpoising, but it is also deduced that an increase of beam is rather unhelpful. Clearly, then, a compromise has to be made and this is often influenced by restrictions other than those imposed by hydrodynamics.

Resistance tests on a series of planing-hull forms (DTMB 62 Series) were performed by Clement and Blount [13] who presented their data in a way suitable for preliminary design calculations. The trim angle and the resistance-to-weight ratio were found to depend primarily on the aspect ratio, the location of the longitudinal centre of gravity and the size-to-weight ratio of the hull. (A deadrise angle of $\bar{\beta} = 12.5$ degrees was used throughout the tests.)

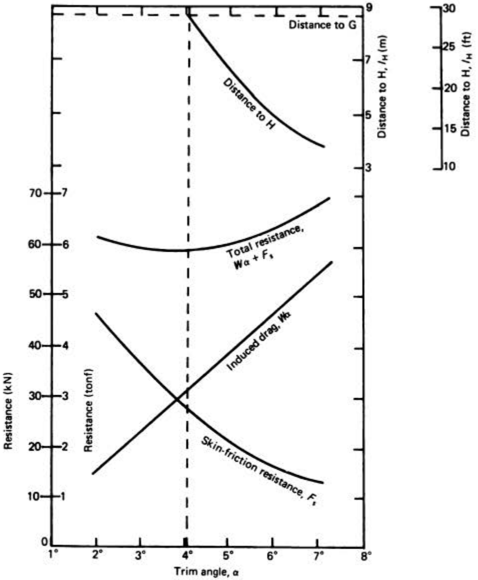

Fig. 6.13 Typical results from a planing craft calculation.

In [13] and later in [14] the high-speed performances of the five planing hull models making up the Series were shown to reduce to a composite plot as indicated in Fig. 6.14. Although these curves are derived for a craft with an all-up weight of $W = 10\,000$ lbf ($\cong 44.5$ kN), they can be used with good accuracy for weights from 7500–15 000 lbf ($\cong 33.38$–66.75 kN). For equilibrium of the forward steady motion l_H is equal to l_G and the latter can be fixed for a given boat. The abscissa of Fig. 6.14 can thus be taken as some known value at the cruise speed. The coefficient C_v is also calculable for a given speed and all-up weight, and the resistance-to-weight ratio then follows. It is then found that the estimated values of resistance lie close to those which were actually measured on the corresponding five models of the Series. A number of other interesting features, characteristic of general planing

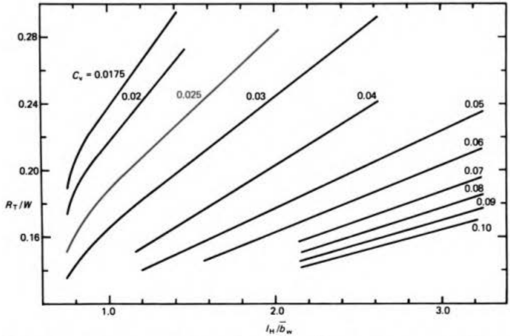

Fig. 6.14 Resistance-to-weight ratio as a function of $l_H/\bar{b}_W$ and C_V for a series of 'V' bottom hulls.

hulls, may be deduced from Fig. 6.14. For a given plan area formed by the chine line a craft of large $\bar{l}_w/\bar{b}_w$ (= $1/\mathcal{R}$) will be elongated in the fore-and-aft direction and consequently the ratio $l_G/\bar{b}_w$ (= $l_H/\bar{b}_w$ at cruise speed) will be large. It is then found that at high speeds long, narrow boats have a somewhat higher total resistance than craft with lower $l_G/\bar{b}_w$, as indicated for a typical example in Fig. 6.15. However, at low speeds the behaviour is significantly reversed as a result of the less pronounced wave-making resistance of the slender craft. Also shown in Fig. 6.15 is the variation of the corresponding trim angle which is seen to vary over a smaller range as $l_G/\bar{b}_w$ increases, though all the results merge at the highest speeds. Finally, as shown in Fig. 6.14, if we consider a craft of constant W, V and $\bar{b}_w$ and change the value of l_G, the total resistance increases as l_G is brought forward. There is thus a desire on the part of designers to keep the centre of gravity well aft. The extent to which this action may be taken is limited by the tendency for the craft to porpoise (bounce from wave crest to wave crest) at high speed and to adopt an excessive trim by the stern when at rest. Consequently, it is recommended in [13] that the centre of gravity should be close to 8 per cent of the projected chine length aft of the centroid of the projected planing bottom area (enclosed by the chine line). It may be noted that for much of the work in [13] correlations were based on the 'volume' Froude number defined as

$$Fr_\nabla = \frac{V}{\sqrt{(g\nabla^{1/3})}} \tag{6.25}$$

where

$$\nabla = \frac{W}{\rho_w g}, \tag{6.26}$$

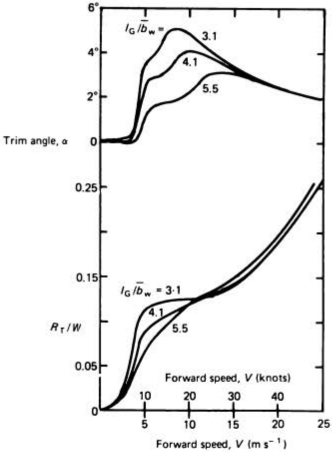

Fig. 6.15 Effects of position of centre of gravity on R_T/W and α.

that is the displacement volume at rest. As shown in Fig. 6.15, the change-over characteristic of R_T/W, which takes place at about 12.5 m s^{-1}($\cong$ 25 knots), corresponds to $Fr_\nabla \cong 3.11$. More recent correlations of total resistance data for the Series 62 and Series 65 hard-chine hulls [15] have shown that the most dominant parameter affecting the resistance at a given speed is the slenderness ratio (i.e. $l_p/\nabla^{1/3}$, where l_p is the projected chine length). Figure 6.16 shows a summary of the typical results in which it is seen that as the slenderness ratio of the hull increases the wave-making hump resistance reduces, but the high-speed resistance increases, confirming the results shown in Fig. 6.15.

We see, therefore, that Murray's method can be used to produce the geometry of a boat consistent with minimum drag or, alternatively, to produce a resistance value for a given location of the longitudinal centre of gravity. These data will, however, refer to only one operating point, that is, at the design cruise speed. On the other hand, the data of Clement and Blount can be used to predict the performance of a boat, similar to the series considered by them, over the whole speed range and for all-up weights to at least 445 kN ($\cong$ 44.5 tonf). These two approaches are complementary and both may be used to deduce optimum operation.

Corresponding data for round-bilge hulls have been given in [16] for the very slender DTMB Series 64 and in [17–19] for the lower slenderness ratios of the

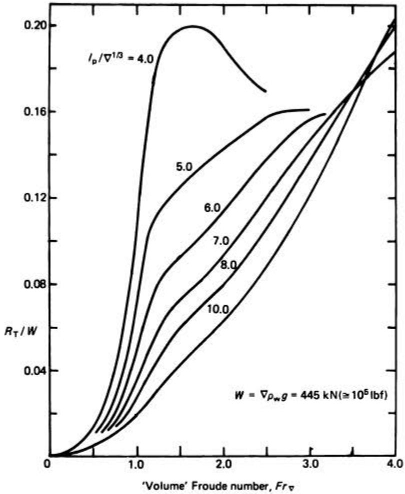

Fig. 6.16 Effect of slenderness ratio on R_T/W for various Fr_∇.

NPL Series. This later series is intended to cover high-speed ships which do not, in fact, plane in the strictest sense. In other words, a significant buoyancy force is present at the cruise speed. However, the question of the fully-planing condition is considered in more detail in Section 6.2.6. For the moment we consider, for the NPL series, that the length Froude number Fr_L ($= V/\sqrt{(gL_{WL})}$, where L_{WL} is the length of the still-water line) is less than 1.1, say. Under these conditions the overall round-bilge characteristics describing resistance and trim angle as functions of Fr_∇ are quite similar to those shown in Fig. 6.15 for the hard-chine hull forms. It is found that trim angles are slightly less and, at lower speeds, the resistance is somewhat less for the round-bilge forms. In [18] it is shown that again the addition of a stern wedge reduces the trim angle (by as much as 50 per cent for a 10 degree wedge) and, for low slenderness ratios, reduces the resistance at the hump speed.

Data from the NPL Series and a collection of hard-chine results are compared in [19] on a resistance against Fr_∇ basis to obtain some idea of the optimum performance range for each type of hull for operation in calm water. Figure 6.17 shows the recommendations derived from these data in terms of speed and ship length. It is thought that the operating régimes illustrated are likely to hold for hull shapes

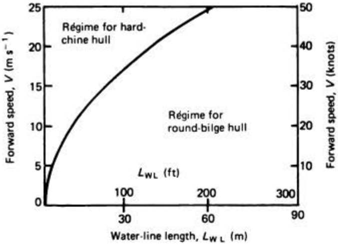

Fig. 6.17 Operating régimes for round-bilge and hard-chine planing craft.

reasonably close to the NPL and DTMB Series. Clearly, the implication is that round-bilge hulls are best for large high-speed craft operating at speeds up to $25\ \mathrm{m\ s^{-1}}$ ($\cong 50$ knots). This may go some way to explaining the often demonstrated superiority in speed of the round-bilge German E-Boats in the Second World War. Nevertheless, North American designers tend to favour the hard-chine hull form and contend that the differences in resistance values at low speeds are not particularly important. Indeed, it is suggested in [15] that the best compromise may be the double chine, which combines the best characteristics of the two basic hull forms and yet retains the shape which offers cheaper and quicker building programmes. The question of which form is best at high speed in waves, measured in terms of seakeeping responses such as displacements and accelerations, still has no definitive answer. Although this question is of great importance, motion in waves is unsteady and the topic is out of context here; but a measure of the seriousness of the problem for several types of high-speed craft may be found in [20] for example.

6.2.5 *Behaviour of a Planing Craft*

The operating characteristics of a successful planing craft hull with a length at the still-water line of approximately 21 m ($\cong 70$ ft) and a length-to-beam ratio of 4 have been given in [21] and are presented in Fig. 6.18. The trim angle is seen to rise to a maximum of about 6 degrees at approximately half the maximum speed and then to reduce steadily to some 4 degrees at the design speed of $25\ \mathrm{m\ s^{-1}}$ ($\cong 50$ knots). Our assumption that α is small is thus seen to be justified for all speeds.

For this craft, and indeed for most planing craft, at low speeds the mid-section falls with respect to the still-water level and only begins to rise at speeds above $7.5\ \mathrm{m\ s^{-1}}$ ($\cong 15$ knots). This settling of the hull in the water suggests that downward (suction) forces are generated on the wetted hull, usually near the stern, which augment the weight. As a result of this submergence $F_B > W$. To balance the moment induced about the centre of gravity by these suction forces α increases so that the centre of buoyancy moves aft; the hydrodynamic centre H is also abaft the centre of gravity. As the speed increases F_V becomes larger with the result that H

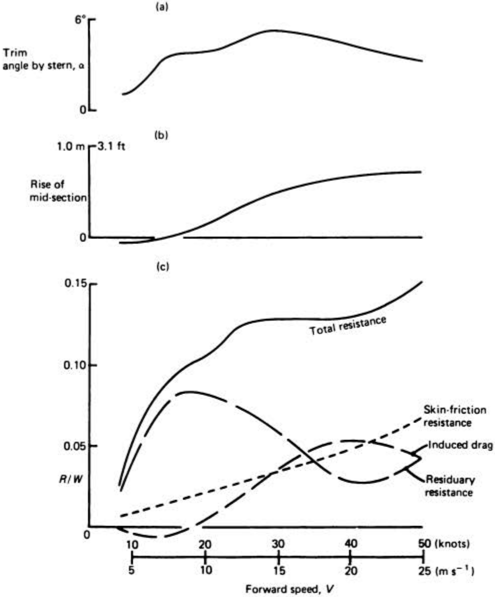

Fig. 6.18 Performance characteristics of a 21 m (70 ft) hard-chine planing craft.

moves forward and F_B diminishes (or rather F_h is small). Between 7.5 and 10 m s^{-1} (≅ 15 and 20 knots) the transom gradually rises clear of water, and to preserve equilibrium the changes in F_v and F_h and the movement of H and X (see Fig. 6.12(a)) take place with little change of trim. As the speed increases further the trim angle reaches a maximum at 15 m s^{-1} (≅ 30 knots). At higher speeds the mid-section emerges slowly and α decreases steadily. This latter trend might be explained, somewhat crudely, for the fully-planing craft by referring to the equation

$$W = F_v = C_v \times (\tfrac{1}{2}\rho_w V^2 \bar{b}_w^2) = \text{constant}.$$

Now as V increases the coefficient C_v must decrease because $\bar{b}_w$ remains constant for hard-chine hulls. The wetted length tends to reduce slowly, and, as we can see in

Equations (A.1)–(A.8) in the Appendix at the end of this chapter, α must also decrease.

Also shown in Fig. 6.18 are the resistance components as functions of the forward speed. In this figure the total resistance was based on measured values, the skin-friction resistance was determined from plank data, the induced drag was deduced from an estimate of F_v and measured angles of trim, and the residuary resistance was obtained by subtraction. The total drag increases rapidly at low speeds, probably at a greater rate than for a displacement ship, but then remains little changed between 12.5 and 20 m s^{-1} ($\cong$ 25 and 40 knots) before rising steadily at higher speeds. Between 5 and 10 m s^{-1} ($\cong$ 10 and 20 knots) the total resistance arises primarily from wave formation. The residuary resistance shows a hump at about 9 m s^{-1} ($\cong$ 18 knots) which corresponds to a Froude number, based on water-line length of the craft at rest, of approximately 0.63. As the speed increases the wave-making resistance decreases, but at high speeds viscous pressure resistance increases so rapidly that it forms the major component of the residuary resistance. As F_v is negative at low speeds, the induced drag is then also negative but becomes increasingly positive as V rises. Above 20 m s^{-1} ($\cong$ 40 knots), F_v changes little but α is seen to decrease, thus causing the product αF_v to pass through a maximum and then decrease gradually. Finally, skin-friction resistance increases steadily throughout the speed range since the V^2 term is always greater than the product $S_w \times C_F$. For the particular craft examined here, the skin-friction resistance becomes the largest component of the total resistance above 20 m s^{-1} ($\cong$ 40 knots). However, the rate at which skin-friction resistance increases is less than that for a displacement vehicle because the wetted surface area decreases with increasing speed.

6.2.6 *Definition of Fully-planing Operation*

We have considered hitherto that the craft is fully planing when speeds are reached for which $F_h \ll F_p$, but some part of the hull must be submerged. Therefore $l_w \neq 0$ and so $F_h \neq 0$. This definition of fully planing is imprecise yet difficult to improve upon. For example, Newton [21] stated that 'it is generally recognised that the definition of fully planing is when the R_T/W curve levels off . . . and the stem trim has reached a maximum'. With this similarly imprecise definition the data shown in Fig. 6.18 suggest that fully-planing motion commences at $V = 14$ m s^{-1} ($\cong$ 28 knots). On the other hand, Mandel [22] considered the craft to be fully planing when 'it ceases to be buoyantly supported and becomes completely dynamically supported'. Clement and Pope [5] found this occurred when $Fr_\nabla \geqslant 3.5$.

We can infer from the results of Fig. 6.18 that this criterion applies for $V \geqslant 20$ m s^{-1} ($\cong$ 40 knots), which is at the upper limit of the level portion of the R_T/W curve.

Our definition is similar to that suggested by Mandel but we know that the craft cannot *cease* to be buoyantly supported. What, then, is the magnitude of $F_h \cos\alpha/W$ ($= F_h/W$ for small α) which could be taken as a reasonable criterion for the inception of 'fully' planing (for only then can we use our design data with accuracy)? Now if F_h/W becomes very small the craft simply skims over the water surface, as may be observed in 'power-boat' races. Should the craft then encounter a disturbance such as a gust of wind or surface waves the hull may emerge completely from the water and become airborne for a short period. When this action occurs repeatedly the craft porpoises violently. The ride becomes extremely uncomfortable, control is poor and structural damage to the hull often takes place. It has been known for some craft to 'flip' right over and break up.

Some idea of the relative magnitudes of F_h/W and F_v/W can be obtained by referring again to Fig. 6.18. The curve of induced drag-to-weight ratio ($\alpha F_v/W$) and trim angle α imply values of F_v from about 0.5 W at 15 m s^{-1} ($\cong$ 30 knots) to about 0.75 W at 20–25 m s^{-1} ($\cong$ 40–50 knots). The vertical component of the hydrostatic force must therefore vary between 0.5 and 0.25 W over the same speed range. (The components of propulsor thrust have been neglected.) Newton suggested that porpoising would occur when V is greater than 25 m s^{-1} ($\cong$ 50 knots) for this craft. The practical maximum value of F_v is therefore 0.75 W and is achieved at 20 m s^{-1} ($\cong$ 40 knots). Du Cane's calculations [11] for a somewhat smaller boat and a length-to-beam ratio of 5.5 show that at the design speed of 21 m s^{-1} ($\cong$ 42 knots) the dynamic force $F_v \cong 0.5$ W.

6.3 Hydrofoil Craft

Unlike the main hull of a planing craft that of the hydrofoil boat is completely clear of the water at high speeds. Hydrodynamic supporting forces are developed on fully – or partially – submerged extensions of appendages fixed to the main hull. The supporting forces result from a suitable distribution of pressure on the wetted surfaces (the hydrofoils) once the craft is in motion. Figure 6.19 shows two typical configurations of hydrofoil craft. The foils, attached by struts to the hull, may either pierce the water surface, or be totally submerged, or be a combination of

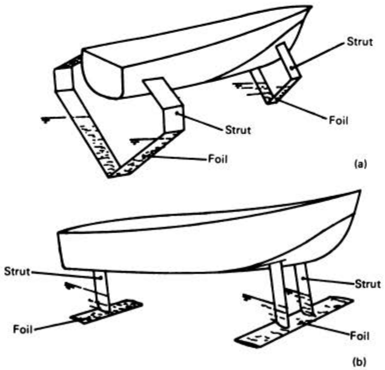

Fig. 6.19 Hydrofoil craft: (a) surface-piercing foils canard configuration; (b) submerged foils conventional (aeroplane) configuration.

both. Further, the main load-bearing foils may either be well aft (the *canard* configuration), or well forward (the conventional *aeroplane* configuration).

The performance of a deeply submerged hydrofoil is equivalent to that of a geometrically similar, isolated aerofoil operating under dynamically similar conditions. However, at high speeds the behaviour of a hydrofoil raises problems which can be solved only with reference to specially designed lifting sections. It is worth pointing out here that although the hull itself is clear of the water the struts, foils and often the propulsor are submerged. These will, therefore, contribute a small buoyancy force to augment the hydrodynamic lift force supporting the craft.

6.3.1 *Generation of Lift Forces*

The lift force on a hydrofoil (or an aerofoil) is defined as that component of the resultant hydrodynamic force which is perpendicular to the direction of the oncoming mainstream velocity. It is worth noting that the lift force may be upwards or downwards, although for a supporting force in horizontal motion we would require an upward vertical lift force. The process by which a lift force is generated on a hydrofoil is fundamentally different from that used by a planing hull to produce a supporting force $\boldsymbol{F}_{\mathrm{V}}$. Let us first postulate that the flow about a stationary, deeply submerged body is steady and irrotational. (It may be recalled that the term 'irrotational' implies that *no* element of the moving fluid undergoes a net rotation.) Since rotation of a fluid particle can be caused only by a torque applied by shear forces on the surface of the particle it follows that in our model shear forces are absent and so the fluid is inviscid. Suppose the body is a long cylinder of uniform, circular cross section set at right angles to the oncoming flow which is of infinite extent. The streamline pattern about a central section of the cylinder appears like that shown in Fig. 6.20(a). Symmetry of the pattern about the axes xx, zz shows, by the application of Bernoulli's equation, that the net forces perpendicular to xx (lift) and perpendicular to zz (drag) must both be zero.

To obtain a lift force it is essential that the streamline pattern about the xx axis should be unsymmetric. This could be achieved by distorting the cross section of the body or by inducing an additional circulatory flow component. If the velocities of the fluid relative to the cylinder over the upper surface of the cylinder are greater than those on the lower surface then Bernoulli's equation shows that the mean pressure on the lower surface is greater than that on the upper surface. A transverse force, in this case a vertical upward (lift) force, is developed as shown in Fig. 6.20(b). The flow is still symmetric about the zz axis and so drag remains zero.

Theoretically, the streamline pattern shown in Fig. 6.20(b) can be obtained from the superposition of a uniform stream and a doublet (which when combined represent the uniform flow about the cylinder) and an irrotational vortex representing a circulatory flow [23–25]. It may then be shown that the lift force per unit span of the cylinder is given by

$$\text{lift/span} = \rho \Gamma V = L' \qquad (6.27)$$

where ρ is the density of the fluid, V is the mainstream approach velocity and Γ is the circulation and corresponds to the strength of the irrotational vortex. We adopt here the convention that positive circulation corresponds to a lift force along the upward perpendicular to the approach flow velocity vector†. Equation (6.27) was

† This sign convention is more suitable for our present purpose; it is not universal and the reverse is often used [23].

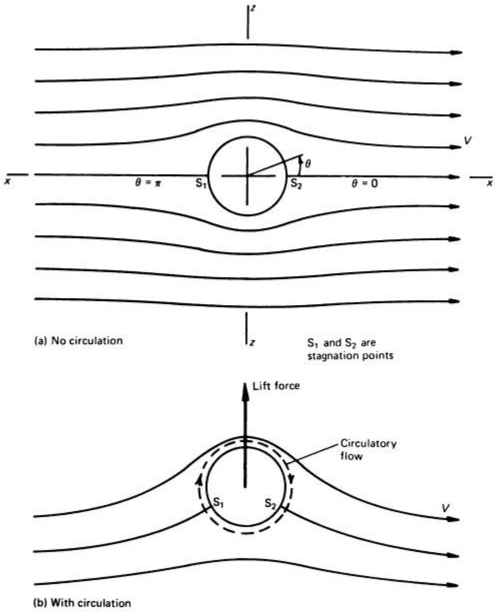

Fig. 6.20

obtained first by Kutta and independently by Joukowski for bodies of arbitrary shape, and the result is often called the Kutta–Joukowski law. Joukowski showed also that the pattern of flow round a cylinder of circular section can be used to deduce the pattern for a body of different (but mathematically related) shape. Using a suitable conformal transformation [24] the body so derived can take the form of a hydrofoil which is symmetric about a mean line (which need not be straight). Velocities and therefore pressures on the surface of the hydrofoil may thus be calculated fairly simply.

Let us now refer specifically to hydrofoil sections of infinite span (i.e. infinite length perpendicular to the plane of the paper) and suppose we transform the flow pattern of Fig. 6.20(a) to that of Fig. 6.21(a). There is no lift force on either the

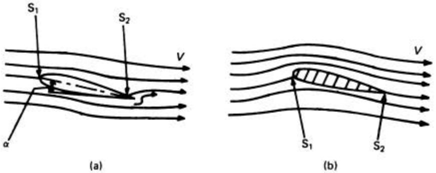

Fig. 6.21

cylinder or the hydrofoil. Whereas for the cylinder the two stagnation points S_1 and S_2 lie on the line $\theta = \pi$ and $\theta = 0$ respectively, the relative positions of the corresponding points S_1 and S_2 on the hydrofoil depend on the angle of incidence α. It may be seen in Fig. 6.20(a) that the result of the transformation is an aerofoil with a sharp (often cusped) trailing edge. However, even for an inviscid fluid, the required instantaneous change in direction cannot actually be sustained. Furthermore, for real fluids the flow over the under surface of the hydrofoil suffers a continuous dissipation of energy by shear stresses in the boundary layer. As a result, the fluid possesses insufficient energy to move round the sharp trailing edge in order to reach the stagnation point S_2 and so breaks away from the surface of the foil.

Actually, the only stable position of S_2 is *at* the trailing edge and the flow pattern of Fig. 6.21(a) lasts only for an instant once motion begins. Now the movement of S_2 to the trailing edge of the hydrofoil corresponds to a shift of the point S_2 on the cylinder (Fig. 6.20(a)) from $\theta = 0$ to $\theta < 0$, that is, below the *xx* axis. Reference to Fig. 6.20(b) shows that a clockwise (and by convention positive) circulation is required with the result that S_1 moves to a position corresponding to $\theta > \pi$, that is, again below the *xx* axis. Transformation of the modified pattern to that for the hydrofoil is shown in Fig. 6.21(b). Thus for stable conditions a circulation round the hydrofoil must be established, and its magnitude depends on the extent to which the rear stagnation point must move to appear on the trailing edge. This is the 'Joukowski hypothesis' which tells us that a circulation about the foil is necessary to produce a lift force on the foil.

To explain how the circulation is generated initially we must draw on the viscous property of real fluids. The separation of the viscous flow near the trailing edge of a hydrofoil causes the fluid on the upper surface to move from S_2 to the trailing edge. This flow is in the opposite direction to that of the ideal flow and so an eddy, called a *starting vortex*, is formed as shown in Fig. 6.22. The starting vortex is washed rapidly downstream from the trailing edge. However, a theorem propounded by Lord Kelvin [26] must be satisfied. This states that in an inviscid fluid the circulation around a closed curve, which moves with the fluid so as always to touch the same particles, does not change with time. Provided that points on the closed curve are well away from the body, then velocity gradients at these points are negligible and the effects of viscosity are small. The behaviour of the flow in that region can then be considered identical with irrotational flow. The vortex induces a circulation (the *bound vortex*) so that the net circulation in the closed curve is zero and S_2 moves towards the trailing edge. A lift force is thus developed by the hydro-

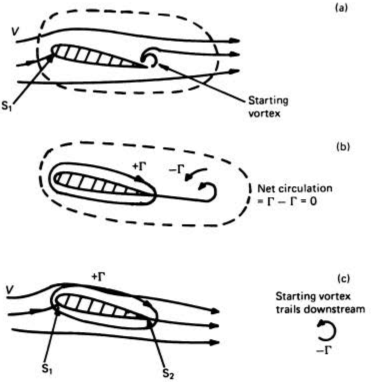

Fig. 6.22

foil. The condition for the circulation in ideal flow to bring S_2 onto the trailing edge is called the 'Kutta–Joukowski condition'. The actual value of circulation needed to satisfy this requirement is slightly less than that for ideal flow because the boundary layer effectively changes the shape of the hydrofoil somewhat.

Whenever the flow pattern is altered by changes in incidence angle α (see Fig. 6.21) or some change in hydrofoil geometry, or if the speed V is changed, then new starting vortices are produced and the circulation adjusted accordingly. The flow round the hydrofoil ceases to be affected by the starting vortex as the latter moves downstream to be dissipated gradually by viscous action. Although viscosity is necessary to generate starting vortices, and therefore circulation, the lift force is affected little by the magnitude of viscosity provided that the boundary layer is thin and separation is avoided. Even so, a wake is always formed as the shear flow in the boundary layer trails downstream and in reality the stagnation point S_2 cannot be readily identified. However, for thin hydrofoils the Kutta–Joukowski law is remarkably accurate.

The lift force on a hydrofoil can be measured directly by using a force balance fixed outside the flow system. Alternatively, we can sum the local vertical components (i.e. perpendicular to the direction of V) of the shear and pressure forces on the surface of the foil. But, as we have noted earlier, the local pressure force on the surface is the major component contributing to the lift force. It is therefore worth examining a typical pressure distribution on a deeply submerged hydrofoil of infinite span in a fluid of infinite extent.

Figure 6.23 shows such a pressure distribution for a NACA 4412 section [27]

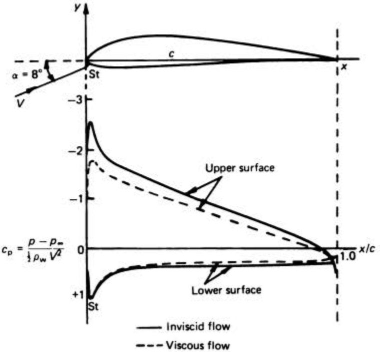

Fig. 6.23 Pressure distribution for NACA 4412 hydrofoil section.

set at an incidence angle of 8 degrees to the oncoming flow. The angle of incidence or, for an isolated hydrofoil (or aerofoil), the angle of attack is the angle α measured between the direction of the upstream approach velocity V and the line of length c joining the leading and trailing edges of the foil as shown in Fig. 6.23. Positive values of α correspond to directions of V from below this line. The reference static pressure p_∞ is taken to be well upstream from the hydrofoil. The flow round the leading edge of the foil accelerates rapidly from the stagnation point St to the upper surface which corresponds to large negative values of the pressure coefficient c_p. The effect of the boundary layer is to reduce the curvature of the upper surface thereby reducing both the 'peak' of the curve and the magnitude of c_p compared with that for inviscid flow. Note also that suction pressures occur over most of the upper surface, whereas positive pressures occur over most of the lower surface. Now the force per unit span, F'_p, on the hydrofoil in the y direction (Fig. 6.23) is proportional to the area enclosed by the pressure contour, and the lift per unit span is thus $F'_p \cos\alpha$. We see, therefore, that suction pressures provide a large contribution to the total lift force. This behaviour contrasts with that of planing surfaces for which c_p is always positive on the wetted surface. Towards the trailing edge of the foil a wake is formed and pressure recovery (to $c_p = +1$) is incomplete. We might thus take the view that the hydrofoil is effectively extended downstream to the point where the wake is dispersed. The magnitude of c_p at the suction peak increases with α to produce a large, adverse pressure gradient beyond the peak. The tendency for boundary-layer separation is therefore increased and this results in a loss of lift force and a rapid increase in drag force (mainly from the viscous pressure component).

6.3.2 *Geometry of Hydrofoil Sections*

In addition to the variation of V and α the geometry of the hydrofoil also affects its performance. The principal geometric parameters of a hydrofoil section suitable for low-speed, non-cavitating flows are shown in Fig. 6.24. These parameters may be identified as follows:

(i) The mean (camber) line is of arbitrary shape (although it is often either straight, part of a circular arc or part of a parabolic arc) on which lie the centres of the leading- and trailing-edge circles. These edges are formed by the intersection of the mean line and the circumference of the circles. The Joukowski transformation produces a leading edge on very nearly a circular arc but the trailing edge is cusped. Such a shape is rather impractical and so most designs have a thickened region over the last 10–15 per cent of the mean line.

(ii) The straight line which connects the leading and trailing edges is called the chord line of length c.

(iii) The thickness distribution t, which is symmetric about the mean line, depends, as does the camber, on the conformal transformation used or on the development of the section from empirical data. For low-speed hydrofoils the maximum thickness t_m is in the range $0.1 \leqslant t_m/c \leqslant 0.25$ and is located at $x/c \cong 0.3$; the maximum camber varies between zero and $0.1c$ and is located in the range $0.4 \leqslant x/c \leqslant 0.5$.

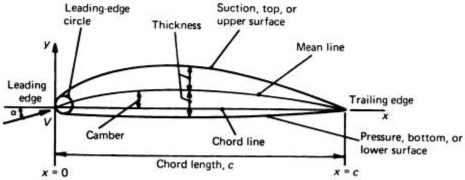

Fig. 6.24 Notation for hydrofoils.

Provided that the foil can be considered thin, that is $t_m/c \leqslant 0.2$, the lift force developed for small angles of incidence is determined primarily by the shape of the mean line. The thickness distribution which clothes the mean line reduces the suction peak at a given α and so reduces the possibility of separation. Further streamlining towards the trailing edge reduces the viscous pressure drag at the expense of a slight increase in skin-friction drag. Maximum values of the section lift coefficient, given by

$$C_l = (\text{lift/span})/\tfrac{1}{2}\rho_w V^2 c = L'/\tfrac{1}{2}\rho_w V^2 c \tag{6.28}$$

can reach 1.8 and the ratio of lift force to drag force can be as high as 100, as shown in [27].

6.3.3 *Data for Hydrofoil Sections*

A typical set of data (for a NACA 4412 section) is shown in Fig. 6.25 for a given value of Reynolds number $Re(= \rho_w Vc/\mu_w)$ and a given roughness geometry. The section drag coefficient is given by C_d, where

$$C_d = (\text{drag/span})/\tfrac{1}{2}\rho_w V^2 c = D'/\tfrac{1}{2}\rho_w V^2 c, \tag{6.29}$$

and the section moment coefficient is given by $C_{m_{c/4}}$, where

$$C_{m_{c/4}} = (\text{moment about quarter-chord point/span})/\tfrac{1}{2}\rho_w V^2 c^2. \tag{6.30}$$

It may be shown from thin-aerofoil theory [25, 27, 28] that for inviscid flow, small α and small camber, $C_{m_{c/4}}$ is independent of C_l. The hydrodynamic centre, through which the resultant hydrodynamic force acts, therefore lies on a line in the section which is perpendicular to the chord line at $x = c/4$. The moment about the quarter-chord point should thus be small, negative (clockwise) and constant, although some variation does occur owing to the influence of boundary layers.

Thin-aerofoil theory may also be used to show that C_l varies linearly with small angles of α according to the equation

$$C_l = C_{l_0} + \alpha\left(\frac{\partial C_l}{\partial \alpha}\right)_{\alpha=0} = C_{l_0} + \alpha a_{l_0} \tag{6.31}$$

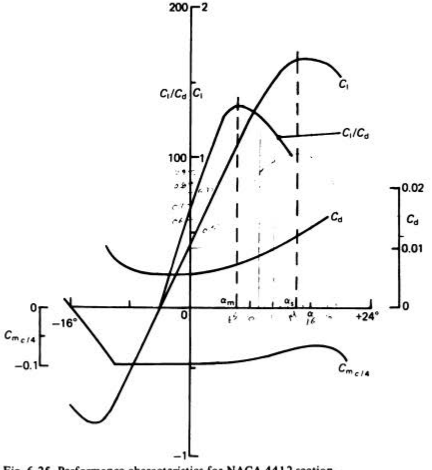

Fig. 6.25 Performance characteristics for NACA 4412 section.

where C_{l_0} is the section lift coefficient at $\alpha = 0$, and is therefore that arising solely from camber, and a_{l_0} is the slope of the lift curve at $\alpha = 0$.

The effect of boundary-layer separation, which occurs at large α, can be seen from Fig. 6.25. As α increases C_l increases until a maximum is reached from which we can infer that the area enclosed by the pressure curve of Fig. 6.23 is also a maximum. There is then a sudden reduction in C_l and a rapid rise in C_d as α increases further. The efficiency of the foil, represented by the ratio C_l/C_d ($= L'/D'$), also drops rapidly, but note that the maximum value is at an angle $\alpha_m \cong 6.5$ degrees compared with the incidence angle at separation $\alpha_s \cong 14$ degrees. Flow separation may be progressive, starting near the leading or trailing edges and then spreading over the entire upper surface of the foil as C_l increases, as shown in Fig. 6.26. In

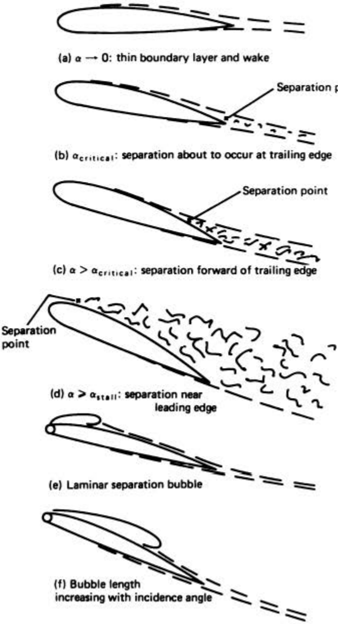

Fig. 6.26 Flow separation on a hydrofoil.

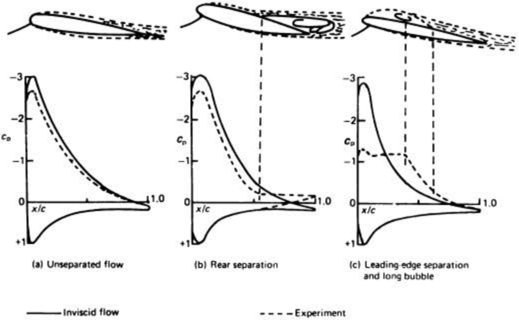

Fig. 6.27 Effect of separation on pressure distribution.

that case the lift curve is well rounded near the maximum, but if separation occurs suddenly over the whole surface the C_l curve is sharply peaked. The effect of separation on the pressure curves is illustrated in Fig. 6.27, and once stall has occurred on a hydrofoil marked changes in $C_{m_{c/4}}$ result. In general, C_l increases and C_d decreases as *Re* increases in the range 3×10^6 to 9×10^6 thus increasing the maximum C_l/C_d.

6.3.4 *Hydrofoils of Finite Span*

The lifting surfaces of a hydrofoil craft cannot, of course, be considered of infinite span and it might be thought that the bound vortex must end abruptly at the ends of the foil. This is, however, at odds with one of the properties of a vortex which does not allow it to terminate in the fluid except at a solid boundary (as proved by Helmholtz and discussed by Kelvin [26]). The difficulty is resolved by recalling that for a given angle of incidence α, a lift force on the hydrofoil implies that the pressure on the under surface must exceed that on the upper surface. Fluid must, therefore, escape round the ends of the foil in the following fashion: outwards to the ends on the under surface and inwards to the centre plane on the upper surface, as shown in Fig. 6.28. At the trailing edge the two flows are discontinuous and so vortices are generated and swept downstream. The vortex pattern is unstable and the separate vortices tend to roll-up quickly to form two strong vortices with strengths of equal magnitude but opposite sign near the tips of the foil as shown Fig. 6.29. The bound vortex is not discontinuous at the tips but joins the tip vortices. In theory, the tip vortices are joined to the starting vortex far downstream to form a complete vortex ring. Thus, Kelvin's theorem is upheld because the pair of trailing tip vortices contribute nothing to the net circulation. The complete system is called a 'horseshoe vortex', because in practice both the tip vortices and the starting vortex are soon dissipated downstream by viscous action. Only the bound vortex and the forward portions of the tip vortices persist.

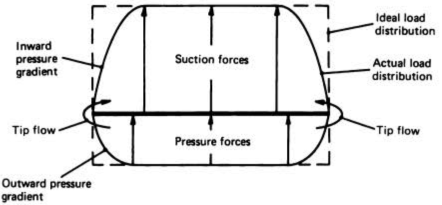

Fig. 6.28 Generation of tip flows.

At the tips of a finite hydrofoil the pressure difference between the upper and lower surfaces must be zero and, therefore, so must the circulation and lift force. As a result, we cannot assume that C_l is constant along the span and thereby obtain the total lift force as the product of lift/span and the span. To account for this the variation of circulation along the wing is assumed to consist of numerous line vortices of different length bound to the wing, the sum of the strengths of the vortices then giving the overall lift distribution. Each bound vortex has its own pair of trailing vortices extending downstream which form a vortex sheet, as shown in Fig. 6.30. This is the classic lifting-line theory expounded by Prandtl and discussed by Glauert [28].

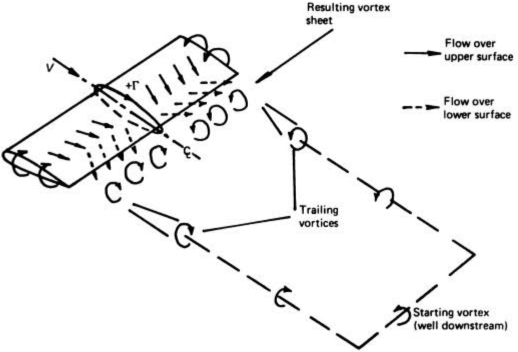

Fig. 6.29 Vortex system for a finite-span hydrofoil (horseshoe vortex).

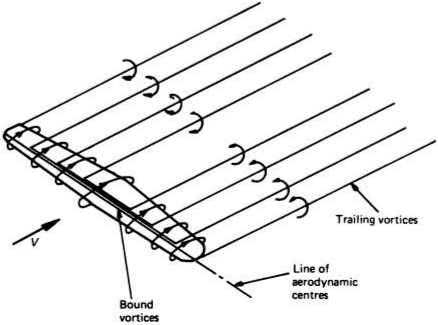

Fig. 6.30 Spanwise distribution of bound vortex strength.

Provided that the aspect ratio† is large, say $AR > 4$, it can be shown that the spanwise variations of circulation and lift approximate to a semi-elliptical form (such as that shown in Fig. 6.31) which agrees closely with measurements. Circulation is again regarded as positive when clockwise viewed from along the span of the hydrofoil with the mainstream flow approaching from the left.

Let us consider for the moment that the flow over a finite foil of constant cross section is inviscid. The tip vortices induce a downwards component of velocity, called the *downwash velocity* v_i. This velocity component can be added vectorially to V to yield a velocity V_0 at an effective angle of incidence $\alpha_0 = \alpha - \alpha_i$ where $\alpha_i = \arctan(v_i/V)$, as shown in Fig. 6.32. In general v_i may vary along the span although it is constant for an elliptical variation of lift, and since V is constant along the span then so are both V_0 and α_i. We now treat the finite foil as equivalent to one of equal span but which forms part of an infinite foil set at an effective incidence angle α_0. The lift force is thus given by $L_0 = \int \rho_w V_0 \Gamma \, dy$ evaluated over the span of the foil and is perpendicular to V_0. The force L_0 can be resolved into a useful lift force L normal to V and a component D_i, called the *induced drag*, parallel to V in a rearward direction. We see, therefore, that although the fluid was assumed inviscid and the foil deeply submerged it experiences a drag component owing to the presence of downwash. The apparent paradox of drag in an inviscid fluid is removed when it is realized that the work done against the induced drag appears as the kinetic energy of the tip vortices which are left behind the trailing edge of the foil.

† Here the aspect ratio AR = (span b)/(mean chord length $\bar{c}$). If S is the plan area of the foil, $S = b \times \bar{c}$ and so $AR = b^2/S$ as before.

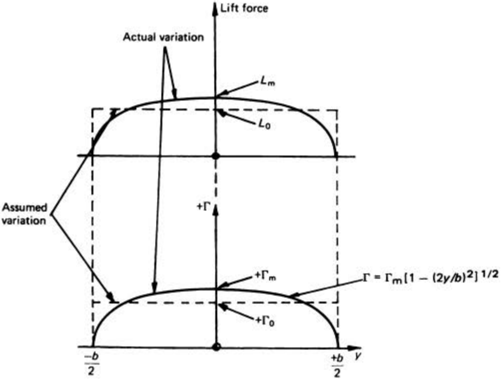

Fig. 6.31

For a hydrofoil in a real fluid D_i augments the viscous drag D_0. Noting that $v_i \ll V$ and α_i is small, and assuming that $D_0 \ll L_0$, we have from Fig. 6.32

$$L = L_0 \cos\alpha_i \cong L_0 \tag{6.32}$$

$$D = D_0 \cos\alpha_i + D_i \cong D_0 + \alpha_i L_0. \tag{6.33}$$

For an elliptic load distribution in the spanwise direction

$$v_i/V_0 = \text{constant} = D_i/L_0$$

that is,

$$D_i = v_i L_0/V_0. \tag{6.34}$$

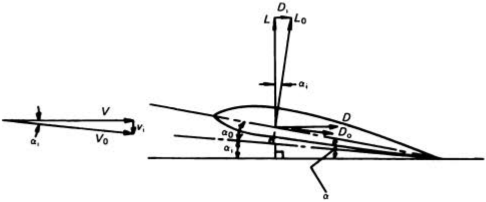

Fig. 6.32 Generation of induced drag.

Furthermore, it can be shown that [29]

$$\nu_i = \Gamma_m/2b \tag{6.35}$$

where Γ_m is the circulation at the mid-span of the hydrofoil (see Fig. 6.31). Therefore, from Equation (6.27)

$$L_0 = \int_{-b/2}^{+b/2} \rho_w V_0 \Gamma dy = \rho_w V_0 \int_{-b/2}^{+b/2} \Gamma_m [1 - (2y/b)^2]^{1/2} dy$$
$$= \rho_w V_0 \Gamma_m \frac{b\pi}{4} = \rho_w V_0 \nu_i \frac{b^2\pi}{2}$$

from Equation (6.35). Whence

$$\nu_i = \frac{2L_0}{\rho_w V_0 \pi b^2}, \tag{6.36}$$

and thus from Equations (6.34) and (6.36)

$$D_i = \frac{2}{\rho_w \pi b^2}\left(\frac{L_0}{V_0}\right)^2 = \frac{2}{\rho_w \pi b^2}\left(\frac{L}{V}\right)^2 \tag{6.37}$$

using the similar triangles in Fig. 6.32. Division by $\frac{1}{2}\rho_w V^2 S$ yields the dimensionless coefficients

$$C_{D_i} = C_L^2\left(\frac{S}{\pi b^2}\right) = C_L^2/(\pi A\!\!\!R). \tag{6.38}$$

Also,

$$\alpha_i = \arctan(\nu_i/V) = \arctan(D_i/L) = \arctan(C_{D_i}/C_L)$$
$$= C_L/(\pi A\!\!\!R) \quad \text{(radian measure)}. \tag{6.39}$$

Division by $\frac{1}{2}\rho_w V^2 S$ throughout Equation (6.33) yields

$$C_D = C_{D_0} + C_{D_i} = C_{D_0} + C_L^2/(\pi A\!\!\!R). \tag{6.40}$$

Note that the profile drag coefficient C_{D_0} is the value of C_D when either $C_L = 0$ or $A\!\!\!R = \infty$ since in either case the downwash velocity is zero and so, therefore, is the induced drag.

Equation (6.38) allows us to separate out the effect of induced drag from Equation (6.40). Data then obtained for one aspect ratio can be converted to those for foils of the same section but a different aspect ratio. This process of conversion is illustrated by Prandtl and Tietjens [29]. The equivalence we have adopted between the flow over an infinite wing at an angle α and that of our finite wing at an angle α_0 means that we can write

$$C_L = \alpha(a_{1_0})_{A\!\!\!R} = C_{L_0} = \alpha_0(a_{1_0})_{A\!\!\!R=\infty} \tag{6.41}$$

where a_{1_0} is the slope of the lift curve and angles of incidence are measured relative to the datum for zero lift. Furthermore

$$\alpha_0 = \alpha - \alpha_i = \alpha - C_L/(\pi A\!\!\!R). \tag{6.42}$$

From Equations (6.41) and (6.42) it is easy to show that

$$\frac{1}{(a_{l_0})_{AR}} = \frac{1}{(a_{l_0})_{AR=\infty}} + \frac{1}{\pi AR}. \tag{6.43}$$

The slope of the lift curve at zero angle of incidence for unit span of an infinite-span, thin aerofoil in inviscid flow may be shown to be 2π/radian ($\cong 0.11$/degree). Equation (6.43) can thus be arranged in the form

$$(a_{l_0})_{AR} = 2\pi\left(\frac{AR}{2+AR}\right). \tag{6.43a}$$

For a given C_L and section geometry, values of C_D and α for an aspect ratio AR are related through Equations (6.40)–(6.42) to C_D' and α' for an aspect ratio AR' as follows, for $\alpha_0' = \alpha_0$

$$C_D' = C_D + \frac{C_L^2}{\pi}\left(\frac{1}{AR'} - \frac{1}{AR}\right) \tag{6.43b}$$

$$\alpha' = \alpha + \frac{C_L}{\pi}\left(\frac{1}{AR'} - \frac{1}{AR}\right). \tag{6.43c}$$

Evidently, the slope of the lift curve decreases as aspect ratio decreases and so it might be expected that foils of large aspect ratio are the more efficient lifting surfaces. Unfortunately, there is considerable difficulty controlling foils for which small changes in α produce large change in C_L. To satisfy both the limitations of strength and the susceptibility of damage to foils of large span, aspect ratios of between 3 and 4 have been adopted for practical hydrofoil craft. In order to attain a high lift force for a limited span, the plan area of the foil can be increased with sweepback accompanied by a reduction of chord along the span (taper) to reduce local bending moments. However, the finite foil may suffer from substantial boundary-layer separation emanating from either the junction between the strut and the foil or from the tips depending on the spanwise lift distribution.

6.3.5 *Hydrofoils Close to a Free Surface*

Hydrofoil lifting surfaces attached to high-speed craft do not usually operate deeply submerged – they may actually pierce the interface. A satisfact ry design must incorporate an acceptable blend of the following issues:

(i) The clearance height between the hull and the air–water interface must be great enough to avoid contact between the hull and the wave crests.

(ii) The size of the strut must be consistent with structural and low drag requirements.

(iii) Fouling between the foils and the sea bottom or jetty wall during docking restricts the length of the strut.

The principal characteristics of low-speed hydrofoils operating close to the surface are similar to those for deeply submerged ones. However, some differences in the flow pattern will occur owing to distortion of the air–water interface, while at higher speeds the performance of the foil may be affected by cavitation and ventilation. A detailed discussion of these matters has been presented by Eames [30], and we shall be content here with a general outline of the effects.

(a) *The Dependence of Lift Force on Depth*

The flow pattern about a hydrofoil must satisfy the condition of no flow across the interface at which the (atmospheric) pressure is usually constant. Now, for positive angles of incidence high velocities, and therefore low pressures (below the corresponding hydrostatic pressure), are developed adjacent to the upper surface of the foil. These low pressures are transmitted through the water so that a depression occurs at the interface which in turn interferes with the flow over the top of the foil. As a result of this blockage effect the fluid velocities over the upper surface of the foil are reduced leading to a concomitant increase in the surface pressure there. Hence, both the lift force and the slope of the lift force–incidence angle curve are less than the corresponding magnitudes for the same hydrofoil deeply submerged. The extent of the interface distortion increases as the depth of immersion decreases. Thus, the lift coefficient of a foil at a given incidence angle decreases as the foil approaches the interface. The significant changes take place over a depth approximately equal to the mean chord length of the hydrofoil. This behaviour is known as the 'depth effect' and can be used in some cases to ensure equilibrium of a hydrofoil craft at various speeds, as will be discussed later.

(b) *Cavitation on Hydrofoils*

When the absolute static pressure p of a liquid is reduced the (absolute) vapour pressure p_v may be reached at which the liquid boils and vaporizes. There are, of course, regions of low pressure on the foil where bubbles and vapour-filled cavities may develop rapidly giving rise to *cavitation*. In principle, cavitation commences when the local absolute pressure

$$p \leqslant p_v$$

or,

$$\sigma = \frac{p - p_v}{\frac{1}{2}\rho_l V^2} \leqslant 0 \tag{6.44}$$

where σ is the cavitation index (or number), V is the velocity of the foil relative to the liquid well upstream and ρ_l is the density of the liquid which we shall consider to be that of water, ρ_w. For several reasons the actual inception of cavitation starts before p is reduced to p_v. Small, solid particles in, for example, sea water act as nuclei for the vapour bubbles and so encourage premature inception. Air bubbles in the water act similarly and further influences arise from the surface roughness of the foil, turbulence of the flow, three-dimensional flows over the foil owing to end effects, non-uniform temperature distribution in the liquid and so on. In other words, inception commences when

$$\sigma \leqslant \sigma_c$$

where σ_c is a critical value obtained empirically.

A pressure coefficient has been defined, in Fig. 6.23, as

$$c_p = \frac{p - p_\infty}{\frac{1}{2}\rho_w V^2} \tag{6.45}$$

where in the present case p_∞ is the upstream, absolute hydrostatic pressure at a depth corresponding to that of the hydrofoil. Thus, cavitation begins when

$$\sigma = \left(\frac{p_\infty - p_v}{\frac{1}{2}\rho_w V^2} + c_p\right) \leqslant \sigma_c. \tag{6.46}$$

Rearrangement of this equation yields the critical velocity

$$V_c = \left(\frac{p_\infty - p_v}{\frac{1}{2}\rho_w(\sigma_c - c_p)} \right)^{1/2} \tag{6.47}$$

and cavitation occurs at all velocities $V \geqslant V_c$. Equation (6.47) shows that to increase V_c it is necessary to increase p_∞, that is, to immerse the foil deeper in the water, or to reduce the maximum suction pressure on the hydrofoil surface.

The following example indicates the limitations imposed by the onset of cavitation. Suppose that a foil is fixed so that the suction peak on the upper surface of the foil corresponds to $c_p = -1$, a modest value. Assume further that $\sigma_c = 0$ and the depth of immersion $h = 1$ m. Now if the ambient atmospheric pressure at the interface is constant at 100 kPa,

$$p_\infty = \rho_w g h + 10^5 \text{ Pa} \cong 110 \text{ kPa},$$

and so with $p_v = 1.8$ kPa for sea water of density 1025 kg m^{-3}, we have

$$V_c = \left(\frac{1.082 \times 10^5}{\frac{1}{2} \times 1.025 \times 10^3} \right)^{1/2} \text{ m s}^{-1} = 14.5 \text{ m s}^{-1} \ (\cong 28 \text{ knots}).$$

When cavitation bubbles are formed near to the surface of the foil they may be swept downstream into the wake. Some remain close to the foil and then collapse violently on reaching regions of higher pressure, especially near to the trailing edge of the foil. Local instantaneous pressures may be as high as 400 MPa (≅ 4000 atmospheres) and it is the shock waves that emanate from the severe impact loading which cause widespread erosion of the material forming the struts and foils. Furthermore, extensive structural vibration and considerable noise generation accompany cavitation in addition to a sudden drop in lift and increase in drag. Instead of remaining individually identifiable the bubbles often coalesce to form a sheet enveloping the complete suction surface of the foil so that the surface is no longer in direct contact with the water. This condition is referred to as 'supercavitation'.

The preceding numerical example shows that the dependence of V_c on depth of immersion is rather small. In any case, strength problems limit the length of supporting struts in addition to the undesirability of excessive draught. An increase in the ratio of foil area to all-up weight would reduce the hydrodynamic loading. However, the aspect ratio of the foil is limited because a craft with excessive underwater beam is vulnerable to damage and difficult to dock. Some hydrofoil sections have been devised to avoid large suction pressures at moderate angles of incidence and these have a more even distribution of pressure on the suction surface. By thus delaying cavitation the maximum operating speed of conventional foils can be raised from 20 m s^{-1} (≅ 40 knots) to, say, 30 m s^{-1} (≅ 60 knots). Some typical shapes of hydrofoil sections are shown in Fig. 6.33.

For speeds above 30 m s^{-1} (≅ 60 knots), a radical change in the design of hydrofoil sections is necessary. The curved wedge section was developed by Tulin [31] to promote cavitation deliberately so that the flow encloses a large cavity over the upper surface as indicated in Fig. 6.34. The sole supporting force is derived from the positive pressure distributed over the lower surface and little useful lift component is generated by the upper surface. The shape of the upper surface may thus be chosen to satisfy manufacturing tolerances, strength requirements, etc., provided that it remains covered by the cavity. The leading edge is sharp to induce a large

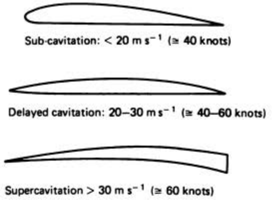

Fig. 6.33 Types of hydrofoil section.

suction peak and precipitate immediate cavitation. It is possible to design the lower surface to generate an acceptable lift force without incurring excessive drag in the supercavitating range. Even so, all hydrofoil craft must operate at low speeds during the run-up to the full-flight, cruise régime during which the supercavitating hydrofoils will have a poor performance.

The flow pattern illustrated in Fig. 6.34 shows some resemblance to that past a planing surface. However, the supercavitating foil is fully submerged and the cavity forms a free surface 'cut out' by the foil itself, thus avoiding the buffetting by waves at the interface which planing craft suffer. Moreover, wave-making drag is absent although the cavity drag will constitute a large component of the total drag force on the hydrofoil. At speeds in the range 25–35 m s^{-1} (≅ 50–70 knots) neither the delayed cavitation nor the supercavitating foils are really satisfactory especially for operating in waves. One solution to the problem has been found by operating the hydrofoil with its suction surface (i.e. the upper surface) partially vented by air, as discussed in the following section.

(c) *Ventilation on Hydrofoils*

Early investigators of hydrofoil craft observed the phenomenon of air entrainment or *ventilation*, as it is often called [32]. The result was a sudden loss of lift, and although the precise nature was not understood practical techniques were developed to restore normal conditions. The low pressures on the top surface of a hydrofoil may be sufficient to draw down the air–water interface to meet the foil. Instead of

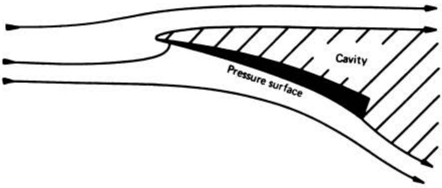

Fig. 6.34 Curved wedge section for supercavitating operation.

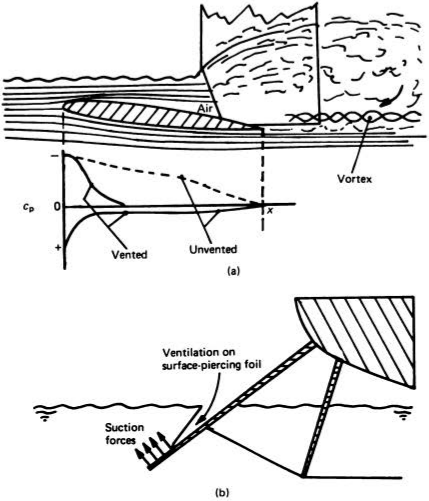

Fig. 6.35 Ventilation on hydrofoils.

the foil being fully submerged it is now substantially enveloped by air and the contribution to lift by the suction pressures is almost totally lost. The effect is shown in Fig. 6.35(a), and Fig. 6.35(b) shows how ventilation can occur on surface-piercing hydrofoils. Ventilation is not, however, confined to foils operating in the proximity of the interface. A sheet of air bubbles can form over the aft part of the suction surface of the foil if a 'suitable' path exists along which air is drawn from the atmosphere. The definition of a suitable path is imprecise but it is often provided by the strut, especially if the boundary layer has separated from it, or the foil [33]. Another flow path is provided by the clearance between the strut and the shaft used to adjust the setting angle of the foil (and therefore the incidence angle) as shown in Fig. 6.36. It is by controlling the flow of air from the atmosphere to the upper surface of the foil that has proved successful in adjusting the lift on hydrofoils to allow stabilization of the craft in the vertical plane [34]. The foils are equipped with pipes so that air can be sucked in at a flow rate controlled by valves operated by sensors which detect the depth of immersion (see Fig. 6.37).

It is generally considered (e.g. [35, 36]) that the dynamic stability of a hydrofoil craft in unsteady motion is probably the most important single design problem.

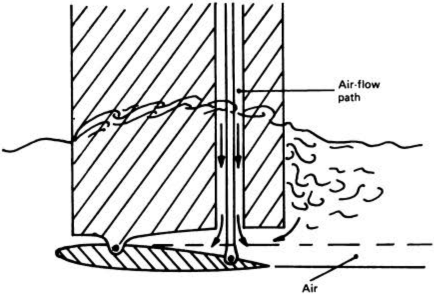

Fig. 6.36 Constantly vented foil.

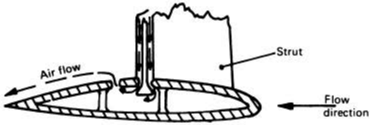

Fig. 6.37 A scheme for controlled ventilation.

Owing to the significant orbital velocities of waves (see Chapter 2) the foils may be subjected to large and rapid changes of incidence angle and therefore loading. The problem is particularly serious in a following sea for a craft with surface-piercing foils when inefficient control of lift forces can result in a sea crash [32, 37]. Complicated combinations of cavitation and ventilation, both of which are influenced by boundary-layer separation [38], may also result. These problems were encountered during the development of the *Bras d'Or*, an open-ocean, anti-submarine, prototype hydrofoil ship of some 2.1 MN (≅ 212 tonf) all-up weight and 46 m (≅ 150.75 ft) overall length [39]. The stability problem was largely solved by adopting a specially designed superventilated foil [40]. Spoilers were fixed to the upper surface of the foil (as shown in Fig. 6.38) which encouraged boundary-layer separation and pre-

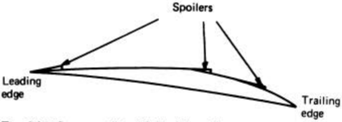

Fig. 6.38 Superventilated foil with spoilers.

vented re-attachment of the flow at low angles of incidence. Ventilation could thus be sustained over the widest possible range of incidence angle, depth of immersion and forward speed. The lift curves for the foils were then continuous with a small slope for operating incidence angles. Of course, drag was high and so the device was used only for the small front foil (the *Bras d'Or* had a canard arrangement of foils). This foil supported about 10 per cent of the all-up weight and operated primarily as a steerable direction controller but it could also adjust the trim of the craft.

A series of systematic tests and analyses, described in [41], have helped to establish more precisely the principal factors which affect ventilation. Compared with calm-water performance the presence of surface waves was found to reduce the angle of incidence of a strut at which ventilation commenced. It was found that the factors favourable for ventilation in a head sea occur at a crest, but for a following sea ventilation may occur at a trough or at other points in the wave system. The results from model tests seemed very sensitive both to small imperfections on the surface of the strut and to slight variations in experimental procedure. Thus, although at cruise speeds in a seaway ventilation on surface-piercing foils may be impossible to prevent its spread is controlled by fixing solid barriers or 'fences' perpendicular to the span as shown in Fig. 6.39.

Further details on cavitation and ventilation, together with a comprehensive bibliography, are given by Acosta [36].

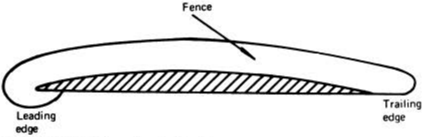

Fig. 6.39 Hydrofoil equipped with a fence.

6.3.6 *Forces on a Foil-borne Vehicle in Steady Motion*

The clearance between the hull of the craft and the water must be sufficiently great so as to avoid physical contact. The vehicle may then maintain a mean clearance relative to the still-water level in a mode called *platforming*, as shown in Fig. 6.40. (This generally requires continuous adjustment of the foil incidence angles as the craft proceeds at a steady forward velocity and a constant trim angle.) In reality, platforming occurs only in calm waters and it is reasonable to expect that in open waters *contouring* or some intermediate response will take place as indicated in Fig. 6.40. Ideally, the intermediate response is sought so that the hull just misses the crests yet the foils remain immersed at the troughs.

Our primary purpose now is to examine the equilibrium conditions for the craft cruising steadily and fully foil-borne. Nevertheless, it must be recognized that for many such craft, particularly those adopted for military assignments, the foil-borne state exists for relatively short periods of time. Foils are used only as a 'dash' facility and for normal patrol duties a conventional displacement mode is employed. However, the hull shape is one designed for fast lift-off from the water and so is not

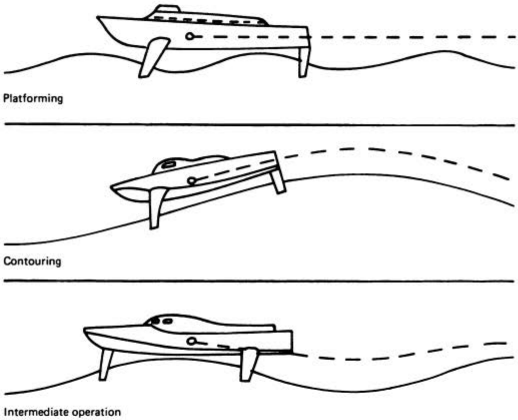

Fig. 6.40 Response of hydrofoil craft in waves.

necessarily conducive to good low-speed performance. Furthermore, as a displacement craft the foil systems including the struts may all be fully submerged thus constituting a large increment of drag. This appendage drag can be eliminated by incorporating separate port and starboard foils which can be retracted from the water and held aloft. The *USS Plainview* is of this type and is, incidentally, the largest hydrofoil boat built so far being 2.9 MN (≅ 290 tonf) all-up weight and 64 m (≅ 210 ft) long. The case for commercial types is different; for these high-speed operation is used most of the time for transportation between ports and hull-borne motion occurs only during docking.

The forces acting on a foil-borne craft of simple fully submerged foil configuration moving steadily forward are shown in Fig. 6.41. The craft moves parallel to its vertical plane of symmetry and so no side forces are developed.† The hull is supported clear of the water by a foil (or foils) forward of the centre of gravity G and a foil (or foils) abaft G. We may assume that in 'flight' the submerged foils and struts displace a negligible volume of water and so buoyancy forces are far smaller than

† In the case of a surface-piercing hydrofoil craft (Fig. 6.19) the lift force, which is perpendicular to both the direction of motion of the craft and the span of the foil, must have components vertically upwards and horizontally inwards to the longitudinal centre plane. Assuming that the motion is parallel to this plane and that both foils are symmetric then the horizontal components of the lift force cancel for each foil and we are left only with the vertical component. This component for each set of surface-piercing foils is usually referred to as the lift force.

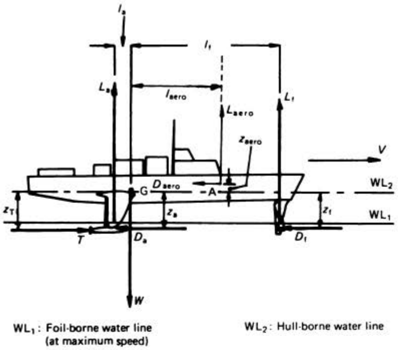

Fig. 6.41 Forces on a hydrofoil craft in steady motion.

dynamic lift forces. The latter forces on the forward and aft hydrofoil systems total L_f and L_a respectively, and the corresponding drag forces are D_f and D_a. It is quite possible for an aerodynamic lift force L_{aero} to act at the aerodynamic centre A of the hull; the corresponding drag force is D_{aero}. At very high speeds, say above 30 m s^{-1} ($\cong$60 knots), the aerodynamic drag can become an appreciable proportion of the total drag. For equilibrium, the all-up weight W will be balanced by the total lift L^* and the propulsor thrust T equals the total drag D^*, that is

$$L^* = W = L_a + L_f + L_{aero} \tag{6.48}$$

$$D^* = T = D_a + D_f + D_{aero}. \tag{6.49}$$

Let us suppose that elevations measured from the horizontal plane through G are given by z identified with appropriate subscripts as shown in Fig. 6.41. Taking clockwise moments as positive the resultant moment about a horizontal axis through G perpendicular to the plane of the diagram must be zero for equilibrium, that is

$$l_a L_a + z_a D_a + z_f D_f - l_f L_f - l_{aero} L_{aero} - z_{aero} D_{aero} - z_T T = 0. \tag{6.50}$$

With the reasonable assumptions that z_a, z_f and z_T are more or less equal and z_{aero} and L_{aero} are often small, Equation (6.50), with the aid of Equation (6.49), reduces to

$$l_a = \frac{L_f}{L_a} l_f. \tag{6.51}$$

Although the forms of these equations are quite simple the estimation of the lift and drag components is far from straightforward, as we have already seen.

The location of G depends on weight distribution, propulsion systems, operational requirements, trim at rest and so on. The positioning of the foils depends primarily on the ability to generate supporting forces, on the control of motion at transient and cruise speeds and on the adjustment of trim angle. Good manoeuvrability leads to one foil (or set of foils) being positioned so that a large moment is imposed on the craft but large control forces within the craft are avoided. Consequently, one foil system develops, at high efficiency, a lift force which is close to G and a large proportion of W. The second foil system develops a small lift force at some distance from G and is often a relatively inefficient lifting surface. This arrangement determines the canard and aeroplane configurations, each being associated with both fully submerged and surface-piercing foil systems. Fully submerged foils are affected little by the presence of moderate waves, provided that the foils are not too close to the interface, but the craft is inherently unstable vertically. Continuously operating incidence control on flaps must be incorporated in the design to counter the effects of lift variation during forward motion. In contrast, surface-piercing foils are certainly affected by waves which results in a harder ride, a considerable loss of speed and a lower longitudinal stability in a following sea, but lift control is far simpler. The characteristics of some significant hydrofoil craft are shown in Table 6.2.

To specify the conditions necessary to achieve and sustain steady motion we introduce the total lift coefficient C_L^* based on the total plan area of the foils S^*. Thus from Equation (6.48) we have

$$L^* = W = L_a + L_f = C_L^*(\tfrac{1}{2}\rho_w V^2 S^*)$$

that is,

$$S^* C_L^* = \frac{2W}{\rho_w V^2} \tag{6.52}$$

and, for simplicity, L_{aero} is taken to be small. For a given vehicle of constant weight it is necessary to vary the product $S^* C_L^*$ in order to secure equilibrium at different forward speeds.

The plan area of fully submerged foils cannot be changed (retractable flaps have not been used to date) and so it is necessary to control C_L^*, for example, by changing the incidence angle. If the foils are fixed relative to the hull then changes of incidence angle result only from changes in trim angle. Clearly, only limited control can be achieved in this way to avoid passenger discomfort at excessive trim and the possibility of the forward foil(s) broaching the interface. A better, but more complicated, method involves the adjustment of foils pivoted to the struts. So that accidental (and uncontrolled) air entrainment is avoided the pivot attached to the control linkage must be located towards the rear of the foil in a region where suction pressures are small. This, however, places the pivot well aft of the centre of pressure of the hydrofoil section (see Fig. 6.36) and so control forces may become excessive. To avoid this difficulty the span of the hydrofoil may be swept back and the foil tapered, as shown in Fig. 6.42. The section lift forces, which act approximately through the quarter-chord line, produce only a small moment about the control pivot because, for example, L_1 and L_2 are designed to yield nearly equal but opposite moments.

Trailing-edge flaps, hinged to the main hydrofoil, may be used to increase the

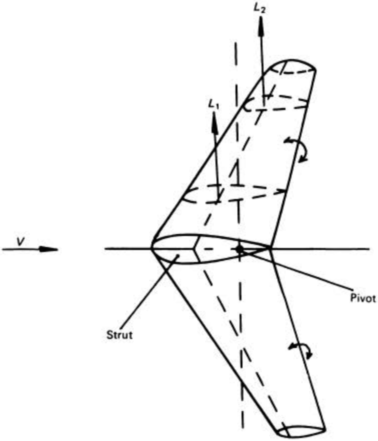

Fig. 6.42

camber. It is then feasible to maintain a constant trim and depth of foil immersion by adjusting independently the forward and rear foils. The US Navy craft ***Plainview*** and ***High Point***, described by Elsworth [42], employ incidence and flap control respectively. The rear foils of the ***Supramar*** PT50 and PT150 are both fitted with flaps. A study of a naval version of Jetfoil (designated 929–115) for use as a Fisheries Patrol Vessel (FPV) in the North Sea has been completed for UK operations [43]. As a result, a hydrofoil FPV named as ***HMS Speedy*** has undergone a trials period with the Royal Navy. In the canard arrangement the front foil is steerable and the boat can bank into a high-speed turn by operating, differentially, the trailing-edge flaps on the main foil. Technical details of these and many other hydrofoil craft may be found in [44].

The product $S^*C_L^*$ can also be changed by varying S^* but keeping C_L^* constant. This is the operating principle of the surface-piercing foils and step-ladder foils (now largely superceded) shown in Fig. 6.43. In both cases, as the forward speed is increased, say, and C_L^* is constant the craft tends to rise because $L^* > W$. However, as the craft rises less of the foil surface remains in the water and so S^* decreases to restore the equilibrium equation $L^* = W$. (The development of these systems has been described by Crewe [45], Hook and Kermode [32], Eames [30], and others.) Surface-piercing foils can also be fitted for incidence control and/or flaps, as for

Table 6.2 Characteristics of some hydrofoil craft.

Country	Craft	Configuration	Use	Foil system	Maximum foil-borne weight MN (tonf)	Proportion of weight taken by foils: Front	Proportion of weight taken by foils: Rear	Length overall m (ft)	Maximum speed: Hull-borne $m\,s^{-1}$ (knots)	Maximum speed: Foil-borne $m\,s^{-1}$ (knots)	Take-off speed $m\,s^{-1}$ (knots)
Canada	Bras d'Or	canard	naval (research)	bow-foil surface piercing, steerable; aft foil mixed fully submerged/ surface piercing	2.1 (212)	0.1	0.9	45.9 (151)	6+ (12+)	25–30 (50–60)	11 (22)
	DHC–MP–100	canard	naval/ coastguard	surface-piercing foils; bow foil diamond-shaped, steerable; main foil trapezium-shaped with fully submerged central portion and surface-piercing, dihedral, outboard surfaces	1.03 (104)	0.1	0.9	36.0 (118)	6 (12)	25 (50)	–
Italy	Swordfish P 420	canard	naval	fully submerged retractable; one bow foil, two aft foils; anhedral in aft foils to prevent broaching when turning, water jet propulsion	0.63 (64)	–	–	28.7 (94.1)	–	18 (36)	–
	RHS 160	conventional	commercial	surface-piercing foils with trailing edge flap control on both foils; craft is one of a series from 0.31–1.2 MN; derivatives used by navy, coastguard, offshore service	0.84 (85)	–	–	31.3 (103)	–	18 (36)	–
	Seaflight L90	conventional	commercial	surface-piercing foils; bow foil of 'W' shape with three struts plus incidence control; aft foil with fully submerged centre portion plus inclined surface-piercing outer surfaces, supports rudders	0.59 (59.5)	0.6	0.4	27.3 (89.3)	–	16–17.5 (32.4–35)	–

Switzerland	Supramar PT20	conventional	commercial	surface piercing with incidence control on bow foil	0.31 (32)	0.58 0.66 (for the PT20B)	0.42 0.34	20.75 (68.1)	–	17 (34)	–
	Supramar PT150	conventional	commercial	bow foil surface piercing with trailing edge flaps; aft foil fully submerged with incidence control and air stabilization	1.64 (165)	0.6	0.4	37.9 (124.2)	–	18.5 (36.5)	11 (22)
USA	Plainview AGEH–1	conventional	naval	all foils fully submerged, retractable and incidence control; aft foil steerable	2.85 (290)	0.9	0.1	64.6 (212)	6.7 (13.4)	25+ (50+)	16.5 (33)
	Pegasus PHM–1	canard	naval	all foils fully submerged, retractable by rotation out of water; trailing-edge flaps fitted to all foils; bow strut steerable; main foil of 'M' shape	2.3 (231)	0.32	0.68	40 (131.2)	5+ (10+)	25+ (50+)	–
	Jetfoil 919–100	canard	commercial/ naval	all foils fully submerged; single inverted 'T' strut/ foil forward; three-strut full-span foil aft; forward strut steerable; trailing-edge flaps on all foils; all foils retractable; water jet propulsion	1.1 (110)	–	–	27.4 (90)	3+ (6+)	25 (50)	10 (20)
	High Point PCH–1	canard	naval	all foils fully submerged with trailing-edge flaps; foils retractable into hull; inverted 'T' bow foil; two struts aft joined by flatted 'M'-shaped foil; subcavitating propellers at base of each aft strut	1.27 (127.2)	0.32	0.68	35.3 (115.75)	12.5 (25)	25 (50)	13.5 (27)
	Flagstaff PGH–1	conventional	naval/ coastguard	all foils fully submerged with incidence control; two inverted 'T' foils forward and one aft which has steerable strut; all foils retractable	0.67 (67.5)	0.7	0.3	22.2 (73)	3.5+ (7+)	20+ (40+)	–

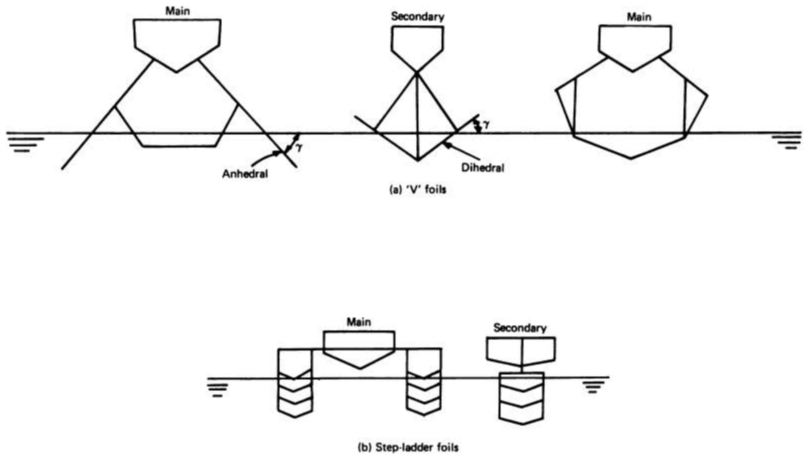

Fig. 6.43 Foil systems showing anhedral and dihedral.

the *Bras d'Or*, and this system, although very complicated, has been shown by Eames and Drummond [46] to be extremely effective in quite severe seas. The surface-piercing system also has the advantage of good lateral stability and control. Owing to the presence of *dihedral* and/or *anhedral* (defined in Fig. 6.43) quite large restoring forces come into play should lateral disturbances arise. Only the supporting struts provide lateral restoring forces for submerged foils unless anhedral is incorporated, as shown in Fig. 6.44. Dihedral cannot be used otherwise broaching takes place when heeling during a tight turn and the craft then experiences a sudden loss of lift.

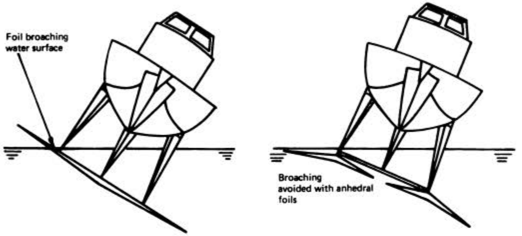

Fig. 6.44

The depth effect, discussed earlier, is used extensively in the USSR for operation on rivers, lakes and inland seas [37]. Many hundreds of hydrofoil craft are used in the USSR and other East European countries, including one type which has carried over 300 passengers. An increase in the forward speed makes the craft rise in the water and the reduced depth of immersion, in a region already close to the interface, causes C_L^* to decrease. A series of equilibrium depths is thus established, but as the range of depths is small over which the depth effect is significant the method cannot be used reliably in a seaway. Eames and Jones [39] quote the following approximate relationship for the effect of depth on the lift force developed by a surface-piercing foil of rectangular plan area:

$$L = \tfrac{1}{2}\rho_w V^2 \left\{ c^2 \left(\frac{h}{c} + \tfrac{1}{2} \right) \cot\gamma \, \cos\gamma \right\} 2\pi\alpha, \tag{6.53}$$

where α is the angle of incidence measured in the vertical plane, c is the chord length of the foil, γ is the angle between the foil and the water plane (see Fig. 6.43) and h is the depth of immersion of the lower tip of the foil. We see that in Equation (6.53) the terms in braces constitute an 'effective area' of the foil, and, further, the lift force varies linearly with both h and α.

6.3.7 *Hydrofoil Vehicle at 'Take-off'*

A gradual increase in forward speed from rest will change the operation of a hydrofoil craft from a conventional displacement mode to a condition in which buoyancy forces are negligible and dynamic lift forces are large. At some particular speed the hull will be just clear of the water and the craft is then said to be foil-borne at the 'take-off' speed. We can thus define the take-off speed as

$$V_{to} = \frac{2W/S^*_{to}}{\rho_W C^*_{L_{to}}} \tag{6.54}$$

where the subscript 'to' refers to take-off. This speed is not, of course, the cruise speed for then a clearance of several metres from the still-water level is required to avoid violent impact with spray and waves. It is advantageous to achieve take-off at the lowest speed possible to minimize hull drag and appendage drag and thereby operate at optimum expenditure of propulsive power. According to Equation (6.54), V_{to} is lowered if S^*_{to} is kept large, as it is for the surface-piercing foil, and/or $C^*_{L_{to}}$ is kept large by adjusting the main-foil incidence angle or flap position. The increment of lift force coefficient from the flaps $C^*_{L_{flap}}$ $(= L^*_{flap}/\frac{1}{2}\rho_W S^* V^2)$ is constant at small α, and so for each foil system

$$C^*_{L_{to}} = C^*_{L_0} + C^*_{L_{flap}} + a_{l_0}\alpha_{to} \tag{6.55}$$

in analogy with Equation (6.31), for example. Take-off speeds for several craft are shown in Table 6.2, where those with surface-piercing main foils can be seen to have the lowest take-off speed.

Two procedures can be envisaged for the take-off manoeuvre, the choice depending on the comprehensiveness of the control system. Suppose the main foils are fixed to struts at a constant angle which corresponds to the incidence angle at the cruise speed. The boat can then be accelerated to the take-off speed with the main foil flaps deflected to the take-off setting. The bow foil, say, can be used as a control foil to raise the bow so that the vehicle rotates to a larger trim angle. When the main-foil incidence angle is α_{to} take-off will follow. This method is similar to that used by aircraft. Large changes of trim are implied, and this is a characteristic unsuitable for vehicles carrying weapons and uncomfortable for passengers in commercial craft.

Alternatively, if all the foils are fully adjustable for incidence angle then α_{to} can be pre-selected. As the forward speed increases the craft maintains a constant trim and simply rises in the water until take-off is achieved. Further adjustments to α then allow the craft to proceed at a given trim angle and water clearance for any speed between take-off and the maximum attainable.

6.3.8 *Drag Force on a Hydrofoil Vehicle*

The hull of a hydrofoil craft is often of the planing-craft type to help increase dynamic lift at speeds just below that corresponding to take-off. Until take-off occurs the total drag force D^* on the craft rises steeply as shown in Fig. 6.45. This behaviour is typical of medium-size craft for which the appendage drag arises from the support struts, shafting, transmission pods and so on. It is only beyond the onset of cavitation that the total drag force rises above the peak corresponding to maximum wave-making drag (the primary hump).

When the hull is clear of the water it is susceptible to both spray drag and aerodynamic drag, although these are reduced by streamlining the craft. The drastic reduction of hydrodynamic-induced drag, as α is decreased, and the reduction in hull drag with higher forward speeds, show as a drop in the total drag force. At

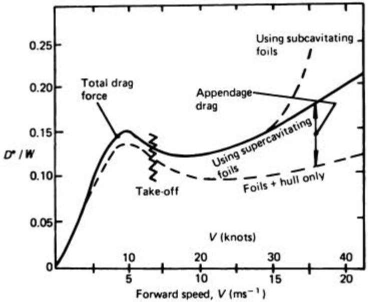

Fig. 6.45 Performance characteristics of a hydrofoil craft of length 30 m (≃ 100 ft).

speeds above take-off the power requirement rises less steeply than it would for hull-borne operation, but again increases rapidly at the higher cruise speeds until a condition is met where the available power at a steady design cruise speed is given by

$$P_{des} = TV_{des} = D^* V_{des}. \tag{6.56}$$

The effectiveness of supercavitating foils is also shown in Fig. 6.45 where their superiority over subcavitating foils at high speeds is clearly demonstrated. Indeed, the usually adopted limit for subcavitating foils is $Fr = V/\sqrt{(gL_{WL})} < 1.6$ where L_{WL} is the water-line length of the hull for the craft at rest.

At the steady foil-borne cruise speed we can express the total drag coefficient in the form,

$$C_D^* = C_{D_0}^* + C_{D_i}^* = D^*/\tfrac{1}{2}\rho_w S^* V^2 \tag{6.57}$$

from Equation (6.40). The coefficient $C_{D_0}^*$ includes contributions from spray drag in addition to the viscous pressure (profile) drag from the foils and struts. These forces can be considered independent of V, but the contribution from skin-friction drag reduces slightly as forward speed increases. Mandel [22] has given the following breakdown of drag for a large hydrofoil craft when cruising steadily at about 22.5 m s^{-1} (45 knots):

skin-friction drag coefficient	= 0.007 (36 %)
spray drag coefficient	= 0.004 (21 %)
form drag coefficient	= 0.002 (11 %)
profile drag coefficient $C_{D_0}^*$	= $\underline{0.013}$ (68 %)
induced drag coefficient $C_{D_i}^*$	= 0.006 (32 %)
total drag coefficient C_D^*	= $\underline{0.019}$ (100 %)

For this example, the lift coefficient C_L^* was 0.24 and the wave-making drag was assumed to be negligible. Thus, the drag-to-weight ratio $C_D^*/C_L^* = 0.079$, and at the cruise speed this ratio is seen to be about one-half the value of the analogous quantity R_T/W for the planing craft whose performance is shown in Fig. 6.18 and about one-third of the value for the craft with the performance shown in Fig. 6.15.

It might be supposed that hydrofoil craft are particularly susceptible to damage from floating debris. If a strut were badly damaged, or even removed in collision, the result could be disastrous with possible capsizing. Perhaps surprisingly, Hook [47] notes that this has not been an outstanding problem to operators. This is mainly because: (i) the struts are strong enough to withstand impact with flotsam; (ii) the pilot has a good view of the water ahead so that he can take avoiding action and, at worst, strike larger obstacles a glancing blow; and (iii) for commercial operations the routes are well planned beforehand and frequent journeys allow continuous observation of prevailing conditions.

6.4 Air Cushion Vehicles (ACV)

There is a wide range of vehicles which depend on the proximity of a solid or water surface below them in order to function effectively, though they need not be in contact with that surface. Some of these are shown in Fig. 6.46, where it can be seen that the 'ground effect machine' may rely on either aerostatic or aerodynamic supporting forces, or possibly a combination of both. For our present purposes, we shall consider aerostatically supported vehicles only, and since we shall not examine air bearings we may refer to hovercraft generally as air-cushion vehicles (ACV). Attention will be primarily focused on plenum and annular jet craft with skirts and with or without solid side walls, that is, those vehicles identified with an asterisk in Fig. 6.46. The ACV depends for its support on the creation and retention of an air cushion between the craft and a land or water surface. Ideally, there is no direct contact between any part of the craft and the surface over which it passes (see Fig. 6.47) and so the hovercraft may therefore be amphibious. It might be supposed that motion over water could be achieved without any contribution from wave-making drag if contact with the water surface is avoided. However, indirect contact with the water occurs through the air cushion. The water surface distorts if subjected to a local pressure different from ambient and this disturbance moves with the ACV.

The over pressure (positive gauge pressure) in the cushion is derived from a fan and maintained by sealing the cushion air along the periphery using either an annular (peripheral) jet, a plenum chamber, or a solid wall in combination with the first two systems. In each of these systems, shown diagrammatically in Fig. 6.48, air must leak from under the cushion if the vehicle is to ride clear of the 'ground'. Thus the cushion pressure must be maintained despite a steady through-flow of air. Various types of fan or compressor have been used for this purpose [48] although centrifugal and mixed-flow fans seem to be favoured most at the present time. Usually, these fans are designed specifically for a particular ACV. Even so, the dynamic behaviour of the fans when subjected to a fluctuating back pressure, such as occurs over rough 'ground' or waves, and the interactions with duct, cushion and skirt flows are still not fully understood. The designer aims to keep the leakage flow as low as possible, thereby reducing the energy of the cushion air, so that the power required by the 'lift' fan is minimized. It is evident, however, that if the leakage, and therefore the clearance height, is small contact will occur between the solid structure of the craft and protruberances in the surface over which the craft is

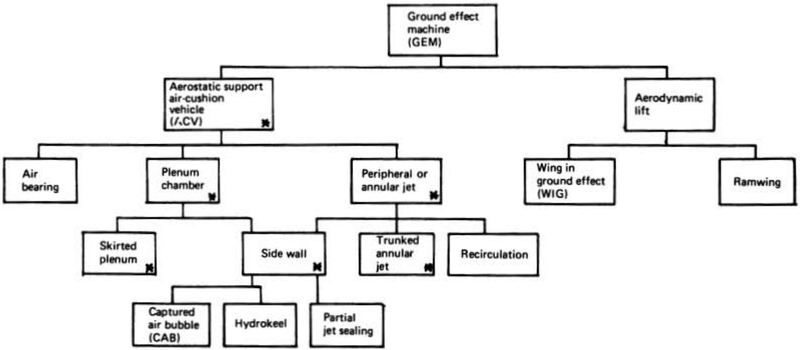

Fig. 6.46 Various types of ground effect machine.

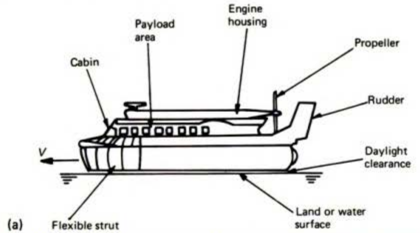

(b)

Fig. 6.47 Amphibious hovercraft: (a) schematic layout; (b) British Hovercraft Corporation SRN-6 Mk 6.

moving. To avoid this, and yet maintain a stable vehicle with small lift power, flexible skirts are now used on most ACV. For the present, we can regard the skirts as extensions of the nozzle through which the leakage flow passes. The advent of the skirt principle has led to a reinstatement of plenum chamber craft after being superseded by the annular (peripheral) jet type following the early development of Cockerell's ideas [37].

In the plenum chamber craft (Fig. 6.48(b)), air is supplied directly to the cushion which is 'pumped up' to an over pressure of 2–3.5 kPa ($\cong 1/50-1/30$ atmosphere).

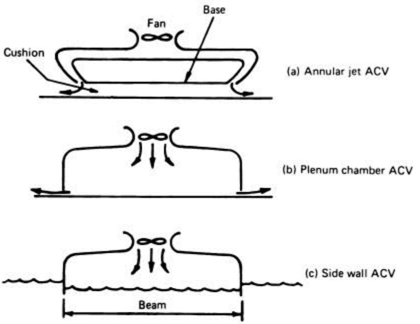

Fig. 6.48 Types of hovercraft (ACV).

The geometry of this craft suggests the use of an axial-flow fan but often this type of fan does not perform well at high cushion pressures and low flow rates. When an annular jet is used (Fig. 6.48(a)) the cushion over pressure results from the inward curvature of the curtain of air flowing to the atmosphere. Rather higher clearances can be obtained compared with the plenum chamber craft at the same leakage flow rate. Both of these ACV are amphibious and forward motion may be obtained from air propellers mounted on the superstructure, although the operation of these is noisy and often inefficient. For operation entirely over water partially immersed side walls may be used (Fig. 6.48(c)) to ensure a complete air seal along most of the jet periphery. In the intended orientation of the craft the side walls are more or less in the direction of motion of the craft and if properly streamlined offer relatively low resistance to movement except at very high speeds. In addition to providing extra support from buoyancy forces each side wall can be used to house the shaft driving a marine propeller. At the bow and stern flexible skirts are fitted to prevent excessive leakage and drag.

The early theoretical and experimental development of ACV from their conception by Cockerell in the 1950s has been described by Crewe and Eggington [49]. More recent advances and future predictions are discussed in, for example, [37, 48, 50–52, 89].

6.4.1 *Hovering Flight: Cushion Pressure*

Simple theories relating the cushion pressure to the geometry of the craft, the jet velocity and the clearance height were given in Chapter 3 for the plenum chamber and annular jet ACV. For the latter an approximate theory based on momentum considerations showed that for steady flow the cushion pressure, p_c, was given by

$$p_c = \rho_a v^2 \left(\frac{a}{h}\right)(1 + \cos\theta) \tag{6.58}$$

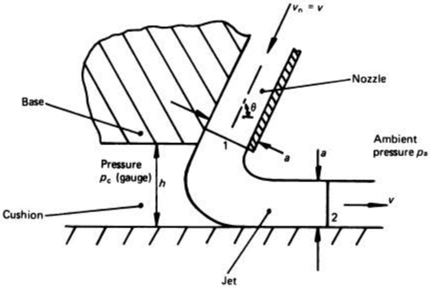

Fig. 6.49

where the symbols are defined in Fig. 6.49 and ρ_a is the density of air. The assumptions in the theory leading to Equation (6.58) are:

(i) the local air velocity v is constant throughout the jet and equal to the velocity v_n, at the nozzle outlet;
(ii) the pressure in the jet is atmospheric;
(iii) p_c is constant;
(iv) the air in the cushion and in the atmosphere is stationary;
(v) the effects of viscosity are negligible;
(vi) the flow is wholly two dimensional;
(vii) ρ_a is constant throughout; and
(viii) atmospheric pressure p_a is constant.

The boundary between the jet and the cushion air marks a discontinuity of both pressure and velocity. The theory is clearly inadequate, because the pressure and the velocity in the curved jet have both been assumed constant. Nevertheless, in some practical arrangements the subsequent predictions of cushion pressure have been found acceptable.

As a result of assumptions (iii)–(v) and neglecting changes in elevation an application of Bernoulli's theorem shows that the total pressure (gauge) in the jet is given by

$$p_t = \tfrac{1}{2}\rho_a v^2$$

whence

$$\frac{p_c}{p_t} = 2\,\frac{a}{h}(1 + \cos\theta) = 2x \tag{6.59}$$

where

$$x = \frac{a}{h}(1 + \cos\theta). \tag{6.60}$$

Equation (6.59) implies that $p_c > p_t$ when

$$\frac{h}{a} < 2(1 + \cos\theta),$$

but this condition is impossible since flow takes place from the fan (the energy source) to the cushion region. This rudimentary theory is, therefore, applicable only when $(a/h)(1 + \cos\theta)$ is small, that is, when h is large for a given craft. Indeed, we can argue that as $h \to 0$ the flow out of the nozzle becomes similar to that for a plenum chamber and so p_c/p_t increases to unity as h becomes small.

A more logical and general approach is obtained by dropping the first two assumptions in the previous list, namely, v is no longer assumed constant nor is the jet pressure taken to be atmospheric. As shown in Fig. 6.50, the pressure in the jet must increase from p_a on streamline S_o to p_c on streamline S_c, and so the velocity v_o on S_o must be greater than the velocity v_c on S_c because the total pressure in the jet p_t is constant (ignoring the small changes in elevation). Furthermore, the velocities v_o and v_c are constant along corresponding streamlines. In the nozzle exit plane the pressure p_n is constant and equal to p_a, the direction of discharge being perpendicular to this plane. Also, since the total pressure is constant throughout, the velocity of the fluid in the nozzle v_n is constant. There must then be a discontinuity of pressure and velocity at the exit plane of the nozzle. However, this mathematical model has an important advantage over the previous postulates in that there are no discontinuities of pressure outside the nozzle. If small changes in

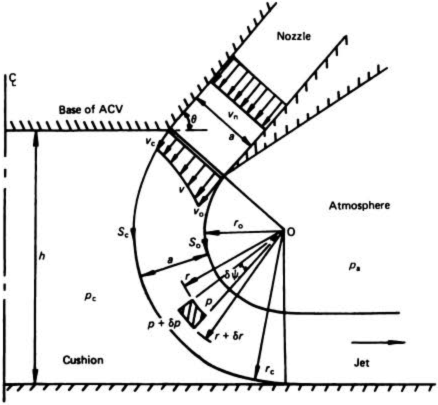

Fig. 6.50

elevation are again neglected Bernoulli's theorem shows that

$$p_t = p + \tfrac{1}{2}\rho_a v^2 = p_n + \tfrac{1}{2}\rho_a v_n^2 = p_a + \tfrac{1}{2}\rho_a v_n^2 = p_a + \tfrac{1}{2}\rho_a v_o^2 = \text{constant} \quad (6.61)$$

and therefore

$$v_n = v_o.$$

For the equilibrium of a fluid element in the jet it is easy to show that

$$\frac{dp}{dr} = \frac{\rho_a v^2}{r} \quad (6.62)$$

where r is the local radius of curvature of the streamline along which the element moves. Since the flow is steady v is constant along a streamline and so is dp/dr. Hence r must be constant and flow therefore occurs along concentric circular streamlines with the point O as the centre of curvature (see Fig. 6.50). The width of the jet a remains constant and equal to the nozzle width. Equation (6.62) forms the basis of numerous inviscid flow theories some of which are summarized by Harting [53].

Substitution for $\rho_a v^2$ from Equation (6.61) into Equation (6.62) yields,

$$\frac{dp}{p_t - p} = 2\frac{dr}{r}$$

whence

$$-\ln(p - p_t) = 2\ln(r) + \text{constant}$$

and so

$$p - p_t = \frac{1}{Kr^2}$$

where K is a constant. When $r = r_o$, $p = p_a$ and therefore

$$\frac{1}{K} = (p_a - p_t)r_o^2.$$

The local pressure in the jet is thus given by

$$p = p_t - (p_t - p_a)\left(\frac{r_o}{r}\right)^2.$$

From Equation (6.61)

$$p_t - p_a = \tfrac{1}{2}\rho_a v_n^2,$$

and so

$$p = p_a + \tfrac{1}{2}\rho_a v_n^2\left\{1 - \left(\frac{r_o}{r}\right)^2\right\}. \quad (6.63)$$

The cushion pressure at the inner streamline of the jet becomes

$$p_c = p_a + \tfrac{1}{2}\rho_a v_n^2\left\{1 - \left(\frac{r_o}{r_c}\right)^2\right\}. \quad (6.64)$$

Noting that

$$r_c = r_o + a = h/(1 + \cos\theta) \tag{6.65}$$

and using Equation (6.60) we can now write

$$p_c = p_a + \tfrac{1}{2}\rho_a v_n^2 \left\{2\frac{a}{r_c} - \left(\frac{a}{r_c}\right)^2\right\} = p_a + \tfrac{1}{2}\rho_a v_n^2(2x - x^2)$$

or,

$$c_{p_c} = \frac{p_c - p_a}{\frac{1}{2}\rho_a v_n^2} = 2x - x^2 \tag{6.66}$$

where c_{p_c} is the cushion-pressure coefficient.

Several theories have been published which are said to be appropriate to jets of small thickness. Thus when a/h is small, x is small and Equation (6.66) reduces to

$$c_{p_c} \cong 2x. \tag{6.67}$$

By making dubious assumptions about the variation of pressure across the jet (just as *we* did to obtain Equation (6.58)) or by contracting the jet to a mean line it is possible to show that

$$c_{p_c} = 2x \quad \text{or} \quad \frac{2x}{1+x} \quad \text{or} \quad 1 - \exp(-2x).$$

The first example is equivalent to Equation (6.58) because then $\nu = \nu_n$. The second and third alternatives for c_{p_c} are often misleadingly portrayed for all x. But, when x is small,

$$\frac{2x}{1+x} \to 2x \quad \textit{and} \quad \{1 - \exp(-2x)\} \to 2x$$

and so all these results, including Equation (6.66), tend to $2x$ as x becomes small. What is perhaps surprising is that the exponential theory yielding

$$c_{p_c} = 1 - \exp(-2x)$$

has been shown in some cases to produce values remarkably close to those obtained from experiment over a wide range of x, as shown in [54].

More accurate theories sometimes assume the streamlines to be elliptical rather than circular or alternatively specify a particular variation of ν across the jet. Exact solutions of the inviscid-flow problem can be obtained by conformal mapping although rather complicated expressions are involved. Finally, we may note that several viscous-flow theories, of varying complexity, have been put forward for both two- and three-dimensional flows. These theories allow entrainment and mixing to be accounted for, and it has been found that the effects of viscosity become important when h is small, that is, for large x.

6.4.2 *Hovering Flight: Cushion Flow*

In all the preceding theories the character of the air in the cushion has been grossly simplified by assuming constant pressure and zero velocity. Figure 6.51(b) adapted from [53] illustrates the complex nature of the flow beneath a simple peripheral

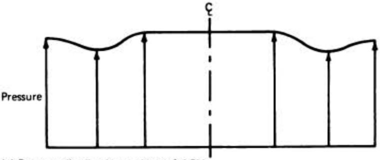

(a) Pressure distribution on base of ACV

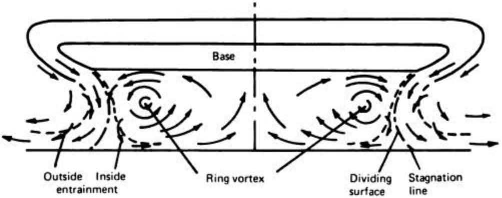

(b) Flow pattern

Fig. 6.51 Hovering ACV over land.

jet ACV model which is hovering horizontally close to the solid ground. Air is drawn in from the atmosphere owing to viscous shear stresses at the outer surface of the jet. Similarly, air is transferred between the cushion region and the inner surface of the jet. Air leaves the cushion by entrainment and is replenished by an inward flow near the ground. Thus, near the ground, the flow divides with one part moving inwards and the other part outwards, the latter consisting of the original jet and the air entrained from the atmosphere. These two parts are separated by a dividing surface which meets the ground at a stagnation line. If the planform of the ACV is circular then the cushion flow consists mainly of a stationary toroidal-shaped ring vortex. A similar, although differently shaped, vortex exists in the cushion region for other planforms.

We see, therefore, that the air under the cushion is actually in motion and that the strength of the vortex depends, among other things, on the thickness and the velocity of the jet. A high-velocity, thin jet generates a stronger vortex than a slow, thick jet. As a result we would expect the pressure on the base of the vehicle to drop near the vortex region as indicated in Fig. 6.51(a). The depression in the pressure profile increases as the strength of the vortex increases. All other things being unchanged, an increase in height increases the diameter of the vortex and thus widens the depression in the pressure profile. At large clearance heights the character of the cushion air changes shape completely to the so-called 'focused' jet described in [53].

When a marine ACV hovers the over pressure in the cushion region causes a depression in the water surface. The craft appears to settle in the water, as shown in Fig. 6.52, so reducing the clearance height relative to the still-water level. Water is scooped out around the perimeter to form spray both outside and, to a lesser extent, inside the cushion region. The details of the flow over a water surface are thus somewhat different from those for motion over land although the principle of generating supporting forces aerostatically remains the same.

Fig. 6.52 Hovering ACV over water.

6.4.3 *Hovering Flight: Performance*

For the sake of simplicity let us proceed from Equation (6.66), and the theory leading to it, in order to find the total aerostatic and aerodynamic components of the overall supporting force. Assuming that p_c is constant and the peripheral jet is uniform then the aerostatic supporting force acting on the base is given by

$$F_c = (p_c - p_a)S = \tfrac{1}{2}\rho_a v_n^2 S(2x - x^2), \tag{6.68}$$

where S is the plan area of the ACV base measured to the inside edge of the jet.

Since the vertical component of the jet momentum flux is destroyed on contact with the ground there must be a vertical supporting force from jet reaction. The vertical component of momentum flux of the air in the jet leaving unit peripheral length of the nozzle between the radii r and $r + \delta r$ (see Fig. 6.50) is

$$\delta F_j' = (\rho_a v \delta r) v \sin\theta .$$

Generally, there are no discontinuities along the periphery of the jet (the ACV planform is usually rectangular with rounded fore and aft ends) and so the unit length can be taken at a mean position in the nozzle. Furthermore, since the nozzle width is constant, the total mean length of the nozzle l_n is the arithmetic mean of the base periphery and the outer periphery of the nozzle. The total supporting force from jet reaction is, therefore,

$$F_j = \rho_a l_n \sin\theta \int_{r_o}^{r_c} v^2 \, dr.$$

Now from Equations (6.61) and (6.63) we see that

$$v = v_n \left(\frac{r_o}{r}\right) \tag{6.69}$$

and so, with the aid of Equation (6.65), we can write

$$F_j = r_o^2 v_n^2 \rho_a l_n \sin\theta \int_{r_o}^{r_c} \frac{dr}{r^2}$$

whence

$$F_j = al_n\rho_a v_n^2(1-x)\sin\theta. \tag{6.70}$$

Pressure also varies across the jet and so we can expect an additional supporting force

$$F_p = l_n\int_{r_0}^{r_c}(p-p_a)\sin\theta\,dr$$

$$= \tfrac{1}{2}\rho_a l_n \sin\theta\int_{r_0}^{r_c}(v_n^2 - v^2)\,dr$$

whence

$$F_p = \tfrac{1}{2}al_n\rho_a v_n^2 x\sin\theta. \tag{6.71}$$

The total vertical supporting force is therefore given by

$$F_v = F_c + F_j + F_p = \tfrac{1}{2}\rho_a v_n^2(2-x)(xS + al_n\sin\theta) \tag{6.72}$$

after some algebraic simplification.

To give a measure of the ground effect F_v may be compared with a reference force. A suitable reference force is that exerted on a nozzle of circular cross section, equal in area to that of the ACV nozzle (i.e. al_n), by a jet directed vertically downwards well clear of the ground. This force is $al_n\rho_a v^2$ and, since the pressure in this cylindrical jet $p = p_a$ because streamlines are straight, we may replace v by v_n. The resulting force $al_n\rho_a v_n^2$ may also be deduced from Equation (6.70) with $\theta = 90°$ and $h \to \infty$. The index of merit is called the *augmentation ratio* A_r and is defined as

$$A_r = \frac{F_v}{al_n\rho_a v_n^2} = \frac{1}{2}(2-x)\left(\frac{xS}{al_n} + \sin\theta\right)$$

$$= \frac{1+\cos\theta}{(hl_n/S)} + \sin\theta - \frac{x}{2}\left(\frac{xS}{al_n} + \sin\theta\right). \tag{6.73}$$

When x is small, that is a/h is small, Equation (6.73) reduces to

$$A_r = \frac{1+\cos\theta}{(hl_n/S)} + \sin\theta \qquad \text{(for small } x\text{)}. \tag{6.74}$$

The benefit of the ground proximity effect is felt only when $A_r > 1$ and so, from Equation (6.74),

$$\frac{hl_n}{S} < \frac{1+\cos\theta}{1-\sin\theta}. \tag{6.75}$$

Inspection of Equation (6.73) shows that the 'thin-jet' theory overestimates A_r for larger values of x. However, the vortex theory breaks down with values of $x \geqslant 2$, for then $A_r \leqslant 0$ and this does not match experimental data.

Again, for the sake of simplicity, let us take x to be small and adopt Equation (6.74) for A_r so that

$$F_v = al_n\rho_a v_n^2\left(\frac{1+\cos\theta}{hl_n/S} + \sin\theta\right). \tag{6.76}$$

Equation (6.76) implies that, for a given vehicle, F_v is related to h as shown in Fig. 6.53. At 'take-off' the vehicle rises until F_v equals the operating all-up weight W at the specified clearance height. However, the real operating conditions are far more complicated than those indicated by Fig. 6.53. Equation (6.76) is approximate and the generation of cushion pressure and nozzle velocity depend on the aerodynamic characteristics of the lift fan(s). A change in h is equivalent to the adjustment of a throttle valve downstream from the fan supplying the cushion air. Different types of fan respond differently although the mass flow rate passing through a given fan running at a constant speed of rotation increases as the back pressure decreases (i.e. as h increases). The augmentation ratio thus depends on the fan characteristics and rather sophisticated control of these using adjustable speeds of rotation, blade angles, bypass circuits and so on are required to maintain the optimum performance. Frequently, it is difficult to interpret the results of model tests in which different air-supply systems have been used.

It is clearly a difficult task to incorporate an accurately modelled lift fan and duct system in small-scale laboratory test work. This has encouraged the use of an external supply system from a fan remote from the model but connected to it by a flexible duct. Although this may be satisfactory for the stationary model hovering, a variety of problems arises when the model is in motion, especially when encountering waves. Variable back pressure on the fan requires a detailed knowledge of the dynamic performance characteristics which often display hysteresis loops over the period of the excitation. The geometry of the ducting leading to the skirt systems is also an important factor in craft behaviour. Furthermore, the resulting oscillations

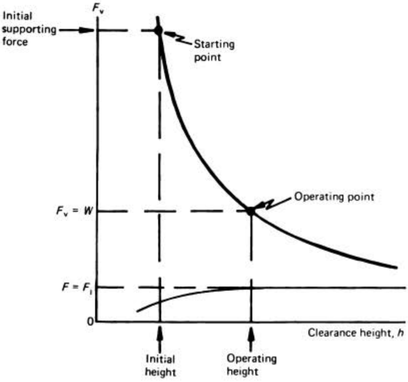

Fig. 6.53 Variation of supporting force for a given ACV and jet flow.

of the air column in the ducting of an external supply system can profoundly alter the response of a hovercraft. Some of these points have been noted in [55]. At least a partial way out of the problem is to incorporate the lift fan system in the model craft and to maintain high enough air velocities to ensure that the flow is fully turbulent. A useful technique is that described in [56] in which a wave belt facility is used. Large models, over 2 m long, can be mounted over a moving continuous belt supporting a prescribed wave system in order to examine the high-speed motion of an ACV passing over head seas.

Figure 6.53 shows that no best operating clearance is predicted; instead a series of equilibrium values of h satisfy a given W. Nevertheless, for a given h there is an optimum nozzle angle and a corresponding maximum augmentation ratio for a given vehicle. The optimum nozzle angle satisfies the relation

$$\frac{\mathrm{d}A_r}{\mathrm{d}\theta} = -\left(\frac{S}{hl_n}\right)\sin\theta + \cos\theta = 0$$

after using Equation (6.74), whence

$$\theta_{opt} = \arctan(hl_n/S). \tag{6.77}$$

The corresponding maximum value of A_r is

$$(A_r)_{max} = \frac{S}{hl_n}\left[1 + \left\{1 + (hl_n/S)^2\right\}^{1/2}\right]. \tag{6.78}$$

The variations of A_r with θ and $(A_r)_{max}$ with hl_n/S, as given by Equations (6.74) and (6.78), are shown in Fig. 6.54. Large values of A_r occur when hl_n/S is small, but small h is, of course, excluded from our analysis. Figure 6.54 indicates that θ_{opt} changes with h and therefore with all-up weight. It is clear, however, that inward-pointing jets are more effective than vertical jets for practical clearances but the added complexity of adjustable nozzles has not yet proved to be a viable proposition.

6.4.4 *Forward Flight Over Land*

The external flow about a simple model of an ACV moving over a flat, solid surface depends significantly on the forward speed as shown for a series of steady states in Fig. 6.55 (see also [53]). The following features are worth emphasizing:

(i) At low speeds the flow under the vehicle resembles that for hovering flight. The efflux from the forward jet is forced upwards from the ground and encloses a larger region of eddies which are then blown over the upper surface of the craft. Over water this régime is characterized by large amounts of spray thrown over the superstructure.

(ii) As the speed increases the eddy region over the upper surface decreases in extent and the flow in the main stream follows the contour of the hovercraft more closely. At the first critical speed the jet flow is carried aft in a thin stream close to the upper surface. For flight over water the spray at the front disappears.

(iii) A stable flow pattern develops in the transition region as the speed increases further. Some of the forward jet enters the cushion and the remainder is deflected upwards to enclose a 'bubble' resulting from the attachment of the jet to the bow structure. At higher speeds more of the jet is deflected aft, the bubble size decreases and it begins to rotate with increasing intensity – rather like a vortex.

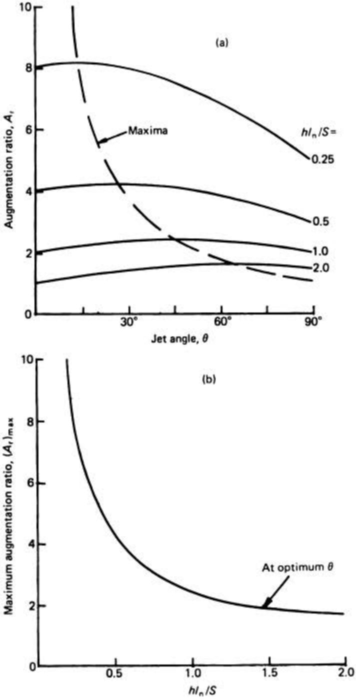

Fig. 6.54 Dependence of augmentation ratio A_r on θ and hl_n/S.

(iv) Eventually, a particular case of transition flow, called the Poisson-Quinton critical condition [57], is reached in which the pressure in the bubble has increased to a value equal to the cushion pressure. The forward jet then has no curvature over most of its length but some of the jet close to the ground is still deflected forwards.

(v) Nevertheless, at speeds higher than this critical condition an increasing

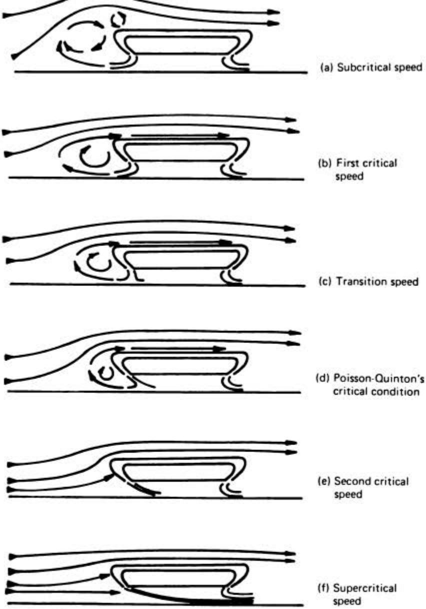

Fig. 6.55 Forward flight of ACV over land.

proportion of the air moves aft. The pressure in the bubble exceeds the cushion pressure and the jet becomes curved concave relative to the cushion. The second critical speed is identified by the absence of any forward air from the leading jet. The passage of the mainstream flow under the cushion is just prevented and the bubble is no longer present.

(vi) Finally, in the supercritical condition, the forward jet is swept under the cushion and mainstream flow occurs between the forward jet and the ground.

A three-dimensional craft has essentially similar external flow patterns.

Although a great amount of experimental work has been published on the flow behaviour around and below ACV it has proved impossible to predict with certainty the occurrence of the régimes shown in Fig. 6.55. However, it has been noticed that with increasing forward speeds:

(i) the cushion (gauge) pressure near the leading edge of the ACV decreases and may become negative, whereas the cushion (gauge) pressure towards the trailing edge remains positive;
(ii) the total supporting force at small clearance heights decreases slightly in the subcritical régime and increases again in the supercritical régime; and
(iii) the total drag increases gradually.

It would seem that in forward flight the augmentation ratios for axially symmetric, annular jet craft are greatest when the jets are inward facing as in the case of hovering flight. In the supercritical régime (Fig. 6.55(f)) the operation of the ACV can be likened to that of a wing fitted with a jet flap. A lift force is developed which increases with forward speed thereby increasing the effective augmentation ratio.

The preceding remarks must be taken as only indicative of the behaviour which may occur because tests in forward flight are difficult to conduct. Dynamic similarity between the model conditions in, say, a wind tunnel and the prototype conditions is often invalidated by the presence of the boundary layer on the bottom wall of the tunnel. This is most profound when the supercritical régime is reached and the clearance height is small.

6.4.5 *Forward Flight Over Water*

When hovering at rest the depression of the water surface below the ACV is symmetric, as shown in Fig. 6.56 (see also [53]). A two-dimensional model is again used here for the purpose of illustration. At low speeds the depression remains nearly parallel to the base of the vehicle but both are tilted to give the craft a small positive

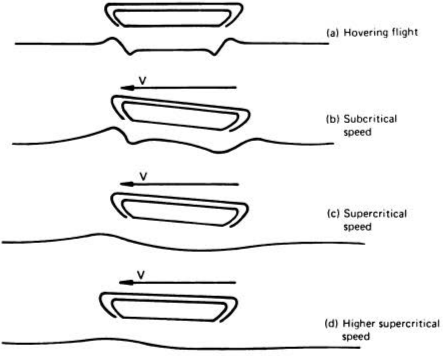

Fig. 6.56 Forward flight of ACV over water.

(nose-up) trim angle, as illustrated in Fig. 6.56(b). This water depression, sometimes called the 'fluid hull', arises from the cushion over pressure and is dragged through the water to produce a wake behind the vehicle. Thus, the AVC appears to settle relative to the still-water level, especially that portion towards the trailing edge. As the speed increases in the subcritical range the slope of the water depression, the trim angle of the vehicle and its clearance height all increase, owing to the piling up of water ahead of the craft, until the trim angle reaches a maximum value at the critical speed. The bow wave and spray then disappear under the front of the vehicle. A further increase in speed, into the supercritical range, produces a longer, shallower depression of greater area and decreased slope owing to the inertial lag of the fluid particles in response to the fast-moving pressure field. This régime is shown in Fig. 6.56(c) where we see that the trim angle is reduced but the clearance height remains unchanged so that the vehicle rises relative to the still-water level. Finally, at high speed, the flow pattern shown in Fig. 6.56(d) resembles that for flight over land.

6.4.6 *Flexible Skirts*

To realize the full potential of hovercraft successful operation over rough surfaces is necessary. An amphibious craft must therefore have a structural clearance related to the height and distribution of obstacles which it would expect to encounter. In open country, over marshes, tundra and deserts it is estimated that 90 per cent of the obstacles met are likely to be less than 0.9 m high. The wave heights in areas such as the English Channel and the North Sea are less than about 1.2 m for 90 per cent of the time. For an acceptably reliable amphibious operation, for example for ferry services and coastal surveillance, we would therefore require a structural clearance of some 1.2 m. However, with a rigid base structure such a clearance would be achieved only with a concomitant increase in nozzle power. The nozzle power, P_n, required for hovering at rest can be obtained from

$$P_n = l_n \int_{r_o}^{r_c} p_t v \, dr = l_n p_t \int_{r_o}^{r_c} v \, dr$$

since the total pressure in the jet is assumed constant. Using Equation (6.69) and inserting the limits of integration yields

$$P_n = l_n p_t v_n r_o \ln \left[1 + \frac{a}{r_o} \right].$$

For the sake of simplicity let us suppose that a/h and therefore a/r_o and x are small. Then

$$P_n = l_n p_t v_n r_o \left(\frac{a}{r_o} \right) = a l_n \left(\frac{2}{\rho_a} \right)^{1/2} (p_t)^{3/2} = a l_n \left(\frac{2}{\rho_a} \right)^{1/2} \left(\frac{p_c}{2x} \right)^{3/2}$$

that is,

$$P_n = \frac{l_n}{2(a\rho_a)^{1/2}} \left(\frac{Wh}{S(1 + \cos\theta)} \right)^{3/2} \tag{6.79}$$

where gauge pressures have been used and the approximation $p_c = W/S$ adopted. For a given craft P_n increases quite rapidly with h and may only be countered by decreasing W/S. However, for a given W an increase in S increases the size of the vehicle and therefore the drag and propulsive power.

This dilemma has been solved – at least in principle – by the development of flexible skirts (sometimes called trunks). At first, these devices took the form of simple extensions of the peripheral nozzle as indicated in Fig. 6.57. The daylight clearance h could be kept at, say, 0.1–0.15 m, yet the structural clearance was sufficient to avoid contact between the base of the ACV and most of the obstacles met in practice. The advent of the skirted design led to the recall of plenum chamber craft since the air from the lift fans could be supplied directly to the cushion and small daylight clearance ensured relatively low nozzle powers. It was found that if the air were pumped through outward-facing apertures adjacent to a skirt attached to the outer periphery of the craft, the skirt could be inflated easily and the bottom edge (hem) of the skirt was pressed down towards the land or water surface. However, a large and continuous skirt was difficult to fit or remove if damaged and it wore quickly in abrasive contact with the ground. Even more unsatisfactory was the uncomfortable pitching response over waves and rough ground. Intensive development since has led to numerous types of skirt, for example, inflated hem, convoluted trunks, bags, segmented skirt and finger-segmented skirt.

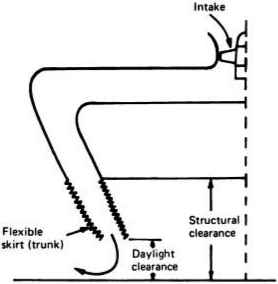

Fig. 6.57 Simple trunk system.

The following air-cushion system may be taken as typical of many. A variable-speed fan draws down air into the craft through inlet cowls situated on the roof. Delivery to the cushion takes place through a duct system containing holes round the periphery which allow the air to pass into and thence inflate a flexible bag surrounding the craft and fixed to the outer edge of the base. Further holes at the bottom of the bag allow the air to pass into a series of fingers which direct the air inwards to the cushion in the manner of the basic annular jet craft. The scheme is illustrated in Fig. 6.58(a). The hovercraft cushion is thus surrounded by a flexible wall; the fingers deflect in sympathy with small obstructions and the bag deforms on contact with larger obstructions to provide the large structural clearance necessary for viable commercial and naval operations. The relative merits of the various skirt

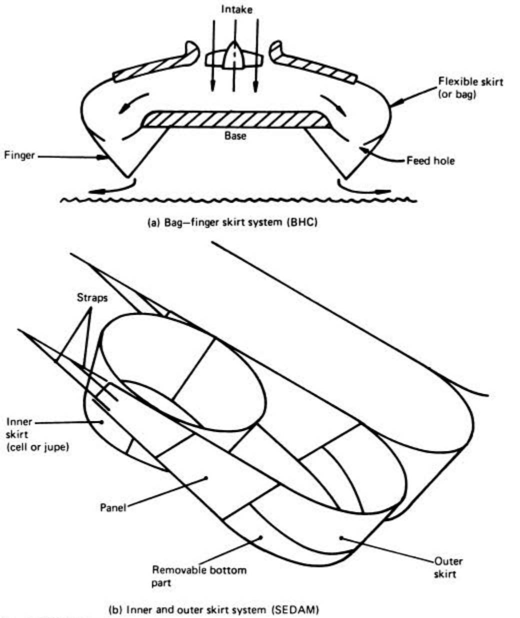

Fig. 6.58 Skirt systems.

systems are summarized in [37, 48, 58]. A fundamentally different scheme is used on the Sedam N500 and is described in [75, 76]. The cushion is formed by a number of separate vertical cells or 'jupes' which have air supplied separately, or in groups, from the lift fans. The 'jupe' is made in the shape of a truncated cone, with the smaller cross section lowermost, so that no chains, belts, etc., are required as the system is laterally stable. The attachment to the hard structure is straightforward in principle and maintenance should be minimal. However, air leakage was found to be excessive with the initial system and so to decrease lift power an outer, peripheral skirt was installed as shown in Fig. 6.58(b). Despite expectations to the contrary test flights showed that tears, wear, fatigue and fixing problems were prevalent.

To give some idea of the reliability of hovercraft in operation we may take as an example the British Hovercraft Corporation SRN-4. This is a plenum chamber craft with a 2.1 m bag-and-finger skirt, an overall weight of 1.5 MN and an operational maximum all-up weight of 2.0 MN. For service across the English Channel in 1969 this ACV was prevented from crossing for only 5 per cent of the total planned trips [59]. The effect of skirts on the steady speed of an ACV over rough water is indicated in Fig. 6.59.

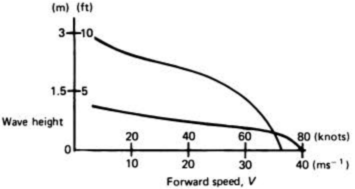

Fig. 6.59 Effect of waves on forward speed of amphibious hovercraft.

Not the least of the many practical problems associated with skirts is the choice of materials. The best to date have been nylon and woven Terylene used to reinforce coatings of pure or synthetic rubber or polyvinylchloride. Reasonable resistance to tearing, abrasion, corrosion and peeling has been obtained. The skirt construction must be robust and flexible to prevent capsizing ('plough-in') during manoeuvres although the advent of the bag-type skirt has considerably reduced this risk.

6.4.7 *Forces on Amphibious ACV*

The total lift (supporting) force exerted on an ACV in steady forward flight with the base horizontal may be expressed as

Total lift = cushion lift + jet lift + pressure lift + aerodynamic lift

and so, for equilibrium,

$$W = (F_c + F_j + F_p)\cos\alpha + L_{aero} = F_v + L_{aero}. \tag{6.80}$$

The aerodynamic lift force results from the distribution of pressure over the superstructure of the ACV. If the vehicle travels over water it does so at a small positive trim angle, as shown schematically in Fig. 6.60. At high cruise speeds the depressed water surface can be assumed parallel tc the base of the craft and so the jet flow and cushion pressure are both uniform.

The aerodynamic lift force is usually small and can be neglected for an analysis consistent with first-order accuracy. Thus, for equilibrium

$$W = (F_c + F_j + F_p)\cos\alpha$$

that is,

$$W \cong F_c + F_j + F_p = F_v \tag{6.81}$$

since α is assumed to be small.

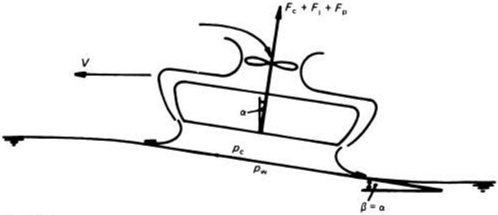

Fig. 6.60

For flight over land the total drag is wholly aerodynamic and is given by

Total drag = profile drag + momentum drag + induced (attitude) drag

that is, for equilibrium,

$$D_T = D_{pr} + D_m + D_i = T \tag{6.82}$$

where T is the thrust from the propulsors.

The profile (pressure) drag consists of skin-friction drag and viscous pressure drag on the vehicle superstructure. As the superstructure cannot generally be regarded as a streamlined body the profile drag can be written in the form

$$D_{pr} = \tfrac{1}{2}\rho_a V^2 S_f C_{D_{pr}} \tag{6.83}$$

where S_f is the frontal area normal to the direction of V and $C_{D_{pr}}$ is the profile drag coefficient assumed independent of V. Typical values of $C_{D_{pr}}$ are: 0.25 for SRN-2; 0.38 for SRN-6; 0.4 for SRN-4. Values can be as high as 0.70, although profile drag coefficients as low as 0.3 or less are now being sought for present-day designs. At cruise speeds the profile drag can be the largest component of the total drag.

The momentum drag is computed on the assumption that relative to the vehicle the horizontal momentum of the air which enters the intake of the lift fan(s) is destroyed. The momentum drag is thus given by

$$D_m = \dot{m}_f V \tag{6.84}$$

where $\dot{m}_f$ is the total mass flow rate of air entering the fan(s) and, in the absence of leakage in the internal ductwork, is equal to the mass flow rate of air in the jet.

If α is the trim angle then the attitude (induced) drag can be written in the form,

$$D_i = (F_c + F_j + F_p)\sin\alpha \cong W\tan\alpha \cong W\alpha \tag{6.85}$$

when α and L_{aero} are small.

In addition to these components of drag account must be taken of drag forces arising from direct contact between parts of the ACV and the ground. Contact with the ground can generate large forces intermittently over rough ground as well as causing damage to the skirting.

It is interesting to note that although the amphibious qualities of hovercraft are often emphasized little use of this attribute is made by commercial craft except when beaching or docking. Most craft in operation spend a major part of their service life over water. However, there have been a number of notable exceptions which include ice-breaking rôles, navigation over river ice and water, and military manoeuvres over desert areas. We must consider, therefore, additional components of drag for marine ACV.

Wave-making drag is transmitted to the vehicle through the air cushion whether or not direct contact is made between the craft and the water. This source of drag can be interpreted as the component of pressure forces on the water depression in the direction parallel but opposite to V. The wave-making drag is thus given by,

$$D_W = \int_{S_d} p_w \sin\beta \, dS_d = \int_{S_d} p_c \sin\beta \, dS_d = p_c \int_{S_d} \sin\beta \, dS_d$$

where S_d and β are the surface area and inclination of the depression respectively, and for equilibrium the water pressure at the interface $p_w = p_c$. The effect of the jet on the deformation of the interface has been neglected. Let us assume that the weight of the craft is supported primarily by cushion pressure forces, then

$$W = \int_{S_d} p_c \cos\beta \, dS_d.$$

If β is constant and the depression is parallel to the base of the craft (see Fig. 6.60) we must have

$$\frac{D_W}{W} = \tan\beta \cong \beta = \alpha \tag{6.86}$$

for small trim angles.

When the craft is hovering at rest it may be shown that the volume of air in the depression measured relative to the still-water level is equal to the volume of water displaced by the vehicle if it were to float at the interface. It is thus reasonable to expect such a criterion to hold at low forward speeds when D_W/W is large. The distortion of the interface reduces as V increases and so, in common with other high-speed vehicles, the wave-making drag of ACV is low at cruising speeds.

Lamb [60] examined the behaviour of a two-dimensional disturbance of constant pressure, say p_c, and length l moving steadily over an initially plane liquid surface. He found that the ratio of the wave-making drag per unit width D'_W, to the applied force per unit width $W' = lp_c$, is given by

$$\frac{D'_W}{W'} = \frac{2p_c}{\rho_w g l}\left[1 - \cos\left\{(Fr)^{-2}\right\}\right] \tag{6.87}$$

where we have considered the liquid to be water of density ρ_w and the Froude number $Fr = V/\sqrt{(gl)}$. The maximum value of $D'_W \rho_w g l / 2p_c W'$ occurs when $\cos\{(Fr)^{-2}\} = -1$, that is, when $(Fr)^{-2} = (2n+1)\pi$ where $n = 0, 1, 2. . .$ Under these conditions the maximum value of wave-making drag is

$$(D'_W)_{max} = \frac{4W'p_c}{\rho_w g l} \tag{6.88}$$

and for $n = 0$ this will correspond to a 'primary hump' at $Fr = 0.56$. A theory has been developed by Barratt [61] to cover three-dimensional ACV over deep water of infinite extent. He found the primary hump to be located at a Froude number between 0.5 and 1.0 depending on the planform. This theoretical analysis has been generally supported by experimental work with models running in a towing tank [62, 63] covering various planforms and angles of yaw. In shallow water the primary hump occurs at a lower Froude number and $(D'_W)_{max}$ increases as the depth of the water decreases.

It is exceedingly difficult to quantify the effects of: (i) spray impact on the hull; (ii) parts of the craft submerged in the water which induce additional components of wave-making and pressure drag; and (iii) an equivalent drag arising from an increase of weight as water is taken on board and retained by various parts of the vehicle. No adequate theory is at present available for the prediction of these items and to obtain a value of the wetting drag D_{wet} the components which can be assessed with reasonable accuracy are thus subtracted from the total drag measured in model and full-scale tests. Hence

$$D_{wet} = D_{T_c} - D_{pr} - D_m - D_i - D_W \tag{6.89}$$

in which D_{T_c} corresponds to the total drag over calm water and D_W is usually assessed on the basis of Equation (6.87) or on Barratt's extensions of the classical theory of wave generation.

An indication of the relative orders of magnitude of the various drag components of a typical, large, amphibious hovercraft (SRN-4) with a peripheral skirt (bag-and-finger system) is given in Fig. 6.61. The wetting drag for calm-water operation accounts for a large proportion of the total throughout the speed range. Also shown is the curve of available thrust and the ideal steady operating speed is that corresponding to the intersection of the thrust and total drag curves. The wetting drag is then about one-third of the total. When operating over waves another drag component arises which includes additional D_{wet} terms together with impact drag in severe conditions. The over-wave drag D_{ow}, is obtained by difference, that is,

$$D_{ow} = (\text{total drag in rough water}) - (\text{total drag in calm water})$$

that is,

$$D_{ow} = D_{T_r} - D_{T_c}. \tag{6.90}$$

6.4.8 *Forces on Non-amphibious ACV*

These craft are usually associated with solid side walls which penetrate the water surface and in the USA are generally referred to as surface effect ships (SES). As a result of the efficient sealing of the cushion by the partially immersed side walls (which are usually parallel to the fore-and-aft vertical plane of symmetry of the craft) the nozzle power is considerably less than for an amphibious craft of the equivalent size. On the other hand, the immersed side walls suffer large drag (mainly from skin friction) at high speeds. Note that the wetted area on the inner surface of the side walls is less than on the outer surface owing to water depression by the over pressure in the cushion.

The power requirements for hypothetical side-wall and amphibious, annular jet

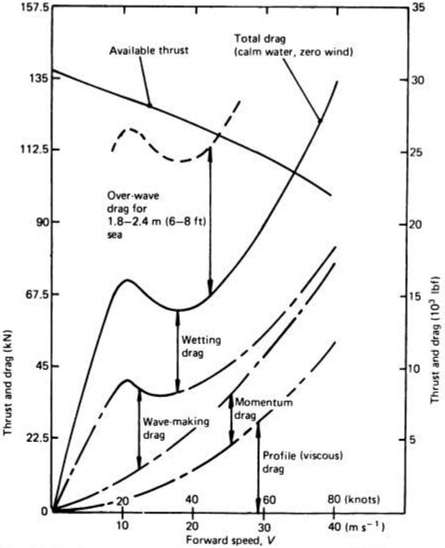

Fig. 6.61 Performance characteristics of amphibious hovercraft (SRN-4).

vehicles of all-up weight 1.2 MN are illustrated in Fig. 6.62. In this case it has been assumed that the water is calm and that each vehicle moves forward parallel to its fore-and-aft axis of symmetry.

For a side-wall craft the walls are able to support water propellers and the transmission leading to them. The air-borne noise associated with air propellers is thus eliminated and, furthermore, buoyancy forces on the side walls support about 10 per cent of the weight of the craft. Such a craft has good manoeuvrability because large side forces can be applied to the walls. Unfortunately, large profile drag then occurs and a considerable drop in forward speed results at constant propeller thrust.

To overcome these disadvantages some recent design exercises have turned to conventional peripheral-skirted craft with a marine propulsion system having a faired shafting and rudders in the water, such as the Vosper–Thorneycroft VT-1. Over the operating speed range drag is relatively low, directional stability and control are

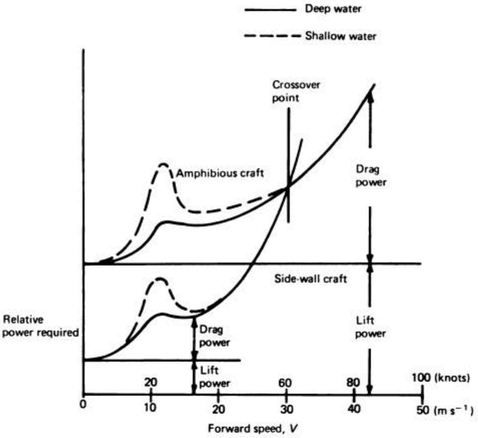

Fig. 6.62 Relative power required by amphibious and side-wall hovercraft of same all-up weight.

superior to amphibious craft, the operation is quieter and with a flexible, bagged skirt the craft can beach on a ramp with the propellers and rudders still submerged.

The principal characteristics of a number of hovercraft are given in Table 6.3.

6.5 Comparative Performances of High-speed Marine Vehicles

Any discussion of the overall performances of high-speed marine vehicles will inevitably involve sea-keeping capability, that is, the response of the vehicle to motion through waves. The state of the sea is referred to by wind speed, sea state or significant wave height, and these data form an essential part of routing selection for commercial operations such as ferry services. Matters are rather more difficult in the case of naval duties because craft may be required to operate in areas for which detailed information on wave spectra is lacking. However, the motion of any marine vehicle in waves will be unsteady and so a thorough analysis of the problem is really out of place here. Consequently, we shall cover the field only briefly in a general, comparative way and offer references for more specialized reading.

A popular method of illustrating the capability of high-speed craft in waves is to plot speed against, for example, significant wave height for a range of craft types and sizes. This has been done in Fig. 6.63 which shows typical, although not necessarily precise, values appropriate to displacement ships, planing craft, hydrofoil

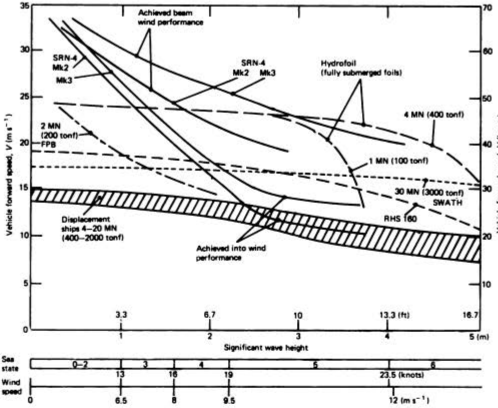

Fig. 6.63 Sea-worthiness of high-speed craft.

craft and hovercraft. Further details of some of the craft may be found in Tables 6.2 and 6.3. Also shown on the abscissa of Fig. 6.63 are equivalent scales for sea state and wind speed. It should be noted here that hovercraft, in particular, are seriously affected by the relative wind direction. Seaworthiness expressed generally in the form of Fig. 6.63 is a fundamental attribute of any marine vehicle whether it be used for commercial or naval applications.

It is immediately apparent that the sea state affects all craft in different ways and thus limits the maximum achievable continuous speed. Although some effects of size are shown, within the context of high-speed craft and therefore small craft, the effects of size are not great enough to cause radical changes in overall trends for curves of a given type or between curves of different types. Up to sea state 3 or 4 and depending on wind direction it is seen that the amphibious hovercraft is presently the fastest practicable form of marine surface vehicle, though the performance deteriorates rapidly with increases in wave height. The hydrofoil craft with fully submerged foils has a lower speed initially but is able to maintain this forward speed up to sea state 5 with larger designs able to achieve sea state 6. Nevertheless, increased size and improved (deeper) skirt design should allow better future performances from large hovercraft. A hydrofoil craft with flap control, initiated by either radar or sonic height sensors at the bow, can transfer the mode of flight from platforming at low wave heights to ccntouring at greater wave heights in order to reduce hull contact with waves yet retain relatively low vertical motion accelerations. A hydrofoil craft with surface-piercing foils is naturally more sensitive to surface waves

Table 6.3 Characteristics of some air-cushion vehicles.

Country	Craft	Configuration	Use	Design all-up weight MN (tonf)	Length overall m (ft)	Beam overall m (ft)	Skirt height m (ft)	Maximum speed (calm water) m s^{-1} (knots)
Canada	Bell 7380 *Voyageur*	amphibious	coastguard/ (ice-breaking)/ army/ commercial	0.4 (41)	20 (65.7)	11.2 (36.7)	1.22 (4)	25 (50)
	Bell 7501 *Viking*	amphibious	coastguard/ army	0.17 (17)	13.6 (44.5)	7.9 (26)	1.22 (4)	26 (52)
France	Sedam Naviplane N300	amphibious	commercial/ naval	0.26 (27)	24 (78.75)	10.5 (34.5)	6.5 (2)	28.5–31 (57–62)
	Sedam Naviplane N500	amphibious	commercial	2.6 (260)	50 (164.1)	23 (75.1)	4 (13.1)	37.5 (75)
Japan	Mitsui MV–PP15	amphibious	commercial	0.5 (50)	26.4 (86.7)	13.9 (45.6)	1.6 (5.25)	32.5 (65)
United Kingdom	BHC SRN–4 (Mk 2)	amphibious	commercial	2.0 (200)	39.7 (130.1)	23.8 (78)	2.44 (8)	35 (70)
	BHC SRN–4 (Mk 3)	amphibious	commercial	2.8 (280)	56.7 (186)	26.52 (87)	3.05 (10)	35 (70)
	BHC SRN–6 *Winchester*	amphibious	commercial/ naval (many variants)	0.1 (10)	17.8 (58)	7.7 (25.3)	1.22 (4)	26 (52)

	BHC BH7 *Wellington*	amphibious	naval (many variants)	0.5 (50)	23.9 (78.3)	13.8 (45.5)	1.67 (5.5)	30 (60)
	Hovermarine HM 2 Mk 3	side wall (front and rear skirts)	commercial	0.19 (19)	15.5 (51)	6.1 (20)	0.91 (3)	17.5 (35)
	Hovermarine HM 2 Mk 4	side wall (front and rear skirts)	commercial	0.2 (20)	18.29 (60)	6.1 (20)	0.63 (2)	17 (34)
	Hovermarine HM 5	side wall (front and rear skirts)	commercial/ naval	0.76 (77)	27.2 (89.25)	10.2 (33.5)	1.15 (3.75)	20 (40)
	Vosper–Thorneycroft VT–1	skirted with water propellers	commercial	0.87 (87)	95.5 (29)	43.5 (13.3)	5.5 (1.67)	19 (38)
	Vosper–Thorneycroft VT–2	amphibious	naval	1.04 (105)	30.17 (99)	13.3 (43.5)	1.7 (5.5)	30+ (60+)
USA	Aerojet/Rohr SES 100 A	side wall (front and rear skirts, water jet propulsion)	naval	0.9 (90)	24.9 (82)	12.7 (42)	–	40 (80)
	Aerojet AALC JEFF(A)	amphibious	naval	1.6 (160)	29.3 (96.1)	14.6 (48)	1.52 (5)	25 (50)
	Bell SES 100 B	Side wall (front and rear skirts, water propellers)	naval	1.04 (105)	23.7 (77.7)	10.7 (35)	–	40+ (80+)†
	Bell AALC JEFF(B)	amphibious	naval	1.6 (160)	26.43 (86.75)	14.32 (47)	1.52 (5)	25 (50)

† Achieved a record speed of 45 m s^{-1} (≃ 90.3 knots) in 1977.

especially when operating in a following sea. Planing craft show good performance in calm water but produce very high accelerations from impact loading in waves so that drastic speed reductions take place over the whole range of operable sea states. Nevertheless, with deep-V bottoms, such as those used in offshore power boats, planing craft can be driven faster up to about sea state 5, provided that sufficient power is available to compensate for the increased resistance of the deep-V forms and that the crew can endure the violent motion which ensues. In the range of sea state 6 the conventional hull displacement ship is capable of greater speeds than any other form of small, high-speed surface vehicle. However, this may change in the future as, for example, large hydrofoil craft are built; there is already an indication that the RHS 160 (see Table 6.2) is superior in rough water. Also shown in Fig. 6.63 are predictions of a 4 MN ($\cong$ 400 tonf) hydrofoil craft with fully submerged foils and a large 30 MN ($\cong$ 3000 tonf) Small-Water-plane-Area, Twin-Hull (SWATH) ship which can maintain a near-constant speed well into waves up to a significant height of 5 m ($\cong$ 16.4 ft).

A major penalty for high speed is cost. Generally speaking, it is still reasonable to assume that

$$\text{propulsive power} \propto \text{displacement} \times (\text{speed})^n$$

where $n = 3$ or more. It is interesting to note that the total resistance of a large, slow ship is about $0.001\Delta^*$, where Δ^* is the weight displacement. This contrasts with resistances of $0.06\Delta^*$ at 15 m s^{-1} ($\cong$ 30 knots) and $0.02\Delta^*$ at 10 m s^{-1} ($\cong$ 20 knots) for a 10 MN ($\cong$ 1000 tonf) corvette and with corresponding figures of $0.1\Delta^*$ and $0.07\Delta^*$ for a 1 MN ($\cong$ 100 tonf) fast patrol boat of a planing hull design. A value of $0.1\Delta^*$ is also quoted in [64] for a 1 MN ($\cong$ 100 tonf) hydrofoil craft travelling at about 25 m s^{-1} ($\cong$ 50 knots).

It has been found that operating limits on speed in a seaway are more likely to be set by the conditions which are acceptable to the crew and passengers rather than by the strength of the craft (although many questions on structural dynamics related to marine vehicles are still largely unanswered in detail [65]). In any given occupation and environment there are usually many stimuli (or stressors) influencing the physiological and mental processes of a crew member or passenger and it is often difficult to separate one effect from another. A general discussion of human factors (or ergonomics) related to ride motions is given by Cole [66]. Noise, vibration and low-frequency motions can all become intolerable to humans in time, but quite high intensities are often sustained for short periods such as ferry crossings and even enjoyed when connected to risk events or sporting activities. Much lower limits are tolerable for a naval patrol lasting days or weeks, especially when frequently repeated. Experience and knowledge of the full facts of an event also influence human response in one way or another. Tolerable noise and vibration levels (above a frequency of 1 Hz) are fairly well defined by the International Standards Organisation (ISO) but it is often difficult to satisfy the specified criteria within the confines of small high-speed craft. Low-frequency motions in the range 0.15–0.25 Hz are particularly important because vertical accelerations in this range lead to widespread sea sickness.

It is difficult to express concisely the relative merits of different craft responding to waves, but Fig. 6.64, adapted from [67], gives a general indication. The excellent characteristics of hydrofoil craft (now being achieved at lower cost) in this respect are clearly evident. An appraisal of the sea-keeping capabilities of high-speed craft

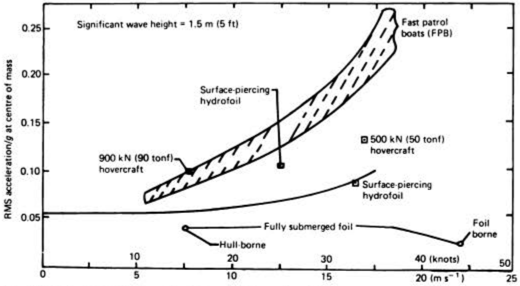

Fig. 6.64 Typical vertical accelerations of high-speed craft.

is given in [20] where the discussion is, in the main, applicable to both commercial and naval craft.

The rôle of commercial high-speed craft is almost exclusively as passenger ferries. The success of hovercraft in this respect has been summarized by, for example, Shaw [68], Mantle [69], Wheeler [70], Stansell and Hewish [71] and Thorpe [72]. The growth of traffic carried by hovercraft across the English Channel has risen spectacularly since operations commenced in 1968. There are now six SRN-4 craft running on the route, and with the five then operating in August 1977 some 24 per cent of cars and 25 per cent of passengers crossing the Channel did so by hovercraft. The corresponding figures for the whole of 1974, given in [70], are 23.9 per cent and 30.9 per cent. Operating reliability is crucial on such an established ferry route and massive efforts have now ensured that lost flights arising from unserviceability are down to 1 per cent and cancellations arising from bad weather are down to less than 3 per cent. The latter figure should be reduced even further with the recent introduction of the stretched SRN–4 Mk–3 hovercraft with improved skirt design (see Fig. 6.65).

A major attraction of hovercraft on sea-route ferries is the car-carrying facility which cannot so far be matched by hydrofoil craft. As pointed out in [67] the latter generally cater for large numbers of passengers without cars on routes less than 160 km (≅ 100 miles). At present, these passengers tend to be attracted by the novelty of the craft, by the sensation of speed and by the hope of a more scenic view than that offered by aircraft. The USSR has many hydrofoil craft carrying over 200 passengers on a variety of river routes which allow simple methods of craft control in the calm water. A successful sea route operating currently is the half-hourly service on the 36 mile journey between Hong Kong and Macao which began in 1963. A number of different craft have been used and now several Boeing Jetfoils are in operation. In such a congested route, particularly around harbours, the main technical problem is the adverse effects of rubbish in the water. Plastic bags floating in the water have been found to block water inlets (for the Jetfoils)

Fig. 6.65 British Hovercraft Corporation SRN 4 Mk 4 – Super 4.

and to wrap round hydrofoils and propellers to cause a serious reduction in lift force and thrust.

Before turning to military applications of high-speed craft it is interesting to examine the rôle of hovercraft being developed by the US and Canadian Coastguard for ice-breaking duties (summarized in, for example, [73, 74]). At first sight it may seem incredible that with such low cushion pressures typical of hovercraft ice up to 0.5 m (≅ 20 in) thick can be rapidly broken up. In fact the mode of operation is rather more subtle than the direct application of aerodynamic forces, for the ice breaks itself. Two principal techniques are used which take advantage of the amphibious quality of the craft. By continually traversing the clear water at the edge of an ice floe, and running up onto it, the hovercraft generates a series of waves which exploits the weak resistance of the ice to bending stresses. In 1978 the *Voyageur* craft (see Table 6.3) was able to break up 18 km^2 (≅ 7 square miles) of ice per hour and in so doing cleared a major ice jam in the St Lawrence and its tributaries every day for three weeks. This greatly reduced flooding of the surrounding countryside during the spring thaw. This high-speed ice-breaking technique can be used to break up fast ice near to banks and in shallow waters where severe limitations on ship draught occur.

The so-called, low-speed ice-breaking technique was developed after trials with a large air-cushion platform, the ACT 100, on the ice of the Great Slave Lake at Yellowknife early in 1972. It was found that as the platform, which carried equipment for oil drilling, moved forward at low speed ice up to 0.7 m (≅ 27 in) below it began to break up. Subsequent tests showed that the overpressure of the cushion air was sufficient to cause a seepage of air streams through fine cracks in the ice which subsequently congregated into a huge bubble of air below the ice. As a result the distributed upward buoyancy force of the ice was lost and the ice then cantilevered across the sides of the bubble. The weakness of ice in bending was insufficient to counter the combined weight and cushion-pressure loadings so that collapse of the ice cover occurred. Present methods of ice clearing now involve the attachment of a cushion platform forward of the bows of an ice-breaker ship so that the combined operation at about 4.5 m s^{-1} ($\cong$ 9 knots) allows thicker ice to be tackled in a shorter time and saves a great deal of fuel compared with the traditional ramming techniques of conventional craft.

A similar ice-breaking programme is underway in the USA, although emphasis is there being placed on the relationships of such techniques to personnel, facilities and support services. Conditions of rapid skirt wear were found in cases where ice was broken and re-frozen over several cycles to produce a very rough and abrasive surface. Consequently, investigations of exceedingly tough skirt materials are now being pursued.

The main tasks likely to be met in non-commercial applications of high-speed craft are surveillance, fishery patrol, protection of offshore resources, customs and immigration, mine counter-measures and assault landings. It is in a number of these tasks that the competition between the main types of high-speed craft is most intense, yet in other applications one high-speed craft remains dominant, e.g. the mine counter-measures vessel, as discussed in [77]. The amphibious hovercraft has a remarkably low underwater noise signature since its noise-generating source is above the air–water interface (see Section 2.4.5.(b)). Furthermore, despite the aircraft-type structure little damage is sustained from the underwater explosion of mines provided that the craft is clear of the explosion plume. Tests have shown that light damage is sustained from metal fragments which have perforated the skirt but operation is not significantly impaired.

Surveillance entails both surface and underwater detection and identification of vessels operating in waters over which control is to be exercized. Limits on equipment height curtail the use of radar to ranges of about 10 km ($\cong$ 6 miles) and therefore the use of aircraft is a necessary adjunct to the overall operation. Clearly a swift response from the well equipped marine craft is called for in order to deal with any violations. There are considerable problems with the detection of submerged submarines owing to the large size of anti-submarine sonars and their poor performance at high water speeds. Nevertheless, some view this type of rôle as promising, especially when the detection vessel operates in the sprint and drift mode where a 'dunking' sonar is used in the stationary or low-speed state and is then followed by a sprint to join, say, the task force. Since speeds of 24 m s^{-1} ($\cong$ 50 knots) may be called for the hydrofoil craft becomes a strong contender for anti-submarine operations. A variety of mission requirements have been examined in [78] and related to a series of hydrofoil craft with payloads up to 2.4 MN ($\cong$ 240 tonf) using a computer-aided program referred to as HANDE. It is interesting to note that the results show, for example, that the mass of the foils appears as a diminishing fraction of the total mass as the size of the craft increases. This is contrary to what might be expected since the lift force increases in proportion to the square of the characteristic length, while mass increases as the cube of the characteristic length. The reason is that strut length does not increase linearly with the size of the craft, nor does the thickness of practical steel plate.

The case for a hydrofoil fishery patrol vessel has been made in [43] based on the Jetfoil concept applied to North Sea conditions. However, probably the most important requirement is the ability to remain in an alert and fit condition when on station. Relatively small periods are spent at the optimum high-speed condition and so some effort must be taken to improve seakindliness at low speeds during long, and often tedious, patrols. Indeed, a survey of trawlers built in 1976 showed that only about 5 per cent were capable of speeds greater than 7.5 m s^{-1} ($\cong$ 15 knots). Thus with the improvements in design examined in [15] a hard-chine planing boat with a speed of 10 m s^{-1} ($\cong$ 20 knots) in sea state 5 may prove to be a desirable option.

In the absence of war, offshore protection may be needed to deal with accidental damage from fire, collisions, or bad weather and with possible terrorism. For the latter situation interception of a terrorist group, intent on, say, the occupation of an installation, is the primary aim with speed, weaponry and manpower to suit. The other tasks could probably be dealt with by craft similar to those used for fishery protection.

Illegal entry and smuggling are likely situations to be dealt with by customs and immigration craft which would probably operate in coastal waters. High speed is of paramount importance since it may be necessary to chase, overtake and subsequently apprehend other high-speed craft. All types of vessels capable of, say 20 m s^{-1} ($\cong$ 40 knots) may be summoned to duty with prevailing sea conditions dictating the final choice.

Work on amphibious assault landing craft (AALC) is being carried out in the USA on two designs designated JEFF(A) (see [79]) and JEFF(B) (see [80] and also Table 6.3). Both are to operate from the well decks of landing ships and also alongside cargo ships. Repeated journeys through surf up to about 2.5 m ($\cong$ 8 ft) high carrying a variety of payloads are called for. The two craft are quite different in a number of respects, such as propulsion and skirt design. The rôles of these craft provide a marked departure from the usual operations of hovercraft and Wheeler [81] offers some other interesting alternatives.

It is clear from the above that the rôles and designs for high-speed craft are extremely diverse and a final choice of one particular type revolves around the solution of a complex set of issues. Future developments are not likely to ease the difficulty of choice because it now seems that size and speed are both necessary for good seakeeping performance. Not surprisingly one finds design studies for surface effect ships of about 30 MN ($\cong$ 3000 tonf) and above [82] and a design for a hydrofoil craft of about 24 MN ($\cong$ 2400 tonf) [83]. There has also been increasing development and support for the Small-Water-plane-Area, Twin-Hull (SWATH) ships. The SWATH configuration consists of twin, submerged, submarine-like hulls providing the bases and hence the buoyancy forces for narrow vertical struts which support the upper deck. The latter is essentially a flat platform which may be used for a whole series of applications as a result of its inherently good lateral stability. Propulsion is obtained from water propellers at the stern of each submerged hull. A summary of some developments of these craft is given in [84] and it is suggested in [85] that SWATH ships have a high development potential for naval applications.

Whether or not any marine vehicle is developed from the design stage to the operational stage depends very largely on economic viability, especially in the case of commercial operations. There is also an increasing awareness of the penalties incurred by high capital, running, maintenance and refitting costs of naval vehicles, and most navies are now applying stringent cost rules. It is clearly a difficult task to predict the overall cost of a marine vehicle for an operational life of perhaps 20 years or more, but there is no doubt that nowadays escalating fuel costs are playing an increasingly important part in cost analyses. Technical excellence can no longer dominate thinking in a cost-conscious environment, as witnessed by the continuing controversy over the future of Concorde. Indeed, the question arises as to what comparisons should be made when different vehicles are under examination. Certainly assessment should be made of direct operating cost, fuel cost, capital cost, passenger and freight rates and so on, as well as passenger and crew comfort and safety criteria.

Costs have not been examined in a number of comparative studies, consideration being given only to performance parameters such as transport efficiency [89] defined as

$$\Omega = \frac{(\text{all-up weight}) \times (\text{maximum cruise speed})}{(\text{total installed power})} = \frac{WV}{P}.$$

This dimensionless parameter is not always expressed in consistent units and so care is needed in the interpretation of data. A wide range of transport vehicles was examined by Gabrielli and Von Karman [86] and they determined a log–log plot of Ω^{-1}, the 'specific resistance', against speed applicable to conditions in 1950. A 'limit' line could be drawn as an upper bound of performance expressed by

$$\Omega V = \frac{WV^2}{P} = 8800 \text{ ft s}^{-1} = 2680 \text{ m s}^{-1} = 5200 \text{ knots}$$

which was approached at low speeds by ships and at high speeds by aircraft. It is at intermediate speeds that a wide range of possibilities arises, especially for marine vehicles. The results have since been updated to include supertankers and subsonic turbojet aircraft. Furthermore, it has been suggested [87] that the limit represents a measure of economic efficiency given by the product ΩV and that this allows for the extent to which speed in its own right can be accounted for in freight carrying.

Crewe [88] recently undertook a detailed investigation of the economic and performance relations between a variety of marine vehicles, concentrating particularly on high-speed marine craft. It is not possible to combine all the factors relating costs, payloads, speeds and distances in a simple graph or equation and so a variety of parametric plots is given. For example, the relationship between normalized fuel cost Υ and payload to all-up weight ratio is shown in Fig. 6.66. Here,

$$\Upsilon = \left(\frac{\text{rsfc}}{\Omega}\right) \bigg/ \left(\frac{W_p}{W}\right),$$

where rsfc is the specific fuel consumption of any engine relative to a datum diesel engine (a value of 1.5 for gas turbines holds at present, but it is gradually being reduced with improvements in design) and W_p is the payload. For the sake of clarity mean hyperbolae are shown in Fig. 6.66, where it is evident that mono-hull displacement ferries stand out in terms of economy at low speeds and W_p/W values and that modern passenger jet aircraft are best at the other extreme. High-speed marine craft are collected in the middle but have favourable values of W_p/W, as a result of their light construction and installed propulsion units of high power-to-weight ratio. The

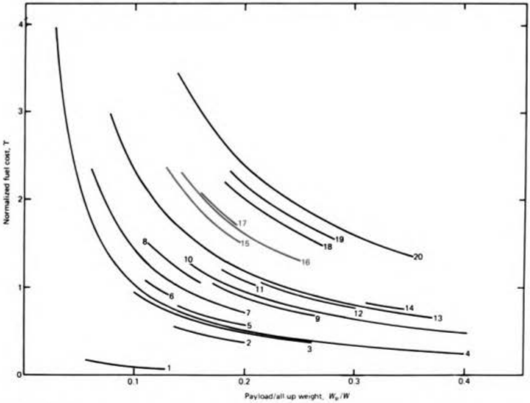

Fig. 6.66 Summary of mean data for normalized fuel cost as a function of payload/all-up weight. (Adapted from [88].) 1. Displacement ferry; 2. SWATH ship (15 MN ≅ 1500 tonf, 14 m s^{-1} ≅ 28 knots); 3. Modern passenger jet aircraft; 4. Airship (3.2 MN ≅ 320 tonf); 5. SWATH ship as 2 but 16.5 m s^{-1} ≅ 33 knots; 6. Westermaen catamaran; 7. Jet surveillance aircraft; 8. Surface-piercing hydrofoil craft; 9. Side-wall hovercraft; 10. Propeller surveillance aircraft; 11. Jetcat and Helicat catamarans; 12. Modern amphibious hovercraft; 13. Water-based aircraft; 14. AD 500 airship; 15. Diesel fast patrol boat; 16. Dynaplane; 17. Jetfoil; 18. Slender planing hulls; 19. Gas-turbine fast patrol boat; 20. Helicopters.

extreme, right-hand end of the amphibious hovercraft line applies to 'stretched' SRN–4 (Mk3–Super 4). A more general plot of the ratio of economic efficiency ΩV to rsfc against V, as shown in Fig. 6.67, reveals that any particular ΩV/rsfc occurs around either of two values of V which are generally widely separated. Note that the scales are 'self-reciprocating' for the sake of clarity and that the 'quadratic nature' of the relationship between the two parameters is emphasized for all craft.

It is concluded in [88] that the escalation of fuel costs allows a simplified comparison of economic efficiency between various types of high-speed marine craft and that these are fulfilling their tasks well. However, there is still considerable room for improvement in detailed design as research continues. The generalization of the original Gabrielli and Von Karman diagram to account for earnings per unit payload per unit distance related to speed allows a more valid comparison for passenger-carrying craft, especially for those classified as high-speed marine craft.

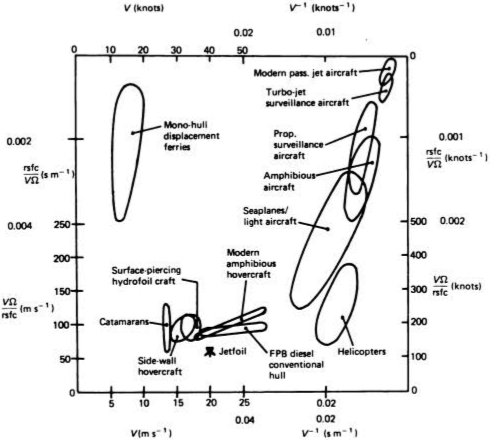

Fig. 6.67 Craft zones of ΩV/rsfc against speed. (Adapted from [88].)

Appendix: Design Equations for Planing Craft

The data of Korvin-Kroukovsky [9] can be assembled into the following empirical relationships. To speed up the preliminary design calculations a number of authors have presented these relations in graphical form.

For a flat plate, when $\bar{\beta} = 0$

$$C_{v_0} = \alpha^{1.1}\{0.0120\lambda^{1/2} + 0.0095\lambda^2(Fr)^{-2}\} \tag{A.1}$$

and for $\bar{\beta} \neq 0$

$$C_v = C_{v_0} - 0.0065\bar{\beta}(C_{v_0})^{0.6} \tag{A.2}$$

in which α and $\bar{\beta}$ are measured in degrees. The wetted length-to-beam ratio

$$\lambda = \frac{\bar{l}_w}{\bar{b}_w} = (AR)^{-1} \tag{A.3}$$

and the definitions of C_v and Fr are given by

$$C_v = \frac{W}{\frac{1}{2}\rho V^2 \bar{b}_w^2}; \qquad Fr = \frac{V}{\sqrt{(g\bar{b}_w)}}. \tag{A.4}$$

In addition,

$$\frac{l_H}{\bar{l}_w} = K\lambda^{-n}; \qquad \frac{l_H}{\bar{b}_w} = \left(\frac{l_H}{\bar{l}_w}\right)\left(\frac{\bar{l}_w}{\bar{b}_w}\right) = K\lambda^{(1-n)} \tag{A.5}$$

where $K = (0.84 + 0.015\bar{\beta})\alpha^{-m}$ (A.6)

$$m = 0.125 + 0.0042\bar{\beta} \tag{A.7}$$

$$n = 0.05 + 0.01\bar{\beta}, \tag{A.8}$$

again with α and $\bar{\beta}$ expressed in degree (protractor) measure.

A design method can now be proposed using the preceding equations and known data for the craft. Thus, using Equation (A.4) the coefficient C_v can be found from the required forward speed V, the specified all-up weight W and the necessary beam $\bar{b}_w$ to accommodate engines, stores, fuel, crew, payload and so on. The mean value of deadrise angle $\bar{\beta}$ is chosen to be consistent with the geometry of the craft and the ride and manoeuvrability sought by the designer. Equation (A.2) can then be manipulated to derive C_{v_0}. From a range of values of α the corresponding values of λ are deduced from Equation (A.1) and hence $\bar{l}_w$ follows from Equation (A.3). Equation (A.5) with the aid of Equations (A.6)–(A.8) yields values of l_H which correspond to the chosen range of α. Now, the position of the centre of gravity is determined from the craft layout so that l_G is known beforehand. We then seek, for steady motion, the condition $l_H = l_G$ from Equation (6.19) and thus identify the operating α and $\bar{l}_w$. The total resistance of the craft at the cruise speed, assuming $\phi = 0$, is given by Equation (6.17), that is

$$R_T = W\alpha + F_s = T. \tag{A.9}$$

The skin-friction force F_s is calculated from, say, the ITTC 1957 correlation line at the corresponding Reynolds number ($=\rho_w V\bar{l}_w/\mu_w$). A further iteration may be necessary to locate the operating condition corresponding to minimum resistance. Finally, the effective power required from the propulsor to drive the boat at speed V is given by the product $R_T V$.

References

1. *Proceedings of the Symposium on Small Fast Warships and Security Vessels* (1978), London, the Royal Institution of Naval Architects, London.
2. *Proceedings of the Conference on High-Speed Surface Craft* (1980), Brighton, England, Kalerghi Publications, London.
3. Du Cane, P. (1974), *High-Speed Small Craft*, 2nd Edn, David and Charles, Newton Abbot.
4. Shoemaker, J. M. (1934), Tank tests of flat and V-bottom planing surfaces. *Nat. Adv. Comm. Aeronaut., Washington, Tech. Note*, No. 509.
5. Clement, E. P. and Pope, J. D. (1961), Stepless and stepped planing hulls – graphs for performance prediction and design. *David Taylor Model Basin Rep.*, No. 1490.
6. Wellicombe, J. F. and Jahangeer, J. M. (1979), The prediction of pressure loads on planing hulls in calm water. *Trans. R. Inst. Nav. Archit.*, 121, 53–70.
7. Murray, A. B. (1950), The hydrodynamics of planing hulls. *Trans. Soc. Nav. Archit. Mar. Engrs*, 58, 658–92.
8. Cole, A. J. and Millward, A. (1978), The measurement of skin friction on a planing hull using a miniature Preston tube. *Trans. R. Inst. Nav. Archit.*, 120, 179–85.
9. Korvin-Kroukovsky, B. V., Savitsky, D. and Lehmen, W. F. (1949), Wetted area and centre of pressure of planing surfaces. *Stevens Inst. Tech., Davidson Lab. Exp. Towing Tank Rep.*, No. 360.

10. Savitsky, D. (1964), Hydrodynamic design of planing hulls. *Mar. Tech.*, 1, 71–95.
11. Du Cane, P. (1964), *High-Speed Small Craft*, 1st Edn, Temple Press, London.
12. Barnaby, K. C. (1967), *Basic Naval Architecture*, Hutchinson, London.
13. Clement, E. P. and Blount, D. L. (1963), Resistance tests of a systematic series of planing hull forms. *Trans. Soc. Nav. Archit. Mar. Engrs*, 71, 491–579.
14. Clement, E. P. (1979), Designing for optimum planing performance. *Int. Shipbuild. Prog.*, 26, 61–4.
15. Hadler, J. B., Hubble, E. N., Allen, R. G. and Blount, D. L. (1978), Planing hull feasibility model – its role in improving patrol craft design. pp. 115–31 of [1].
16. Yeh, H. Y. H. (1965), Series 64 resistance experiments on high speed displacement forms. *Mar. Tech.*, 2, 248–72.
17. Marwood, W. J. and Bailey, D. (1969), Design data for high speed displacement hulls of round bilge form. *NPL Rep.* No. 99.
18. Bailey, D. (1976), The NPL high speed round bilge displacement hull series. *R. Inst. Nav. Archit., Mar. Tech. Monogr.*, No. 4.
19. Bailey, D. (1974), Performance prediction – fast craft. *R. Inst. Nav. Archit., Occas. Publ.*, No. 1, Paper C.
20. Heather, R. G., Nicholson, K. and Stevens, M. J. (1978). Seakeeping and the small warship. pp. 31–46 of [1].
21. Newton, R. N. (1962), Contribution to the discussion on 'The combination of sail with an alternative source of power', by K. C. Barnaby, *Trans. R. Inst. Nav. Archit.*, 104, 90–2.
22. Mandel, P. (1969), *Water, Air and Interface Vehicles*, MIT Press, Boston, Mass.
23. Massey, B. S. (1979), *Mechanics of Fluids*, 4th Edn, Van-Nostrand Reinhold, London.
24. Milne-Thomson, L. M. (1968), *Theoretical Hydrodynamics*, 5th Edn, Macmillan, London.
25. Thwaites, B. (ed.), (1960), *Incompressible Aerodynamics*, Clarendon Press, Oxford.
26. Thomson, Sir W. (later Lord Kelvin), 1869, On vortex motion. *Trans. R. Soc. Edinb.*, 25, 217–60. (See also: *Mathematical and Physical Papers*, (1910), Vol. 4, Paper 2, 13–66, Cambridge University Press, Cambridge.)
27. Abbott, I. H. and Von Doenhoff, A. E. (1959), *Theory of Wing Sections*, Dover, New York.
28. Glauert, H. (1948), *The Elements of Aerofoil and Airscrew Theory*, Cambridge University Press, Cambridge.
29. Prandtl, L. and Tietjens, O. G. (1957), *Applied Hydro-Aeromechanics*, Dover, New York.
30. Eames, M. C. (1974), *Principles of Hydrofoils*, Chapter 3 of [3].
31. Tulin, M. P. (1956), Supercavitating flows past foils and struts. *NPL Symposium on Cavitation in Hydrodynamics*, HMSO, London.
32. Hook, C. and Kermode, A. C. (1967), *Hydrofoils*, Pitman, London.
33. Wadlin, K. L. (1958), Mechanics of ventilation inception. *2nd Symposium on Naval Hydrodynamics*, (ed. R Cooper), ONR/ACR-38, 425–45.
34. Von Schertel, H. (1974), The design and application of hydrofoils and their future prospects. *Trans. Inst. Mar. Engrs*, 86, 53–64.
35. Silverleaf, A. (1970), Developments in high-speed craft. *Proc. Inst. Mech. Engrs*, 184, 1221–44.
36. Acosta, A. J. (1973), Hydrofoils and hydrofoil craft. *Ann. Rev. Fluid Mech.*, 5, 161–84.
37. Gunston, W. (1969), *Hydrofoils and Hovercraft*, Aldus Books, London.
38. Swales, P. D. and Rothblum, R S. (1977), Ventilation and separation on surface piercing struts and foils, *Leeds University Press*, Leeds.
39. Eames, M. C. and Jones, E. A. (1971), *HMCS Bras d'Or* – an open-ocean hydrofoil ship. *Trans. R. Inst. Nav. Archit.*, 113, 111–38.
40. Davis, B. V. (1969), Problems and prospects of the superventilating foil. *CASI/AIAA Subsonic Aero/Hydro-dynamics Meeting*, AIAA Paper 69-754.
41. McGregor, R. C., Wright, A. J., Swales, P. D. and Crapper, G. D. (1973), An examination of the influence of waves on the ventilation of surface piercing struts. *J. Fluid Mech.*, 61, 85–96.
42. Ellsworth, W. M. (1967), The US Navy hydrofoil development program – a status report. *AIAA/SNAME Advanced Marine Vehicles Symposium*, AIAA Paper 67–351.
43. Coates, J. T. S. (1978), A hydrofoil fisheries patrol vessel for the United Kingdom. pp. 71–85 of [1].
44. McLeavy, R. (ed.), (1978), *Jane's Surface Skimmers – Hovercraft and Hydrofoils*, Macdonald and Jane's, London.

45. Crewe, P. R. (1958), The hydrofoil boat: its history and future prospects. *Trans. Inst. Nav. Archit.*, 100, 329–73.
46. Eames, M. C. and Drummond, T. G. (1973), *HMCS Bras d'Or* – sea trials and future prospects. *Trans. R. Inst. Nav. Archit.*, 115, 69–87.
47. Hook, C. (1969), The hydrofoil boat and the floating log hazard. *Transpo 69: 3rd Symposium of the Society of Environmental Engineers*, London.
48. Trillo, R. L. (1971), *Marine Hovercraft Technology*, Leonard Hill, London.
49. Crewe, P. R. and Eggington, W. J. (1960), The hovercraft – a new concept in maritime transport, *Trans. R. Inst. Nav. Archit.*, 102, 315–65.
50. Stanton Jones, R. (1968), Hovercraft. *J. R. Aeronaut. Soc.*, 72, 911–14.
51. Silverleaf, A. (1968), A review of hovercraft research in Britain. *J. R. Aeronaut. Soc.*, 72, 1019–28.
52. Summers, B. J., Winter, A. and Marks, J. (1974), *Hovercraft*, Chapter 4 of [3].
53. Harting, A. (1969), A literature survey of the aerodynamics of air cushion vehicles. *AGARD Rep.*, No. 565.
54. Elsley, G. H. and Devereux, A. J. (1968), *Hovercraft Design and Construction*, David and Charles, Newton Abbot.
55. Christopher, P. A. T. and Lim, K. H. (1980), Hovercraft research on the Cranfield whirling arm facility. pp. 28–36 of [2].
56. Clayton, B. R., Discussion of [55].
57. Poisson-Quinton, P. (1959), Two-dimensional studies of a ground effect platform. *Symposium on Ground Effect Phenomena*, Princeton University.
58. Stanton Jones, R. (1968), Hovercraft skirt development: an engineering and performance review. *Trans. R. Inst. Nav. Archit.*, 110, 499–524.
59. Stanton Jones, R. (1971), Operational experience with the SRN 4, *Aeronaut. J.*, 75, 375–8.
60. Lamb, Sir H. (1945), *Hydrodynamics*, Cambridge University Press, Cambridge.
61. Barratt, M. J. (1965), The wave drag of a hovercraft. *J. Fluid Mech.*, 22, 39–47.
62. Everest, J. T. and Hogben, N. (1967), Research on hovercraft in calm water. *Trans. R. Inst. Nav. Archit.*, 109, 311–26.
63. Everest, J. T. and Hogben, N. (1969), A theoretical and experimental study of the wavemaking of hovercraft of arbitrary planform and angle of yaw. *Trans. R. Inst. Nav. Archit.*, 111, 343–65.
64. Eckersley-Maslin, D. M. and Coates, J. F. (1978), Operational requirements and choice of craft. pp 1–13 of [1].
65. Bishop, R. E. D. and Price, W. G. (1980), Structural dynamics. *Nav. Archit.*, No. 6, November, 247–8.
66. Cole, S. H. (1980), The human factor aspects of ride motion. pp 218–29 of [2].
67. Brown, D. K. (1980), Hydrofoils, a review of their history, capability and potential. *Trans. Inst. Engrs Shipbuild. Scotland*, 123, 49–56.
68. Shaw, R. A. (1975), British Hovercraft Corporation. *Hovering Craft and Hydrofoil*, 14, 10, 13–21.
69. Mantle, P. J. (1975), Background to air cushion vehicles. *Hovering Craft and Hydrofoil*, 15, 2, 5–15.
70. Wheeler, R. L. (1975), An appraisal of present and future large commercial hovercraft. *Trans. R. Inst. Nav. Archit.*, 117, 221–44.
71. Stansell, J. and Hewish, M. (1978), Could the hovercraft's rough ride be over? *New Scientist*, 25 May, 498–501.
72. Thorpe, D. A. R. (1979), Stretching of the Mountbatten class SRN 4 hovercraft. *J. R. Elec. Mech. Engrs*, No. 29, April, 15–8.
73. Buck, J., Dennis, B., Anthony, J. and Neal, E. (1979), Air cushion vehicle icebreaker test and evaluation program. *US Coastguard Rep.*, CG-D-21 and 22. (Available from National Technical Information Services, Springfield, Virginia 22161, USA.)
74. Hindley, K. (1978), A breakthrough for Canadian icebreaking. *New Scientist*, 25 May, 502–3.
75. Herrouin, G. and Lafont, A. (1980), Skirt design and development on the Naviplane. pp. 315–25 of [2].
76. Guienne, P. (1978), The 260 tons French amphibious hovercraft Naviplane N500. *AIAA/SNAME Advanced Marine Vehicles Conference*, Paper No. 78–762.

77. Plumb, C. M. and Brown, D. K. (1980), Hovercraft in mine counter measures. pp 286–97 of [2].
78. Clark, D. J., O'Neill, W. C. and Wight, D. C. (1978), Balancing mission requirements and hydrofoil design characteristics. *AIAA/SNAME Advanced Marine Vehicles Conference*, Paper No. 78–725.
79. Davison, E. F. and Fink, M. D. (1980), The amphibious assault landing craft JEFF(A). pp. 298–314 of [2].
80. Coles, A. V. and Kidd, M. A. (1980), Demonstrated performance of the amphibious assault landing craft JEFF(B). pp 366–83 of [2].
81. Wheeler, R. L. (1978), The amphibious hovercraft as a warship. pp. 87–99 of [1].
82. McGhee, G. D. (1977), US Navy 3000-LT surface-effect ship (3KSES) Program. *Trans. Soc. Nav. Archit. Mar. Engrs*, 85, 396–418.
83. Pieroth, G. (1978), Grumman design M163, a 2400 metric ton air capable hydrofoil ship. *AIAA/SNAME Advanced Marine Vehicles Conference*, Paper No. 78–749.
84. Burnett, R. F. (1980), The advent of semi-submersible twin-hull ships. *Nav. Archit.*, No. 5, September, 193–5.
85. Eames, M. C. (1980), Advances in naval architecture for future surface warships. *Trans. R. Inst. Nav. Archit.*, 122, 93–118.
86. Gabrielli, G. and Von Karman, Th. (1950), What price speed? *Mech. Engng, J. Am. Soc. Mech. Engrs*, 72, 775–81.
87. Magnuson, A. H. and Sahin, I. (1979), Marine vehicle performance limits and economic potential. *AIAA Paper* No. 79–2007.
88. Crewe, P. (1980), Hovercraft in relation to other advanced marine vehicles, some particular advantages and problems. Lecture on *Advanced Marine Vehicles Course*, Southampton University, October 1980.
89. Mantle, P. J. (1975), A technical summary of air cushion craft development. *David W. Taylor Naval Ship Research and Development Centre Rep.* No. DTNSRDC 4727.

7 Propulsion

7.1 Introduction

In earlier chapters we have seen that to induce and maintain the motion of a vehicle in a viscous fluid, or at the interface between two viscous fluids, a resistance to motion must be overcome. By definition, viscous fluids will deform continuously when subjected to shear stresses and it is the resultant shear force necessary to produce this deformation which provides a contribution to the total resistance. Other contributions arise from (i) the incomplete pressure recovery at the aft end of a body owing to the thickening of the boundary layer there and the consequent formation of a wake, and (ii) wave making, if the vehicle operates at the interface. A vehicle at rest can therefore be set in motion by quite a small applied force, but should this force be removed then the vehicle will decelerate to rest according to Newton's Second Law of Motion. A continuous propulsive force is therefore required to sustain the motion and it is the means by which this force is developed that is now our concern.

A simple example of forces producing motion can be seen when a body rises or falls in a fluid owing to the inequality of weight and buoyancy. Movement then takes place along a radius extending from the centre of the Earth. However, our main interest here concerns 'horizontal' motion for which gravitation forces play no direct part. It is then necessary to attach to the outside of the vehicle some form of propulsor supplied with energy from a prime mover. We shall examine the propulsor which is that part of the propulsion system in contact with the fluid(s) comprising the external environment of our marine-vehicle system. To create a propulsive thrust the propulsor must exert a force on the environment† in such a way that the reaction force on the propulsor (to conform with Newton's Third Law of Motion) urges the vehicle forward. Although the majority of vehicles are self-propelled certain types, such as barges, oil rigs, dracones, floating docks, etc., are propelled by towing. The tow rope can therefore be regarded as the propulsor. For operation in restricted or shallow waterways propulsion of a floating vehicle can be derived from the reaction to a force applied directly to an immovable surface, for example, by the use of punt

† A rocket motor may be regarded as creating its own environment consisting of the products of combustion which issue from the nozzle. It is thus independent of the vehicle environment and so is an ideal device for space travel, but fuel consumption is enormous. For example, suppose we design a rocket motor to propel a frigate with a displacement of, say, 27 MN at $10\ \mathrm{m\ s^{-1}}$ (i.e. approximately 2700 tonf at 20 knots). The results published by Canham [1] suggest that the total resistance of such a ship would be about 3×10^5 N ($\simeq$ 30 tonf). A typical specific fuel consumption for a rocket is about $1\ \mathrm{kg\ N^{-1}\ h^{-1}}$ ($\simeq 10\ \mathrm{ton\ tonf^{-1}\ h^{-1}}$) and so the mass of fuel to be carried aboard the ship would amount to 3×10^5 kg ($\simeq$ 300 ton) per hour of cruising. Thus, to cruise even for 9 hours a .nass of fuel approximately equal to the mass of the ship would be required; such a situation is clearly unacceptable.

and barge poles, chain ferries and bottom-crawling vehicles. However, our interest will be focused on vehicles operating well away from solid boundaries.

The force exerted by a propulsor on the fluid environment will cause particles of that fluid to move. Thus, energy is expended not only in moving the vehicle but also wastefully in setting the fluid in motion which therefore leads to an augmentation of resistance as we saw in Chapter 5.

From the propulsion viewpoint, the chief difference between marine animals and marine vehicles lies in the non-rigidity of the body of animals. Motion can be induced by muscular actions which control the adjustment of appendages [2] such as hairs, fins, tails, legs and so on, in addition to changing the geometry of the main body. Nature infers that there is no unique method of propulsion and so it is perhaps not surprising that in technology numerous propulsors exist. These are summarized briefly to provide some understanding of the main problems to be solved in order to satisfy the basic requirements for the design of a marine propulsor.

7.2 A Review of Propulsors

To achieve steady motion of a marine vehicle over a range of speeds the following factors influencing the propulsion system need to be satisfied:

(i) Capability to produce a net forward thrust which is steady and continuous;
(ii) Capability to produce a net thrust which can be varied readily in magnitude;
(iii) Good matching between the performance of the prime mover and the propulsor;
(iv) Compatibility with the design and performance of the vehicle to which the propulsor is attached;
(v) Economic viability;
(vi) Ability to produce a stern thrust.

The question of steady motion was raised in Chapter 5 and it is an ideal which we cannot reach in practice – indeed, there is no reason why we should do so. Quite apart from the difficulty of ensuring a steady thrust from the propulsor, the vehicle itself may be subjected to unsteady forces in the environment. We cannot exercise complete control over wind, waves and currents, but we can, of course, reduce their effect by appropriate design and in some instances by planning carefully the routes over which operation is to take place.

Essentially we require that the thrust

$$T = \bar{T} + T'$$

where $\bar{T}$ is the time average value of the instantaneous thrust T and T' is the fluctuating component of T. For an acceptable propulsor we simply propose that $T' \ll \bar{T}$ and that T is produced continuously. We then regard the result as steady motion.

The resistance to motion experienced by a marine vehicle varies with forward velocity and so to proceed at any particular steady speed the control of thrust is essential. The resistance usually increases as the forward speed increases. However, as we saw, notably in Chapter 6, the resistance to motion of some high-speed vehicles does not increase uniformly but reaches a local maximum value at the hump speed. In fact, the hump resistance may, in some cases, exceed the cruise resistance even though the hump speed may be less than half the cruise speed.

The range over which the propulsive thrust may be required to vary depends on the type, the size and the desired performance of the vehicle. Although not necessarily independent, the methods of thrust control may be summarized as follows:

(i) Control of the output of the prime mover by, for example, varying the rate of fuel supply (which is proportional to the input energy) or by changing the geometry of the prime mover in terms of valve settings, blade angles and so on;
(ii) Control of the power transmitted to the propulsor by altering gear ratios and braking mechanisms;
(iii) Control of the output of the propulsor by adjusting its size, geometry, speed, etc.

To satisfy efficiently the thrust requirements over a range of specified service speeds the various components comprising the complete propulsion system must be well matched and each component must be compatible with the others. Bad matching may be said to occur if the propulsor operates most efficiently at low rotational speeds, whereas the prime mover is most effective when running at high rotational speeds. (We may note in passing that at this stage in the technical development of the prime movers for marine propulsion the output source of energy usually takes the form of a rotating shaft. The same, or a connecting, shaft then passes through a suitably sealed orifice in the hull to the propulsor.) Poor matching of the propulsor to the prime mover can result in low efficiency, mechanical complexity, overloading of one or both components, excessive vibration, and high rates of wear.

In addition to adequate matching of components of the propulsion system the complete system must be well matched to the vehicle. The complex interactions between the individual parts comprising the vehicle demand that we consider the vehicle system as a whole. For example, tugs with paddle wheels may be quite satisfactory, but owing to the large change in draught between the empty and the loaded conditions of a very large crude carrier (VLCC) a paddle wheel would offer a poor match. For steady motion the resistance at the service speed must always be matched with the propulsion system installed in the vehicle and this is often difficult to ensure on the basis of results obtained from the system before installation. There will clearly be an interaction between the flow about the bare hull of a ship and the flow about a propulsor in the proximity of the hull. The assessment of interaction effects is an extremely difficult problem to solve analytically and experimentally determined 'correction' factors are thus generally used.

Economic operation is essential but often many desirable features, such as good stability, control and load-carrying capacity, have conflicting specifications. For example, fuel economy is often linked with high capital and maintenance cost and exactly where the boundary of economic compromise is drawn frequently depends on considerations seemingly quite remote from engineering solutions.

A propulsion system must be capable of producing astern thrust in order to reduce stopping distance and to assist manoeuvrability in confined waters. In general, commercial and military vehicles are powered by either steam or gas turbines (the steam being produced by oil-fired boilers or by nuclear reactors) or high-speed diesel engines. The latter can provide reverse motion but the former, owing to a preferred direction of rotation, cannot. Astern thrust may then be developed by reversing the direction of rotation of the transmission shaft through a gear box. However, reversible mechanical gear boxes transmitting large torques are bulky and expensive. The difficulties may be overcome by the use of electrical transmission (the turbine being coupled to a generator which supplies a reversible electric motor driving the propulsor) or by the installation of a separate turbine specifically used for reverse thrust. Alternatively, the geometry of the propulsor itself may be changed without altering the direction of rotation (e.g. by adjusting the pitch of the blades while the propeller is rotating, as in the case of controllable pitch propellers).

Let us now consider some means of propulsion and assess how they meet the general requirements discussed above.

7.2.1 *Oars, Paddles and Paddle Wheels*

The oldest man-made propulsor is the paddle or oar and it may be conveniently considered as an extension of the arm and hand. These are good examples of compatible matching of the propulsor and the prime mover (a human) and this is the principal advantage of the systems. Motion of the blade of an oar or paddle relative to the water surrounding the boat will accelerate water particles in the vicinity of the blade. If the velocity of the blade relative to the water is greater than that of the boat and in the opposite direction then a forward thrust will be exerted on the blade by the water according to Newton's Second Law of Motion. For paddling this thrust is transmitted to the hull by the paddler, while in rowing the thrust is transmitted to the hull through the rowlock.

Thrust generation by rowing and paddling is not continuous and consequently the forward motion of the boat is unsteady. Furthermore, using humans as the power source limits the magnitude of thrust and so the method is used only for small boats. Steadier motion of the vehicle may be approached by developing thrust from multi-bladed paddle wheels. However, side-paddle wheels mounted on a horizontal axis suffer from many drawbacks, the most important being:

(i) the variable immersion under different loading conditions of the ship;
(ii) the high risk of damage in rough seas;
(iii) the alternate rise and fall of the wheels about the water level when the ship is rolling, which results in erratic course keeping;
(iv) the increase in overall width of the ship, which can cause difficulty when docking; and
(v) the wheels are essentially slow running and need to be matched to compatible prime movers. The reciprocating steam engine is suited to this purpose but the lighter, smaller, steam turbines and diesel engines are fast running and must therefore be equipped with large reduction gears. Most of these limitations also apply to stern-wheel ferry boats.

Many of the disadvantages of the horizontal-axis paddle wheel are overcome by making the axis of rotation vertical. The paddles and the disc to which they are attached can then be fully immersed in the water below a flat portion of the ship's hull. The first such wheel was invented by Fowler in 1870 [3]. As the wheel rotated linkages adjusted the angular setting of the blades in order to control the direction and magnitude of the thrust. These propulsors were therefore able to provide the added benefit of steering control and so eliminated the need for rudders. At the present time there exist two variants of the vertical-axis propeller, namely, the Kirsten–Boeing and the Voith–Schneider types [4]. In the former each blade performs half a revolution about its own axis per revolution of the wheel, whereas in the latter each blade performs one revolution per revolution of the wheel. Figures 7.1 and 7.2 show the relative orientation of the blades in each case for

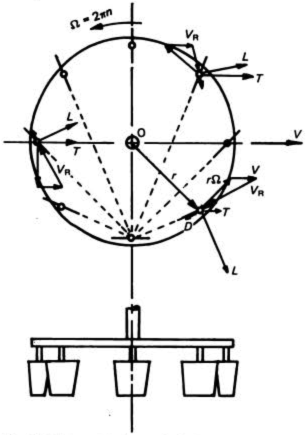

Fig. 7.1 Kirsten–Boeing vertical-axis propeller.

ahead thrust. The velocity of the water relative to the blade, V_R, is the vector sum of the velocity of the vehicle relative to the water V and the tangential velocity of the blade $r\Omega$. Each blade pivot is the same radial distance r from the axis of rotation of the propeller and Ω is the angular velocity of the propeller. Provided that the hydrodynamic force normal to the blade has a component in the direction of V then a thrust force is produced, as shown in Figs. 7.1 and 7.2. These propellers have been found particularly useful in applications calling for a high degree of maneouvrability (e.g. in ferries and tugboats) but a number of disadvantages remain, such as structural complexity, large weight and vulnerability to damage owing to the relatively sparse protection offered by the hull.

7.2.2 *Wind-generated Thrust*

Sails are most often used to develop a propulsive thrust from the energy of the wind. To propel a sailing boat in a following wind requires no more than a simple transverse sail. Alteration of the sail area then allows adjustment of the forward speed. The efficiency of the sail, whether mounted transversely or obliquely to the wind, may be improved by using flexible material for the sail so that it will billow, that is, a convex surface is presented to the air in the direction of motion. The maximum speed attainable by a given boat depends on the velocity of the wind (which may not necessarily be uniform across the sail area) and upon the strength of the material making up the sails, mast and rigging. In this condition the boat is

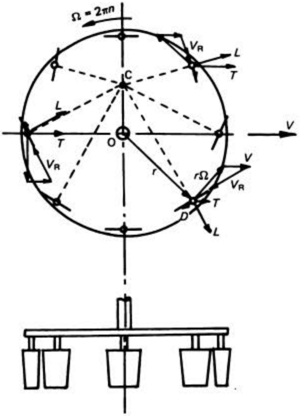

Fig. 7.2 Voith–Schneider vertical-axis propeller.

said to be 'running before the wind' and thrust is thus developed by placing a bluff body (i.e. one that has a large drag coefficient) across the path of the wind.

The mechanism of thrust generation by a sail is rather more complicated when the boat is 'beating into the wind', that is, when its heading is somewhat greater than about 45 degrees to the oncoming wind, as shown in Fig. 7.3. When the sail is properly sheeted the flexibility of the material enables the sail to 'fill out' and take up a cambered shape to become quite an efficient aerodynamic lifting surface. The

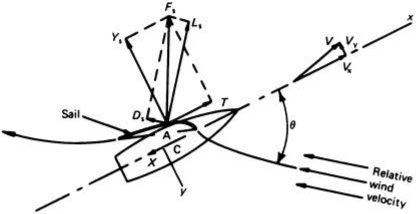

Fig. 7.3 Forces on a simple sail.

net forces on each side of the sail may be resolved into lift and drag components normal and parallel to the relative wind direction. It can be seen in Fig. 7.3 that the resultant of these local forces F_s can itself be resolved into lift and drag components L_s and D_s, or alternatively, into a propulsive thrust T in the Cx direction, where C is the centre of mass of the vessel, and a (larger) side force Y_s which induces a drift. The conventional hull of a sailing boat offers a large resistance to drift owing to the installation of a centre board, dagger board or fin keel and so drift can be kept small. On the other hand, the resistance to forward motion X (along $-Cx$) is small because the hull is streamlined for this mode of operation. The boat therefore moves forward with velocity V_x along Cx but with a smaller velocity of drift V_y along Cy so that the vector sum of these components is V directed off the beam. By beating first to one side of the relative wind direction and then to the other (i.e. to 'tack') it becomes possible to progress in a 'zig-zag' fashion against the wind. Further details on the aerodynamics of sails and yachts generally are given by Kay [5].

It is worth noting, however, that the use of wind forces for the propulsion of ships is not necessarily reserved for small craft. There have been several recent conferences, see for example [6–9], which have discussed the wind propulsion of ships having displacements up to 200 MN ($\cong$ 20000 tonf) or so. Some interesting propulsion devices have been investigated and, at least on the question of aerodynamic effectiveness, many can be considered to offer viable techniques either as total or supplementary power sources. These have been discussed and compared in [10, 11]. Considerable development on the design of sails and their automatic control has taken place in recent years and the adoption of aerofoil sections with faired masts, into which the flexible sails may be furled, appear to offer a significant challenge to conventionally powered ships. However, the careful selection of routing is crucial if competitiveness, in terms of size and speed, is to be made available. Arguments have been put forward to support the use of wind turbines on ships in [12]. Probably, the vertical-axis type of rotor will prove the best alternative as it is independent of wind direction. Use may be made of (i) power in the rotating shaft to drive a propeller, through as yet unspecified auxiliary machinery, or (ii) the aerodynamic force on the rotor in the direction of the relative wind, that is a kind of sail. In principle it is possible to sail into the wind but there are many problems, mainly structural [13], which have yet to be investigated, let alone overcome. Another, quite different, form of wind propulsion is to use the towing forces of, possibly, a series of high-flying kites as suggested in [14]. At high altitude, say above 1.5 km ($\cong$ 5000 ft), wind speeds rising up to 50 m s^{-1} ($\cong$ 100 knots) are common and so, for large kites, substantial towing forces may be obtained. Even at 300 m ($\cong$ 1000 ft) the wind velocity can be 2.5 times that at mast height. Another important characteristic of winds at high altitude is that the direction of motion is often quite different from that of the surface winds. This veering effect is the result of the Ekman Spiral in the aerodynamic boundary layer (which may be compared with the same phenomenon in the oceans referred to in Section 2.5.2). It is then possible to sail into the surface winds, but there are likely to be problems of stability and it will be also necessary to improve kite efficiency. Improvements in winch design and remote-control systems are the probable aims for the future progress of wind propulsion.

Another interesting device for wind propulsion is the Flettner Rotor [15] which takes the form of a vertical cylinder that rotates about its vertical axis of symmetry and is mounted above the deck of the ship. As a result of the Magnus Effect [16] a cross-wind force is generated on the cylinder perpendicular to the oncoming relative wind. Substantial cross-wind forces can be obtained by rotating several cylinders at high speed and so even in moderate winds the cylinders can be quite small (relative to sails, say). The demands on auxiliary power, which must be available, can be large and the rather high drag of the cylinder is also a disadvantage when sailing to windward. As with all ships driven by surface winds limitations arise from the unpredictability of wind speed, direction and duration. No control can be exercized over the wind and no propulsion can be achieved in a dead calm. This means that commercial scheduling of cargo and passengers and the potency of naval ships become unreliable. Even though this energy from the wind would cost nothing, and despite the escalating cost of conventional fuels, the only wind-powered vessels in common use are sporting, survival and training craft. However, we may see significant use of wind power once optimization criteria for routing, proportion of auxiliary power requirements and systems control have been established.

7.2.3 *Jet Propulsion*

Unlike the rocket motor the jet engine does not create its own environment but reacts with the environment surrounding it. Essentially, the device operates by transferring energy to the fluid entering the engine so as to increase the momentum flux of that fluid. The reaction to this increase of momentum flux provides the propulsive thrust exerted on the engine (and thus on the vehicle to which it is rigidly attached) giving rise to forward motion.

Air entering a gas-turbine jet engine passes through a compressor in which the air pressure is raised by a factor of about 5 or 6 before entry to the combustion chamber. Here, mixing with atomized fuel takes place with subsequent combustion and ejection of the air–fuel mixture at high temperature through a nozzle. Before reaching the nozzle, however, the exhaust gases pass through a turbine stage which drives the compressor once ignition has commenced. The main benefit of the gas-turbine engine accrues from its high power-to-weight ratio which is an essential requirement for high-speed aircraft. The application to marine vehicles is limited owing to the low propulsive efficiency and large specific fuel consumption for low-speed operation. However, there has been some call for these propulsion devices in high-speed craft, particularly for hovercraft on commercial and rescue operations and naval patrol boats.

In a hydraulic-jet propulsion system (the earliest mechanical system proposed for ships, patents having been granted to Toogood and Hayes [3] in 1661) the momentum flux of the oncoming water, relative to the vehicle, is increased by an externally driven pump housed in a duct. The duct consists of an inlet region and an exhaust nozzle as shown schematically in Fig. 7.4. The intake is usually positioned either close to the bows or in the form of a scoop near to the keel of the craft. Typical water-jet systems are illustrated in [17] and it is clear from these examples that the flow approaching the intake is non-uniform owing to the presence of the hull boundary layer, interference from appendages and three-dimensional flow near the bows. As a result, the performance of the installed propulsion system may be significantly inferior to that predicted on the basis of uniform flow at entry to the pump.

Let us now derive a simple theory of hydraulic-jet propulsion. Suppose that, relative to the vehicle, water of density ρ enters the intake uniformly with a steady rearward velocity V equal to the forward velocity of the vehicle, and is ejected

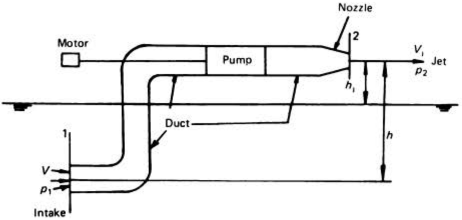

Fig. 7.4 Schematic of hydraulic-jet propulsion.

through a nozzle of area A_n with a steady, uniform rearward velocity V_j relative to the vehicle. The rearward force exerted by the vehicle on the water is equal to the rate of increase of momentum of the water and must also be equal and opposite to the forward thrust the water exerts on the vehicle. Thus the propulsive thrust T is given by

$$T = \rho V_j A_n (V_j - V). \tag{7.1}$$

The useful power obtained in propelling the vehicle is then TV (= $R_T V$, where R_T is the total resistance to motion of the vehicle).

We may now apply the steady-flow energy equation to a fluid particle entering the duct at plane 1 with a velocity V and pressure p_1 and leaving the duct at the nozzle exit plane 2 where the jet velocity is V_j and the pressure is p_2. From Fig. 7.4 it can be seen that

$$\frac{p_1}{\rho g} + \frac{V^2}{2g} + \Delta H = \frac{p_2}{\rho g} + \frac{V_j^2}{2g} + h + h_l \tag{7.2}$$

where the energy datum is taken to be the centre line of the intake. The term ΔH accounts for the increase of energy per unit weight of water supplied by the pump and h_l is the *total* loss of head (i.e. energy per unit weight) in the complete jet system. We here group together all the losses which occur at the intake and in the duct, pump and nozzle; the separate assessment of these components is exceedingly complicated. Assuming that the ambient pressure above the water line is constant and that the water into which the vehicle moves is stationary, then Equation (7.2) reduces to

$$\Delta H = \frac{1}{2g}(V_j^2 - V^2) + h_j + h_l. \tag{7.3}$$

The energy per unit time (i.e. power) transferred to the fluid by the pump is, therefore,

$$\rho g V_j A_n \Delta H = \rho V_j A_n \{\tfrac{1}{2}(V_j^2 - V^2) + g(h_j + h_l)\}$$

that is,

$$P_{\text{pump}} = \rho V_j A_n \{\tfrac{1}{2}(V_j^2 - V^2) + \tfrac{1}{2}kV^2 + gh_j\} \tag{7.4}$$

where we have made the substitution $h_l = kV^2/2g$ and since the flow in practice may be considered fully turbulent k is virtually independent of V.

The propulsive efficiency of the jet system can be written in the form

$$\eta = \frac{TV}{P_{\text{pump}}} = \frac{\rho V_j A_n (V_j - V)V}{\rho V_j A_n \{\frac{1}{2}(V_j^2 - V^2) + \frac{1}{2}kV^2 + gh_j\}}$$

which may be rearranged to yield

$$\eta = \frac{2V(V_j - V)}{V_j^2 - V^2 + kV^2 + 2gh_j}. \tag{7.5}$$

For the sake of simplicity, let us suppose $h_j = 0$ so that with $V_j/V = \lambda_j$ Equation (7.5) becomes

$$\eta = \frac{2(\lambda_j - 1)}{\lambda_j^2 - 1 + k}. \tag{7.6}$$

The ideal efficiency (for inviscid flow) occurs when $k = 0$; then Equation (7.6) shows that $\eta \to 1$ as $\lambda_j \to 1$. However, there is then no thrust exerted by the water on the vehicle. The variations of η with λ_j for given values of k are shown in Fig. 7.5. Evidently, for each value of k there is a maximum value of η and the effect of friction is seen to be most marked at small values of λ_j. The maximum efficiency is given by

$$\eta_{\max} = \frac{2\sqrt{k}}{2\sqrt{k} + k + k^2} \tag{7.7}$$

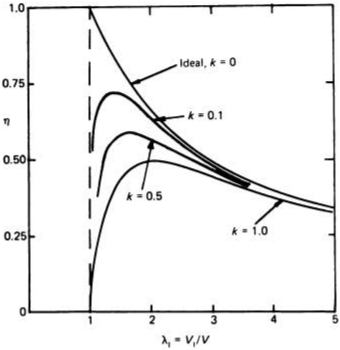

Fig. 7.5 Efficiency of hydraulic-jet propulsion accounting for losses.

and this occurs when

$$\lambda_j = 1 + \sqrt{k}. \tag{7.8}$$

For a given thrust large values of V_j imply a concomitant decrease in mass flow rate ($= \rho A_n V_j$) for a given forward speed of the craft. Consequently, inlets, ducts, pumps and nozzles then become smaller and lighter. Propulsion systems are therefore chosen so that $\lambda_j > 1 + \sqrt{k}$, and the resulting reduction in efficiency from the optimum given by Equation (7.7) must be accepted. Furthermore, sufficient thrust must be available from the system to overcome the hump resistance which can be especially large for high-speed craft (see Chapter 6). At the relatively low speed corresponding to the hump the large thrust necessary to accelerate the vehicle to the cruise speed requires ΔH to be large as shown in Equation (7.3). Since the pump is often located closer to the nozzle than the inlet, the pressure of the water at entry to the pump may be so low that cavitation may occur. This problem can be lessened by ensuring that the 'static lift' h_j is kept as small as possible. However, the simple drive from the prime mover indicated in Fig. 7.4 cannot then be adopted. The difficulty is particularly acute in the case of hydrofoil craft where the intake must be located on the main struts just above the foil. Provided that cavitation inception can be avoided at the hump speed the subsequent 'ram' pressure at higher speeds should ensure cavitation-free operation, but an additional 'resistance' component must be accepted. The methods of selecting the necessary pump to match the system energy losses and thrust requirements are out of context here but details are given in [18, 19]. Pump sizes can be reduced for a given thrust requirement by dividing the total discharge into a number of parallel units. For example, the hydrofoil test craft *Tucumcari* used several double-suction centrifugal pumps all mounted on a common shaft [20] and this principle was used to drive the Jetfoil with a pair of jets each produced by a pump absorbing some 2.475 MW (≅ 3320 hp).

For steady motion of the vehicle a thrust coefficient (equivalent to the total resistance coefficient discussed in Chapters 5 and 6) may be formed as follows:

$$C_T' = \frac{T}{\frac{1}{2}\rho V^2 S_w} = \frac{R}{\frac{1}{2}\rho V^2 S_w} = 2\frac{A_n}{S_w}\left(\frac{V_j}{V}\right)\left(\frac{V_j}{V} - 1\right) \tag{7.9}$$

where S_w is the wetted surface area of the underwater hull and appendages. Let us consider a conventional surface ship for which a value of C_T' of 0.005 is typical and suppose that $V_j = 2V$. For $k = 1$ we have $\eta_{max} = 0.5$ from Equation (7.7) and so $A_n/S_w = 0.001\,25$ from Equation (7.9). A ship of length 300 m (≅ 1000 ft), draught 20 m (≅ 67 ft) and beam 30 m (≅ 100 ft) would require a nozzle exit area A_n of about 25 m^2 (≅ 280 ft^2) and an intake area of about 50 m^2 (≅ 560 ft^2) for a simple, straight-through jet system with the intake at the bows and the nozzle at the stern. The volume occupied by the propulsion system could be as much as 15000 m^3 (≅ 5.56×10^5 ft^3) and this represents a considerable loss of space. Moreover, a 4 or 5 per cent increase in size would be needed to accommodate the propulsion system, which would result in a higher hull resistance from the increased surface area. Little benefit is gained by increasing V_j/V, and so the hydraulic-jet propulsion system does not really commend itself to large-scale, low-speed applications.

An interesting assessment of efficiency for a variety of craft is given in [3] and it is clear from these results that propulsion efficiencies greater than 60 per cent are unlikely. However, as alternative propulsion systems for small high-speed craft have efficiencies no better hydraulic jets become more competitive. If the craft runs in clean water the inlet grilles may be left off, so that large energy losses there can be avoided and a consequent saving in space made with the smaller duct/pump system. Furthermore, by using nozzles which are directionally adjustable in the horizontal plane a high degree of manoeuvrability is achieved without incorporating a rudder. The added safety of a fully shrouded propulsor is also a significant factor for sporting craft.

7.2.4 *Screw Propeller*

The introduction of steam turbines into ship propulsion would have been greatly hindered by the limitations of the paddle wheel owing to the necessary installation of large reduction gears. A new propulsor was therefore needed and this proved to be the screw propeller (Fig. 7.6). It was first used on a large ship by Brunel for the *Great Britain* in 1845 and has since remained the most common method of ship propulsion. R. E. Froude pioneered much of the early development of marine propellers which in turn laid the foundation for the design of airscrews.

The present-day screw propeller consists of 2–20 but generally 3–7 blades of hydrofoil section mounted symmetrically on a boss fixed to a shaft. The shaft passes through glands and seals in the hull of the vehicle before connecting to the prime mover. Relative motion between a blade and the water results from forward motion of the vehicle and from rotation of the propeller. As the surface of each blade lies on a helicoid generated about the shaft axis this combined motion may be likened to that of a screw.

The propeller usually takes the form of a 'pushing' device placed near the stern of the vehicle with the shaft passing through and supported by an extension of the hull called the stern tube. In this location the propeller is protected by the hull from damage and the flow downstream from the propeller does not interfere with that round the major part of the hull. Unfortunately, the flow approaching the blades is very disturbed at the stern, but as we shall see later the operation of a propulsor in a wake can be an advantage. Some 60–65 per cent of the power available at the shaft may be converted by the propeller for useful propulsive purposes. Thrust is continuous and reversible and is easily controlled by adjustment of the shaft speed and/or the angular setting of the blades. The optimum performance of a

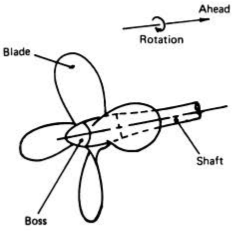

Fig. 7.6 Screw propeller.

screw propeller is compatible with both steam turbines and marine diesel engines, although (relatively small) gear boxes are necessary, and the capital cost of a propeller even though high is a relatively small proportion of the total cost of the vehicle.

In sea-going ships the propeller must be kept below the water surface so that the phenomenon of air draw-down, with subsequent ventilation, is avoided. Broaching of the surface by the blades and thus racing of the propeller must also be prevented by deep submersion. However, when the draught is shallow the propeller may be surrounded by a short duct. Indeed, it has been found that a ducted propeller is often quieter, more efficient and produces a greater thrust than its unshrouded counterpart in the same location. There are two principal variants of the ducted propeller; the pump jet and the Kort nozzle. The precise ways in which the improvements in performance are achieved are still not fully clear and a detailed examination of these propulsors is beyond our present scope. Nevertheless, the main principles governing the behaviour of ducted propellers will now be discussed briefly.

(a) *Pump Jet*

The pump jet consists of a rotating impeller with fixed guide vanes (stator) either ahead of it or astern, or both, the whole unit being enclosed in a short duct concentric with the impeller. The area of the duct increases between the inlet and the impeller (see Fig. 7.7) which results in a gradual increase of static pressure from the upstream value. In this way cavitation in the vicinity of the blades can be delayed. The formation of trailing vortices (see Chapter 6) from the tips of the impeller blades is inhibited if the tip clearance between the blades and the duct is kept small, and this leads to a somewhat higher efficiency compared with the equivalent 'open' propeller. However, the *total* surface area of the duct gives rise to an additional increment of skin-friction resistance.

(b) *Kort Nozzle (Ducted Propeller)*

The main features of this device, introduced in 1933 by Kort [21], are shown in Fig. 7.8. The longitudinal sections of the axisymmetric duct are of hydrofoil shape and often the NSMB.19A design is now used [22]. The length of the nozzle is generally about one-half its diameter, and in contrast to the pump jet it is seen that the cross sectional area of the duct decreases between the inlet and the propeller. Compared with an 'open' propeller of the same size the ducted propeller draws in a greater mass of water. For a given thrust this larger quantity of water must be

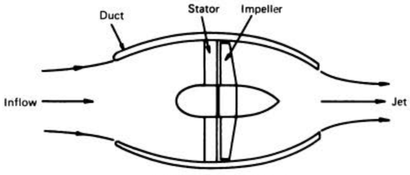

Fig. 7.7 Pump jet.

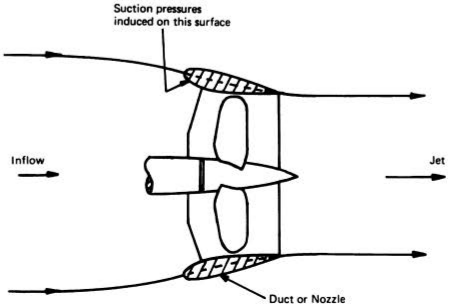

Fig. 7.8 Kort nozzle.

given a smaller acceleration so that a higher propulsive efficiency results. Moreover, the accelerating water induces suction pressures on the inner surface of the duct in the inlet region and there is, therefore, a forward thrust on the nozzle and thus on the hull to which it is attached.

In the past the Kort nozzle has been found especially effective when large thrusts are required from vehicles moving at low forward speeds or when stationary. Kort nozzles are often to be found on tugs and result in an increase of up to 40 per cent of the static thrust exerted by an identical open propeller. More recently, such a ducted propeller was fitted to a VLCC of over 2 GN (≅ 200 000 tonf) displacement (the *Golar Nichu*) and during the first two years of service this ship showed a propulsive efficiency gain of 6 per cent and a small increase in speed over her sister ships, which were powered by conventional screw propellers [23]. A theoretical investigation [24] has indicated that tip clearance should be kept to about 0.5 per cent of the propeller diameter, but by adjusting the radial distribution of thrust on the blades, so that increments of thrust developed near to the tip region are reduced, rather larger clearances are possible without large reductions in efficiency.

As in the case of the nozzle of a hydraulic-jet system directional thrust, and thus manoeuvrability without rudders, can be obtained from both the pump jet and the Kort nozzle by pivoting the duct about a vertical axis. Incidentally, there appears to be no readily available data on astern thrust for ducted propellers but clearly their effectiveness is likely to be severely curtailed. An appraisal of many aspects of ducted propeller design and performance can be found in the proceedings of the symposium referred to in [23].

With the preceding advantages it is no small wonder that the screw propeller reigns supreme, at least for the propulsion of vehicles at speeds up to 15 m s^{-1}

($\cong$ 30 knots). Many series of blade geometries have been devised and tested and more recent investigations have turned to types operating satisfactorily at vehicle speeds in excess of 25 m s^{-1} ($\cong$ 50 knots). Because of its vital importance and unique standing as a propulsor we shall devote the remainder of this chapter to a discussion of the behaviour and performance of the screw propeller. Before doing so it is worth summarizing the principal features of the various propulsors we have examined so far and this is done most effectively by referring to Table 7.1. A more detailed investigation of the comparative attributes and performances of many kinds of

Table 7.1 Principal characteristics of marine propulsors.

System of propulsion	Principal advantage(s)	Principal disadvantage(s)	Remarks
Oars, paddles	well matched to manpower	low, unsteady thrust	use confined to small boats
Paddle wheels	efficient; can provide directional control	require low-speed engines; easily damaged	use eliminated by steam turbines and diesel engines
Vertical-axis propellers	efficient; mechanical adjustment of blades; does not broach surface of water; provides high degree of steering control and thrust	heavy; costly	use on ferries and in confined waters
Sails	do not require mechanical power	ineffective in absence of wind	use largely restricted to sport but possible future importance for commercial operations
Flettner rotors	only require mechanical power to rotate cylinders	ineffective in absence of wind	possible adoption of variable height cylinders for adjustment in gales
Rocket motors	can operate in a vacuum; can give very large thrust	very high fuel consumption	might be used in emergencies
Hydraulic jets	no parts external to vehicle	large duct losses can lead to low efficiency	efficiency increases at higher vehicle speeds
Pump jet	duct length reduced from preceding device; cavitation delayed	expensive to build and install	used in shallow-draught ships
Kort nozzle	high thrust at zero forward speed	cavitation occurs earlier than pump jet	used on tugs and large tankers
Screw propeller	simple, efficient and reliable	cavitation limits performance	used on all types of marine vehicle

propulsor is given by Silverleaf [25] and the selection of propulsion systems for high-speed marine vehicles has been reviewed in [26].

7.3 Thrust and Efficiency of an Actuator Disc

A simple model of the steady flow of a fluid through a screw propeller can be obtained by replacing the propeller by a thin, isolated 'actuator disc'. The fluid passing through the disc is assumed to experience a sudden increase in pressure, whereas the axial velocity of the fluid remains continuous. Fortunately, the detailed mechanism by which such an artificial propulsor generates thrust need not detain us – we seek only the overall behaviour. The magnitude of the thrust developed by the disc can be explained entirely in terms of the changes of axial momentum taking place in the fluid, but no details of the particular propeller to produce a given thrust can be deduced. This representation of a propeller was introduced by R. E. Froude [27], among others.

There are two cases to be considered: first we shall assume that the flow downstream from the propeller possesses no rotational component of velocity; and second we shall assume that a weak rotation is present.

7.3.1 *Axial Acceleration Without Downstream Rotation*

(a) *Open Propeller Actuator Disc*

The flow relative to the disc is illustrated in Fig. 7.9(a). The disc moves forward at a steady velocity of advance V_A, parallel to its axis of rotation, into a stationary, constant-density inviscid fluid of infinite extent into which it is deeply immersed. The propeller disc is assumed to impart a uniform acceleration to all the fluid passing through it so that the thrust generated is uniformly distributed over the disc. (Glauert [28] has shown that as a uniform thrust loading leads to minimum energy losses the efficiency of this system will be the maximum attainable.) The stream tube containing all the fluid which passes through the disc must therefore contract in the downstream direction. The contraction cannot take place suddenly at the disc because the axial velocity of the fluid is continuous there; the actual contraction and acceleration must occur outside the disc and extend for some distance upstream and downstream as shown in Fig. 7.9(a). We shall, however, consider the disc to be lightly loaded so that the contraction is small and therefore the radial component of fluid velocity, v, is also small. It follows that the axial velocity of the fluid relative to the disc increases from V_A at section 1, which is effectively an infinite distance upstream from the disc, to $V_A(1+a)$ through the disc and to $V_A(1+b)$ at section 2, which is effectively an infinite distance downstream from the disc. The absolute induced velocities at the disc and at section 2 are, therefore, aV_A and bV_A. In the present context a is known as the 'axial inflow factor'.

Uniform loading of the disc also ensures that both pressure and velocity are constant across any given section of the stream tube. In particular, the pressure across the cylindrical tube at section 1 is p_0. Since the fluid extends to infinity the pressure is also p_0 at the cylindrical section 2 and indeed over the whole curved surface of the stream tube. No net pressure force is therefore exerted on the fluid contained in the stream tube between sections 1 and 2, as demonstrated in [29]. The constancy of pressure and velocity over a cross section of the tube leads to a point worth noting. The pressure on the surface of the tube is p_0 and this implies

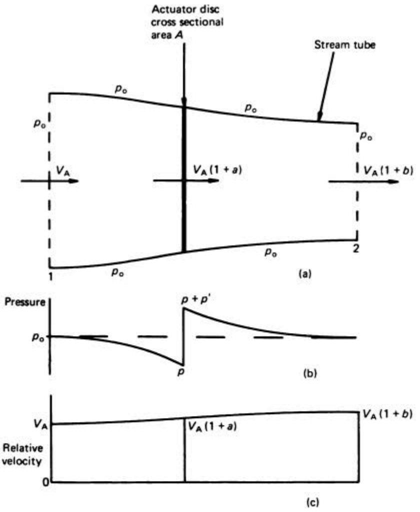

Fig. 7.9

that the velocity on that surface is V_A (since $p_0 + \frac{1}{2}\rho V_A^2$ is constant along the streamlines in that surface). Thus both pressure and velocity are discontinuous at the curved surface of the stream tube.

The uniform pressure at the upstream face of the disc is p and at the downstream face, following a jump in pressure p', it is $p + p'$. We may now apply Bernoulli's theorem to any streamline in the approach flow from section 1 to the disc and ignore the small changes in elevation, whence

$$p_0 + \tfrac{1}{2}\rho V_A^2 = p + \tfrac{1}{2}\rho[\{V_A(1+a)\}^2 + v^2] \tag{7.10}$$

where v is the (small) radial component of velocity of the fluid. Similarly, we can apply the same theorem to a streamline emanating from the downstream face of the disc (at the same radius as that corresponding to the radial velocity v) and extending to section 2:

$$p + p' + \tfrac{1}{2}\rho[\{V_A(1+a)\}^2 + v^2] = p_0 + \tfrac{1}{2}\rho\{V_A(1+b)\}^2. \tag{7.11}$$

The increment of pressure p' is thus obtained from Equations (7.10) and (7.11):

$$p' = \tfrac{1}{2}\rho b(2 + b)V_A^2 \tag{7.12}$$

and is uniform over the disc. The thrust exerted by the fluid on the disc of area A is given by

$$T = Ap' = \tfrac{1}{2}\rho A b(2 + b)V_A^2. \tag{7.13}$$

Now the equal and opposite reaction, that is the force exerted by the disc on the fluid passing through the disc, can be equated to the rate of increase of axial momentum of the fluid passing through the stream tube (there is no rotation far downstream from the disc) and so

$$T = (\text{mass flow rate})\,\{V_A(1 + b) - V_A\}$$
$$= \rho A V_A(1 + a)bV_A$$

that is,

$$T = \rho A b(1 + a)V_A^2. \tag{7.14}$$

Equations (7.13) and (7.14) can be combined to show that

$$b = 2a \tag{7.15}$$

and so

$$T = 2\rho A a(1 + a)V_A^2. \tag{7.16}$$

The velocity at the disc is, therefore, the arithmetic mean of the velocities well upstream and well downstream and so the same overall change in velocity occurs in the upstream and downstream flows. It follows that the same change in static pressure occurs in the upstream and downstream flows. The variations of static pressure and velocity relative to the disc are shown in Figs 7.9(b) and 7.9(c).

The energy per unit time (power) supplied to the fluid gives rise only to an increase in kinetic energy per unit time. The absolute velocity of the fluid passing through the disc increases from zero to $bV_A(= 2aV_A)$ and thus the power absorbed by the fluid is

$$\left.\begin{aligned} P_{ke} &= \tfrac{1}{2}(\text{mass flow rate})4a^2 V_A^2 \\ &= 2\rho A(1 + a)a^2 V_A^3 \end{aligned}\right. \tag{7.17}$$

which is contained by the slipstream. The useful work done per unit time is the output power absorbed in propelling the disc through the fluid, that is,

$$P_{out} = TV_A = 2\rho A a(1 + a)V_A^3. \tag{7.18}$$

The input power to the propeller is, therefore,

$$P_{in} = P_{ke} + P_{out} = 2\rho A a(1 + a)^2 V_A^3 \tag{7.19}$$

and so the ideal efficiency η_i of the actuator-disc model of a propeller is given by

$$\eta_i = \frac{P_{out}}{P_{in}} = \frac{1}{1 + a}. \tag{7.20}$$

We may use Equation (7.16) to define a thrust coefficient for the actuator disc which takes the form

$$C_T = \frac{T}{\frac{1}{2}\rho A V_A^2} = 4a(1 + a). \tag{7.21}$$

Hence the inflow factor, a, is given by

$$a = \tfrac{1}{2}\{(1 + C_T)^{1/2} - 1\} \tag{7.22}$$

where the radical is taken with the positive sign since a and T must vanish together. Substitution of a from Equation (7.22) into Equation (7.20) yields, for the ideal propulsive efficiency,

$$\eta_i = \frac{2}{1 + (1 + C_T)^{1/2}}. \tag{7.23}$$

The relationship (7.23), shown in Fig. 7.10, must be regarded as representing the highest possible limit for the propulsive efficiency; practical values are considerably less than shown, although 0.7 is quite common for lightly loaded propellers. Evidently, the ideal (or Froude) efficiency increases with increasing ρ, A and V_A but decreases with increasing thrust. The designer consequently aims generally for low thrust coefficients, say less than 3.† Since ρ, V_A and T are set by conditions other than those pertaining directly to the propeller it is advantageous to use the largest practicable propeller diameter.

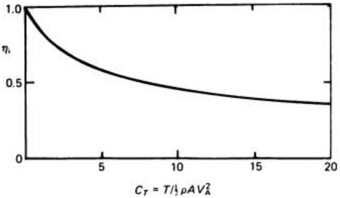

Fig. 7.10 Ideal efficiency of an actuator disc.

Figure 7.10 and Equations (7.21) and (7.23) can be used to show the expected superiority of water propellers over corresponding air propellers. Suppose each is the same diameter, advances at the same speed and develops the same thrust. The ratio of water to air densities is about 830 and so the thrust coefficient for the water propeller will be far less than that of the air propeller. The former will thus be more lightly loaded and possess a higher ideal efficiency. Alternatively, to achieve the same ideal efficiency for a given T and V_A the diameter of the air propeller must be nearly thirty times greater than the corresponding water propeller. At least from the viewpoint of ideal efficiency it would seem preferable to use water propellers

† It should be noted that the thrust coefficient defined here is not the one commonly used for propellers. We shall use subsequently another definition which will be justified later.

whenever possible, but there are many other factors which may invalidate such a choice.

We can now show that the power required to produce a given thrust by a propeller in the wake of a ship is less than that required by the same propeller in open water. Uniform flow is again assumed, even in the wake, and the two arrangements of the actuator disc are as shown in Fig. 7.11. Application of Equation (7.16) to the 'disc in wake' and the 'disc in open water' yields, for a given thrust,

$$T = 2\rho A a_w(1 + a_w)V_A^2 = 2\rho A a(1 + a)V^2 \tag{7.24}$$

where a_w is the axial inflow factor for the 'disc in wake', that is

$$\left(\frac{V_A}{V}\right)^2 = \frac{a(1 + a)}{a_w(1 + a_w)}. \tag{7.25}$$

The input power to the propeller disc is given by Equation (7.19) and hence the ratio of input power of the 'disc in wake' to that of the 'disc in open water' is, after using Equation (7.25),

$$\frac{P'_{in}}{P_{in}} = \frac{2\rho A a_w(1 + a_w)^2 V_A^3}{2\rho A a(1 + a)^2 V^3} = \frac{(1 + a_w)V_A}{(1 + a)V}. \tag{7.26}$$

From Equation (7.24)

$$a_w^2 + a_w - T/2\rho A V_A^2 = 0$$

whence

$$a_w = \tfrac{1}{2}\{-1 + (1 + 2T/\rho A V_A^2)^{1/2}\}$$

and the positive sign in the radical is taken because a_w has the same sign as T. Thus

$$1 + a_w = \tfrac{1}{2}\{1 + (1 + 2T/\rho A V_A^2)^{1/2}\} \tag{7.27a}$$

and similarly

$$1 + a = \tfrac{1}{2}\{1 + (1 + 2T/\rho A V^2)^{1/2}\}. \tag{7.27b}$$

(a) Actuator disc in wake

(b) Actuator disc in open water

Fig. 7.11

Substitution from Equations (7.27a) and (7.27b) into Equation (7.26) shows that

$$\frac{P'_{\text{in}}}{P_{\text{in}}}=\frac{\{1+(1+2T/\rho A V_{\text{A}}^2)^{1/2}\}V_{\text{A}}}{\{1+(1+2T/\rho A V^2)^{1/2}\}V}=\frac{V_{\text{A}}+(V_{\text{A}}^2+2T/\rho A)^{1/2}}{V+(V^2+2T/\rho A)^{1/2}}. \tag{7.28}$$

This ratio must be less than unity because the wake is a region of retarded flow and so $V_{\text{A}} < V$. However, as we shall see later, the presence of a propeller close to the hull effectively increases the resistance of the vehicle.

(b) *Ducted Propeller Actuator Disc*

The previous analysis can be extended to include a duct round the propeller (see Fig. 7.12) provided that we again consider the flow to be steady, axisymmetric, inviscid and of constant density. Clearance between the duct and the very thin actuator disc is considered to be exceedingly small. Other conditions on pressure and velocity within and on the surface of the stream tube containing the disc remain as before. We now need to examine the combined effect of both the propeller plus duct and of the propeller alone. We shall not examine the theoretical details leading to the design of the cylindrical duct and its hydrofoil section. Suffice it to say that the hydrofoil shape is designed around part of the surface of a stream tube so that it forms the camber line. Thus, the thickness of the hydrofoil section making up the duct wall reduces the diameter of the disc for given areas at sections 1 and 2.

For the uniformly loaded disc we may now apply Bernoulli's theorem along a streamline between section 1 and the disc and between the disc and section 2. Equation (7.13) is again derived but it must now be identified as applying only to

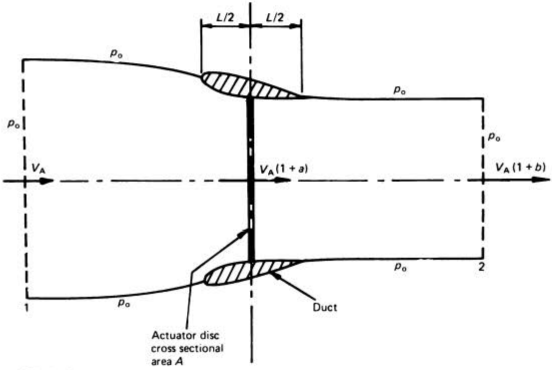

Fig. 7.12

the 'propeller alone' thrust

$$T_p = \tfrac{1}{2}\rho Ab(2+b)V_A^2. \tag{7.29}$$

Application of the axial momentum equation to the flow in the stream tube then leads to Equation (7.14), but here the thrust is that exerted on the fluid by the combined propeller-plus-duct arrangement and so

$$T = \rho Ab(1+a)V_A^2. \tag{7.30}$$

The kinetic energy lost per unit time in the slipstream is

$$P_{ke} = \tfrac{1}{2}(\text{mass flow rate})b^2 V_A^2 = \tfrac{1}{2}\rho A(1+a)b^2 V_A^3. \tag{7.31}$$

The ideal efficiency is given, as before, by

$$\eta_i = \frac{TV_A}{TV_A + P_{ke}} = \frac{2}{2+b} \tag{7.32}$$

after substitution from Equations (7.30) and (7.31). The value of b can be found from Equation (7.29), that is

$$b = (1+\tau C_T)^{1/2} - 1 \tag{7.33}$$

where

$$\tau = T_p/T \tag{7.34}$$

and C_T is given by Equation (7.21). The expression for η_i which corresponds to

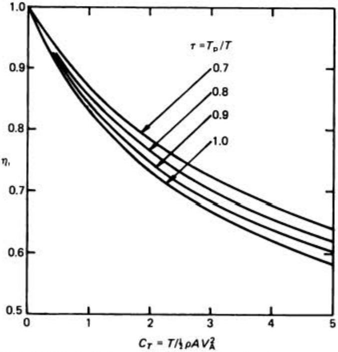

Fig. 7.13 Ideal efficiency of an actuator disc in a duct.

Equation (7.23) is obtained by substituting for b from Equation (7.33) into Equation (7.32) with the result that

$$\eta_i = \frac{2}{1 + (1 + \tau C_T)^{1/2}}. \tag{7.35}$$

Equation (7.35) differs from (7.23) by the presence of τ in the denominator and clearly for the duct to be effective $T > T_p$ and so $\tau < 1$. The variation of η_i for different values of τ is shown in Fig. 7.13. It should be noted that the application of the preceding theory is strictly concerned only with lightly loaded propellers for which C_T might be less than unity. We may then deduce that the advantage of the ducted propeller is that its diameter is smaller and the ideal efficiency higher than an open propeller with the same C_T. Similar deductions can also be made when the theory is extended to cover high values of C_T as shown in [30].

In practice, the overall efficiency is reduced owing to the presence of shear stresses on both the propeller and the duct. Nevertheless, it has been found that for high propeller loadings (e.g. $C_T > 3$) the ducted propeller has a substantial advantage, in terms of efficiency, compared with the corresponding open propeller. A particularly appropriate application of the ducted propeller is for the propulsion of fast modern tankers [23].

7.3.2 *Effect of Rotation in the Slipstream*

The power developed by a prime mover inside the vehicle is transmitted as torque in a rotating shaft to which the propeller is connected. Thus, the fluid passing through the actuator disc model experiences an increase of angular momentum as a reaction to this torque, and so the fluid downstream of the disc possesses both an axial and a rotational velocity component. Far downstream from the disc the path traced by a given particle takes the form of a helix. We therefore have an idealization of the screw propeller and the effect of rotation on the ideal propulsive efficiency must now be examined. A detailed development of the theory is given by Glauert [28] but here we shall be content to introduce a number of reasonably tenable assumptions in order to provide a simple modification to the preceding analysis. Attention will also be restricted to an examination of the open propeller.

Compared with the axial velocity component we assume that the actuator disc imparts only a small tangential velocity component to the fluid. This assumption is made partly for the sake of simplicity and partly on the basis of physical evidence from propellers with small values of C_T. Hence, in the equation describing radial equilibrium of a fluid particle,

$$\frac{\partial p}{\partial r} = \rho \omega^2 r \tag{7.36}$$

(where p is the pressure at the point occupied by the particle and ω is the angular velocity of the particle at radius r measured from the axis of rotation of the disc) the right-hand side is negligibly small. To good accuracy, therefore, the static pressure at a given section of the flow can again be considered constant over that section.

Reference to Fig. 7.9 shows that the absolute axial velocity of the fluid in a rearward direction at section 1, the disc and section 2 is $0, aV_A$ and bV_A respectively. These components are taken to be constant over the cross section considered and we now make a similar assumption about the induced absolute angular velocity at the same sections; these are taken as 0, $a'\Omega$ and $b'\Omega$ respectively, where Ω is the angular velocity of the disc. These velocity components are in the same sense as the angular velocity of the disc. The rotational inflow factor a' arises from the rotation of the fluid induced by the disc at entry to the disc.

Let us now consider the passage of an elementary mass of fluid δm in unit time between section 1 and section 2 shown in Fig. 7.9. In analogy with the expressions leading to Equation (7.14) we can write

$$\delta T = (\delta m) b V_A \tag{7.37}$$

where δT is the increment of axial downstream force exerted on the mass δm and is equal in magnitude to the forward thrust exerted by this element of fluid on the disc. It is implied here that at any cross section the element δm is contained between radii r and $r + \delta r$ and that there exists no mutual interference between adjacent annular elements. It is thought that in practice such an assumption is not seriously in error. The torque δQ applied to the element by the actuator disc can be equated to the increase in angular momentum of the element, that is

$$\delta Q = (\delta I) b' \Omega \tag{7.38}$$

where δI is the moment of inertia of the element about the axis of rotation of the disc at section 2.

The power absorbed by the disc during the passage of the element through it is $(\delta Q)\Omega$ and this must provide the useful work per unit time $(\delta T)V_A$ and also the increase in axial and rotational kinetic energy per unit time. That is,

$$(\delta Q)\Omega = (\delta T)V_A + \tfrac{1}{2}(\delta m)(bV_A)^2 + \tfrac{1}{2}(\delta I)(b'\Omega)^2. \tag{7.39}$$

Substitution for δm and δI from Equations (7.37) and (7.38) into (7.39) gives

$$(\delta Q)\Omega(2 - b') = (\delta T)V_A(2 + b),$$

and so the ideal propulsive efficiency of the element is

$$\eta_i = \frac{(\delta T)V_A}{(\delta Q)\Omega} = \frac{2 - b'}{2 + b}. \tag{7.40}$$

It may be shown [28] that the relationship $b = 2a$ derived for the axial momentum theory is not strictly true when rotation of the slipstream is taken into account. However, for the torque and thrust loadings normally adopted for open screw propellers operating at maximum efficiency the departure from this relationship is small enough to be neglected. Furthermore, it can be shown that $b' = 2a'$, and so one-half of the final angular velocity of the fluid at section 2 is acquired prior to entry into the disc. Equation (7.40) may now be written in the form

$$\eta_i = \frac{1 - a'}{1 + a} \tag{7.41}$$

and this may be compared with the ideal efficiency of the simple theory given by Equation (7.20), namely

$$\eta_i = \frac{1}{1 + a}.$$

It is clear that, as a' is positive, the ideal efficiency obtained when rotation in the slipstream is accounted for is less than that obtained when rotation is ignored. Within the limitations of our assumptions this arises from the additional increment of rotational kinetic energy supplied by the disc and contained in the slipstream. Finally, the condition of minimum energy losses results in Equation (7.41) applying not only to a particular annular element of the disc but also to the disc as a whole. The subsequent distribution of thrust and torque over the propeller must then be consistent with this constant-efficiency condition.

7.4 Flow Through a Screw Propeller

In order to determine the shape of the blades making up the propeller we must investigate the nature of the flow about each blade element. Figure 7.14 shows a

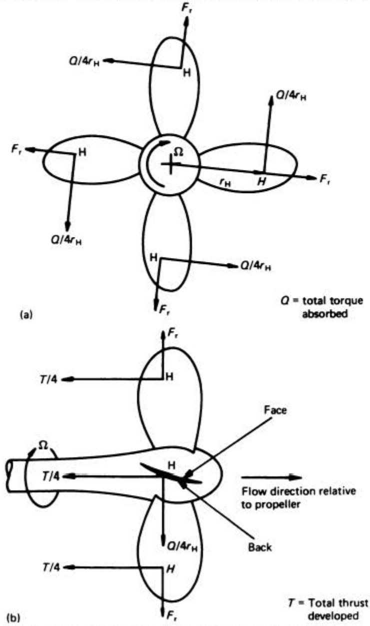

Fig. 7.14 Resultant forces and moments on a screw propeller.

four-bladed propeller attached to a shaft which rotates at a steady angular velocity Ω. The flow approaching the propeller is considered to be steady and uniform and so the forces and moments on each (identical) blade must also be steady. The resultant hydrodynamic force on each blade acts at the hydrodynamic centre H, a distance r_H from the axis of rotation. This resultant force may be resolved into three components: a propulsive thrust parallel to the shaft axis, a tangential force, and a radial force F_r. The total tangential force on the propeller gives rise to a torque Q, resisting rotation, which must be supplied by the shaft. Reference to Fig. 7.14 shows that the net radial hydrodynamic force on the propeller is zero.

The problem now is to determine the geometry of each section of the blade so that we can achieve the desired total thrust from the propeller. At the same time, the input torque to the shaft must be kept to a minimum. In general, blade design is so complex that here we shall only hint at the procedure and refrain from the detail.

7.4.1 *Vortex System of a Propeller*

Let us first take a simple case of the flow about a thin element of one blade located between the radii r and $r + \delta r$ and assume that the behaviour of the fluid is unaffected by either adjacent elements or the remaining blades. A typical section geometry might be as that shown in Fig. 7.15 which represents an inward (towards the hub) view of the element. This element rotates with a tangential velocity Ωr and moves

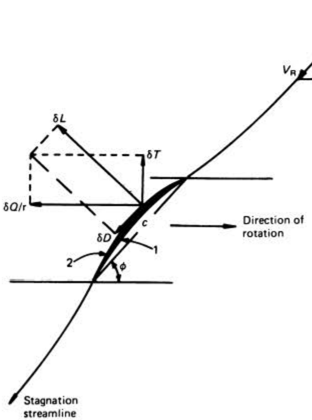

Fig. 7.15

forward with a velocity of advance V_A relative to the water well upstream from the propeller. The resultant velocity of the water ahead of the propeller relative to the blade element is therefore V_R and this vector is inclined at an angle β to the tangential direction. If the chord line of the element, of length c, makes an angle ϕ to the tangential direction then the nominal incidence angle for that element is $\phi - \beta$ relative to the direction of V_R.

The shape of the element shown in Fig. 7.15 is evidently similar to a hydrofoil section. In each case circulation about the section leads to the generation of incremental lift and drag forces δL and δD respectively, which may be resolved into a thrust δT and a tangential force $\delta Q/r$. The complete blade is therefore analogous to the foil of hydrofoil craft or the wing of an aircraft. The generation of lift also implies that the pressure at points on side 1 of the element is higher than that at corresponding points on side 2. (When referred to the complete blade these sides are usually called the 'face' and 'back' respectively.) Although we can say that the mechanism by which a propeller blade generates thrust is similar to that by which a hydrofoil develops lift, some differences remain. Rotation of the propeller causes particles of fluid within the blade passages to take on a spanwise (radial) motion. Furthermore, significant interference may occur between the flows about adjacent blades, especially near the hub. Fortunately, for many applications these factors have only a minor influence on propeller performance under design conditions and we shall pursue them no further.

In Chapter 6 it was shown that the flow about a foil of finite span could be represented by the addition of a horseshoe vortex to the basic flow, and we may follow a similar argument to model the flow round a propeller blade. For the sake of simplicity, let us assume that the circulation about each circumferential element of the blade is the same. We can then adopt the notion of a line vortex of constant strength bound to the blade and extending from tip to root. However, we know that as such a line vortex cannot terminate abruptly in the fluid each end must continue as a free vortex. Consequently, a pair of free vortices must spring from each blade of the propeller, one at the tip and the other at the root. According to Kelvin's theorem of constant circulation these must join the starting vortex. The vortex emanating from the root of each blade will combine to form a single vortex along an extension of the propeller axis. The total strength of this axial line vortex equals the sum of the strengths of the individual root vortices and it rotates in the same sense as the propeller. Each tip vortex is located approximately on the path traced out by the rotating blade tip as it advances through the fluid and so the locus is roughly helical. The sense of rotation of the tip vortices is opposite to that of the propeller. Clearly, the bound vortex rotates with each blade and will have a sense opposite to that of the starting vortex.

Figure 7.16 shows a typical system of vortices for a two-bladed propeller advancing through the fluid from right to left. Viewed in the direction 'A' the rotation of the propeller is clockwise and so, therefore, is the rotation of the axial line vortex. The rotation of the tip vortices is anticlockwise when viewed along the appropriate helix in a direction towards the corresponding tip. The bound vortex rotates anticlockwise when viewed from the tip of the blade towards the root in a spanwise (radial) direction. These vortex lines give rise to the slipstream and the motion in the slipstream can be determined from the induced velocities of this system. The sense of rotation of each line vortex shown in Fig. 7.16 is such that the fluid in the slipstream experiences an increased axial velocity and an angular velocity in the

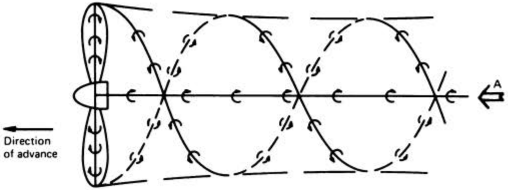

Fig. 7.16

same sense as the rotation of the propeller. This is precisely the nature of the flow downstream from the actuator disc that was postulated in Section 7.3.2.

In general, the circulation about a blade will not be constant; indeed, it may be shown that constant circulation along the whole blade is physically impossible. As a result of the variation of circulation along the blade trailing vortices will stem not only from the blade root and tip but also from every point on the trailing edge of the blades, as was suggested for finite hydrofoils in Chapter 6. Consequently, the slipstream consists of helical vortex sheets and the fluid contained between them.

To develop the detailed mathematics of the various vortex theories of propellers is beyond the scope of the present text, but some general discussion is given later. The concepts certainly allow us to predict the flow about a blade element more accurately than that shown in Fig. 7.15 so that a better estimation of the torque and thrust of a screw propeller can be made.

7.4.2 *Blade Element Theory*

It was shown in Section 7.4.1 that a thin element of a propeller blade between any radii r and $r + \delta r$ could be considered to behave as a hydrofoil. Interference between adjacent elements and between one blade and another were ignored and, furthermore, the velocity of the fluid relative to the blade was assumed to be the vector sum of the components V_A and Ωr reversed. Experience has shown that these interference effects can be neglected without incurring significant inaccuracies. The forces on each blade element can then be summed to provide the performance characteristics of the complete propeller.

The second assumption is clearly invalid owing to the influence of the induced velocities generated by the vortex system described in Section 7.4.1. Thus, if we refer to Fig. 7.17, it can be seen that the effective incidence angle of the blade element $\alpha = \phi - \beta_i$ is less than the nominal incidence angle $\alpha_N = \phi - \beta$. The velocity of the fluid relative to the blade element is therefore taken as the vector sum of an axial component $V_A(1 + a)$ and a rotational component $\Omega r(1 - a')$ and drawn in the reverse direction. In Fig. 7.17 the elements of lift and drag are perpendicular and parallel to the resultant velocity vector V_R, whereas the elements of thrust and torque are parallel and perpendicular to the direction of advance.

The pitch angle ϕ is related to the geometric pitch P by the expression

$$\tan \phi = \frac{P}{2\pi r}. \tag{7.42}$$

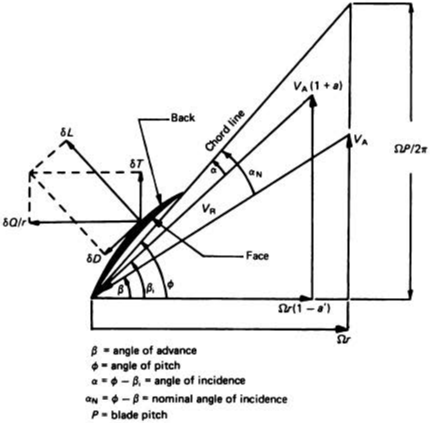

Fig. 7.17

(If a blade element is considered to be part of a screw then P is the distance moved forward by the screw in one revolution and the locus of a point on the element is a helix.) For most modern propellers the pitch varies along the span of a blade, especially near the root, and so for the sake of convenience a reference 'nominal pitch' is taken at a radius equal to 0.7 times the tip radius.

The hydrodynamic forces on each blade element can be calculated assuming the flow pattern to be the same as that about a two-dimensional hydrofoil of infinite span and with the same section geometry set at an incidence angle α in a flow of velocity V_R. Hydrofoil-section data may thus be used for each element to deduce the lift and drag forces per unit span which can be resolved into thrust and tangential forces per unit span. We may, therefore, derive the thrust and torque loadings on each element in the form $\mathrm{d}T/\mathrm{d}r$ and $\mathrm{d}Q/\mathrm{d}r$, as shown typically in Fig. 7.18, and integration of these along the blade span provides the total thrust and torque, respectively, of that blade. In practice, known satisfactory thrust and torque loadings are specified first and blade shapes are then determined to satisfy the required propeller performance.

7.5 Propeller–Hull Interaction

Up to now the propeller has been considered in isolation and no account has been taken of the interaction between the flows around a hull and those in the vicinity

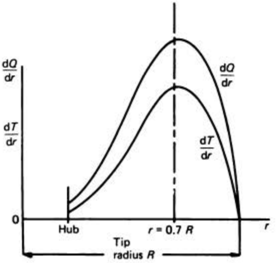

Fig. 7.18

of the propulsor. Although the possible superiority of a propeller mounted in an idealized, uniform wake over that situated in open water was demonstrated, other interaction effects were ignored. In Chapter 5 we saw that the departure from a vehicle at rest to one in motion is marked by a redistribution of local hydrodynamic forces on the hull. For a viscous fluid the sum of the local forces in the streamwise direction is no longer zero but equals the resistance R_T. To maintain a steady forward motion the propeller, now considered part of the hull of the vehicle, must alter the overall local force distribution so that the sum of the local forces is zero.

Three summations of the local streamwise forces may now be considered:

(i) For the vehicle without the propeller; this evaluates the 'bare-hull' resistance R_T.

(ii) For the vehicle with interaction effect of the propeller on the vehicle but without including the propeller surface; this yields the resistance $R_T^\dagger$.

(iii) For the propeller installed in, or on, the vehicle to deduce the thrust T.

For steady motion T will equal $R_T^\dagger$, but $R_T^\dagger$ will not necessarily equal R_T because: (i) in addition to T the propeller may generate vertical and side forces as well as pitch, yaw and rolling moments, and so to maintain steady motion alteration of the attitude of the hull and control surface settings may be required; and (ii) the flow pattern around the hull, particularly near to the propeller (usually in the vicinity of the stern), may be modified. These effects may be present separately or together.

As we have seen, the velocity of flow into an actuator disc increases as the disc is approached and so the pressure decreases. Consequently, the pressure over the stern of the vehicle is reduced and the resistance is increased compared with the respective values for the bare hull. The difference between R_T and $R_T^\dagger$ may therefore be attributed to propeller–hull interaction. Since $R_T^\dagger$ is usually greater than R_T we can adopt a so-called 'augment of resistance fraction' given by

$$a_R = \frac{R_T^\dagger - R_T}{R_T}. \tag{7.43}$$

For steady flow $T = R_T^*$, and so

$$T = R_T(1 + a_R). \tag{7.44}$$

Alternatively, a more recent (although perhaps less logical) view is to regard this increase of resistance as a reduction of propeller thrust. We can therefore define a 'thrust deduction fraction' in the form

$$t = \frac{T - R_T}{T} \tag{7.45}$$

and so

$$R_T = T(1 - t) \tag{7.46}$$

where t is invariably positive so that $R_T < T$.

The interaction between the flow about the hull and the flow through a ship's propeller was noted originally by Rankine [31]. It is clear that the design and development of propellers should be an integral part of the vehicle design because to treat each in isolation leads to poor predictions of performance. In practice this is often very difficult and so, not surprisingly, a number of empirical interaction coefficients are used to correlate both theoretical and model results with those achieved from full-scale operation.

The actual flow in the wake behind a marine vehicle is both non-uniform and unsteady and defies precise description. However, the main effects which contribute to the development of the wake are:

(i) A viscous boundary layer which forms over the wetted surfaces of the hull, shaft, shaft brackets, etc., and which reduces the kinetic energy of the fluid at these locations. Consequently, the fluid approaching the propeller is retarded and therefore has a substantial forward velocity relative to the surrounding stationary water.

(ii) The displacement of the streamlines around the hull which gives rise to a non-uniform distribution of axial, tangential and radial velocity components near the stern. There is also a rise in static pressure near to the stern of the immersed hull where the velocity of the fluid relative to the hull is reduced. Again, therefore, particles in the stern region experience a forward velocity with the vehicle.

(iii) The air–water interface which distorts during the passage of surface vehicles so that waves are generated by the hull. Orbital velocities of fluid particles below the waves may have a forward component below a wave crest and a rearward component below a trough. A trough is formed close to the stern so that then the effect of surface waves on the overall wake is opposite to those of (i) and (ii).

The overall effect of these contributions to the wake is to yield a velocity of advance V_A (i.e. the velocity of flow at the propeller location but with the propeller absent) which is somewhat less than the forward velocity V of the vehicle. This led Taylor [32] to advocate the use of a 'wake fraction' defined by

$$w = \frac{V - V_A}{V} \tag{7.47}$$

or

$$V_A = V(1 - w). \tag{7.48}$$

R. E. Froude put forward an alternative and earlier definition of a wake fraction which took the form $w_F = (V - V_A)/V_A$. However, this version will not be used hereafter owing to the wider adoption of the Taylor wake fraction.

The wake fraction is generally positive but occasionally exceptions occur for high-speed ships of fine form, such as frigates. For these the effect of a wave trough at the stern outweighs the effect of the narrow viscous wake. The need for large thrusts then calls for propellers of large diameter so that some of the propeller disc lies outside the viscous wake.

The wake velocity can be deduced from the axial, tangential and radial components measured by, for example, a pitot rake in a position corresponding to the propeller location. A typical measured distribution of w (axial velocities only) for a single-screw ship is shown in Fig. 7.19(a). It is clear that the axial velocity of flow

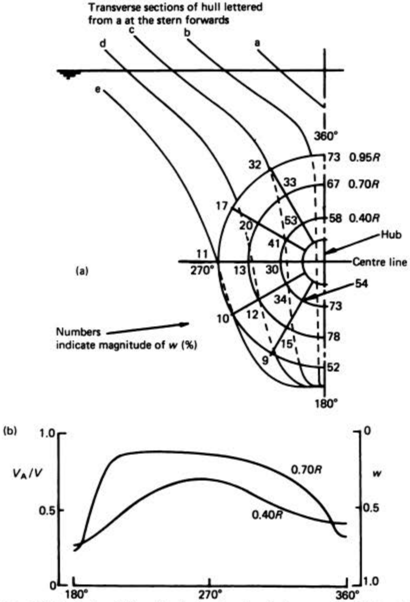

Fig. 7.19 Typical variation of wake fraction for single-screw ship. (Adapted from [3].)

onto a blade of the propeller varies with distance from the hub and with angular position. Figure 7.19(b) shows the corresponding circumferential variation of w and V_A/V at two radii $0.7R$ and $0.4R$, where R is the radius of the propeller. Note the intense wake, that is large w and small V_A/V, along the vertical centre line of the propeller. It is in this centre plane that the maximum effect of the viscous wake from the hull is felt and conditions there will thus depend on the ship Reynolds number. In other words, the wake fraction depends on the forward speed of a given ship. Based on model tests, for example, the characteristics of the wake of the prototype may be assessed and the propeller designed to ensure optimum (i.e. high-efficiency) operation of each blade element taken as a mean over the wake. Even then, however, a fluctuating, resultant fluid force will be exerted on each propeller blade and thus a fluctuating thrust and torque will be exerted on the hull. Furthermore, as a result of the asymmetry of the wake fraction the fluctuating forces on the blades will be out of phase with each other, so that a side force may well be present. This effect will also be unsteady and may result in a nonzero average couple on the vehicle which must be balanced by the continuous activation of a control surface such as a rudder.

We have concentrated here on describing the variations of the axial velocity component of the fluid approaching the stern propeller in terms of the wake fraction w. In general, there will also be variations of fluid velocity in both the radial and tangential directions which contribute further to the non-uniformity and unsteadiness of the flow. Moreover, unsteady loading of the propeller blades may result in the intermittent occurrence of flow separation from, and cavitation on, the blade surfaces which could lead to severe vibration of the propeller, the transmission system and the adjacent hull structure. These matters are taken up later in Section 7.10.

7.6 *Propulsive Efficiency*

When the propeller operates in open water, that is away from the influence of the hull, let Q_O be the shaft torque required to deliver a thrust T_O at a rotational speed n (revolutions per unit time) when the velocity of advance is V_A. The 'open-water efficiency' for the propeller is thus defined as

$$\eta_O = \frac{T_O V_A}{2\pi n Q_O}. \tag{7.49}$$

When positioned behind the hull and with the same n and V_A the given propeller will require a torque Q to deliver a thrust T. (Note that T and Q are not independent variables, whereas n and V_A are.) Thus the efficiency of the propeller behind the hull will be

$$\eta_B = \frac{TV_A}{2\pi n Q}. \tag{7.50}$$

The ratio of 'behind-to-open' efficiencies is called the 'relative rotative efficiency' given by

$$\eta_R = \eta_B/\eta_O = Q_O T/Q T_O. \tag{7.51}$$

The power required to move the vehicle at a steady speed V against a total resistance R_T is $R_T V$. The power expended by the propeller in delivering a thrust T

at a speed of advance V_A is TV_A. Consequently, we can define a 'hull efficiency' as

$$\eta_H = \frac{R_T V}{TV_A} = \frac{1-t}{1-w} \tag{7.52}$$

from Equations (7.46) and (7.48).

Finally, the overall efficiency of the propeller, sometimes called the 'quasi-propulsive coefficient' (QPC), can be defined as,

$$\eta_T = \frac{R_T V}{2\pi n Q} \tag{7.53}$$

where $2\pi nQ$ is the power supplied to the propeller. Substitution from Equations (7.49), (7.51) and (7.52) into Equation (7.53) leads to the expression

$$\eta_T = \eta_O \eta_H \eta_R = \left(\frac{1-t}{1-w}\right) \eta_O \eta_R . \tag{7.54}$$

We see, therefore, that the overall efficiency of a propeller is estimated from open-water propeller tests, hull resistance tests and hull–propeller tests.

Some typical values of the Taylor wake fraction, thrust deduction fraction, hull efficiency, relative rotative efficiency and overall efficiency are given in Table 7.2.

7.7 *Propeller Tests*

A full-size screw propeller can be large and costly but, of course, its behaviour is vital to the performance of the vehicle. Consequently, the design and assessment of a marine propeller when it is attached to the vehicle must be substantiated by model tests. Two kinds of tests are generally needed to develop the necessary techniques for predicting the prototype performance from that of the model. The first establishes the 'open-water' characteristics by running the submerged model, mounted at the end of a long sleeve containing the shaft, in a water tunnel† or suspended from the carriage of a towing tank†. Measurements of torque and thrust can then be obtained for different velocities of advance and rotational speeds of the propeller. In the second series of experiments an even smaller model propeller is installed on the model hull in its proper location. Such appendages as may affect the propeller, for example stern tubes, shafting, brackets, etc., are also included. The hull is then suspended from the carriage of a towing tank at the operating draught and again torque and thrust are measured for a series of carriage and propeller speeds.

7.7.1 *Open-water Performance*

Suppose that a given propeller, which may be one of a geometrically similar (homologous) series, is deeply immersed in a uniform, homogeneous, steady, constant-density flow approaching the propeller in a direction parallel to its axis of rotation. The thrust developed T and the torque absorbed Q may be considered to depend on the following parameters: V_A, the velocity of advance; D, the diameter, which specifies the size of the propeller; n, the rotational speed of the propeller; ρ, the density of the fluid; μ, the dynamic viscosity of the fluid; and $\bar{p} - p_v$, the pressure

† Some aspects of these facilities are discussed in Chapter 4.

Table 7.2 *Typical values of efficiency, wake fraction and thrust deduction fraction.*

Vehicle	$(1-w)$	$(1-t)$	η_H	η_R	η_T
Single-screw submarine	0.50–0.80	0.80–0.90	1.10–1.45	1.00–1.10	0.72–0.93
Single-screw merchant ship	0.55–0.85	0.75–0.85	1.10–1.30	0.99–1.09	0.72–0.86
Twin-screw merchant ship	0.83–0.95	0.82–0.89	0.96–0.97	–	0.62–0.70
Twin-screw destroyer at maximum speed	0.93–1.01	0.90–0.99	–	–	0.61–0.70
Large, fast, four-screw ship	0.87–0.99	0.82–0.95	–	–	0.60–0.67
VLCC with ducted propeller	0.66	0.80	1.21	0.98	~0.80

of the fluid relative to vapour pressure. Here, $\bar{p}$ is the upstream static pressure acting at a point on an extension of the propeller centre line and p_v is the vapour pressure of the water at that point. For the moment, we shall include in our analysis the possible effects of cavitation, although a more detailed discussion of the phenomenon is reserved until later. The diameter D is also assumed to include the effects of roughness height, that is, the ratio of roughness height to diameter is considered constant for the series of propellers. (We know already that this is extremely difficult to achieve and that the distribution and shape of the roughness are also important.)

The application of dimensional analysis to the preceding parameters shows that,

$$K_T = \text{function}\,(J, Re_D, \sigma_N) \tag{7.55}$$

and

$$K_Q = \text{function}\,(J, Re_D, \sigma_N), \tag{7.56}$$

where

$$\left.\begin{aligned}
K_T &= \frac{T}{\rho n^2 D^4}, && \text{thrust coefficient}\\
K_Q &= \frac{Q}{\rho n^2 D^5}, && \text{torque coefficient}\\
J &= \frac{V_A}{nD}, && \text{advance coefficient}\\
Re_D &= \frac{\rho D V_A}{\mu}, && \text{propeller Reynolds number}\\
\sigma_N &= \frac{\bar{p} - p_v}{\frac{1}{2}\rho V_A^2}, && \text{nominal cavitation index.}
\end{aligned}\right\} \tag{7.57}$$

Were we to include the possibility of the propeller operating in close proximity to the free surface of the water the effects of distortion there would need to be taken into account. Another variable, weight per unit mass g, must then be included in the original list of parameters even though for a propeller g may be considered constant. The result of dimensional analysis is an additional dimensionless group $V_A/\sqrt{(gD)}$ which is the propeller Froude number Fr_D. Then, of course, K_T and K_Q would also depend on Fr_D. Furthermore, under these operating conditions 'draw-down' of air from above the free surface is a real possibility and thus the effect of surface tension, giving rise to the propeller Weber number, may become significant. However, for our present purpose we shall not consider these latter two effects.

The local flow past the blades of a propeller operating at the design condition is invariably fully turbulent and so Re_D has relatively little influence. Nevertheless, when fluid velocities near the propeller surfaces are low, for example in model testing, Re_D may become significant. However, V_A and therefore Re_D are kept as large as possible and n adjusted accordingly to give the necessary range of J. Thus, for a non-cavitating propeller the principal independent parameter is J. Hence, in the case of open-water tests, we can write

$$K_{T_O} = \text{function}\,(J_O); \qquad K_{Q_O} = \text{function}\,(J_O). \tag{7.58}$$

It can be seen from Fig. 7.17 that the advance coefficient is related to the advance angle as follows,

$$\tan\beta = \frac{V_A}{\Omega r} = \frac{V_A}{2\pi nr} = J\left(\frac{D}{2\pi r}\right). \tag{7.59}$$

For a given blade section at radius r and pitch angle ϕ large values of J give large values of β and thus small angles of incidence, and vice versa.

Using Equation (7.49) we can write, for the open-water efficiency,

$$\eta_O = \frac{T_O V_A}{2\pi n Q_O} = \frac{J_O K_{TO}}{2\pi K_{QO}}. \tag{7.60}$$

When $V_A = 0$, so that $J_O = 0$, then $\eta_O = 0$ since no useful work is done by the propeller. However, the incidence angle of the flow onto the blade is high and so K_{TO} and K_{QO} are both large (actually the largest values induced by the propeller). As J_O increases the incidence angle decreases, as do both K_{TO} and K_{QO}. The ratio K_{TO}/K_{QO} decreases slowly and η_O thus reaches a maximum value.

From Equation (7.42)

$$\tan\phi = \frac{P}{2\pi r} = \frac{P}{D}\left(\frac{D}{2\pi r}\right). \tag{7.61}$$

Together with Equation (7.59) this equation shows that $\phi = \beta$ when $J = P/D$, provided that the blade pitch P does not vary radially. The angle of incidence will therefore be close to zero over the whole blade span under these conditions and so blade stall (and additionally cavitation) with consequent high drag can be avoided. In practice, P does vary radially and, furthermore, the blades are cambered. As a result the thrust falls to zero at a value of J_O slightly higher than P/D. Typical open-water performance curves of a non-cavitating screw propeller are shown in Fig. 7.20.

The maximum diameter of the propeller is usually fixed by structural and clearance limitations, but the rotational speed which gives the required thrust must then be found. From the definitions of K_T and J given in Equation (7.57) it is clear that both depend on n. However, by combining these two coefficients in the form

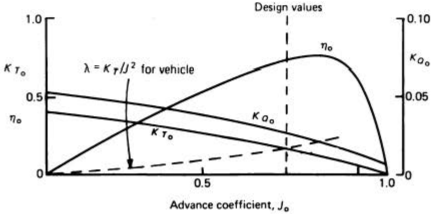

Fig. 7.20 Typical propeller performance curves.

K_T/J^2 we can eliminate n to give

$$\frac{K_T}{J^2} = \left(\frac{T}{\rho n^2 D^4}\right)\left(\frac{n^2 D^2}{V_A^2}\right) = \frac{T}{\rho V_A^2 D^2} = \left(\frac{T}{\frac{1}{2}\rho A V_A^2}\right)\left(\frac{\pi}{8}\right) = \frac{\pi C_T}{8} \tag{7.62}$$

where C_T is the thrust-loading coefficient of an actuator disc of swept area A, defined by Equation (7.21). As the value of C_T can be estimated for a given application and hull–propeller combination the right-hand side of Equation (7.62) may be considered to be some known constant factor λ, say. We may therefore plot in Fig. 7.20 the parabola

$$K_T = \lambda J^2, \tag{7.63}$$

and the intersection of this line with the curve of K_{T_O} against J_O for the propeller denotes the required operating point. Corresponding values of J_O (and thus n_O), K_{Q_O} and η_O can be obtained. The principal aim of the designer is to achieve operation at the highest value of η_O possible over a range of propeller loadings.

A great deal of data has been collected on the performance of several series of propellers by numerous authors [e.g. 3, 33–37]. Composite plots of K_{T_O}, K_{Q_O} and η_O against J_O are drawn on charts onto which can be laid the $K_T = \lambda J^2$ curve for a given design requirement. The propeller can then be chosen to optimize such parameters as pitch ratio (P/D), the blade area ratio (abbreviated BAR), the number of blades and so on.

7.7.2 *Self-propulsion Tests*

For each model self-propulsion test at a given V_M and n_M the dynamometer on the towing tank carriage indicates values of $(R_T^*)_M - T_M$ where R_T^* is the augmented total resistance defined in Section 7.3.4 and the subscript M refers to the model. Low values of n_M give values of $T_M < (R_T^*)_M$, whereas high values of n_M result in $T_M > (R_T^*)_M$. When the reading on the dynamometer is zero $T_M = (R_T^*)_M$, and this is known as the 'self-propulsion point'. Under these conditions the forward velocity of the hull–propeller combination is sustained by the propeller alone. The value of n_M at the self-propulsion point depends on V_M for a given model. Readings are taken of the corresponding values of torque Q_M and thrust T_M to complete the test data.

A typical performance curve for a model self-propulsion test is shown in Fig. 7.21. It might be supposed that the self-propulsion point A, corresponding to the rotational speed n_{M_1}, for which $(R_T^*)_M - T_M = 0$, is the 'operating point' of the model propeller and thus of the scaled prototype propeller. However, for ship propulsion V_M is determined from V_P (the prototype velocity) on the basis of identical Froude numbers and so the Reynolds number for the model hull is less than that for the prototype. Consequently, the model resistance coefficient is greater than the ship resistance coefficient. (We recall that dynamic similarity is also impossible to achieve with a submarine even though the Froude number has no significance for deep submersion. Here again $Re_M < Re_P$.) We may therefore expect the model propeller to be overloaded compared with the prototype. Consequently, K_T will be too large and the predicted efficiency of the propeller will be too low.

The solution to this dilemma is far from clear and although methods have been suggested none are fully satisfactory. Essentially, the operating point should not

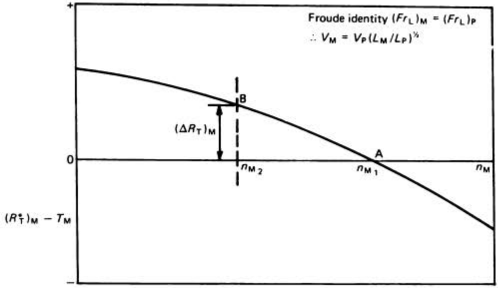

Fig. 7.21

be at A, in Fig. 7.21, but at another point corresponding to a lower rotational speed. Mandel [38] and others have argued that a more realistic operating point B (in Fig. 7.21) can be located, the ordinate of which is given by

$$(R_T^*)_M - T_M = (\Delta R_T)_M = \tfrac{1}{2}\rho(S_W)_M V_M^2 \{(C_F)_M - (C_F)_P - C_A\}, \quad (7.64)$$

where $(S_W)_M$ is the wetted surface area of the model hull, $(C_F)_M$ and $(C_F)_P$ are the skin-friction coefficients of the model and the prototype hulls respectively, and C_A is the correlation allowance discussed previously. The operating speed of the propeller is thus n_{M_2}. In practice, $(\Delta R_T)_M$ is calculated first and the ordinate plotted as $(R_T^*)_M - T_M - (\Delta R_T)_M$, and when this is zero the propeller operating speed is n_{M_2}. Alternatively, the self-propulsion point A may still be adopted and use made of the speed n_{M_1} with an appropriate thrust 'allowance' made subsequently to account for the scale effects.

7.8 Estimation of Propeller Efficiency

The procedure required for an accurate estimate of η_T is extremely complex and for the sake of clarity only a relatively simple approach is given here. Our primary purpose is to indicate the ways in which the various tests described previously can be used and to note the various limitations of the procedure as applied to the power requirements of ships. The power to propel a ship, that is the effective power, is given by

$$(P_E)_P = (R_T)_P V_P. \quad (7.65)$$

The resistance $(R_T)_P$, which includes appendage resistance, is obtained from model tests and/or calculations as outlined in Chapter 5.

Essentially, we need to determine for the prototype ship the value of λ in Equation (7.63) and then use this equation to obtain the most efficient propeller. Experience has shown that provided the model hull is run at a steady speed the wake pattern approaching the propeller is only weakly dependent on the actual detailed design of the propeller of given diameter. This is especially so at the operating (or self-propulsion) point and it is indeed a most fortunate state of affairs. Thus, in the self-propulsion and open-water experiments, the model propeller used is one chosen from perhaps a set of existing propellers or one actually made to fill a gap in a standard range. The sizes of the hull and propeller are in the same ratio for both the model and the prototype so that the propeller disc is subjected to the same proportion of the wake.

We may now proceed as follows:

1. A self-propulsion test is carried out with the model hull and appendages installed but with a model propeller of diameter D_M reasonably similar to the contemplated design. The forward speed is given by

$$V_M = V_P(L_M/L_P)^{1/2}. \tag{7.66}$$

At the adopted operating point the model propeller speed n_M, torque Q_M and thrust T_M are measured. The magnitude of $(K_T)_M$, that is $T_M/\rho n_M^2 D_M^2$, can thus be calculated. For similar operating conditions $(K_T)_M = (K_{T_O})_M$, that is, the thrust coefficient of the *same* model propeller in the open-water test.

2. The open-water test on the model is conducted at a high value of $(V_A)_M$ in order to maintain a high propeller Reynolds number, the rotational speed being adjusted accordingly to give a range of advance coefficients. At the $(K_{T_O})_M$ deduced in 1 we can read off from the open-water curves the corresponding values of $(J_O)_M$ and $(K_{Q_O})_M$.

3. The appended resistance $(R_T)_M$ of the model hull without the propeller is obtained from a towing test at the speed V_M given by Equation (7.66).

From tests 1 and 3 we have measured T_M and $(R_T)_M$, and so from Equation (7.45) the model thrust deduction fraction is given by

$$t_M = 1 - \left(\frac{R_T}{T}\right)_M. \tag{7.67}$$

From test 2 we have $(J_O)_M$ at the operating point and from test 1 the corresponding operating n_M can be obtained. Hence, assuming that $J_M = (J_O)_M$ at the operating point,

$$(V_A)_M = (J_O nD)_M. \tag{7.68}$$

Equation (7.47) yields the model wake fraction

$$w_M = 1 - \left(\frac{V_A}{V}\right)_M. \tag{7.69}$$

Using Equation (7.52) we can therefore write for the hull efficiency of the model

$$(\eta_H)_M = \frac{1 - t_M}{1 - w_M}. \tag{7.70}$$

The relative rotative efficiency for the model hull is given by Equation (7.51), that is

$$(\eta_R)_M = \left(\frac{Q_O T}{Q T_O}\right)_M = \left(\frac{D_O}{D}\right)_M \left(\frac{K_{Q_O}}{K_Q}\right)_M \left(\frac{K_T}{K_{T_O}}\right)_M.$$

However, at the operating point $(K_{T_O})_M = (K_T)_M$, and for the same propeller $(D_O)_M = D_M$. Hence

$$(\eta_R)_M = \left(\frac{K_{Q_O}}{K_Q}\right)_M = \left(\frac{\rho}{\rho_O}\right)_M \left(\frac{Q_O}{Q}\right)_M \left(\frac{n}{n_O}\right)_M^2 \tag{7.71}$$

where ρ_M need not necessarily equal $(\rho_O)_M$.

When the prototype ship operates at its design speed V_P it is tacitly assumed that

$$t_P = t_M; \quad w_P = w_M; \quad (\eta_H)_P = (\eta_H)_M; \quad (\eta_R)_P = (\eta_R)_M. \tag{7.72}$$

However, as the conditions for dynamic similarity cannot be fully satisfied the equalities expressed in (7.72) are not necessarily valid. Nevertheless, we can proceed with the selection of a propeller on this basis and subsequently make adjustments using trials data from previous ships to compensate for the present deficiencies.

The variables in expressions (7.72) are thus known for the prototype ship and $(R_T)_P$ can be obtained from model tests on a geometrically similar hull. Thus we can deduce $(V_A)_P$:

$$(V_A)_P = V_P(1 - w_P), \tag{7.73}$$

and the prototype propulsor thrust T_P:

$$T_P = \frac{(R_T)_P}{1 - t_P}. \tag{7.74}$$

Combining the results of Equations (7.73) and (7.74) we can now write, from Equation (7.62),

$$\left(\frac{K_T}{J^2}\right)_P = \frac{\pi(C_T)_P}{8} = \left(\frac{T_P}{\frac{1}{2}\rho A_P(V_A^2)_P}\right)\left(\frac{\pi}{8}\right) = \lambda_P. \tag{7.75}$$

We now return to open-water tests for the final phase of the analysis. This time, however, the open-water data are obtained for the prototype propeller in one of the following ways. Based on the vortex and blade element theories described in Section 7.4 and prescribed radial distributions of torque and thrust together with cavitation data the shape of the propeller blade can be deduced. A model of this propeller is then built and the open-water $(K'_{T_O})_M$, $(K'_{Q_O})_M$ and $(J'_O)_M$ characteristics obtained as outlined earlier. Here the prime on the coefficients denotes that these values correspond to a model propeller which is geometrically similar (within manufacturing limits) to the prototype ship propeller. Alternatively, published open-water data for K_{T_O} of various series of propeller geometries can be used on which the curve $(K_T)_P = (\lambda J^2)_P$ from Equation (7.75) can be superimposed. If it is assumed that the open-water and behind-the-hull flows are dynamically similar at the same advance coefficient then $(K'_{T_O})_M = (K_T)_P$ and the intersection of the two K_T curves indicates the operating point. We can now ascertain $(J'_O)_M = J_P$ corresponding to the operating conditions:

$$(J'_O)_M = J_P = \left(\frac{V_A}{nD}\right)_P. \tag{7.76}$$

Hence, as $(V_A)_P$ is known from Equation (7.73), n can be found for a given diameter of the prototype propeller. The corresponding $(\eta_O)_P = (\eta'_O)_M$ and $(K_{QO})_P = (K'_{QO})_M$ are also obtained from the open-water curves. Consequently, the overall efficiency of the prototype propeller can now be determined from

$$(\eta_T)_P = (\eta_O \eta_R \eta_H)_P. \tag{7.77}$$

The power delivered to the propeller by the shaft external to the ship is then

$$(P_D)_P = \left(\frac{P_E}{\eta_T}\right)_P = \left(\frac{R_T V}{\eta_T}\right)_P \tag{7.78}$$

Finally, the relative rotative efficiency $(\eta_R)_P$ can be used to determine the operating torque for the prototype propeller since, for dynamic similarity,

$$(\eta_R)_P = \left(\frac{(D'_O)_M}{D_P}\right)\left(\frac{(K'_{QO})_M}{(K_Q)_P}\right)\left(\frac{(K_T)_P}{(K'_{TO})_M}\right) = \left(\frac{(D'_O)_M}{D_P}\right)\left(\frac{(K'_{QO})_M}{(K_Q)_P}\right).$$

as identical thrust coefficients are assumed at the operating point. Whence

$$Q_P = (\rho n^2 D^5)_P \left(\frac{(D'_O)_M}{D_P}\right)\left(\frac{(K'_{QO})_M}{(\eta_R)_P}\right). \tag{7.79}$$

The principal parameters for the prototype propeller have therefore been found. The full-scale ship will be propelled at a forward speed V_P (related to V_M by equating Froude numbers) by a propeller of diameter D_P rotating at a speed n_P (from Equation (7.76)) which develops a thrust T_P (from Equation (7.74)) and absorbs a torque Q_P (from Equation (7.79)). It is clear, however, that the reliance on dynamic similarity between the model hull–propeller combination and its full-scale counterpart is hardly justified. Use must therefore be made of trials data and previous experience of propeller design and performance. Nevertheless, despite the various shortcomings of the analytical techniques the rated output from full-scale propellers can be predicted with good accuracy.

A similar approach to that above may be adopted for ducted propellers [39]. However, the open-water tests now apply to the propeller–duct combination. Model propulsor–hull interaction effects are obtained from towing and self-propulsion tests with the models, but the flow over the model duct and appendages is at low Reynolds numbers. The results must therefore be interpreted with some care. Since the effect of the ducted propeller on interaction phenomena is different from that of the open propeller we could expect, for example, a change in correlation allowance. As pointed out in [39] the performance of a ship fitted with a ducted propeller depends critically on the afterbody–duct configuration. A number of interesting examples of ducted propeller installations on large ships are described in [40]. The applicaton of design processes has been extended to include twin-propeller systems as well as a single, large, middle-line ducted propeller. The designers of naval ships and submarines see the reduced noise and cavitation associated with the ducted propeller as a valuable device for decreasing vulnerability to detection by sonar or acoustic mines and torpedoes. Incidentally, ducted propellers are also used on high-speed torpedoes for similar reasons, but the duct then decelerates the water after entry.

7.9 Cavitation

Reference has already been made to the phenomenon of cavitation as it affects the flow about a hydrofoil (see Chapter 6). Furthermore, we have established in Section 7.4 that the flow past a propeller blade can be likened to that in the vicinity of a hydrofoil. In both cases suction pressures are induced close to some parts of the solid surface of the blade (or hydrofoil) which encourage the inception of cavitation. Should the local pressure p fall below the local vapour pressure p_v at a particular point in the flow then cavitation occurs. The vapour pressure of sea water is influenced by many factors, not the least being water temperature and the size and concentration of solid and gas particles in the bulk of the water which act as nuclei for cavitation bubbles. As in the case of hydrofoils the results of cavitation erosion can produce disastrous failure of propeller blades. The performance of a propeller is seriously curtailed by the presence of sheet cavitation or the change in blade profile arising from erosion of the metal surface.

A local pressure coefficient c_p, applicable to any given blade section, can be defined as

$$c_p = \frac{p - p_r}{\frac{1}{2}\rho V_R^2}, \tag{7.80}$$

where the resultant velocity of the flow onto the section is V_R, the local static pressure on the surface of the section is p, p_r is a reference static pressure in the flow just upstream from the leading edge of the section and ρ is the density of the liquid. A cavitation index σ can now be formed:

$$\sigma = \frac{p - p_v}{\frac{1}{2}\rho V_R^2} = \sigma_L + c_p \tag{7.81}$$

where

$$\sigma_L = \frac{p_r - p_v}{\frac{1}{2}\rho V_R^2} \tag{7.82}$$

is the local cavitation index referred to upstream conditions. Cavitation occurs when $\sigma < 0$, and we must therefore determine the minimum value of c_p for a propeller of a given geometry.†

The minimum value of c_p on the surface of conventional, low-speed hydrofoil sections is usually located within the first 50 per cent of the chord length measured from the leading edge. For positive angles of incidence $c_{p_{min}}$ occurs on the back of the blade, but on the face for negative angles of incidence. The flow accelerates to a maximum velocity corresponding to a minimum pressure which is less than p_r so that $c_{p_{min}}$ is negative. For a given section the magnitude of $c_{p_{min}}$ depends primarily on α and increases with α. At and near the operating design point of the propeller it is likely that the induced velocities will be small. Thus, neglecting a and a' we see from Fig. 7.17 and Equation (7.59) that an increase in $\alpha(=\alpha_N)$ implies a decrease in $V_A/\Omega r$, which is proportional to the advance coefficient J. If α remains unchanged $c_{p_{min}}$ will not change with V_R provided that free-surface and Reynolds number

† Whereas the nominal cavitation index σ_N, defined in Equation (7.57), can be used to indicate an overall cavitation pattern of a series of geometrically similar propellers we must use σ to assess when and where cavitation commences on a particular blade.

effects are negligible. However, p_{min} may then become so small that p_v is approached and cavitation encouraged. Excessive fluid velocities must, therefore, always be avoided.

Let us assume that the propeller disc is vertical and the horizontal axis of rotation is at a depth h below the air–water interface. Furthermore, suppose that the flow into the propeller is steady, horizontal and uniform. The pressure distribution in the upstream flow can be considered hydrostatic and so for a blade element at radius r from the hub the minimum value of p_r occurs when the blade, of which the element is part, is in the upper vertical position. Thus

$$(p_r)_{min} = p_a + \rho g(h - r) \tag{7.83}$$

where p_a is the ambient pressure at the interface. When the propeller operates at and near the design point we see from Fig. 7.17 that the resultant velocity of the flow relative to the blade is given by

$$V_R^2 = V_A^2 + \Omega^2 r^2 = V_A^2 + 4\pi^2 n^2 r^2 \tag{7.84}$$

where a and a' have been put equal to zero.

Substitution from Equations (7.83) and (7.84) for p_r and V_R into Equation (7.81) yields

$$\sigma_L = \frac{p_a - p_v + \rho g(h - r)}{\frac{1}{2}\rho(V_A^2 + 4\pi^2 n^2 r^2)}. \tag{7.85}$$

For a given propeller the likelihood of cavitation increases as σ_L decreases, which implies (i) a decrease in p_a and/or h; and, (ii) an increase in V_A and/or n. Furthermore, for given values of V_A, n, p_a and h, the minimum value of σ_L occurs when $r = R$, the radius of the propeller, that is at the tip of the blade in the uppermost position.

7.9.1 *Development of Cavitation on Propeller Blades*

Cavitation can be observed most readily from open-water tests in a water tunnel. Variations in σ_L can be obtained by keeping the velocity of advance constant and varying the speed of rotation. The ambient pressure of the water p_a can also be varied, but h is of course constant. Since V_A and D are constant then it follows from Equation (7.57) that the advance coefficient J_O is inversely proportional to n.

At very low rotational speeds (high values of J_O) the propeller thrust may be so low that over substantial portions of the span the angle of incidence may be negative. Low pressures on the face of the blade may therefore lead to cavitation on that surface near to the leading edge. Behind the suction peak the positive pressure gradient is so high that collapse of the bubbles occurs after only a short distance.

With an increase in rotational speed face cavitation disappears and the next type is generated close to the blade tips. As a result of developing thrust vortices are shed in helical spirals from the tips of the blades. The pressure at the centre of these trailing vortices is relatively low and becomes lower as the thrust increases, that is, as J_O decreases. A spiral of tip vortex cavitation forms close to the blade tip and extends downstream as shown in Fig. 7.22. The overall performance of the propeller is not affected appreciably but considerable noise is generated.

As the rotational speed increases further cavitation begins to appear on the back of the blade extending downstream from a region close to the leading edge. A silvery

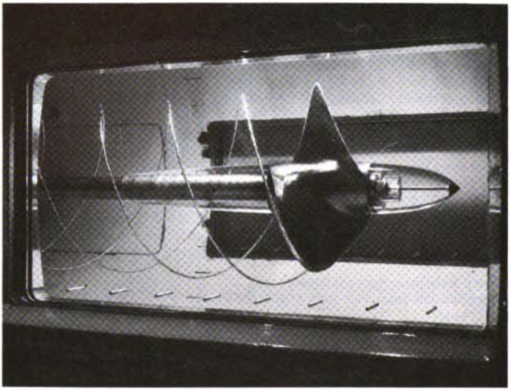

Fig. 7.22 Cavitating tip vortices in flow downstream from a propeller.

sheet is thus formed as suggested in Fig. 7.23(a). Tests must usually be carried out on small propellers in a water tunnel so that the pattern of cavitation which develops on a blade in the upper vertical position differs little from that on the blade in any other position. This is not true in the case of the full-scale prototype. In reality intermittent cavitation prevails and this induces longitudinal vibrations along the shaft owing to fluctuations of thrust.

Increased blade loading (n increases, J_O decreases) leads to the sheet covering additional outer areas of the blade. Discrete bubbles may also be produced at about mid-chord and are swept downstream. These larger bubbles collapse on entry to zones of higher pressure near the trailing edge of the blade. This collapse may occur on the blade surface and cause severe impact loads. In addition, a great deal of noise and vibration develops, which are indicative of overloading of the propeller blades and which will result in a deterioration of performance. The continuing spread of cavitation as J_O decreases is shown in Figs. 7.23(b), (c) and (d).

Eventually, the rotational speed becomes so high (and therefore J_O so low) that the whole of the back surface of the blade is covered in a sheet of cavitation bubbles, as shown in Figs. 7.23(e) and 7.24. This condition is called full cavitation (or super-cavitation) in which the back surface of the blade is no longer in contact with the water and thrust can only be generated from the region of positive c_p on the face. The trailing vortex from the hub section of each blade may also possess a cavitation core under these conditions.

The general effects of cavitation on thrust, torque and efficiency are shown in Fig. 7.25 (which corresponds to the pictorial representation of cavitation in Fig. 7.23).

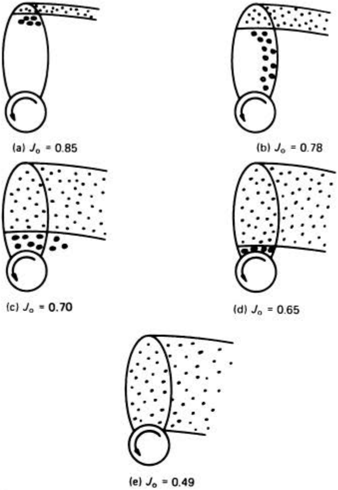

Fig. 7.23 Typical progression of back cavitation on a propeller obtained from open-water tests.

The data [41] refer to open-water tests on a three-bladed propeller of 200 mm ($\cong$ 8 in) diameter in a water tunnel under normal and depressurized conditions. Perhaps we should recall that Fig. 7.25 shows the effects of cavitation on the overall performance of a given propeller and that details of cavitation inception cannot be obtained from it for the purposes of design data. The use of σ_N is therefore quite justified in typifying cavitation régimes. It is worth noting that many different forms of cavitation index (or number) exist and the appropriate form depends largely on convenience and the purpose to which the data are put. Often $\bar{p} - p_v$ is referred to the propeller centre line, but instead of V_A the velocity V_R is used and may be taken as the value corresponding to the flow conditions approaching a blade section at a position 70 per cent of the propeller radius from the hub, namely, at $r = 0.7R$.

We see in Fig. 7.25 that as cavitation develops on the back of each blade ($0.95 < J_O < 0.55$) the thrust generated by the face increases but the contribution from the back decreases. The net result is that both thrust and torque increase with n (i.e. decreasing J_O) at a rate less than that for cavitation-free operation. In the super-cavitating mode the thrust obtained from the back is negligible and so both

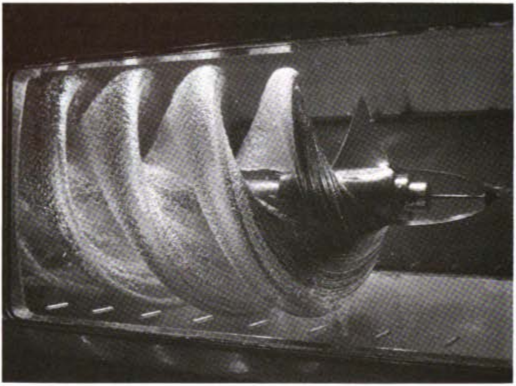

Fig. 7.24 Fully developed sheet of back cavitation on a propeller.

thrust and torque increase at a somewhat greater rate. The reduction in maximum efficiency for this propeller is small because cavitation has only just been initiated at the corresponding speed. However, at $J_O = 0.64$ (when $n = 20$ revolutions per second) cavitation is well advanced and the open-water efficiency of the propeller drops from 0.61 to 0.49.

Accurate observation and interpretation of cavitation patterns on propeller blades attached to models and full-scale ships require carefully developed techniques and rather sophisticated equipment [42]. Stroboscopic pictures are useful, but often difficulties are experienced owing to the unperiodic nature of the unsteady wake flows and consequent confused cavitation pattern. Furthermore, equipment must be mounted inboard at the stern above transparent windows so that a high-speed camera can be focused on the back of the propeller blades. An intense light source, also inboard, must illuminate both the face and back of the blades so that pictures of face and back cavitation can be taken. For the observation of face cavitation a periscope can be placed downstream from the propeller and pointing upstream. Simultaneous film and video recordings provide permanent records for subsequent analysis. The preceding techniques, described in detail in [42], have been used for cavitation tests in the NSMB depressurized towing tank (see Table 4.1 for dimensional details). Although it is possible with this tank to scale the full-size ship cavitation index accurately, this does not necessarily give a true indication of cavitation inception phenomena. The formation of cavitation bubbles depends on the nature, size, and distribution of particles in the water. By reducing the surface

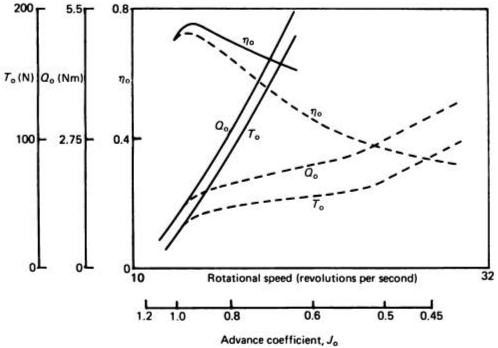

Fig. 7.25 Effects of cavitation on propeller performance. ——, full pressure condition in tunnel; – – –, reduced pressure condition in tunnel.

pressure of water in a towing tank air in the water comes out of solution. The air bubbles will then form the nuclei to precipitate cavitation. Clearly, the distribution and concentration of the nuclei at model and full scale are unlikely to be the same.

A number of cavitation experiments have been performed at full scale and a particularly interesting discussion is given in [43]. In contrast with model tests there is usually sufficient space at full scale to allow external filming and lighting. As a result, equipment can be moved from ship to ship without necessitating major structural alterations. This was done for seven large ships, including oil tankers, an ore carrier and an LPG (liquid petroleum gas) carrier, all of which were fitted with ducted propellers. Experience with ships having ducted propellers indicated that the main region of cavitation erosion was not on the blades but on the inner surface of the duct. Generally, good agreement was found between model and full-scale cavitation patterns, although the latter appeared to be of somewhat larger relative area. Tip vortex cavitation was the probable cause of duct erosion and, presumably, if the hydrodynamic loading at the tip could be reduced by redesigning the blades (after the method of Glover [50, 52] for open propellers) damage to the duct might be avoided. Apparently, no success along these lines was achieved and so examples are given of patching techniques, using anti-erosive materials on the inner duct wall, and of air injection into the main cavitation regions. It was found that only a modest injection of air bubbles into the flow significantly reduced the impact loads from the shock waves and microjets of collapsing vapour bubbles. This evidence was deduced from a metallurgical survey of the eroded areas of the duct. It is thought that the effectiveness of the method derives from the cushioning effect of air bubbles and works in the same way as controlled ventilation on the foils of hydrofoil craft (see Section 6.3.5).

7.10 Propeller Design

A detailed description of propeller design, which necessarily requires an analysis of hydrofoil section performance followed by an optimum stacking of the sections to form the blade geometry, is outside the scope of this book. However, it was hinted earlier that an examination of the behaviour of hydrofoil sections could be carried out on the basis of blade element theory or by adopting one of a number of vortex theories. With the development of large-capacity digital computers it has been the vortex theories which have dominated present-day design analyses. It is possible to account for non-uniformity of the flow approaching the propeller (i.e. the hull wake in the presence of the propeller if this is known, or if not by an iteration process), blade thickness and width in the axial direction, and variations in cross section of the slipstream.

Two principal aims of propeller design are to calculate the pitch of each blade section to suit the mean circumferential wake velocity and direction at each radius and to derive the section shape compatible with minimum cavitation and other energy losses. Although the use of blade element theory (Section 7.4.2) attempts to do this it is unable to account for tip losses and the interference to the flow through the propeller by the blades themselves (which induces streamline curvature and velocity changes in the flow). A better description of the flow through a propeller is obtained from vortex theory (Section 7.4.1) which allows for radial variation in circulation and thus of the strength of the bound vortex (Sections 6.3.1 and 6.3.4) along each blade. As implied by Fig. 7.16, the system of vortices may be assumed to be concentrated along lines of corresponding vortex strength and so the associated theory is usually referred to as 'lifting-line theory'. Lifting-line theory was initially developed for ship propellers which could be considered lightly or moderately loaded (e.g. [44–46]). This theory then takes account of the velocities induced at the propeller by the vortex system, which represents the propeller and its slipstream, the bound circulation at the propeller and the circulation and pitch of the free vortex lines. No account is taken of the downstream variation of the induced velocities since it is assumed that a typical free vortex line lies along the surface of a cylinder of constant radius and is of constant axial pitch. In fact, the variation of the induced velocities causes the radius of the helicoidal free vortex line to decrease with increasing distance downstream whereas the pitch angle increases.

Each blade has, of course, a width in the flow direction, measured by the chord length, and so the blade should be considered a surface defined by the product of the chord length and the span. Furthermore, the streamline curvature resulting from the vortex system requires the mean line of the blade section to possess a camber (Section 6.3.2). Finally, for high efficiency and to minimize cavitation the mean line is clothed with a surface of finite thickness to produce a hydrofoil section. These additional factors are included in the lifting-surface theory as described in, for example, [47–49].

The assumption of moderate loading has in the past been considered satisfactory for ships at service speeds. In any case, it is thought that deficiencies in the lifting-line theory are largely swamped following the application of lifting-surface corrections. However, with present-day trends towards high-speed, large, single-screw tankers and bulk carriers the effects of slipstream deformation cannot be ignored. Thus, a method has been developed in [50] to adapt lifting-line theory for designs of highly loaded propellers. First, the lightly loaded analysis is worked out to give an initial approximation to the radial distribution of bound circulation and hydrodynamic pitch. The slipstream velocities and the deformation of the slipstream can then be determined. In the final part of the method a second lifting-line design is obtained for which the induced velocities are calculated as functions of the geometry of the deformed slipstream. Designs worked out by this theory show that propeller efficiencies are less than those deduced by the methods described in, for example, [44] and [51], sometimes by 6 per cent in the former case and 3 per cent in the latter. It is vital that energy conversion efficiencies are calculated as accurately as possible, otherwise the power installed could be insufficient to reach the desired service speed under the optimum operating conditions of the propulsion system.

Usually, propeller designs are based on established series using data from water tunnel tests and various propeller theories. Although a number of series now exist the most well known are probably those associated with the names of Troost, Gawn and Burrill. The results are generally presented in the form of charts and some examples are shown in [3]. The charts illustrate the relationship between open-water efficiency, advance coefficient, pitch-to-diameter ratio, and the delivered power of the propeller for propellers with different numbers of blades. A set of charts is also required to show the effect of blade area ratio (BAR), that is, the ratio of the total face area of the blades to the area of the propeller disc. For conventional propellers an empirical, overall blade pressure in the range 70–80 kPa ($\cong$ 0.65–0.75 tonf ft^{-2}) has often been adopted to avoid excessive cavitation effects. From the required thrust the BAR can then be calculated.

It has been implied so far that the blades are fixed to the hub; indeed the propeller and hub may be cast in bronze as one complete unit. However, there are some applications for which controllable pitch (CP) propellers are of great advantage. In these designs the blades can rotate about a radial pivot at the root which is activated by hydraulic pistons connected to crossheads in the hub. Thus, by adjusting the pitch angle of the blades, torque and thrust can be altered at a constant rotational speed so that a high efficiency is maintained over a wide range of operating conditions. The CP propeller can be made almost as efficient as the fixed pitch propeller at a given design condition, the only difference arising from the somewhat larger hub-to-tip diameter ratio needed to house the pitch-changing mechanism.

If the blade pitch can be changed sufficiently then astern thrust can be produced without the necessity for reversing gear boxes (in the case of reciprocating engines, such as the diesel) or astern turbines (for turbine-powered ships). Since changes in blade angle can often be carried out quicker than changes in shaft speed it is possible to obtain greater manoeuvrability. Typical examples of the use of CP propellers are (i) tugs which are either towing or running free and (ii) trawlers when trawling and when on passage to or from fishing grounds.

In recent years considerable attention has been brought to bear on the problem of hull vibration excited by strongly cavitating propellers. Attempts to alleviate the problem rely either on reducing the problem at source, that is at the propeller design stage, or applying some kind of palliative treatment to an existing hull–propeller combination. Clearly, the first technique is preferable but presents many difficulties as a result of the complex nature of the hull wake and the compromises called for in the overall ship design. The high amplitudes of the pressure fluctuations experienced by the hull arise from the unsteady nature of the cavitation, in particular the appearance followed by disappearance of back sheet and tip vortex cavitation over an angular range of 30° either side of top dead centre. This is a consequence of the wake distribution (see, for example, Fig. 7.19) and seriously curtails the propeller performance at maximum efficiency when the loading is high.

A technique for the control of cavitation under these adverse flow conditions is given in [52] where use is made of non-optimum, or arbitrary, spanwise load distributions to control the pressure amplitudes. The method is based on an earlier theory [50], but instead of using a minimum energy loss criterion for the optimum propeller an arbitrary radial distribution of the bound vortex is specified. Coefficients describing the prescribed vortex must then satisfy the basic design conditions. The principal dimensions of the propeller, for example diameter, blade width and thickness, can be deduced from combinations of the assessments in Sections 7.7–7.9, lifting-line and lifting-surface theories. The blade section camber and pitch angle can thus be deduced, making various viscous 'allowances', to produce the optimum blade based on the radial mean wake variation. However, it is now necessary to consider further the cavitation behaviour, especially near the propeller tip, by calculating the lift coefficient and the corresponding pressure distribution on blade sections as the given blade rotates through the complete wake. To avoid problems with tip cavitation the outer blade sections require reduced circulation compared with those at smaller radii. Thus, the slope $\partial\Gamma/\partial r$ of the optimum circulation curve shown in Fig. 7.26 (which may be likened to that of the finite-span aerofoil in Fig. 6.31) must be reduced at the tip and examples are shown for $|\partial\Gamma/\partial r|$ equal to unity and zero. In order to maintain a total lift force on the blade consistent with the appropriate contribution to the total thrust it is clear that Γ must be increased at the middle sections, as indicated in Fig. 7.26. Experiments have confirmed that a reduction of the tip circulation considerably delays the inception of tip cavitation and the associated hull and shaft vibration. It would appear that only a small penalty on efficiency and ship speed has to be paid.

An alternative solution of the cavitation excitation problem is described in [53]. Here the philosophy is to change the character of the ship wake so that the flow into the propeller is more uniform. The optimum propeller design using a mean wake is therefore a more realistic analytical tool since fluctuations of blade loading become less severe. It is not possible to alter the shape of the hull at the stern for a ship in service, and so to avoid fitting a new propeller the wake is modified by

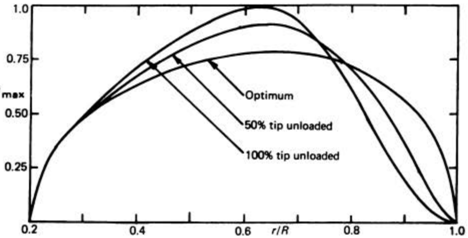

Fig. 7.26

adding small vanes, which act as flow deflectors, on each side of the hull close to the stern. The size and location of these vanes can be assessed in relation to the growth of the boundary layer. Although, as we have noted, the theory of viscous flows near the sterns of ships is far from complete it is, nevertheless, possible to predict the best position for the vanes at locations ahead of regions of low energy. Thus, by deflecting the boundary-layer flow the energy in the wake can be distributed more evenly. A check on predicted improvements was carried out with a series of model tests [53] which subsequently revealed a number of difficulties. Owing to Froude number scaling $(Re)_M < (Re)_P$ and so the boundary layer at the model stern was excessively thick. As a result, any full-scale predictions from model vanes fitted to model hulls which improved the model wake would most likely be of excessive span and too far forward for success at full scale. In this technique of vibration reduction it is therefore necessary to construct an empirical prediction method based jointly on theory and model testing so that the correct size and location of the vanes can be found.

7.11 Propulsion for High-speed Craft

If the conventional propeller is used for the propulsion of a high-speed vehicle it is clear that severe cavitation will take place. However, it is possible to design a supercavitating propeller which, although noisy, avoids cavitation damage and is relatively efficient. A supercavitating propeller system was incorporated in the design of the hydrofoil research ship HMCS *Bras d'Or* [54].

The discussion in Chapter 6 on supercavitating hydrofoils applies generally to the design of propeller blades. Curved, wedge-shaped hydrofoil sections based on those proposed by Tulin [55] and Johnson [56] are often used. Supercavitating propeller blade sections operate best when they are wedge-shaped with a sharp leading edge and an abrupt cut-off at the trailing edge. The surface corresponding to the back of the blade is then enveloped by a vapour cavity and collapse of this cavity does not occur near the blade.

An alternative series of propellers for operation up to and including the fully cavitating régime has been used to drive fast patrol boats [57]. The blade sections were not wedge-shaped and it was found that blades with a concave face showed superior performance in partially cavitating conditions. The use of this series and the Gawn–Burrill series of propellers in the context of high-speed craft is discussed in [58]. It is pointed out that efficiency is not the only criterion by which to select the dimensions of a fully cavitating propeller. When the Newton–Rader Series [57] are used and the BAR is large, for strength reasons, it is vital that the fully cavitating conditions are met at the design point. If the design speed is too low to yield sufficiently low local cavitation numbers the propeller loading represented by K_T/J^2 has to be increased above that corresponding to maximum efficiency. Unless this is done partially cavitating conditions prevail which could lead to face cavitation on propellers fitted to an inclined shaft. Propellers on fast craft normally operate in an oblique flow owing to the inclination of the shaft to the forward direction of the craft. Whereas blade forces fluctuate substantially under normal operation these fluctuations are significantly reduced when fully cavitating operation prevails.

It has also be found experimentally [59, 60] that the value of σ_L, defined by Equation (7.85), evaluated at $r = 0.7R$ must be less than 0.045 to give the best results. The practical zones of operation for screw propellers in terms of J and the cavitation indexes σ_N and σ_L are shown in Fig. 7.27. Note that for a given hull geometry and vehicle speed, with the shaft therefore at a fixed location, σ_N cannot be changed because V_A and $\bar{p}$ are set values. However, in Fig. 7.27 movement from one zone to another can be selected by changing J as a result of an adjustment to the rotational speed or, possibly, the diameter of the propeller. Provided that a propeller is designed initially for the fully cavitating condition its efficiency is superior to that of a conventional propeller which is cavitating.

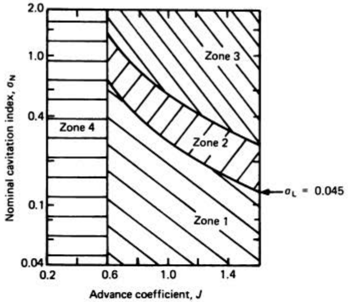

Fig. 7.27 Practical zones of operation for propellers. Zone 1, fully cavitating propeller best choice; zone 2, neither propeller is good choice; zone 3, conventional propeller best choice; zone 4, all propellers inefficient.

Controllable pitch propellers have also found use in high-speed marine vehicles, both in terms of water propulsion and air propulsion, for amphibious ACV [61–64]. There are two principal reasons why CP propellers are used. The first arises from the resistance characteristics of high-speed vehicles which show two distinct operating conditions of the propeller, namely, that at the design cruise speed and that at an off-design condition corresponding to the low- or medium-speed hump in the resistance. Although not always particularly noticeable for slender, round-form displacement hulls the problem can be severe at the shallow-water resistance hump of hovercraft. Furthermore, hydrofoil craft may require the same thrust at a take-off speed of, say, 10 m s^{-1} ($\cong$ 20 knots) as at the cruising foil-borne speed of 25 m s^{-1} ($\cong$ 50 knots). Use of fully cavitating, fixed pitch propellers for the design point will always result in overspeeding the prime mover at the hump speed, whereas non-cavitating propellers may become incompatible with the available torque. In both cases CP propellers use the full power available at the maximum rotational speed. The second reason for the popularity of CP propellers results from the need to shut off one or several prime movers when, for example, low-speed patrols are called for. Excessive resistance to motion by 'windmilling' propellers can be avoided by feathering if CP propellers are installed. The additional rapid stopping and reversing feature of CP blades when put into negative pitch is as important here as it is for conventional ships (see Section 7.10). Controllable pitch propellers, both conventional and fully cavitating, were used on HMCS *Bras d'Or* and are described in [54]. A similar dual system is advocated for the design study of a large hydrofoil ship of 24 MN (≅ 2400 tonf) displacement [65] but here, surprisingly, the identical propeller form is to be used for both foil-borne and hull-borne operation.

A rather special problem applies to hovercraft where the same power plant drives the lift fans and the air, or water, propeller. By using fixed gear ratios, lift-fan control requires changes in the output speed of the prime mover. If the propulsion power is to be varied simultaneously, but independently, then a CP propeller is required. An interesting development along these lines has been applied to the Vosper–Thorneycroft VT-2 (see Table 6.3 and [64]). Controllable pitch has been combined with a ducted propeller to reduce noise and the craft is fitted with two rotors each of about 4.1 m (13.5 ft) diameter as shown in Fig. 7.28.

A number of hydraulic-jet propulsion systems have been installed in high-speed vehicles, for example the Boeing Jetfoil (see Fig. 7.29), the Aerojet/Rohr SES 100A (see Table 6.3) and the *American Enterprise* (see [66]). It is suggested in [66] that a well designed jet system will be as efficient as the equivalent water-propeller system for planing craft up to 20 m (≅ 67 ft) long. Excellent manoeuvrability is obtained by using directional nozzles to provide a vectored thrust, even without forward motion. This technique has been included in the design study of a large surface-effect ship [67].

A fundamental principle of all high-speed vehicles is the minimization of resistance by raising as much of the craft out of the water as possible. This means that

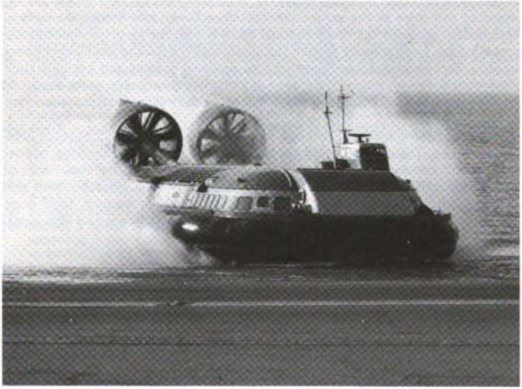

Fig. 7.28 Vosper–Thorneycroft VT-2 hovercraft showing ducted propellers.

Fig. 7.29 Boeing Jetfoil.

propellers run close to the air–water interface and may even broach the surface. Nevertheless, provided that the rotational speed is high the propeller remains fully wetted on the face (pressure side) of the blades with the back of the blades becoming dry. The additional conditions of high propeller loading and low cavitation number make the operation of this type of partially submerged propeller similar to the fully cavitating condition. Further details of partially submerged propellers may be found in [68].

It is clear, then, that a wide range of possible propulsors is available for high-speed vehicles. The choice largely depends on the duties required of the vehicle. Very careful assessment of fuel consumption is vital owing to the importance of cost, weight and space restrictions. Ease of maintenance and reliability must also be taken into account for both commercial and naval applications. Until more operational experience is gained these matters cannot easily be assessed with accuracy.

References

1. Canham, H. J. S. (1975), Resistance, propulsion and wake tests with HMS *Penelope*. *Trans. R. Inst. Nav. Archit.*, 117, 61–94.
2. Lighthill, M. J. (1960), Note on the swimming of slender fish. *J. Fluid Mech.*, 9, 305–17.
3. Todd, F. H. (1967), *Resistance and Propulsion*, Chapter 7 of *Principles of Naval Architecture* (ed. J. P. Comstock), Society of Naval Architects and Marine Engineers, New York.
4. Mueller, H. F. (1955), Recent developments in the design and application of vertical axis propellers. *Trans. Soc. Nav. Archit. Mar. Engrs*, 63, 4–30.

5. Kay, H. F. (1971), *The Science of Yachts: Wind and Water*, G. T. Foulis and Company Ltd, Henley-on-Thames, Oxfordshire.
6. *Symposium on the Future of Commercial Sail* (1975), Occasional Publication No. 2, Royal Institution of Naval Architects, London.
7. *Symposium on the Technical and Economic Feasibility of Commercial Sailing Ships* (1979), Liverpool Polytechnic.
8. *Symposium on the Viability of Commercial Sailing Ships* (1979), Ship and Marine Technology Requirements Board, Department of Industry, London.
9. *Symposium on Wind Propulsion of Commercial Ships* (1980), Royal Institution of Naval Architects, London.
10. Wellicombe, J. (1975), A broad appraisal of the economic and technical requisites for a wind driven merchant vessel. pp 57–80 of [6].
11. Nance, C. T. (1980), Wind power for ships – a general survey. Paper No. 1 of [9].
12. Rainey, R. C. T. (1980), The wind turbine ship. Paper No. 8 of [9].
13. Clayton, B. R. (1980), Discussion of [12].
14. Schaefer, G. W. and Allsopp, K. (1980), Kite sails for wind-assisted ship propulsion. Paper No. 9 of [9].
15. Flettner, A. (1924), Die Anwendung der Erkenntnisse der Aerodynamik zum Windantrieb von Schiffen. *Jahr. Schiffbautech. Ges.*, Hamburg.
16. Massey, B. S. (1979), *Mechanics of Fluids*, 4th Edn, Van Nostrand Reinhold, London.
17. Johnson, V. E. (1968), Waterjet propulsion. *Proc. 7th Symposium on Naval Hydrodynamics*, (ed. R. D. Cooper and S. W. Doroff), Office of Naval Research, Department of the Navy, Arlington, Virginia, DR-148, 1045–58.
18. Johnson, V. E. (1966), Waterjet propulsion for high-speed hydrofoil craft. *AIAA, J. Aircr.*, 3, 174–9.
19. Venturini, G. (1980), Waterjet propulsion in high-speed surface craft. *Proc. Conference on High-Speed Surface Craft*, 125–42, Kalhergi Publications, London.
20. Gunston, W. (1969), *Hydrofoil and Hovercraft*, Aldus Books, London.
21. Kort, L. (1934), The new nozzle screw propulsor. (in German), *Werft Reederei Hafen*, 15, No. 4, 41–3.
22. Van Manen, J. D. and Oosterveld, M. W. C. (1966), Analysis of ducted propeller designs. *Trans. Soc. Nav. Archit. Mar. Engrs*, 74, 522–62.
23. Anderson, O. and Tani, M. (1973), Experience with SS *Golar Nichu*. *Proc. Symposium on Ducted Propellers*, Royal Institution of Naval Architects, London, Paper No. 12.
24. Gibson, I. S. (1974), Theoretical studies of tip clearance and radial variation of blade loading on the operation of ducted fans and propellers. *J. Mech. Engng Sci.*, 16, 367–76.
25. Silverleaf, A. (1968), Prospects for unconventional marine propulsion devices. *Proc. 7th Symposium on Naval Hydrodynamics*, (ed. R. D. Cooper and S. W. Doroff), Office of Naval Research, Department of the Navy, Arlington, Virginia, DR-148, 885–917.
26. Barr, R. A. and Etter, R. J. (1975), Selection of propulsion systems for high-speed advanced marine vehicles. *Mar. Tech.*, 12, 33–49.
27. Froude, R. E. (1889), On the part played in propulsion by differences of fluid pressure. *Trans. Inst. Nav. Archit.*, 30, 390–405.
28. Glauert, H. (1963), *Aerodynamic Theory*, (ed. W. F. Durand), Chapter 4, Dover, New York.
29. Milne-Thomson, L. M. (1966), *Theoretical Aerodynamics*, 4th Edn, Macmillan, London.
30. Gibson, I. S. and Lewis, R. I. (1973), Ducted propeller analysis of surface vorticity and actuator disc theory. *Proc. Symposium on Ducted Propellers*, Royal Institution of Naval Architects, London, Paper No. 1.
31. Rankine, W. J. M. (1865), On the mechanical principles of the action of propellers. *Trans. Inst. Nav. Archit.*, 6, 13–39.
32. Taylor, D. W. (1911), *The Speed and Power of Ships*, John Wiley, New York. (Revised edition published by US Government Printing Office, 1943.)
33. Troost, L. (1950), Open water tests on modern propeller forms. *Trans. North-East Coast Inst. Engrs Shipbuild.*, 67, 89–130.
34. Gawn, R. W. L. (1953), Effect of pitch and blade width on propeller performance. *Trans. Inst. Nav. Archit.*, 95, 157–93.
35. O'Brien, T. P. (1962), *The Design of Marine Screw Propellers*, Hutchinson, London.
36. Van Manen, J. D. (1966), The choice of the propeller. *Mar. Tech.*, 3, 158–71.

37. Van Manen, J. D. (1960), *Fundamentals of Ship Resistance and Propulsion – Part B: Propulsion*, Publication No. 132a, Netherlands Ship Model Basin, Wageningen.
38. Mandel, P. (1969), *Water Air and Interface Vehicles*, MIT Press, Cambridge, Mass.
39. Oosterveld, M. W. C. and Van den Berg, W. (1976), Research in a depressurised towing tank on ducted propeller–hull interaction. *Proc. 3rd Lips Propeller Symposium*, Drunen, Netherlands, 97–110. (See also: *Int. Shipbuild. Prog.*, 23, 218–31, 1976.)
40. Meyerhoff, L., Hill, J. G. and Meyerhoff, S. (1972), Ducted propeller applications for modern ships. *Trans. Soc. Nav. Archit. Mar. Engrs*, 80, 136–69.
41. Todd, F. H. (1944), Discussion of the Paper 'On the working of supercavitating screw propellers', by V. L. Posdunine. *Trans. Inst. Nav. Archit.*, 86, 138–49. (See also [3] and [38].)
42. Boshuisen, D. C. and Versmissen, A. G. P. (1978), Cavitation observation techniques in the NSMB depressurised towing tank. *Int. Shipbuild. Prog.*, 25, 55–64.
43. Okamoto, H., Okada, K., Saito, Y. and Takahei, T. (1975), Cavitation study on ducted propellers on large ships. *Trans. Soc. Nav. Archit. Mar. Engrs*, 83, 168–90.
44. Lerbs, H. W. (1952), Moderately loaded propellers with a finite number of blades and an arbitrary distribution of circulation. *Trans. Soc. Nav. Archit. Mar. Engrs*, 60, 73–117.
45. Eckhart, M. K. and Morgan, W. B. (1955), A propeller design method. *Trans. Soc. Nav. Archit. Mar. Engrs*, 63, 325–74.
46. Kerwin, J. E. and Leopold, R. (1964), A design theory for subcavitating propellers. *Trans. Soc. Nav. Archit. Mar. Engrs*, 72, 294–335.
47. Cox, G. G. (1961), Corrections to the camber of constant pitch propellers. *Trans. R. Inst. Nav. Archit.*, 103, 227–43.
48. Pien, P. C. (1961), The calculation of marine propellers based on lifting surface theory. *J. Ship. Res.*, 5, 1–14.
49. Morgan, W. B., Silovic, V. and Payer, S. B. (1968), Propeller lifting-surface corrections. *Trans. Soc. Nav. Archit. Mar. Engrs*, 76, 309–47.
50. Glover, E. J. (1974), A design method for the heavily loaded marine propeller. *Trans. R. Inst. Nav. Archit.*, 116, 111–25.
51. Burrill, L. C. (1955–6), The optimum diameter of marine propellers: a new design approach. *Trans. North-East Coast Inst. Engrs Shipbuild.*, 72, 57–82 and D1–D22.
52. Glover, E. J., Thorn, J. F. and Hawdon, L. (1979), Propeller design for minimum hull excitation. *Trans. R. Inst. Nav. Archit.*, 121, 267–84.
53. Gadd, G. E. (1980), Flow-deflectors – a cure for vibration. *Nav. Archit*, No. 6, November, 238.
54. Davis, B. V. and English, J. W. (1968), The evolution of a fully-cavitating propeller for a high-speed hydrofoil ship. *Proc. 7th Symposium on Naval Hydrodynamics*, (ed. R. D. Cooper and S. W. Doroff), Office of Naval Research, Department of the Navy, Arlington, Virginia, DR-148, 961–1017.
55. Tulin, M. P. (1951), Supercavitating flows past foils and struts. *Proc. NPL Symposium on Cavitation in Hydrodynamics*, HMSO, London. (See also: Tulin, M. P. and Burkhart, M. P. (1955), Linearised theory for flows about lifting foils at zero cavitation number. *David Taylor Model Basin Rep.*, C-638.)
56. Johnson, V. E. (1957), Theoretical determination of low drag supercavitating hydrofoils and their two-dimensional characteristics at zero cavitation number. *NACA Rep. Memo.* No. L57 G1 1a.
57. Newton, R. N. and Rader, H. P. (1961), Performance data of propellers for high-speed craft. *Trans. R. Inst. Nav. Archit.*, 103, 93–129.
58. Kruppa, C. (1974), *The Design of Screw Propellers*, Chapter 18 of *High-Speed Small Craft*, (ed. P. Du Cane), David and Charles, Newton Abbot.
59. Tachmindji, A. J. and Morgan, W. B. (1958), The design and estimated performance of a series of supercavitating propellers. *Proc. 2nd Symposium on Naval Hydrodynamics*, Office of Naval Research, Department of the Navy, Washington, DC.
60. Venning, E. and Haberman, W. L. (1962), Supercavitating propeller performance. *Trans. Soc. Nav. Archit. Mar. Engrs*, 70, 354–417.
61. Hafström, H. G. (1973), Experiences of a multiple gas turbine machinery in fast patrol craft. *Trans. Am. Soc. Mech. Engrs, J. Engng Power*, 95, Ser. A, 2, 124–31.
62. Pehrsson, L. (1974), *Controllable Pitch Propellers*, Chapter 9 of *High-Speed Small Craft*, (ed. P. Du Cane), David and Charles, Newton Abbot.

63. Norrby, R. (1978), Controllable pitch propellers for small fast warships and patrol craft. *Proc. Symposium on Small Fast Warships and Security Vessels*, Paper No. 18, Royal Institution of Naval Architects, London, 241–52.
64. Wheeler, R. L. (1978), Recent United Kingdom hovercraft development, *J. Hydronaut.*, 12, 3–17.
65. Pieroth, G. (1978), Grumman design M163, a 2400 metric ton air capable hydrofoil ship. *AIAA/SNAME Advanced Marine Vehicles Conference*, Paper 78–749, San Diego, California.
66. Davison, G. H. (1979), Modern marine jet propulsion. *Nav. Archit.*, No. 6, November, 234–5.
67. McGhee, C. D. (1977), US Navy 3000-LT surface effect ship (3K SES) program. *Trans. Soc. Nav. Archit. Mar. Engrs*, 85, 396–418.
68. Kruppa, C. (1976), Practical aspects in the design of high-speed small propellers. *Proc. 3rd Lips Propeller Symposium*, Drunen, Netherlands, 39–49.

8
Control in Steady Planar Motion

8.1 Introduction

Any vehicle that is moving in or on a fluid must be capable of being controlled so that (i) a desired path can be maintained and (ii) the path may be changed in a controlled manner. It is normal to use the same device for both maintaining and changing the path and this device usually takes the form of one or more 'control surfaces'. These control surfaces are widely used because they are simple, cheap and reliable, and the main types are shown in Table 8.1.

In all its generality the theory of control-surface operation is very complicated. In this introductory chapter we shall therefore discuss only a simplified form of it in which:

(i) All motions are assumed *either* to occur parallel to a fixed plane, horizontally or vertically, or to involve roll alone;
(ii) Transient effects are ignored so that only *steady* manoeuvres are contemplated;
(iii) The actual flow conditions round the control surfaces and vehicles are not examined in any detail.

In practice adjustment of a rudder setting, for instance, causes a vehicle to drift, yaw *and* roll. The first two of these motions allow the helmsman to change direction.

Roll motion is strictly an angular *velocity* about a fore-and-aft axis and may occur in the steady motion of vehicles such as aircraft, missiles and rockets. The only comparable steady effect with marine vehicles entails a constant angular *heel* about a fore-and-aft axis. We shall not discuss the case in any detail although a simple theory (for constant angle of heel in terms of a constant stabilizer fin

Table 8.1 Common types of control surfaces.

Control surface	Motions chiefly affected when setting adjusted			
	Aircraft	Airship	Ship	Submarine
Aileron	roll	–	–	–
Elevator	heave and pitch		–	–
Hydroplane	–	–	–	heave and pitch
Rudder		drift and yaw		
Stabilizer	–	–	roll	–

deflection) is straightforward to formulate. (If on the basis of the theory a subsequent calculation is made of roll, it must be remembered that the calculation is not strictly compatible with the initial assumptions.) Dynamics problems in which allowance *is* made for three-dimensional motions are studied in Chapter 10 and as we shall see the theory is then rather more sophisticated.

Problems concerned with transient motion are also discussed in Chapter 10 and so only *steady* motion, in which fluid forces are not dependent on time, will be discussed here. Inertia forces do occur of course, but we shall assume that, if they are applied to a body, they are constant.

It is difficult to analyse the flow round any fluid-borne vehicle with any precision and practically impossible for a conventional control surface, particularly where marine vehicles are concerned. This statement may be reinforced, in the case of marine vehicles, by considering the following three sources of difficulty:

(i) the control surfaces of marine vehicles have low aspect ratios so that the effects of three-dimensional flow are marked;

(ii) usually one tip moves near a relatively large hull; and

(iii) flow round a control surface is usually greatly influenced by flow into or out of a propeller.

Obviously something more 'practical' is needed than, for example, the rather refined theory of oblique inviscid flow round a symmetric body. Consequently, the present treatment consists of a linear theory of the motions specified by the above limitations.

8.2 Steady Two-dimensional Parasitic Motion of a Symmetric Body

Consider a rigid body which possesses a plane of symmetry and which moves in such a way that its plane of symmetry remains always in the same fixed plane. The body then executes what may be thought of as a 'steady reference motion' when proceeding in this 'intended attitude' at a fixed speed V_{ref}, as shown in Fig. 8.1. Our purpose now is to examine the execution, in a controlled manner, of departures from this reference motion – departures that can conveniently be referred to as 'parasitic motions'.

There are two distinct ways in which the body may depart from the reference motion. The parasitic motion may be one of translation, or one of rotation. (A combination of the two is also possible, as we shall see.) Assuming that all points of the body move only parallel to a fixed plane the motions are of the types shown in Figs. 8.2(a) and (b) where, in each case, the second diagram indicates the combined motion due to the reference motion and the parasitic motion shown in the first. The reference point C lies on the plane of symmetry, and for the parasitic motion

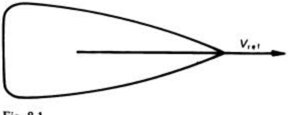

Fig. 8.1

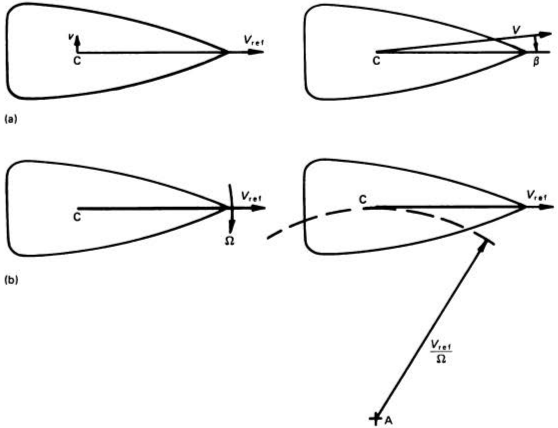

Fig. 8.2

of translation the resultant velocity V of the body is the vector sum of the reference velocity V_{ref} and the parasitic transverse velocity of translation v. The resultant velocity vector is thus at an angle β to the reference direction and Fig. 8.2(a) shows the chosen direction for positive β. Figure 8.2(b) shows the chosen positive direction for rotation about C, represented by angular velocity Ω, imposed on the reference velocity. The path followed by the body is circular (for constant V_{ref} and Ω) with centre at A and a radius given by V_{ref}/Ω. The parasitic motions have different names according to whether the motion occurs in the vertical or the horizontal plane, as shown in Table 8.2.

Table 8.2 Definitions of parasitic motions.

	Parasitic motion	
Plane of motion	Translation (Fig. 8.2(a))	Rotation (Fig. 8.2(b))
Horizontal	drift (or 'sway')	yaw
Vertical	heave	pitch

Although these motions may exist separately we need also to consider combinations of them. There are two possibilities for steady combined motion and these are illustrated in Fig. 8.3. A parasitic transverse velocity to starboard is shown in Fig. 8.3(a) and Fig. 8.3(b) depicts a parasitic transverse velocity to port.

The problem before us is the control of marine vehicles as they execute steady plane motions of the types shown in Figs. 8.2 and 8.3. No motion is contemplated perpendicular to the plane of the diagrams. It follows, therefore, that the body must experience no net applied force out of the plane of motion and no net applied couple about an axis in that plane. The distribution of the fluid forces must therefore conform to these requirements.

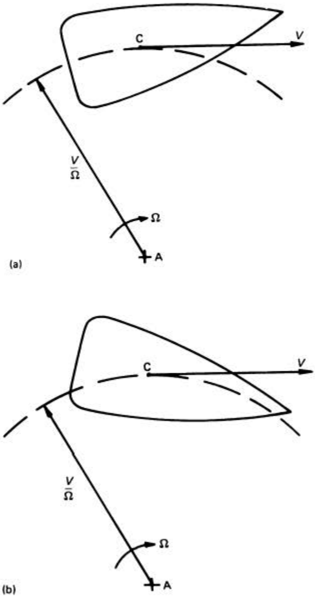

Fig. 8.3

8.2.1 *Parasitic Motion of Translation*

Suppose that the body executes a parasitic motion of translation alone, either in heave or drift. In discussing the fluid forces exerted on it we shall purposely obscure the distinction between two- and three-dimensional régimes. It will be helpful to consider the body as being infinitely long perpendicular to the plane of the diagram in Fig. 8.4. The point C represents the centre of mass of a transverse slice of the body and rectangular coordinates Cx, Cy are centred on C as shown. We now consider motion only parallel to the plane Cxy; let this motion be one of translation V so that β is an angle of incidence and is positive in Fig. 8.4.

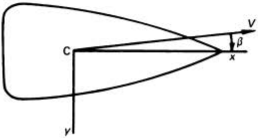

Fig. 8.4

Now instead of considering flow round the body in any detail a number of far-reaching, and admittedly gross, simplifying assumptions are made. First, however, it may be noted that the fluid force per unit span F' (the span being measured along the Cz axis perpendicular to the plane Cxy) can be resolved into lift and drag components, respectively perpendicular and parallel to the direction of V. Alternatively, F' may be resolved in the directions Cx, Cy to obtain fluid forces per unit span X' and Y'. In either case the component of fluid force exerted *on* the body is always in the opposite direction to the corresponding component of the velocity. This means that X' acts along $-$Cx for the configuration shown in Fig. 8.4 and Y' acts parallel to Cy. We now assume that:

(i) These forces X' and Y' (both per unit span) act on the axis Cx at an identifiable point H called the 'hydrodynamic centre'. (This is the usage *we* shall adopt; it is not unique.)

(ii) The first assumption remains true even though the body is not of infinite length in the Cz direction. Indeed, most marine vehicles have quite a small aspect ratio (i.e. small span) and some have a large degree of taper and no plane of symmetry parallel to Cxy.

In other words, F', X' and Y' are taken as forces F, X and Y (and not forces per unit span) and C is taken as the centre of mass of a finite body. The fluid forces applied to this body are therefore as shown in Fig. 8.5 in which X is positive rearwards and Y is positive to starboard. We shall now consider that this system is identified with a control surface, the immersed portion of a ship's hull and the hull of a submarine. It must, of course, be admitted that the accuracy of the resulting predictions for all but the smallest departures from the reference motion would be unacceptable in practice. Nevertheless, it is possible to examine the nature of some important features without recourse to complicated analysis.

Unless the centre of mass C happens to lie on the line of action of F – and in

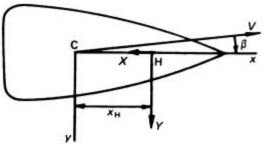

Fig. 8.5

general it does not – the fluid force will have a moment $M_C = Yx_H$ about C. Note that the magnitude and sense of M_C depends not only on the magnitude and line of action of F, but also on the position of C *relative* to H. For most bodies (in which C is more or less amidships) H is forward of C.

The value of dimensional analysis, applied to the physical variables affecting the motion of a body in a fluid, has been discussed in earlier chapters. The same principles may be used here in order to assemble a collection of dimensionless groups and thence describe the problem in the form of a functional relationship between the groups. Thus, the fluid forces X and Y and moment M_C may be expressed as

$$C_X = \frac{X}{\frac{1}{2}\rho V^2 l^2} = \phi_1(Re, Fr, Ma, \beta, \text{shape}) \tag{8.1}$$

$$C_Y = \frac{Y}{\frac{1}{2}\rho V^2 l^2} = \phi_2(Re, Fr, Ma, \beta, \text{shape}) \tag{8.2}$$

$$C_{M_C} = \frac{M_C}{\frac{1}{2}\rho V^2 l^3} = \phi_3(Re, Fr, Ma, \beta, \text{shape}) \tag{8.3}$$

where ϕ again means 'some function of' and all of the preceding functions are different. The definitions of Reynolds number (*Re*), Froude number (*Fr*) and Mach number (*Ma*) are given in Chapter 4. The length l represents a characteristic length of the body (e.g. its overall length in the plane Cxy) and ρ represents the density of the fluid. Clearly, the force and moment coefficients are functions of the angle β and also of parameters representing the shape of bodies of different homologous series. It is not uncommon to see l^2 replaced by the projected area A of the body in either the Cxy plane or the Cxz plane, or alternatively l replaced by $\nabla^{1/3}$, where ∇ is the immersed volume.

In addition to the above dimensionless groups, others may be required for a study of control problems. For example, if the 'body' is a marine rudder aeration may occur so that air is drawn down from the water surface to form a tip bubble, depending largely on how close the root is to the water surface. If this happens it may be necessary to introduce the Weber number

$$We = \frac{V^2 R}{K}$$

where R represents, for example, the radius of the leading edge of the rudder and K represents the coefficient of kinematic capillarity (i.e. surface tension/ρ).

Again it may be necessary to consider a 'cavitation number' σ if the body is, say, a hydroplane on the surface of which cavitation takes place. Nevertheless, we shall ignore these latter possibilities along with *Ma* since speeds are low enough to ignore the effects of compressibility. Thus, for a given body and a given fluid, the only dimensionless independent variables we need are *Re*, *Fr* and β.

Suppose an experiment is conducted on a given body in which *Re* and *Fr* are held constant as β is varied. (This does not mean that β will be a function of time, but rather that we examine a series of steady states.) According to Taylor's theorem we should expect that, for C_Y as an example,

$$C_Y = \beta\left(\frac{\partial C_Y}{\partial \beta}\right)_{\beta=0} + \frac{\beta^2}{2!}\left(\frac{\partial^2 C_Y}{\partial \beta^2}\right)_{\beta=0} + \ldots, \tag{8.4}$$

there being no constant term because the body is symmetric. Since the sign of C_Y must change when that of β changes, and since the body is symmetric about Cx, partial derivatives of even order will be zero. Thus, to a first approximation for small β, we should expect that

$$C_Y = \beta\left(\frac{\partial C_Y}{\partial \beta}\right)_{\beta=0} \tag{8.5}$$

where $(\partial C_Y/\partial\beta)_{\beta=0}$ is a function of *Re* and *Fr*.

By a similar argument we may conclude that, for small β,

$$C_{M_C} = \beta\left(\frac{\partial C_{M_C}}{\partial \beta}\right)_{\beta=0}. \tag{8.6}$$

The coefficient C_X is rather different because it is not equal to zero when $\beta = 0$ and it is also an even function of β. The predicted proportionality of C_Y and C_{M_C} to β can be examined by experiment, and it is found that the accuracy of the approximation is often quite acceptable.

As we have already noted

$$M_C = Yx_H, \tag{8.7}$$

where positive M_C is taken as acting clockwise in Fig. 8.5. In dimensionless form we may write

$$C_{M_C} = C_Y x'_H \tag{8.8}$$

where

$$x'_H = \frac{x_H}{l}. \tag{8.9}$$

It is important to note that while the value of x'_H is constant for a given steady motion, it is not the same for all operating conditions.

8.2.2 *Parasitic Motion of Rotation*

Let us return to the body of infinite span perpendicular to the plane Cxy but this time suppose the body has an angular velocity Ω superimposed on the reference velocity V_{ref}, as shown in Fig. 8.2(b). The fluid force per unit span F' can be resolved into components X' and Y' parallel to Cx, Cy respectively. Again X' acts along −Cx. We now make similar assumptions to those in the previous section, that is,

(i) The forces X' and Y' (both referred to unit span) act at an identifiable hydrodynamic centre J on the axis Cx.
(ii) This remains true for a body of finite span so that C is taken as the centre of mass of the body and X' and Y' are replaced by X and Y forces.

The fluid forces and positive Ω are therefore as shown in Fig. 8.6.

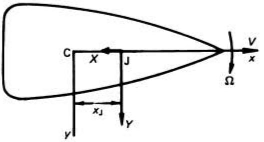

Fig. 8.6

A somewhat rudimentary line of reasoning suggests that the fluid exerts (i) a large net couple acting in such a direction as to oppose the yaw (i.e. counterclockwise in Fig. 8.6) and also (ii) a small side force Y of uncertain sign whose line of action may intersect Cx on either side of C.

If these two actions are combined to give the statically equivalent system of Fig. 8.6, it is easy to show that

(i) x_J is of uncertain sign and may be extraordinarily large, and
(ii) the net fluid moment

$$M_C = Yx_J \tag{8.10}$$

will act in the opposite direction to Ω and so be negative.

If required, X, Y and M_C may again be put in dimensionless form as before and l used as a characteristic length. Consequently, it is assumed that, in particular

$$C_Y = \frac{Y}{\frac{1}{2}\rho V^2 l^2} = \phi_4(Re, Fr, Ma, \Omega', \text{shape}), \tag{8.11}$$

where ϕ_4 represents another unknown function. In Equation (8.11) the dimensionless form of the angular velocity is given by

$$\Omega' = \frac{\Omega l}{V}. \tag{8.12}$$

For marine applications the effects of Ma are negligible and so the relevant independent variables for a given body are Re, Fr and Ω'. Following the preceding development we again imagine a series of experiments to be performed, all at the same Re and Fr, so that for small angular velocities

$$C_Y = \Omega' \left(\frac{\partial C_Y}{\partial \Omega'}\right)_{\Omega'=0}. \tag{8.13}$$

A similar result holds for C_{M_C}. Furthermore,

$$C_{M_C} = C_Y x'_J \tag{8.14}$$

where

$$x'_J = \frac{x_J}{l}. \tag{8.15}$$

Again, x'_J is only constant for given values of V and Ω.

8.2.3 *Combined Translation and Rotation*

Figure 8.3 shows that there are two admissible forms of steady combined motion in which both parasitic motions are performed simultaneously. In theory we could at least proceed as before and define a 'hydrodynamic centre' for the combined motion. If this were done an appropriate sign convention for the components of the resultant fluid force F would need to be defined. We should also have to accept the complication that may be seen in Fig. 8.3, namely, that the angle of incidence and the velocity vary from point to point along Cx.

Instead of proceeding along these lines we shall now make a fresh assumption: henceforth we shall consider only 'small' parasitic motions.

Suppose the composite motion is as shown in Fig. 8.7. The velocity V and angle of incidence β are arbitrarily defined as those prevailing at C. There will once more be a resultant fluid force F which can be resolved into components X and Y. These components may be made dimensionless as before so that we may expect the following functional relationship to hold:

$$C_Y = \phi_5(Re, Fr, \beta, \Omega'). \tag{8.16}$$

Thus, to a first approximation for small parasitic motions, Taylor's theorem shows that

$$C_Y = \beta \left(\frac{\partial C_Y}{\partial \beta}\right)_{\beta=0=\Omega'} + \Omega' \left(\frac{\partial C_Y}{\partial \Omega'}\right)_{\beta=0=\Omega'}. \tag{8.17}$$

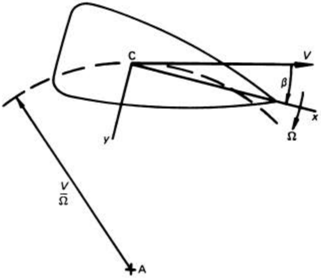

Fig. 8.7

Similarly

$$C_{M_\mathrm{C}} = \beta \left(\frac{\partial C_{M_\mathrm{C}}}{\partial \beta}\right)_{\beta=0=\Omega'} + \Omega' \left(\frac{\partial C_{M_\mathrm{C}}}{\partial \Omega'}\right)_{\beta=0=\Omega'}. \tag{8.18}$$

In other words, both C_Y and C_{M_C} have the values obtained from superimposing the translation and the rotation separately on the reference motion. The dimensionless force C_X, on the other hand, is given approximately by

$$C_X = C_\mathrm{T} + \frac{\beta^2}{2!}\left(\frac{\partial^2 C_X}{\partial \beta^2}\right)_{\beta=0=\Omega'} + \frac{\Omega'^2}{2!}\left(\frac{\partial^2 C_X}{\partial \Omega'^2}\right)_{\beta=0=\Omega'} \tag{8.19}$$

where C_T is the coefficient of total resistance in the absence of parasitic motion. We may recall that the force X and the total resistance for the reference motion R_T are both in the opposite direction to V_{ref} and are therefore directed along $-\mathrm{C}x$.

Equations (8.17) and (8.18) suggest that the body shown in Fig. 8.7 can best be thought of as having the fluid forces indicated in Fig. 8.8 acting on it. Subscripts H and J are used to distinguish the two transverse forces. That is, Y_H would act at H if there were no angular velocity Ω, and Y_J would act at J if there were no angle of incidence β. The total force X merely acts along $-\mathrm{C}x$ and there is no point in separating it into identifiable components in the same way.

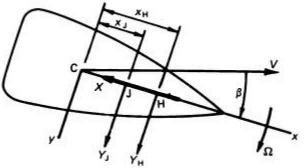

Fig. 8.8

The fluid forces X, Y and the moment M_C are of major importance in the problems to be investigated. It is therefore natural to ask whether or not they can be calculated. Briefly and roughly they are far easier to estimate for a parasitic translation than for a rotation. A great deal of relevant data from the field of aerodynamics are available for the steady flow of a constant-density fluid past a symmetric body when there is a constant angle of incidence.

Data are rather more scarce for the effects of the parasitic angular velocity Ω. This is not because the problem is of less importance in aeronautics, but rather it is far more difficult to solve. The reason is that yawing cannot be studied as a problem of steady flow, but some ground can be gained by developing the techniques suggested in Chapter 5.

In the discussion of the dynamics of marine vehicles in Chapter 10 we shall examine ways of *measuring* the various components of fluid force. It transpires that all of those mentioned so far can be measured fairly readily by means of models.

8.3 Steady Motion of Control Surfaces

We have referred so far to a body rather than to a control surface or a hull. From now on it will be necessary to distinguish between the motion of a control surface and that of the vehicle to which it is attached. The convention shown in Table 8.3 will therefore be adopted.

Table 8.3 Convention for symbols.

Quantity	Symbol used for: Discussion in Section 8.2	Control surface	Vehicle or hull
Velocity of C	V	U	V
Angle of incidence	β	α	β

Suppose that the 'body' referred to in the previous section now has a symmetric hydrofoil section. For our present purposes it is assumed to be well separated from the hull (or fuselage) to which it is attached so that the flow onto it is 'clear'. The body has our postulated symmetry and can be thought of as moving always in a plane (and never parallel to its own axis of rotation). Within our assumptions it is thus possible to describe the motion of a control surface such as that shown in Fig. 8.9(a) in terms of that shown in Fig. 8.9(b). That is, the body will now be identified with a control surface.

The control surface represented in Fig. 8.9(a) may be taken to be typical of spade rudders (used extensively on naval ships), hydroplanes on submarines and stabilizers. More details on these devices are given later, but here we need only note that for the trapezoidal planform shown b_H is the span corresponding to the section containing the hydrodynamic centre H. The overall size of a conventional control surface is usually far smaller than the vehicle to which it is attached and, furthermore, the linear dimensions are a good deal less than the radius of its turning circle during rotation. This implies that U and α scarcely vary along the fore-and-aft axis of symmetry (the chord length) at any spanwise location on the control surface. Consequently, the effects of rotation on the behaviour of the control surface are negligible and so only translation needs to be examined.

If the angular velocity Ω can be neglected in *steady* motion, it is permissible to neglect inertia forces also since the body translates only with constant speed. With negligible inertia forces the centre of mass C is no longer of concern, and only the hydrodynamic centre and the axis of the stock OO are therefore shown in Figs. 8.9(a) and (b). The position of H is determined by (i) the angle of incidence α, (ii) the velocity U, and (iii) the geometry of the control surface, all of which are constant (or are assumed so) for steady flow. Thus for operation in clear flow the geometry of the motion will be as shown in Fig. 8.10. The angle of incidence α and the angle of deflection ξ depicted in Fig. 8.10 are considered positive. The forward velocity U of the control surface relative to the fluid has neither the magnitude nor the direction of the velocity V of the vehicle. This is because (i) the presence of the vehicle in the fluid may significantly change the streamline pattern about the control

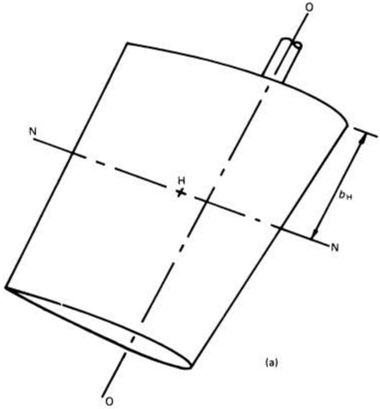

Fig. 8.9

surface from that experienced by the control surface with the vehicle absent and (ii) the point O on the control surface lies at a greater distance from A than does C.

8.3.1 *Forces and Moment Applied to the Hull*

The fluid forces X and Y act at H. (The subscripts H and J are dropped for the control surface as there is no significant force associated with J.) The resultant fluid force F may be resolved into any pair of convenient directions (not only those of X and Y, along and perpendicular to the NN axis respectively, as shown in Fig. 8.11). Now a designer will be concerned principally with the directions along and across Cx, the axis of symmetry of the parent vehicle, for it is to obtain the force component perpendicular to Cx that the control surface is installed. Let us therefore resolve F accordingly, as in Fig. 8.12, and thereby obtain

$$P = X \cos \xi + Y \sin \xi \tag{8.20}$$

$$Q = -X \sin \xi + Y \cos \xi \tag{8.21}$$

where the deflection of the control surface, ξ, is positive. Clearly, when ξ is negative

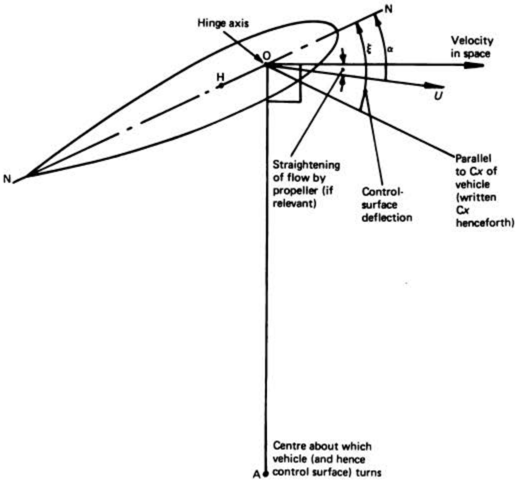

Fig. 8.10

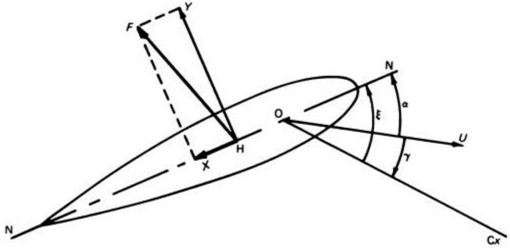

Fig. 8.11

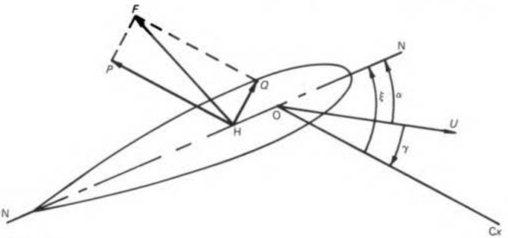

Fig. 8.12

we must replace Y in Equations (8.20) and (8.21) by $-Y$. It follows that P always acts in the $-Cx$ direction, but the sign of Q is opposite to that of ξ. The system of fluid forces acting on the control surface can be represented as shown in Fig. 8.13, where 'flow straightening' is neglected.

A positive clockwise moment M_O is applied *by the fluid to the control surface* about the axis OO and will be given by (see Fig. 8.11)

$$M_O = Y \cdot \overline{OH} \tag{8.22}$$

if H is abaft O. This moment is counteracted by a torque in the stock whose magnitude is equal to M_O but in the opposite direction. Thus

$$G_O = Y \cdot \overline{HO} = -M_O \tag{8.23}$$

as shown in Fig. 8.13. The signs of M_O and G_O are reversed, of course, when α is negative.

The control surface has to be dragged through the fluid by the vehicle, which must overcome the force P (i.e. a resistance) to do so. We would normally wish the magnitude of P to be a minimum, which suggests that the magnitudes of α and γ must be kept small for control purposes. The force Q is applied (y the stock and its reaction on the parent vehicle provides the reason why the control surface is

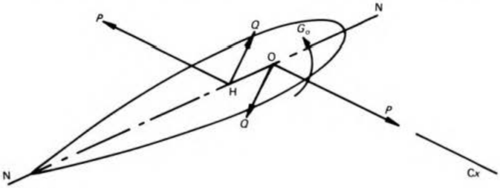

Fig. 8.13

installed. As far as possible, therefore, we wish to maximize the magnitude of Q for given values of α and γ. The torque G_O must be applied to the control surface by its operating gear.

If the magnitude of the deflection angle ξ is always small, then to a first approximation

$$P = X \tag{8.24}$$

$$Q = Y. \tag{8.25}$$

It follows that a designer would prefer to have a fairly large value for the magnitude of

$$\left(\frac{\partial C_Y}{\partial \alpha}\right)_{\alpha=0}.$$

Unfortunately, a large value of this parameter usually implies that a hydrofoil section will stall (see Section 6.3.3) at a small angle of incidence. Furthermore, problems of control become severe since one would then be concerned with very small changes in α accompanied by large forces and torques.

The question of how large the operating shaft of a control surface should be is a vitally important one. In general, it must sustain the operating torque, bending, and direct loading, and it must be stressed accordingly. The stress calculations are often based on drastic simplifications. In particular it is usual to regard the loading as being essentially static, and thus the theory of Chapter 3 can be used where appropriate. While it is not our purpose to discuss this subject here it will be of use to introduce it briefly by reference to 'spade'-type control surfaces, that is surfaces supported solely by their stocks, such as the example shown in Fig. 8.9. The bending moment in the stock at the root of the control surface might be taken as

$$(X^2 + Y^2)^{1/2} \times b_H.$$

in view of the equivalent force system shown in Fig. 8.11. Note that the position of H depends *inter alia* on the angle of incidence.

8.3.2 *Lift and Drag Forces*

It has been explained that, to all intents and purposes, control surfaces perform only a significant parasitic motion in translation. Without rotation and the uncertainty of locating the side force, there is no ambiguity in the definition of α. When this is the case it is common to refer to lift and drag components rather than to X and Y (or X_H, Y_H). Since the literature is largely based on this alternative approach it is worthwhile illustrating it here.

The theoretical approach and the assumptions made for the fluid forces remain as before, so that, in particular, we may still refer to a 'hydrodynamic centre' H. The fluid force F is resolved in the directions along (the drag force, D) and perpendicular to (the lift force, L) the velocity U, as shown in Fig. 8.14. (The directions of L and D shown in Fig. 8.14 are by convention positive.) The dimensionless force coefficients are then

$$C_L = \frac{L}{\frac{1}{2}\rho U^2 l^2}; \qquad C_D = \frac{D}{\frac{1}{2}\rho U^2 l^2} \tag{8.26}$$

and the fluid moment about the centre of mass C is exactly as before (except that

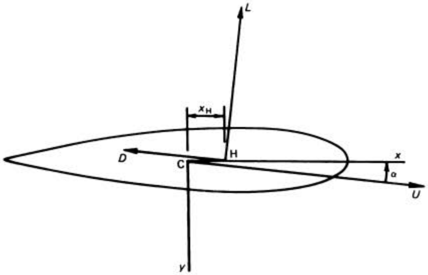

Fig. 8.14

both L and D contribute to M_C instead of just Y). Moreover, for small α,

$$C_L = \alpha \left(\frac{\partial C_L}{\partial \alpha} \right)_{\alpha=0} \tag{8.27}$$

where the slope of the lift curve at $\alpha = 0$ depends principally on *Re* and *Fr* for most marine vehicles.

The relationship that exists between X and Y on the one hand and L and D on the other is easily shown to be

$$X = -L \sin \alpha + D \cos \alpha \tag{8.28}$$

$$Y = -L \cos \alpha - D \sin \alpha. \tag{8.29}$$

Both X and Y are negative quantities for the system shown in Fig. 8.14. If the angle of incidence is small, then to a first-order approximation

$$X = D \tag{8.30}$$

$$Y = -L \tag{8.31}$$

$$M_C = -Yx_H = Lx_H, \tag{8.32}$$

which is an anticlockwise moment.

Most of the data available for control surfaces are presented in terms of lift and drag forces [1], but note that this approach is not so helpful for bodies which can possess significant angular velocity (such as hulls).

Care has been taken always to relate fluid forces and moments to α, the angle of incidence, and not to ξ, the angle of deflection. If the 'straightening of flow' effect that is sometimes allowed for (as shown in Fig. 8.10) is neglected the situation shown in Fig. 8.15 arises. It is necessary to distinguish carefully between three angles: α the angle of incidence; γ the angle of incidence that the control surface would have (due to motion of the parent vehicle) if it were undeflected; and ξ the angle of deflection.

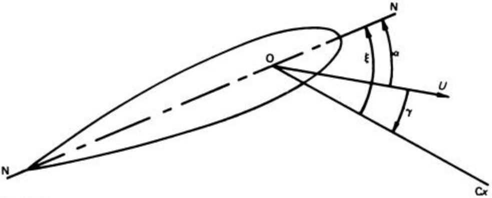

Fig. 8.15

The fluid forces X, Y and the moment M_O applied to the control surfaces correspond to the angle of incidence α, which means that P, Q and G_O also correspond to this angle of incidence. However, these quantities may be equally thought of as corresponding to $\xi - \gamma$. This is a convenient approach in the *dynamics* of marine vehicles.

8.3.3 *Some Practical Considerations*

It has been shown that a designer would like to have large values of both (i) $(\partial C_L/\partial\alpha)_{\alpha=0}$ or $(\partial C_Y/\partial\alpha)_{\alpha=0}$ and (ii) the stalling angle. These two requirements are to some extent mutually opposed. The first is promoted by having a suitable foil section for the control surface and by having a large aspect ratio. The effect of aspect ratio on the lift coefficient for a given hydrofoil section is shown schematically in Fig. 8.16. For thin hydrofoil sections, operating at high Reynolds numbers,

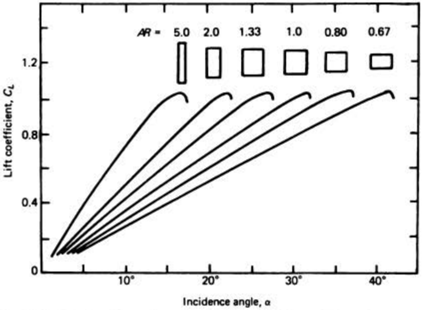

Fig. 8.16 Relative effect of aspect ratio $\mathcal{R}$ on the lift coefficient of rectangular plan aerofoils.

Equation (6.43c) of Section 6.3.4 can be used to determine the slope of the lift curve of a rectangular-plan hydrofoil. It can be seen in Fig. 8.16 that aspect ratio has little effect on the maximum value of C_L for a given hydrofoil. Unfortunately, a high aspect ratio not only tends to produce early stall (i.e. at low α) but also raises questions of strength and of vulnerability to obstructions.

The quantities $(\partial C_L/\partial\alpha)_{\alpha=0}$ and stalling angle are clearly of great importance. As a consequence they are studied experimentally in wind tunnels, water tunnels and water channels. The results of these tests are tabulated for different profiles (i.e. shapes in side view), section shapes, tip shapes, directions (ahead or astern) and so on. In addition, a variety of *ad hoc* model tests are conducted on control surfaces, including simulated hull effects and free-running models. The best response from control surfaces occurs when they are fitted close to the hull. This precept is followed in warship design but is often completely discarded where ships such as tankers are concerned.

Inevitably empiricism creeps into the theory of control surfaces, because any usably simple theory must perforce be very highly idealized. Considerable emphasis is therefore made on the compilation and mode of presenting data[1]. Some of these data will be summarized and discussed in Section 8.6.

8.4 Control of Steady Motion in the Horizontal Plane

We turn now from an isolated control surface to something which at first sight may seem very different – the hull of a marine vehicle. To a very good approximation it may be assumed that the forces acting on a hull in a direction normal to the water surface are in equilibrium. Unless there is an excessive list a vertical plane of symmetry will determine Cx for most vessels, again at least to good accuracy. In short, the conditions of our earlier discussions are met. The hull itself acts as a very large control surface, albeit an inefficient one.

Motion is taken to be in the horizontal plane and, for the sake of definiteness, reference is made to a conventional surface ship. It must be noted at the outset that yaw motion is not negligible. (The minimum diameter of a ship's turning circle is as little as three or four ship lengths; thus V and β vary significantly from point to point along the centre line.) It has already been explained that H normally lies forward of C when C is placed in the midships region. Moreover, x_J may be positive or negative according to whether J is forward or aft of C (although the product $Y_J x_J$ is always negative). Note that, in the figures, H and J are both placed forward of C so as to indicate what positive x_H and x_J imply.

Suppose that a ship under way performs a small parasitic motion of drift only, so that it is subjected to a fluid force which has a nonzero moment M_C. The ship will therefore commence to accelerate in yaw. In other words, a steady motion cannot generally exist in which the ship drifts without yawing. If instead the ship yaws without drift (so that its fore-and-aft axis is always tangential to its circular path), the fluid force again produces an unbalanced moment about C. This will tend to swing the centre line Cx out of the tangential direction and so produce drift. We conclude that *steady* motion must either take place along a straight path containing Cx or else it must entail both yaw and drift together.

The purpose of a rudder is to control the combined motions of yaw and drift. The question of how a rudder functions in this capacity is considered shortly. First, however, the possibility of yaw and drift of the hull *without* a rudder needs to be examined, and this requires an investigation of directional stability.

8.4.1 *Directional Stability of a Hull*

A ship with its rudder held undeflected (i.e. in the fore-and-aft direction) would be expected to be capable of only motion ahead. It is found in Chapter 10 that under certain circumstances motion ahead can be only a theoretical possibility rather than an actual capability. If the vehicle is directionally unstable, steady motion in the horizontal plane without any parasitic motion is not possible, for any slight departure from straight ahead motion will be magnified by the fluid forces. On the other hand, if the ship is directionally stable a slight disturbance will tend to die away.

The phenomenon of directional instability is now introduced in a preliminary and elementary fashion. The discussion is based on the fact that when a ship is actually *at* the boundary of instability it will depart from motion ahead infinitely slowly. During this departure we assume that steady conditions prevail and suppose that the ship turns to starboard. The forces acting on the ship are then as shown in Fig. 8.17, except that those in the fore-and-aft direction have been omitted. (The force X is balanced by the propulsor thrust T.) Evidently, for small β and Ω,

$$Y_J + Y_H = mV\Omega \tag{8.33}$$

for equilibrium of forces perpendicular to Cx and, on taking moments about an axis through C perpendicular to the plane Cxy we obtain, for steady motion,

$$Y_J x_J + Y_H x_H = 0. \tag{8.34}$$

However, if the sum of the moments of the external fluid forces obeys the condition

$$Y_J x_J + Y_H x_H < 0, \tag{8.35}$$

there is a net moment about the centre of mass C tending to nullify the angular velocity Ω (and hence β). This, then, is a rough-and-ready criterion of directional stability. When we discuss unsteady motion we shall examine the implication of this criterion. (This is in fact a degraded form of the correct inequality which must be satisfied if directional stability is to prevail, and it is not suggested that this

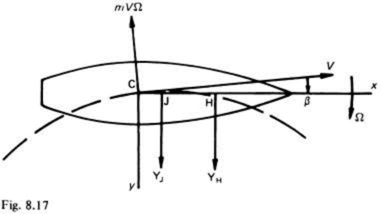

Fig. 8.17

derivation of it is satisfactory, or even persuasive. Our purpose at this stage is merely to point out that there is the possibility of a problem.)

8.4.2 *Hull–Rudder Combination*

By installing a rudder, forces P and Q can be applied along and perpendicular to the centre line of the hull. Suppose initially that a ship has its rudder attached at the point O shown in Fig. 8.18(a). This is, admittedly, an odd place to put it but we can always place O aft of C if required. The forces applied to the hull may be regarded in the alternative way shown in Fig. 8.18(b). The simplification of the second approach (in which G_O is omitted) arises because the torque is *internal* – the system comprises the hull *plus rudder*. It is the second approach, which uses the hydrodynamic centre of the rudder R as depicted in Fig. 8.18(b), that will now be developed.

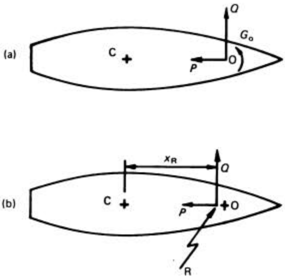

Fig. 8.18

If the motion of the ship may be regarded as being (a) performed solely in the horizontal plane, and (b) steady, so that Ω is constant (and hence β measured at C is also constant), then the forces acting on the ship reduce to: (i) thrust T; (ii) hull side force Y_H arising from drift; (iii) hull side force Y_J arising from yaw; (iv) total hull resistance X; (v) rudder resistance P; (vi) rudder side force Q; and (vii) inertia force $mV\Omega$ applied at C. Note that a further assumption related to the rudder and hull forces has been included. These forces are taken to act in the same horizontal plane or, at least, departures from one plane are negligible. With R kept at the strange position forward of C for the moment, we see that the forces acting on the ship are as shown in Fig. 8.19 (but with either x_J or Y_J negative).

The forces P and Q are, in effect, placed at the command of the helmsman and it is with these that he controls Ω. But variations of Ω call fluid forces into being which tend to alter β, the angle of incidence at C. Hence the helmsman controls Ω and β by adjustment of P and Q (although these latter forces are not independent of each other). By resolving forces along Cx, Cy and taking moments about C the

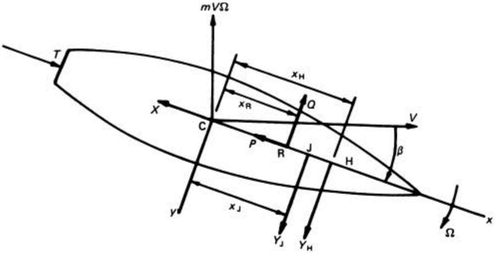

Fig. 8.19

equations of motion are obtained as follows:

$$T - X - P = mV\Omega \sin \beta \tag{8.36}$$

$$Y_H + Y_J - Q = mV\Omega \cos \beta \tag{8.37}$$

$$x_H Y_H + x_J Y_J - Qx_R = 0 \tag{8.38}$$

where either x_J or Y_J is negative.

8.4.3 *Position of the Rudder*

It is well known that the rudder of a ship is normally placed at the stern and we may now give one reason why this is so. The object of installing a rudder is to cause the ship to yaw and by so doing to obtain an angular velocity Ω. Its performance may be assigned a figure of merit based, for example, on the ratio Ω/Q. In forming this ratio β is assumed to be small so that Equation (8.37) is reduced to

$$Y_H + Y_J - Q = mV\Omega. \tag{8.39}$$

Unfortunately, Y_J depends upon Ω and so we cannot use Equation (8.38) with Equation (8.39) to obtain Ω/Q directly. If, however, the approximation

$$Y_J \cong \Omega \left(\frac{\partial Y_J}{\partial \Omega} \right)_{\Omega=0} = \Omega Y_\Omega \tag{8.40}$$

is used for small Ω, it is found that

$$\frac{\Omega}{Q} = \frac{x_R - x_H}{(mV - Y_\Omega)x_H + Y_\Omega x_J}. \tag{8.41}$$

A dimensionless figure of merit is therefore obtained as

$$\frac{\Omega l}{V} \bigg/ \frac{Q}{\frac{1}{2}\rho l^2 V^2} = \frac{\Omega'}{Q'} = \frac{x_R' - x_H'}{(m' - C_{Y_\Omega})x_H' + C_{Y_\Omega} x_J'} \tag{8.42}$$

where the primes on x denote dimensionless ratios of lengths. In addition

$$m' = m/\tfrac{1}{2}\rho l^3; \qquad C_{Y_\Omega} = Y_\Omega/\tfrac{1}{2}\rho l^3 V. \tag{8.43}$$

Note that the dependence of x_J on Ω is ignored because, by Taylor's theorem, the moment $Y_J x_J$ and the force Y_J are both roughly proportional to Ω. For a good rudder performance $|\Omega'/Q'|$ must be as large as possible.

If the rudder were mounted so that its hydrodynamic centre R coincided with the hydrodynamic centre H of the hull in drift, then $x_R = x_H$ and the rudder would produce no steady yawing motion. The largest value of $|\Omega'/Q'|$ is obtained if R is as far away from H as possible, that is, if x_R is large and negative. This accounts (at least in large measure) for the location of the rudder at the stern of a ship.

With reference to the normal stern-fitted rudder, it is of interest to see how a ship behaves when this rudder is put over. When a vessel executes a 'circle manoeuvre' it first proceeds in a straight line at constant speed. The rudder is then moved to some selected deflection and the ship's path is noted. The path is usually of the general form shown in Fig. 8.20. After an initial transient motion the vessel begins to turn

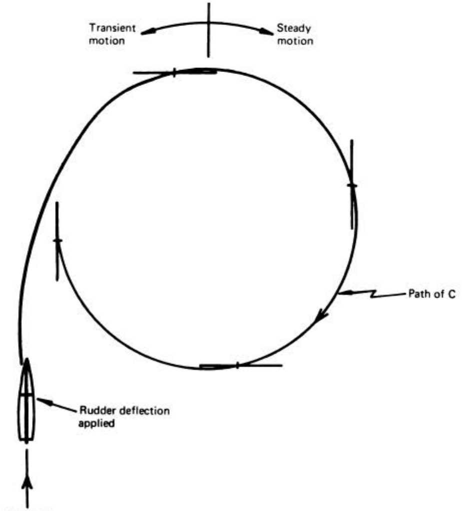

Fig. 8.20 The circle manoeuvre.

in a circle. We are concerned here only with this second phase, during the course of which the forces applied to the ship are as shown in Fig. 8.21, where it is assumed that $x_J < 0$ and $Y_J > 0$. Figure 8.22 shows an actual model executing a circle manoeuvre in a large test tank. A number of positions of the model have been exposed on one negative in order to produce a composite picture.

We must also mention the locations of the hydrodynamic centres H and J. It is tempting to refer to these points as if they are fixed in the ship. This, however, is not strictly true, and indeed dimensional analysis indicates that

$$x'_H = \frac{x_H}{l} = \text{function } (Re, Fr, \beta) \tag{8.44}$$

$$x'_J = \frac{x_J}{l} = \text{function } (Re, Fr, \Omega'). \tag{8.45}$$

How sensitive these functions are on the values of the dimensionless groups is itself a quite important matter.

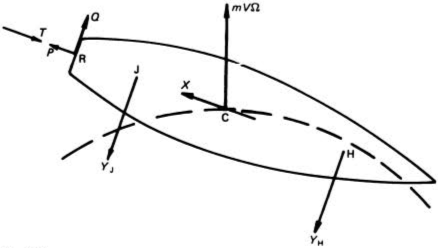

Fig. 8.21

8.4.4 *Some Comments on Rudder Design*

In the above discussion it was assumed that the ship proceeds normally in calm water and calm weather so that its response is dictated entirely by the rudder. This is a simplification because wind and waves significantly affect manoeuvrability and control. For example, a large superstructure forward may hinder a ship turning into the wind.

A more subtle, yet equally basic, assumption has been made, namely, that the ship *possesses* the ability to proceed in a straight line. As we have indicated, problems of dynamic instability do arise in ships, notably in large tankers. These problems are also common in aircraft, the behaviour of which can be materially affected by the shape and position of control surfaces and the elasticity of their control circuits.

In the design of ships' rudders, although some consideration is given to berthing and manoeuvring in confined waters, attention is mainly directed at manoeuvring and control under way at normal ahead speeds in open water (as assumed up to

Fig. 8.22 A model ship performing a circle manoeuvre.

now.) A variety of other techniques are available for 'low-speed' manoeuvring, for example, the use of tugs, restraint of motion ahead by wires and ropes (or 'springs'), the differential use of propellers, the use of thrusters and so forth.

The design of a rudder is – or should be – determined by the requirements of performance in manouevring, directional stability and control. Unfortunately, as things stand at present, these requirements are neither very specific nor quantitatively expressed, so that rudder design is not an exact science. Consequently, for surface ships, rudder features such as size, speed of operation, maximum deflection and so on are usually based on the 'evolution' of previous practice. Although the present discussion is restricted to steady motions transient conditions are also important. In particular, there can be no question in the design process of ignoring the speed of operation of control surfaces.

Now the design of a rudder is inextricably linked with hull design, since the latter determines the types of rudder that could be used, the position of the rudder and some limiting dimensions. The process of evolution of rudder–hull combinations can be demonstrated in the approximate way depicted in Fig. 8.23. To improve the turning characteristics of earlier vessels (although at the same time, presumably, decreasing directional stability) the deadwood (area of skeg) was reduced and, to reduce operating torques, 'balanced rudders' were introduced. Little deadwood is needed on 'knife-like' naval hulls with their large propellers, but there is a need for 'feathers on the arrow' in beamier vessels for directional stability. Note that, in the latter case, the 'feathers' will be totally ineffective in improving directional stability if they do not protrude through the region of separated flow near the stern.

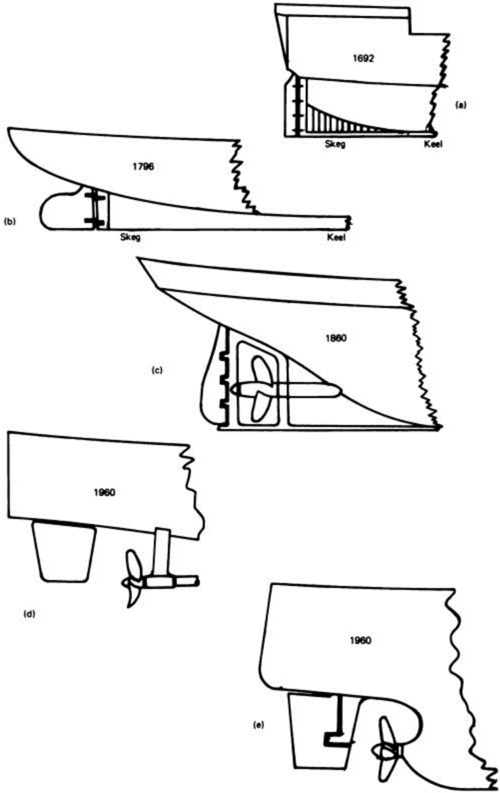

Fig. 8.23 A visual summary of the development of rudders.

Figure 8.23(c) shows an unbalanced rudder, of the type used on Brunel's *Great Britain*, for which a number of pintles were used to support the limited strength of the rudder and its shaft. The rudder in Fig. 8.23(d) is the balanced spade type, which is on many naval ships and fast craft. In naval ships, the after cut-up is long and the rudder can be sufficiently small so that strength problems with the rudder stock are not too severe. Furthermore, steering gear can be kept compact, an important feature for small, fast marine vehicles. The 'gnomen' or 'skeg' rudder in Fig. 8.23(e) is used largely on merchant ships, where the size of the rudder calls for additional support to the rudder bearing. However, the lower portion of the rudder can be used to balance the torque partially if required.

Whenever possible, rudders are placed in a propeller race for greater effect, so that $U > V$. The flow downstream from a propeller operating in a wake is exceedingly complex and yet the rudder is still required to operate effectively. Remarkably, this type of arrangement works well and is a great asset when manoeuvring at slow speeds or from rest. The augmentation of V by a propeller race at normal ahead speeds usually means that U is 10–30 per cent greater than V.

Although many semi-empirical rules exist for estimating rudder forces and torques, these are at present very crude. (The basis on which bending moment and torque in a rudder stock is normally assessed has already been mentioned.) The rules adopted [1–3] are most often based on statics, although the largest angles of incidence are likely to occur during transient manoeuvres. Unsteady conditions of transient motion into or out of a turn (during the process of applying a deflection or arising from any other source) may require special considerations, however, and estimates of rudder forces are often checked by *ad hoc* model tests.

The designer must remember that hydrodynamic centres shift when a vessel runs astern, and that the rudder then operates in clear water and not in the propeller race. A rudder is not the most robust part of a ship; when a ship is docked for overhaul it is often found that the back end, comprising the propeller *and the rudder*, needs care and attention.

8.5 Control of Steady Motion in the Vertical Plane

For reasons of pressure-hull strength, most submarines are confined to a depth range of only two or three times their own length. This means that the handling characteristics in the vertical plane are of crucial importance, particularly at high speed.

As speeds of less than 5 m s^{-1} ($\cong$ 10 knots) hydrostatic forces become increasingly important and eventually predominate. But, for speeds greater than this (and 15 m s^{-1}, about 30 knots, is the likely maximum for the present), hydrodynamic effects begin to predominate. These hydrodynamic effects arise from flow over:

(i) the hull, which (as with a ship) acts like an inefficient, but very large, lifting surface; and

(ii) hydroplanes, that is, control surfaces whose interaction with the hull requires examination.

Modern submarines usually have circular frames which have a common longitudinal axis. It is convenient to take Cx parallel to this axis and to make this the direction of V in translation for zero fluid force in the perpendicular direction by suitably choosing the zero settings of the hydroplanes. Even if there were no such readily identifiable axis in the structure, Cx can still be selected arbitrarily (so determining the 'level keel' condition) and then made the direction of V for zero fluid force in the perpendicular direction during translation parallel to Cx.

As with the previous example of a surface vessel, the system of forces applied to a submarine (in Fig. 8.24) in the direction normal to the plane of the diagram is in equilibrium. Here, however, the equilibrium is a result of symmetry. In other words, the submerged submarine moving in the vertical plane provides a problem to which the theory of Section 8.2 can be readily adapted. (We have already seen that motion in the horizontal plane is also of this type.)

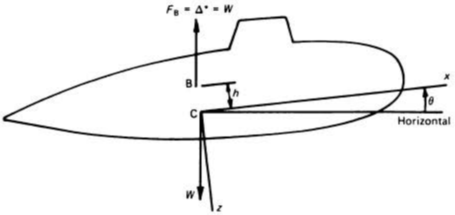

Fig. 8.24

Once more we consider small but steady perturbations of a steady reference motion along Cx. Motion in the vertical plane will be referred to the axes Cx, Cz (rather than Cx, Cy) with z measured positive downwards. The relevant perturbations are now: (i) heave velocity of translation, which is positive downwards; and (ii) angular velocity of pitching, which is positive when the bows rise.

It may be recalled that the steady motion of a control surface permits a useful simplification to be made, namely that rotation can be ignored. For a completely different reason the same assumption can be made for submarine manoeuvres in the vertical plane. If the submarine is in trim the upward buoyancy force equals the weight. This means that when Cx is inclined at an angle θ to the horizontal, as shown in Fig. 8.24, there is a hydrostatic righting couple $Wh\sin\theta \cong Wh\theta$, where h is the distance between the centres of mass and buoyancy. It is therefore impossible for a *steady* state of motion to exist in which pitching occurs, for pitching entails variations of θ. (Note that this argument does not apply to aeronautical vehicles because buoyancy effects are then usually negligible.)

8.5.1 *Hydroplanes*

It is common practice to provide hydroplanes both forward and aft. Nevertheless, satisfactory control can be achieved with after hydroplanes alone, although forward hydroplanes are very useful at low speeds. However, the boat can only maintain constant depth with an even keel, that is with Cx horizontal, when both forward and after hydroplanes are fitted. This cannot be done with only after hydroplanes because, unlike a torpedo, a submarine is not axially symmetric (owing to the presence of a bridge fin). Consequently, the hull of the boat experiences both a fluid force and a fluid moment about C in the vertical plane when Cx is horizontal. Only if both forward and after hydroplanes are fitted is it possible with Cx *horizontal* to counter both the force and moment. The settings of the hydroplanes required to do this are termed the 'balance angles'.† If after hydroplanes alone are fitted, the boat can proceed at constant depth only by running with Cx inclined (as well as with the after hydroplanes deflected).

Note that these considerations apply to a boat that is in trim, that is, in a state of 'neutral buoyancy'. There is no real need for a boat to be exactly in trim, however, except at very low speeds where hydrostatics prevail. In fact submarines are often run somewhat light (or 'positively buoyant'). In such circumstances rather different hydroplane settings are necessary 'to hold the boat down' and these will vary with speed.

When the hydroplanes are aligned with the local flow they do not produce a lift force; the settings are then known as the 'no-lift' (or 'inoperative') angles. Usually the no-lift settings are virtually parallel to Cx. Now for the purpose of reference it is desirable to decide what the 'zero' setting shall be. Generally, it is the setting parallel to Cx, but if this differs greatly, by more than 5°, say, from the no-lift condition then the latter is taken to define the zero angles. For the least hydrodynamic resistance the balance and no-lift angles of a set of hydroplanes should be close together, but this depends on the symmetry of the boat.

At each pair of control surfaces (i.e. hydroplanes) the forces P and Q, respectively parallel and perpendicular to Cx, may be adjusted. Thus, if there are hydroplanes fore and aft the forces exerted upon the hull are as shown in Fig. 8.25. Let the resultant of Q_F and Q_A be Q, so that Q is the resultant hydroplane force parallel to Cz. The force Q may be found from the equation defining (i) the resultant force

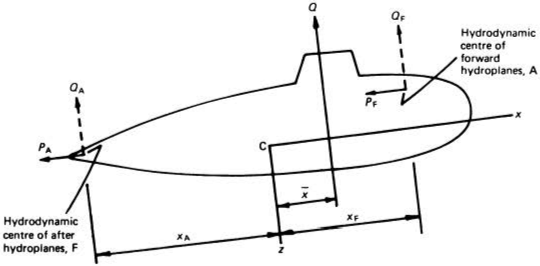

Fig. 8.25

† In some cases the balance angles are not set for a horizontal Cx as this would require excessive deflections, limiting the scope of control on one side and increasing the resistance to motion of the boat. Under these conditions the balance angles are chosen for a small trim angle on the boat.

normal to Cx and (ii) the net moment about C as shown, respectively, in Equations (8.46) and (8.47):

$$Q = Q_A + Q_F \tag{8.46}$$

$$\bar{x}Q = -x_A Q_A + x_F Q_F \tag{8.47}$$

Whence,

$$\bar{x} = \frac{x_F Q_F - x_A Q_A}{Q_F + Q_A}. \tag{8.48}$$

Thus, by adjusting the hydroplane settings Q may be moved along the Cx axis so that, in theory,

$$-\infty < \bar{x} < \infty.$$

For the sake of convenience and conciseness, the following analysis of submarine motion will be developed in terms of the equivalent force Q rather than the separate hydroplane forces Q_F and Q_A.

8.5.2 *Hull–Hydroplane Combination*

The resultant fluid force F acting on the hull may be resolved into components X which is positive in the direction $-$Cx and Z (the sign of which depends upon the sense of the angle of incidence β) in the direction Cz. These components act at H, the hydrodynamic centre for translation, as indicated in Fig. 8.26(a), a statically

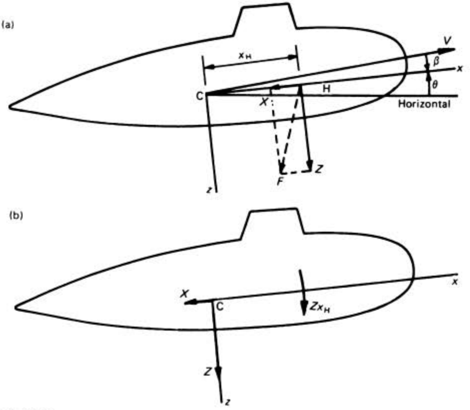

Fig. 8.26

equivalent system being that of Fig. 8.26(b). A positive value of β produces a downward positive force Z; that is, $\beta > 0$ when Cx is inclined below the direction of V, as in Fig. 8.26(a). (Of course we could consider hull lift and drag forces, so that F may be resolved in directions parallel and perpendicular to the velocity V. But for reasons that will become apparent the directions Cx, Cz are more convenient.)

The complete assembly of forces and moments applied to the submarine during steady motion is as shown in Fig. 8.27. There are no inertia forces since the vessel is supposed only to perform a motion of translation at constant speed. In what follows the moments of P_F, P_A and T about Cy are disregarded on the grounds that they are all undirectional and (in the cases to be examined) more or less constant. We shall also assume that the angles θ and β are small.

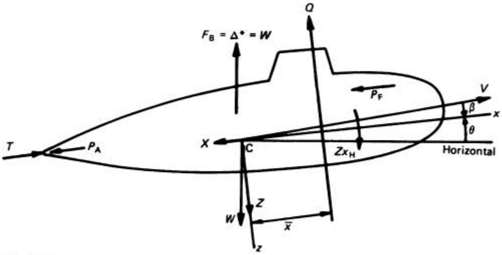

Fig. 8.27

The equations governing the steady motion of translation are derived by resolving forces along Cx and Cz and by taking moments about an axis through C which is perpendicular to the Cxz plane (in Fig. 8.27). The results are, respectively,

$$T - P_F - P_A - X = 0 \tag{8.49}$$

$$Z - Q = 0 \tag{8.50}$$

$$Zx_H + Wh\theta - Q\bar{x} = 0 \tag{8.51}$$

The assumption of steady motion implies, from Equation (8.50), that Z adjusts to the magnitude of Q, applied by the hydroplanes, through a change of β. Moreover, θ will adjust itself to ensure equilibrium. If Q is eliminated from Equations (8.50) and (8.51) it is found that

$$\bar{x} = x_H + \frac{Wh\theta}{Z} \tag{8.52}$$

and we may note that in any normal craft $x_H > 0$ and also that x_H varies little with forward speed for small β.

Equation (8.50) shows that if Q is negative (upwards) Z is positive (downwards) and thus $\beta > 0$, that is Cx is depressed below the direction of V. If, on the other hand, $Q > 0$ then $Z < 0$ and $\beta < 0$ and Cx is above the direction of V. This leads us, therefore, to two important operating conditions for submarines, namely, level trim and constant depth.

(a) *Maintenance of Level Trim*
To maintain level trim, that is forward motion with Cx horizontal, $\theta = 0$ and so Equation (8.52) gives

$$\bar{x} = x_H. \tag{8.53}$$

That is, the equivalent hydroplane force Q must be applied at the hydrodynamic centre of the hull as indicated in Fig. 8.28. The hydrodynamic centre is sometimes known as the 'neutral point' in this context.

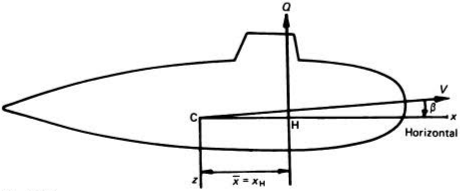

Fig. 8.28

(b) *Maintenance of Constant Depth*
If the direction of V is horizontal and Q acts upwards, Z must be positive. To give the necessary angle of hull incidence β, Cx is depressed so that θ is negative. On the other hand, if Q acts downwards so that $Z < 0, \beta < 0$ and Cx is raised giving $\theta > 0$. In either case, therefore, Equation (8.52) becomes

$$\bar{x} = x_H - \left| \frac{Wh\theta}{Z} \right| \tag{8.54}$$

so that $\bar{x} < x_H$.

In analogy with, for example, Equations (8.2) and (8.5) for steady motion of a ship in the horizontal plane the force Z may be expressed in the form

$$Z = \tfrac{1}{2}\rho V^2 l^2 \beta \left(\frac{\partial C_Z}{\partial \beta}\right)_{\beta=0} = aV^2 l\beta. \tag{8.55}$$

The coefficient a is given by

$$a = \tfrac{1}{2}\rho l \left(\frac{\partial C_Z}{\partial \beta}\right)_{\beta=0} \tag{8.56}$$

and is positive. Provided that V is not too low a can be considered independent of hull Reynolds number. Since $\theta = -\beta$ in this case

$$\bar{x} = x_H - \frac{Wh}{aV^2 l} = x_{crit}, \tag{8.57}$$

say. Equation (8.57) shows that $x_{crit} < x_H$ and so Q must now be applied aft of the neutral point H at a distance that varies inversely with V^2. Consequently, Q must be applied at the 'critical point' S in conformity with Fig. 8.29. On the basis of these two special cases three significant points can be identified on the Cx axis of a submarine, namely, S, C and H as shown.

For a given submarine moving forward at a constant velocity V all three points S, C and H are fixed. In general, therefore, the hydroplanes may be adjusted so that Q is forward of H, or in SH, or abaft S. These cases will now be examined in turn.

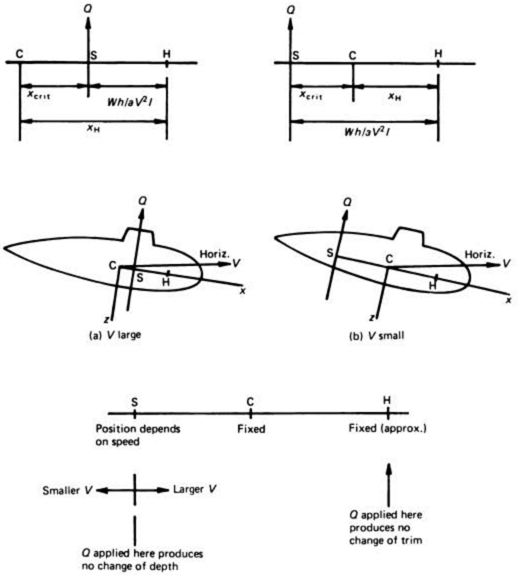

Fig. 8.29

(c) *Q Applied forward of* H
With Q upwards (and hence $Z>0$ and $\beta>0$) we now require $\theta>0$ in Equation (8.52) since $\bar{x}>x_H$. The motion is thus of the form shown in Fig. 8.30.

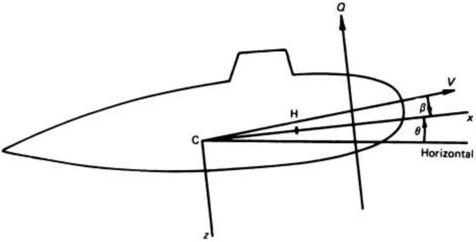

Fig. 8.30

(d) *Q Applied in* SH
In this case, $\bar{x}-x_{crit}>0$ whether the critical point S is forward or aft of C. That is,

$$\bar{x}-x_{crit}=\left(x_H+\frac{Wh\theta}{Z}\right)-\left(x_H-\frac{Wh\beta}{aV^2l\beta}\right)=\frac{Wh}{Z}(\theta+\beta)>0. \qquad (8.58)$$

In addition, $\bar{x}<x_H$ so that, since $Z>0$ for upward Q, Equation (8.52) gives $\theta<0$. Consequently, Cx is inclined below the horizontal. Moreover, $\beta>0$ to give $Z>0$. It follows that $\beta>|\theta|$ and the system is as shown in Fig. 8.31.

(e) *Q Applied abaft* S
Now $\bar{x}-x_{crit}<0$ whether S is forward or aft of C. Therefore

$$\frac{Wh}{Z}(\theta+\beta)<0. \qquad (8.59)$$

But $Z>0$, so that $\beta>0$ as always for upward Q, and also $\bar{x}<x_H$ so that $\theta<0$ from Equation (8.52). Therefore, $\theta<0<\beta$ and $|\theta|>|\beta|$ to give the system shown in Fig. 8.32.

In the above examples an upward Q (and therefore positive Z) has been chosen by way of illustration. The argument for Q acting downwards is straightforward to develop and results in a 'mirror image' about the horizontal of the systems depicted in Figs. 8.28–8.32.

(f) *Position of Q for Most Effective Depth Changing*
The ability of a submarine to dive or surface is clearly of paramount importance. Now the rate of change of depth for a given magnitude of Q is proportional to the

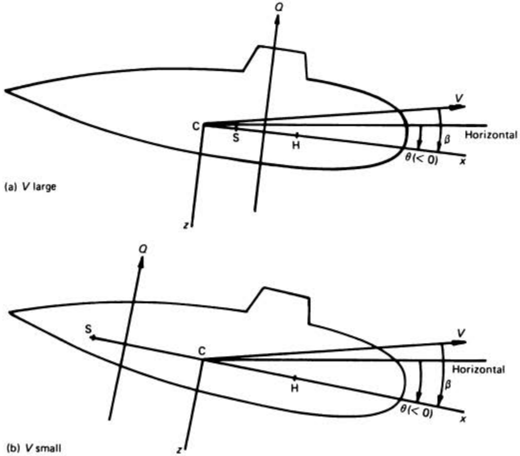

Fig. 8.31

inclination of V to the horizontal, that is to $\theta + \beta$, as shown in Fig. 8.27. The expression (8.58) allows the following identity to be written:

$$\bar{x} - x_{\text{crit}} = \frac{Wh}{Z}(\theta + \beta) \tag{8.60}$$

Hence, for a given Q we require the maximum value of $\bar{x} - x_{\text{crit}}$. That is, the distance of Q forward of S must be as large as possible.

8.5.3 *Some Practical Notes on Hydroplanes*

The force Q in the foregoing analysis is obtained by the use of hydroplanes. As already mentioned, they are usually fitted fore and aft, the arrangement being as shown in Fig. 8.33. Sometimes (on American boats for example) the forward hydroplanes are mounted on the bridge fin, almost exactly over the neutral point H, so that they therefore become depth controllers only. Moreover, this location removes them from the vicinity of the forward sonar transducers and also makes them useful as gangways when the submarine is alongside.

Sections 8.5.2(c) and (d) show that if the equivalent hydroplane force Q is forward of S an upward (negative) Q causes the boat to rise. Section 8.5.2(e) shows that an upward Q causes the boat to dive if Q is applied aft of S. The practical

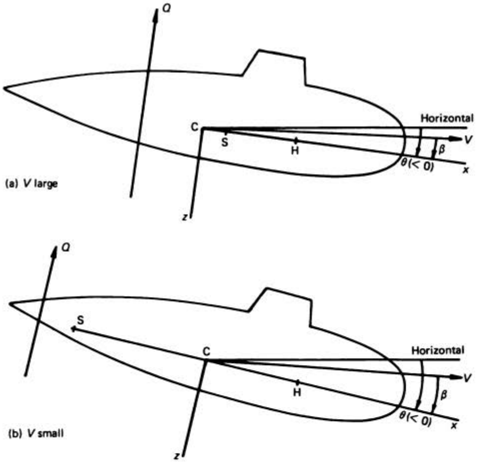

Fig. 8.32

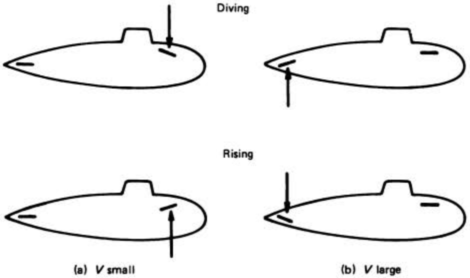

Fig. 8.33

arrangement shown in Fig. 8.33 is therefore based on the assumption that S is forward of the after hydroplanes. It has been shown that S moves further aft at low speeds. In a practical submarine S lies *at* the after hydroplanes when V is about $1–2\ \mathrm{m\ s^{-1}}$ ($\cong$ 2–4 knots). This is known as the 'critical speed', and below it S lies abaft the after hydroplanes. When V is less than the critical speed control by the after hydroplanes therefore reverses, a fact which causes problems with deep-diving, low-speed submersibles.

Suppose that a submarine has to rise and that an upward Q is applied. Assuming that V is not too small, and that the cases examined in Sections 8.5.2(c) and (d) are therefore relevant, $\bar{x} - x_{\mathrm{crit}}$ must be as large as possible. In accordance with Section 8.5.2(f), Q must be applied as far forward of S as possible. Now at low speeds S is well aft, so we should use the forward hydroplanes for maximum rate of rise. But at high speeds S is well forward, so that the after hydroplanes will provide the maximum rate of rise with a downward force Q†.

The main argument in favour of installing both forward and after hydroplanes is that Q can thereby be placed where it is wanted, that is, $\bar{x}$ can be adjusted. This means that trim (i.e. tilt) and depth can be controlled independently, for if Q is applied at H, depth and not trim is altered, but if Q is applied at S (whose location varies with speed) trim and not depth is changed.

8.6 Performance of Control Surfaces

Although of vital importance, it is extremely difficult to calculate accurately the hydrodynamic forces and moments on control surfaces. The principal reasons for this lie in the exceedingly complex nature of the flow in which control surfaces operate. For example, the forward hydroplanes of a submarine are partially immersed, at the root, in the hull boundary layer. The after hydroplanes and rudder may be totally immersed in the turbulent boundary layer, or even in the separated flow, at the stern of the boat and may be affected by the forward influence of the propeller. The rudder of a displacement ship or planing craft is deliberately placed downstream from the propeller in order to take advantage of the high axial velocities in the propeller race. However, there will be occasions when the rotational velocities in the wake are a significant proportion of the axial velocities, for example, when the propeller is highly loaded during acceleration phases such as getting underway from rest. The flow passing the rudder is then strongly three-dimensional and will, of course, contain cavitation bubbles shed from the propeller blades and boss. Consequently, rudders are not placed too close to propellers – say at one propeller radius downstream – and, furthermore, are offset somewhat from the centre line of the propeller shaft. A given rudder may therefore operate partially in a propeller race but with the remainder of its surface in the hull wake. It is also usual for the shafts of high-speed craft to be inclined downwards in order to ensure propeller immersion under cruise conditions. The race then passes over the rudder obliquely.

As a result of the complexity of the flows about control surfaces it is, perhaps, not surprising to find that a number of rough-and-ready design criteria are in current use. Many of these rely on previous experience with ships of similar form and must therefore be employed with care when applied generally. In some instances desirable

† Note that if H were very far forward and S moved close behind it at very high speeds, the forward hydroplanes if aft of S, would operate in reverse fashion.

features become mutually opposed; one case has been discussed in Section 8.3.1 and another concerns the turning qualities in response to rudder deflection which improve for a ship inherently unstable in motion ahead, such as some warships. Guidelines that have been adopted for the principal rudder parameters are as follows:

(i) *Size*. Rudder area is selected as a proportion of the product of the length of the hull at the water line (L_{WL}) and the mean draught ($\bar{T}$) in the fully laden condition. This proportion, or rudder area coefficient ϵ, given by

$$\epsilon = \text{rudder area}/\bar{T}L_{WL} \tag{8.61}$$

is chosen in the light of previous designs.

(ii) *Speed of operation*. Commonly, 2.33 deg s^{-1} is taken as a minimum requirement in order to provide a reasonable limit to the transient motion displayed, for example, in the circle manoeuvre illustrated in Fig. 8.20. (Although we are concerned here with steady motion the time taken to reach that state is clearly important and will be discussed in Chapter 10.) An alternative criterion is given in [1] which uses the 'degree rate of rudder deflection' $\dot{\xi}_R$ as a proportion of the ratio of ship speed (V) to water-line length. Based on the work in [4] the criterion is given by

$$\dot{\xi}_R = 46.7 \frac{V}{L_{WL}} \text{ degrees,} \tag{8.62}$$

where ξ_R is the rudder deflection angle and V and L_{WL} are measured in consistent units of, for example, m s^{-1} and m respectively. We then see that the rate of change of rudder deflection depends on the size and speed of the ship so that, as might be expected, small, fast ships call for fast operation of the rudder.

(iii) *Maximum Deflection*. The effectiveness of a rudder is largely lost when stall occurs along the whole span. This, therefore, limits both the deflection rate and the maximum deflection which is often set at 35 degrees. At a rate of 2.33 deg s^{-1} it takes 15 seconds to reach the maximum. Because the angle of incidence at the rudder is less than the deflection angle a maximum angle of 45 degrees has sometimes been adopted in the knowledge that the nature of the hull forces and moments and not stall phenomena limits the useful rudder deflection angle [1].

(iv) *Number of Rudders*. The choice depends on the number of propellers installed so that use can be made of speed augmentation by the propeller race. Multiple, for example twin, rudders must be well separated to avoid flow interference (cascade effect) between them. Two rudders with a total area equal to a single, middle-line rudder would generally each have the same span and therefore each of the pair would have an aspect ratio about twice that of the single rudder. Thus, at a given lift coefficient each twin rudder would have a lower angle of incidence than the single rudder, as indicated in Fig. 8.16, appropriate to the ideal conditions described in Section 7.5. The flow onto the twin rudders during a turn is rather complicated, but in effect the rudders should be staggered across the flow rather in the form of the wings of biplanes.

(v) *Rudder Balance*. The location of the shaft attached to the rudder dictates the torque required to change or maintain the deflection of a given rudder–hull combination. The choice depends on the capability of operating gear, the type of rudder and the extent to which rudder vibration can be tolerated.

8.6.1 *Approximate Formulae for Rudders*

Many formulae have been suggested for the calculation of rudder forces and an old one, used widely, is

$$Y_R = 577 S_R U^2 \sin \xi_R (\mathrm{N\,s^2\,m^{-4}}) = 1.12 S_R U^2 \sin \xi_R (\mathrm{lbf\,s^2\,ft^{-4}}), \quad (8.63)$$

where S_R is the plan area of the rudder normal to the rudder side force Y_R and ξ_R is the rudder deflection angle. The velocity U is that approaching the rudder and, for operation in the propeller race, is often taken as 30 per cent higher than the ship speed V. For a centre-line rudder of a twin-screw ship the augmentation is 20 per cent.

Gawn [5] examined the formulae (8.63) in the light of additional tests and data from aircraft controls. As a result, the following expressions were recommended for the estimation of the side force on rudders in ahead and astern motion for ships with twin rudders fitted behind wing propellers:

Ahead

$$Y_R = 21.1 S_R V^2 \xi_R (\mathrm{N\,s^2\,m^{-4}\,deg^{-1}}) = 0.041 S_R V^2 \xi_R (\mathrm{lbf\,s^2\,ft^{-4}\,deg^{-1}}) \quad (8.64)$$

Astern

$$Y_R = 19.1 S_R V^2 \xi_R (\mathrm{N\,s^2\,m^{-4}\,deg^{-1}}) = 0.037 S_R V^2 \xi_R (\mathrm{lbf\,s^2\,ft^{-4}\,deg^{-1}}). \quad (8.65)$$

In these expressions the true ship speed V is used, allowance being made in the coefficient for the effects of the propeller race. For middle-line rudders behind single screws the coefficient in Expression (8.64) becomes $18.0\ \mathrm{N\,s^2\,m^{-4}\,deg^{-1}}$ ($\cong 0.035\ \mathrm{lbf\,s^2\,ft^{-4}\,deg^{-1}}$) for both ahead and astern motions. The corresponding coefficient for a middle-line rudder fitted to twin- and quadruple-screw ships is $15.5\ \mathrm{N\,s^2\,m^{-4}\,deg^{-1}}$ ($\cong 0.03\ \mathrm{lbf\,s^2\,ft^{-4}\,deg^{-1}}$). It should be noted that these results were obtained from model and full-scale warships of generally fine form. Ships of higher block coefficient, such as many cargo carriers, have a greater wake (i.e. the wake fraction is high) and so the preceding numerical factors are reduced, perhaps by 10 per cent or so.

The hydrodynamic centre (i.e. centre of pressure) of the rudder must be located in order to calculate the shaft torque. The appropriate rudder balance, consistent with the capability of the installed steering gear, may then be determined. On the basis of the data in [5] Gawn suggested that the hydrodynamic centre of the rudder could be calculated by dividing the rudder into horizontal strips (normally perpendicular to the axis of the shaft) according to the actual planform and whether the strips of the rudder were in 'open' flow or immediately behind a skeg. The fore-and-aft (chordwise) position of the hydrodynamic centre of each strip was taken to be 0.35 times the chord length aft of the leading edge for strips behind a skeg, with this figure becoming 0.31 for strips in 'open' water. The rudder is essentially in 'open' water for astern motion and so the latter figure applies for the complete rudder. The local side forces can be summed to give the total side force and the local moments can be summed to give the total rudder torque which, after division by the total side force, yields the location of the hydrodynamic centre of the rudder relative to the axis of the shaft.

Although the preceding equations allow a straightforward calculation of forces and moments the results must be regarded as only approximate. Sometimes good predictions are obtained, fortuitously, but it must be appreciated that the formulae are based on rudder deflection angles and not local angles of incidence. Furthermore, the relationships are only likely to be applicable for high Reynolds number flows and for small angles of incidence.

8.6.2 *All-movable Control Surfaces*

A typical example of an all-movable control surface is that shown in Fig. 8.34 and it may be identified with a spade rudder or a submarine hydroplane. The geometry of such a control surface may be specified in terms of the variables given in Fig. 8.34, although the cross section usually varies from point to point along the span. At the root and tip of the control surface the chord length and section maximum thickness are, respectively, c_r, c_t and t_r, t_t. The mean chord length $\bar{c} = (c_r + c_t)/2$ and the corresponding mean section maximum thickness $\bar{t} = (t_r + t_t)/2$ if t varies linearly along the span. The hydrodynamic centre H is located a spanwise distance b_H

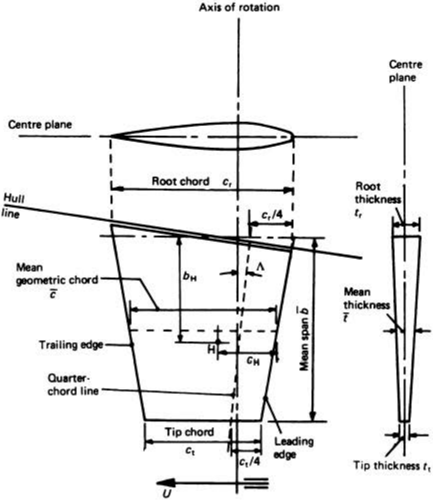

Fig. 8.34 Geometry of all-movable (spade) rudder.

from the root and a distance c_H aft of the leading edge at its intersection with the mean chord line. The line joining the quarter-chord points is, from thin-aerofoil, inviscid-flow theory, that about which zero hydrodynamic moment occurs. The mean span $\bar{b}$ is the average of the spans at the leading and trailing edges and so for a trapezoidal planform the profile area $S = \bar{b}\bar{c}$. The ratio $\bar{b}/\bar{c}$ ($= \bar{b}^2/S$) is the geometric aspect ratio $\mathcal{R}$, the ratio t/c is the thickness-to-chord ratio, the ratio $c_t/c_r = \lambda$ is the taper ratio and Λ is the sweep angle. The sections of control surfaces are symmetric about the chord line (i.e. no camber is present) so that the magnitude of the side force, for a given magnitude of incidence angle, is the same whether deflection is to port or starboard. The velocity U is that of the fluid relative to the control surface.

Comprehensive data on model control surfaces of the type shown in Fig. 8.34 were obtained by Whicker and Fehlner [6] from models fixed to the bottom of a wind tunnel. A number of section shapes were used including the NACA 0015 (see [7] for details) and ranges of taper ratios, sweepbacks and aspect ratios along with different tip shapes were examined. Because the root section was close to an 'infinite' plane no free flow of air took place there from the high- to the low-pressure side of the control surface. Consequently, the effect of aspect ratio on the performance of the control surface is equivalent to that of the actual control surface plus its mirror image, as shown in Fig. 8.35. In other words, the performance of a control surface, profile area S, with its root adjacent to a plane is equivalent to that of the control surface plus its mirror image in the plane to produce a planform of area $2S$ and twice the original span. Thus, the effective aspect ratio $\mathcal{R}'$ of the original control surface is twice the geometric aspect ratio $\mathcal{R}$. The same comments apply to the actual operation of rudders and hydroplanes, except in these instances

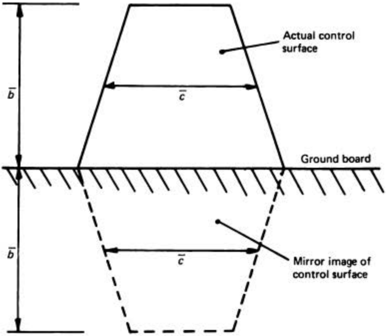

Fig. 8.35

the hull is not often plane but has transverse curvature. As the control surface is deflected the root section is no longer closely seated to the hull and some flow takes place through the gap. However, it is probable that in most instances AR' is not likely to drop below, say, $1.7AR$ even for large deflections.

In the practical case of a ship's rudder the span is limited by the distance between the top of the after cut-up and the keel to avoid grounding and damage in docking. The chord length is governed by the distance between the propeller(s) and the stern, bearing in mind the small clearance at the root and the possibility of aeration if the water surface is approached. Consequently, for most ships geometric aspect ratios are limited to about 1.5 (i.e. $AR' = 3$). The thickness-to-chord ratio has a significant effect on performance , as too great a thickness will increase drag (and therefore the force P in Fig. 8.12) and yet a sufficient thickness at the root must be present in order to accommodate the shaft and sustain bending stresses. Usually, t/c at the root does not exceed 0.25, whereas t/c at the tip does not fall below about 0.10. Hydrofoil sections having values of t/c between 0.12 and 0.18 appear to be the best hydrodynamically.

There is great advantage in utilizing a control surface which yields only a small variation in the position of the hydrodynamic centre. When the type of control surface shown in Fig. 8.34 has an elliptic distribution of lift force along the span a unique relationship, independent of aspect ratio, exists between the taper ratio λ and the sweep angle Λ. In particular, $\lambda = 0.45$ then corresponds to $\Lambda = 0$, but it has been found experimentally that when $\lambda = 0.45$ a wide variation of Λ does not materially affect the *free-stream* performance of the control surface.

All the profiles examined in [6] were tested with tips either squared-off or faired with circular arcs. It was found that profiles with the squared-off tips invariably achieved a substantially greater maximum lift coefficient and higher angle of incidence at stall than the corresponding profiles with faired tips. Although a small drag penalty has to be paid with the former these are generally adopted nowadays because of their easier construction.

In addition to the substantial quantity of experimental data in [6] it was also shown that good correlation could be found between the data and the following theoretical and semi-empirical equations describing the free-stream, low aspect ratio, all-movable control-surface characteristics for motion ahead.

Lift Coefficient:

$$C_L = \alpha\left(\frac{\partial C_L}{\partial \alpha}\right)_{\alpha=0} + \frac{C_{DC}}{AR'}\left(\frac{\alpha}{57.3\ \text{deg}}\right)^2 = \frac{L}{\frac{1}{2}\rho S U^2} \tag{8.66}$$

where

$$\left(\frac{\partial C_L}{\partial \alpha}\right)_{\alpha=0} = \frac{1.8\pi AR'}{57.3\left\{\left(\dfrac{(AR')^2}{\cos^4\Lambda} + 4\right)^{1/2}\cos\Lambda + 1.8\right\}}\ (\text{deg}^{-1}) \tag{8.67}$$

= slope of lift coefficient curve at $\alpha = 0$

AR' = effective aspect ratio = $2AR$

Λ = sweep angle of quarter-chord line

α = angle of incidence expressed in protractor measure (degrees)

C_{DC} = cross-flow drag coefficient

= $1.6\lambda + 0.08$ for square tips or

$0.72\lambda + 0.08$ for faired tips

λ = taper ratio.

Drag Coefficient:

$$C_D = C_{D_0} + \frac{C_L^2}{0.9\pi \mathcal{R}'} = \frac{D}{\frac{1}{2}\rho S U^2} \tag{8.68}$$

where

C_{D_0} = minimum drag coefficient

= 0.0065 at $C_L = 0 = \alpha$ for NACA 0015 section.

Moment Coefficient: This coefficient is determined from the pitching moment about an axis perpendicular to the mean chord line and at a distance $\bar{c}/4$ from the leading edge. Thus,

$$C_M = \alpha \left\{ 0.25 - \left(\frac{\partial C_M}{\partial C_L} \right)_{C_L=0} \right\} \left(\frac{\partial C_L}{\partial \alpha} \right)_{\alpha=0} - \frac{C_{DC}}{2\mathcal{R}'} \left(\frac{\alpha}{57.3 \text{ deg}} \right)^2 \tag{8.69}$$

where,

$$\left(\frac{\partial C_M}{\partial C_L} \right)_{C_L=0} = \frac{1}{2} - \frac{1.11\{(\mathcal{R}')^2 + 4\}^{1/2} + 2}{4(\mathcal{R}' + 2)}$$

= slope of quarter-chord moment coefficient at $C_L = 0$.

Hydrodynamic Centre (Centre of Pressure): The chordwise location, measured from the intersection between the leading edge and the mean chord line, is given by

$$c_H = \left(0.25 - \frac{C_M}{C_Y} \right) \bar{c} \tag{8.70}$$

where,

$C_Y = C_L \cos\alpha + C_D \sin\alpha$

= side (normal) force coefficient.

The spanwise location, measured from the root section, is given by

$$b_H = \frac{\left\{ \left(\frac{4}{3\pi} \right) C_L \cos\alpha + C_D \sin\alpha \right\} \bar{b}}{C_L \cos\alpha + C_D \sin\alpha} \tag{8.71}$$

$$\cong \frac{4\bar{b}}{3\pi} \text{ for small } C_D \text{ and/or } \alpha.$$

The preceding equations produce accurate estimates of the quantities listed for geometries and flow conditions similar to those tested in [6]. For practical applications the derived numerical values can only be regarded as approximate and so reliance is still placed on model testing and previous full-scale data.

The semi-balanced rudder supported by a skeg or horn fixed to the hull, illustrated in Fig. 8.23(e) and in more detail in Fig. 8.36, is being fitted increasingly to vessels of all types. The skeg is adjacent to the rudder and must therefore be considered part of it. This type of rudder is therefore a combination, geometrically, of an all-movable and a flapped rudder although it does not follow that the operating characteristics are intermediate between these two. A comprehensive set of data, based on the NACA 0020 hydrofoil section, is given by Goodrich and Molland [8] for several geometries of skeg rudders mounted on the floor of a wind tunnel. That part of the rudder abaft the skeg acts as a variable-camber hydrofoil. The performance of this arrangement depends on the camber, dictated by the movable part of the rudder, and the angle of incidence of the local flow on the skeg which is nonzero during turning of the hull. The area of the rudder below the skeg operates as though it were part of an all-movable surface. There is a discontinuity between the two parts of the rudder as seen in Fig. 8.36, so that tip vortices are formed at that location and inevitably alter the whole flow about the combined rudder. In some cases, the skeg extends to the base of the rudder and so no discontinuity in geometry occurs. However, compared with the preceding arrangement it is found that this combination tends to be hydrodynamically inferior in terms of the overall side-force development. A clear advantage of the skeg rudder over the spade rudder lies in the

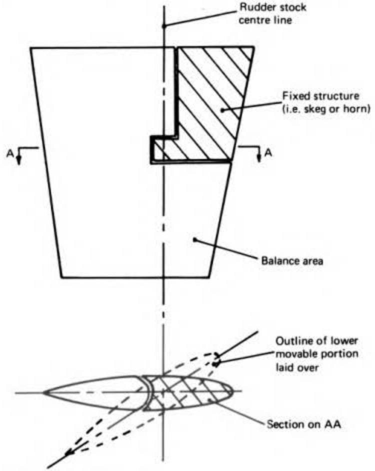

Fig. 8.36 The skeg rudder.

means of attachment to the rudder stock and the simpler construction of the rudder itself.

Comparisons were made in [8] between the performance of the all-movable rudder and the equivalent skeg rudder for the three planforms tested. It was found that $(\partial C_L/\partial \alpha)_{\alpha=0}$ for the skeg rudder was consistently less than that for the all-movable equivalent and that α at stall was over 10 degrees higher. The maximum lift coefficient was only about 10 per cent lower than that of the all-movable rudder. In fact, the effect on the lift curve is rather similar to that of decreasing the aspect ratio of the all-movable rudder, which is precisely the effect of the geometric discontinuity. The discontinuity also accounts for the increase in total drag force for a given lift force owing in part to the generation of tip vortices and therefore an increased induced drag. It was also found that the movement of the hydrodynamic centre, both chordwise and spanwise, was significantly greater for the skeg rudder than for the all-movable equivalent. In general terms, the measured data indicated that the attitude of the skeg to the oncoming flow did not have a large effect on the lift force produced by the movable part of the rudders. The skeg accounted for about 20 per cent of the *total* profile area of each rudder. The largest proportion of the change in the total lift force of the rudder-plus-skeg combination for a variation of skeg angle arose from the change in lift force on the skeg itself.

There is no doubt that the work in [8] and earlier data discussed briefly in [1] provide valuable information on the performance of skeg rudders in uniform flow. The same may be said of the data from [6] and other similar work. Equally there is no doubt that the interaction between the propeller and the rudder is very intimate, as pointed out in [9]. Whether or not the effects of the propeller race on the rudder are separable from the uniform-flow behaviour of rudders is certainly open to question. It is clear, however, that thorough investigations are urgently required into this rather difficult area of hydrodynamics.

References

1. Mandel, P. (1967), *Ship Manoeuvring and Control*, Chapter 8 of *Principles of Naval Architecture* (ed. J. P. Comstock), Society of Naval Architects and Marine Engineers, New York.
2. Rawson, K. J. and Tupper, E. C. (1976), *Basic Ship Theory*, 2nd Edn, Vol. 2, Longmans, London.
3. Okada, S. (1966), *On the Performance of Rudders and Their Design*, Vol. 11 of the 60th Anniversary Series of the Society of Naval Architects of Japan (a book entitled *Researches on the Manoeuvrability of Ships in Japan*), 61–82.
4. Haruzo, E. and Crane, C. L. (1965), Steering characteristics of ships in calm water and in waves. *Trans. Soc. Nav. Archit. Mar. Engrs*, 73, 135–77.
5. Gawn, R. W. L. (1943), Steering experiments: part 1., *Trans. Inst. Nav. Archit.*, 85, 35–73.
6. Whicker, L. F. and Fehlner, L. F. (1958), Free-stream characteristics of a family of low aspect ratio all movable control surfaces for application to ship design., *David Taylor Model Basin Rep.*, No. 933.
7. Abbott, I. H. and Von Doenhoff, A. E. (1959), *Theory of Wing Sections*, Dover, New York.
8. Goodrich, G. J. and Molland, A. F. (1979), Wind tunnel investigation of semi-balanced ship skeg-rudders. *Trans. R. Inst. Nav. Archit.*, 111, 285–307.
9. English, J. W. (1979), Discussion of [8].

9
Structural Dynamics

9.1 Introduction

Strictly speaking, no marine vehicle ever performs an absolutely steady motion. Some parasitic motion is inescapable and this will involve distortion of the vehicle to some extent. We are concerned, then, with the motion of a deformable body through a fluid. If the fluid is a gas the study of this motion is the science of 'aeroelasticity', and if the fluid is a liquid the study is that of 'hydroelasticity'.

It is often possible to obtain useful information about 'rigid-body' parasitic motions by simply ignoring the distortions that accompany them. (This is the basis on which seakeeping and directional stability and control are usually investigated.) The reasons for this concentration on rigid-body motions are that they are often large and that they are not usually affected much by the distortions. But there is an obvious and important class of investigation in which this approach is valueless. The distortion itself must frequently be studied, simply because it cannot be ignored, and it may be accompanied by excessive stresses (which could cause breakage or failure by fatigue). If the distortion is in the nature of a vibration, it may radiate undue noise – possibly into the sea, which is a most efficient noise transmitter – or it may be unpleasant. For a simple introduction to the study of such motions [1] may be consulted.

We shall limit our attention here to distortions that are not accompanied by actual structural failure. That is to say, we shall be concerned with problems of time-dependent elastic deformations (as the word 'hydroelasticity' suggests) and so various types of vibration problem will be discussed.

Vibration is a common phenomenon in ships [2]. Plates in the hull near a propeller may vibrate at 'blade frequency' owing to the transmission of hydrodynamic forces through the water. Again, a radio antenna whips to some extent when the ship rolls (though this is unlikely to be a serious matter in practice). Now these two problems differ in a significant way. In the former motion, sea water must be regarded as part of the vibrating system since the plates cannot move independently of the surrounding water. We shall refer to 'wet sea' problems when confronted by this state of affairs. In contrast, even though local vibration of an antenna is caused ultimately by waves on the sea, the motion can validly be investigated using a system – the antenna, suitably supported – of which water does not form a part. This is typical of what we shall call 'dry land' problems.

The distinction between wet sea and dry land problems is quite fundamental, as we shall discover. When the flowing water must be counted as part of the oscillatory system, there exists the possibility (though usually not the probability in ships) of 'self-excitation'. The situation is familiar to the aeronautical engineer, who must contend with possible 'divergence' or with 'flutter'. On the other hand, systems typified by the antenna, in which the flow of fluid plays no significant part in defining the system, are usually 'passive' and self-excitation by the flow is not possible. These dry land systems raise problems that are more akin to those commonly studied by mechanical engineers.

Both of the vibrations mentioned – those of the hull plating and the antenna – are 'forced'. That is, the motion occurs with the frequency of the imposed disturbance. (The danger is, of course, that it may become resonant.) In the following we shall refer mainly to this type of vibration. Self-excitation, transient oscillation and random loading will be referred to only briefly since, in practice, they represent highly specialized subjects, though very important ones in this context.

In all their generality problems of structural dynamics are usually exceedingly complex. The difficulties are of two sorts – physical and mathematical – and the structural analyst has to possess skills of both sorts. In this chapter we shall attempt to identify 'problem areas' in physical terms, and only in the barest outline shall we indicate how actual numerical solutions may be reached by mathematical means. It must be remembered that practical structural dynamics problems usually make severe demands on the purely computational side. In particular, the use of an electronic digital computer is often essential in practical vibration analysis.

9.2 General Linear Theory

It will help to fix ideas if we consider a very simple problem first. Consider an anchored mechanical system that may be represented as shown in Fig. 9.1. Let $\bar{x}$, a constant, be the extension of the spring under the steady (i.e. constant) force $\bar{F}$. The instantaneous extension of the spring during excitation by the force

$$F(t) = \bar{F} + f(t)$$

is $\bar{x} + x$. The equation of motion is

$$m\ddot{x} = -b\dot{x} - k(\bar{x} + x) + \bar{F} + f(t)$$

and, since $\bar{F} = k\bar{x}$, this reduces to

$$m\ddot{x} + b\dot{x} + kx = f(t). \tag{9.1}$$

Suppose that an extra force F acts on the mass and that this force is applied in some way by a flowing fluid. Plainly the quantity F will depend on (i) the nature of

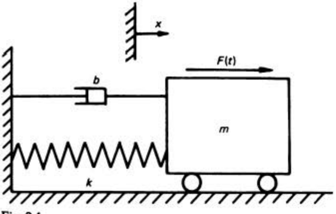

Fig. 9.1

the undisturbed flow, (ii) the configuration and geometry of the system in the flow, and, (iii) the motion of the system. The first two of these features must be thought of as 'given' and it is the last that is now considered. In specifying a fluid force of this sort it is almost invariably the custom to make the assumption of 'linearity'. This means that $\mathbf{F}$ is assumed to depend in a linear manner on x, $\dot{x}$ and $\ddot{x}$ such that

$$\mathbf{F} = \bar{\mathbf{F}} - \alpha\ddot{x} - \beta\dot{x} - \gamma(\bar{x} + x). \tag{9.2}$$

Here, $\bar{\mathbf{F}}$ is a constant contribution to $\mathbf{F}$ and α, β, γ are constants of proportionality so chosen as to permit use of the minus signs.

With this extra force $\mathbf{F}$ acting, the equation of motion becomes

$$m\ddot{x} = -b\dot{x} - k(\bar{x} + x) + \bar{F} + f(t) + \bar{\mathbf{F}} - \alpha\ddot{x} - \beta\dot{x} - \gamma(\bar{x} + x),$$

and if $\bar{x}$ is now taken as being defined by

$$\gamma\bar{x} + k\bar{x} = \bar{F} + \bar{\mathbf{F}} \tag{9.3}$$

this becomes

$$(m + \alpha)\ddot{x} + (b + \beta)\dot{x} + (k + \gamma)x = f(t). \tag{9.4}$$

At first sight this equation appears to differ very little from its predecessor. It seems that the mass, damping and stiffness are merely augmented. But while this is true in a sense it is necessary to make one or two observations.

In the first place, the mass m is not augmented *by an identifiable mass of fluid*. The mass m is augmented by a quantity α which must not be assumed to possess all the attributes of a mass. Thus if $f(t) = A \sin \omega t$ and the steady resulting sinusoidal motion $x = B \sin(\omega t - \theta)$ is sought, the constant α will depend in general on the constant ω. Similar conclusions may be drawn in respect of the constants β and γ.

Secondly, it will be seen that one or more of the constants $(m + \alpha)$, $(b + \beta)$, $(k + \gamma)$ may be negative for an exponential form of motion. If this *is* so, a question of instability arises since the free motion concerned (corresponding to the complementary function) may mask the forced motion of the particular integral. The growth of the motion under these circumstances is possible because the system is capable of extracting energy from the fluid flow.

It is worth while to pursue this line of discussion further. Figure 9.2 shows an *unanchored* system having two degrees of freedom. Suppose that it moves in the direction indicated so as to oscillate about a steady motion under the influence of the applied forces $F_1(t)$ and $F_2(t)$, and fluid forces $\mathbf{F}_1$ and $\mathbf{F}_2$. The mass m_1 moves with a velocity $U_1(t)$ which varies with respect to a mean value so that

$$U_1(t) = \bar{U}_1 + u_1(t). \tag{9.5}$$

This may be regarded as the bodily motion of the whole system. The distortion of the system is measured by $X_2(t)$ where

$$X_2(t) = \bar{x}_2 + x_2(t) \tag{9.6}$$

and $\bar{x}_2$ represents the distortion of the spring in the steady state.

The applied forces are

$$F_1(t) = \bar{F}_1 + f_1(t); \qquad F_2(t) = \bar{F}_2 + f_2(t) \tag{9.7}$$

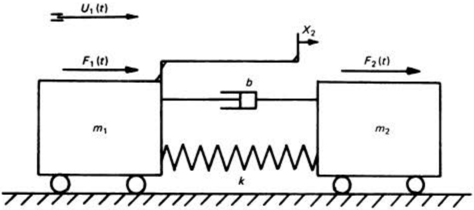

Fig. 9.2

and the fluid forces are

$$\mathbf{F}_1 = \bar{\mathbf{F}}_1 + \text{(component depending on motion and distortion)} \tag{9.8}$$

$$\mathbf{F}_2 = \bar{\mathbf{F}}_2 + \text{(component depending on motion and distortion).} \tag{9.9}$$

To represent the variable components of $\mathbf{F}_1$ and $\mathbf{F}_2$ we may employ the assumption of linearity. The components are:

$$-\alpha_{11}\dot{u}_1 - \beta_{11}u_1 - \alpha_{12}\ddot{x}_2 - \beta_{12}\dot{x}_2 - \gamma_{12}(\bar{x}_2 + x_2)$$

$$-\alpha_{21}\dot{u}_1 - \beta_{21}u_1 - \alpha_{22}\ddot{x}_2 - \beta_{22}\dot{x}_2 - \gamma_{22}(\bar{x}_2 + x_2)$$

respectively, where the α's, β's and γ's are constants. Note that, since $u_1(t)$ is a velocity, there are no $\ddot{u}_1$ terms under the assumption of linearity. Nor are there any terms depending on the quantity,

$$\int_0^t u_1 \, dt = x_1$$

since the overall position of the system is of no consequence.

The equations of motion are therefore given by

$$m_1\dot{u}_1 = \{\bar{F}_1 + f_1(t)\} + \{\bar{\mathbf{F}}_1 - \alpha_{11}\dot{u}_1 - \beta_{11}(\bar{U}_1 + u_1) - \alpha_{12}\ddot{x}_2 - \beta_{12}\dot{x}_2 - \gamma_{12}(\bar{x}_2 + x_2)\} + b\dot{x}_2 + k(\bar{x}_2 + x_2) \tag{9.10}$$

and

$$m_2(\dot{u}_1 + \ddot{x}_2) = \{\bar{F}_2 + f_2(t)\} + \{\bar{\mathbf{F}}_2 - \alpha_{22}\ddot{x}_2 - \beta_{22}\dot{x}_2 - \gamma_{22}(\bar{x}_2 + x_2) - \alpha_{21}\dot{u}_1 - \beta_{21}(\bar{U}_1 + u_1)\} - b\dot{x}_2 - k(\bar{x}_2 + x_2). \tag{9.11}$$

Both may be simplified, since

$$\bar{F}_1 + \bar{\mathbf{F}}_1 - \beta_{11}\bar{U}_1 - \gamma_{12}\bar{x}_2 + k\bar{x}_2 = 0 \tag{9.12}$$

in Equation (9.10) and

$$\bar{F}_2 + \bar{\mathbf{F}}_2 - \gamma_{22}\bar{x}_2 - \beta_{21}\bar{U}_1 - k\bar{x}_2 = 0 \tag{9.13}$$

in Equation (9.11). This will be seen by considering the steady motions of the isolated masses when $U_1(t) = \bar{U}_1$ and $X_2(t) = \bar{x}_2$. We are thus left with a pair of equations which may be written in the matrix form

$$\begin{bmatrix} m_1 + \alpha_{11} & \alpha_{12} \\ m_2 + \alpha_{21} & m_2 + \alpha_{22} \end{bmatrix} \begin{bmatrix} \ddot{x}_1 \\ \ddot{x}_2 \end{bmatrix} + \begin{bmatrix} \beta_{11} & -(b - \beta_{12}) \\ \beta_{21} & b + \beta_{22} \end{bmatrix} \begin{bmatrix} \dot{x}_1 \\ \dot{x}_2 \end{bmatrix} + \begin{bmatrix} 0 & -(k - \gamma_{12}) \\ 0 & k + \gamma_{22} \end{bmatrix} \begin{bmatrix} x_1 \\ x_2 \end{bmatrix} = \begin{bmatrix} f_1(t) \\ f_2(t) \end{bmatrix} \tag{9.14}$$

where $u_1 \equiv \dot{x}_1$, $\dot{u}_1 \equiv \ddot{x}_1$. The analogy with the system that possessed but one degree of freedom is at once apparent. It is therefore natural to enquire if further generalisation is possible.

9.2.1 *Use of Lagrange's Equations*

At the risk of over-exploiting the simple systems of Figs. 9.1 and 9.2, we shall again derive the equations of motion. This time, however, we shall employ Lagrange's equations for the purpose [3, 4]. The reason for adopting this fresh approach is that we shall subsequently shift emphasis on to linear hydroelastic systems *in general* and the Lagrangean technique provides a method of doing so.

The kinetic energy T and potential energy V of the system of Fig. 9.1 are

$$T = \tfrac{1}{2} m\dot{x}^2; \tag{9.15a}$$

$$V = \tfrac{1}{2} k(\bar{x} + x)^2. \tag{9.15b}$$

From the (single) Lagrange equation

$$\frac{\mathrm{d}}{\mathrm{d}t}\left(\frac{\partial T}{\partial \dot{x}}\right) - \frac{\partial T}{\partial x} + \frac{\partial V}{\partial x} = Q \tag{9.16}$$

therefore, we have

$$m\ddot{x} + k(\bar{x} + x) = Q. \tag{9.17}$$

The generalized force Q corresponds to all the non-conservative forces, that is, those not taken into account by V. Thus Q represents the effects of damping, the fluid force and the applied force. Let δW be the work done by these forces in the virtual displacement δx, so that

$$\delta W = \{-b\dot{x} + F(t) + \mathsf{F}\}\, \delta x. \tag{9.18}$$

By definition, $Q = \delta W/\delta x$ so that, under the assumption of linearity of the fluid forces,

$$Q = -b\dot{x} + \bar{F} + f(t) + \bar{\mathsf{F}} - \alpha\ddot{x} - \beta\dot{x} - \gamma(\bar{x} + x). \tag{9.19}$$

We thus arrive at the same equation as before.

The use of Lagrange's technique here is distinctly unhelpful. Indeed this approach is very seldom used in practical problems of hydroelasticity. But, as we shall discover, Lagrange's equations do provide a useful and powerful means of unifying what would otherwise be a very large and diffuse subject. Without some unification, hydroelasticity is little more than a collection of *ad hoc* investigations.

For the unanchored system of Fig. 9.2,

$$T = \tfrac{1}{2}m_1(\bar{U}_1 + u_1)^2 + \tfrac{1}{2}m_2(\bar{U}_1 + u_1 + \dot{x}_2)^2 \tag{9.20a}$$

$$V = \tfrac{1}{2}k(\bar{x}_2 + x_2)^2. \tag{9.20b}$$

The Lagrangean equations are

$$\frac{\mathrm{d}}{\mathrm{d}t}\left(\frac{\partial T}{\partial \dot{x}_1}\right) - \frac{\partial T}{\partial x_1} + \frac{\partial V}{\partial x_1} = Q_1 \tag{9.21a}$$

$$\frac{\mathrm{d}}{\mathrm{d}t}\left(\frac{\partial T}{\partial \dot{x}_2}\right) - \frac{\partial T}{\partial x_2} + \frac{\partial V}{\partial x_2} = Q_2 \tag{9.21b}$$

where $\dot{x}_1 \equiv u_1$. To find the generalized forces it is necessary to consider the work done during virtual displacements $\delta x_1, \delta x_2$. That is

$$\begin{aligned} Q_1 &= \frac{\delta W}{\delta x_1} = \frac{\{F_1(t) + F_2(t) + \mathsf{F}_1 + \mathsf{F}_2\}\delta x_1}{\delta x_1} \\ &= F_1(t) + F_2(t) + \mathsf{F}_1 + \mathsf{F}_2 \end{aligned} \tag{9.22a}$$

$$Q_2 = \frac{\delta W}{\delta x_2} = \frac{\{-b\dot{x}_2 + F_2(t) + \mathsf{F}_2\}\delta x_2}{\delta x_2} = F_2(t) + \mathsf{F}_2 - b\dot{x}_2. \tag{9.22b}$$

Hence

$$\begin{aligned} (m_1 + m_2)\dot{u}_1 + m_2\ddot{x}_2 &= \{\bar{F}_1 + f_1(t)\} + \{\bar{F}_2 + f_2(t)\} \\ &\quad + \{\bar{\mathsf{F}}_1 - \alpha_{11}\dot{u}_1 - \beta_{11}(\bar{U}_1 + u_1) \\ &\quad - \alpha_{12}\ddot{x}_2 - \beta_{12}\dot{x}_2 - \gamma_{12}(\bar{x}_2 + x_2)\} + \{\bar{\mathsf{F}}_2 - \alpha_{21}\dot{u}_1 \\ &\quad - \beta_{21}(\bar{U}_1 + u_1) - \alpha_{22}\ddot{x}_2 - \beta_{22}\dot{x}_2 - \gamma_{22}(\bar{x}_2 + x_2)\} \end{aligned} \tag{9.23a}$$

$$\begin{aligned} m_2(\dot{u}_1 + \ddot{x}_2) + k(\bar{x}_2 + x_2) &= \{\bar{F}_2 + f_2(t)\} \\ &\quad + \{\bar{\mathsf{F}}_2 - \alpha_{21}\dot{u}_1 - \beta_{21}(\bar{U}_1 + u_1) \\ &\quad - \alpha_{22}\ddot{x}_2 - \beta_{22}\dot{x}_2 - \gamma_{22}(\bar{x}_2 + x_2)\} - b\dot{x}_2. \end{aligned} \tag{9.23b}$$

The sum of Equations (9.12) and (9.13) may be used to simplify Equation (9.23a), while (9.13) simplifies (9.23b). We thus arrive at a pair of equations that may be written in the matrix form

$$\begin{aligned} &\begin{bmatrix} m_1 + m_2 + \alpha_{11} + \alpha_{21} & m_2 + \alpha_{12} + \alpha_{22} \\ m_2 + \alpha_{21} & m_2 + \alpha_{22} \end{bmatrix} \begin{bmatrix} \ddot{x}_1 \\ \ddot{x}_2 \end{bmatrix} \\ &\quad + \begin{bmatrix} \beta_{11} + \beta_{21} & \beta_{12} + \beta_{22} \\ \beta_{21} & b + \beta_{22} \end{bmatrix} \begin{bmatrix} \dot{x}_1 \\ \dot{x}_2 \end{bmatrix} \\ &\quad + \begin{bmatrix} 0 & \gamma_{12} + \gamma_{22} \\ 0 & k + \gamma_{22} \end{bmatrix} \begin{bmatrix} x_1 \\ x_2 \end{bmatrix} = \begin{bmatrix} f_1(t) + f_2(t) \\ f_2(t) \end{bmatrix} \end{aligned} \tag{9.24}$$

or, in symbols

$$(\mathbf{A} + \mathsf{A})\ddot{\mathbf{q}} + (\mathbf{B} + \mathsf{B})\dot{\mathbf{q}} + (\mathbf{C} + \mathsf{C})\mathbf{q} = \mathbf{f}(t). \tag{9.25}$$

The matrices **A**, **B**, **C** relate to the mechanical characteristics of the system in the absence of the fluid flow. The effects of the flowing fluid are reflected in the matrices A, B, C. The elements of these two sets of matrices are dependent on the coordinates chosen and arranged in the coordinate matrix $\mathbf{q} = \{x_1 \quad x_2\}$.

The pair of equations of motion in (9.24) may be brought into coincidence with Equation (9.14) by subtracting the second from the first. (The second of Equations (9.24) is already the same as the second of (9.14).) The present form of the matrix equation is in fact the better one though. This is because the Lagrangean technique can readily be used in general terms rather than by reference only to specific systems. When used in this way it produces results that conform to certain general rules.

This point may readily be illustrated by the above results. When the equations of motion are arrived at by the method of Lagrange, the matrices **A**, **B**, **C** are found to be symmetric. Moreover they are positive semi-definite, since the kinetic energy T, the rate of energy dissipation and the potential energy V are all essentially non-negative [5]. While this is true of the equations we have just found, the previous matrices for the mechanical constants were

$$\begin{bmatrix} m_1 & 0 \\ m_2 & m_2 \end{bmatrix}; \quad \begin{bmatrix} 0 & -b \\ 0 & b \end{bmatrix}; \quad \begin{bmatrix} 0 & -k \\ 0 & k \end{bmatrix}$$

which are all asymmetric.

(a) *Added Mass from Lagrange's Equations*

It is sometimes possible to obtain the hydrodynamic coefficients directly from a generalization of Lagrange's equations. Consider a very special case, namely the system of Fig. 9.1 immersed in an infinite ideal fluid; that is, the fluid is incompressible and inviscid, and extends to infinity in all directions. Suppose, further, that the surface of the body, whose mass is m, is a sphere, and assume that the spring, dashpot, and rigid support have no influence on the flow. It is shown in [6] that the influence of the motions of the mass on the fluid may be accounted for entirely by including the kinetic energy of the fluid in Lagrange's equation for the system. Now the kinetic energy of flow around a sphere may be obtained quite simply. For a sphere of radius a moving with velocity $\dot{x}$ in a fluid of density ρ, the fluid kinetic energy T_f is given by [6]

$$T_f = \tfrac{1}{3}\pi\rho a^3\dot{x}^2. \tag{9.26}$$

Hence the total kinetic energy of the system is

$$T = \tfrac{1}{2}m\dot{x}^2 + \tfrac{1}{3}\pi\rho a^3\dot{x}^2, \tag{9.27}$$

and this is the modified quantity to be used in Lagrange's equations. Equation (9.15b) can again by used for V. The corresponding expression for Q is

$$Q = -b\dot{x} + \bar{F} + f(t). \tag{9.28}$$

(Note that were it not for the damping b and the applied force $F(t)$, this would be a conservative system: the effect of the fluid is entirely represented by including the fluid kinetic energy T_f in Lagrange's equations.) If we now substitute T, V and Q from Equations (9.27), (9.15b) and (9.28) into the Lagrangean equation for the one degree of freedom system, we obtain

$$(m + \tfrac{2}{3}\pi\rho a^3)\ddot{x} + b\dot{x} + kx = f(t). \tag{9.29}$$

The fluid forces have therefore been found explicitly and for this particular case the added mass is

$$\alpha = \tfrac{2}{3}\pi\rho a^3. \tag{9.30}$$

The added damping and added stiffness are both zero, since the body is immersed in an ideal fluid extending to infinity in all directions.

(b) *Generalized Coordinates*

The method of Lagrange owes its power to the fact that Lagrange's equations are framed in terms of 'generalized coordinates'. Such coordinates may be used to specify the configuration of a hydroelastic system. In order to describe the passage of a deformable vehicle through a liquid it is clearly necessary to employ variables of two basic kinds:

(i) generalized coordinates specifying bodily motions about a steadily moving reference configuration†;

(ii) generalized coordinates specifying distortions – both those imposed by intent for the purposes of control and those that 'just happen'.

Suppose that a suitable set of generalized coordinates has been chosen. Those specifying bodily motions can be set out in the form of a column matrix, $\mathbf{q_B}$, say. The distortion coordinates (whose selection in practice is a matter in which skill can pay handsome dividends) can be arranged to form a column matrix, $\mathbf{q_D}$, say. The complete matrix of generalized coordinates may be assembled from $\mathbf{q_B}$ and $\mathbf{q_D}$ to give the partitioned matrix

$$\mathbf{q} = \begin{bmatrix} \mathbf{q_B} \\ \cdots \\ \mathbf{q_D} \end{bmatrix}. \tag{9.31}$$

A Lagrange equation may be used for each element of $\mathbf{q}$ in the manner employed for the system of Fig. 9.2. In this way a set of equations of motion may be derived. The approach appears to be due to Duncan, who introduced it in the context of aeroelasticity [7]. It is not our purpose to discuss the theory in detail here, however. (It is not, in fact, particularly simple.) But it is not difficult to see that the general form of the theory is fundamentally the same as that already found. The equations of motion are of the type

$$(\mathbf{A} + \mathbf{A})\ddot{\mathbf{q}} + (\mathbf{B} + \mathbf{B})\dot{\mathbf{q}} + (\mathbf{C} + \mathbf{C})\mathbf{q} = \mathbf{f}(t) \tag{9.32}$$

† Where these are not associated with changes of potential energy, they are sometimes referred to as 'ignorable coordinates' since only their rates of change and higher derivatives appear in equations of motion; for example see [5].

where

- $\mathbf{q}$ is a column vector of generalized coordinates, some ignorable and others not,
- $\mathbf{A}, \mathbf{B}, \mathbf{C}$ are inertia, damping and stiffness matrices of the structure,
- $\mathsf{A}, \mathsf{B}, \mathsf{C}$ are added inertia, added damping and added stiffness matrices of the flow,
- $\mathbf{f}(t)$ is a column vector of generalized external excitations.

9.3 'Dry Land' and 'Wet Sea' Problems

It is not suggested that our general matrix equation occurs constantly – indeed it almost never does in practice. The point is that, with its sole (and fairly mild) restriction to linear analysis, the equation is one of great generality which readily suggests those problems likely to be encountered.

9.3.1 *Practical 'Dry Land' Problems*

As far as the mechanics is concerned, many of the vibration problems that arise in marine vehicles are effectively just sea-going versions of problems that arise in mechanical engineering. The fluid forces then play no significant part in determining the characteristics of the vibrating system so that

$$\mathsf{A} = \mathbf{0} = \mathsf{B} = \mathsf{C}.$$

Thus in many practical cases there is (at least in a sense) nothing essentially nautical about the investigations that have to be performed. This still leaves tremendous scope for difficulties, however, as will be readily appreciated.

The system concerned is usually a localized one, for otherwise the flowing fluid would augment the mechanical system in some manner. It follows that $\mathbf{q}$ contains none of the rigid-body or distortion coordinates of the vehicle as a whole. Generally speaking the elements of $\mathbf{q}$ will refer to local distortions (though, for example, rigid rotation of a shaft would be quite normal). We shall now review these 'dry land' problems in the briefest possible terms.

(a) *Free vibration*

Free vibration is seldom of intrinsic importance yet it has nevertheless to be studied for the determination of principal modes, natural frequencies and levels of damping, for those features of a mechanical system *are* important. In the derivation of principal modes and natural frequencies, the matrix $\mathbf{B}$ is assumed to be null.

Free vibration of a marine structure over some frequency range of interest may well be exceedingly complex. This is because natural frequencies are very numerous, with many near equalities. This particular difficulty has led to the development of an interesting technique of vibration analysis which is based on a study of the free vibration following a blow of limited duration. The salient points of the method are explained in Appendix I (at the end of this chapter).

(b) *Periodic forced vibration*

Forced vibration is a common phenomenon in marine vehicles. The relevant equation of motion is

$$\mathbf{A}\ddot{\mathbf{q}} + \mathbf{B}\dot{\mathbf{q}} + \mathbf{C}\mathbf{q} = \mathbf{F} \sin \omega t \tag{9.33}$$

and the commonest source of excitation is a reciprocating engine or auxiliary machinery. The idea of 'displacement excitation' is sometimes invoked to study localized vibration. While this type of excitation, too, may be due to unbalanced machinery, it may also be of hydrodynamic origin. Thus it may be necessary to stress a mast during rolling oscillation, since the metacentric height of the vehicle could be sufficiently large to produce excessive stresses. It may therefore be convenient to specify a sinusoidal motion of the base of the mast, a technique which is discussed in [8].

Little need be said here about these types of motion as they will already be familiar. It must be remembered that resonance has usually to be avoided. It is worth recalling, however, that there are certain general approaches to the control of forced vibrations, which are

(i) Reduction of excitation:

– by modifying the process by which it occurs (e.g. by 'balancing' of rotors);
– by reducing the effectiveness of the process of excitation (e.g. by shifting the source to a less sensitive location within the offending principal mode);

(ii) Increase of damping:
(iii) Detuning so that ω is not near coincidence with a natural frequency:
(iv) Modification of the vibrating system:

– by installing an absorber;
– by changing **A** or **C** (e.g. by the introduction of suitable 'mounts').

(c) *Transient Vibration*

Transient vibration is not as widely studied as periodic forced vibration, yet it is by no means unimportant. The equation of motion is now

$$\mathbf{A}\ddot{\mathbf{q}} + \mathbf{B}\dot{\mathbf{q}} + \mathbf{C}\mathbf{q} = \mathbf{f}(t)$$

and appropriate analytical techniques of solution are described in the literature [9]. Some modification of traditional methods may occasionally be necessary because the driving may be in the nature of a 'displacement excitation'. The underlying theory of this type of vibration analysis is dealt with elsewhere [10].

This particular type of vibration analysis is often of great difficulty. Consequently it is something of a Cinderella, thus although much of the electronic apparatus in a warship has to be protected by shock mounts, the choice of these mounts is unlikely to be a highly scientific business.

(d) *Self excitation*

Conditions can arise with *active* systems [1] in which the equation

$$\mathbf{A}\ddot{\mathbf{q}} + \mathbf{B}\dot{\mathbf{q}} + \mathbf{C}\mathbf{q} = \mathbf{0} \tag{9.34}$$

has an exponentially growing solution of the form

$$\mathbf{q} = \mathbf{\Psi}\exp(\alpha t) \sin \beta t \tag{9.35a}$$

or, alternatively,

$$\mathbf{q} = \mathbf{\Psi}\exp(\gamma t). \tag{9.35b}$$

This is not particularly common in marine vehicles (although it could conceivably happen with a rapidly rotating shaft having high internal damping) and the matter need therefore be taken no further here.

(e) *Nonlinear vibration*
There are many 'dry land' vibration phenomena whose nature cannot be described even approximately by linear theory. This difficulty commonly arises from the violence of the motion, which is sufficiently large to be of the same order of magnitude as a dynamically significant dimension of the system. For example, the amplitude of vibration of a plate may not be 'much smaller than' the thickness (as linear theory usually requires). This state of affairs requires the techniques of nonlinear vibration theory, a highly specialized subject that lies outside the scope of this book.

9.3.2 *Practical 'Wet Sea' Problems*

The linear theory of hydroelasticity requires, in general, that the matrices A, B, C be retained in the equations of motion

$$(\mathbf{A} + \mathsf{A})\ddot{\mathbf{q}} + (\mathbf{B} + \mathsf{B})\dot{\mathbf{q}} + (\mathbf{C} + \mathsf{C})\mathbf{q} = \mathbf{f}(t). \tag{9.36}$$

But a complete analysis of this equation would represent a formidable task if $\mathbf{q}$ contained more than two or three elements. Consequently relatively few *types* of system have been studied with any generality and extreme idealization has invariably to be practised. Our purpose here is to outline briefly the more important types of problem that have arisen.

When a *rigid* vehicle has a fore-and-aft plane of symmetry and performs a symmetric reference motion, small deviations from that motion are of two distinct and mutually independent types, namely, 'symmetric' and 'antisymmetric'. This fact is used extensively in the study of directional stability and control (see Chapter 10). The same arguments apply to a *flexible* marine vehicle provided it is symmetric in all respects about the plane *Cxz* of body axes *Cxyz* and has a symmetric reference motion. (In selecting body axes we shall follow the convention adopted for the rigid vehicle.) This simplification is used when ship hull vibration is classified as (i) vertical flexure, or 'symmetric vibration'; and (ii) horizontal flexure coupled with torsion, or 'antisymmetric vibration'.

The main areas of investigation that involve significant fluid effects have been: ship hull vibration (both general and local); marine shafting problems; and propeller blade vibration ('singing'). As these are all serious matters it is not surprising to find that an enormous (and highly specialized) literature now exists on all of them. Furthermore, in view of the considerable difficulties of practical cases it is understandable that the techniques of analysis normally adopted rely heavily on empirical results. Helpful rules of thumb abound in this field and it will be appreciated that particular care should be exercised when using them.

9.4 Hull Vibration

The hulls of marine vehicles are subjected to three main types of excitation:

periodic – main engine, propeller, auxiliary machinery;
random – waves;
transient – particularly heavy seas with wave impact, jetty impact, slamming, weapon firing, anchor drop manoeuvres, mine detonation, etc.

In this chapter we shall concentrate mainly on periodic excitation since it is not only of intrinsic interest but is also relevant in other investigations.

In the general subject of periodic forced vibration of hulls we again find that a question of 'scale' arises. It is therefore common to distinguish between two extremes:

(i) 'ship-girder' vibrations in which the entire hull is treated as a free–free beam on some sort of foundation; and

(ii) local vibration in which attention is focused on a plate, or some other geographically limited sub-system in which a troublesome motion occurs.

We shall refer almost exclusively to problems of type (i), that is to vibrations whose frequency is low enough not to invalidate the 'hull-girder' idealization. Unfortunately, the distinction between types (i) and (ii) is not a sharp one and the analyst has sometimes to consider the hull as a more or less crudely made structure with many close natural frequencies and very uncertain damping. Under these conditions the techniques of statistical energy analysis may have to be used.

9.4.1 *Excitation of Periodic Vibration by a Propeller*

A common source of periodic excitation in symmetric vibration is a propeller. Although the nature of the excitation has been the subject of much research [2, 11, 12], it is a very difficult field and progress is understandably slow. Excitation of two distinct types may be identified, arising from (i) bearing forces and (ii) surface forces.

(a) *Propeller-bearing Forces*

Even under perfectly steady flow conditions, the propeller runs in a non-uniform wake. The drag and lift forces and fluid moments applied to each blade therefore fluctuate as the propeller rotates at constant speed. This fluctuation causes periodic forces to be applied to the hull. From the point of view of forced hull vibration, two features of this excitation are of vital importance – the amplitude and the frequency. As might be expected, the amplitude is difficult to calculate. Fortunately, the more important matter of frequency is straightforward. Our purpose now is to discuss the frequency and, in doing so, to indicate what the calculation of amplitude would imply.

Suppose that an N bladed propeller rotates at constant speed Ω in a steady wake and let us consider the nth blade. A thin slice cut from the surface at radius r (see Fig. 9.3(a)) generates a lift force δL_n. We now wish to determine the manner in which δL_n may vary and hence account for a fluctuating force δF_y in the vertical direction Oy. The contribution δL_n has the general form

$$\delta L_n = \mathrm{Re}\left[\sum_{k=0}^{\infty} C_k \exp\{ik(\Omega t + \theta_n)\}\right]\delta r \tag{9.37}$$

where Re implies that real parts are to be taken, and

$$\theta_n = \left(\frac{n-1}{N}\right) 2\pi.$$

This is because the flow conditions, assumed steady, produce a fluctuating force (i.e. δL_n may be expressed as a Fourier series). Inevitably the flow is influenced by the hull, by A-brackets, by the rudder, and so on. Note that determination of the

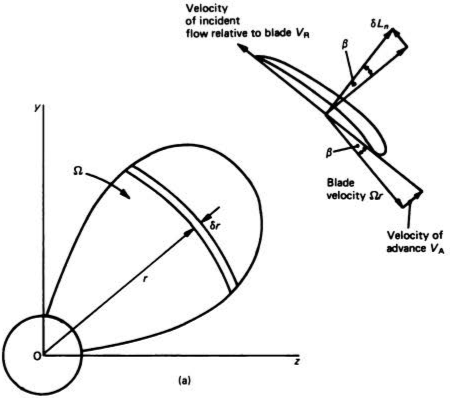
Velocity
of incident
flow relative to blade V_R
δL_n
β
β
Blade
velocity Ωr
Velocity of
advance V_A
Ω
δr
r
y
O
z

(a)

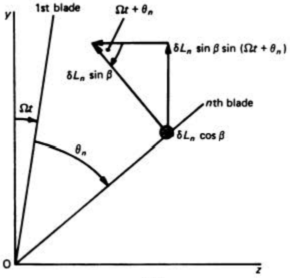
y
1st blade
$\Omega t + \theta_n$
$\delta L_n \sin\beta \sin(\Omega t + \theta_n)$
$\delta L_n \sin\beta$
nth blade
Ωt
$\delta L_n \cos\beta$
θ_n
O
z

(b)

Fig. 9.3

coefficients C_k from a *specified* wake distribution would be no mean task. They are dependent upon such factors as blade shape, wake distribution, cavitation effects (which must be assumed periodic), etc.

The contribution of δL_n to the bearing force δF_y is given by

$$\delta L_n \sin\beta \sin(\Omega t + \theta_n),$$

where β is the local helix angle of the blade which depends only on r. Summing the contributions over the N blades, we have

$$\delta F_y = \mathrm{Re}\left[\sum_{k=0}^{\infty}\sum_{n=1}^{N} C_k \exp\{ik(\Omega t + \theta_n)\}\sin(\Omega t + \theta_n)\right]\sin\beta \,.\, \delta r. \quad (9.38)$$

It is shown in Appendix II at the end of the chapter that this expression reduces to

$$\delta F_y = \mathrm{Re}\left[\frac{iN}{2}\sum_{\substack{k=1,\\ N+1,\\ 2N+1\\ \dots}}^{\infty} C_k \exp\ i(k-1)\Omega t\} - \frac{iN}{2}\sum_{\substack{k=N-1\\ 2N-1,\\ 3N-1,\\ \dots}}^{\infty} C_k \exp\{i(k+1)\Omega t\}\right]\sin\beta \,.\, \delta r$$

or, expressed rather more elegantly,

$$\delta F_y = \mathrm{Re}\left[\frac{iN}{2}\left\{C_1 + \sum_{\lambda=1}^{\infty}(C_{\lambda N+1} - C_{\lambda N-1})\exp(i\lambda N\Omega t)\right\}\right]\sin\beta \,.\, \delta r. \quad (9.39)$$

This result confirms what would be expected intuitively. That is, the total bearing force obtained by summing components of this sort for all δr acting in the vertical direction contains: (i) a steady component; (ii) a sinusoidal component of frequency $N\Omega$, the 'blade frequency'; and (iii) harmonics with multiples of the blade frequency. By the same token, if the moment of δL_n about the axis Oz is determined, a fluctuating bending moment of the same general character is found.

(b) *Propeller-induced Surface Forces*

Surface forces are likely to be more important than bearing forces and are caused by the periodic approach of blades to the surface of the hull. The fundamental frequency of excitation is, of course, that 'of the blades' but, since the pressure fluctuation at the hull surface will not in general be sinusoidal, harmonics will also be present. The amplitude of forcing is far more difficult to calculate than it is with bearing forces and reference should be made to the literature for details of techniques that have been proposed [13]. (A major difficulty is the dominant rôle played by propeller cavitation (see Chapter 7).) In practice it is essential to keep the blades well away from the hull surface and not to allow other design considerations to permit the clearance to be pared away.

9.4.2 *Excitation of Periodic Vibration by Waves*

If the motion and distortion of a hull in a confused sea are to be investigated these responses have to be treated as random processes. It might be necessary to determine the statistics of, say, bending moment amidships or vertical acceleration at the bow given details of a ship, the operating conditions and statistics of the waves. This type of analysis requires preliminary estimates to be made of steady-state responses to regular sinusoidal waves [14, 15]. Hull response to a sinusoidal sea is of cardinal importance in ship dynamics and it is significant that the frequencies at which perceptible responses occur are usually low enough for the hull-girder idealization to be tenable.

9.5 Structural Dynamics of a Uniform Beam in Symmetric Motion

In order to gain an appreciation of the vertical flexural response of ship hulls, it is useful to consider first the simple idealization of a uniform beam. For this we shall develop an admittedly rough-and-ready theory which shows why the simple quasi-static approach to the stressing of ships in waves has been so successful. In the interests of clarity at this stage we shall make use of the simplest possible beam theory, with the Bernoulli–Euler assumptions that shear and rotary inertia effects may be neglected. This is plausible for a long slender beam in the lowest modes of vibration. A more detailed treatment of the subject is given in [15].

Consider the hull girder as a uniform free–free beam floating in the water and subject to a distributed excitation force $f(x, t)$ per unit length. By describing the excitation in general terms we shall be able to handle both local forces, such as propeller excitation, and forces distributed along the complete hull length as in wave excitation. We shall, however, restrict our attention to harmonic motions, bearing in mind that this is frequently the first step of a more general dynamic analysis, and in particular of a random vibration analysis.

Under the influence of the distributed exciting force $f(x, t)$, the vertical equation of motion of an element of draught d and length δx, subject to the forces shown in Fig. 9.4, is

$$S + \frac{\partial S}{\partial x}\delta x - S + (mg + f)\delta x - \rho g b(d + v)\delta x = m'\delta x \frac{\partial^2 v}{\partial t^2}$$

where m represents the mass per unit length of the beam, ρ represents the water density, and, for the element, b and v represent the breadth and deflection. The shear force is represented by S and the bending moment by M. The section is assumed to have an associated added mass per unit length α, which when added to the distributed mass per unit length of the beam gives a 'virtual' mass per unit length m'. Note in this simple idealization that m' is assumed constant along the length of the beam and that no attempt is made to allow for damping forces, either hydrodynamic or structural. As $\delta x \to 0$ this equation becomes

$$\frac{\partial S}{\partial x} + mg + f - \rho g b(d + v) = m' \frac{\partial^2 v}{\partial t^2}.$$

Now in the equilibrium condition the weight of the element equals the buoyancy

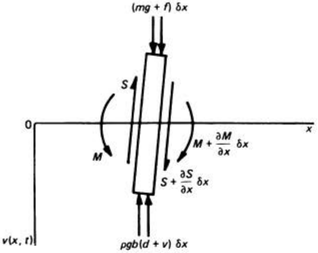

Fig. 9.4

force acting upon it; thus

$$mg = \rho gbd$$

so that the vertical equation of motion reduces to

$$\frac{\partial S}{\partial x} + f - \rho gbv = m' \frac{\partial^2 v}{\partial t^2}. \tag{9.40}$$

Since we are neglecting rotary inertia of the cross section, the rotational equation of motion is

$$M + \frac{\partial M}{\partial x}\,\delta x - M + S\delta x = 0$$

or in the limit $\delta x \to 0$

$$\frac{\partial M}{\partial x} = -S. \tag{9.41}$$

As we are also neglecting the influence of shear deformation, we may use the moment–curvature relation of simple beam theory:

$$M = EI\frac{\partial^2 v}{\partial x^2}. \tag{9.42}$$

Combining Equations (9.40), (9.41) and (9.42) we obtain the one governing equation

$$EI\frac{\partial^4 v}{\partial x^4} + \rho gbv + m'\frac{\partial^2 v}{\partial t^2} = f. \tag{9.43}$$

9.5.1 *Free Vibration*

By considering free vibration we may attempt to find 'natural frequencies' and 'principal modes' of the floating beam†. For free vibrations Equation (9.43) becomes

$$EI\frac{\partial^4 v}{\partial x^4} + \rho g b v + m'\frac{\partial^2 v}{\partial t^2} = 0, \tag{9.44}$$

which is satisfied by a solution of the form

$$v(x, t) = \phi(x)\sin\omega t$$

where

$$EI\frac{d^4\phi}{dx^4} + \rho g b\phi - m'\omega^2\phi = 0. \tag{9.45}$$

Let us take

$$\beta^4 = \frac{m'\omega^2 - \rho g b}{EI} \tag{9.46}$$

so that we may express Equation (9.45) in the form

$$\frac{d^4\phi}{dx^4} - \beta^4\phi = 0, \tag{9.47}$$

which has the general solution

$$\phi = A\cos\beta x + B\sin\beta x + C\cosh\beta x + D\sinh\beta x \tag{9.48}$$

where the constants A, B, C, D are determined by the boundary conditions, two at each end of the beam. For the free–free boundary conditions representing the conditions at the ends of the floating beam:

$$\left.\begin{aligned} M &= 0 \quad \text{at } x = 0, l \\ S &= 0 \quad \text{at } x = 0, l. \end{aligned}\right\} \tag{9.49}$$

Thus for the uniform beam

$$\left.\begin{aligned} \frac{d^2\phi}{dx^2} &= 0 \quad \text{at } x = 0, l \\ \frac{d^3\phi}{dx^3} &= 0 \quad \text{at } x = 0, l, \end{aligned}\right\} \tag{9.50}$$

and hence a set of four homogeneous equations are obtained for A, B, C, D. The determinant of the coefficients must therefore be set to zero, yielding a transcendental equation for β. This has an infinite number of solutions β_r, to each of which corresponds a frequency ω_r, and a set of four constants A_r, B_r, C_r, D_r defining a characteristic mode shape ϕ_r.

It is found [4] that these functions and mode shapes may be written

$$\phi_{-1}(x) = \frac{2\sqrt{3}}{l}\left(x - \frac{l}{2}\right) \quad \text{with } \beta_{-1} = 0 \quad (\text{i.e. } r = -1) \tag{9.51}$$

$$\phi_0(x) = 1 \quad \text{with } \beta_0 = 0 \quad (\text{i.e. } r = 0) \tag{9.52}$$

$$\phi_r(x) = (\cosh\beta_r x + \cos\beta_r x) - \sigma_r(\sinh\beta_r x + \sin\beta_r x) \tag{9.53}$$

† There are a number of objections to this on theoretical grounds [15], but these are ignored in the present treatment.

where

$$\sigma_r = \frac{\cosh \beta_r l - \cos \beta_r l}{\sinh \beta_r l - \sin \beta_r l}$$

with β_r given by

$$\cosh \beta_r l \cos \beta_r l - 1 = 0 \quad \text{for } r = 1, 2, \ldots .$$

Note that these functions are indeterminate to the extent of a multiplying constant in each. The amplitude of the response in free vibration is undefined if the initial conditions have not been specified. Note also that the index r has been chosen to start from -1 to emphasize the special characteristics of the lowest two modes ($r = -1, 0$) of the uniform beam. These modes are seen to be rigid-body modes, and are associated with the values $\beta_{-1} = 0 = \beta_0$.

Thus

$$\omega_{-1}^2 = \frac{\rho g b}{m'} = \omega_0^2.$$

Indeed, for the uniform free–free beam *in vacuo* ($\rho = 0$)

$$\omega_{-1} = 0 = \omega_0.$$

The distinction between these lowest two modes for the uniform free–free beam *in vacuo* and its higher modes ($r = 1, 2, \ldots$) is particularly clear. It is less evident for the uniform floating beam, in that the frequencies associated with the rigid-body motions are no longer zero. Any distinction between the lowest two and higher modes of a non-uniform floating beam becomes somewhat artificial, as the theory of the non-uniform beam illustrates, although in practice it is still useful to make this distinction. The characteristic modes for the uniform beam are shown in Fig. 9.5.

(a) *Orthogonality of the Principal Modes*

Let $\phi_r(x)$ and $\phi_s(x)$ be the principal modes corresponding to the frequencies ω_r, ω_s so that, from Equation (9.47),

$$\frac{d^4\phi_r}{dx^4} - \beta_r^4 \phi_r = 0 \tag{9.54a}$$

and

$$\frac{d^4\phi_s}{dx^4} - \beta_s^4 \phi_s = 0. \tag{9.54b}$$

When Equation (9.54a) is multiplied by ϕ_s and Equation (9.54b) is multiplied by ϕ_r, and the results combined and integrated over the range $0 \leqslant x \leqslant l$, then

$$(\beta_r^4 - \beta_s^4) \int_0^l \phi_r \phi_s dx = \int_0^l \left(\phi_s \frac{d^4\phi_r}{dx^4} - \phi_r \frac{d^4\phi_s}{dx^4} \right) dx.$$

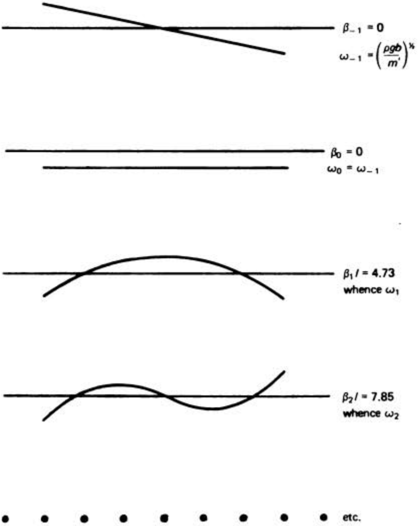

Fig. 9.5 Some characteristic modes of a floating beam.

Integrating the right-hand side twice by parts, we obtain

$$(\beta_r^4 - \beta_s^4)\int_0^l \phi_r\phi_s \mathrm{d}x = \left[\phi_s\frac{\mathrm{d}^3\phi_r}{\mathrm{d}x^3} - \phi_r\frac{\mathrm{d}^3\phi_s}{\mathrm{d}x^3} - \frac{\mathrm{d}\phi_s}{\mathrm{d}x}\frac{\mathrm{d}^2\phi_r}{\mathrm{d}x^2} + \frac{\mathrm{d}\phi_r}{\mathrm{d}x}\frac{\mathrm{d}^2\phi_s}{\mathrm{d}x^2}\right]_0^l$$
$$+\int_0^l\left(\frac{\mathrm{d}^2\phi_s}{\mathrm{d}x^2}\frac{\mathrm{d}^2\phi_r}{\mathrm{d}x^2} - \frac{\mathrm{d}^2\phi_r}{\mathrm{d}x^2}\frac{\mathrm{d}^2\phi_s}{\mathrm{d}x^2}\right)\mathrm{d}x,$$

which is equal to zero at $x = 0$ and l since the boundary term is zero for any combination of ideal supports. In this case, the appropriate conditions are, at $x = 0$ and l,

$$\frac{\partial^2\phi_r}{\partial x^2} = \frac{\partial^3\phi_r}{\partial x^3} = \frac{\partial^2\phi_s}{\partial x^2} = \frac{\partial^3\phi_s}{\partial x^3} = 0.$$

Therefore,

$$(\beta_r^4 - \beta_s^4) \int_0^l \phi_r \phi_s \mathrm{d}x = 0.$$

Now except for $r = -1$ and $s = 0$, or vice versa, $\beta_r \neq \beta_s$ if $r \neq s$. Hence,

$$\int_0^l \phi_r \phi_s \mathrm{d}x = 0, \quad r \neq s.$$

This is the orthogonality property for the characteristic functions of the floating uniform beam. By substituting the values given above for the characteristic functions it may in fact be shown that

$$\left.\begin{aligned} \int_0^l \phi_r \phi_s \mathrm{d}x &= 0, \quad r \neq s \\ &= l, \quad r = s \end{aligned}\right\} \text{for } r, s = -1, 0, 1, 2, \ldots, . \tag{9.55}$$

9.5.2 *Forced Vibration*

Equation (9.43) may be written in the form

$$\frac{\partial^2 v}{\partial t^2} + \gamma^2 \frac{\partial^4 v}{\partial x^4} + \omega_0^2 v = \frac{f}{m'} \tag{9.56}$$

where

$$\gamma^2 = \frac{EI}{m'}, \qquad \omega_0^2 = \frac{\rho g b}{m'}.$$

The response $v(x, t)$ may be expressed in terms of principal coordinates $p_r(t)$ in the form

$$v(x, t) = \sum_{r=-1}^{\infty} p_r(t)\phi_r(x).$$

The principal coordinates therefore satisfy the equation

$$\sum_{r=-1}^{\infty} \ddot{p}_r(t)\phi_r(x) + \gamma^2 \sum_{r=-1}^{\infty} p_r(t) \frac{\mathrm{d}^4 \phi_r(x)}{\mathrm{d}x^4} + \omega_0^2 \sum_{r=-1}^{\infty} p_r(t)\phi_r(x) = \frac{1}{m'} f(x, t).$$

But, since

$$\frac{\mathrm{d}^4 \phi_r(x)}{\mathrm{d}x^4} = \beta_r^4 \phi_r(x), \quad r = -1, 0, 1, 2, \ldots$$

the former equation may be written as

$$\sum_{r=-1}^{\infty} \ddot{p}_r(t)\phi_r(x) + \sum_{r=-1}^{\infty} (\gamma^2 \beta_r^4 + \omega_0^2) p_r(t)\phi_r(x) = \frac{1}{m'} f(x, t). \tag{9.57}$$

By noting that

$$\gamma^2\beta_r^4 + \omega_0^2 = \omega_r^2$$

we may multiply the equation of motion (9.57) throughout by $\phi_s(x)$ and integrate over the range $0 \leqslant x \leqslant l$. It turns out that, because of the orthogonality of the modes,

$$\ddot{p}_r + \omega_r^2 p_r = \frac{1}{m'l}\int_0^l f(x,t)\phi_r(x)\mathrm{d}x, \quad r = -1, 0, 1, 2, \ldots .$$

As we are concerned with harmonic excitation at frequency ω, the force $f(x, t)$ may be written in the form

$$f(x, t) = \mathrm{Re}[\bar{f}(x)\exp(\mathrm{i}\omega t)]$$

where Re denotes the real part of the complex number contained within the brackets. Note that although $f(x, t)$ is real, $\bar{f}(x)$ may be a complex quantity; indeed this is the case for the wave excitation to be examined subsequently.

We may now define the generalized force $\bar{f}_r$ associated with the rth mode. Thus,

$$\bar{f}_r = \int_0^l \bar{f}(x)\phi_r(x)\mathrm{d}x, \quad r = -1, 0, 1, 2, \ldots .$$

The uncoupled differential equations for the principal coordinates may therefore be written

$$\ddot{p}_r + \omega_r^2 p_r = \mathrm{Re}\left[\frac{\bar{f}_r}{m'l}\exp(\mathrm{i}\omega t)\right], \quad r = -1, 0, 1, 2, \ldots . \tag{9.58}$$

The steady-state modal responses are the particular integrals of this set of equations and are given by

$$p_r(t) = \mathrm{Re}\left[\frac{\bar{f}_r}{m'l(\omega_r^2 - \omega^2)}\exp(\mathrm{i}\omega t)\right] \tag{9.59}$$

for all modes. The response to the harmonic excitation is

$$v(x, t) = \mathrm{Re}\left[\sum_{r=-1}^{\infty} \frac{\bar{f}_r\phi_r(x)}{m'l(\omega_r^2 - \omega^2)}\exp(\mathrm{i}\omega t)\right]. \tag{9.60}$$

We note that resonance is possible in any mode r if $\omega \to \omega_r$. Moreover the response in any mode r is dependent on the generalized force associated with that mode. The latter observation is crucial to the behaviour of the beam under the influence of wave excitation, as we shall see, and it is also relevant to machinery excitation and propeller excitation. Consider, for example, propeller-induced vertical forces at the stern bearing of a ship, which we shall represent as acting at the point $x = x_s$ of our uniform beam. If the magnitude of the force is P, the rth generalized force is

$$\bar{f}_r = \int_0^l \bar{f}(x)\phi_r(x)\mathrm{d}x = P\phi_r(x_s). \tag{9.61}$$

Hence the response in mode r is proportional to the magnitude of the rth modal ordinate at the point of application of the force. If the excitation occurs at a node of the rth mode (i.e. at a point where $\phi_r(x) = 0$), then the response in that mode will be zero. In practice, however, this possibility is rarely achieved because of the large number of modes excited during the service conditions of a real ship.

(a) *Response to Wave Excitation*

The uniform beam is assumed to be excited by deep-water sinusoidal waves possessing a time-dependent depression

$$\zeta(x, t) = a\cos(\omega_e t - kx) \tag{9.62}$$

where ω_e represents the frequency of encounter with the waves, a represents the wave amplitude and k the wave number. The excitation force is then taken as the crude and simple approximation†

$$\begin{aligned} f(x, t) &= \rho g b \zeta(x, t) \\ &= \mathrm{Re}\left[a\rho g b \exp(-\mathrm{i}kx)\exp(\mathrm{i}\omega_e t)\right]. \end{aligned}$$

Hence for wave excitation

$$\bar{f}(x) = a\rho g b \exp(-\mathrm{i}kx)$$

and the generalized force is, say,

$$\bar{f}_r = a\rho g b\int_0^l \exp(-\mathrm{i}kx)\phi_r(x)\mathrm{d}x = a\rho g b l\bar{g}_r.$$

The response of the beam to wave excitation is, following substitution in Equation (9.60),

$$\begin{aligned} v(x, t) &= \mathrm{Re}\left[\sum_{r=-1}^{\infty} \frac{a\rho g b\bar{g}_r\phi_r(x)}{m'(\omega_r^2 - \omega_e^2)}\exp(\mathrm{i}\omega_e t)\right] \\ &= a\sum_{r=-1}^{\infty} \frac{\omega_0^2\phi_r(x)}{\omega_r^2 - \omega_e^2}\frac{1}{l}\int_0^l \phi_r(x)\cos(\omega_e t - kx)\mathrm{d}x \end{aligned} \tag{9.63}$$

where use is made of the relation

$$m'\omega_0^2 = \rho g b. \tag{9.64}$$

Evidently, the possibility of resonance arises if the wave encounter frequency ω_e equals a natural frequency ω_r. It may also be noted that the generalized force $\bar{f}_r$ is a function of the product kl, and hence of the ship length/wavelength ratio l/Λ, since

$$k = \frac{2\pi}{\Lambda}. \tag{9.65}$$

† Such an approach completely ignores scattering of the incident wave by the hull, a behaviour discussed in [16].

The modal responses will therefore be dependent on the ratio l/Λ. These matters may be illustrated by formulating a rudimentary theory of seakeeping. To do this responses in the -1 and 0 modes only are considered and the subsequent theory of seakeeping may be regarded as a study of motion in these modes. We are therefore concerned with the response

$$v(x,t)=a\left(\frac{\omega_0^2}{\omega_0^2-\omega_e^2}\right)\mathrm{Re}\left[\left\{\bar{g}_{-1}\left(\frac{l}{\Lambda}\right)\frac{2\sqrt{3}}{l}\left(x-\frac{l}{2}\right)+\bar{g}_0\left(\frac{l}{\Lambda}\right)\right\}\exp(\mathrm{i}\omega_e t)\right]$$

where $\bar{g}_r(l/\Lambda)$ indicates that $\bar{g}_r$ is a function of l/Λ.

It is convenient to think in terms of the slope and vertical displacement of the centroid. For the uniform ship these are

$$\frac{\partial v}{\partial x}=2\sqrt{3}\left(\frac{a}{l}\right)\left(\frac{\omega_0^2}{\omega_0^2-\omega_e^2}\right)\mathrm{Re}\left[\bar{g}_{-1}\left(\frac{l}{\Lambda}\right)\exp(\mathrm{i}\omega_e t)\right] \tag{9.66}$$

$$v=a\left(\frac{\omega_0^2}{\omega_0^2-\omega_e^2}\right)\mathrm{Re}\left[\bar{g}_0\left(\frac{l}{\Lambda}\right)\exp(\mathrm{i}\omega_e t)\right] \tag{9.67}$$

respectively. The integrals defining $\bar{f}_{-1}, \bar{f}_0$ can now be evaluated:

$$\bar{g}_{-1}\left(\frac{l}{\Lambda}\right)=\frac{\sqrt{3}}{2\pi^2}\left(\frac{\Lambda}{l}\right)^2\left\{\left(\cos\frac{2\pi l}{\Lambda}+\frac{\pi l}{\Lambda}\sin\frac{2\pi l}{\Lambda}-1\right)\right.$$
$$\left.-\mathrm{i}\left[\sin\frac{2\pi l}{\Lambda}-\frac{\pi l}{\Lambda}\left(1+\cos\frac{2\pi l}{\Lambda}\right)\right]\right\}$$

$$\bar{g}_0\left(\frac{l}{\Lambda}\right)=\frac{1}{2\pi}\left(\frac{\Lambda}{l}\right)\left\{\sin\frac{2\pi l}{\Lambda}-\mathrm{i}\left(1-\cos\frac{2\pi l}{\Lambda}\right)\right\}.$$

Let us now briefly examine the variation of the slope and vertical displacement with the ratio ship length/wavelength. Consider first three special cases:

(i) a very short ship ($l/\Lambda \to 0$);
(ii) a 'Reed' ship whose length equals the wavelength ($l/\Lambda = 1$); and
(iii) a very long ship ($l/\Lambda \to \infty$).

(i) *The short uniform ship*. If $l/\Lambda = \epsilon$, a small quantity, we find that

$$\bar{g}_{-1}\left(\frac{l}{\Lambda}\right)=-\frac{\pi^2}{\sqrt{3}}\epsilon^2-\mathrm{i}\frac{\pi}{\sqrt{3}}\epsilon$$

and

$$g_0\left(\frac{l}{\Lambda}\right)=1-\mathrm{i}\pi\epsilon.$$

It follows that, amidships,

$$\frac{\partial v}{\partial x}\triangleq\left(\frac{a}{l}\right)\left(\frac{\omega_0^2}{\omega_0^2-\omega_e^2}\right)2\pi\epsilon\sin\omega_e t$$

and

$$\nu \simeq a\left(\frac{\omega_0^2}{\omega_0^2 - \omega_e^2}\right) \cos \omega_e t.$$

Now the corresponding wave depression and wave slope at the centre of mass of the short ship are, respectively,

$$\begin{aligned}\zeta &= a \cos \pi\epsilon \cos \omega_e t + a \sin \pi\epsilon \sin \omega_e t \\ &\simeq a \cos \omega_e t\end{aligned}$$

and

$$\begin{aligned}\frac{\partial \zeta}{\partial x} &= \left(\frac{a}{l}\right) 2\pi\epsilon(\cos \pi\epsilon \sin \omega_e t - \sin \pi\epsilon \cos \omega_e t) \\ &\simeq \left(\frac{a}{l}\right) 2\pi\epsilon \sin \omega_e t.\end{aligned}$$

Hence for the short ship

$$\frac{\partial \nu}{\partial x} \simeq \frac{\omega_0^2}{\omega_0^2 - \omega_e^2} \frac{\partial \zeta}{\partial x} \tag{9.68}$$

and

$$\nu \simeq \frac{\omega_0^2}{\omega_0^2 - \omega_e^2} \zeta \tag{9.69}$$

Thus the ship follows the surface of the sea. However, the ship motion may resonate if $\omega_e \to \omega_0$.

(ii) *The uniform 'Reed' ship.* If $l/\Lambda = 1$, we find that

$$\bar{g}_{-1}\left(\frac{l}{\Lambda}\right) = i\frac{\sqrt{3}}{\pi}, \qquad g_0\left(\frac{l}{\Lambda}\right) = 0.$$

Thus,

$$\frac{\partial \nu}{\partial x} = \left(\frac{a}{l}\right)\left(\frac{\omega_0^2}{\omega_0^2 - \omega_e^2}\right)\frac{6}{\pi} \cos \omega_e t \tag{9.70}$$

and

$$\nu = 0 \tag{9.71}$$

for the motion amidships. The ship thus performs a sinusoidal motion in which the slope fluctuates, without vertical motion of the centre of mass, as shown in Fig. 9.6. Note again that the motion will resonate if $\omega_e \to \omega_0$.

(iii) *The long uniform ship.* If $l/\Lambda \to \infty$, it is found that $\bar{g}_{-1}$ and $\bar{g}_0 \to 0$. Responses in the -1 and 0 modes therefore become very small, although theoretically resonance is possible if $\omega_e \to \omega_0$.

For the more general case of a ship of length l, the amplitude of the oscillating

Fig. 9.6 Response of a 'Reed' ship to harmonic wave excitation.

slope and displacement amidships may now be examined. These are, respectively,

$$\left|\frac{\partial v}{\partial x}\right| = \left(\frac{a}{l}\right)\left(\frac{\omega_0^2}{\omega_0^2-\omega_e^2}\right)\left(\frac{\Lambda}{l}\right)^2\frac{3}{\pi^2}\left\{\left(\cos\frac{2\pi l}{\Lambda}+\frac{\pi l}{\Lambda}\sin\frac{2\pi l}{\Lambda}-1\right)^2\right.$$

$$\left.+\left(\sin\frac{2\pi l}{\Lambda}-\frac{\pi l}{\Lambda}\left(1+\cos\frac{2\pi l}{\Lambda}\right)\right)^2\right\}^{1/2}$$

$$= \left(\frac{a}{l}\right)\left(\frac{\omega_0^2}{\omega_0^2-\omega_e^2}\right)\left(\frac{\Lambda}{l}\right)^2\frac{6}{\pi^2}\left(\sin\frac{\pi l}{\Lambda}-\frac{\pi l}{\Lambda}\cos\frac{\pi l}{\Lambda}\right)$$

$$= \left(\frac{a}{l}\right)\left(\frac{\omega_0^2}{\omega_0^2-\omega_e^2}\right)h_{-1}\left(\frac{l}{\Lambda}\right)$$

$$|\,v\,| = a\left(\frac{\omega_0^2}{\omega_0^2-\omega_e^2}\right)\left(\frac{\Lambda}{l}\right)\frac{1}{2\pi}\left\{\sin^2\frac{2\pi l}{\Lambda}+\left(1-\cos\frac{2\pi l}{\Lambda}\right)^2\right\}^{1/2}$$

$$= a\left(\frac{\omega_0^2}{\omega_0^2-\omega_e^2}\right)\left(\frac{\Lambda}{l}\right)\frac{1}{\pi}\sin\frac{\pi l}{\Lambda} = a\left(\frac{\omega_0^2}{\omega_0^2-\omega_e^2}\right)h_0\left(\frac{l}{\Lambda}\right)$$

with the dimensionless functions $h_{-1}(l/\Lambda)$ and $h_0(l/\Lambda)$ defined accordingly. These quantities are plotted in Fig. 9.7. We see that for a given wave height the maximum

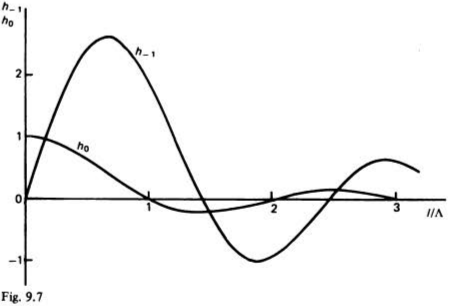

Fig. 9.7

variation of slope $|\partial v/\partial x|$ arises in waves with a length approximately equal to the length of the beam.

(b) *Wave-excited Bending Moments in the Uniform Beam*

If the hydrodynamic force on the beam is F_H per unit length, the bending moment at any section x_0 is

$$M(x_0, t) = \int_0^{x_0} (F_H - m\ddot{v})(x_0 - x)dx. \tag{9.72}$$

Now in terms of our crude theory of the uniform beam

$$F_H = \rho g b(\zeta - v) - \alpha\ddot{v}. \tag{9.73}$$

Thus, from Equations (9.72) and (9.73),

$$M(x_0, t) = \rho g b \int_0^{x_0} \left((\zeta - v) - \frac{m + \alpha}{\rho g b}\ddot{v}\right)(x_0 - x)dx$$

$$= \rho g b \int_0^{x_0} \left((\zeta - v) - \frac{\ddot{v}}{\omega_0^2}\right)(x_0 - x)dx \tag{9.74}$$

where use is made of Equation (9.63) and the relation

$$m + \alpha = m'. \tag{9.75}$$

Substituting for $\zeta(x, t)$, from Equation (9.62), and for $v(x, t)$, from Equation (9.63), we obtain from Equation (9.74)

$$M(x_0, t) = a\rho g b \,\mathrm{Re}\left[\int_0^{x_0} \left(\exp(-ikx) + \sum_{r=-1}^{\infty} \frac{\omega_e^2 - \omega_0^2}{\omega_r^2 - \omega_e^2}\bar{g}_r\phi_r(x)\right)(x_0 - x)dx \exp(i\omega_e t)\right]. \tag{9.76}$$

For the sake of simplicity, consideration is given to the amidships bending moment at $x_0 = l/2$. Symmetry arguments then show that all the terms of the series for even values of r are zero. The integral in Equation (9.76) may be evaluated and, for convenience, separated into two sets of terms: the summation for $r = 1, 3, 5, \ldots, \infty$, and the others. This leads to the expression

$$M\left(\frac{l}{2}, t\right) = a\rho g b l^2 \left(\frac{\sin \pi l/\Lambda}{8(\pi l/\Lambda)} - \frac{1 - \cos \pi l/\Lambda}{4(\pi l/\Lambda)^2}\right) \cos\left(\omega_e t - \frac{\pi l}{\Lambda}\right)$$

$$+ a\rho g b(\omega_e^2 - \omega_0^2) \sum_{r=1,3,\ldots}^{\infty} \frac{1}{\omega_r^2 - \omega_e^2} \frac{1}{l}\int_0^l \phi_r(x)\cos(\omega_e t - kx)dx \int_0^{l/2} \phi_r(x)\left(\frac{l}{2} - x\right)dx. \tag{9.77}$$

It is thus found that resonant contributions to the amidships bending moment are obtained only from the modes $1, 3, 5, \ldots$. In particular, there is no resonant contribution to the amidships bending moment in a uniform beam from the −1 mode.

Let us now consider the limit of the right-hand side of Equation (9.77) for an infinitely rigid ship. In this case

$$\gamma^2 = \frac{EI}{m'} \to \infty.$$

Hence

$$\omega_r^2 = (\gamma^2 \beta_r^4 + \omega_0^2) \to \infty, \quad r = 1, 2, 3, \ldots$$

and all the terms of the summation tend to zero. It follows that the amidships bending moment in a perfectly rigid beam is given by

$$M\left(\frac{l}{2}, t\right) = a\rho g b l^2 M^{\mathrm{W}}\left(\frac{l}{\Lambda}\right) \cos\left(\omega_e t - \frac{\pi l}{\Lambda}\right) \tag{9.78}$$

where $M^{\mathrm{W}}(l/\Lambda)$ is the dimensionless quantity

$$M^{\mathrm{W}}\left(\frac{l}{\Lambda}\right) = \left(\frac{\sin \pi l/\Lambda}{8(\pi l/\Lambda)} - \frac{1 - \cos \pi l/\Lambda}{4(\pi l/\Lambda)^2}\right). \tag{9.79}$$

Furthermore, this is the exact value of the amidships bending moment in a flexible beam at the particular encounter frequency $\omega_e = \omega_0$. It is also a close approximation at other values of encounter frequency, provided that $\omega_e \ll \omega_1$; this is because all terms of the summation in Equation (9.77) are then negligible. In other words, a small change of ω_e away from ω_0 causes little direct change in the bending moment in the flexible beam. The only indirect influence is through the term $M^{\mathrm{W}}(l/\Lambda)$ since ω_e is related to the wave frequency and hence to Λ.

It is clear that the nature of the response of the beam at low frequencies ($\omega_e \ll \omega_1$) differs qualitatively from that at higher frequencies. When ω_e coincides with one of the natural frequencies $\omega_1, \omega_2, \omega_3, \ldots$, high stresses are set up due to resonance. The stresses are infinite in our theoretical model, although in practice they are of course limited by damping. It is convenient to refer to this phenomenon as a condition of 'resonant encounter'. At the lower frequencies, this phenomenon does not exist in the uniform beam. The possibility of high stresses then arises because of the nature of the function $M^{\mathrm{W}}(l/\Lambda)$, which is plotted in Fig. 9.8. We see that there is an absolute maximum when

$$\frac{l}{\Lambda} = 1.11. \tag{9.80}$$

In the lower frequency range an absolute maximum amplitude of amidships bending moment exists if the ship length is a little greater than the wavelength. We refer to this condition as ship–wave matching.

9.6 Application of Beam Analysis to Ship Hulls in Steady Motion

The uniform beam analysis which has been outlined, and which is discussed in more detail in [17], indicates many of the features of the behaviour of real ship hulls. The response to dynamic excitation may be written as the sum of responses in an infinite series of modes, of which only the lowest few modes will generally be of

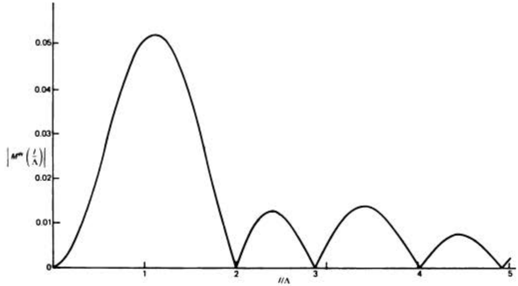

Fig. 9.8

interest in the range of frequencies excited in practice. In the higher modes it is unlikely that the simple assumptions of beam theory will be tenable. It may be misleading to assume that at the higher frequencies plane cross sections remain sensibly plane: thus in the higher modes of a tanker with longitudinal stiffening, the instantaneous distortion at a cross section may be as indicated in Fig. 9.9 (see [18]). This, however, is a specialized subject beyond the scope of this book, as are the details of introducing corrections for the influences of shear and rotary inertia on the lowest beam modes. We simply observe that it may be necessary to make allowance for these, since a ship is unlikely to be very long and thin; but this is relatively straightforward when use is made of the approximate numerical techniques which become obligatory when dealing with the complex non-uniformity of ship hulls.

It is clear that interest centres on the lowest modes of a ship hull, acting as a beam, and on the responses in those modes to various excitations. Methods of performing these calculations will be described in the following sections. The response of real ship hulls is discussed in a qualitative manner [19].

For the uniform ship the lowest two modes were found to be rigid-body modes having equal natural frequencies. Neither of these characteristics generally holds for

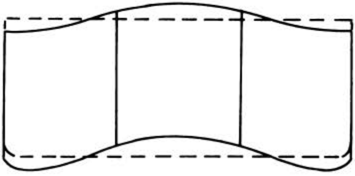

Fig. 9.9

a real ship, represented by a non-uniform beam: the lowest two modes are not without distortion, and the corresponding frequencies differ (although they are, nevertheless, close to each other). Furthermore, a real ship does not usually have fore-and-aft symmetry, and the strict symmetry and antisymmetry of successive modes does not always apply. For most ships the distortion in the 'heave' and 'pitch' modes is negligible, an assumption that has always been made in the past. If the higher modes are ignored, this then leads to the idea of the ship as a rigid body, which has for many years been the basis for ship stressing. It can now be shown how this is related to the quasistatic approach which was discussed in Chapter 3.

9.6.1 *Rigid Ship Approximation for Behaviour in Waves*

Our study of the uniform beam in waves has shown how, in the rigid modes, the displacement and slope of the centre of mass are subject to a condition of resonant encounter. This is true also of a non-uniform beam, but for a real ship damping due to wave making in these modes is so high that resonant magnification factors greater than 1.5 are most unlikely. Large motions of a real ship are therefore predominantly the result of some type of ship-wave matching phenomenon. Maximum pitching motions occur somewhere in the region of wavelength equal to ship length.

The overall strength of the ship is related to the maximum hull girder bending moment, and this has been examined for the uniform beam. Qualitatively, the analytical results for a real ship are very similar, if it is assumed to respond as a rigid body. Ship–wave matching is again the governing phenomenon, and the maximum amidships bending moment is given in a wave whose length is approximately equal to the ship length. This indicates why the traditional quasistatic approach of balancing the ship on a wave of the same length has worked so well. For a simple uniform beam the quasistatic approach gives an identical value of bending moment to the amplitude of fluctuating moment obtained from a dynamic analysis of the rigid beam. Now the dynamic analysis of the rigid-body motions of a *real* ship in waves introduces several complexities beyond our previous discussion. Nevertheless, the resulting bending moments are found to be of the same order (in fact somewhat smaller) as those obtained from a quasistatic analysis.

This discussion is not intended as a justification for the quasistatic approach, but rather as an indication of why it has worked satisfactorily before more sophisticated analytical tools became available. The reasons for abandoning it are clear. Not only does the quasistatic analysis generally give unnecessarily conservative results when compared with a well formulated, deterministic, rigid-body dynamic analysis, but it has no possibility of extension to deal with the random nature of waves. The advance in the 1950s to the rigid-ship dynamic approach allowed a fundamental switch in the philosophy underlying ship stressing. By using certain reasoned assumptions about the statistical properties of waves, together with the mathematics of random process theory, it became possible to estimate the maximum bending moment likely to be applied once in the life-time of the ship.† The ship is then designed to resist this without demanding major repairs.

It is worth while to outline the procedure involved in a thorough dynamic analysis of the rigid ship. The equations of motion are written in terms of appropriate generalized coordinates, which for symmetric motions correspond to heave and

† This corresponds to a probability of about 10^{-8} that the bending moment will not be exceeded.

pitch measured at the centre of mass. The two equations are coupled by the hydrodynamic terms for added inertia, damping and stiffness. An additional complexity is that these hydrodynamic terms are generally frequency-dependent, and involve contributions proportional to the forward speed of the ship. The wave-exciting force has terms proportional to the free-surface elevation and to the velocities and accelerations of wave particles. All these hydrodynamic forces are evaluated on the basis of strip theory, in which the flow past hull cross sections is assumed to be two-dimensional. For a given ship velocity and wave frequency, the resulting coupled equations may be solved and the heave and pitch amplitudes determined. As for the uniform beam the bending moment at any section may then be calculated. In this way a transfer function is derived, giving the vertical bending moment resulting from an incident wave of unit amplitude, over a range of frequencies. This transfer function is used in conjunction with wave statistics provided by the oceanographer to yield probabilistic estimates of extreme bending moments.

The procedure we have summarized in the preceding paragraph is quite complex. Even so it is based on fairly sweeping assumptions. Quite apart from the strip-theory hypothesis for obtaining hydrodynamic forces, it is assumed that the ship responds in rigid modes and in no others. This latter simplification is reasonable provided that (i) the lowest two modes are indeed essentially rigid, and (ii) the relevant frequencies of excitation are well below the natural frequencies of the higher modes. Condition (i) is not a matter that has been examined in the past, and seems to call for further investigation. The behaviour of the ship when condition (ii) is not satisfied will now be examined.

9.6.2 *Response in the Two-node and Higher Modes*

Some very large and flexible ships may be induced to resonate in the two-node mode by waves. This is a relatively new problem, caused by the decrease in natural frequency associated with increase in ship size. It is particularly relevant to tankers and Great Lakers, and a correction, distinguished by the name 'springing', is then sometimes applied for the analysis [20]. The analysis of springing stresses may form an integral part of the assessment of the strength of large ships.

Response to wave excitation ('springing') has also been well illustrated by the uniform beam analysis, but there are certain aspects which should be considered in order to emphasize the similarities and contrasts with wave-induced response in the lowest modes. Flexural stresses due to springing are associated with the phenomenon of resonant encounter, and they are therefore strongly dependent on a ship's forward speed. In contrast, large bending moments due to response in the lowest modes arise predominantly from ship–wave matching, and these are only weakly dependent on speed. Full-scale measurements at service speeds have shown springing stresses in current ships, including tankers in the 3 GN ($\cong$ 300 000 tonf) displacement range, to be generally smaller than low-frequency wave stresses, except in large Great Lakers, where they have been found to be of the same order. The difficulty, however, is that of designing for fatigue. In order to predict accurately the fluctuating stress ranges to which a vessel will be subjected, it is essential that the designer should have reliable methods of dynamic analysis.

It will be appreciated that the separation of a 'springing' response from that in the lowest modes rests upon certain empirical assumptions, and there is consequently some difficulty in attempting to develop a rational theory for use with very large ships. It has been pointed out [15] that difficulty of this nature can be avoided quite simply by adopting a rather different approach *ab initio*.

It has been noted that a rotating propeller stimulates a ship's hull into forced vibration and there exists a real possibility that the response might be resonant. Generally speaking, the frequency of such motion is sufficiently large to throw doubt on the concept of the 'hull-girder'; the hull does not act as a non-uniform beam. But at the lower end of the propeller frequency spectrum this form of idealization may still be adequate and much research in this field is based upon this assumption. We are then concerned with the two-node and higher modes.

To examine the response of a ship hull to propeller (and for that matter, other machinery) excitation in these rather restricted conditions it is necessary to determine the excitation forces. Once this information has been obtained, by experiment or by theoretical calculations, the appropriate generalized forces may be calculated. The modes of interest are those whose natural frequencies are close to a major driving frequency. Modal responses are calculated on the basis of assumed values of damping, which is discussed below. In contrast with calculations of springing, responses to propeller excitation are usually made with the aim of keeping amplitudes within tolerable limits for environmental (as opposed to strength) reasons.

9.6.3 *Numerical Methods for Hull-girder Vibrations*

In the discussion of the structural dynamics of ship hulls in symmetric motions, it is seen how the first step in the analysis is to obtain the first few natural frequencies and characteristic modes. For complex non-uniform beams of the type that might be used to idealize a real ship hull, exact solution of the free vibration equations will seldom, if ever, be possible. Approximate numerical methods are required, and we shall briefly outline two possible approaches based on methods applicable to a very wide variety of problems in structural mechanics. For very rapid, approximate solutions to certain ship vibration problems other methods may also be useful, as for example those due to Rayleigh and Stodola. These are powerful methods which may be clearly illustrated in the context of beam vibrations, but they are unlikely to be of direct relevance to analysis of the highly complex structure of a ship hull. The Rayleigh and Stodola methods are of more use for simpler configurations; an example of their use might be in the estimation of the lowest natural frequency of an antenna, idealized as a tapered cantilever.

In this chapter we shall continue to adopt the simplifying assumptions used in Section 9.5. That is, we shall not employ the far more powerful methods of hydroelastic ship analysis but will continue to use the basic ideas that underly much contemporary practice.

(a) *Transfer Matrix Methods*

These methods are well suited to analysis of non-uniform beams, and the effects of shear deformation and rotary inertia may be included in a straightforward manner. To keep our explanation simple, however, these latter effects will again be considered negligible.

In the general form of the method, the beam is idealized as a set of uniform beams joined end to end. In considering one of these elementary uniform beams, the displacement, slope, bending moment and shear force at one end are expressed in terms of the corresponding quantities at the other end by means of a so-called 'transfer matrix'. This matrix is obtained from the general solution for free vibration of a uniform beam. By proceeding from one end of the beam to the other, and multiplying transfer matrices for adjacent elements, the bending moment and shear force at one end may be expressed in terms of the displacement and slope at the other for a certain frequency of vibration. Because of the free–free boundary conditions this leads to a homogeneous set of equations; the determinant of coefficients should therefore be zero. The value of the determinant will, however, depend on the chosen frequency for which the calculation was made, and by iteration the natural frequency may be found. The corresponding mode shape may then be readily obtained.

A somewhat simpler variant of this approach is the Myklestad–Prohl method, which is now described in some detail. The non-uniform beam is again divided into a series of beams, but the mass of each elementary beam is apportioned between its ends and concentrated there. The continuous beam is thus approximated (as indicated in Fig. 9.10) as a system possessing

$$\{(\text{number of cuts}) + 2\} = n$$

degrees of freedom.

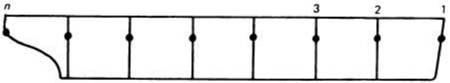

Fig. 9.10

Each degree of freedom may be associated with the deflection of a mass, and that deflection may be considered as an element of a matrix $\mathbf{q}$. In terms of our present approach, each such deflection must in some way be associated with an 'added mass'. In practice, an added mass is found for each 'slice' of the hull, being given by

$$\begin{pmatrix}\text{added mass per unit length}\\ \text{for appropriate 'average'}\\ \text{cross section}\end{pmatrix} \times (\text{length of slice}).$$

This quantity is added to the mass of the slice and the sum is then divided (usually equally) between the appropriate cuts.

The concentrated masses are connected by lengths of beam which, being massless and undamped, distort according to the laws of statics, and if the cuts are close enough together these short lengths are effectively uniform. If the hull can indeed be treated as a beam (rather than a shell)† we may find flexibilities for the segments, treating each in turn as a cantilever of small span. Thus for the rth slice, of span l_r, the flexibilities are

$$\xi_r = \frac{l_r^3}{3EI_r}; \quad \eta_r = \frac{l_r^2}{2EI_r}; \quad \zeta_r = \frac{l_r}{EI_r}$$

as indicated in Fig. 9.11.

† It has been suggested that this is acceptable provided that an equivalent, reduced width (i.e. beam dimension) is assumed.

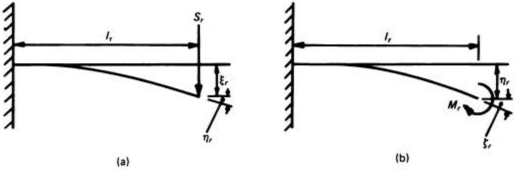

Fig. 9.11

Consider a vibration of the complete free–free beam with some assumed frequency ω. Starting at the right-hand end of Fig. 9.10 we have a mass m_1 representing half the mass of the first slice and half the added mass of that slice (assuming that the masses were divided equally). This mass is acted upon by a shear force S_1 and bending moment M_1, both of which vary sinusoidally with time (see Fig. 9.12(a)). Evidently

$$S_1 = m_1 \ddot{v}_1 = -m_1 \bar{v}_1 \omega^2 \sin \omega t = \bar{S}_1 \sin \omega t$$

$$M_1 = \bar{M}_1 \sin \omega t = 0$$

so that the amplitudes $\bar{S}_1$ of S_1 and $\bar{M}_1$ of M_1 can be written down in terms of the assumed amplitudes $\bar{v}_1$ of deflection v and $\bar{\theta}_1$ of slope θ at mass 1. Now consider

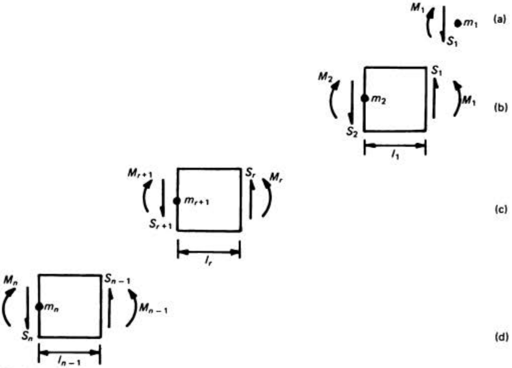

Fig. 9.12

the first slice together with the second mass (Fig. 9.12(b)). The deflection (positive downwards) and slope (positive for clockwise rotation) at mass m_2 are given by v_2 and θ_2, where

$$\theta_1 = \theta_2 - \eta_1 S_1 - \zeta_1 M_1$$

$$v_1 = v_2 - \xi_1 S_1 - \eta_1 M_1 + l_1 \theta_2$$

respectively. Hence

$$\theta_2 = \theta_1 + \eta_1 S_1 + \zeta_1 M_1 = (\bar{\theta}_1 + \eta_1 \bar{S}_1)\sin \omega t = \bar{\theta}_2 \sin \omega t$$

$$v_2 = v_1 + \xi_1 S_1 + \eta_1 M_1 - l_1 \theta_2 = (\bar{v}_1 + \xi_1 \bar{S}_1 - l_1 \bar{\theta}_2)\sin \omega t = \bar{v}_2 \sin \omega t.$$

Furthermore,

$$S_2 = S_1 + m_2 \ddot{v}_2 = (\bar{S}_1 - m_2 \bar{v}_2 \omega^2)\sin \omega t = \bar{S}_2 \sin \omega t$$

$$M_2 = M_1 + l_1 S_1 = l_1 \bar{S}_1 \sin \omega t = \bar{M}_2 \sin \omega t.$$

Starting with assumed amplitudes $\bar{v}_1$, $\bar{\theta}_1$ we first found $\bar{S}_1$ and $\bar{M}_1$. Now we have deduced $\bar{v}_2$, $\bar{\theta}_2$, $\bar{S}_2$ and $\bar{M}_2$. It is possible to move along the whole beam in this way for the assumed frequency since, at the rth slice (Fig. 9.12(c)),

$$\bar{\theta}_{r+1} = \bar{\theta}_r + \eta_r \bar{S}_r + \zeta_r \bar{M}_r \tag{9.81a}$$

$$\bar{v}_{r+1} = \bar{v}_r + \xi_r \bar{S}_r + \eta_r \bar{M}_r - l_r \bar{\theta}_{r+1} \tag{9.81b}$$

$$\bar{S}_{r+1} = \bar{S}_r - m_{r+1} \bar{v}_{r+1} \omega^2 \tag{9.81c}$$

$$\bar{M}_{r+1} = \bar{M}_r + l_r \bar{S}_r. \tag{9.81d}$$

The calculations may be done in a tabular form or, much more effectively, on a computer.

The results of the calculation are the quantities

$$S_n = \bar{S}_n \sin \omega t \tag{9.82a}$$

$$M_n = \bar{M}_n \sin \omega t \tag{9.82b}$$

at the left-hand end of the beam (Fig. 9.12(d)). They are expressed in the form

$$\bar{S}_n = A_n \bar{v}_1 + B_n \bar{\theta}_1 \tag{9.83a}$$

$$\bar{M}_n = C_n \bar{v}_1 + D_n \bar{\theta}_1 \tag{9.83b}$$

But since the left-hand end is free, $\bar{M}_n = 0$ so that

$$\bar{\theta}_1 = -\frac{C_n}{D_n} \bar{v}_1$$

and hence

$$\bar{S}_n = \left(A_n - \frac{B_n C_n}{D_n}\right) \bar{v}_1$$

or

$$\frac{\bar{v}_1}{\bar{S}_n} = \frac{D_n}{A_n D_n - B_n C_n} = \alpha_{1n}. \tag{9.84}$$

The quantity α_{1n} is a cross receptance between the two ends of the beam. If a curve of $1/\alpha_{1n}$ is plotted against ω, the initially assumed driving frequency, the zeros occur at the natural frequencies since they correspond to $S_n = 0$. The corresponding sequences of values $\bar{v}_1, \bar{v}_2, \ldots, \bar{v}_n$ define the principal modes.

Strictly speaking, the added masses that should be used depend upon the assumed value of ω. This is because, with sinusoidal motion, **A**, **B** and **C** are in general frequency-dependent. This is a matter of some consequence in wave excitation and it further emphasizes the superiority of a more complete hydroelastic analysis. It has been found, however, that this dependence is usually very weak and can be ignored in cases where the excitation is that of a propeller and yet the frequency is not high enough to invalidate the hull-girder idealizations [21].

It must be understood that the Myklestad–Prohl method of calculation has been described merely by way of illustration. The method is capable of refinement, notably in regard to the corrections for rotary inertia and shear deflection. A discussion of practical results relating to surface ships is given by Lewis [22].

(b) *Finite Element Methods*

A more general technique which may be applied to a system of any degree of complexity, within the limits of computer technology, is the finite element method [23]. In ship structural dynamics this has great potential for solving complex vibration problems such as the interaction between the main hull and local vibrations [24]. The application of the method to dynamic problems is now briefly illustrated by again considering symmetric flexure of the main hull as a non-uniform beam.

The beam is divided into a series of elements, and frequencies and mode shapes are calculated by what may be considered an extension of the Rayleigh–Ritz method. We consider a uniform element (indicated in Fig. 9.13) and assume that it deforms according to the *static* deflected shape, as in the Rayleigh–Ritz method. Note that in the Myklestad–Prohl method the static deflection curve is also used, but this is a consequence of concentrating the mass at the ends of the elements. In the finite element method to be described here, the mass is assumed to be distributed uniformly along the element; it is also possible to incorporate concentrated masses simultaneously. If the deflections and slopes at either end are as indicated in Fig. 9.13, it may be shown by simple beam theory that the static deflection curve is given by

$$\begin{aligned}\bar{v}(\xi) = {} & (1 - 3\xi^2 + 2\xi^3)\bar{v}_r + (\xi - 2\xi^2 + \xi^3)l_r\bar{\theta}_r \\ & + (3\xi^2 - 2\xi^3)\bar{v}_{r+1} + (-\xi^2 + \xi^2)l_r\bar{\theta}_{r+1}\end{aligned} \tag{9.85}$$

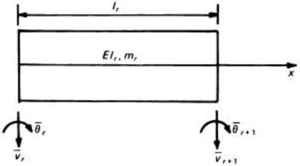

Fig. 9.13

where ξ is the dimensionless coordinate x/l_r. In matrix form this may be written

$$\bar{v}(\xi) = \mathbf{a}'(\xi)\bar{\mathbf{v}}^{(r)}. \tag{9.86a}$$

Also,

$$\frac{d^2\bar{v}}{dx^2} = \mathbf{b}'(\xi)\bar{\mathbf{v}}^{(r)} \tag{9.86b}$$

where the superscript r indicates that a matrix is associated with the rth element and a prime signifies a transposed matrix. In fact

$$\bar{\mathbf{v}}^{(r)} = \begin{bmatrix} \bar{v}_r \\ \bar{\theta}_r \\ \bar{v}_{r+1} \\ \bar{\theta}_{r+1} \end{bmatrix}; \qquad \mathbf{a}(\xi) = \begin{bmatrix} 1 - 3\xi^2 + 2\xi^3 \\ (\xi - 2\xi^2 + \xi^3)l_r \\ 3\xi^2 - 2\xi^3 \\ (-\xi^2 + \xi^3)l_r \end{bmatrix}$$

and $\mathbf{b}(\xi)$ is obtained by differentiating Equation (9.85) twice with respect to ξ.

Now for harmonic motions $\bar{v}\sin\omega t$, we may write expressions for the strain energy and kinetic energy in the element. These are respectively

$$V^{(r)} = \frac{EI_r}{2}\int_0^{l_r}\left(\frac{d^2\bar{v}}{dx^2}\right)^2 dx\,\sin^2\omega t \tag{9.87a}$$

$$T^{(r)} = \frac{\omega^2 m_r}{2}\int_0^{l_r}\bar{v}^2\,dx\,\cos^2\omega t. \tag{9.87b}$$

Hence

$$V^{(r)} = \tfrac{1}{2}\bar{\mathbf{v}}^{(r)'}\left\{EI_r l_r\int_0^1 \mathbf{b}(\xi)\mathbf{b}'(\xi)d\xi\right\}\bar{\mathbf{v}}^{(r)}\sin^2\omega t = \tfrac{1}{2}\mathbf{v}^{(r)'}\mathbf{K}^{(r)}\mathbf{v}^{(r)} \tag{9.88}$$

where $\mathbf{K}^{(r)}$ is the 'stiffness' matrix of the element and is given by the expression within the braces, and $\mathbf{v}^{(r)}$ is the matrix of generalized coordinates

$$\mathbf{v}^{(r)} = \bar{\mathbf{v}}^{(r)}\sin\omega t.$$

Furthermore

$$T^{(r)} = \tfrac{1}{2}\omega^2\bar{\mathbf{v}}^{(r)'}\left\{m_r l_r\int_0^1 \mathbf{a}(\xi)\mathbf{a}'(\xi)d\xi\right\}\bar{\mathbf{v}}^{(r)}\cos^2\omega t = \tfrac{1}{2}\dot{\mathbf{v}}^{(r)'}\mathbf{M}^{(r)}\dot{\mathbf{v}}^{(r)} \tag{9.89}$$

where $\mathbf{M}^{(r)}$ is the 'consistent mass' matrix of the element and $\dot{\mathbf{v}}^{(r)}$ stands for $d(\mathbf{v}^{(r)})/dt$.

Thus for the total assembly of n elements we have, from Equations (9.88) and (9.89),

$$V = \sum_{r=1}^{n} V^{(r)} = \frac{1}{2}\sum_{r=1}^{n}\mathbf{v}^{(r)'}\mathbf{K}^{(r)}\mathbf{v}^{(r)} \tag{9.90a}$$

$$T = \sum_{r=1}^{n} T^{(r)} = \frac{1}{2}\sum_{r=1}^{n}\dot{\mathbf{v}}^{(r)'}\mathbf{M}^{(r)}\dot{\mathbf{v}}^{(r)}. \tag{9.90b}$$

Consider now a matrix of all the generalized coordinates ($2n + 2$ in all):

$$\mathbf{q} = \begin{bmatrix} v_1 \\ \theta_1 \\ v_2 \\ \theta_2 \\ \cdot \\ \cdot \\ \cdot \\ v_{n+1} \\ \theta_{n+1} \end{bmatrix} = \bar{\mathbf{q}} \sin \omega t. \tag{9.91}$$

The quantities for V and T may be rearranged in the form

$$V = \tfrac{1}{2}\mathbf{q}'\mathbf{K}\mathbf{q}; \tag{9.92a}$$

$$T = \tfrac{1}{2}\dot{\mathbf{q}}'\mathbf{M}\dot{\mathbf{q}} \tag{9.92b}$$

In these expressions, **K** and **M** represent, respectively, the total beam stiffness and consistent mass matrices.

We now use the Lagrangean equations for the beam in free vibrations. There are $2n + 2$ such equations for this system, of which the $(2r - 1)$th and the $2r$th are

$$\frac{\mathrm{d}}{\mathrm{d}t}\left(\frac{\partial T}{\partial \dot{v}_r}\right) - \frac{\partial T}{\partial v_r} + \frac{\partial V}{\partial v_r} = 0 \tag{9.93a}$$

$$\frac{\mathrm{d}}{\mathrm{d}t}\left(\frac{\partial T}{\partial \dot{\theta}_r}\right) - \frac{\partial T}{\partial \theta_r} + \frac{\partial V}{\partial \theta_r} = 0. \tag{9.93b}$$

The combination of Equations (9.91)–(9.93) yields, in matrix form,

$$-\omega^2\mathbf{M}\bar{\mathbf{q}} + \mathbf{K}\bar{\mathbf{q}} = 0$$

or,

$$(\mathbf{K} - \omega^2\mathbf{M})\bar{\mathbf{q}} = 0. \tag{9.94}$$

The natural frequencies are thus the square roots of the eigenvalues of this set of equations, and from their solution the characteristic modes can be obtained.

This method is ideally suited for implementation on a digital computer, and it may be used with a wide variety of elements for more complex vibration problems, for example beam, plate and shell elements. It may also be easily developed for the calculation of the dynamic response to a complicated distributed excitation force.

9.6.4 *Section Properties*

The methods previously described require knowledge of structural properties for a discrete set of sections along the length of the hull. Some of these, such as flexural rigidity and mass per unit length (or possibly lumped mass at a point), may be found in a relatively straightforward manner, although the numerical work involved should not be underestimated. There are two properties, however, on which we must elaborate.

(a) *Added Mass in Symmetric Vibration*

The above treatment assumes that values of 'added mass' are known. We shall now explain briefly how these values are found, noting first of all that there is no suggestion that mass is really 'added' in the sense that an identifiable body of water is 'entrained by' the hull. Note also that it is an 'added mass' *per unit length* that is required.

Consider an infinitely long, circular cylinder moving along a perpendicular to its axis in an infinite, incompressible, inviscid liquid which is at rest at infinity. Let the velocity of the cylinder at any instant be U so that its kinetic energy per unit length is $\frac{1}{2}mU^2$. As the cylinder moves it causes particles of liquid to move out of its way and round to its 'rear'. The liquid thus acquires kinetic energy and the value of this at any instant per unit length of cylinder is $\frac{1}{2}\rho\pi b^2 U^2$, where ρ is the density of the liquid and b is the radius of the cylinder [6]. The total kinetic energy of the cylinder and liquid per unit length of cylinder is thus

$$\tfrac{1}{2}(m + \alpha)U^2$$

where $\alpha = \pi\rho b^2$. Note that α is equal to the mass of liquid displaced by unit length of the cylinder and that, generally speaking, this is far from negligible. If an external force f per unit length acts on the cylinder in the direction of U, then

$$Uf = \frac{\mathrm{d}}{\mathrm{d}t}\left(\tfrac{1}{2}mU^2 + \tfrac{1}{2}\alpha U^2\right)$$

so that

$$f = (m + \alpha)\dot{U},$$

assuming that there is no change in potential energy. The quantity $m + \alpha$ is the 'virtual mass' and α is the 'added mass', both per unit length.

This result for a moving circular cylinder is central to any discussion of added mass. Its derivation by consideration of kinetic energy is convenient but it may also be found by the use of a time-dependent potential function [6, 25]. Being readily amenable to analysis, the potential flow round an accelerating circular cylinder provides a convenient basis of comparison. Let

$$C = \frac{\begin{pmatrix}\text{added mass per unit length of other body}\\ \text{in two-dimensional flow}\end{pmatrix}}{\begin{pmatrix}\text{added mass per unit length of circular cylinder}\\ \text{having the appropriate 'comparable' size}\end{pmatrix}}.$$

For a ship floating at a free surface there will be two such coefficients: C_V for vertical (i.e. symmetric) motion; and C_H for horizontal (i.e. antisymmetric) motion. We are here concerned with C_V, and values of it were first found by Lewis using conformal transformations [26].

Two features of Lewis's coefficients C_V must be mentioned. First, the basis of comparison used in defining C_V is that the radius of the cylinder is taken as half the beam of the hull. Second, all of Lewis's sections are vertical at the water line so that the added mass of the totally immersed, non-circular cylinder may be calculated. It is then assumed that the added mass of a cylinder (whether circular or not) whose waterplane section bisects the cross section is half that of the same cylinder fully immersed. A typical result is illustrated in Fig. 9.14; for the given shape, in which $b/d = 0.6$, it is found that $C_V = 1.20$.

The quantities C_V are based entirely on two-dimensional potential flow. Both the circular cylinder and the hull are assumed to be of infinite length. Some improvement of accuracy is obtained by treating the flow as three-dimensional, though still for potential flow. The values of C_V are accordingly multiplied by a factor J ($J < 1$) that is determined by the length-to-beam ratio of the hull [15]. In reality, this three-dimensional flow is accompanied by a steady flow along the cylinder axis, but its effects are generally ignored.

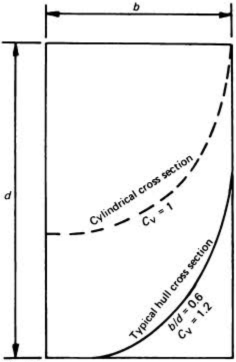

Fig. 9.14

(b) *Damping*

One of the major uncertainties in the analysis of modal responses lies in the figures assigned to damping. Except at low frequencies, associated with response in the lowest two symmetric modes, damping occurs mostly in the hull. Beam theory suggests that damping might be ascribed ***per unit length***. The figure

$$b = 0.03\, m\omega \tag{9.95}$$

has been quoted empirically [21] and further information on damping can be found in [12]. In Equation (9.95),

b = damping force/unit velocity/unit length

m = mass/unit length (including added mass)

ω = driving frequency in radians per second.

Such an approximation as this makes the calculation of steady response possible, provided the excitation is specified and the hull-girder idealization remains tenable.

As is almost always the case, damping virtually defies estimation (and even accurate measurement). It is known that damping levels differ markedly between nominally similar vehicles, for instance. Moreover, even the vibration analyst's trick of associating a damping factor with each principal mode is not always helpful. There is a fair degree of agreement on the following points, however:

(i) riveted vehicles are more heavily damped than welded ones;

(ii) 'added damping' is seldom great, except in the lowest two symmetric modes for which it is crucial;

(iii) damping increases with frequency and high modes are generally much more heavily damped than low ones (although whether or not the hull can continue to be regarded as a beam becomes questionable); and

(iv) more data are needed.

This side of structural dynamics is in a most unsatisfactory state.

9.7 Structural Dynamics of Ship Hulls in Antisymmetric Motion

'Torsion' and 'bending' are forms of behaviour that are associated with prismatic bodies and they are individually observable phenomena only under certain special conditions. Pure bending occurs only if all loads acting on the beam pass through the elastic axis (or locus of shear centres). Rarely, if ever, are those conditions likely to prevail in a marine hull. In practice, therefore, torsion and bending are 'coupled' in antisymmetric vibration. Moreover, the nature of the coupling is made complicated by the departure of the hull from a uniform prismatic form.

Coupled torsion and lateral bending may be examined by the same techniques as those described above. Finite elements may be used, and the transfer matrix method has also been applied in this context to ship hulls. In this way, principal modes and natural frequencies may be obtained. By including structural and fluid damping, we may find the response to forced sinusoidal excitation, either directly or by a modal approach. But it has to be accepted that the theory is much more complicated and can give rise to numerous levels of simplification. In order to illustrate what is involved we shall now outline an approach which is, in effect, another home-grown adaptation of that due to Myklestad [27].

9.7.1 *Free Vibration*

Let us first examine briefly an elementary theory of coupled bending and torsion. Figure 9.15 shows a uniform beam (or rudimentary hull) in which the axis Ox is

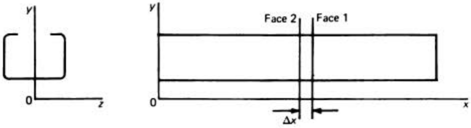

Fig. 9.15

associated with the axis of shear centres. It is assumed that the distances of K and C from Ox are known, K being the keel and C the centre of mass of the cross section. Consider an element of the beam that is isolated by the faces 1 and 2 as shown. A static force $q\Delta x$ applied to the slice at the shear centre causes no rotation so that the element is as shown in Fig. 9.16. (It is assumed that the transverse loading at all points of the beam lies in the plane Oxz.) The bending moment M and shear force S are given by the relations,

$$M_1 - M_2 = S\Delta x \qquad \text{or} \qquad \frac{dM}{dx} = S$$

$$S_1 - S_2 = -q\Delta x \qquad \text{or} \qquad \frac{dS}{dx} = -q.$$

But,

$$M = -EI_y \frac{d^2w}{dx^2}$$

where I_y is the second moment of area of the section about the centroidal axis parallel to Oy. Therefore

$$EI_y \frac{d^4w}{dx^4} = q. \tag{9.96}$$

If, instead of passing through the shear centre, the horizontal load $q\Delta x$ passes through C – and we assume that this is true all along the beam – then the slice will be rotated (as well as deflected) as illustrated in Fig. 9.17. There are now twisting

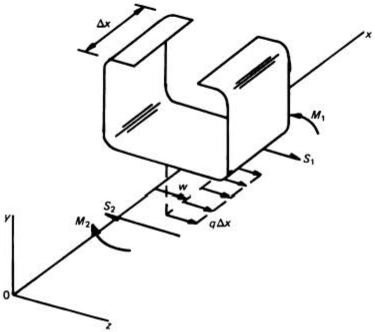

Fig. 9.16

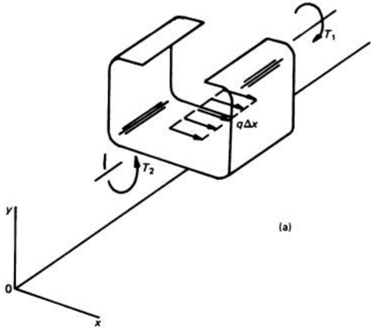

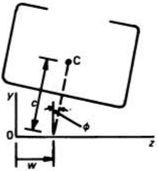

Fig. 9.17

moments T, and those applied to the element are given by

$$T_1 - T_2 = -(q\Delta x)c$$

whence, as $\Delta x \to 0$,

$$\frac{dT}{dx} = -qc. \tag{9.97}$$

The quantity T is related to the angle of rotation ϕ by a relationship of the form

$$T = K\frac{d\phi}{dx} - K'\frac{d^3\phi}{dx^3} \tag{9.98}$$

in which K is the 'torsional stiffness' for uniform torsion and K' is the 'warping stiffness'. In practical analysis – certainly with ship hulls – it is usually assumed, however, that the form

$$T = K\frac{d\phi}{dx} \tag{9.99}$$

will suffice.

A simple theory of vibration is now obtained by assuming that the loading q is in the nature of an inertia force, so that

$$q = -A\rho\frac{\partial^2}{\partial t^2}(w + c\phi) \tag{9.100}$$

where $A\rho$ is the mass per unit length of beam. It is further assumed that, instead of Equation (9.97), we may write

$$T_1 - T_2 = -(q\Delta x)c + (I_p\rho\Delta x)\frac{\partial^2\phi}{\partial t^2}$$

or, in the limit $\Delta x \to 0$,

$$\frac{\partial T}{\partial x} = -qc + I_p\rho\frac{\partial^2\phi}{\partial t^2} \tag{9.101}$$

where I_p is the polar second moment of area about the centroidal axis. Equations (9.96), (9.98), (9.100) and (9.101) now give a pair of simultaneous equations of motion:

$$EI_y\frac{\partial^4 w}{\partial x^4} = -A\rho\frac{\partial^2 w}{\partial t^2} - A\rho c\frac{\partial^2\phi}{\partial t^2} \tag{9.102}$$

$$K\frac{\partial^2\phi}{\partial x^2} - K'\frac{\partial^4\phi}{\partial x^4} = A\rho c\frac{\partial^2 w}{\partial t^2} + A\rho c^2\frac{\partial^2\phi}{\partial t^2} + I_p\rho\frac{\partial^2\phi}{\partial t^2}. \tag{9.103}$$

These equations are examined in the literature, for example in [28].

Let us now see how a practical technique of analysis might be formulated for a hull. We again start by imagining the hull cut into slices, as shown in Fig. 9.18, each slice being supposed uniform. The mass of each slice is concentrated at its two bounding 'cuts', as is its polar moment of inertia $(I_p\rho)\Delta x$. Corresponding to Fig. 9.17(b) we now have, at the rth cross sectional 'cut', the concentrated mass m_r and moment of inertia J_r as indicated in Fig. 9.19.

Starting at the right-hand end, we can again work along the hull to the left-hand end. In so doing the following notation is used:

$\bar{w}_r$ = amplitude of deflection w_r

$\bar{\theta}_r$ = amplitude of slope, $(\partial w/\partial x)_r \equiv \theta_r$

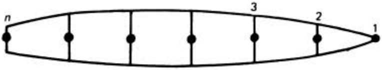

Fig. 9.18

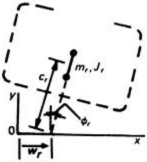

Fig. 9.19

$\bar{\phi}_r$ = amplitude of rotation ϕ_r

$\bar{S}_r$ = amplitude of shearing force S_r

$\bar{M}_r$ = amplitude of bending moment M_r

$\bar{T}_r$ = amplitude of twisting moment T_r.

Let us assume that $\bar{w}_1, \bar{\theta}_1, \bar{\phi}_1$ may take any arbitrary (although as yet unspecified) value and then consider the sinusoidal motion of the mass m_1 with arbitrary frequency ω (refer to Fig. 9.20(a)). Evidently

$$T_1 = J_1\ddot{\phi}_1 = -J_1\omega^2\bar{\phi}_1 \sin \omega t = \bar{T}_1 \sin \omega t \tag{9.104a}$$

$$M_1 = 0 \tag{9.104b}$$

$$S_1 = -m_1(\ddot{w}_1 + c_1\ddot{\phi}_1) = m_1\omega^2(\bar{w}_1 + c_1\bar{\phi}_1) \sin \omega t = \bar{S}_1 \sin \omega t \tag{9.104c}$$

Thus, we can find $\bar{T}_1, \bar{M}_1$ (= 0), $\bar{S}_1$ in terms of $\bar{w}_1, \bar{\theta}_1, \bar{\phi}_1$.

To proceed to the next concentrated mass, m_2, consider the system shown in Fig. 9.20(b). Inspection shows that

$$\theta_1 = \theta_2 + \eta_1 S_1 - \zeta_1 M_1 \tag{9.105a}$$

$$w_1 = w_2 + l_1\theta_2 + \xi_1 S_1 - \eta_1 M_1 \tag{9.105b}$$

$$\phi_1 = \phi_2 + \chi_1 T_1. \tag{9.105c}$$

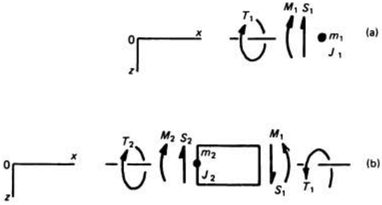

Fig. 9.20

Here the flexibilities ξ_1, η_1, ζ_1 are the same as those defined previously (see Fig. 9.11) for pure bending. The fresh flexibility χ_1 is for torsion and of the type suggested by Equation (9.99). The estimation of flexibilities χ may present some difficulty in practice. Often, however, it is permissible to use the theory of torsion of closed, thin-walled sections; when this is so,

$$\chi_r = \frac{l_r}{4GA_0^2} \oint \frac{ds}{t(s)} \tag{9.106}$$

for the appropriate (rth) slice, where G is the shear modulus, A_0 is the enclosed cross sectional area, t is the wall thickness and s is the distance round the wall.

Returning to Equations (9.105a, b, c) for the first slice we see that

$$\theta_2 = \theta_1 - \eta_1 S_1 + \zeta_1 M_1 = (\bar{\theta}_1 - \eta_1 \bar{S}_1) \sin \omega t = \bar{\theta}_2 \sin \omega t \tag{9.107a}$$

$$\begin{aligned} w_2 &= w_1 - l_1\theta_2 - \xi_1 S_1 + \eta_1 M_1 = (\bar{w}_1 - l_1\bar{\theta}_2 - \xi_1 \bar{S}_1) \sin \omega t \\ &= \bar{w}_2 \sin \omega t \end{aligned} \tag{9.107b}$$

$$\phi_2 = \phi_1 - \chi_1 T_1 = (\bar{\phi}_1 - \chi_1 \bar{T}_1) \sin \omega t = \bar{\phi}_2 \sin \omega t. \tag{9.107c}$$

Thus $\bar{\theta}_2, \bar{w}_2, \bar{\phi}_2$ are found in terms of $\bar{\theta}_1, \bar{w}_1, \bar{\phi}_1$ and it is possible to find $\bar{T}_2, \bar{M}_2, \bar{S}_2$:

$$T_2 = T_1 + J_2\ddot{\phi}_2 = (\bar{T}_1 + J_2\omega^2\bar{\phi}_2) \sin \omega t = \bar{T}_2 \sin \omega t \tag{9.108a}$$

$$M_2 = -l_1 S_1 = -l_1 \bar{S}_1 \sin \omega t = \bar{M}_2 \sin \omega t \tag{9.108b}$$

$$\begin{aligned} S_2 &= S_1 - m_2(\ddot{w}_2 + c_2\ddot{\phi}_2) = \{\bar{S}_1 + m_2\omega^2(\bar{w}_2 + c_2\bar{\phi}_2)\} \sin \omega t \\ &= \bar{S}_2 \sin \omega t \end{aligned} \tag{9.108c}$$

We can then turn our attention to the second slice to calculate $\bar{\theta}_3, \bar{w}_3, \bar{\phi}_3, \bar{T}_3, \bar{M}_3, \bar{S}_3$ *in that order*.

Without going into detail it is possible to see that this process may be carried on until $\bar{\theta}_n, \bar{w}_n, \bar{\phi}_n, \bar{T}_n, \bar{M}_n, \bar{S}_n$ are found. In theory a tabular calculation might be performed, but in practice a computer would be essential. All of these six quantities are found as linear algebraic functions of $\bar{\theta}_1, \bar{w}_1, \bar{\phi}_1$. If the requirements

$$\bar{T}_n = 0 = \bar{M}_n \tag{9.109}$$

say, are imposed, a suitable cross receptance between the two ends may be found. Thus, suppose that the condition at the nth mass is

$$\bar{T}_n = \hat{A}\bar{\theta}_1 + \hat{B}\bar{w}_1 + \hat{C}\bar{\phi}_1 \tag{9.110a}$$

$$\bar{M}_n = \hat{D}\bar{\theta}_1 + \hat{E}\bar{w}_1 + \hat{F}\bar{\phi}_1 \tag{9.110b}$$

$$\bar{S}_n = \hat{G}\bar{\theta}_1 + \hat{H}\bar{w}_1 + \hat{I}\bar{\phi}_1 \tag{9.110c}$$

where $\hat{A}, \hat{B}, \ldots, \hat{I}$ are known. The requirements in (9.109) permit us to find $\bar{\theta}_1$ and $\bar{w}_1$ in terms of $\bar{\phi}_1$ (say). That is,

$$\bar{\theta}_1 = \hat{X}\bar{\phi}_1 \tag{9.111a}$$

$$\bar{w}_1 = \hat{Y}\bar{\phi}_1 \tag{9.111b}$$

where $\hat{X}$, $\hat{Y}$ are known. It follows that

$$\bar{S}_n = (\hat{G}\hat{X} + J\hat{H}\hat{Y} + \hat{I})\bar{\phi}_1 = \hat{Z}\bar{\phi}_1 \tag{9.112}$$

say. The ratio $\bar{\phi}_1/\bar{S}_n$ is the 'cross receptance between rotation at the bow and transverse displacement at the stern'. In other words, the quantity

$$\hat{Z} = \frac{\bar{S}_n}{\bar{\phi}_1} \tag{9.113}$$

(which is known for the given frequency ω) gives the transverse shear force at the stern per unit rotation at the bow.

If $\hat{Z}$ is plotted as a function of ω it is found that for certain values of ω, $\hat{Z}$ vanishes, so that a finite response is produced without excitation. These frequencies are the natural frequencies of the hull in antisymmetric vibration. The corresponding principal modes are found from the values $\bar{\theta}$, $\bar{w}$, $\bar{\phi}$ when ω has the appropriate natural frequency.

The above outline of a method to determine the free antisymmetric vibrations of a hull obviously embodies many sweeping assumptions, and in most cases these assumptions are capable of refinement or adaptation. But it is not our purpose to examine them here in any detail.

(a) *Added Mass in Antisymmetric Vibration*

The values of m_r and J_r in the previous calculations are assumed, within the context of this rather crude formulation, to include allowances for added mass and added moment of inertia respectively.† (Note that the concept of an added moment of inertia is fully in accord with Lagrangean theory since rotation, like displacement, is represented by a generalized coordinate.) These contributions have been estimated in the same manner as those referred to in Section 9.6.4(a). They are quoted in the literature in the form of dimensionless coefficients of added mass – or moment of inertia – per unit length.

It will be recalled that in two-dimensional potential flow round an accelerating cylinder of radius b, the added mass per unit length is $\pi\rho b^2$. Suppose that instead of being fully immersed in an infinite fluid the cylinder lies on the surface with its axis lying in the water-plane section. If the cylinder moves in a direction perpendicular to its axis but so that that axis remains in the water-plane section, it is reasonable to assume that the added mass is $\frac{1}{2}\pi\rho b^2$. A similar argument for two-dimensional flow round a non-circular cylinder representing a section of the hull gives α_H, the added mass per unit length in horizontal motion. The quantity α_H is normally quoted in non-dimensional form as

$$C_H = \frac{\alpha_H}{\frac{1}{2}\pi\rho d^2} \tag{9.114}$$

where d is the draught of the section.

The added moment of inertia per unit length of a circular cylinder rotating in an inviscid fluid is zero. The added moment of inertia J' of a hull is therefore compared

† Once again, far more accurate techniques of analysis exist and are discussed in, for example, [15].

arbitrarily with the quantity $\pi\rho d^4$. Thus

$$C_T = \frac{J'}{\pi\rho d^4}. \tag{9.115}$$

For actual values of C_H and C_T the reader is referred to Chapter 4 of [21].

It is a matter of conjecture whether or not it is appropriate to concentrate the masses m_r in the calculations referred to above at the centres of mass of the sections shown in Fig. 9.18 when m_r contains an allowance for added mass. It must be understood that the distance c' from the shear centre to the point C_A at which the added mass is located is significant. Calculation of the position of C_A is discussed in [29] and values for Lewis forms have been given in [30] from which c' may be determined. The complete form of Equation (9.100) is, therefore,

$$q = -A\rho \frac{\partial^2}{\partial t^2}(w + c\phi) - \alpha_H \frac{\partial^2}{\partial t^2}(w + c'\phi). \tag{9.116}$$

Consequently, in the formulation we have given, the term $m_r c_r$ implies $A\rho c + \alpha_H c'$ evaluated at the section r.

As with the coefficient C_V, corrections are made to C_H and C_T to allow for three-dimensional effects of flow from strip to strip. The effects of shallowness of water (which tends to increase added masses) may also be allowed for on a semi-empirical basis, or use may be made of complex numerical techniques for solving three-dimensional potential flow problems (e.g. see [31]).

9.8 Marine Shafting Vibrations

In technology generally, rotating shafts are commonly subject to vibration of the 'dry land' variety. The parasitic motion can usually be recognized as torsional, longitudinal or flexural; that is, these motions are usually uncoupled. Moreover, except in such specialized problems as the short-circuit loading of generators (which causes violent transient motion), the motions are usually sinusoidal. There is, of course, a very extensive literature on shaft vibration [32].

All of these types of motion are encountered in marine craft and they often crop up as 'wet sea' problems. The fact that the water may effectively modify the vibrating system can lead to coupling of the motions [33]. (As might be expected, a screw propeller can cause some coupling of longitudinal and torsional vibrations.) It is seldom found necessary to allow for this coupling in calculations, however. We shall therefore discuss torsional, longitudinal and flexural vibration separately. It must be borne in mind, then, that some reappraisal might be necessary on occasion because of possible coupling. In any event, rather little needs to be said as far as the effects of the water are concerned.

9.8.1 *Torsional Vibration*

The drive of a marine vehicle may be direct, geared or branched and the prime mover may be a reciprocating engine or some sort of turbine. Torsional vibration may be caused by:

(i) fluctuating gas torques and unbalanced inertia forces (in reciprocating engines),
(ii) operation of the propeller in a non-uniform wake,

(iii) misaligned gears, and
(iv) partial emergence of a propeller in a rough sea.

There exist standard techniques of torsional vibration analysis which may be employed in the study of this motion (e.g. see [34]) but certain features of marine problems require special mention.

(a) *The System*
The torsional system under discussion must be idealized for the purposes of analysis and there are well known methods of doing this. Now, however, it is necessary to consider one or more propellers and necessary to consider how it (or they) can best be represented. The general linear theory indicates that there must be an 'added moment of inertia' term and a fluid damping effect.

The added moment of inertia is often taken empirically as some fraction of the true moment of inertia. A crude approximation is simply to increase the latter by 25 per cent. Attempts have been made to calculate the added moment of inertia and more refined corrections are made in the design of high-performance propellers. It is not normal, however, to allow for frequency dependence of the added moment of inertia.

Damping at the propeller is a matter of considerable uncertainty (needless to say). A common assumption is that the damping torque is $-b\dot{\theta}$, where θ is the angular departure from steady rotation and

$$b = \frac{\text{steady average torque}}{2 \times \begin{pmatrix}\text{rotational speed} \\ \text{measured in} \\ \text{revolutions per second}\end{pmatrix}}.$$

There are many other assumptions available, however, and the literature should be consulted in case of need [35].

(b) *The Excitation*
As already mentioned, there are two main sources of torsional vibration, namely, the engine and the propeller. The means by which a reciprocating engine excites a system are well known and will not be reviewed here (but see Chapter 5 of [36]). All we need to note is that the exciting torque has the general form

$$\mathrm{Re}\left[\sum_{n=1}^{\infty} T_n \exp(-\mathrm{i}\alpha_n)\exp(in\omega t)\right]$$

where T_n is the amplitude of the nth torque harmonic, α_n the phase of the nth torque harmonic, and $\omega = 2\pi \times$ (rotational speed).

In order to examine the nature of the propeller torque fluctuations, let us return to the crude theory introduced in Section 9.4.1. Figure 9.3(b) shows that the contribution to the torque provided by the elementary lift force δL_n is

$$-\delta L_n r \sin\beta.$$

Summing like contributions over the N blades we find that the torque is

$$\delta T_x = -\mathrm{Re}\left[\sum_{k=0}^{\infty}\sum_{n=1}^{N} C_k \exp\{ik(\Omega t + \theta_n)\}\right](r\sin\beta)\delta r.$$

The summation over n may be performed readily because

$$\sum_{n=1}^{N} \exp\{i2\pi k(n-1)/N\} = \begin{cases} N & \text{if } k = \lambda N \ (\lambda = 0, 1, 2, \ldots) \\ 0 & \text{if } k \neq \lambda N \end{cases}$$

as may be seen by adding vectors in the Argand diagram. Hence,

$$\delta T_x = -\text{Re}\left[N \sum_{\substack{k=0,N,\\2N,\ldots}}^{\infty} C_k \exp(ik\Omega t)\right](r \sin\beta)\delta r$$

$$= -\text{Re}\left[NC_0 + \sum_{\lambda=1}^{\infty} C_{\lambda N} \exp(i\lambda N\Omega t)\right](r \sin\beta)\delta r.$$

In other words, the steady torque has a fluctuating component with 1, 2, 3, . . . , times the blade frequency superimposed on it. This again is in line with what intuition suggests.

If it is wished to ascertain the amplitude and phase of this propeller excitation it would be necessary to evaluate the complex quantities $C_{\lambda N}$ and to integrate the expression for δT_x with respect to r. The calculations are far from simple but some success has been achieved in this type of endeavour (e.g. see [37]).

(c) *Principal Modes and Natural Frequencies*

The Holzer technique of calculation is particularly well suited to the system now under discussion, being easily adapted to geared and branched systems (e.g. see [4]). The principal modes and natural frequencies may be calculated by the Holzer method after the system has been idealized into a series of rigid discs and massless shafts. An allowance for added moment of inertia must be included in the disc(s) representing the propeller(s). All damping is ignored when the system is idealized (as is required by the definitions of principal modes and natural frequencies).

(d) *Steady Forced Vibration*

In most practical analyses of steady forced vibration it is hoped that a knowledge of the relevant principal modes and natural frequencies will suffice. A check is made for coincidence (or near coincidence) of the driving frequency and a natural frequency. This may require that the system be detuned, although detuning may not be necessary if the excitation is close to a node in the principal mode concerned or if the damping is heavy. Unfortunately, torsional systems are seldom heavily damped. Moreover, with the propeller-induced excitation applied at an extremity of the system, modal excitations are likely to be high. Consequently, the practical problem may well be to minimize vibration rather than to suppress it. Calculations of forced vibration have therefore to be made.

Two methods of approach suggest themselves: (i) modal analysis, and (ii) direct calculation using physical coordinates such as the rotations of the discs of a Holzer-type system. Of these, the first is likely to be the more easily interpreted. (Note particularly, however, that if the drive embodies a fluid coupling special care is needed [38].) But it requires preliminary calculation of principal modes and natural frequencies and also requires that a level of damping be assigned to each principal mode.

The second type of calculation is likely to be the more easily made, although here again the estimation of damping is difficult. The actual technique of calculation for a system with n degrees of freedom effectively requires the solution of n simultaneous algebraic equations for a given driving frequency. A convenient way of avoiding direct solution of the equations is to employ a modified version of Holzer's method.

9.8.2 *Longitudinal Vibration*

Longitudinal vibration occurs in marine shafting largely as a consequence of propeller excitation. (The motion is often thought to be coupled significantly to torsional vibration but evidence on the point is sparse and, as mentioned already, allowance is seldom made for it in calculations.) Longitudinal vibration does not often raise problems in 'dry land' mechanical systems, partly because of a lack of excitation and partly because the relevant natural frequencies are very high. In marine shafting there *is* a significant source of excitation. Moreover, the shafting in question is often sufficiently long for its lowest natural frequency to make low-order resonance a possibility.

(a) *The System*
Unlike the system in torsion, which is necessarily free at its extremities, the present one is nominally clamped at (or near) a thrust bearing. The idealization of this bearing is in fact a matter requiring much thought. In terms of lumped parameters, then, the system consists of a light shaft (which is restrained, or clamped, at some point) to which masses are attached. Apart from the added mass and the fluid damping at the propeller, the system is essentially of the 'dry land' sort.

The concentrated mass at the free end represents the propeller and its magnitude is the actual mass of the propeller plus an 'added mass' to allow for the water. The value of this latter contribution is usually assumed empirically to be of the order of 20 per cent of the actual mass of the propeller and to be independent of frequency. The damping that is attributable to the water is also a matter of some uncertainty.

(b) *The Excitation*
Intuitively, the frequency of excitation would be expected to be the blade frequency and integral multiples thereof. This is supported by the following argument. The contribution to the axial force along Ox (see Fig. 9.3(b)) made by the slice of width δr of the nth blade is $\delta L_n \cos\beta$. The N blades together thus provide a contribution

$$\delta F_x = \mathrm{Re}\left[\sum_{k=0}^{\infty}\sum_{n=1}^{N} C_k \exp\{\mathrm{i}(\Omega t + \theta_n)\}\right]\cos\beta\,\delta r$$

to the thrust. It follows that

$$\delta F_x = \mathrm{Re}\left[NC_0 + \sum_{\lambda=1}^{\infty} C_{\lambda N}\exp(\mathrm{i}\lambda N\Omega t)\right]\cos\beta\,\delta r,$$

so the frequency is what we would expect. The amplitude of the excitation again depends on the values of the complex constants C_k, and we have already mentioned the difficulty of their evaluation.

(c) *Calculations*
In principle, the calculation of principal modes and natural frequencies of the undamped system and of the forced response when the damping is included is mathematically the same as that for the torsional system [4]. But, in practice, the present calculations are likely to be the simpler because the system concerned is usually without gearing or branches.

9.8.3 *Flexural Vibration*

Flexural vibration of marine shafting is not a frequent occurrence but it is not impossible, and whirling has been reported in 'wet sea' systems such as a propeller shaft between an A-bracket and the hull bearing (see Fig. 9.21). The same problem may arise with the propeller shaft of a hydrofoil craft, which has to be long enough to drive the craft when it is foil-borne. In practice, flexural vibration of this sort, arising from a slight initial bend or lack of balance, may be suppressed either by balancing or by detuning. Of these two possibilities the latter is by far the better, since the maintenance of a good balance may be difficult.

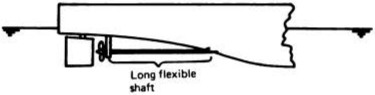

Fig. 9.21

Comparatively little has been reported on this type of motion. It is likely, however, that it may be analysed by standard techniques assuming that added mass of the water increases the mass per unit length of shaft by about 12 per cent. Elementary discussions of this somewhat specialized aspect of vibration analysis have been given elsewhere [39, 40].

9.9 Concluding Note

This treatment of ship vibrations does no more than scratch the surface of the subject. It is the rule, rather than the exception, that idealization of the vibrating system is difficult, and we have really concentrated only on excitation of very low frequency in order to simplify this particular aspect as much as possible. Some vibration problems, of considerable significance from the standpoint of military need, extend well up the frequency range to hundreds of kHz. Although it tends to become a little easier with very high frequencies, analysis of vibration in the vitally important intermediate range of, say, 15 Hz–10 kHz poses very difficult problems indeed. Far from lying within the scope of an elementary textbook, these matters demand attention from the most experienced dynamicists.

Appendix I: Theoretical Basis of 'Transient Resonance Testing'

Suppose that a linear system has an excitation $Q_s(t)$ applied at its sth generalized coordinate and that this produces a response $q_r(t)$ at the rth generalized coordinate.

Under certain modest restrictions the Fourier integral theorem states that $Q_s(t)$ may be expressed in the form

$$Q_s(t) = \frac{1}{2\pi}\int_{-\infty}^{\infty} Q_s(\omega)\exp(\mathrm{i}\omega t)\mathrm{d}\omega \tag{A.1}$$

where

$$Q_s(\omega) = \int_{-\infty}^{\infty} Q_s(t)\exp(-\mathrm{i}\omega t)\mathrm{d}t. \tag{A.2}$$

Now the harmonic response at q_r resulting from the excitation

$$\frac{Q_s(\omega)\mathrm{d}\omega\, \exp(\mathrm{i}\omega t)}{2\pi}$$

is, by the definition of a cross receptance,

$$\frac{\alpha_{rs}(\omega)Q_s(\omega)\mathrm{d}\omega\, \exp(\mathrm{i}\omega t)}{2\pi}.$$

The total response at q_r is thus

$$q_r(t) = \frac{1}{2\pi}\int_{-\infty}^{\infty} \alpha_{rs}(\omega)Q_s(\omega)\exp(\mathrm{i}\omega t)\mathrm{d}\omega. \tag{A.3}$$

But according to the Fourier integral theorem

$$q_r(t) = \frac{1}{2\pi}\int_{-\infty}^{\infty} q_r(\omega)\exp(\mathrm{i}\omega t)\mathrm{d}\omega. \tag{A.4}$$

Therefore

$$\alpha_{rs}(\omega) = \frac{q_r(\omega)}{Q_s(\omega)}, \tag{A.5}$$

where $q_r(\omega)$, $Q_s(\omega)$ are the Fourier transforms of $q_r(t)$, $Q_s(t)$ respectively.

The various cross receptances $\alpha_{1s}, \alpha_{2s}, \ldots$, corresponding to the one excitation coordinate contain information about the shapes, frequencies and damping factors of the principal modes. (It will be recalled that some conventional methods of resonance testing entail the derivation of α_{rs} and then extraction of the required data). Let us now consider whether or not an input $Q_s(t)$ of known frequency content $Q_s(\omega)$ can be applied and the frequency content $q_r(\omega)$ of the response $q_r(t)$ measured.

In theory, at least, this idea is attractive and, furthermore, it is simple for a system with one degree of freedom q_1. Thus suppose that $Q_1(t)$ is a unit impulse $\delta(t)$ applied at the instant $t = 0$. For this excitation $Q_1(\omega) = 1$ for all ω and the response $q_1(t)$ is the unit impulse response

$$h(t) = \frac{1}{m\omega_1\sqrt{(1-\upsilon^2)}}\exp(-\upsilon\omega_1 t)\sin\sqrt{(1-\upsilon^2)}\omega_1 t \tag{A.6}$$

where

$$\upsilon = \frac{b}{2m\omega_1}; \qquad \omega_1^2 = \frac{k}{m}$$

the system being that of Fig. 9.1. Hence

$$\alpha_{11}(\omega) = \int_0^\infty h(t)\exp(-\mathrm{i}\omega t)\mathrm{d}t = \frac{1/m}{\omega_1^2 - \omega^2 + 2\mathrm{i}\upsilon\omega\omega_1}. \tag{A.7}$$

If $\alpha_{11}(\omega)$ were obtained as a curve in the Argand diagram, ω_1 and υ could be measured from it.

If, instead of one, there were in fact several degrees of freedom, then loci $\alpha_{1s}(\omega)$, $\alpha_{2s}(\omega)$, . . . , could be obtained by measuring the corresponding responses $q_1(t)$, $q_2(t)$, . . . , produced by the impulse $Q_s(t) = \delta(t)$ and then finding their Fourier transforms. The shapes, natural frequencies and levels of damping for the various principal modes could then be found from the loci. The obvious way of finding them would be by the use of the Kennedy and Pancu method [41].

There are two major drawbacks, unfortunately. First, the responses $q_r(t)$ cannot be measured for infinite time and so $q_r(\omega)$ cannot be computed accurately. (A computer is essential in this type of work.) This is because $q_r(t)$ rapidly dies away and so becomes lost and because, in any case, analysis time must be limited. The errors that this implies have been examined in [42]. It is found that this particular difficulty does not restrict the use of the technique.

The second drawback is that a true impulse function cannot be applied. It is therefore necessary to use other functions $Q_s(t)$ and, hence, $Q_s(\omega)$. Suitable excitations have been devised and used by White [43] who reports some success with the method.

Appendix II: Some Mathematical Results Used in the Theory of Propeller Excitation

The quantity

$$\exp\{\mathrm{i}k(\Omega t + \theta_n)\}\sin(\Omega t + \theta_n)$$

may be written in the form

$$\begin{aligned}\exp(\mathrm{i}kp)\sin p &= \cos kp \sin p + \mathrm{i}\sin kp \sin p\\ &= \tfrac{1}{2}\{\sin(k+1)p - \sin(k-1)p\}\\ &\quad + \tfrac{1}{2}\mathrm{i}\{\cos(k-1)p - \cos(k+1)p\}\\ &= \tfrac{1}{2}\mathrm{i}\,[\exp\{\mathrm{i}(k-1)p\} - \exp\{\mathrm{i}(k+1)p\}].\end{aligned} \tag{A.8}$$

It follows that Equation (9.38) can be written in the form

$$\begin{aligned}\delta F_y &= \mathrm{Re}\left[\tfrac{1}{2}\sum_{k=0}^{\infty}\sum_{n=1}^{N} C_k\,[\exp\{\mathrm{i}(k-1)(\Omega t + \theta_n)\} - \exp\{\mathrm{i}(k+1)(\Omega t + \theta_n)\}]\right]\sin\beta\,\delta r\\ &= \mathrm{Re}\left[\tfrac{1}{2}\sum_{k=0}^{\infty} C_k\,[\exp\{\mathrm{i}(k-1)\Omega t\}\sum_{n=1}^{N}\exp\{\mathrm{i}(k-1)\theta_n\}\right.\\ &\quad \left. - \exp\{\mathrm{i}(k+1)\Omega t\}\sum_{n=1}^{N}\exp\{\mathrm{i}(k+1)\theta_n\}]\right]\sin\beta\,\delta r.\end{aligned} \tag{A.9}$$

The two summations over n may be performed by inspection since

$$\sum_{n=1}^{N} \exp\{i2\pi(k-1)(n-1)/N\} = \begin{cases} N & \text{if } k-1=\lambda N, \text{ where} \\ & \lambda = 0, 1, 2, \ldots \\ 0 & \text{if } k-1 \neq \lambda N \end{cases} \tag{A.10}$$

$$\sum_{n=1}^{N} \exp\{i2\pi(k+1)(n-1)/N\} = \begin{cases} N & \text{if } k+1=\lambda N \\ 0 & \text{if } k+1 \neq \lambda N. \end{cases} \tag{A.11}$$

These results may be seen to be true by adding vectors in the Argand diagram. It follows that the first of these sums is N if $k = \lambda N + 1$, while the second is N if $k = \lambda N - 1$; otherwise both vanish. It is this result which is used in the text.

References

1. Bishop, R. E. D. (1979), *Vibration*, 2nd Edn, Cambridge University Press, Cambridge.
2. *Proceedings of the Symposium on Propeller Induced Ship Vibration* (1979), Royal Institution of Naval Architects, London.
3. Ramsey, A. S. (1944), *Dynamics*, Part II, 2nd Edn, Chapter 9, Cambridge University Press, Cambridge.
4. Bishop, R. E. D. and Johnson, D. C. (1979), *The Mechanics of Vibration*, Chapter 2, Cambridge University Press, Cambridge.
5. Bishop, R. E. D., Gladwell, G. M. L. and Michaelson, S. (1979), *The Matrix Analysis of Vibration*, Cambridge University Press, Cambridge.
6. Milne-Thomson, L. M. (1968), *Theoretical Hydrodynamics*, 5th Edn, Macmillan, London.
7. Duncan, W. J. (undated), Introductory survey. *AGARD Manual on Aeroelasticity*.
8. Mahalingam, S. (1968), Displacement excitation of vibrating systems. *J. Mech. Engng Sci.*, 10, 74–80.
9. Bishop, R. E. D., Parkinson, A. G. and Pendered, J. W. (1969), Linear analysis of transient vibration. *J. Sound Vib.*, 9, 313–37.
10. Bishop, R. E. D. and Mahalingam, S. (1971), The response of an oscillatory system to excitation by a transient displacement. *Proc. Roy. Soc. (A)*, 324, 67–77.
11. Breslin, J. (1960), Ship vibration, Part I: propeller generated vibrations. *Appl Mech. Rev.*, 13, 463–6.
12. *Proceedings of the 7th ISSC* (1979), Rep. Committee II.4, Paris.
13. *Proceedings of the 15th ITTC* (1978), Wageningen.
14. Price, W. G. and Bishop, R. E. D. (1974), *Probabilistic Theory of Ship Dynamics*, Chapman and Hall, London.
15. Bishop, R. E. D. and Price, W. G. (1979), *Hydroelasticity of Ships*, Cambridge University Press, Cambridge.
16. Liapis, N. and Faltinsen, O. M. (1980), Diffraction of waves around a ship. *J. Ship Res.*, 24, 147–55.
17. Bishop, R. E. D., Eatock Taylor, R. and Jackson, K. L. (1973), On the structural dynamics of ship hulls in waves. *Trans. R. Inst. Nav. Archit.*, 115, 257–74.
18. Ohtaka, K., Kagawa, K. and Yamamoto, T. (1969), Higher mode vertical vibration of a giant tanker. *J. Soc. Nav. Archit. Japan*, 125, 157–88.
19. Bishop, R. E. D. (1971), On the strength of large ships in heavy seas. *S. Afr. Mech. Engr*, 21, 338–53.
20. Goodman, R. A. (1971), Wave-excited main hull vibration in large tankers and bulk carriers. *Trans. R. Inst. Nav. Archit.*, 113, 167–84.
21. Todd, F. H. (1961), *Ship Hull Vibration*, Edward Arnold, London.
22. Lewis, F. M. (1967), *Vibration of Ships*, Chapter 10 of *Principles of Naval Architecture* (ed. J. P. Comstock), Society of Naval Architects and Marine Engineers, New York.
23. Zienkiewicz, O. C. (1977), *The Finite Element Method*, 3rd Edn, McGraw-Hill, New York.
24. *Proceedings of the 5th ISSC* (1973), Rep. Committee IX, Hamburg.
25. Lamb, H. (1932), *Hydrodynamics*, 6th Edn, Cambridge University Press, Cambridge.

26. Lewis, F. M. (1929), The inertia of the water surrounding a vibrating ship. *Trans. Soc. Nav. Archit. Mar. Engrs*, 37, 1–20. (See also [15].)
27. Myklestad, N. O. (1956), *Fundamentals of Vibration Analysis*, McGraw-Hill, New York.
28. Timoshenko, S., Young, D. H. and Weaver, W. (1974), *Vibration Problems in Engineering*, 4th Edn, Van Nostrand Reinhold, New York.
29. Vossers, G. (1962), Resistance, propulsion and steering of ships, C: behaviour of ships in waves. *H. Stam. NV*, Netherlands.
30. Umezaki, K., Miyamoto, K., Ohtaka, K. and Kagawa, K. (1969), Vibration of container ships. *J. Soc. Nav. Archit. Japan*, 126, 187–207.
31. Orsero, P. and Armand, J. L. (1978), A numerical determination of the entrained water in ship vibrations. *Int. J. Num. Meth. Engng*, 13, 35–48.
32. Bishop, R. E. D. and Parkinson, A. G. (1968), Vibration and balancing of flexible shafts. *Appl. Mech. Rev.*, 21, 439–51.
33. Lewis, F. M. and Auslaender, J. (1960), Virtual inertia of propellers, *J. Ship Res.*, 3, 37–46.
34. Nestorides, E. J. (1958), *A Handbook on Torsional Vibration*, Cambridge University Press, Cambridge.
35. Wereldsma, R. (1965), Experiments on vibrating propeller models. *TNO Rep*. No. 70M.
36. Den Hartog, J. P. (1956), *Mechanical Vibrations*, 4th Edn, McGraw-Hill, New York.
37. Tsakonas, S., Breslin, J. and Miller, M. (1967), Correlation and applications of an unsteady flow theory for propeller forces. *Trans. Soc. Nav. Archit. Mar. Engrs*, 75, 158–93.
38. Bishop, R. E. D., Price, W. G. and Tam, P. K. Y. (1978), On damping of torsional vibration in a propulsion system having a fluid drive. *Trans Inst. Mar. Engrs, (TM)*, 95, 109–23.
39. Parkinson, A. G. (1967), An introduction to the vibration of rotating flexible shafts, *Bull. (now Int. J.) Mech. Engng Educ.*, 6, 47–62.
40. Bishop, R. E. D. (1966), An introduction to the balancing of flexible rotors. *Engng Mater. Des.*, 9, 1468–74.
41. Kennedy, C. C. and Pancu, C. D. P. (1947), Use of vectors in vibration measurement and analysis. *J. Aeronaut. Sci.*, 14, 603–25.
42. Clarkson, B. L. and Mercer, C. A. (1965), Use of cross-correlation in studying the response of lightly damped structures to random forces. *AIAA J.*, 12, 2287–91.
43. White, R. G. (1969), Use of transient excitation in the dynamic analysis of structures. *J. R. Aeronaut. Soc.*, 73, 1047–50.

10
Directional Stability and Control

10.1 Introduction

It is a matter of common experience that fluid-borne vehicles do not execute only steady motions. In fact unsteady motion may be

(i) voluntarily performed (as when manoeuvring or accelerating);
(ii) involuntary (as in response to waves or – perhaps more surprisingly – when steady motion is simply not possible); and
(iii) semi-voluntary (as in the response of a ship's hull to excitation by, say, a rotating propeller).

Predictably, the problem of unsteady motion is a considerable one.

Strictly speaking, we are concerned with the motion of a flexible vehicle moving through a fluid. The motion is described through the variation of 'coordinates' and these are of three distinct types:

(i) bodily displacements and changes of orientation measured by reference to the overall steady motion (if any);
(ii) imposed deflections of control surfaces;
(iii) coordinates used to specify distortions of the vehicle.

It is desirable to set up equations governing all these types of coordinates and embodying suitable disturbance 'inputs'. But such a formulation would be far too complicated to be useful as equations with any claim to reality would be very involved.

The present chapter is concerned with 'Directional Stability and Control' in the sense that is discussed in the following section. The subject is enormous and our purpose is only to introduce it. As far as conventional displacement ships and submarines are concerned, more detailed presentations are to be found in the literature of naval architecture [1–3].

10.2 Unsteady Motions in General

With certain reservations that will be mentioned later, progress can only be made on the basis of linear theory. This means that a process of approximation is adopted in which the differential equations of motion are expressed in a particular form. Now there are grounds for suggesting that once it has been found – *if* it can be found – the linear form of the equations of motion will have additive solutions. This means that the motion for 'disturbance A' plus that for 'disturbance B' is the motion that will be executed when disturbances A and B coexist. This strongly suggests that we should study separately (i) manoeuvring in a flat calm, (ii) motion in a disturbed sea, and (iii) structural vibration resulting from other sources. If necessary we can then add the motions, in the expectation that the results will bear some resemblance to reality.

To a limited extent this approach has indeed been found to work adequately for the separated sub-problems, although the proviso must be made that, generally speaking, the departures from any steady reference motion (or from a state of rest) must not be excessive. As to whether or not sensible answers can be obtained by superposition, it is difficult to say with certainty. It is, in fact, an exaggeration to suggest that all the usual conditions of a linear theory can be met, and indeed the very basis of linearized dynamics of fluid-borne vehicles is by no means as firm as one would wish.

The three problems of handling in a flat calm, motion in a disturbed sea, and structural vibration from some other source sometimes occur singly. Thus the manoeuvring of a deeply submerged submarine is essentially a problem of the first type, the response of a ship to waves when it is not manoeuvring is of the second, and the hull vibration of a deeply submerged submarine due to propeller excitation in straight and level motion is of the third type. When this is so, one may not wish to accept the limitation to *small* unsteady motions, and in this event the simplifications of linear theory will not be made.

When, in contrast, these three problems arise together and have to be separated artificially for the purposes of analysis, a linear theory can be used. But once the separation has been made, a nonlinear theory may nevertheless be employed. This is not strictly logical and is really an empirical matter of judgement. Thus the three types of analysis (which are commonly referred to, respectively, as 'Directional Stability and Control', 'Seakeeping' and 'Structural Dynamics') are usually investigated with linear theory but may sometimes be tackled with nonlinear theory. Generally speaking the nonlinear theory raises by far the more difficult *mathematical* questions.

There is another type of simplification which must be considered. Three distinct types of coordinates have been referred to, namely, (i) 'rigid-body' coordinates, (ii) 'imposed deflection' coordinates, and (iii) 'distortional' coordinates. In the study of directional stability and control of *marine* vehicles it is often possible to disregard coordinates of type (iii) altogether. The justification for this is that distortion of the vehicle is either so small or of such a form that the handling characteristics are not seriously affected. However, this is not always true and, indeed, is nonsense where a vehicle like a dracone is concerned.

In the same way, only coordinates of type (i) are employed in much analytical work on involuntary transient motion. This, again, is not always justifiable and in the aeronautical context, for instance, distortion of an airliner as it flies through turbulent air is not only plainly visible but also profoundly important. Equally, there are circumstances at sea in which one would wish to examine the effects of distortion of vehicles moving in waves. This may well be the case for instance with highly loaded hydrofoils, control surfaces such as stabilizers (which are elastically supported) or with inflatable craft. But, commonly, the theory of seakeeping relates to rigid ships.

By now it will be clear that we have entered a field of study that can become extremely difficult. Even the necessity to explain what this subject of vehicle dynamics covers raises problems. Arbitrary divisions have to be made somewhere and, for the present purposes:

'Directional Stability and Control' will relate to a rigid vehicle and coordinates of types (i) and (ii) only will be used; and

'Seakeeping' will refer to a rigid vehicle so that only coordinates of type (i) will be employed.

All matters in which distortion is allowed for are encompassed by 'Structural Dynamics', not that present knowledge can get us far in that particular direction (as we saw in Chapter 9). Note that this is not entirely logical because it means that some aspects of 'Stability and Control' and some of 'Seakeeping' – those in which distortions matter – will not be referred to under the appropriate titles.

10.3 Axes Fixed to a Rigid Body

Consider a set of body axes fixed to a rigid vehicle as shown in Fig. 10.1. (For the sake of definiteness a ship will be taken by way of example.) Let the origin of this frame be the centre of mass of the vehicle, C. For some analyses these body axes *Cxyz* have distinct advantages over the inertial frame *OXYZ* that is fixed to the Earth.

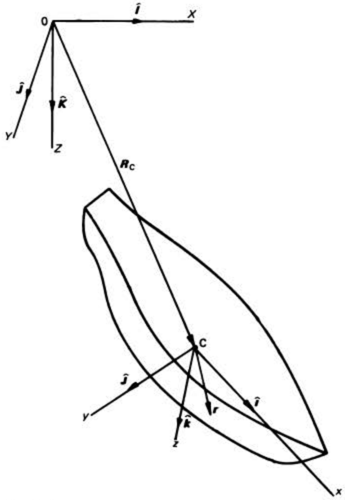

Fig. 10.1

For navigational purposes reference is made, in effect, to OXYZ. Thus in local navigation C may be located relative to the Earth by means of coordinates on a chart. But in describing motions of the vehicle it is almost instinctive to refer to such terms as surge, drift (or sway), heave, and roll, pitch, yaw. These are motions in which use of the body axes is implied, since the first three quantities refer to translations along Cx, Cy, Cz respectively and the second three refer to rotations about Cx, Cy, Cz respectively.

Using the axes shown in Fig. 10.1, we may specify the position of C by the quantities X_C, Y_C, Z_C where

$$\boldsymbol{R}_C = X_C\hat{\boldsymbol{I}} + Y_C\hat{\boldsymbol{J}} + Z_C\hat{\boldsymbol{K}}. \tag{10.1}$$

in which $\hat{\boldsymbol{I}}$, $\hat{\boldsymbol{J}}$, $\hat{\boldsymbol{K}}$ are unit vectors in the directions OX, OY, OZ respectively. The velocity of C is

$$\dot{\boldsymbol{R}}_C \equiv \boldsymbol{U} = U\hat{\boldsymbol{\imath}} + V\hat{\boldsymbol{\jmath}} + W\hat{\boldsymbol{k}} \tag{10.2}$$

in which $\hat{\boldsymbol{\imath}}, \hat{\boldsymbol{\jmath}}, \hat{\boldsymbol{k}}$ are unit vectors in the directions Cx, Cy, Cz respectively. The location of a point within the ship may be specified as

$$\boldsymbol{r} = x\hat{\boldsymbol{\imath}} + y\hat{\boldsymbol{\jmath}} + z\hat{\boldsymbol{k}}. \tag{10.3}$$

The equations of motion for the rigid vehicle contain the total external force $\boldsymbol{F}$ and the moment about C of the external forces, $\boldsymbol{G}$. In terms of the unit vectors associated with the body axes, these will be written in the form†

$$\boldsymbol{F} = X\hat{\boldsymbol{\imath}} + Y\hat{\boldsymbol{\jmath}} + Z\hat{\boldsymbol{k}} \tag{10.4}$$

$$\boldsymbol{G} = K\hat{\boldsymbol{\imath}} + M\hat{\boldsymbol{\jmath}} + N\hat{\boldsymbol{k}}. \tag{10.5}$$

The vectors $\boldsymbol{U}, \boldsymbol{r}, \boldsymbol{F}, \boldsymbol{G}$ have been specified in terms of $\hat{\boldsymbol{\imath}}, \hat{\boldsymbol{\jmath}}, \hat{\boldsymbol{k}}$, although they could equally well be specified in terms of $\hat{\boldsymbol{I}}, \hat{\boldsymbol{J}}, \hat{\boldsymbol{K}}$. As has already been indicated, however, the former specification is usually the more useful.

10.3.1 *Position and Orientation of the Vehicle*

The position of the vehicle can only be specified by reference to the axes OXYZ and the most obvious approach is to use the rectangular coordinates X_C, Y_C, Z_C. (Other possibilities, such as spherical and cylindrical coordinates, are of little practical interest here.)

The orientation of the vehicle can also be specified with respect to OXYZ, but the method is less obvious. The usual approach (at least for ships and aircraft) is to start with Cxyz parallel to OXYZ and bring the vehicle from this reference orientation to its actual one by:

(i) A 'swing' Ψ to the actual azimuth;
(ii) A 'tilt' Θ to the actual elevation; and
(iii) A 'heel' Φ to the actual orientation.

It is important to note that these rotations *must* be performed *in this order*. The quantities Ψ, Θ, Φ can now be used as the required 'orientation coordinates' and,

† Note that in aeronautics the components of the moment are usually taken as L, M, N, whereas the less elegant notation K, M, N, is common in marine technology [4].

when used in this manner, are a modified form of 'Euler's Angles'. It should be noted that unless these rotations are applied in an agreed order these coordinates are ambiguous.

To sum up, then, the rigid vehicle may be located in space by

(i) three position coordinates X_C, Y_C, Z_C, and
(ii) three angular coordinates Ψ, Θ, Φ,

with the latter set only meaningful if the rotations in swing, tilt and heel are applied in the agreed order.

(a) *Variation of the Orientation*

It has been pointed out that the order in which the rotations Ψ, Θ, Φ are applied is important because it partially determines the resulting orientation. It can also be demonstrated easily that the orientation may *not* be specified in terms of vectors.

Consider for example the special case in which Ψ, Θ, Φ are all equal to π in radian measure and that, instead of a ship, we rotate a prayer book as in Fig. 10.2(a). If we were (wrongly) to use a vector formulation of this process, we should arrive at the spurious vector polygon shown in Fig. 10.2(b). Since the polygon has to be closed, there is apparently a resultant rotation, whereas Fig. 10.2(a) shows that this is not in fact so.

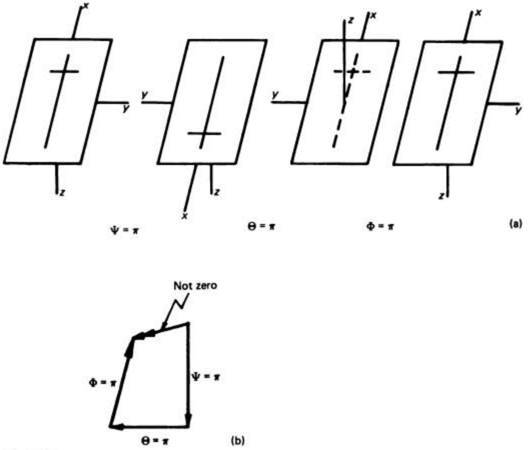

Fig. 10.2

If the velocity components U, V, W are given, the coordinates X_C, Y_C, Z_C vary in a manner that depends on the prevailing values of Ψ, Θ, Φ. Our purpose now is to examine this dependence, bearing in mind that Ψ, Θ, Φ are *not* to be thought of as components of a vector.

The velocity of C may be written as

$$\mathbf{U} = U_1 \hat{\imath}_1 + V_1 \hat{\jmath}_1 + W_1 \hat{k}_1 \tag{10.6a}$$

with respect to the axes $Cx_1y_1z_1$ which represent the initial orientation of the axes $Cxyz$ and are parallel to the axes $OXYZ$ (see Fig. 10.3(a)). If the axes are

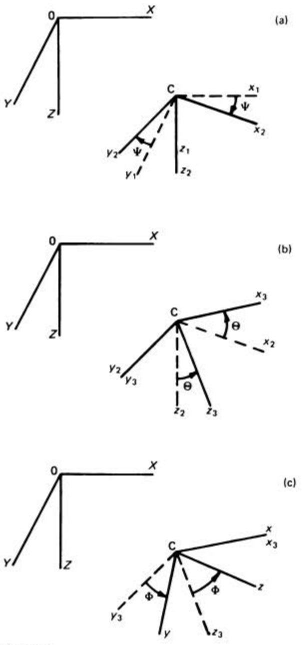

Fig. 10.3

rotated through an angle Ψ about the Cz_1 axis to the position $Cx_2y_2z_2$ in Fig. 10.3(a), the velocity of C may also be written in the form,

$$U = U_2\hat{\imath}_2 + V_2\hat{\jmath}_2 + W_2\hat{k}_2 \tag{10.6b}$$

by reference to the axes $Cx_2y_2z_2$. By inspection it can be seen that,

$$\begin{bmatrix} U_1 \\ V_1 \\ W_1 \end{bmatrix} = \begin{bmatrix} \cos\Psi & -\sin\Psi & 0 \\ \sin\Psi & \cos\Psi & 0 \\ 0 & 0 & 1 \end{bmatrix} \begin{bmatrix} U_2 \\ V_2 \\ W_2 \end{bmatrix}$$

or

$$\mathbf{U}_1 = \mathbf{T}_1(\Psi)\mathbf{U}_2. \tag{10.7a}$$

Next, the tilt angle Θ must be applied by rotating $Cx_2y_2z_2$ to $Cx_3y_3z_3$ as indicated in Fig. 10.3(b). The velocity of C may be written

$$U = U_3\hat{\imath}_3 + V_3\hat{\jmath}_3 + W_3\hat{k}_3.$$

It can be now seen that

$$\begin{bmatrix} U_2 \\ V_2 \\ W_2 \end{bmatrix} = \begin{bmatrix} \cos\Theta & 0 & \sin\Theta \\ 0 & 1 & 0 \\ -\sin\Theta & 0 & \cos\Theta \end{bmatrix} \begin{bmatrix} U_3 \\ V_3 \\ W_3 \end{bmatrix}$$

or

$$\mathbf{U}_2 = \mathbf{T}_2(\Theta)\mathbf{U}_3. \tag{10.7b}$$

Finally the heel Φ must be applied, as in Fig. 10.3(c), so that $Cx_3y_3z_3$ takes up the actual position $Cxyz$. The velocity of C is

$$U = U\hat{\imath} + V\hat{\jmath} + W\hat{k}.$$

Now by inspection it can be seen that

$$\begin{bmatrix} U_3 \\ V_3 \\ W_3 \end{bmatrix} = \begin{bmatrix} 1 & 0 & 0 \\ 0 & \cos\Phi & -\sin\Phi \\ 0 & \sin\Phi & \cos\Phi \end{bmatrix} \begin{bmatrix} U \\ V \\ W \end{bmatrix}$$

or

$$\mathbf{U}_3 = \mathbf{T}_3(\Phi)\mathbf{U}. \tag{10.7c}$$

The matrix $\mathbf{U}_1$ is the same thing as

$$\dot{\boldsymbol{R}}_C = \dot{X}_C\hat{\boldsymbol{I}} + \dot{Y}_C\hat{\boldsymbol{J}} + \dot{Z}_C\hat{\boldsymbol{K}}$$

so that

$$\mathbf{U}_1 \equiv \{\dot{X}_C, \dot{Y}_C, \dot{Z}_C\}.$$

It follows that

$$\begin{bmatrix} \dot{X}_C \\ \dot{Y}_C \\ \dot{Z}_C \end{bmatrix} = \mathbf{T}_1(\Psi)\mathbf{U}_2 = \mathbf{T}_1(\Psi)\cdot\mathbf{T}_2(\Theta)\mathbf{U}_3 = \mathbf{T}_1(\Psi)\cdot\mathbf{T}_2(\Theta)\cdot\mathbf{T}_3(\Phi)\mathbf{U} = \mathbf{TU}\ (\text{say}) \tag{10.8}$$

If the matrix product $\mathbf{T}$ is formed it is found that

$$\begin{bmatrix} \dot{X}_C \\ \dot{Y}_C \\ \dot{Z}_C \end{bmatrix} = \begin{bmatrix} \cos\Psi\cos\Theta & \cos\Psi\sin\Theta\sin\Phi - \sin\Psi\cos\Phi & \cos\Psi\sin\Theta\cos\Phi + \sin\Psi\sin\Phi \\ \sin\Psi\cos\Theta & \sin\Psi\sin\Theta\sin\Phi + \cos\Psi\cos\Phi & \sin\Psi\sin\Theta\cos\Phi - \cos\Psi\sin\Phi \\ -\sin\Theta & \cos\Theta\sin\Phi & \cos\Theta\cos\Phi \end{bmatrix} \begin{bmatrix} U \\ V \\ W \end{bmatrix} \tag{10.9}$$

In principle, a knowledge of $\Psi, \Theta, \Phi, U, V, W$ as functions of time will permit step-by-step integration (with a computer). This yields X_C, Y_C, Z_C and hence $\boldsymbol{R}_C$ as functions of time.

(b) *Angular Velocity Expressed in Terms of Modified Euler Angles*

Even though finite rotations are not vector quantities, angular velocity is. (This is demonstrated in elementary dynamics.) If we let the angular velocity of a vehicle be

$$\boldsymbol{\Omega} = P\hat{\imath} + Q\hat{\jmath} + R\hat{k} \tag{10.10}$$

then clearly the way in which the components P, Q, R vary with time depends on the way in which Ψ, Θ, Φ vary with time. We shall now examine the relationship that exists between the two sets of quantities P, Q, R and Ψ, Θ, Φ.

By superimposing a suitable velocity of translation (in which $\boldsymbol{\Omega} = 0$) on a rigid body, any chosen point of the body may be brought to rest without changing its angular velocity. It is convenient to imagine point C fixed in this way so that only the orientation of the frame $Cxyz$ varies with time. This means that, as time goes on, the frames $Cx_2y_2z_2$, $Cx_3y_3z_3$, $Cxyz$ all rotate about C (while, of course, $Cx_1y_1z_1$ remains stationary and parallel to $OXYZ$). To specify the orientation of $Cxyz$ at any instant it is necessary to 'freeze' the frames and measure the angles Ψ, Θ, Φ.

Since angular velocity is a vector quantity we may add:

(i) Angular velocity of $Cxyz$ relative to $Cx_3y_3z_3$ ($= \dot{\Phi}\hat{\imath}$);
(ii) Angular velocity of $Cx_3y_3z_3$ relative to $Cx_2y_2z_2$ ($= \dot{\Theta}\hat{\jmath}_3$); and
(iii) Angular velocity of $Cx_2y_2z_2$ relative to $Cx_1y_1z_1$ ($= \dot{\Psi}\hat{k}_2$),

where $Cx_1y_1z_1$ is fixed. Therefore,

$$\boldsymbol{\Omega} = \dot{\Phi}\hat{\imath} + \dot{\Theta}\hat{\jmath}_3 + \dot{\Psi}\hat{k}_2 \tag{10.11}$$

and, in order to find expressions for P, Q, R, we must express $\hat{\jmath}_3$ and $\hat{k}_2$ in terms of $\hat{\imath}, \hat{\jmath}, \hat{k}$.

Let

$$\hat{\jmath}_3 = a\hat{\imath} + b\hat{\jmath} + c\hat{k}$$

so that

$$\begin{bmatrix} 0 \\ 1 \\ 0 \end{bmatrix} = \mathbf{T}_3(\Phi) \begin{bmatrix} a \\ b \\ c \end{bmatrix}.$$

This is easily inverted because $|\mathbf{T}_3| = 1$, whence

$$\begin{bmatrix} a \\ b \\ c \end{bmatrix} = \begin{bmatrix} 0 \\ \cos\Phi \\ -\sin\Phi \end{bmatrix}.$$

Again, let

$$\hat{k}_2 = d\hat{\imath} + e\hat{\jmath} + f\hat{k}$$

so that

$$\begin{bmatrix} 0 \\ 0 \\ 1 \end{bmatrix} = \mathbf{T}_2(\Theta)\mathbf{T}_3(\Phi) \begin{bmatrix} d \\ e \\ f \end{bmatrix}.$$

Since $|\mathbf{T}_2| = 1$, this too is easily inverted to give

$$\begin{bmatrix} d \\ e \\ f \end{bmatrix} = \begin{bmatrix} -\sin\Theta \\ \sin\Phi\cos\Theta \\ \cos\Phi\cos\Theta \end{bmatrix}.$$

It follows that

$$\begin{aligned} \Omega &= (\dot{\Phi} - \dot{\Psi}\sin\Theta)\hat{\imath} + (\dot{\Theta}\cos\Phi + \dot{\Psi}\sin\Phi\cos\Theta)\hat{\jmath} \\ &\qquad + (\dot{\Psi}\cos\Phi\cos\Theta - \dot{\Theta}\sin\Phi)\hat{k} \\ &= P\hat{\imath} + Q\hat{\jmath} + R\hat{k}. \end{aligned} \tag{10.12}$$

The components P, Q, R are thus expressed in terms of Ψ, Θ, Φ and their derivatives. The result may be put in matrix form and then inverted. This is found to produce the result

$$\begin{bmatrix} \dot{\Phi} \\ \dot{\Theta} \\ \dot{\Psi} \end{bmatrix} = \begin{bmatrix} 1 & \sin\Phi\tan\Theta & \cos\Phi\tan\Theta \\ 0 & \cos\Phi & -\sin\Phi \\ 0 & \sin\Phi\sec\Theta & \cos\Phi\sec\Theta \end{bmatrix} \begin{bmatrix} P \\ Q \\ R \end{bmatrix}. \tag{10.13}$$

At least in theory, then, the variation of the orientation coordinates can be traced in terms of the angular velocities of roll, P, pitch, Q, and yaw, R.

10.3.2 *Equations of Motion*

Let the velocity $\boldsymbol{R}_C$ be written in the form

$$U = U\hat{\imath} + V\hat{\jmath} + W\hat{k}. \tag{10.14}$$

According to Newton's laws, then,

$$\boldsymbol{F} = m\,\frac{\mathrm{d}\boldsymbol{U}}{\mathrm{d}t}. \tag{10.15}$$

This is a general result that applies to a swarm of particles and, in particular, to the rigid vehicle. It follows that

$$\begin{aligned}\boldsymbol{F} &= m\,\frac{\mathrm{d}}{\mathrm{d}t}(U\hat{\imath} + V\hat{\jmath} + W\hat{k}) \\ &= m(\dot{U}\hat{\imath} + \dot{V}\hat{\jmath} + \dot{W}\hat{k}) + m(U\dot{\hat{\imath}} + V\dot{\hat{\jmath}} + W\dot{\hat{k}}).\end{aligned} \tag{10.16}$$

From elementary dynamics we know that, for a rigid body,

$$\dot{\hat{\imath}} = \boldsymbol{\Omega} \times \hat{\imath} \qquad \dot{\hat{\jmath}} = \boldsymbol{\Omega} \times \hat{\jmath} \qquad \dot{\hat{k}} = \boldsymbol{\Omega} \times \hat{k}$$

so that, using the convenient notation,

$$\dot{U}\hat{\imath} + \dot{V}\hat{\jmath} + \dot{W}\hat{k} = \frac{\delta \boldsymbol{U}}{\delta t}$$

we may write

$$\boldsymbol{F} = m\,\frac{\delta \boldsymbol{U}}{\delta t} + m\left\{U(\boldsymbol{\Omega} \times \hat{\imath}) + V(\boldsymbol{\Omega} \times \hat{\jmath}) + W(\boldsymbol{\Omega} \times \hat{k})\right\}. \tag{10.17}$$

This equation of motion may thus be written

$$\boldsymbol{F} = m\,\frac{\delta \boldsymbol{U}}{\delta t} + m\boldsymbol{\Omega} \times \boldsymbol{U}. \tag{10.18}$$

A second equation of motion refers to the moment of external forces about the centre of mass C (i.e. to the vector $\boldsymbol{G}$). Before examining it, however, consider the moment of momentum vector $\boldsymbol{h}$. For a swarm of particles (whose typical member is the ith),

$$\boldsymbol{h} = \sum_i \boldsymbol{r}_i \times \delta m_i \dot{\boldsymbol{R}}_i \tag{10.19}$$

where δm_i is the mass of the typical particle. As Fig. 10.4 shows, it follows that

$$\begin{aligned}\boldsymbol{h} &= \sum_i \boldsymbol{r}_i \times \delta m_i(\boldsymbol{U} + \dot{\boldsymbol{r}}_i) \\ &= \left(\sum_i \delta m_i \boldsymbol{r}_i\right) \times \boldsymbol{U} + \sum_i \boldsymbol{r}_i \times \delta m_i \dot{\boldsymbol{r}}_i\end{aligned}$$

the sum in parentheses vanishing because C is the centre of mass. The quantity $\boldsymbol{r}_i$ is a position vector of fixed length in a rigid body so that

$$\dot{\boldsymbol{r}}_i = \boldsymbol{\Omega} \times \boldsymbol{r}_i$$

and therefore

$$\boldsymbol{h} = \sum_i \delta m_i \left\{\boldsymbol{r}_i \times (\boldsymbol{\Omega} \times \boldsymbol{r}_i)\right\}. \tag{10.20}$$

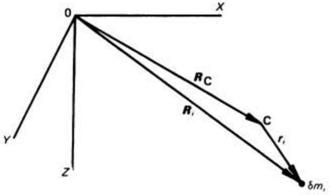

Fig. 10.4

But r_i represents the position of the ith particle with respect to the centre of mass C which is the origin of the axes Cxyz. Accordingly, let

$$r_i = x_i\hat{\imath} + y_i\hat{\jmath} + z_i\hat{k}$$

so that in the 'determinantal form' for a cross product

$$\Omega \times r_i = \begin{vmatrix} \hat{\imath} & \hat{\jmath} & \hat{k} \\ P & Q & R \\ x_i & y_i & z_i \end{vmatrix}.$$

If, now, $r_i \times (\Omega \times r_i)$ is formed in this way, and the appropriate summation is performed, it is found that

$$\begin{aligned} h = & \left\{P\sum_i (y_i^2 + z_i^2)\delta m_i - Q\sum_i x_iy_i\delta m_i - R\sum_i x_iz_i\delta m_i\right\}\hat{\imath} \\ & + \left\{-P\sum_i x_iy_i\delta m_i + Q\sum_i (x_i^2 + z_i^2)\delta m_i - R\sum_i y_iz_i\delta m_i\right\}\hat{\jmath} \\ & + \left\{-P\sum_i x_iz_i\delta m_i - Q\sum_i y_iz_i\delta m_i + R\sum_i (x_i^2 + y_i^2)\delta m_i\right\}\hat{k} \end{aligned}$$

$$= h_x\hat{\imath} + h_y\hat{\jmath} + h_z\hat{k} \tag{10.21}$$

say.

Some abbreviation is obviously desirable and it is usual to introduce the notion of 'products' and 'moments of inertia'. Thus the product of inertia

$$I_{xy} = \sum_i x_iy_i\delta m_i \tag{10.22a}$$

or, if it is preferred to think of the swarm of particles as being a continuous distribution of matter,

$$I_{xy} = \int_V \rho xy \, \mathrm{d}V \tag{10.22b}$$

where V is the volume of the rigid body and ρ is its density. Again

$$I_x = \sum_i (y_i^2 + z_i^2)\delta m_i \quad \text{or} \quad \int_V \rho(y^2 + z^2)\mathrm{d}V. \tag{10.23}$$

The components of $\boldsymbol{h}$ can then be written in the convenient matrix form

$$\mathbf{h} = \begin{bmatrix} h_x \\ h_y \\ h_z \end{bmatrix} = \begin{bmatrix} I_x & -I_{xy} & -I_{xz} \\ -I_{yx} & I_y & -I_{yz} \\ -I_{zx} & -I_{zy} & I_z \end{bmatrix} \begin{bmatrix} P \\ Q \\ R \end{bmatrix} = \mathbf{I}\boldsymbol{\Omega}. \tag{10.24}$$

Note that the elements of $\mathbf{I}$ are all constants because we have adopted body axes fixed in the rigid vehicle.

The moment equation of motion for a swarm of particles is

$$\boldsymbol{G} = \dot{\boldsymbol{h}}. \tag{10.25}$$

In the present context, this becomes

$$\boldsymbol{G} = \frac{\mathrm{d}}{\mathrm{d}t}(h_x\hat{\imath} + h_y\hat{\jmath} + h_z\hat{k})$$

or

$$\boldsymbol{G} = \frac{\delta \boldsymbol{h}}{\delta t} + \boldsymbol{\Omega} \times \boldsymbol{h}. \tag{10.26}$$

This, then, is the second of the two vector equations of motion.

In applying the equations of motion to totally immersed vehicles it is necessary to include the mass of fluid trapped in the vehicle with the mass of the vehicle itself. In particular the mass of water trapped in the free-flooding spaces of a submerged submarine contributes to the mass and moments of inertia of the boat. This is because that water is constrained to perform the same motions as the boat.

(a) *The Component Form of the General Equations of Motion*

It is of practical value to express the vector equations of motion in component form. It is also desirable to separate the gravity forces from fluid forces. Consider first the force equation (10.18),

$$\boldsymbol{F} = m\frac{\delta \boldsymbol{U}}{\delta t} + m\boldsymbol{\Omega} \times \boldsymbol{U}. \tag{10.18}$$

If the symbols X, Y, Z are reserved for the components of fluid forces, we have

$$\boldsymbol{F} = X\hat{\imath} + Y\hat{\jmath} + Z\hat{k} + mg\hat{K} \tag{10.27}$$

where $\hat{K}$, it will be recalled, is a unit vector pointing vertically downwards. Since it will be convenient to express $\boldsymbol{F}$ entirely in terms of the unit vectors $\hat{\imath}, \hat{\jmath}, \hat{k}$, let

$$mg\hat{K} = F_x\hat{\imath} + F_y\hat{\jmath} + F_z\hat{k}. \tag{10.28}$$

To find F_x, F_y, F_z we shall trace the effects of applying successively the orientation angles Ψ, Θ, Φ to bring the vehicle to its actual orientation. First apply the swing Ψ, so that $Cx_1y_1z_1$ swings to $Cx_2y_2z_2$. The components $(F_x)_2, (F_y)_2, (F_z)_2$

in the new directions are obviously 0, 0, *mg* respectively. These results may be found by using appropriate scalar products. Thus, from Fig. 10.5(a),

$$(F_x)_2 = mg\hat{k}_2 \cdot \hat{\imath}_2 = 0 \tag{10.29a}$$

$$(F_y)_2 = mg\hat{k}_2 \cdot \hat{\jmath}_2 = 0 \tag{10.29b}$$

$$(F_z)_2 = mg\hat{k}_2 \cdot \hat{k}_2 = mg. \tag{10.29c}$$

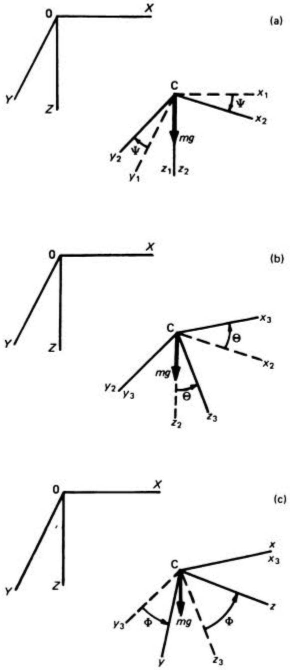

Fig. 10.5

Next apply the angle of tilt Θ, as in Fig. 10.5(b):

$$
\begin{aligned}
(F_x)_3 &= mg\hat{k}_2 \cdot \hat{\imath}_3 \\
&= mg\hat{k}_2 \cdot (\cos\Theta\,\hat{\imath}_2 - \sin\Theta\,\hat{k}_2) \\
&= -mg\sin\Theta
\end{aligned}
\tag{10.30a}
$$

$$
\begin{aligned}
(F_y)_3 &= mg\hat{k}_2 \cdot \hat{\jmath}_3 \\
&= mg\hat{k}_2 \cdot \hat{\jmath}_2 \\
&= 0
\end{aligned}
\tag{10.30b}
$$

$$
\begin{aligned}
(F_z)_3 &= mg\hat{k}_2 \cdot \hat{k}_3 \\
&= mg\hat{k}_2 \cdot (\sin\Theta\,\hat{\imath}_2 + \cos\Theta\,\hat{k}_2) \\
&= mg\cos\Theta.
\end{aligned}
\tag{10.30c}
$$

Finally, apply the angle of heel Φ to bring the vehicle to its actual orientation (Fig. 10.5(c)):

$$
\begin{aligned}
F_x &= \{(F_x)_3\hat{\imath}_3 + (F_z)_3\hat{k}_3\} \cdot \hat{\imath} \\
&= (-mg\sin\Theta\,\hat{\imath}_3 + mg\cos\Theta\,\hat{k}_3) \cdot \hat{\imath}_3 \\
&= -mg\sin\Theta
\end{aligned}
\tag{10.31a}
$$

$$
\begin{aligned}
F_y &= (-mg\sin\Theta\,\hat{\imath}_3 + mg\cos\Theta\,\hat{k}_3) \cdot \hat{\jmath} \\
&= (-mg\sin\Theta\,\hat{\imath}_3 + mg\cos\Theta\,\hat{k}_3) \cdot (\cos\Phi\,\hat{\jmath}_3 + \sin\Theta\,\hat{k}_3) \\
&= mg\cos\Theta\sin\Phi
\end{aligned}
\tag{10.31b}
$$

$$
\begin{aligned}
F_z &= (-mg\sin\Theta\,\hat{\imath}_3 + mg\cos\Theta\,\hat{k}_3) \cdot \hat{k} \\
&= (-mg\sin\Theta\,\hat{\imath}_3 + mg\cos\Theta\,\hat{k}_3) \cdot (-\sin\Theta\,\hat{\jmath}_3 + \cos\Phi\,\hat{k}_3) \\
&= mg\cos\Theta\cos\Phi.
\end{aligned}
\tag{10.31c}
$$

The results of Equations (10.29), (10.30) and (10.31) may now be collected to give

$$
\begin{aligned}
\boldsymbol{F} = (X - mg\sin\Theta)\hat{\imath} &+ (Y + mg\cos\Theta\sin\Phi)\hat{\jmath} \\
&+ (Z + mg\cos\Theta\cos\Phi)\hat{k}.
\end{aligned}
\tag{10.32}
$$

When written out entirely in terms of the unit vectors the force equation (10.18) now becomes

$$
\begin{aligned}
(X - mg\sin\Theta)\hat{\imath} + (Y + mg\cos\Theta\sin\Phi)\hat{\jmath}& \\
+ (Z + mg\cos\Theta\cos\Phi)\hat{k}& \\
= m(\dot{U}\hat{\imath} + \dot{V}\hat{\jmath} + \dot{W}\hat{k}) + m&\begin{vmatrix} \hat{\imath} & \hat{\jmath} & \hat{k} \\ P & Q & R \\ U & V & W \end{vmatrix}.
\end{aligned}
\tag{10.33}
$$

The scalar equations can now be separated out:

$$X - mg\sin\Theta = m(\dot{U} + QW - RV) \tag{10.34a}$$

$$Y + mg\cos\Theta\sin\Phi = m(\dot{V} + RU - PW) \tag{10.34b}$$

$$Z + mg\cos\Theta\cos\Phi = m(\dot{W} + PV - QU). \tag{10.34c}$$

These are the required force equations in surge, drift (or 'sway'), and heave, respectively.

Unlike the force vector $\boldsymbol{F}$, $\boldsymbol{G}$ contains no contribution from the gravity force because it represents a moment about the centre of mass C, that is about the centre of gravity. To obtain the scalar equations from the vector equation, therefore, is straightforward. The vector equation is, from Equation (10.26),

$$Ki + Mj + Nk = \dot{h}_x\hat{\imath} + \dot{h}_y\hat{\jmath} + \dot{h}_z\hat{k} + \boldsymbol{\Omega} \times \boldsymbol{h} \tag{10.35}$$

where K, M, N are the components of the moment of the external fluid forces about the centre of mass C. When expressed in terms of the products and moments of inertia and split up into component form Equation (10.35) becomes

$$K = I_x\dot{P} - I_{xy}\dot{Q} - I_{xz}\dot{R} + (I_zR - I_{zx}P - I_{zy}Q)Q \\ - (I_yQ - I_{yz}R - I_{yz}P)R \tag{10.36a}$$

$$M = -I_{yx}\dot{P} + I_y\dot{Q} - I_{yz}\dot{R} + (I_xP - I_{xy}Q - I_{xz}R)R \\ - (I_zR - I_{zx}P - I_{zy}Q)P \tag{10.36b}$$

$$N = -I_{zx}\dot{P} - I_{zy}\dot{Q} + I_z\dot{R} + (I_yQ - I_{yz}R - I_{yx}P)P \\ - (I_xP - I_{xy}Q - I_{xz}R)Q. \tag{10.36c}$$

These are the required moment equations in roll, pitch and yaw.

10.3.3 *Uses of the General Equations*

In deriving the set of six equations we have made no significant simplifying assumptions other than that the vehicle is rigid. It is therefore to be expected that the equations are fundamental in the dynamics of ships, submarines, small (i.e. relatively stiff) aircraft, and so forth. Unfortunately, they are not at all easy to use in practical investigations, because the quantities X, Y, Z, K, M, N are invariably difficult to specify.

At the outset the origin of the body axes was placed at the centre of mass C, which considerably simplifies the theory (by removing gravity contributions from $\boldsymbol{G}$, for example). It is sometimes possible, however, to simplify the fluid forces and moments by placing the origin elsewhere in the vehicle†, so that advantage can be taken of symmetry. When a different origin is used the equations of motion are more complex than those we have derived. They are quoted for reference in the Appendix (at the end of the chapter), but they do not have the same degree of importance as the equations we have derived.

To return to the basic equations and to the practical difficulty of specifying X, Y, Z, K, M, N, we should expect that certain simplifying techniques would be employed. This is indeed the case. It is natural, for example, to separate out identifiable contributions to X, Y, Z, K, M, N. Notable among these contributions are buoyancy effects, and the effects of control surfaces, which are usually treated separately in the hope that serious error will not result. So difficult is it to specify

† There are other reasons why a different choice of origin may be helpful, as we shall see.

X, Y, Z, K, M, N in practice that one of two approximate approaches has to be employed:

(i) either empirical expressions are used† – and there is no complete agreement as to what expressions are best – or
(ii) the theory is 'linearized'.

10.4 'Linearized' Equations of Motion

Generally speaking, the equations that have been found are too complicated for practical use, and accordingly they are commonly simplified by a process of 'linearization', that is, they are recast in a form that is linear in the mathematical sense. The underlying idea is a common one in applied mathematics. It is then possible to study small departures from a steady (or 'reference') motion, rather than the motion in any more general form, as we did in a rather restricted way in Chapter 8.

Let us consider first the steady reference motion, which is normally taken as one of translation. For a rigid aircraft or submarine this motion may well involve climbing or descent but not a banking or sideways movement. Thus, a steady *symmetric* reference motion is contemplated in which

$$V = 0; \quad \dot{U} = 0; \quad \Omega = 0; \quad \Phi = 0 = \Psi. \tag{10.37}$$

Under these conditions the equations of motion reduce to

$$\bar{X} - mg \sin \bar{\Theta} = 0 \tag{10.38a}$$
$$\bar{Y} = 0 \tag{10.38b}$$
$$\bar{Z} + mg \cos \bar{\Theta} = 0 \tag{10.38c}$$
$$\bar{K} = 0 = \bar{M} = \bar{N} \tag{10.38d}$$

where the bars over the symbols mean 'steady value'. The equations governing the steady reference motion of an interface vehicle are simpler still. For if the body axes are such that Cx, Cy are always parallel to the water surface during the steady motion – strictly, the water surface at infinity – then

$$\bar{X} = 0 = \bar{Y} \tag{10.39a}$$
$$\bar{Z} + mg = 0 \tag{10.39b}$$
$$\bar{K} = 0 = \bar{M} = \bar{N}. \tag{10.39c}$$

10.4.1 *Theory of Small Disturbances*

In any real steady reference motion small disturbances will inevitably occur as a result of small departures from the highly idealized conditions that are assumed to prevail in the reference motion. It is necessary to enquire whether or not a small departure from the reference motion will subside as time goes on, for if it grows it will eventually mask the reference motion, or at least seriously modify it. It is necessary to investigate the 'stability' of the reference motion and this will now be

† For example, for expressions relating to violent manoeuvres of submarines; see [5].

done in a more rigorous manner than that presented in Section 8.4.1. We must first examine the behaviour of small disturbances: if they subside, the reference motion is stable; if they grow, the reference motion is unstable and a parasitic motion will become more and more apparent. This parasitic motion may be undirectional or oscillatory. Examination of the behaviour of small disturbances is a main use of the linear theory.

A second use of the linear theory is rather more obvious. The theory relates to small departures from a steady reference motion and it can therefore be expected to apply to handling characteristics, provided that violent manoeuvres are excluded. This is the basis of the linear theory of directional control. As we shall discover, the theories of directional stability and of control are not to be considered as being independent of each other, however. They are, in fact, closely allied subjects.

In our discussion of small departures from a steady reference motion we shall have to consider:

(i) components of fluid force

$$\bar{X} + \Delta X, \quad \bar{Y} + \Delta Y, \quad \bar{Z} + \Delta Z$$

(ii) components of the moment of fluid force about C

$$\bar{K} + \Delta K, \quad \bar{M} + \Delta M, \quad \bar{N} + \Delta N.$$

If the steady reference motion is

$$\boldsymbol{U} = \bar{U}\hat{\imath} + \bar{W}\hat{k} \tag{10.40a}$$

$$\boldsymbol{\Omega} = 0 \tag{10.40b}$$

then disturbed motion will be of the form

$$\boldsymbol{U} = (\bar{U} + u)\hat{\imath} + v\hat{\jmath} + (\bar{W} + w)\hat{k} \tag{10.41a}$$

$$\boldsymbol{\Omega} = p\hat{\imath} + q\hat{\jmath} + r\hat{k}. \tag{10.41b}$$

Not only must we admit small departures from the reference motion, but also

(i) small displacements from the position that would be occupied at any given instant in the reference motion, and

(ii) small angles of departure from the orientation in the reference motion (which we denote by ψ, θ, ϕ).

(Although the small displacements from the 'steady-motion position' do not appear explicitly in the equations of motion, they may radically affect the fluid forces and moments.)

The disturbed motion must satisfy the six basic equations of motion (10.34a, b, c) and (10.36a, b, c):

$$\bar{X} + \Delta X - mg \sin(\bar{\Theta} + \theta) = m\{\dot{u} + q(\bar{W} + w) - rv\}$$

$$\bar{Y} + \Delta Y + mg \cos(\bar{\Theta} + \theta) \sin\phi = m\{\dot{v} + r(\bar{U} + u) - p(\bar{W} + w)\}$$

$$\bar{Z} + \Delta Z + mg \cos(\bar{\Theta} + \theta) \cos\phi = m\{\dot{w} + pv - q(\bar{U} + u)\}$$

and

$$\bar{K} + \Delta K = I_x\dot{p} - I_{xy}\dot{q} - I_{xz}\dot{r} + (I_z r - I_{zx}p - I_{zy}q)q - (I_y q - I_{yz}r - I_{yx}p)r$$

$$\bar{M} + \Delta M = -I_{yx}\dot{p} + I_y\dot{q} - I_{yz}\dot{r} + (I_x p - I_{xy}q - I_{xz}r)r - (I_z r - I_{zx}p - I_{zy}q)p$$

$$\bar{N} + \Delta N = -I_{zx}\dot{p} - I_{zy}\dot{q} + I_z\dot{r} + (I_y q - I_{yz}r - I_{yx}p)p - (I_x p - I_{xy}q - I_{xz}r)q.$$

It will save time henceforth to take account of the symmetry that is usual in fluid-borne vehicles. If Cxz is a fore-and-aft plane of symmetry, then

$$I_{xy} = 0 = I_{yx} = I_{yz} = I_{zy}.$$

If these simplifications are made in the above equations and if, moreover, all products of small perturbations are discarded from those equations, we find

$$\bar{X} + \Delta X - mg\sin\bar{\Theta} - mg\,\theta\cos\bar{\Theta} = m(\dot{u} + q\bar{W}) \tag{10.42a}$$

$$\bar{Y} + \Delta Y + mg\,\phi\cos\bar{\Theta} = m(\dot{v} + r\bar{U} - p\bar{W}) \tag{10.42b}$$

$$\bar{Z} + \Delta Z + mg\cos\bar{\Theta} - mg\,\theta\sin\bar{\Theta} = m(\dot{w} - q\bar{U}) \tag{10.42c}$$

and

$$\bar{K} + \Delta K = I_x\dot{p} - I_{xz}\dot{r} \tag{10.43a}$$

$$\bar{M} + \Delta M = I_y\dot{q} \tag{10.43b}$$

$$\bar{N} + \Delta N = I_z\dot{r} - I_{xz}\dot{p}. \tag{10.43c}$$

Substitution for $\bar{X}$, $\bar{Y}$, $\bar{Z}$, $\bar{K}$, $\bar{M}$, $\bar{N}$ from Equations (10.38) into Equations (10.42) and (10.43) yields

$$\Delta X - mg\,\theta\cos\bar{\Theta} = m(\dot{u} + q\bar{W}) \tag{10.44a}$$

$$\Delta Y + mg\,\phi\cos\bar{\Theta} = m(\dot{v} + r\bar{U} - p\bar{W}) \tag{10.44b}$$

$$\Delta Z - mg\,\theta\sin\bar{\Theta} = m(\dot{w} - q\bar{U}) \tag{10.44c}$$

and

$$\Delta K = I_x\dot{p} - I_{xz}\dot{r} \tag{10.45a}$$

$$\Delta M = I_y\dot{q} \tag{10.45b}$$

$$\Delta N = I_z\dot{r} - I_{xz}\dot{p}. \tag{10.45c}$$

This set of six equations governs the small parasitic motions of a symmetric vehicle (such as a rigid aircraft or submarine) whose steady symmetric reference motion can involve climbing or descent. Owing to the way in which these equations have been derived, any mathematical expressions which may be developed for ΔX, ΔY, ΔZ, ΔK, ΔM, ΔN must also be restricted to linear forms and the products of small perturbations neglected.

A rigid, symmetric displacement ship will have slightly simpler equations because

$$\bar{W} = 0 = \bar{\Theta} \tag{10.46}$$

and so

$$\Delta X - mg\,\theta = m\dot{u} \tag{10.47a}$$

$$\Delta Y + mg\,\phi = m(\dot{v} + r\bar{U}) \tag{10.47b}$$

$$\Delta Z = m(\dot{w} - q\bar{U}) \tag{10.47c}$$

along with Equations (10.45) which remain unchanged.

10.4.2 *Symmetric and Antisymmetric Disturbances from a Steady Symmetric Reference Motion*

Suppose a small symmetric departure takes place from the reference motion. During the course of it

x, u, z, w, θ, q and their higher derivatives with respect to time will in general be nonzero,

y, v, ϕ, p, ψ, r and their higher derivatives with respect to time will all be zero.

(Here, x, y, z are displacements of the body in the Cx, Cy, Cz directions respectively.) In view of the symmetry of the body, the components ΔY, ΔK, ΔN will all remain zero. This can be seen from physical considerations. (If in difficulty here, the reader should examine the *directions* in which these increments would act.)

Inspection of the mathematical form of Equations (10.44) and Equations (10.45) reveals that three of these equations remain identically zero. There are thus three equations governing the symmetric disturbance, namely

$$\Delta X - mg\,\theta \cos\bar{\Theta} = m(\dot{u} + q\bar{W}) \tag{10.44a}$$

$$\Delta Z - mg\,\theta \sin\bar{\Theta} = m(\dot{w} - q\bar{U}) \tag{10.44c}$$

$$\Delta M = I_y\dot{q}. \tag{10.45b}$$

Consider next a small antisymmetric departure from the symmetric reference motion. During the course of it

y, v, ϕ, p, ψ, r and their higher derivatives with respect to time will in general be nonzero,

x, u, z, w, θ, q and their higher derivatives with respect to time will all be zero.

Although physical reasoning does not suggest that ΔX, ΔZ, ΔM will all be zero, it does indicate that they will be very small. To illustrate this, suppose that the disturbance is one of pure drift v and that the vehicle is as shown in Fig. 10.6. This disturbance would probably produce a negative force ΔX, but a negative value of v would then also produce a negative force ΔX of the same magnitude. Certainly, if ΔX depends on the instantaneous value of v in a well behaved manner, a small value of v must produce a very small magnitude for ΔX (see Fig. 10.6(b)).

If ΔX, ΔZ, ΔM can be neglected during an antisymmetric disturbance, then three of the six equations of motion are identically zero. We thus have as the equations

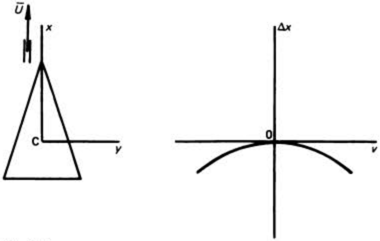

Fig. 10.6

governing the disturbance,

$$\Delta Y + mg\,\phi \cos\bar{\Theta} = m(\dot{v} + r\bar{U} - p\bar{W}) \tag{10.44b}$$

$$\Delta K = I_x\dot{p} - I_{xz}\dot{r} \tag{10.45a}$$

$$\Delta N = I_z\dot{r} - I_{xz}\dot{p}. \tag{10.45c}$$

Once again, some simplification can be made where interface vehicles are concerned and as before,

$$\bar{W} = 0 = \bar{\Theta}.$$

Finally, suppose that the vehicle is given a small *arbitrary* disturbance from the symmetric reference motion so that Equations (10.44) and Equations (10.45) are relevant. Moreover, it must be recalled that any mathematical representation of the small increments, ΔX, ΔY, ΔZ, ΔK, ΔM, ΔN in these equations must be restricted to appropriate linear forms. In these circumstances the symmetry of the ship with respect to the Cxz plane will result in the six equations of motion being uncoupled into two independent sets of three linear simultaneous equations, namely, Equations (10.44a), (10.44c) and (10.45b) for a symmetric disturbance and Equations (10.44b), (10.45a) and (10.45c) for an antisymmetric disturbance.

An element of caution should be introduced at this stage. The simplifications developed in this section really depend upon the fluid flow relative to the vehicle having certain properties of symmetry relative to the plane Cxz. The corresponding symmetry of the vehicle itself is, of course, a necessary requirement for the flow to exhibit the desired characteristics, but it is not sufficient. Thus the flow around a symmetric body, such as a circular cylinder, may exhibit a non-symmetric wake. Moreover, the presence of a propeller (or propellers) at the stern of the ship may distort the symmetry of the flow around the ship's hull. In addition, if the flow displays the 'memory' effects which are introduced in Section 10.4.3(c), then the implications of symmetry may require further examination, at least if the disturbances are not small.

10.4.3 *Nature of the Deviations $\Delta X, \ldots, \Delta N$ for a Totally Immersed Vehicle*

By referring at this stage to a totally immersed vehicle such as a deep-running torpedo, a submarine or an aircraft, we can postpone discussion of the effects associated with a surface. (Surface effects will be examined later, as they raise some complicated points.) We shall consider the component $\Delta Y\bar{j}$ by way of example. This component will be a function of the instantaneous perturbed motion, the previous motion of the vehicle and constant factors, such as the hull geometry and trim. Since it is agreed that in many instances the small perturbation $\Delta Y\bar{j}$ will be independent of all the small symmetric disturbances, it must be possible to express ΔY in the form†

$$\Delta Y = \text{function}\,(\phi,\, v,\, p,\, r,\, \dot{v},\, \dot{p},\, \dot{r}\text{: previous values of these variables: } t\text{: } \bar{U},\, \bar{W},\, \bar{\Theta}). \tag{10.48}$$

One of the main problems in ship dynamics arises from the need to reduce expressions like this to a mathematical form which is both simple and a reasonable approximation to reality. Several techniques are available for this purpose. The conventional method, which has been used for many years, is to express increments like ΔY in terms of the instantaneous motion of the vehicle by means of 'slow motion derivatives'. More recently an alternative approach using oscillatory coefficients has been developed which is more appropriate in some applications. Finally, a more comprehensive technique employing a form of impulse response function has been proposed. We shall discuss the more conventional approaches first, although the presentation will be more general than usual, and then describe briefly the fundamentals of the impulse response function technique.

Consider the variation of, say, the drift velocity v with time. If the variation is sufficiently well behaved then

$$v(t-\tau) = v(t) - \tau\dot{v}(t) + \frac{\tau^2}{2!}\ddot{v}(t) - \frac{\tau^3}{3!}\dddot{v}(t) + \ldots\,. \tag{10.49}$$

This expansion is only strictly valid if Lagrange's form of the remainder, that is

$$R_n = (-1)^n \frac{\tau^n}{n!}\left|\frac{\mathrm{d}^n v}{\mathrm{d}t^n}\right|_{t=t-\tau\theta}$$

in the range $0 < \theta < 1$ is such that

$$\lim_{n\to\infty} |R_n| = 0.$$

Such a condition is certainly satisfied [6] by a disturbance of the form

$$v = v_0 \exp(\mu t) \sin(\omega t + \epsilon).$$

Similar observations may be made in respect of ϕ and r. This merely means that these parameters (ϕ, v, r) can be expanded in a Taylor series. Provided that we may express ϕ, v, p, r, $\dot{v}$, $\dot{p}$, $\dot{r}$ in terms of Taylor series in this way, therefore, we may

† Note that ΔY does not depend on any small displacement but that it does depend on the small angle of heel ϕ, through the buoyancy force.

write

$$\Delta Y = \text{function}\,(\phi, v, p, r, \dot{v}, \dot{p}, \dot{r}, \ddot{v}, \ddot{p}, \ddot{r}, \dddot{v}, \ldots; t). \tag{10.50}$$

Here, 'the previous values of ϕ, v, p, r, $\dot{v}$, $\dot{p}$, $\dot{r}$' are determined by the higher instantaneous derivatives $\ddot{v}$, $\ddot{p}$, $\ddot{r}$, $\dddot{v}$, ... The functional form function ( ) is partly determined by $\bar{U}$, $\bar{W}$, $\bar{\Theta}$ and the other constant parameters.

If ΔY can be expressed as a function in this way, and if that function is a reasonably well behaved one, it may also be expressed in the form of a Taylor series. To the first order, therefore,

$$\begin{aligned}\Delta Y = Y_\phi \phi &+ Y_p p + Y_{\dot{p}} \dot{p} + Y_{\ddot{p}} \ddot{p} + \ldots \\ &+ Y_v v + Y_{\dot{v}} \dot{v} + Y_{\ddot{v}} \ddot{v} + \ldots \\ &+ Y_r r + Y_{\dot{r}} \dot{r} + Y_{\ddot{r}} \ddot{r} + \ldots \\ &+ Y(t)\end{aligned} \tag{10.51}$$

where, for example,

$$Y_v = \left| \frac{\partial \Delta Y}{\partial v} \right|_{\text{steady reference motion}} \tag{10.52}$$

Similar series representations may be found for ΔX, ΔZ, ΔK, ΔM and ΔN in terms of the appropriate motion parameters. Even so, infinite series are not convenient and further simplification is necessary. This may take one of two forms, introducing (i) slow motion derivatives, and (ii) oscillatory coefficients.

(a) *Slow Motion Derivatives*

It will be convenient to continue referring to ΔY by way of example. The easiest and most common method of simplifying the infinite series representation is simply to curtail it. Thus we write

$$\Delta Y = Y_\phi \phi + Y_v v + Y_p p + Y_r r + Y_{\dot{v}} \dot{v} + Y_{\dot{p}} \dot{p} + Y_{\dot{r}} \dot{r} + Y(t) \tag{10.53}$$

where Y_ϕ, Y_v, . . . , $Y_{\dot{r}}$ are called 'slow motion derivatives'.

A proper mathematical justification for this curtailment is not straightforward. Roughly, however, it requires that the departure from the reference motion shall be 'slow'. This suggests that the approximation is acceptable if

$$\frac{|v|}{|\dot{v}|}, \frac{|\dot{v}|}{|\ddot{v}|}, \frac{|\ddot{v}|}{|\dddot{v}|}, \ldots \gg \frac{L}{\bar{U}}$$

where $L/\bar{U}$ is the time taken to travel one length of the vehicle during the initial steady motion. The approach is useful because, at a stability boundary, departure from the reference motion $\bar{U}\hat{\imath} + \bar{W}\hat{k}$ is often infinitely slow.

Generally speaking, calculation of the constants Y_ϕ, Y_v, . . . is in most cases rather primitive and anything approaching accurate theory is exceedingly complicated. No doubt computer techniques will gradually make numerical methods available, but at present reliance has to be placed on measurement by means of model tests.

It is now possible to write the equations of motion for a totally immersed vehicle. For a symmetric disturbance from a steady *straight and level* reference motion (in which $\bar{W} = 0 = \bar{\Theta}$),

$$(X_{\dot{u}}\dot{u} + X_u u + X_{\dot{w}}\dot{w} + X_w w + X_{\dot{q}}\dot{q} + X_q q + X_\theta \theta)$$
$$- mg\theta = m\dot{u} - X(t) \tag{10.54a}$$

$$(Z_{\dot{u}}\dot{u} + Z_u u + Z_{\dot{w}}\dot{w} + Z_w w + Z_{\dot{q}}\dot{q} + Z_q q + Z_\theta \theta)$$
$$= m(\dot{w} - q\bar{U}) - Z(t) \tag{10.54b}$$

$$(M_{\dot{u}}\dot{u} + M_u u + M_{\dot{w}}\dot{w} + M_w w + M_{\dot{q}}\dot{q} + M_q q + M_\theta \theta)$$
$$= I_y\dot{q} - M(t). \tag{10.54c}$$

For an antisymmetric disturbance from a steady straight and level reference motion (in which $\bar{W} = 0 = \bar{\Theta}$),

$$(Y_{\dot{v}}\dot{v} + Y_v v + Y_{\dot{p}}\dot{p} + Y_p p + Y_\phi \phi + Y_{\dot{r}}\dot{r} + Y_r r)$$
$$+ mg\phi = m(\dot{v} + r\bar{U}) - Y(t) \tag{10.55a}$$

$$(K_{\dot{v}}\dot{v} + K_v v + K_{\dot{p}}\dot{p} + K_p p + K_\phi \phi + K_{\dot{r}}\dot{r} + K_r r)$$
$$= I_x\dot{p} - I_{xz}\dot{r} - K(t) \tag{10.55b}$$

$$(N_{\dot{v}}\dot{v} + N_v v + N_{\dot{p}}\dot{p} + N_p p + N_{\dot{r}}\dot{r} + N_r r)$$
$$= I_z\dot{r} - I_{xz}\dot{p} - N(t). \tag{10.55c}$$

(Note that there is no $N_\phi \phi$ term in the last equation.)

These, then, are the equations we seek. They are linear, simultaneous, ordinary differential equations of the second order, with constant coefficients.

It is often assumed that the hydrostatic components of ΔX, ΔY, . . . , ΔN are unchanged in the reference motion from their values when $\bar{U} = 0$. In the equations for symmetric disturbances, then,

$$X_\theta = mg; \quad Z_\theta = 0; \quad M_\theta = -mgh \tag{10.56}$$

where $h = \overline{BC}$, the height of the centre of buoyancy *above* the centre of mass. Similarly in the equations for antisymmetric disturbances

$$Y_\phi = -mg; \quad K_\phi = -mgh. \tag{10.57}$$

It should be noted that these values of the 'hydrostatic derivatives' obtain only for a neutrally buoyant vehicle.

(b) *Oscillatory Coefficients*

We shall still consider the deviation ΔY for a totally immersed vehicle by way of example. Suppose that, by some means, a sinusoidal displacement of drift†

$$y = y_0 \sin \omega t$$

is superimposed on the steady reference motion. In practice, of course, this is only possible with models. The expression for ΔY is

$$\Delta Y = Y_v v + Y_{\dot{v}}\dot{v} + Y_{\ddot{v}}\ddot{v} + \ldots + Y(t) \tag{10.58}$$

† It should be noted that this is one of the unsteady motions for which the Taylor series expansion for $v(t - \tau)$ is certainly valid.

where $Y(t)$ must be such as to produce this sinusoidal displacement (or, rather, to help to produce it). Equation (10.58) becomes

$$\begin{aligned}\Delta Y &= (Y_v - \omega^2 Y_{\ddot{v}} + \ldots)(y_0 \omega \cos \omega t)\\ &\quad + (Y_{\dot{v}} - \omega^2 Y_{\dddot{v}} + \ldots)(-y_0 \omega^2 \sin \omega t) + Y(t)\\ &= \bar{Y}_v v + \bar{Y}_{\dot{v}} \dot{v} + Y(t) \end{aligned} \tag{10.59}$$

say.

In this expression for the sinusoidally varying ΔY, $\bar{Y}_v v$ is a sinusoidal fluid force that is in quadrature with the imposed displacement y, and $\bar{Y}_{\dot{v}} \dot{v}$ is a sinusoidal fluid force that is in phase (or anti-phase) with y.

Similar arguments to these hold good if a sinusoidal roll or yaw is applied to a model. But if a sinusoidal roll is imposed, there will be no term $\bar{Y}_{\dot{p}} \dot{p}$ because it is impossible to distinguish between $\bar{Y}_{\dot{p}}$ and $\bar{Y}_\phi$, both being in phase with the roll.

The usefulness of these 'oscillatory coefficients' arises because although $\bar{Y}_v$ is frequency-dependent (as may be shown by model testing),

$$\lim_{\omega \to 0} \bar{Y}_v = Y_v,$$

and this suggests a way of measuring slow motion derivatives by means of model tests. The technique involves use of the 'planar motion mechanism' as will be explained in Section 10.5.2. Indeed, oscillatory coefficients provide a better interpretation of these tests than slow motion derivatives.

Oscillatory coefficients may also prove useful in their own right, because at the boundary of an oscillatory instability the unsteady motion is sinusoidal (e.g. the flutter of an aircraft wing).

(c) *Impulse response functions*

The principal deficiency in slow motion derivative theory probably lies in the neglect of fluid 'memory' or time history effects. Hydrodynamic forces and moments can be shown to depend significantly on the previous unsteady motion of the ship. A simple example will illustrate this aspect. If a fully immersed hydrofoil is moving through the water at a steady speed and constant angle of incidence, then the lift force generated by the foil is constant and proportional to the angle of incidence, provided that the latter is not greater than the stall value. If the incidence of the foil is sufficiently changed, then eventually the lift force on the foil attains a new steady-state value proportional to the new angle of incidence. For a perceptible time after the change in incidence, however, the lift force on the foil is still adjusting to the change and in this period the lift force is not proportional to the instantaneous angle of incidence. This phenomenon is the well known Wagner effect of aeronautics.

Time history or 'memory' effects are known to arise from surface waves and from vortex shedding. Although they are ignored in the slow motion derivative approach, they may be of considerable importance in many problems of unsteady ship dynamics.

An alternative approach has been proposed [7] in which the effects of the previous motion of the vehicle are more comprehensively represented in ΔY than is possible with slow motion derivatives. Increments in hydrodynamic loading, such as ΔY, can be expressed in the form of Volterra series, which in the linear form appropriate to the present discussion reduce to Duhamel (or convolution) integrals.

Consider, for example, the increment in the sway force produced by a disturbance in sway. This can be expressed to the first order as

$$\Delta Y\{v(t)\} = \int_{-\infty}^{\infty} y_v(\tau)\, v(t-\tau)\, \mathrm{d}\tau \tag{10.60}$$

where $y_v(\tau)$ is the variation in ΔY produced by a 'unit impulse' in v at $\tau = 0$ (see Fig. 10.7); $y_v(\tau)$ is thus comparable to an impulse response function. In addition,

$$y_v(\tau) = 0, \qquad \tau < 0 \tag{10.61a}$$

$$v(t-\tau) = 0, \qquad \tau > t. \tag{10.61b}$$

Thus, although the convolution integral for ΔY is apparently to be evaluated over the range $-\infty < \tau < \infty$ it is actually determined for the range $0 < \tau < t$. That is, the unsteady motion is assumed to commence at time $t = 0$ and ΔY is determined at time t. Moreover, the values of $v(t')$ at time $t' > t$ cannot influence ΔY at time t. It should be observed that, insofar as the convolution integral admits all values of $v(\tau)$ in the range $0 \leqslant \tau \leqslant t$, it automatically includes the effect of sway acceleration $\dot{v}(t)$, that is variations in $v(t)$, in producing a contribution to ΔY.

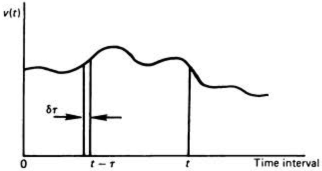

Fig. 10.7

For a vessel in which Cxz is a plane of symmetry, therefore, the total sway force can be written, to the first order, in the form

$$\Delta Y\{v(t), r(t), \phi(t)\} = \int_{-\infty}^{\infty} y_v(\tau)\, v(t-\tau)\, \mathrm{d}\tau + \int_{-\infty}^{\infty} y_r(\tau)\, r(t-\tau)\, \mathrm{d}\tau + \int_{-\infty}^{\infty} y_\phi(\tau)\, \phi(t-\tau)\, \mathrm{d}\tau \tag{10.62}$$

where $y_r(\tau)$ and $y_\phi(\tau)$ are impulse response functions which relate respectively to disturbances in yaw and roll. In a similar manner integral expressions can be formulated for ΔK and ΔN in terms of the appropriate response functions, as far as antisymmetric motion is concerned. For example,

$$\Delta N = \int_{-\infty}^{\infty} n_v(\tau)\, v(t-\tau)\, d\tau + \int_{-\infty}^{\infty} n_r(\tau)\, r(t-\tau)\, d\tau$$

$$+ \int_{-\infty}^{\infty} n_p(\tau)\, p(t-\tau)\, d\tau \qquad (10.63)$$

where $n_v(\tau)$, $n_r(\tau)$ and $n_p(\tau)$† are the relevant impulse response functions.

These response functions are of fundamental importance in ship dynamics. Although they are difficult to measure directly with any accuracy, their Fourier transforms can be determined from models by oscillatory testing (see Section 10.5.2). A full discussion of the properties and applications of the response functions is beyond our scope here but a few of their characteristics will next be examined briefly.

Let $Y_v(\omega)$ be the Fourier transform of $y_v(t)$, so that

$$Y_v(\omega) = \int_{-\infty}^{\infty} y_v(\tau) \exp(-i\omega\tau)\, d\tau \qquad (10.64a)$$

$$y_v(\tau) = \frac{1}{2\pi} \int_{-\infty}^{\infty} Y_v(\omega) \exp(i\omega\tau)\, d\omega \qquad (10.64b)$$

where, of course, $y_v(\tau)$ must be mathematically well behaved to ensure the existence of $Y_v(\omega)$. To illustrate the physical significance of $Y_v(\omega)$, consider a sinusoidal sway motion of the vehicle executed about a steady reference motion, such that

$$y = y_0 \sin \omega t$$

$$v = y_0 \omega \cos \omega t = v_0 \cos \omega t.$$

The associated increment of sway force can be written as

$$\Delta Y\{v(t)\} = \int_{-\infty}^{\infty} y_v(\tau)\, v_0 \cos \omega(t-\tau)\, d\tau$$

$$= \Delta Y_{\mathrm{IN}} \sin \omega t + \Delta Y_{\mathrm{QUAD}} \cos \omega t$$

where

$$\Delta Y_{\mathrm{IN}} = v_0 \int_{-\infty}^{\infty} y_v(\tau) \sin \omega\tau\, d\tau$$

$$\Delta Y_{\mathrm{QUAD}} = v_0 \int_{-\infty}^{\infty} y_v(\tau) \cos \omega\tau\, d\tau.$$

† It should be noted that p and not ϕ is used here as the basic variable in roll, as a fully submerged vehicle experiences no yaw moment due to roll angle.

Moreover, the Fourier transform $Y_v(\omega)$ can be rewritten as

$$Y_v(\omega) = \int_{-\infty}^{\infty} y_v(\tau) \cos \omega\tau \, \mathrm{d}\tau - \mathrm{i} \int_{-\infty}^{\infty} y_v(\tau) \sin \omega\tau \, \mathrm{d}\tau$$

$$= Y_v^{\mathrm{Re}}(\omega) + \mathrm{i} Y_v^{\mathrm{Im}}(\omega)$$

where

$$Y_v^{\mathrm{Re}}(\omega) = \int_{-\infty}^{\infty} y_v(\tau) \cos \omega\tau \, \mathrm{d}\tau$$

$$Y_v^{\mathrm{Im}}(\omega) = -\int_{-\infty}^{\infty} y_v(\tau) \sin \omega\tau \, \mathrm{d}\tau.$$

Thus

$$Y_v^{\mathrm{Re}}(\omega) = \frac{\Delta Y_{\mathrm{QUAD}}}{v_0}$$

$$Y_v^{\mathrm{Im}}(\omega) = -\frac{\Delta Y_{\mathrm{IN}}}{v_0}$$

and

$$\Delta Y = v_0 \left\{ Y_v^{\mathrm{Re}}(\omega) \cos \omega t - Y_v^{\mathrm{Im}}(\omega) \sin \omega t \right\}$$

$$= \mathrm{Re}\left[Y_v(\omega) y_0 \exp(\mathrm{i}\omega t) \right]. \tag{10.65}$$

It follows that $Y_v(\omega)$ is the sway force per unit amplitude of $v_0 \exp(\mathrm{i}\omega t)$ and it is a complex quantity, since ΔY is not in phase with $v(t)$. In vibration terminology $Y_v(\omega)$ is an inverse receptance.

Comparison with Slow Motion Derivatives. It is not easy to establish a general relationship between slow motion derivatives and impulse response functions. For purposes of illustration we will continue to consider a sway disturbance, and by restricting our attention to cases for which $v(t - \tau)$ can be expanded in a Taylor series (see Section 10.4.3) we shall be able to make some progress. In these circumstances the convolution integral for ΔY can be expanded in the form

$$\Delta Y = \int_{-\infty}^{\infty} y_v(\tau) \left\{ v(t) - \tau \dot{v}(t) + \frac{\tau^2}{2!} \ddot{v}(t) - \frac{\tau^3}{3!} \dddot{v}(t) + \ldots \right\} \mathrm{d}\tau$$

$$= v(t) \int_{-\infty}^{\infty} y_v(\tau) \, \mathrm{d}\tau - \dot{v}(t) \int_{-\infty}^{\infty} \tau y_v(\tau) \, \mathrm{d}\tau$$

$$+ \left\{ \frac{\ddot{v}(t)}{2!} \int_{-\infty}^{\infty} \tau^2 y_v(\tau) \, \mathrm{d}\tau - \frac{\dddot{v}(t)}{3!} \int_{-\infty}^{\infty} \tau^3 y_v(\tau) \, \mathrm{d}\tau + \ldots \right\}. \tag{10.66}$$

The slow motion approximation is equivalent to neglecting all but the first and second terms in the above expression and writing

$$Y_v = \int_{-\infty}^{\infty} y_v(\tau)\, d\tau \tag{10.67a}$$

$$Y_{\dot v} = -\int_{-\infty}^{\infty} \tau y_v(\tau)\, d\tau \tag{10.67b}$$

These expressions for Y_v and $Y_{\dot v}$ can be evaluated by noting that

$$\int_{-\infty}^{\infty} y_v(\tau)\, d\tau = \lim_{\omega \to 0} \int_{-\infty}^{\infty} y_v(\tau) \cos \omega\tau\, d\tau = \lim_{\omega \to 0} Y_v^{\mathrm{Re}}(\omega) = Y_v(0)$$

$$\int_{-\infty}^{\infty} \tau y_v(\tau)\, d\tau = \lim_{\omega \to 0} \int_{-\infty}^{\infty} \tau y_v(\tau) \frac{\sin \omega\tau}{\omega\tau}\, d\tau = \lim_{\omega \to 0} \left[-\frac{Y_v^{\mathrm{Im}}(\omega)}{\omega} \right]$$

$$= -Y_{\dot v}(0) \tag{10.68a, b}$$

where $Y_v(0)$ and $Y_{\dot v}(0)$ is a convenient notation. Moreover, experiments with models indicate that the limits $Y_v(0)$ and $Y_{\dot v}(0)$ are finite. Thus the slow motion approximation is equivalent to neglecting the terms in $\ddot v(t)$, $\dddot v(t)$, . . . in Equation (10.66) for ΔY and writing

$$Y_v = Y_v(0); \tag{10.69a}$$

$$Y_{\dot v} = Y_{\dot v}(0). \tag{10.69b}$$

Comparison with Oscillatory Coefficients. Once again, for sinusoidal unsteady motions it is possible to expand motion variables such as

$$v(t - \tau) = v_0 \cos \omega(t - \tau)$$

in a Taylor series. Consequently, ΔY can be expressed in the form

$$\Delta Y = \left\{ Y_v(0) - \frac{\omega^2}{2!} \int_{-\infty}^{\infty} \tau^2 y_v(\tau)\, d\tau + \frac{\omega^4}{4!} \int_{-\infty}^{\infty} \tau^4 y_v(\tau)\, d\tau - \dots \right\} v_0 \cos \omega t$$

$$+ \left\{ Y_{\dot v}(0) - \frac{\omega^2}{3!} \int_{-\infty}^{\infty} \tau^3 y_v(\tau)\, d\tau + \frac{\omega^4}{5!} \int_{-\infty}^{\infty} \tau^5 y_v(\tau)\, d\tau - \dots \right\} (-v_0 \omega \sin \omega t). \tag{10.70}$$

This result is equivalent to that derived in terms of oscillatory coefficients, namely,

$$\Delta Y = \bar{Y}_v v + \bar{Y}_{\dot v} \dot v \tag{10.71}$$

if we define

$$\bar{Y}_v = Y_v(0) - \frac{\omega^2}{2!} \int_{-\infty}^{\infty} \tau^2 y_v(\tau)\, d\tau + \frac{\omega^4}{4!} \int_{-\infty}^{\infty} \tau^4 y_v(\tau)\, d\tau \dots$$

$$\bar{Y}_{\dot v} = Y_{\dot v}(0) - \frac{\omega^2}{3!} \int_{-\infty}^{\infty} \tau^3 y_v(\tau)\, d\tau + \frac{\omega^4}{5!} \int_{-\infty}^{\infty} \tau^5 y_v(\tau)\, d\tau \dots .$$

Apart from establishing expressions for the oscillatory coefficients $\tilde{Y}_v$ and $\tilde{Y}_{\dot{v}}$ in terms of the appropriate impulse response function, these results serve an additional purpose. We have deduced in Section 10.4.3(b) that

$$\lim_{\omega \to 0} \tilde{Y}_v = Y_v; \qquad \lim_{\omega \to 0} \tilde{Y}_{\dot{v}} = Y_{\dot{v}}$$

where Y_v, $Y_{\dot{v}}$ are the corresponding slow motion derivatives. There was the possibility of some confusion in that Y_v, $Y_{\dot{v}}$, $Y_{\ddot{v}}$, $Y_{\dddot{v}}$, . . . might have been functions of frequency, when measured from oscillatory model testing. Now, however, the impulse response function $y_v(\tau)$ and also $Y_v(0)$ and $Y_{\dot{v}}(0)$ are clearly independent of frequency, so that the limits

$$\lim_{\omega \to 0} \tilde{Y}_v = Y_v(0) = Y_v; \qquad \lim_{\omega \to 0} \tilde{Y}_{\dot{v}} = Y_{\dot{v}}(0) = Y_{\dot{v}}$$

can be established in a more satisfactory manner.

It is also to be noted that, since

$$\Delta Y = \tilde{Y}_{\dot{v}}(-v_0 \omega \sin \omega t) + \tilde{Y}_v(v_0 \cos \omega t),$$

it follows that

$$Y_v = \tilde{Y}_v^{\mathrm{Re}}(\omega); \qquad Y_{\dot{v}} = \frac{\tilde{Y}_v^{\mathrm{Im}}(\omega)}{\omega}$$

which can also be subjected to the above limiting process ($\omega \to 0$).

(d) *Matrix Form of the Equations of Motion of a Totally Immersed Body*

Equations (10.54) relate to symmetric and Equations (10.55) relate to antisymmetric departures from a steady, symmetric, straight and level reference motion of a totally immersed vehicle. Inspection reveals that they are of a type that can conveniently be put into a matrix form. This is

$$\mathbf{A}\ddot{\mathbf{q}} + \mathbf{B}\dot{\mathbf{q}} + \mathbf{C}\mathbf{q} = \mathbf{Q}(t) \tag{10.72}$$

where $\mathbf{q}$ must not be mistaken for q.

For symmetric disturbances,

$$\mathbf{A} = \begin{bmatrix} m - X_{\dot{u}} & -X_{\dot{w}} & -X_{\dot{q}} \\ -Z_{\dot{u}} & m - Z_{\dot{w}} & -Z_{\dot{q}} \\ -M_{\dot{u}} & -M_{\dot{w}} & I_y - M_{\dot{q}} \end{bmatrix}$$

$$\mathbf{B} = \begin{bmatrix} -X_u & -X_w & -X_q \\ -Z_u & -Z_w & -(m\bar{U} + Z_q) \\ -M_u & -M_w & -M_q \end{bmatrix}$$

$$\mathbf{C} = \begin{bmatrix} 0 & 0 & mg - X_\theta \\ 0 & 0 & -Z_\theta \\ 0 & 0 & -M_\theta \end{bmatrix} \xrightarrow[\substack{\text{submerged} \\ \text{submarine} \\ \text{with neutral} \\ \text{buoyancy}}]{\text{for a deeply}} \begin{bmatrix} 0 & 0 & 0 \\ 0 & 0 & 0 \\ 0 & 0 & mgh \end{bmatrix}$$

$$\mathbf{Q}(t) = \begin{bmatrix} X(t) \\ Z(t) \\ M(t) \end{bmatrix}; \quad \mathbf{q} = \begin{bmatrix} \int u\,dt \\ \int w\,dt \\ \theta \end{bmatrix} = \begin{bmatrix} x \\ z \\ \theta \end{bmatrix}.$$

For antisymmetric disturbances,

$$\mathbf{A} = \begin{bmatrix} m - Y_{\dot{v}} & -Y_{\dot{p}} & -Y_{\dot{r}} \\ -K_{\dot{v}} & I_x - K_{\dot{p}} & -(I_{xz} + K_{\dot{r}}) \\ -N_{\dot{v}} & -(I_{xz} + N_{\dot{p}}) & I_z - N_{\dot{r}} \end{bmatrix}$$

$$\mathbf{B} = \begin{bmatrix} -Y_v & -Y_p & m\bar{U} - Y_r \\ -K_v & -K_p & -K_r \\ -N_v & -N_p & -N_r \end{bmatrix}$$

$$\mathbf{C} = \begin{bmatrix} 0 & -(mg + Y_\phi) & 0 \\ 0 & -K_\phi & 0 \\ 0 & 0 & 0 \end{bmatrix} \xrightarrow[\substack{\text{for a deeply} \\ \text{submerged} \\ \text{submarine} \\ \text{with neutral} \\ \text{buoyancy}}]{} \begin{bmatrix} 0 & 0 & 0 \\ 0 & mgh & 0 \\ 0 & 0 & 0 \end{bmatrix}$$

$$\mathbf{Q}(\mathrm{t}) = \begin{bmatrix} Y(t) \\ K(t) \\ N(t) \end{bmatrix}; \quad \mathbf{q} = \begin{bmatrix} \int v\,dt \\ \phi \\ \psi \end{bmatrix} = \begin{bmatrix} y \\ \phi \\ \psi \end{bmatrix}.$$

It should be noted that in formulating the two column matrices **q**, we have deduced from Section 10.3.1(b) that for small parameters ϕ, θ, ψ,

$$p = \dot{\phi}, \quad q = \dot{\theta}, \quad r = \dot{\psi} \tag{10.73}$$

if the reference motion is symmetric and level.

In these two sets of matrices, slow motion derivatives have been used. The equations can also be expressed in matrix form in terms of oscillatory coefficients, although the structure of some of the matrices will be somewhat different.†

10.4.4 *Nature of the Deviations $\Delta X, \ldots, \Delta N$ for an Interface Vehicle*

We now return to a question that was previously avoided. We have seen that the force and moment deviations depend on

(i) a number of constant parameters, such as
   the postulated reference motion
   the shape of the vehicle
   the properties of the fluid supporting the vehicle,

† It has been shown that, by employing Fourier transforms, a matrix formulation can be developed in conjunction with impulse response functions [8].

(ii) the position of the centre of mass C with respect to the position it would occupy if the vehicle did not depart from the reference motion,

(iii) the orientation of the vehicle with respect to its orientation in the reference motion,

(iv) the instantaneous motion,

(v) the history of the instantaneous motion.

Provision has been made for all of these except (ii) by limiting our discussion to totally immersed vehicles.

With surface vehicles, and conventional ships in particular, the dependence (ii) is fundamentally important. To examine it, it is helpful to introduce the concept of the 'equilibrium vehicle' which does *not* depart from the reference motion

$$\mathbf{U} = \bar{U}\hat{\imath}$$

$$\mathbf{\Omega} = 0.$$

(Note that we need not consider nonzero $\bar{W}$ or $\bar{\Theta}$ with interface vehicles.) If body axes $C^*x^*y^*z^*$ are attached to the equilibrium vehicle, then the axes $Cxyz$ will move out of coincidence with them during a disturbance (as shown in Fig. 10.8).

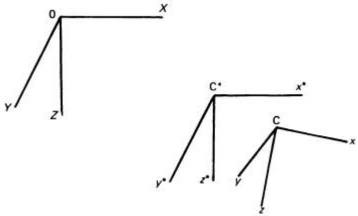

Fig. 10.8

The disturbance displacement upon which ΔX, ΔY, ΔZ, ΔK, ΔM, ΔN partly depend is

$$\mathbf{C^*C} = x^*\hat{I} + y^*\hat{J} + z^*\hat{K} \tag{10.74}$$

where, to the first order,

$$\dot{x}^* = u \tag{10.75a}$$

$$\dot{y}^* = v + \bar{U}\psi \tag{10.75b}$$

$$\dot{z}^* = w - \bar{U}\theta. \tag{10.75c}$$

Suppose that the disturbance commences at the instant $t = 0$. Then, from

Equations (10.75),

$$x^* = \int_0^t u \, dt = x \tag{10.76a}$$

$$y^* = \int_0^t v \, dt + \bar{U} \int_0^t \psi \, dt = y + \bar{U} \int_0^t \psi \, dt \tag{10.76b}$$

$$z^* = \int_0^t w \, dt - \bar{U} \int_0^t \theta \, dt = z - \bar{U} \int_0^t \theta \, dt \tag{10.76c}$$

to the first order. Now variation of x^* and y^* will not affect any of the components $\Delta X, \ldots, \Delta N$, since they merely represent changes of position on the surface. On the other hand, z^* will affect at least some components, so z^* *and its time history* must be introduced into the theory.

By our previous reasoning, we must now include

$$z^*, \dot{z}^*, \ddot{z}^*, \dddot{z}^*, \ldots$$

as arguments in the functions governing $\Delta X, \Delta Y, \ldots$. But z^* and its history introduce z and θ and their histories only (although in a complicated way). Hence z^* must be regarded as a symmetric variable in the sense that it influences only symmetric departures from the reference motion. The equations governing antisymmetric disturbances of an interface vehicle are thus the same as those for a totally immersed vehicle, except that the stiffness matrix is now

$$\mathbf{C} = \begin{bmatrix} 0 & -(mg + Y_\phi) & 0 \\ 0 & -K_\phi & 0 \\ 0 & -N_\phi & 0 \end{bmatrix} \simeq \begin{bmatrix} 0 & 0 & 0 \\ 0 & mgh & 0 \\ 0 & -N_\phi & 0 \end{bmatrix}$$

for N_ϕ is only zero for a fully immersed vehicle.

To examine the effect of the introduction of z^*, we consider the deviation ΔM. This quantity now has the form

$$\Delta M = \text{function}\,(z^*, \theta, \dot{z}^*, u, w, q, \ddot{z}^*, \dot{u}, \dot{w}, \dot{q}, \dddot{z}^*, \ddot{u}, \ldots; t). \tag{10.77}$$

But as z^* and its derivatives depend on z, θ and their derivatives, we cannot proceed as before to expand ΔM 'to the first order' as a Taylor series. In fact there are more ways than one of expressing ΔM in terms of derivatives. The best method of approach is by no means obvious and so we shall therefore now leave this topic.

To sum up, the position for surface vehicles is that

(i) the equations governing antisymmetric disturbances are of the same form as those for the totally immersed vehicle, but the **C** matrix is modified in the manner outlined above;

(ii) the equations for symmetric disturbances require modification to allow for the motions z^*, but the nature of the modification is not simple and it is not treated here.

10.4.5 *Uses of the Linear Equations of Motion*

It has been shown that the equations governing both symmetric and antisymmetric disturbances from a symmetric reference motion may be expressed in the general matrix form of Equation (10.72), namely,

$$\mathbf{A}\ddot{\mathbf{q}} + \mathbf{B}\dot{\mathbf{q}} + \mathbf{C}\mathbf{q} = \mathbf{Q}(t). \tag{10.72}$$

This is true for totally immersed as well as for interface vehicles, although the equations for the symmetric motion of the latter have not been dealt with in detail. The matrices **A**, **B**, **C** contain constant elements which are mostly slow motion derivatives or (possibly) oscillatory coefficients. In practice, however, only slow motion derivatives are really relevant, since oscillatory coefficients are seldom used in the study of directional stability and control.

As has already been indicated there are two main types of problem for which solutions to these equations have to be sought. In the first of these $\mathbf{Q}(t)$ is specified; this is the typical problem of 'manoeuvring'. The second type of investigation concerns directional stability and relates to a small disturbance of the reference motion. In this latter case there is no continuous excitation, so that

$$\mathbf{Q}(t) = \mathbf{0}.$$

If the equations are to be used in these ways, it is plainly essential to ascertain the values of the derivatives in the matrices **A**, **B**, **C**. In general there are two ways of finding the required constants:

(i) By calculation (which must surely become a practical proposition *some* day, although it is at present a very long way off!);

(ii) By measurement with the use of models (which is by no means as straightforward as one would wish and is, strictly speaking, virtually impossible!).

The first of these approaches is rather too specialized for treatment here, but we shall examine the second in Section 10.5.

(a) *'Horizontal Motion' of Interface Vehicles*

A special case of the theory above is commonly considered as being of particular importance. The motion referred to is an antisymmetric disturbance of a surface vehicle from its reference motion. It is assumed that, during the disturbance, although rolling may occur it does not affect yaw or drift.

On the basis of this assumption, all ϕ and p terms are omitted from Equations (10.55a) and (10.55c), which leads to the equations

$$(m - Y_{\dot{v}})\dot{v} - Y_v v - Y_{\dot{r}}\dot{r} + (m\bar{U} - Y_r)r = Y(t) \tag{10.78}$$

$$-N_{\dot{v}}\dot{v} - N_v v + (I_z - N_{\dot{r}})\dot{r} - N_r r = N(t). \tag{10.79}$$

Since drift and yaw are the only parasitic motions admitted we now have equations governing 'horizontal motion', that is 'flat' motion in which all points of the vehicle are confined to motion parallel to the fixed plane OXY. The externally applied components $Y(t)$ and $N(t)$ are normally obtained by the use of a rudder, and this aspect will be discussed later. Directional stability problems of interface vehicles such as large tankers are normally studied by means of these equations, taking

$$Y(t) = 0 = N(t).$$

The two simultaneous equations of horizontal motion (10.78) and (10.79) are somtimes augmented by a third, namely,

$$(m - X_{\dot{u}})\dot{u} - X_u u = X(t). \tag{10.80}$$

This is, of course, a simplified form of Equation (10.54a). The reason for this apparently arbitrary inclusion of an equation for a symmetric disturbance is that horizontal motion really concerns perturbations in u, v and r, although considerations of symmetry uncouple deviations in u from those in v and r in linear theory. It is an observed fact, however, that forward speed may fall off sharply during horizontal motion. Indeed, if the rudder of a ship travelling at speed under power is put hard over, the fall in speed may be as much as 40 per cent, but this is a matter for analysis using a nonlinear theory.

10.5 Measurement of the Deviations $\Delta X, \ldots, \Delta N$ with Models

The linearized equations of motion have been shown to contain 'derivatives' (or, possibly, 'oscillatory coefficients'). Direct calculation of these quantities is notoriously difficult and generally speaking the most reliable approach is to use models (unless one can test the full-size vehicle, as with torpedoes). Such action demands that similarity conditions be satisfied.

For a model that is geometrically similar to its prototype we shall assume that, even for unsteady flow, any representative fluid force may be expressed in the form discussed in Chapter 4, namely,

$$F = \tfrac{1}{2}\rho V^2 L^2 \text{ function}(Re, Fr) \tag{10.81}$$

where ρ represents the density of the fluid, V is any representative velocity (such as $\bar{U}$) and L is a representative length (such as the length of the model). Thus if the Reynolds number Re and the Froude number Fr are the same for the model as they are for the prototype (so that function(Re, Fr) is the same), then $F/\tfrac{1}{2}\rho V^2 L^2$ will be the same for the model and the prototype.

In this context, a typical fluid force might be $Y_v v$. With Re and Fr the same for model and prototype we should have, for *both*,

$$\begin{aligned}\frac{F}{\tfrac{1}{2}\rho V^2 L^2} \equiv \frac{F}{\tfrac{1}{2}\rho \bar{U}^2 L^2} = \frac{Y_v v}{\tfrac{1}{2}\rho \bar{U}^2 L^2} &= \frac{Y_v}{\tfrac{1}{2}\rho \bar{U} L^2}\,\frac{v}{\bar{U}} \\ &= Y'_v v' = \text{function}(Re, Fr).\end{aligned} \tag{10.82}$$

Here, and henceforth, a prime is used to signify a dimensionless quantity. Thus Y'_v is the dimensionless form of the derivative Y_v.

Let the subscript M refer to the model and P to its prototype. Equality of the Reynolds and Froude numbers requires that

$$\left(\frac{\bar{U}\rho L}{\mu}\right)_{\mathrm{M}} = \left(\frac{\bar{U}\rho L}{\mu}\right)_{\mathrm{P}}; \qquad \left(\frac{\bar{U}}{\sqrt{(gL)}}\right)_{\mathrm{M}} = \left(\frac{\bar{U}}{\sqrt{(gL)}}\right)_{\mathrm{P}},$$

where μ represents the dynamic viscosity of the fluid. If the model and prototype are to move in the same fluid, then:

(i) equality of *Re* requires that

$$\frac{\bar{U}_M}{\bar{U}_P} = \frac{L_P}{L_M}$$

so a one-fiftieth scale model must travel fifty times as fast as its prototype, and

(ii) equality of *Fr* requires that

$$\frac{\bar{U}_M}{\bar{U}_P} = \left(\frac{L_M}{L_P}\right)^{1/2}$$

so a one-fiftieth scale model must travel about one-seventh as fast as its prototype.

There is thus a fundamental difficulty in the measurement of fluid forces for marine vehicles which we noted as the 'ship-model tester's dilemma' in Chapter 4.

Fortunately it is usually true – or at least alleged to be so – that the function in Equation (10.82) depends only insensitively on *Re provided* precautions are taken to preserve reasonable turbulence. For a submerged submarine model one can disregard the Froude number *Fr* but turbulence must still be promoted in the boundary layer. Errors of scaling arising from low Reynolds numbers have simply to be accepted.

A propeller (or propellers) must be installed in the model and run during tests as it has a profound effect on the flow near the stern. But the speed at which the propeller should run is open to question (see Section 7.7.2) and a number of techniques may be adopted. For example:

(i) use a self-propelling model; this probably overemphasizes the effect of the propeller;

(ii) attempt to make an empirical correction of the results obtained with a self-propelled model;

(iii) under-run the propeller (so that the model is not quite self-propelled) and assist it with a propeller running in air if necessary.

During tests, the model is

either passed through still water along some path – usually being towed or guided along a long tank or round in a circle,

or held stationary as water is pumped past it.

We shall refer principally to the former approach in which the model is given an appropriate reference motion $\boldsymbol{U} = \bar{U}\boldsymbol{i}$ and must be permitted to take up its appropriate attitude. In addition to this steady reference motion the model is given some relevant perturbation of motion. The technique is to measure incremental fluid forces and moments that are applied to the model by the fluid as a consequence of the perturbation of motion.

Our purpose now is to discuss briefly the measurement of particular derivatives. But it must be understood that the mounting and instrumentation of models call for considerable skill and the following remarks should be regarded only as a bare outline.

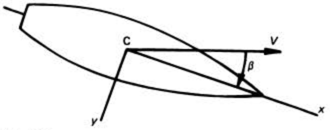

Fig. 10.9

10.5.1 *Measurement of Slow Motion Derivatives*

(a) *Towing Tests*
The derivatives Y_v and N_v of interface and submerged vehicles are commonly measured by means of towing tests. For interface vehicles the towing speed V is chosen on the basis of Froude number identity. The model is towed along the tank at various angles β to the direction of motion (see Fig. 10.9), so that for small angles

$$\bar{U} = V\cos\beta \triangleq V \tag{10.83}$$

$$v = -V\sin\beta \triangleq -\bar{U}\beta. \tag{10.84}$$

The parasitic disturbances ΔY and ΔN are measured for a number of small angles β (i.e. for various values of v), all for the same towing speed V. The results are plotted as shown in Fig. 10.10. The slopes of the curves at the origin are the required quantities Y_v and N_v, which can be made dimensionless by forming

$$Y_v' = \frac{Y_v}{\frac{1}{2}\rho\bar{U}L^2}; \tag{10.85a}$$

$$N_v' = \frac{N_v}{\frac{1}{2}\rho\bar{U}L^3} \tag{10.85b}$$

where L can conveniently be taken as the length of the model.

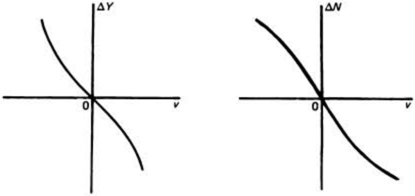

Fig. 10.10

This method has been described in terms of the slow motion derivatives Y'_v and N'_v for an interface model. It can also be used for a submerged vehicle, but there is then no need to match the Froude number. Instead, the test should be run at as high a speed as possible in order to minimize the disparity of Re. For the measurement of Z'_w and M'_w the submerged model is towed either upright or inverted and the ΔM gauge is calibrated to remove a nonzero $M_\theta \theta$ component; by mounting the model on its side, Y'_v and N'_v can be found in the same way.

These tests all require the rudder and/or hydroplanes to be undeflected. Now it will be shown later that these control surfaces are themselves associated with 'slow motion derivatives' and these, too, may be measured in towing tests. If ζ is the rudder deflection, the derivatives Y'_ζ and N'_ζ are found for a surface model from tests in which $\beta = 0, \zeta \neq 0$.

For a submerged submarine model held upright or inverted, the hydroplane derivatives are found in a similar way. Let the hydroplane setting be η and the forward and after hydroplanes be referred to by a subscript F or A respectively. Then,

(i) to determine $(Z'_\eta)_F$ and $(M'_\eta)_F$, take $\eta_F \neq 0$ and $\eta_A = 0 = \beta$;
(ii) to determine $(Z'_\eta)_A$ and $(M'_\eta)_A$, take $\eta_A \neq 0$ and $\eta_F = 0 = \beta$.

In the same way, the rudder derivatives Y'_ζ, N'_ζ may be found for a submerged submarine model mounted on its side.

The significance of these derivatives will become clear later when control surfaces are examined.

(b) *Rotating Arm Tests*

In the past curved models were towed along a straight path in an effort to measure the slow motion derivatives of a straight model following a curved path. This technique (whose origins lay in airship practice) is no longer used and a 'rotating arm' is now employed to measure Y_r and N_r, as shown in Fig. 10.11.

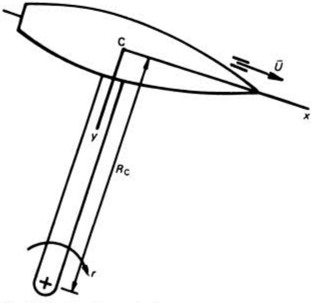

Fig. 10.11 Rotating arm test.

By fixing the model to an arm and then rotating the arm, the model is given a fixed forward speed and known imposed angular velocity of yaw. The force F_y that must be applied to the model in the radial direction and also the moment G_z about a vertical axis through C are both measured for a given forward speed and various angular velocities. Here,

$$\bar{U} = rR_C \tag{10.86}$$

where R_C is the radius of the path of C, and this product is kept constant in a given series of tests so that r and R_C are both varied. The model is accelerated to the test speed and measurements of F_y and G_z are made. The readings are taken before one revolution is completed since otherwise the model runs in its own wake (although this is sometimes regarded as an unnecessary refinement). Then

$$F_y + \Delta Y = m_M r^2 R_C = m_M \bar{U} r \tag{10.87}$$

$$G_z + \Delta N = 0 \tag{10.88}$$

whence ΔY and ΔN may be found.

For a given value of $\bar{U}$, curves may be plotted of ΔY and ΔN against r as shown in Fig. 10.12. From the slopes at the origin the derivatives Y_r and N_r may be determined and then the dimensionless derivatives formed:

$$Y_r' = \frac{Y_r}{\frac{1}{2}\rho \bar{U} L^3}; \tag{10.89a}$$

$$N_r' = \frac{N_r}{\frac{1}{2}\rho \bar{U} L^4}. \tag{10.89b}$$

When an interface model is used in such a test the speed $\bar{U}$ is chosen so as to satisfy the requirement of 'equality of Froude number'. If a deeply submerged model of a submarine vehicle is used, however, the Froude number is disregarded and the model speed is made as large as possible in order to reduce the (unknown) error caused by having $(Re)_M$ too small. The slow motion derivatives Y_r' and N_r' can be found for the submerged model as before, and by mounting the submerged model on its side one can measure the (important) derivatives Z_q' and M_q'.

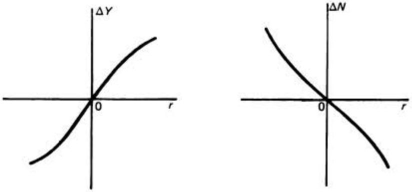

Fig. 10.12

(c) *Comments on the Measurement of Slow Motion Derivatives*

By returning to the definition of a slow motion derivative we have seen how some derivatives may be measured by towing a model suitably in a straight line or round a circular path. It is worth while to mention certain features of the method.

1. Some slow motion derivatives – namely the 'acceleration derivatives' such as $Y'_{\dot{v}}, N'_{\dot{r}}, \ldots$ – cannot be measured in this way. To obtain these the more sophisticated approach of the planar motion mechanism (or PMM) must be used.

2. Furthermore, 'orientation derivatives' such as M_θ, K_ϕ cannot be measured in this way, at least not without modifying the tests. This is not so serious, however, as they can be calculated without difficulty or measured by means of an 'inclining experiment'.

3. For ship and submarine models the rotating arm has to be of enormous size if it is to cope with small values of r. This means that the experimental curves are difficult to draw in the region of the origin, where accuracy is needed most. This drawback, too, is overcome with the PMM.

4. In theory, at least, it is possible to dispense with the straight-line towing tests. In this case the quantities ΔY, ΔN are measured on the rotating arm as before and then the model is slewed round so as to add $Y_v v, N_v v$ components to $Y_r r, N_r r$. The former can then be found by subtracting the latter from $\Delta Y, \Delta N$.

5. In practice, measurements are sometimes 'faired' by drawing a 'carpet' of results. Thus one might plot ΔY in an isometric form taking v and r as the independent variables.

10.5.2 *Oscillatory Model Testing*

It has been shown how, for sinusoidal disturbances superimposed on a steady reference motion, fluid forces and moments may be expressed in terms of oscillatory coefficients. These quantities are usually used merely as a means of finding slow motion derivatives, since a derivative may be regarded as the limit to which an oscillatory coefficient tends as the driving frequency is made infinitely small. But although slow motion derivatives (rather than the corresponding oscillatory coefficients) are conventionally employed in equations of motion, the indirect approach of oscillatory coefficients is particularly useful, as we shall now show.

To be more precise, these model tests are a means of measuring the real and imaginary parts of the Fourier transform of the corresponding impulse response functions. In addition an impulse response function can be calculated from either the real *or* the imaginary part of the associated Fourier transform provided the latter can be measured over a sufficiently wide range of frequency.

The subsequent discussion in this section is couched in terms of oscillatory coefficients, but it must be realized that it could be expressed equally well in terms of the Fourier transforms of the impulse response functions. For example, if $z_w(\tau)$ is the impulse response function relating a heave disturbance, w, to the heave force ΔZ then

$$\Delta Z = \int_{-\infty}^{\infty} z_w(\tau)\, w(t-\tau)\, \mathrm{d}\tau$$

$$Z_w(\omega) = Z_w^{\mathrm{Re}}(\omega) + \mathrm{i} Z_w^{\mathrm{Im}}(\omega) = \int_{-\infty}^{\infty} z_w(\tau) \exp(-\mathrm{i}\omega\tau)\, \mathrm{d}\tau.$$

Consequently, in the following section, the oscillatory coefficients $\tilde{Z}_w$ and $\tilde{Z}_{\dot{w}}$ could be replaced by

$$\tilde{Z}_w = \tilde{Z}_w^{\text{Re}}(\omega); \qquad \tilde{Z}_{\dot{w}} = \frac{\tilde{Z}_w^{\text{Im}}(\omega)}{\omega}$$

and the related slow motion derivatives may be calculated from the experimental data through the limiting process

$$Z_w = \lim_{\omega \to 0} Z_w^{\text{Re}}(\omega) = Z_w(0)$$

$$Z_{\dot{w}} = \lim_{\omega \to 0} \frac{Z_w^{\text{Im}}(\omega)}{\omega} = Z_{\dot{w}}(0).$$

Furthermore, since $Z_w^{\text{Re}}(\omega)$ and $Z_w^{\text{Im}}(\omega)$ are known to be even and odd functions of ω respectively, the impulse response function can be calculated from either one of them. In fact it may be shown that

$$z_w(\tau) = \frac{2}{\pi} \int_0^\infty Z_w^{\text{Re}}(\omega) \cos \omega\tau \, d\omega$$

or

$$z_w(\tau) = -\frac{2}{\pi} \int_0^\infty Z_w^{\text{Im}}(\omega) \sin \omega\tau \, d\omega.$$

Consequently, the 'in-phase' or the 'quadrature' results of a test in which the model is given a sinusoidal disturbance in heave provide a means of calculating $z_w(\tau)$.

As we have already remarked, a full discussion of the use of impulse response functions in ship dynamics is beyond the scope of this book. It is, however, worth while to refer briefly to some simple experimental verifications of the theory [7, 9] which have been made with the results from oscillatory tests with a surface ship model. From the observed values for ΔY_{QUAD}, $y_v(\tau)$ can be calculated from

$$y_v(\tau) = \frac{2}{\pi} \int_0^\infty Y_v^{\text{Re}}(\omega) \cos \omega\tau \, d\omega$$

for which the value $Y_v^{\text{Re}}(0)$ is measured by a towing test described in Section 10.5.1(a). The direct Fourier transform can then be performed to determine $Y_v^{\text{Im}}(\omega)$ in the form

$$Y_v^{\text{Im}}(\omega) = -\int_{-\infty}^{\infty} y_v(\tau) \sin \omega t \, d\tau.$$

The numerical values produced in this way agree remarkably well with the values for $Y_v^{\text{Im}}(\omega)$ deduced from ΔY_{IN} and so confirm the validity of the concept of the impulse response functions. In addition, the computed values for $Y_v^{\text{Im}}(\omega)$ provide further information concerning this function at small values of ω and consequently clarify the limiting process, whereby the slow motion derivative $Y_{\dot{v}}$ is calculated from

$$Y_{\dot v} = \lim_{\omega \to 0} \left(\frac{Y_v^{\mathrm{Im}}(\omega)}{\omega} \right).$$

(a) *Oscillatory Coefficients of a Submerged Submarine in Heave*

Suppose that a model submarine is mounted on 'swords' as shown in Fig. 10.13 and that it is deeply submerged. It is held upside down to minimize interference of the flow round the fin caused by the swords. While the model moves forward with the reference velocity $\bar{U}$ it oscillates in heave so that

$$z_F = z_o \sin \omega t = z_A. \tag{10.90}$$

In a test of this sort, $\bar{U}$ should ideally satisfy the condition

$$(Re)_M = (Re)_P,$$

but this is usually quite impractical and so $\bar{U}$ has simply to be as large as is conveniently possible. (Matching of Froude numbers is here assumed to be unnecessary because the model is sufficiently deeply submerged for surface effects to be negligible.)

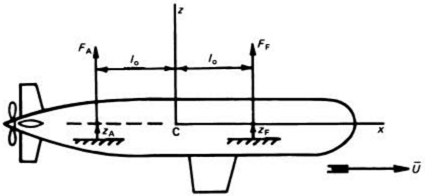

Fig. 10.13 Measurement of heave oscillatory coefficient for a submarine.

The reference motion $\bar{U}\bar{t}$ has a superimposed sinusoidal disturbance described by, say

$$w = z_o \omega \cos \omega t = w_o \cos \omega t \tag{10.91}$$

and

$$\dot{w} = -z_o \omega^2 \sin \omega t = -w_o \omega \sin \omega t. \tag{10.92}$$

To impose this motion it is necessary to apply forces at the swords:

$$F_F = F_{F\bullet} + (F_F)_{\mathrm{IN}} \sin \omega t + (F_F)_{\mathrm{QUAD}} \cos \omega t \tag{10.93}$$

$$F_A = F_{A\bullet} + (F_A)_{\mathrm{IN}} \sin \omega t + (F_A)_{\mathrm{QUAD}} \cos \omega t. \tag{10.94}$$

That is, each force consists of a constant component, an 'in phase' component and a 'quadrature' component. Observe that, in practice, the model is usually mounted on the swords in such a way that the difference between the weight and the buoyancy force is balanced out at $\bar{U} = 0$. The constant contributions $F_{F\bullet}$ and $F_{A\bullet}$ are accounted for by lift forces when $\bar{U} \neq 0$. (It is well to remember that a submarine hull acts like a very inefficient lifting surface, but *not* a negligible one because of its great size.)

The heave equation (10.54b) for a totally immersed vehicle now becomes

$$\begin{aligned} \bar{\bar{Z}}_{\dot{w}}\dot{w} + \bar{\bar{Z}}_w w &= m\dot{w} - Z(t) \\ &= m\dot{w} - [Z_* + F_{F\bullet} + F_{A\bullet} \\ &\quad + \{(F_F)_{IN} + (F_A)_{IN}\} \sin \omega t \\ &\quad + \{(F_F)_{QUAD} + (F_A)_{QUAD}\} \cos \omega t]. \end{aligned} \tag{10.95}$$

The right-hand side of this equation may be abbreviated to give the equation in the form

$$\bar{\bar{Z}}_{\dot{w}}\dot{w} + \bar{\bar{Z}}_w w = m\dot{w} - (Z_* + F_* + F_{IN} \sin \omega t + F_{QUAD} \cos \omega t). \tag{10.96}$$

In this equation Z_* is a constant fluid force acting in the direction Cz. If w and $\dot{w}$ are now substituted into this equation from Equations (10.91) and (10.92) it is found that

$$Z_* = -F_* = -(F_{F\bullet} + F_{A\bullet}) \tag{10.97a}$$

$$\bar{\bar{Z}}_w = -\frac{F_{QUAD}}{w_o} = -\frac{1}{w_o}\{(F_F)_{QUAD} + (F_A)_{QUAD}\} \tag{10.97b}$$

$$\bar{\bar{Z}}_{\dot{w}} = m + \frac{F_{IN}}{w_o\omega} = m + \frac{1}{w_o\omega}\{(F_F)_{IN} + (F_A)_{IN}\}. \tag{10.97c}$$

These oscillatory coefficients may be found for a range of the driving frequency ω and then the slow motion derivatives found, since

$$Z_w = \lim_{\omega \to 0} \bar{\bar{Z}}_w; \qquad Z_{\dot{w}} = \lim_{\omega \to 0} \bar{\bar{Z}}_{\dot{w}}.$$

(b) *Oscillatory Coefficients of a Submerged Submarine in Pitch*

It is possible to impose a sinusoidal disturbance of pitching on the model, instead of heaving as previously. If this is done the path of the centre of mass C is sinusoidal, as shown in Fig. 10.14. We must first examine the problem of imposing a pure pitching motion on the model by imparting suitable motions to the two swords.

Fig. 10.14

The angle made at any instant by the body axis Cx with the horizontal is

$$\theta = \arcsin\left(\frac{z_A - z_F}{2l_o}\right) \tag{10.98}$$

from Fig. 10.15, in which the symbols are defined. The vertical upward velocity of C is

$$\frac{d}{dt}\left(\frac{z_F + z_A}{2}\right).$$

The resultant velocity of C is therefore inclined upward at an angle λ with the horizontal, where

$$\lambda = \arctan\left\{\frac{d}{dt}\left(\frac{z_F + z_A}{2}\right)\bigg/\bar{U}\right\}. \tag{10.99}$$

For pure pitching, the velocity of C must always be in the direction Cx (since $w = 0 = \dot{w}$). Therefore

$$\theta = -\lambda$$

or, approximately,

$$\frac{z_A - z_F}{2l_o} = -\left\{\frac{d}{dt}\left(\frac{z_F + z_A}{2}\right)\bigg/\bar{U}\right\}. \tag{10.100}$$

If z_F and z_A satisfy Equation (10.100) they produce a pure pitching motion. In fact this is so (as the reader should check) if

$$z_F = z_o \cos\left(\omega t + \frac{\epsilon}{2}\right) \tag{10.101a}$$

$$z_A = z_o \cos\left(\omega t - \frac{\epsilon}{2}\right) \tag{10.101b}$$

where the phase advance of z_F with respect to z_A is

$$\epsilon = 2 \arctan\left(\frac{\omega l_o}{\bar{U}}\right). \tag{10.101c}$$

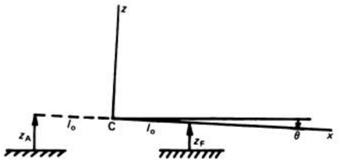

Fig. 10.15

Note that ϵ depends on ω and $\bar{U}$. It is therefore possible to arrange that

$$\theta = \theta_o \sin \omega t \qquad (10.102a)$$

$$q = \theta_o \omega \cos \omega t = q_o \cos \omega t \qquad (10.102b)$$

$$\dot{q} = -\theta_o \omega^2 \sin \omega t = -q_o \omega \sin \omega t \qquad (10.102c)$$

(where $q_o = \theta_o \omega$) while $w = 0 = \dot{w}$.

The equation of motion of the model *in heave* along Cz is

$$\begin{aligned}\tilde{Z}_{\dot{q}}\dot{q} + \tilde{Z}_q q &= -mq\bar{U} - Z(t)\\ &= -mq\bar{U} - (Z_* + F_* + F_{\mathrm{IN}} \sin \omega t\\ &\quad + F_{\mathrm{QUAD}} \cos \omega t)\end{aligned} \qquad (10.103)$$

where F_{IN} and F_{QUAD} are measured by reference to θ (and not to z_F or z_A). From Equation (10.103) it is found that

$$Z_* = -F_* \qquad (10.104a)$$

$$\tilde{Z}_q = -m\bar{U} - \frac{F_{\mathrm{QUAD}}}{q_o} \qquad (10.104b)$$

$$\tilde{Z}_{\dot{q}} = +\frac{F_{\mathrm{IN}}}{q_o \omega}. \qquad (10.104c)$$

And then

$$Z_q = \lim_{\omega \to 0} \tilde{Z}_q; \qquad Z_{\dot{q}} = \lim_{\omega \to 0} \tilde{Z}_{\dot{q}}. \qquad (10.105)$$

(c) *Other Uses of the Planar Motion Mechanism*

The above tests to determine oscillatory coefficients are performed with a planar motion mechanism (or PMM) attached to the carriage of a towing tank. Two types of measurement only have been described by way of examples, but in fact the PMM is sufficiently versatile to provide all the oscillatory coefficients (and, hence, slow motion derivatives) required by linear theory. We shall now briefly describe the nature of the necessary modifications of the test procedure.

1. To obtain the derivatives M_w, $M_{\dot{w}}$, M_q, $M_{\dot{q}}$ it is only necessary to employ the 'pitch equations' rather than the 'heave equations'. Note that

$$\tilde{M}_\theta = M_\theta - \omega^2 M_{\dot{q}} + \omega^4 M_{\dddot{q}} - \ldots \qquad (10.106)$$

whence

$$M_\theta = \lim_{\omega \to 0} \tilde{M}_\theta \qquad (10.107a)$$

$$M_{\dot{q}} = \lim_{\omega \to 0} \left(-\frac{1}{\omega^2} (\tilde{M}_\theta - M_\theta) \right). \qquad (10.107b)$$

The curve of $\tilde{M}_\theta$ plotted against ω^2 might thus have the form shown in Fig. 10.16 in the region where ω is small. Note also that, here, M_θ is a 'hydrostatic derivative' whose value may be checked fairly readily by calculation.

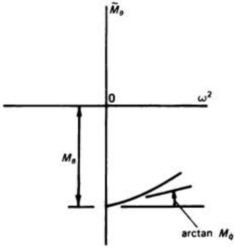

Fig. 10.16

2. In order to obtain derivatives for the antisymmetric motions of drift and yaw of a submerged submarine model, it is necessary to mount the model on its side.

3. The PMM may readily be adapted to give the roll derivatives of a submerged submarine model (as indicated in Fig. 10.17).

4. The PMM can readily be adapted to models of interface vehicles. When it is used in this way it is, of course, necessary to employ the appropriate equations of motion (i.e. not those for a totally immersed vehicle). It is also necessary to run at the correct Froude number.

5. The PMM can also be used to determine control-surface derivatives. For example the slow motion derivatives associated with the forward hydroplanes of a submarine can be deduced from the corresponding oscillatory coefficients if the submerged

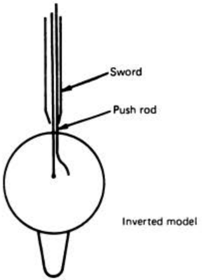

Fig. 10.17 Planar motion mechanism adapted for roll of a submarine.

submarine model is towed along the tank with $w = 0 = q$ but with the forward hydroplanes oscillating so that $\eta = \eta_o \sin \omega t$.

(d) *Comments on Use of the Planar Motion Mechanism*
A few matters relating to the PMM deserve special mention.

1. In practice, all moments of fluid forces applied to the prototype are reckoned with respect to the centre of mass of the prototype. Thus, to find $\tilde{M}_q q$ for the prototype we measure $\tilde{M}'_q q'$ for a geometrically similar model, taking moments about that point of the model at which the scaling ratio suggests the centre of mass should lie. The model is mounted with the swords equidistant from that point, as shown in Fig. 10.18(a). (If it is a surface model the driving points are equidistant from that point, as in Fig. 10.18(b).) The moment applied about that point is then, for the submarine,

$$G_y = (F_A - F_F)l_o \tag{10.108}$$

and for the surface vehicle

$$G_z = (F_F - F_A)l_o. \tag{10.109}$$

It is from this measurement of an applied moment that the required fluid moment is found, by using the appropriate equation of motion.

Now it has been assumed here that the sword attachments (or driving points) are equidistant from the *centre of mass* of the model. That is, it has been assumed that scaling has been such as to preserve the correct position of C. In fact it may well be difficult to place the centre of mass of the model at the correct (i.e. scaled) position.

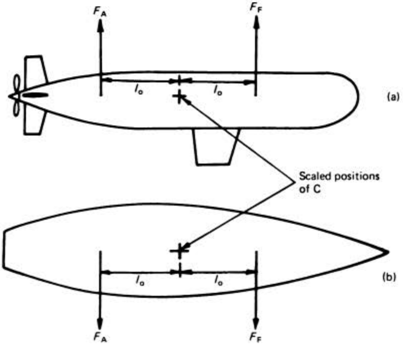

Fig. 10.18

The engine has to be placed in the stern because the 'strongback' attachment of the PMM occupies approximately the middle third of the length, and to place C correctly, therefore, it will normally be necessary to ballast the bows substantially, which may well raise a stressing problem. It does not matter if the centre of mass of the model is not at the correct position, however, so long as its actual location is known.

Suppose it is wished to measure $\tilde{M}_q$ for a submerged submarine. Let A correspond to the centre of mass of the prototype as in Fig. 10.19 and let C be the actual centre of mass of the model. The sword attachments are equidistant from A (not C) and the body axes are erected with A as the origin so that, in the notation of the Appendix at the end of this chapter, the distance $\overline{AC}$ is given by

$$\rho_C = \xi_C \hat{\imath}$$

where ξ_C is negative. The applied moment G_y about A is given by Equation (10.108), and this is the quantity measured during tests.

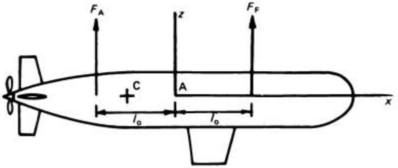

Fig. 10.19

It is now possible to calculate the moment of fluid forces about A (i.e. ΔM_a) using a linearized form of the equations of motion, as quoted in the Appendix at the end of this chapter. In fact it is found that a simple correction term is introduced into the expression for M_q as shown in [6].

2. It was explained previously that symmetric disturbances from the reference motion of a surface vehicle require special thought. A PMM can be made to impart a sinusoidal heaving motion w (with $q = 0$) or a sinusoidal pitching motion q, and hence varying tilt θ (with $w = 0$ but $z^* \neq 0$). Alternatively,

$$\dot{z}^* = w - \bar{U}\theta$$

can be made to vary sinusoidally. But the interpretation of results is by no means straightforward and will not be dealt with here.

3. The PMM was first designed as a device for measuring slow motion derivatives [10, 11] and these quantities permit us to specify fluid forces and moments approximately. We have seen, however, that the PMM has wider applications in that it can enable us to measure the Fourier transforms of the impulse response functions. It thus provides data for the calculation of these response functions. In this way fluid forces and moments can be specified in a far more realistic manner and the

scope of linear theory considerably extended. The need for nonlinear theory, especially as far as the PMM is concerned, is reduced. This simplification is fortunate for practical purposes, as in this context nonlinear theory is very difficult to interpret and to apply logically. It is a field which requires extensive research and is well beyond the scope of this book.

10.6 Control Surfaces

The employment of control surfaces in steady motion has already been discussed in Chapter 8. It is plain that control surfaces raise questions as regards unsteady, as well as steady, motion. For example:

How does the presence of the surfaces affect the stability of the complete vehicle?
What is the nature of the vehicle's response to deflection of a control surface?

Our aim now is to incorporate the effects of control-surface deflections into the equations of motion.

In the following discussion the forward hydroplanes of a submarine will be used for the purposes of analysis and, for simplicity, we shall regard the problem as being essentially a two-dimensional one. The forces acting on a hydroplane are shown in Fig. 10.20 and are:

$\boldsymbol{F}_s, \boldsymbol{G}_s$ the force and moment exerted through the actuating shaft;
$\boldsymbol{F}_h$ the force exerted by the fluid.

(There will, in addition, be a bending moment in the actuating shaft but we shall disregard it.) The moment of $\boldsymbol{F}_h$ about the actuating shaft is

$$\boldsymbol{G}_h = \boldsymbol{r}_h \times \boldsymbol{F}_h \tag{10.110}$$

where $\boldsymbol{r}_h$ is any vector from the shaft to the line of action of $\boldsymbol{F}_h$. The deflection of the hydroplane is η, the angle being measured from the appropriate datum position. For our present purposes we shall take this datum as being parallel to the plane Cxy. Now when $\eta(t)$ varies it is clear that it alters (i) $\boldsymbol{F}_s, \boldsymbol{G}_s$; and (ii) $\boldsymbol{F}_h, \boldsymbol{G}_h$.

It is necessary to study the variation (i) for the purposes of design, both as regards strength and in the design of control engines. This demands a study of the equations of motion of the isolated control surface, but unfortunately this is

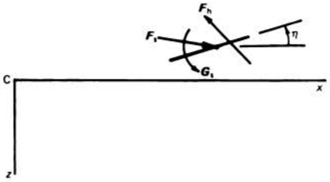

Fig. 10.20

complicated when carried out with any generality, because the hinge line is itself accelerating.

The study of the variation (ii) is obviously necessary in the prediction and analysis of handling characteristics. It is necessary to know how X, Y, Z, K, M, N or, in terms of departures from a steady reference motion, $\Delta X, \Delta Y, \Delta Z, \Delta K, \Delta M, \Delta N$, vary with $\eta(t)$.

We have therefore to consider two distinct types of problem. It should be noted that this applies not only to hydroplanes but also to rudders and stabilizers. We now deal with each variation separately.

10.6.1 *Elementary Analysis of Control-surface Motion*

By way of illustration a very rudimentary form of analysis will be used in variation (i) for a pair of hydroplanes. Our sole purpose now is to indicate how very rough estimates may be obtained – no more.

Assume that the hydroplanes are adequately represented by laminae which lie in the plane Cxy when a totally submerged vehicle performs the reference motion

$$\boldsymbol{U} = \bar{U}\hat{\imath}, \qquad \boldsymbol{\Omega} = 0.$$

Consider a small deflection η of the hydroplanes and a small departure

$$\boldsymbol{u} = u\hat{\imath} + v\hat{\jmath} + w\hat{k}$$

$$\boldsymbol{\Omega} = p\hat{\imath} + q\hat{\jmath} + r\hat{k}$$

from the reference motion. (In short, let us immediately make the simplifying assumptions that have been associated with the linear equations of motion.)

The position of any point B on a hydroplane is given by

$$\boldsymbol{R} = \boldsymbol{R}_C + \boldsymbol{r} = \boldsymbol{R}_C + x\hat{\imath} + y\hat{\jmath} + z\hat{k}$$

(see Fig. 10.21). The velocity of B is therefore

$$\dot{\boldsymbol{R}} = \dot{\boldsymbol{R}}_C + \dot{x}\hat{\imath} + \dot{y}\hat{\jmath} + \dot{z}\hat{k} + \boldsymbol{\Omega} \times \boldsymbol{r}$$

and if the commonly used abbreviation

$$\dot{x}\hat{\imath} + \dot{y}\hat{\jmath} + \dot{z}\hat{k} = \frac{\delta \boldsymbol{r}}{\delta t}$$

is adopted, this becomes

$$\dot{\boldsymbol{R}} = \boldsymbol{U} + \frac{\delta \boldsymbol{r}}{\delta t} + \boldsymbol{\Omega} \times \boldsymbol{r}.$$

The acceleration of B is

$$\ddot{\boldsymbol{R}} = \dot{\boldsymbol{U}} + \ddot{x}\hat{\imath} + \ddot{y}\hat{\jmath} + \ddot{z}\hat{k} + \boldsymbol{\Omega} \times \frac{\delta \boldsymbol{r}}{\delta t} + \dot{\boldsymbol{\Omega}} \times \boldsymbol{r} + \boldsymbol{\Omega} \times \dot{\boldsymbol{r}}.$$

Noting that

$$\boldsymbol{U} = \frac{\delta \boldsymbol{U}}{\delta t} + \boldsymbol{\Omega} \times \boldsymbol{U}$$

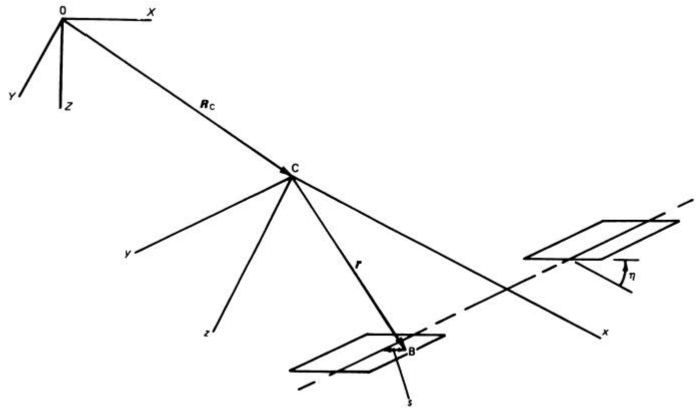

Fig. 10.21

and adopting the abbreviation

$$\frac{\delta^2 \boldsymbol{r}}{\delta t^2} = \ddot{x}\hat{\imath} + \ddot{y}\hat{\jmath} + \ddot{z}\hat{k}$$

we see that

$$\ddot{\boldsymbol{R}} = \frac{\delta \boldsymbol{U}}{\delta t} + \boldsymbol{\Omega} \times \boldsymbol{U} + \frac{\delta^2 \boldsymbol{r}}{\delta t^2} + 2\boldsymbol{\Omega} \times \frac{\delta \boldsymbol{r}}{\delta t} + \dot{\boldsymbol{\Omega}} \times \boldsymbol{r} + \boldsymbol{\Omega} \times (\boldsymbol{\Omega} \times \boldsymbol{r}).$$

By neglecting higher powers of $\eta, \dot{\eta}, \ddot{\eta}$ than the first we may express the acceleration of B in the form

$$\ddot{\boldsymbol{R}} \simeq \frac{\delta \boldsymbol{U}}{\delta t} + \begin{vmatrix} \hat{\imath} & \hat{\jmath} & \hat{k} \\ p & q & r \\ \bar{U}+u & v & w \end{vmatrix} - s\ddot{\eta}\hat{k} + 2\begin{vmatrix} \hat{\imath} & \hat{\jmath} & \hat{k} \\ p & q & r \\ 0 & 0 & -s\dot{\eta} \end{vmatrix}$$

$$+ \begin{vmatrix} \hat{\imath} & \hat{\jmath} & \hat{k} \\ \dot{p} & \dot{q} & \dot{r} \\ x & y & -s\eta \end{vmatrix} + \begin{vmatrix} \hat{\imath} & \hat{\jmath} & \hat{k} \\ p & q & r \\ -qs\eta - ry & rx + ps\eta & py - qx \end{vmatrix}. \qquad (10.111)$$

This vector may be written out in full by expanding the determinants. Suppose that this is done to give $\ddot{R}_x, \ddot{R}_y, \ddot{R}_z$ where

$$\ddot{\boldsymbol{R}} = \ddot{R}_x\hat{\imath} + \ddot{R}_y\hat{\jmath} + \ddot{R}_z\hat{k}. \qquad (10.112)$$

It will be found that, when all products of the small quantities ($u, v, w, p, q, r, \dot{p}, \dot{q}, \dot{r}, \eta, \dot{\eta}$) are neglected,

$$\ddot{R}_x \simeq \dot{u} - \dot{r}y \qquad (10.113a)$$

$$\ddot{R}_z \simeq \dot{w} - q\bar{U} - s\ddot{\eta} + \dot{p}y - \dot{q}x. \qquad (10.113b)$$

The inertia force applied to a particle of the hydroplane located at B is $-(\delta m)\ddot{\boldsymbol{R}}$. If this is resolved as shown in Fig. 10.22 and moments are taken about the hinge line in accordance with d'Alembert's Principle, it is found that

$$G_s + G_h + \sum s(\ddot{R}_z + \eta \ddot{R}_x)\delta m = 0 \qquad (10.114)$$

to the first order in η. The summation is over all particles of the hydroplanes (both

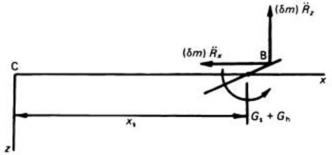

Fig. 10.22

port and starboard). It follows that

$$G_s + G_h + \sum s(\dot{w} - q\bar{U} - s\ddot{\eta} + \dot{p}y - \dot{q}x)\delta m = 0$$

again to the first order (so that, as expected, $\ddot{R}_x$ is irrelevant). Therefore

$$G_s + G_h + m_h e_h(\dot{w} - q\bar{U}) - I_h\ddot{\eta} + P_{hy}\dot{p} - P_{hx}\dot{q} = 0 \tag{10.115}$$

where

$$\begin{aligned}
m_h e_h &= \sum s\,\delta m \ (= 0 \text{ if so designed})\\
I_h &= \sum s^2 \delta m\\
P_{hy} &= \sum sy\delta m = 0 \text{ by symmetry}\\
P_{hx} &= \sum sx\delta m = \sum s(x_s + s)\delta m = m_h e_h x_s + I_h\\
&= I_h \text{ (if so designed).}
\end{aligned}$$

It follows that if the analysis is simplified as much as is reasonably possible the equation governing motion of the hydroplane is

$$G_s + G_h = I_h(\ddot{\eta} + \dot{q}). \tag{10.116}$$

This last equation has at least the merit of appearing to be correct, although a number of assumptions have been made in its derivation. Even so, the practice in naval architecture is to simplify even further on the grounds that $\ddot{\eta}$ and $\dot{q}$ are invariably small quantities. That is, the motions of control surfaces – not only hydroplanes – are analysed on the basis that

$$G_s + G_h = 0 \tag{10.117}$$

even during unsteady motion. A more rigorous approach is needed for aeronautical vehicles, however.

10.6.2 *Control-surface Derivatives*

We now turn to variation (ii), that is to the question of how $X, Y, \ldots, N$ (or ΔX, $\Delta Y, \ldots, \Delta N$) vary when a control surface moves. It is convenient once more to discuss a pair of forward hydroplanes by way of example.

Now considerations of symmetry and antisymmetry imply that only ΔX, ΔZ and ΔM vary with $\eta(t)$. (Note that we prefer to deal here with the perturbations rather than with X, Z and M.) Making the usual assumption that these variations are mathematically well behaved, we can again invoke the idea of 'slow motion derivatives'.† For small departures of the deeply submerged vehicle from its horizontal motion, then, *to the first order*

$$\begin{aligned}
\Delta X &= X_u u + X_{\dot{u}}\dot{u} + X_w w + X_{\dot{w}}\dot{w} + X_\theta\theta + X_q q + X_{\dot{q}}\dot{q} + X_\eta\eta + X_{\dot{\eta}}\dot{\eta} + X_{\ddot{\eta}}\ddot{\eta}\\
\Delta Z &= Z_u u + Z_{\dot{u}}\dot{u} + Z_w w + Z_{\dot{w}}\dot{w} + Z_q q + Z_{\dot{q}}\dot{q} + Z_\eta\eta + Z_{\dot{\eta}}\dot{\eta} + Z_{\ddot{\eta}}\ddot{\eta}\\
\Delta M &= M_u u + M_{\dot{u}}\dot{u} + M_w w + M_{\dot{w}}\dot{w} + M_\theta\theta + M_q q + M_{\dot{q}}\dot{q} + M_\eta\eta + M_{\dot{\eta}}\dot{\eta} + M_{\ddot{\eta}}\ddot{\eta}.
\end{aligned}$$

† It should be noted that an alternative approach using impulse response functions can also be developed.

These expressions may now be used in the equations of motion governing symmetric departures from the symmetric motion. The resulting equations can be expressed in matrix form as follows:

$$\begin{bmatrix} m - X_{\dot{u}} & -X_{\dot{w}} & -X_{\dot{q}} \\ -Z_{\dot{u}} & m - Z_{\dot{w}} & -Z_{\dot{q}} \\ -M_{\dot{u}} & -M_{\dot{w}} & I_y - M_{\dot{q}} \end{bmatrix} \begin{bmatrix} \dot{u} \\ \dot{w} \\ \dot{q} \end{bmatrix} + \begin{bmatrix} -X_u & -X_w & -X_q \\ -Z_u & -Z_w & -(m\overline{U} + Z_q) \\ -M_u & -M_w & -M_q \end{bmatrix} \begin{bmatrix} u \\ w \\ q \end{bmatrix}$$

$$+ \begin{bmatrix} 0 & 0 & 0 \\ 0 & 0 & 0 \\ 0 & 0 & mgh \end{bmatrix} \begin{bmatrix} x \\ z \\ \theta \end{bmatrix} = \begin{bmatrix} X_{\ddot{\eta}} & X_{\dot{\eta}} & X_\eta \\ Z_{\ddot{\eta}} & Z_{\dot{\eta}} & Z_\eta \\ M_{\ddot{\eta}} & M_{\dot{\eta}} & M_\eta \end{bmatrix} \begin{bmatrix} \ddot{\eta} \\ \dot{\eta} \\ \eta \end{bmatrix}. \qquad (10.118)$$

This is generally the case when analysis of this type is applied to

$$\left.\begin{array}{l}\text{forward}\\ \text{after}\\ \text{both sets of}\end{array}\right\} \text{hydroplanes in symmetric motion}$$

$$\left.\begin{array}{l}\text{rudder}\\ \text{stabilizers}\end{array}\right\} \text{in antisymmetric motion.}$$

It is usual in marine practice to specify $\eta(t)$ – or whatever the deflection variable is – so that the appropriate deflection is 'inexorable'. This is quite satisfactory as the deflecting agency must always be sufficient to meet a coxwain's demands. With aeronautical vehicles, on the other hand, one might well have to use extra simultaneous equations arising from analysis of type (i) (i.e. Section 10.6.1). The coefficients $X_{\ddot{\eta}}, X_{\dot{\eta}}$, etc., are of course constants and their values have to be calculated, estimated, measured or ignored.

10.6.3 *'Horizontal Motion' of a Surface Ship*

The handling characteristics of surface vehicles – and we shall here refer specifically to conventional ships – raise a number of complicated problems. Our purpose now is to discuss in greater detail the approximate linear theory of 'horizontal motion'. It should be noted, however, that although this theory is widely used it is not at all accurate.

Arguments of symmetry and antisymmetry suggest that, for small deflections ζ of a ship's rudder, one need only consider the equations governing antisymmetric disturbances from the steady reference motion (see Fig. 10.23). That is, only ΔY,

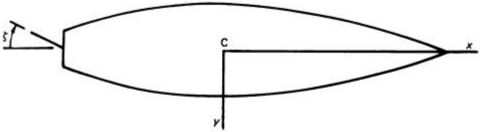

Fig. 10.23

ΔK and ΔN are affected by variations of ζ. It is to be expected, therefore, that terms containing slow motion derivatives

$$Y_\zeta, Y_{\dot\zeta}, Y_{\ddot\zeta}, K_\zeta, K_{\dot\zeta}, K_{\ddot\zeta}, N_\zeta, N_{\dot\zeta}, N_{\ddot\zeta}$$

must be introduced into the relevant equations, which now become

$$\mathbf{A}\ddot{\mathbf{q}} + \mathbf{B}\dot{\mathbf{q}} + \mathbf{C}\mathbf{q} = \mathbf{E}\boldsymbol{\zeta} \tag{10.119}$$

where

$$\mathbf{q} = \{y \quad \phi \quad \psi\}; \tag{10.120a}$$

$$\zeta = \{\ddot\zeta \quad \dot\zeta \quad \zeta\} \tag{10.120b}$$

and

$$\mathbf{A} = \begin{bmatrix} m - Y_{\dot v} & -Y_{\dot p} & -Y_{\dot r} \\ -K_{\dot v} & I_x - K_{\dot p} & -(I_{xz} + K_{\dot r}) \\ -N_{\dot v} & -(I_{zx} + N_{\dot p}) & I_z - N_{\dot r} \end{bmatrix} \tag{10.121a}$$

$$\mathbf{B} = \begin{bmatrix} -Y_v & -Y_p & m\bar{U} - Y_r \\ -K_v & -K_p & -K_r \\ -N_v & -N_p & -N_r \end{bmatrix} \tag{10.121b}$$

$$\mathbf{C} = \begin{bmatrix} 0 & 0 & 0 \\ 0 & mgh & 0 \\ 0 & 0 & 0 \end{bmatrix} \tag{10.121c}$$

$$\mathbf{E} = \begin{bmatrix} Y_{\ddot\zeta} & Y_{\dot\zeta} & Y_\zeta \\ K_{\ddot\zeta} & K_{\dot\zeta} & K_\zeta \\ N_{\ddot\zeta} & N_{\dot\zeta} & N_\zeta \end{bmatrix}. \tag{10.121d}$$

It has already been explained that, under the assumptions relating to 'horizontal motion', a number of coefficients in **A**, **B** and **C** are ignored. The additional assumption is also made that only the third column of **E** is significant. The equations of motion† thus become

$$(m - Y_{\dot v})\dot v - Y_v v - Y_{\dot r}\dot r + (m\bar{U} - Y_r)r = Y_\zeta \zeta \tag{10.122}$$

$$-N_{\dot v}\dot v - N_v v + (I_z - N_{\dot r})\dot r - N_r r = N_\zeta \zeta. \tag{10.123}$$

Equations (10.122) and (10.123) refer to motions of drift and yaw only (i.e. to 'horizontal motion'). The linear theory of manoeuvrability is commonly based on

† If the third equation of antisymmetric motion (that for K) is assumed to be completely uncoupled from these two, it becomes

$$(I_x - K_{\dot p})\dot p - K_p p - K_\phi \phi = K_\zeta \zeta.$$

This, however, would usually be too great a simplification and the dependence on v and r has to be retained.

them, although its usefulness appears to be a matter for debate. To obtain these equations in their more useful dimensionless form, it is convenient to divide (10.22) by $\rho\bar{U}^2L^2/2$ and (10.123) by $\rho\bar{U}^2L^3/2$, to obtain

$$\left(\frac{m}{\frac{1}{2}\rho L^3}-\frac{Y_{\dot v}}{\frac{1}{2}\rho L^3}\right)\left(\frac{\dot v L}{\bar U^2}\right)-\left(\frac{Y_v}{\frac{1}{2}\rho\bar U L^2}\right)\left(\frac{v}{\bar U}\right)-\left(\frac{Y_{\dot r}}{\frac{1}{2}\rho L^4}\right)\left(\frac{\dot r L^2}{\bar U^2}\right)$$

$$+\left(\frac{m\bar U}{\frac{1}{2}\rho\bar U L^3}-\frac{Y_r}{\frac{1}{2}\rho\bar U L^3}\right)\left(\frac{rL}{\bar U}\right)=\left(\frac{Y_\zeta}{\frac{1}{2}\rho\bar U^2L^2}\right)\zeta;$$

$$-\left(\frac{N_{\dot v}}{\frac{1}{2}\rho L^4}\right)\left(\frac{\dot v L}{\bar U^2}\right)-\left(\frac{N_v}{\frac{1}{2}\rho\bar U L^3}\right)\left(\frac{v}{\bar U}\right)+\left(\frac{I_z}{\frac{1}{2}\rho L^5}-\frac{N_{\dot r}}{\frac{1}{2}\rho L^5}\right)\left(\frac{\dot r L^2}{\bar U^2}\right)$$

$$-\left(\frac{N_r}{\frac{1}{2}\rho\bar U L^4}\right)\left(\frac{rL}{\bar U}\right)=\left(\frac{N_\zeta}{\frac{1}{2}\rho\bar U^2L^3}\right)\zeta.$$

That is,

$$(m' - Y'_{\dot v})\dot v' - Y'_v v' - Y'_{\dot r}\dot r' + (m' - Y'_r)r' = Y'_\zeta\zeta \tag{10.124}$$

$$-N'_{\dot v}\dot v' - N'_v v' + (I'_z - N'_{\dot r})\dot r' - N'_r r' = N'_\zeta\zeta. \tag{10.125}$$

Note that the quantities $Y'_\zeta\zeta$, $N'_\zeta\zeta$ refer to changes of force and moment due to deflection of the rudder and *not* the fluid force and moment acting on the rudder.

(a) *Rudder and Skeg Theory*

It is natural – and, up to a point, proper – to think of slow motion derivatives as built-in properties of a vehicle. A vehicle 'comes with its derivatives', so to speak. In fact, the derivatives can be modified to some extent by the addition of fins, control surfaces and skegs, and our purpose now is to illustrate the broad principles involved. The reader must be warned, however, that the theory is an extremely idealized one. In particular, the introduction or modification of a surface may not be even remotely as effective in modifying a derivative as the theory would indicate if that surface is not placed on the vehicle's hull so as to protrude into a region of clear flow. (It should also be recalled that a displacement ship's trim can modify its derivatives sufficiently to affect directional stability quite substantially.)

When a surface ship executes a horizontal motion, it is assumed that the fluid force acting on the rudder at any instant is proportional to the prevailing angle of incidence α. Consider the ship in plan view so that the side force exerted on the rudder is F_R (as shown in Fig. 10.24). The force F_R is in fact a 'lift force' or, more

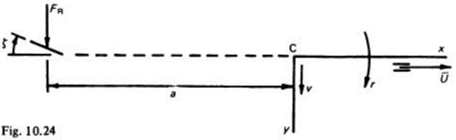

Fig. 10.24

precisely, a 'side force'. According to the elementary theory of control surfaces described in Chapter 8,

$$\frac{F_R}{\frac{1}{2}\rho \bar{U}^2 L^2} = C_L = \alpha \left(\frac{\partial C_L}{\partial \alpha} \right)_0$$

where C_L is the dimensionless lift coefficient and $(\partial C_L/\partial\alpha)_0$ is the slope of the lift curve at zero angle of incidence. Therefore if a is the distance of C from the hydrodynamic centre of the rudder,

$$\frac{F_R}{\frac{1}{2}\rho \bar{U}^2 L^2} = \left(\zeta - \frac{v}{\bar{U}} + \frac{ar}{\bar{U}} \right) \left(\frac{\partial C_L}{\partial \alpha} \right)_0$$

$$= (\zeta - v' + a'r') \left(\frac{\partial C_L}{\partial \alpha} \right)_0 \qquad (10.126)$$

where $a' = a/L$.

This result may be written in the alternative form

$$\frac{F_R}{\frac{1}{2}\rho \bar{U}^2 L^2} = Y'_\zeta \zeta + {}_R Y'_v v' + {}_R Y'_r r' \qquad (10.127)$$

where ${}_R Y'_v$ is the contribution of the undeflected rudder to Y'_v for the ship, and ${}_R Y'_r$ is the undeflected rudder's contribution to Y'_r. In the same way, we may write

$$-\frac{F_R a'}{\frac{1}{2}\rho \bar{U}^2 L^2} = N'_\zeta \zeta + {}_R N'_v v' + {}_R N'_r r' \qquad (10.128)$$

where again the prefixed subscript R means 'contribution of the undeflected rudder'. By inspection it is evident that

$$\left.\begin{aligned} Y'_\zeta &= \left(\frac{\partial C_L}{\partial \alpha} \right)_0 \quad & {}_R Y'_v &= -\left(\frac{\partial C_L}{\partial \alpha} \right)_0 \quad & {}_R Y'_r &= a' \left(\frac{\partial C_L}{\partial \alpha} \right)_0 \\ N'_\zeta &= -a' \left(\frac{\partial C_L}{\partial \alpha} \right)_0 \quad & {}_R N'_v &= a' \left(\frac{\partial C_L}{\partial \alpha} \right)_0 \quad & {}_R N'_r &= -a'^2 \left(\frac{\partial C_L}{\partial \alpha} \right)_0 . \end{aligned}\right\} \qquad (10.129)$$

A skeg may be thought of as a fixed rudder and the above results may readily by adapted to it. If the distance of the hydrodynamic centre of the skeg from the centre of mass C is b (as shown in Fig. 10.25) and $b' = b/L$, we may write

$$\left.\begin{aligned} {}_S Y'_v &= -\left(\frac{\partial \mathbf{C}_L}{\partial \alpha} \right)_0 \quad & {}_S Y'_r &= b' \left(\frac{\partial \mathbf{C}_L}{\partial \alpha} \right)_0 \\ {}_S N'_v &= b' \left(\frac{\partial \mathbf{C}_L}{\partial \alpha} \right)_0 \quad & {}_S N'_r &= -b'^2 \left(\frac{\partial \mathbf{C}_L}{\partial \alpha} \right)_0 \end{aligned}\right\} \qquad (10.130)$$

where $\mathbf{C}_L$ is the lift coefficient of the skeg and the prefixed subscript S means 'contribution of the skeg'.

To illustrate how these results may sometimes be useful, consider the horizontal motion of a ship with a fixed rudder deflection ζ_c. With $\dot{v}' = 0 = \dot{r}'$ in the steady

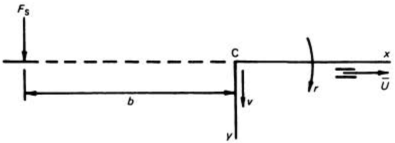

Fig. 10.25

state, Equations (10.124) and (10.125) become

$$-Y'_v v' + (m' - Y'_r)r' = Y'_\zeta \zeta_c \tag{10.131}$$

$$-N'_v v' - N'_r r' = N'_\zeta \zeta_c. \tag{10.132}$$

If v' (which is now a constant) is eliminated from Equations (10.131) and (10.132) it is found that

$$\frac{r'}{\zeta_c} = \frac{N'_\zeta Y'_v - N'_v Y'_\zeta}{N'_v(Y'_r - m') - N'_r Y'_v}. \tag{10.133}$$

In Equation (10.133), the derivatives Y'_v, N'_v, Y'_r, N'_r must be thought of as sums of contributions from the rudder, skeg and hull. Thus

$$Y'_v = {}_\mathrm{R}Y'_v + {}_\mathrm{S}Y'_v + (Y'_v \text{ for remainder of hull}).$$

In this way, r'/ζ_c (whose importance is obvious) is found in terms of C'_α and $\mathbf{C}'_\alpha$, along with the derivatives of the bare hull, where

$$C'_\alpha = \left(\frac{\partial C_L}{\partial \alpha}\right)_0; \qquad \mathbf{C}'_\alpha = \left(\frac{\partial \mathbf{C}_L}{\partial \alpha}\right)_0.$$

These two slopes of 'lift curves' may then be chosen to provide an adequate degree of control.

(b) *Longitudinal Position of a Rudder*
In Equation (10.133) we know that

$$N'_\zeta = -a'\left(\frac{\partial C_L}{\partial \alpha}\right)_0 = -a' Y'_\zeta.$$

It follows that

$$\frac{r'}{\zeta_c} = \frac{-Y'_\zeta(a'Y'_v + N'_v)}{N'_v(Y'_r - m') - N'_r Y'_v}. \tag{10.134}$$

Now it will be seen later that, for directional stability to prevail, the denominator of this expression must be negative. Moreover, in a normal ship, N'_v is negative (as one expects with C abaft amidships) and Y'_v is negative, of course. Hence in simple terms r'/ζ_c is greatest when a' is positive and as large as possible; and for this reason the rudder is placed aft (so that $a' \triangleq 1/2$). This result confirms that found with the elementary approach of Section 8.4.3.

10.6.4 Steering Indices

If the quantities $\dot{v}'$ and v' are eliminated from Equations (10.124) and (10.125) it is found that

$$A\ddot{r}' + B\dot{r}' + Cr' = E\zeta + F\dot{\zeta}'. \tag{10.135}$$

Here

$$A = (m' - Y'_{\dot{v}})(I'_z - N'_{\dot{r}}) - Y'_{\dot{r}}N'_{\dot{v}}$$
$$B = (m' - Y'_r)N'_{\dot{v}} - N'_vY'_{\dot{r}} - (m' - Y'_{\dot{v}})N'_r - (I'_z - N'_{\dot{r}})Y'_v$$
$$C = (m' - Y'_r)N'_v + Y'_vN'_r$$
$$E = N'_vY'_\zeta - Y'_vN'_\zeta$$
$$F = (m' - Y'_{\dot{v}})N'_\zeta - N'_{\dot{v}}Y'_\zeta.$$

In theory, if ζ is prescribed as a function of time it is possible to solve the equation for r; it is the sum of a particular integral and the complementary function. In practice, however, this is not particularly helpful because the significance of the quantities A, B, C, E, F is not clear.

A more useful approach is described in [12] where a simplified form of the equation is examined – or, rather, the predictions of a simplified form. The equation may be written in terms of the operator D:

$$(AD^2 + BD + C)r' = (E + FD)\zeta. \tag{10.136}$$

The rate of yaw r' is thus related to the rudder deflection by the transfer operator

$$r' = \left(\frac{E + FD}{C + BD + AD^2}\right)\zeta.$$

This can be written as

$$r' = \frac{E}{C}\left\{1 + \left(\frac{B}{C} - \frac{F}{E}\right)D + \left(\frac{A}{C} - \frac{BF}{CE} + \frac{F^2}{E^2}\right)D^2 + \ldots\right\}^{-1}\zeta.$$

Letting

$$K' = \frac{E}{C}; \qquad T' = \frac{B}{C} - \frac{F}{E}$$

and truncating the power series, we have

$$r' = \frac{K'}{1 + T'D}\zeta.$$

That is, we now contemplate solutions of the approximate first-order equation

$$T'\dot{r}' + r' = K'\zeta. \tag{10.137}$$

It is not easy to see in what sense this equation *is* approximate; indeed a theoretical investigation of its range of validity is complicated and obscure. Care has therefore to be exercised in using the equation, particularly near the boundary of instability, since the first-order equation does not even admit the possibility of directional instability.

If this simplified equation is adopted, however, it relates the rate of turn r' to the rudder deflection by the two constants K' and T'. These may be identified for a ship or a model and used to specify its handling qualities. The constants are referred to as 'steering indices' and they have useful physical interpretations.

Although a step change of ζ is strictly inadmissible, since it casts grave doubt on the validity of slow motion derivatives in the equations of motion, suppose, nevertheless, that with $t' = t\bar{U}/L$

$$\zeta = 0 \quad \text{for } t' < 0$$

$$\zeta = \zeta_c \quad \text{for } t' > 0.$$

The appropriate solution of Equation (10.137) is then

$$r' = K'\zeta_c[1 - \exp\{-(t'/T')\}] \tag{10.138}$$

and this is sketched in Fig. 10.26. As the sketch indicates, K' is a measure of sensitivity to rudder deflection, whereas the constant T' is a measure of 'sluggishness' in responding to the helm. If Equation (10.138) is now integrated with respect to time interval the ship's variation of heading with time can be found:

$$\psi = K'\zeta_c(t' - T'[1 - \exp\{-(t'/T')\}]) \tag{10.139}$$

and the appropriate curve is as shown in Fig. 10.27.

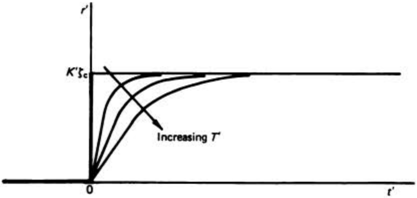

Fig. 10.26

10.6.5 *Dimensionless Linear Equations of Motion*

It has been shown that the equations of horizontal motion may be put into a dimensionless form. The use of dimensionless equations is quite common and it is worthy of some extra thought, for the point is not simply that the terms in the dimensionless equations are independent of the systems of units used (although this is of course true).

Suppose that a ship executes a steady reference motion upon which a steady drift is superimposed. Let us consider the component ΔY of the fluid force by way of example. Dimensional analysis (see Chapter 4) tells us that for a given shape of hull

$$\frac{\Delta Y}{\frac{1}{2}\rho\bar{U}^2L^2} = \text{function } (Re, Fr, \beta)$$

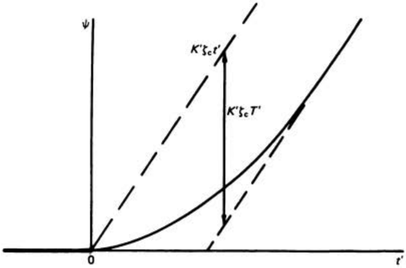

Fig. 10.27

and hence, by Taylor's theorem, we find that

$$\frac{\Delta Y}{\frac{1}{2}\rho\bar{U}^2L^2} = \beta\{\text{function}(Re, Fr)\}$$

approximately. Now

$$\beta = \frac{v}{\bar{U}} = v',$$

so we can write

$$\Delta Y' = Y'_v v'.$$

The quantity $\{\text{function }(Re, Fr)\}$ is therefore a dimensionless derivative which depends on Re and Fr only. Since the dependence is not normally a sensitive one, the quantity Y'_v is more or less independent of speed over a substantial range of operating conditions. This is really the main reason for using dimensionless derivatives; without them, the equations of motion have different coefficients for different operating conditions. Note too that Y'_v is not dependent on the scale of the model, so a value obtained with a model may be used for a prototype.

Contrast this with the result when ΔY is not expressed in the dimensionless form. We have

$$\Delta Y = \tfrac{1}{2}\rho\bar{U}^2L^2\,\frac{v}{\bar{U}}\,\{\text{function}(Re, Fr)\} = Y_v v$$

where

$$Y_v = \tfrac{1}{2}\rho\bar{U}L^2\{\text{function}(Re, Fr)\}.$$

Here the derivative depends on $\bar{U}$ directly (as well as through Re and Fr) and also on L^2 and ρ. When this quantity Y_v is found for a model it cannot be used immediately for the prototype, since it has to be 'corrected' for speed and scale.

This is true generally; if model measurements are made with the appropriate scaling of operating conditions – of *Fr* for a surface ship and its model – it is usually possible to use the same values of dimensionless derivatives for model and prototype.

It is as well to note that the use of dimensionless derivatives is not without drawbacks. This can be illustrated by means of the various equations of motion already referred to:

1. Since the reference speed $\bar{U}$ is taken as the magnitude of velocity it vanishes from the equations. (Thus $m\bar{U}$ becomes m' in the ΔY equation of horizontal motion.) This can be misleading.

2. Although all the dimensionless derivatives for a given hull form depend on *Re and Fr*, dimensionless inertial terms (e.g. m' and I_z' in the equations of horizontal motion) are constants for the hull form.

3. The derivative $M_\theta = -mgh$ which appears in the pitch equation for a submerged submarine cannot be expressed as a dimensionless derivative M_θ' which is the same for model and prototype since

$$\begin{aligned} M_\theta' &= -\frac{mgh}{\frac{1}{2}\rho\bar{U}^2L^3} \\ &= -m'\frac{h}{L}\frac{gL}{\bar{U}^2} \\ &= -m'h'g\frac{L}{\bar{U}^2}, \end{aligned}$$

that is, a dependence on $L/\bar{U}^2$. But this at least has the merit of showing that the stability and control of a submerged submarine are markedly affected by speed.

4. This process of rendering equations dimensionless is lost when the ship is not moving ahead, since $\bar{U} = 0$, yet there may well be significant motions of yaw or of drift. In that event $\bar{U}$ is not used as the basis for yielding dimensionless parameters. This case arises not only with certain types of ship but also with 'hovering' submerged vehicles and with hovercraft.

10.7 Manoeuvring Trials

It is useful to perform manoeuvring trials with free-running models and/or full scale vehicles. The advantage of free model tests is that they do not demand mathematical representation by a 'mathematical model' (although this does not mean, of course, that interpretation of results for the purposes of the prototype is without difficulty). When full-scale vehicles have been built, tests are carried out on them to assess their directional stability and manoeuvrability, for it would not be realistic to rely solely on calculations, even for a conventional ship – let alone for nautical oddities!

There is never any question of aimless testing *ad hoc* and consequently definite, standard tests and trials have come to be accepted. Briefly, the most important of these are

(i) stability trials – the 'pull-out' manoeuvre
– the 'spiral' (or Dieudonné) manoeuvre

(ii) control trials – the 'circle' manoeuvre
– the 'zig-zag' (or Kempf) manoeuvre.

It should be noted that, although the trials are placed here in two categories, the designer is *not* concerned with stability and control as two distinct phenomena. This is because large stability implies difficulty of control, whereas marginal stability implies 'touchiness' (which, to be sure, may not be disastrous).

The compromise that must be achieved between stability and sensitivity is particularly important where the motion of a submarine in the vertical plane is concerned, for vehicles of this type must possess directional stability of vertical motion for safety and yet too much stability reduces the submarine's essential capabilities.

Although calculations are backed up by actual trials, it cannot be assumed that a vehicle's degree of stability is easily assessed, and even the question of whether or not a particular vehicle is directionally stable is sometimes difficult to answer with any conviction. From an analyst's point of view the study of directional stability and control is somewhat unrewarding and rather untidy.

10.7.1 *The Pull-out Manoeuvre*

The equation governing horizontal motion of a ship with its rudder amidships is, from Equation (10.135),

$$A\ddot{r}' + B\dot{r}' + Cr' = 0. \qquad (10.140)$$

Any yawing motion is therefore described by

$$r' = r_1' \exp(\alpha t) + r_2' \exp(\beta t) \qquad (10.141)$$

where r_1' and r_2' are constants whose values are determined by the initial conditions and α, β are given by

$$\frac{-B \pm \sqrt{(B^2 - 4AC)}}{2A}.$$

It is a matter of observation that ships never behave in the manner suggested by the complex solution. Thus $B^2 > 4AC$, and therefore directional stability requires that α and β must both be real and negative.

In practice, the constants A and B are both positive. (As we have seen, they are combinations of derivatives and inertia terms and the signs of the derivatives determine the signs of A, B and C.) Since A and B are always real and positive, C must also be real and positive if directional stability is to prevail, although as we have already noted it is never large enough to make $4AC > B^2$.

The values of α and β provide measures of directional stability. Now if the stability is in question at all, that is if C is small,

$$\beta \ll \alpha$$

(assuming that β is associated with the negative root and α with the positive). That is, β will be large and negative. Thus in free motion with rudder amidships the solution

$$r' = r_1' \exp(\alpha t) \qquad (10.142)$$

will quickly become dominant.

In the 'pull-out' manoeuvre the ship or free model is put into a turn and then the rudder is restored to zero deflection. The subsequent decay of r' from its initial value provides a means of determining α. Since the root β is large and negative the decaying motion assumes the form $r'_1 \exp(\alpha t)$ whence

$$\ln(r') = \ln(r'_1) + \alpha t. \tag{10.143}$$

A curve of $\ln(r')$ plotted against t eventually becomes a straight line of slope α, and the tendency of this slope to approach zero indicates that a state of instability is at hand.

Although a pull-out manoeuvre may be commenced in a violently nonlinear fashion, the majority of the $\ln(r')$ curve that is obtained usually conforms well to linear theory. In particular it is found that different initial yawing rates produce little effect on the results.

It is because of the normally large difference between the roots α and β that the reduction to a first-order equation [12] may be justified. (Unfortunately a rigorous demonstration of this appears to be complicated.) But whether or not Equation (10.137) gives sensible results does not rest solely on this; it also depends on whether or not a linear régime can decently be assumed to exist at all. In fact, in the form in which they are usually determined the 'constants' K' and T' are not unique, mainly because they are deduced from manoeuvres that can only be described adequately by highly nonlinear equations.

10.7.2 *The Spiral Manoeuvre*

The equation governing horizontal motion may be written in the form

$$A\ddot{r}' + B\dot{r}' + Cr' = E\zeta + F\dot{\zeta}'.$$

If $\zeta(t)$ is prescribed, a solution can be sought as the sum of a complementary function (whose nature is determined by the stability since it corresponds to $\zeta = 0$) and a particular integral (which is determined by the given $\zeta(t)$). It has already been pointed out that the constants A and B are both positive and that the sign of C determines whether or not directional stability prevails, for if C is also positive the motion is stable. In effect, the spiral manoeuvre is a check on the sign of C.

If $\zeta = \zeta_c$, a constant, then

$$r' = (\text{complementary function}) + \frac{E}{C}\zeta_c.$$

If the motion is stable, so that the transient complementary function subsides, we should then expect

$C > 0$ for stability,

$E < 0$ both from the analytical form of E (and the signs of the derivatives that comprise it) and also from consideration of the sign convention we are using.

(The apparent contradiction in Fig. 10.28 clearly indicates that r'/ζ_c should be negative.) In a spiral manoeuvre, $r' = rL/\bar{U}$ is measured for various values of ζ_c after the transient motion has subsided, and the results are plotted in Fig. 10.29.

If the resulting curve is of type I the motion is stable, since $dr'/d\zeta_c < 0$ when $\zeta_c \to 0$. When stability is marginal, the slope of the curve at the origin becomes

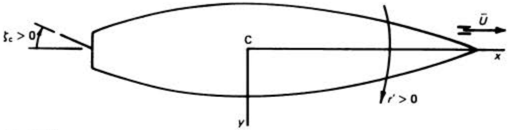

Fig. 10.28

more nearly vertical as in II. This is because

$$\frac{d\zeta_c}{dr'} = \frac{C}{E} \to 0$$

as C approaches zero. Unfortunately, the slope is also large when E is large and it is a weakness of this technique that it cannot distinguish between (i) an unexpectedly powerful rudder, and (ii) marginal stability. Unstable motion produces a curve of type III, which indicates that the rudder only takes effect correctly when it has a large deflection.

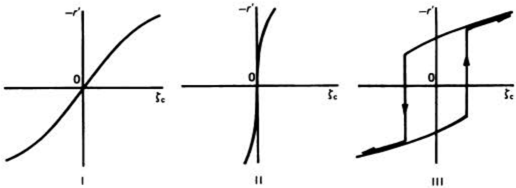

Fig. 10.29

Case III has been the subject of considerable investigation, but it is still not entirely elucidated. It has been suggested, in particular, that an unstable motion is such that $C < 0$ and $E < 0$ so that $r'/\zeta_c > 0$ as $\zeta_c \to 0$. This implies that the curve of type III should really have the form shown in Fig. 10.30. But if the system is truly

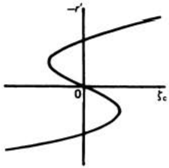

Fig. 10.30

unstable, there is no guarantee that the motion corresponding to a small deflection ζ_c will not be masked by an excessive transient. This aspect has been investigated further by means of the reverse spiral manoeuvre, proposed by Bech, which provides a quicker and more suitable procedure, especially for directionally unstable ships (see [13]).

In practice the spiral manoeuvre is carried out on conventional surface ships using constant shaft speed. The following routine is employed:

1. rudder 15° to starboard,
2. when the turning rate has become steady, record it,
3. repeat with 10° starboard rudder,
4. repeat with 5°, 4°, 3°, 2°, 1° starboard rudder,
5. increase rudder deflection in these steps to 15° port,
6. reverse the above routine and repeat measurements until rudder deflection is again 15° starboard.

The whole operation is repeated with different shaft speeds.

It should be noted that it is common to plot r' against $-\zeta_c$ (rather than $-r'$ against ζ_c) because a starboard rudder deflection is then plotted to the right-hand side.

(a) *Theory of the Spiral Manoeuvre*

We shall now consider in a little more detail the condition of a vehicle that executes a steady turn in horizontal motion. This is the motion previously represented by Equation (10.133):

$$\frac{r'}{\zeta_c} = \frac{N'_\zeta Y'_v - N'_v Y'_\zeta}{N'_v(Y'_r - m') - N'_r Y'_v} = \frac{-E}{-C}\,.$$

The motion is a combined one of yaw and drift and of the form shown in Fig. 10.31. The velocity V_C of the centre of mass C is tangential to the turning circle.

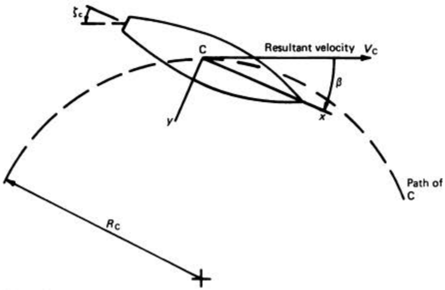

Fig. 10.31

If, as has been supposed, linear theory is applicable it is necessary that u, v be much smaller than the reference velocity $\bar{U}$. The vector diagram for the velocity of C is thus of the form shown in Fig. 10.32, with β a small angle. That is

$$v = (\bar{U} + u)\beta \simeq \bar{U}\beta \tag{10.144}$$

$$r = \frac{V_C}{R_C} = \frac{\{(\bar{U} + u)^2 + v^2\}^{1/2}}{R_C} \simeq \frac{\bar{U}}{R_C} \tag{10.145}$$

where both of these quantities are constant. Thus $\dot{v} = 0 = \dot{r}$, as assumed when Equation (10.133) was derived.

The expression for r'/ζ_c becomes infinite if

$$N_v'(Y_r' - m') - N_r'Y_v' = 0. \tag{10.146}$$

This, then, is the condition $C = 0$ that marks the stability boundary.

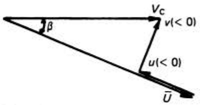

Fig. 10.32

10.7.3 *The Circle Manoeuvre*

The circle manoeuvre is the most primitive of the standard trials evolutions. As it is mainly for surface craft, it is conducted in a calm sea when there is little wind. The manoeuvre is commenced with a straight run at constant speed. With the throttle settling constant, some chosen rudder deflection ζ_c is applied, and the trial consists of determining the subsequent path of the vehicle during a change of heading of 360°. The trial is repeated for different throttle settings† and different values of ζ_c. A number of techniques (e.g. the sighting of a free buoy) are available for tracking the model or ship.

Once the path has been found and plotted as in Fig. 10.33, the following measurements can be made:

tactical diameter;
advance (after 90° change of heading);
transfer (after 90° change of heading).

In addition, it is usual to determine

time to change heading by 360°.

Also, after steady turning conditions have been achieved, it is usual to record

speed ahead;
drift angle;
angle of heel (by photographing a 'vertical' pole against the horizon).

† During a circle manoeuvre, both the ship speed and propeller rotational speed may drop markedly.

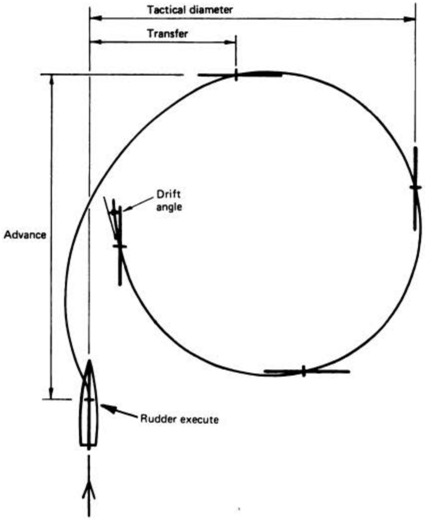

Fig. 10.33 The circle maneouvre.

These data are used for the purposes of comparison with those of 'successful' designs. Sometimes, when these data have been recorded and the ship is still turning, the rudder is restored to zero deflection and a 'pull-out' manoeuvre is performed.

10.7.4 *The Zig-zag Manoeuvre*

The zig-zag manoeuvre, as it was originally conceived, is akin to the circle manoeuvre in that it is a standard test the results from which are really only suitable for making comparisons between vehicles. That is, the results originally had little intrinsic value. They have, however, been used by Nomoto to evaluate the K' and T' indices [12].

The zig-zag is simple to perform, the only apparatus needed being a stopwatch and a gyrocompass. An initial straight run is made at constant speed and then, with the throttle setting kept constant, the rudder is set at 20° to starboard 'as quickly and smoothly as possible'. This rudder setting is maintained constant as the ship changes heading. When the heading has changed 20° the rudder setting is reversed to 20° to port, again 'as quickly and smoothly as possible', and this fresh rudder setting is held while the ship changes heading. When the heading has altered to 20° in the opposite direction, the rudder setting is again reversed 'as quickly and smoothly as possible'.

The whole procedure is repeated four or five times, by which time a steady periodic motion will have been achieved, and the rudder angle and heading are recorded and plotted against time, as in Fig. 10.34. From the periodic portion of the curve, measurements are made of overshoot, period, and time to overshoot.

The whole exercise is repeated for various throttle settings† and the variations of the three parameters are then plotted and used in making comparisons with results obtained from 'successful' designs. One of the major weaknesses of this technique, which makes accurate comparisons difficult, is the fundamental obscurity of the phrase 'as quickly and smoothly as possible'.

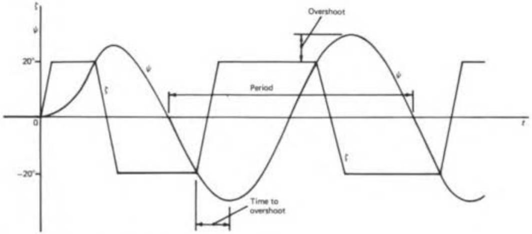

Fig. 10.34 The zig-zag manoeuvre.

10.8 Final Remarks

This chapter is only intended to give a bare introduction to the subject and it will readily be seen that, even where linear theory is concerned, we have done little more than scratch the surface. Perhaps the most obvious topics that have been left out are:

stability theory;
a full discussion of impulse response functions;
nonlinear representations of fluid forces and moments;
solutions of nonlinear equations;
calculation of derivatives and the dependence of the accuracy needed upon the degree of directional stability;
analogue techniques;
automatic control;

† When steering indices K' and T' are determined from zig-zags, it is found that the values vary from one manoeuvre to another. For this reason the International Towing Tank Conference (ITTC) now recommends that 10°–10° and 20°–10° zig-zags be performed, as well as 20°–20°. The 20°–10° manoeuvre is performed with rudder settings of 20°, but the rudder is reversed whenever the ship's heading has changed to 10° in the appropriate direction.

special techniques for directional stability and control in restricted and shallow water and for shallow immersion of underwater vehicles;

peculiarities of hovercraft and hydrofoils;

towing;

effects of waves;

the use of means other than control surfaces for control.

Moreover we have omitted all discussion of distorting vehicles. In short, this chapter represents only an elementary introduction to a field of some size and complexity.

Appendix: Equations of Motion of a Rigid Vehicle with Body Axes whose Origin is not at the Centre of Mass

Let the velocity of the origin A of the body axes shown in Fig. 10.35 be

$$\boldsymbol{U}_a = U_a\hat{\boldsymbol{i}} + V_a\hat{\boldsymbol{j}} + W_a\hat{\boldsymbol{k}}.$$

Referred to the body axes A$\xi\eta\zeta$, the position of a point P in the vehicle is given by

$$\boldsymbol{\rho} = \xi\hat{\boldsymbol{i}} + \eta\hat{\boldsymbol{j}} + \zeta\hat{\boldsymbol{k}}.$$

In particular the position of the centre of mass C is given by

$$\boldsymbol{\rho}_C = \xi_C\hat{\boldsymbol{i}} + \eta_C\hat{\boldsymbol{j}} + \zeta_C\hat{\boldsymbol{k}}.$$

The equations of motion are derived elsewhere [14] and will merely be quoted here.

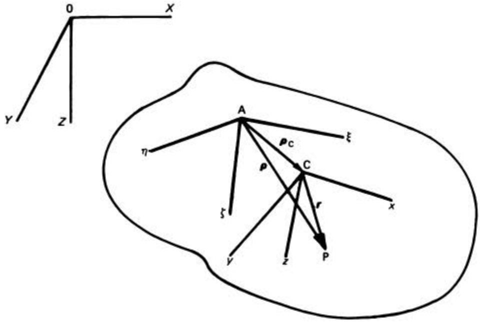

Fig. 10.35

The three force equations are

$$\begin{aligned} X - mg\sin\Theta &= m\{(\dot{U}_a + QW_a - RV_a) + (\dot{Q}\zeta_C - \dot{R}\eta_C) \\ &\quad + P(Q\eta_C + R\zeta_C) - \xi_C(Q^2 + R^2)\} \\ Y + mg\cos\Theta\sin\Phi &= m\{(\dot{V}_a + RU_a - PW_a) + (\dot{R}\xi_C - \dot{P}\zeta_C) \\ &\quad + Q(R\zeta_C + P\xi_C) - \eta_C(R^2 + P^2)\} \\ Z + mg\cos\Theta\cos\Phi &= m\{(\dot{W}_a + PV_a - QU_a) + (\dot{P}\eta_C - \dot{Q}\xi_C) \\ &\quad + R(P\xi_C + Q\eta_C) - \zeta_C(P^2 + Q^2)\}. \end{aligned}$$

The moment about A of the momentum *relative to* A is †

$$\boldsymbol{h}'_a = \sum_i \boldsymbol{\rho}_i \times \delta m_i \dot{\boldsymbol{\rho}}_i.$$

This expression may be reduced to the form

$$\boldsymbol{h}'_a = h'_\xi \hat{\imath} + h'_\eta \hat{\jmath} + h'_\zeta \hat{k}$$

where

$$\begin{bmatrix} h'_\xi \\ h'_\eta \\ h'_\zeta \end{bmatrix} = \begin{bmatrix} I_\xi & -I_{\xi\eta} & -I_{\xi\zeta} \\ -I_{\eta\xi} & I_\eta & -I_{\eta\zeta} \\ -I_{\zeta\xi} & -I_{\zeta\eta} & I_\zeta \end{bmatrix} \begin{bmatrix} P \\ Q \\ R \end{bmatrix}$$

in which

$$I_\xi = \sum_i (\eta_i^2 + \zeta_i^2)\delta m_i; \quad I_{\xi\eta} = \sum_i \xi_i \eta_i \delta m_i; \quad \text{etc.}$$

The three moment equations may now be written as follows:

$$\begin{aligned} &K_a + mg(\eta_C\cos\Theta\cos\Phi - \zeta_C\cos\Theta\sin\Phi) = (\dot{h}'_\xi + Qh'_\zeta - Rh'_\eta) \\ &\quad + m(\eta_C\dot{W}_a - \zeta_C\dot{V}_a) + m\{\eta_C(PV_a - QU_a) - \zeta_C(RU_a - PW_a)\} \\ &M_a - mg(\zeta_C\sin\Theta + \xi_C\cos\Theta\cos\Phi) = (\dot{h}'_\eta + Rh'_\xi - Ph'_\zeta) \\ &\quad + m(\zeta_C\dot{U}_a - \xi_C\dot{W}_a) + m\{\xi_C(QW_a - RV_a) - \xi_C(PV_a - QU_a)\} \\ &N_a + mg(\xi_C\cos\Theta\sin\Phi + \eta_C\sin\Theta) = (\dot{h}'_\zeta + Ph'_\eta - Qh'_\xi) \\ &\quad + m(\xi_C\dot{V}_a - \eta_C\dot{U}_a) + m\{\xi_C(RU_a - PW_a) - \eta_C(QW_a - RV_a)\} \end{aligned}$$

where K_a, M_a, N_a are, respectively, the moments about $A\xi$, $A\eta$, $A\zeta$ of the net fluid force.

References

1. Mandel, P. (1967), *Ship Manoeuvring and Control*, Chapter 8 of *Principles of Naval Architecture* (ed. J. P. Comstock), Society of Naval Architects and Marine Engineers, New York.
2. Abkowitz, M. A. (1969), *Stability and Motion Control of Ocean Vehicles*, MIT Press, Boston, Mass.

† The prime is used in $\boldsymbol{h}'_a$ as a reminder that momentum is referred relative to A and not relative to the fixed origin O, as is more usual.

3. Fedyayevskiy, K. K. and Sobolev, G. V. (1964), *Control and Stability in Ship Design* (English transl.), Joint Publication Research Service, Washington, D.C.
4. International Towing Tank Conference Standard Symbols (1965), *NPL Ship Division* (now National Maritime Institute), *Ship Rep*, No. 77.
5. Gertler, M. and Hagen, G. R. (1967), Standard equations of motion for submarine simulation. *NSRDC, R and D Rep.*, No. 2510.
6. Bishop, R. E. D. and Parkinson, A. G. (1970), On the planar motion mechanism used in ship model testing. *Phil. Trans. R. Soc. (A)*, 266, 35–61.
7. Bishop, R. E. D., Burcher, R. K. and Price, W. G. (1973), On the linear representation of fluid forces and moments in unsteady flow; 5th Annual Fairey Lecture. *J. Sound Vib.*, 29, 113–28.
8. Bishop, R. E. D., Burcher, R. K. and Price, W. G. (1973), Directional stability analysis of a ship allowing for time history effects of the flow. *Proc. R. Soc.*, 335A, 341–54.
9. Bishop, R. E. D., Burcher, R. K., Parkinson, A. G. and Price, W. G. (1974), Oscillatory testing for the assessment of ship manoeuvrability. *10th Symposium on Naval Hydrodynamics*, Boston, Mass.
10. Gertler, M. (1959), The DTMB planar motion mechanism. *Symposium on Towing Tank Facilities*, Zagreb.
11. Goodman, A. (1960), Experimental techniques and methods of analysis used in submerged body research. *3rd Symposium on Naval Hydrodynamics*, Scheveningen.
12. Nomoto, K. (1966), *Response Analysis of Manoeuvrability and its Application to Ship Design*, Chapter 2 of *Researches on the Manoeuvrability of Ships in Japan*, pp. 17–59 of Vol. 11 of the 60th Anniversary Series of the Society of Naval Architects of Japan, Tokyo. (Note: This is a most useful reference book.)
13. Wagner Smitt, L. (1967), The reversed spiral test. *Hydro- and Aerodynamics Laboratory Rep.* No. HY-10, Lyngby, Denmark.
14. Bishop, R. E. D. and Parkinson, A. G. (1969), Choice of origin for the body axes attached to a rigid vehicle. *J. Mech. Engng Sci.*, 11, 551–5.

Notation

The wide range of subject matter covered in this book has necessitated the use of a large number of symbols from both the Roman and Greek alphabets. Duplication of symbols is therefore inevitable, occasionally within a given chapter, but the distinction between the meanings should be clear. In any event, all symbols are defined within the text where they first occur. The following list of symbols, chapter by chapter, is provided for the sake of convenience.

General

A	area
$\mathcal{R}$	aspect ratio
g	weight per unit mass
Fr	Froude number
L_{PP}	length between perpendiculars
L_{WL}	length at still-water line
L_{OV}	length overall
Re	Reynolds number
V	forward velocity of vehicle (excluding Chapter 9)
W	weight (excluding Chapters 9 and 10)
Δ^*	weight displacement
∇	immersed volume; volume displacement
μ	dynamic viscosity
υ	kinematic viscosity
ρ	density of fluid

Subscripts

a	air
l	liquid
WL	water line
w	water; wetted

Other Symbols

d	ordinary derivative
ln	natural logarithm, that is logarithm to base e

log	logarithm to base 10
Δ	an increment of
δ	a very small increase of
∂	partial derivative
Σ	summation
$\lvert x \rvert$	modulus of x, that is the magnitude of x without regard to its direction or sign
$\bar{}$	(bar) over letters identifying locations implies the distance between those locations; for example $\overline{BG}$ means the distance between B and G.

Chapter 2

D	depth of frictional resistance
F	centrifugal force
f	frequency
H	wave height
h	depth of water from free surface
K	bulk modulus
L	lunar force
Q	rate of heat transfer per unit area of the sea surface. Subscript s refers to solar radiation transferred to ocean, subscripts h, e and b refer, respectively, to convection, evaporation and back radiation from ocean.
T	tide raising force
t	period
v	mean velocity of particle at water surface
λ	wavelength. Subscripts d and s refer to deep and shallow water respectively
$\sigma_{s,t,p}$	= (relative density -1) $\times$ 1000; *in situ* density
σ_t	potential 'density'

Other symbols are defined in Table 2.2.

Chapter 3

A_{WL}	water-plane are of hull
A	water-plane area of body
a	see Fig. 3.38; width of jet
B	beam

C	moment (for changes of trim)
C_c	contraction coefficient
C_d	$= C_v \times C_c$, discharge coefficient
C_v	velocity coefficient
d	distance moved by deck weight
E	Young's modulus (modulus of elasticity)
F_A	aerostatic force
F_B	buoyancy force
F_T	thrust
H	height
h	daylight clearance; distance $\overline{BG}$
I	second moment of area of water-plane section about the neutral axis
k	radius of gyration
l	perimeter of nozzle
M	bending moment
MCT	moment to cause trim
$\dot{m}$	mass flow rate
P	tensile force; contact force
p	pressure
p_a	ambient (atmospheric) pressure
p_c	cushion pressure
q	force/unit length of a prismatic vehicle
q_B	buoyancy force/unit length
q_g	gravity force/unit length
q_h	hydroynamic force/unit length
q_i	inertia force/unit length
r	radius of curvature of buoyancy curve
S	shear force; planform area of hovercraft
T	draught
T_A	draught aft
T_F	draught forward
TPI	tonne force (ton force) parallel immersion
t	trim by the stern ($= T_A - T_F$) or trim by the bow ($= T_F - T_A$); time interval
V_j	jet velocity
v	hull deflection relative to water plane
W	weight (see Equation (3.2) for components)
w	movable deck weight

x	distance along prismatic vehicle
y	distance from neutral axis
z	distance below interface
β	angle of rotation
θ	small angle of trim or tilt (positive when bows up); angle of nozzle of hovercraft (see Fig. 3.43)
ρ	density (i.e. mass/volume)
$\bar{\rho}$	relative density
σ	direct stress
τ	shear stress
Φ	finite angle of heel (positive to starboard)
ϕ	small angle of heel (positive to starboard)

Superscript

*	refers to pressure hull of submarine

Axes

OXYZ	a right-handed frame of reference fixed to the Earth with OXY horizontal and OZ pointing vertically downwards.
Oxyz	a right-handed set of body axes with O at the centroid of the water-plane section. Before the application of required angular displacements about Ox or Oy, Oz points vertically downwards.
A$\xi\eta\zeta$	a right-handed set of body axes with A placed at any convenient point. Before the application of required linear and angular displacements about Aξ or Aη, Aζ points vertically downwards.

Chapter 4

A	area
A_o	area of orifice
A_1	area of flow some way upstream of orifice
a	linear acceleration
$a, a_1, a_2, a_3, \ldots$	exponents
B	beam of vehicle
$b, b_1, b_2, b_3, \ldots$	exponents
C	velocity of propagation of water waves
Ca	$= \rho V^2/K$, Cauchy number
C_d	(dimensionless) coefficient of discharge of orifice

C_P	(dimensionless) power coefficient
C_R	(dimensionless) resistance coefficient
c	velocity of propagation of sound waves
c_f	$= \tau_s/\frac{1}{2}\rho V^2$, local skin-friction coefficient
c_p	$= \Delta p/\frac{1}{2}\rho V^2$, pressure coefficient
$c, c_1, c_2, c_3, \ldots$	exponents
d	internal diameter of a pipe of circular cross section; exponent
F	force in prototype system
Fr	$= V/\sqrt{(gl)}$, Froude number
f	force in model system; friction factor of pipe
h	head over orifice
h_f	head lost to friction
K	bulk modulus of elasticity of fluid
K_1, K_2, K_3	(dimensionless) coefficients
k	number of fundamental magnitudes
$\bar{k}$	mean height of surface roughness
$k_1, k_2, k_3, \ldots$	(dimensionless) coefficients
L	fundamental magnitude of length
l	characteristic length; length of pipe
M	fundamental magnitude of mass
Ma	$= V/c$, Mach number
N	wave frequency
n	number of magnitudes influencing the behaviour of a system
$n_1, n_2, n_3, \ldots, n_a, n_b, n_c, \ldots$	numerics
P	power
p	static pressure
Δp	difference of static pressure
p_a	atmospheric pressure
p_v	vapour pressure of liquid
Δp_v	$= p - p_v$
Δp^*	drop of piezometric pressure in pipe; over orifice
$Q, Q_1, Q_2, Q_3, \ldots$	magnitudes of physical quantities
Q_v	volume flow rate through orifice
q	number of fundamental magnitudes
R	resistance
R'	resistance per unit surface area of pipe
Re	$= Vl\rho/\mu$, Reynolds number

Re_o	$= (gh)^{1/2} l\rho/\mu$, Reynolds number of orifice
S	length scale factor
T	fundamental magnitude of time interval
T	draught
t	time interval
$U, U_1, U_2, U_3, \ldots$	units of measurement
$\bar{V}$	mean velocity of fluid in pipe
$\bar{V}_c$	critical mean velocity of fluid in pipe
We	$= V(\rho l/\gamma)^{1/2}$, Weber number
γ	surface tension at air–water interface
λ	ratio of forces in model system to corresponding forces in prototype system
$\Pi, \Pi_1, \Pi_2, \Pi_3, \ldots$	dimensionless parameters
σ	$= (p - p_v)/\frac{1}{2}\rho V^2$, cavitation number
τ	shear stress
τ_s	shear stress at solid surface
ϕ	(with and without numerical subscripts) 'some unknown function of'
ψ	(with and without numerical subscripts) 'some unknown function of'
[ ]	'having the dimensional formula of'

Subscripts

e	arising from elasticity
g	arising from gravity
i	arising from inertia
M	refers to model
P	refers to prototype
p	arising from difference of pressure
s	arising from shear
st	arising from surface tension

Chapter 5

A	area
A_m	cross sectional area at midship transverse plane
A_{max}	maximum cross sectional area of submarine
B	beam
b	half-breadth of control volume
C_1, C_2, C_3	coefficients

C_A	correlation allowance (coefficient)
C_F	skin-friction resistance coefficient
C_{FORM}	form resistance coefficient
C_{F_o}	'basic' two-dimensional, skin-friction resistance coefficient
C_{PV}	viscous pressure resistance coefficient
C_R	residuary resistance coefficient
C_T	total resistance coefficient
C_V	viscous resistance coefficient
C_W	wave-making resistance coefficient
$(C_T)_{s/p}$	total 'ship–propeller' resistance coefficient
C_{aero}	aerodynamic resistance coefficient for above-water profile
C_{app}	appendage resistance coefficient
C_{att}	attitude resistance coefficient
C_{ice}	ice resistance coefficient
$C_{p/h}$	propeller–hull interaction coefficient
c_p	$= (p - p_\infty)/\frac{1}{2}\rho V^2$, local pressure coefficient
D	drag force
d_{max}	maximum diameter of submarine
e	energy dissipation per unit weight
F	fluid dynamic force resulting from motion of vehicle
F_B	buoyancy force
F_T	total fluid force
F_{aero}	aerodynamic force
F_v	fluid force in a direction perpendicular to that of motion of vehicle
H	total energy per unit weight
h	depth of control volume below still-water level
h_i	thickness of ice
h_s	height of superstructure
k	$= r - 1$
L	lift force
L_{app}	virtual appendage length
n	an integer 1, 2, 3, . . .
P_T	towing force
p	local static pressure
p_a	atmospheric pressure at air–water interface

p_{st}	stagnation pressure
p_∞	reference static pressure
q	local velocity at surface in inviscid flow
R	resistance
R_F	skin-friction resistance
R_{Pr}	pressure resistance
R_{PV}	viscous pressure resistance
R_R	residuary resistance
R_T	total resistance
R_V	viscous resistance
R_W	wave-making resistance
R_{aero}	aerodynamic resistance
R_{ice}	ice resistance
R_{ov}	overall resistance
r	$= 1 + (C_{FORM})/C_{F_0}$
S	surface area
S_T	transverse projected surface area of above-water profile
S_{app}	wetted surface area of appendages
S_{tot}	$= S_{app} + S_w$
S_w	wetted surface area of hull
T	thrust
U_∞	steady velocity approaching a flat plate
u, v, w	local velocities of fluid in Ox, Oy, Oz directions respectively
u_{abs}	$= u - V$
V	$= \bar{V} + V'$, forward velocity of vehicle
$\bar{V}$	steady component of forward velocity
V'	time-dependent component of forward velocity
V_a	velocity of air relative to ship
ζ	wave height measured relative to the still-water level
θ	angle between wave crest line and direction of V
θ_d	value of θ for divergent waves
θ_t	value of θ for transverse waves
λ	wavelength
λ'	$= \lambda \cos^2 \theta$
ρ_i	density of ice
σ_i	flexural yield stress of ice

Subscripts

M	refers to model
P	refers to prototype
t	theoretical
v	viscous effect
w	wave effect

Axes

$Oxyz$	a set of body axes with plane Oxy horizontal, Oz measured downwards and Ox in the direction of V.

Chapter 6

The following are common throughout this chapter.

T	thrust of propulsor
$'$	denotes quantity evaluated per unit length or width

Planing Craft

$\mathcal{R}$	$= \bar{b}_w^2/S$, aspect ratio
$\bar{b}_w$	mean wetted beam
C_v	$= W/\frac{1}{2}\rho_w V^2 \bar{b}_w^2$, vertical supporting force coefficient
C_{F_s}	$(\equiv C_F) = F_s/\frac{1}{2}\rho_w V^2 S_w$
$C_{F'_v}$	$= F'_v/\frac{1}{2}\rho_w V^2 l$
C_{v_0}	value of C_v at $\bar{\beta} = 0$
c_p	$= (p - p_a)/\frac{1}{2}\rho_w V^2$, pressure coefficient
Fr	$= V/\sqrt{(g\bar{b}_w)}$, Froude number based on wetted beam
F_B	buoyancy force
Fr_L	$= V/\sqrt{(gL_{WL})}$, Froude number based on length at still-water surface
F_h	hydrostatic force
F_p	pressure force
F_s	skin-friction force
F_v	vertical dynamic supporting force
Fr_∇	$= V/\sqrt{(g\nabla^{1/3})}$, Froude number based on immersed volume
K	defined in Equation (A.6)
L_{WL}	hull length of boat at rest measured in the still-water surface, that is length at water line
l	characteristic length

l_G, l_H, l_X	distances defined in Fig. 6.12(a)
l_p	projected chine length
l_w	wetted length
$\bar{l}_w$	mean wetted length
m	defined in Equation (A.7)
n	defined in Equation (A.8)
p	pressure
p_a	ambient (atmospheric) pressure
q	local velocity
Re	$= \rho_w V \bar{l}_w / \mu_w$, Reynolds number
R	hydrodynamic resistance
R_T	total resistance
S	plan area of wetted surface
S_w	area of wetted surface
z	distance measured vertically downwards from the still-water surface
z_H, z_T	distances defined in Fig. 6.12(a)
α	angle of trim
$\alpha + \phi$	inclination of F_p to the vertical
$\alpha + \psi$	inclination of F_h to the vertical
β	deadrise angle
$\bar{\beta}$	mean deadrise angle
δ	depth of stagnation streamline below still-water surface
λ	$= \bar{l}_w / \bar{b}_w = (\mathcal{R})^{-1}$

Hydrofoil Craft

$\mathcal{R}$	$= b^2/S$, aspect ratio
a_{l_0}	slope of section lift curve at $\alpha = 0$
b	span of hydrofoil
$C_D; C_D^*$	total drag coefficient for hydrofoil; craft
$C_{D_i}; C_{D_i}^*$	induced drag coefficient for hydrofoil; craft
$C_{D_0}; C_{D_0}^*$	profile drag coefficient for hydrofoil; craft
$C_L; C_L^*$	lift coefficient for hydrofoil; craft
C_{L_0}	lift coefficient for hydrofoil at $\alpha = 0$
$C_{L_{flap}}^*$	increment of lift coefficient for craft arising from flap deflection
$C_{L_{to}}^*$	lift coefficient at take-off for craft

C_d	drag coefficient for hydrofoil section
C_l	lift coefficient for hydrofoil section
C_{l_0}	lift coefficient for hydrofoil section at $\alpha = 0$
$C_{m_{c/4}}$	section moment coefficient about quarter-chord point
c	chord length of hydrofoil
c_p	$= (p - p_\infty)/\frac{1}{2}\rho_w V^2$
$D; D^*$	total drag force for hydrofoil; craft
$D_a; D_f$	drag force on aft; front hydrofoil
D_{aero}	aerodynamic drag for hull of craft
$D_i; D_i^*$	induced drag for hydrofoil; craft
$D_0; D_0^*$	profile drag for hydrofoil; craft
Fr	$= V/\sqrt{(gL_{WL})}$, Froude number
F_p	pressure force
h	depth of immersion of lower tip of hydrofoil
$L; L^*$	total lift force for hydrofoil; craft
L_{WL}	hull length of boat at rest measured in the still-water surface
$L_a; L_f$	lift force on aft; front hydrofoil
L_{aero}	aerodynamic lift force for hull of craft
L_0	$= \int_{-b/2}^{+b/2} \rho_w V_0 \Gamma \, dy = L \sec\alpha_i$
l_a, l_{aero}, l_f	distances defined in Fig. 6.41
P_{des}	design power from propulsors
p	pressure
p_v	vapour pressure of water
p_∞	pressure at an upstream reference position
Re	$= \rho Vc/\mu$, Reynolds number
S	plan area of hydrofoil
S^*	total plan area of hydrofoils on given craft
S_{to}^*	total plan area of hydrofoils at take-off
t	thickness of hydrofoil section
V_c	critical velocity at which cavitation commences
V_o	$= V \sec\alpha_i$
V_{to}	take-off velocity
V_{des}	design forward velocity
v_i	downwash velocity
x	distance measured along chord line from the leading edge of hydrofoil

y	coordinate along span centred at mid-span
z_a, z_{aero}, z_f, z_T	distances defined in Fig. 6.41
α	angle of incidence (attack) of hydrofoil
α_i	$= \arctan (v_i/V)$
α_m	value of α for which C_l/C_d is a maximum
α_o	$= \alpha - \alpha_i$
α_s	value of α for which flow separation (stall) occurs
α_{to}	incidence angle at take-off
Γ	circulation of vortex strength
Γ_m	maximum value of Γ
γ	dihedral angle
$\rho_l; \rho_w$	density of liquid; of water
σ	$= (p - p_v)/\frac{1}{2}\rho_w V^2$, cavitation index
σ_c	critical value of σ

Air-Cushion Vehicles **(ACV)**

A_r	augmentation ratio
a	width of nozzle outlet
$C_{D_{pr}}$	profile drag coefficient
c_{p_c}	$= (p_c - p_a)/\frac{1}{2}\rho_a v_n^2$, cushion pressure coefficient
D_T	total drag force
D_W	wave-making drag force
D_i	induced drag force
D_m	momentum drag force
D_{pr}	profile drag force
D_{ow}	over-wave drag force
D_{wet}	wetting drag force
Fr	$= V/\sqrt{(gl)}$, Froude number
F_c	aerostatic cushion force on base of ACV
F_j	jet force on nozzle of ACV
F_p	pressure force
F_v	vertical supporting force
h	daylight clearance
K	a constant
L_{aero}	aerodynamic force on superstructure
l	length of pressure disturbance
l_n	mean length along periphery of nozzle
$\dot{m}_f$	mass flow rate of air through lift fan

n	integer 0, 1, 2, . . .
P	total installed power
P_n	nozzle power
p	pressure in jet
p_a	ambient (atmospheric) pressure
p_c	cushion pressure
p_n	pressure at nozzle exit plane
p_t	total pressure in jet
p_w	pressure at surface of water depression below air cushion
r	radius of curved jet
r_c	inner radius of curved jet
r_o	outer radius of curved jet
S	plan area of base of ACV measured to inside of jet
S_d	surface area of water depression below air cushion
S_f	frontal area of vehicle projected in direction of V
v	local velocity of air in jet
v_c	velocity of particle on inner radius of jet
v_n	local velocity of air in nozzle
v_o	velocity of particle on outer radius of jet
W_p	payload
x	$= (a/h)(1 + \cos\theta)$
α	angle of trim (attitude)
β	slope of water depression below air cushion
θ	angle of nozzle measured inwards to horizontal
θ_{opt}	optimum nozzle angle for maximum A_r
ρ_a	density of air
Υ	normalized fuel cost
Ω	transport efficiency

Chapter 7

A	$= \pi D^2/4$, area of propeller disc
A_n	area of nozzle cross section
a	axial inflow factor
a'	rotational inflow factor
a_R	$= (T - R_T)/R_T$, augment of resistance fraction
a_w	axial inflow factor for 'disc in wake'
b	axial propeller-race velocity factor

b'	rotational propeller-race velocity factor
C_A	correlation allowance
C_T	$= T/\frac{1}{2}\rho A V_A^2$, propeller disc thrust-loading coefficient
C'_T	$= T/\frac{1}{2}\rho S V^2$
c	chord length
c_p	$= (p - p_r)/\frac{1}{2}\rho V_R^2$, local pressure coefficient
$c_{p\min}$	minimum value of the local pressure coefficient
D	drag force; diameter of propeller
Fr_D	$= V_A/\sqrt{(gD)}$, Froude number of propeller
F_r	radial fluid force on propeller blade.
ΔH	energy per unit weight of fluid supplied by pump
h	difference in elevation between nozzle and intake; depth of immersion of propeller axis
h_j	elevation of jet above still-water surface
h_l	total loss of energy per unit weight of fluid in hydraulic-jet system
I	moment of inertia of particle about axis of actuator disc
J	$= V_A/nD$, coefficient of advance
K_Q	$= Q/\rho n^2 D^5$, coefficient of torque
K_T	$= T/\rho n^2 D^4$, coefficient of thrust
k	$= h_l/(V^2/2g)$
L	lift force
m	mass of fluid
n	rotational speed of propeller (revolutions/time)
P	blade pitch
P_D	shaft power delivered to propeller
P_E	effective power to propel vehicle
P_{in}	total input power to actuator disc in open water
P'_{in}	total input power to actuator disc in wake
P_{ke}	power supplied to fluid by actuator disc
P_{out}	output power absorbed in propelling actuator disc
P_{pump}	power supplied by pump
p	local static pressure
p'	static pressure rise across actuator disc
$\bar{p}$	static pressure on the upstream extension of a propeller axis
p_a	ambient static pressure at air–water interface
p_{min}	minimum value of local static pressure

p_0	static pressure on surface of stream tube
p_r	local reference static pressure
p_v	vapour pressure of liquid
Q	propeller torque
R	$= D/2$, radius of propeller
R_T	total resistance of vehicle without propeller
R_T^*	total resistance of vehicle with propeller
ΔR_T	$= R_T^* - T$
Re_D	$= \rho D V_A/\mu$, Reynolds number of propeller
r	local radius of propeller
r_H	radial distance to hydrodynamic centre
S_w	wetted surface area of hull and appendages
T	thrust of hydraulic-jet propulsor; thrust of actuator disc; thrust of propeller-plus-duct; thrust of propeller
T_P	thrust of propeller alone for ducted arrangement
$\bar{T}$	time average thrust
T'	fluctuating component of thrust
t	$= (T - R_T)/T$, thrust deduction fraction
V_A	velocity of advance of propeller relative to upstream fluid
V_R	relative velocity of fluid
V_j	velocity of jet relative to vehicle
v	radial velocity at actuator disc
w	$= (V - V_A)/V$, Taylor wake fraction
α	$= \phi - \beta_i$, angle of incidence
α_N	$= \phi - \beta$, nominal angle of incidence
β	angle of advance
β_i	defined in Fig. 7.17
Γ	circulation
η	propulsive efficiency of hydraulic-jet system
η_B	$= TV_A/2\pi nQ$, efficiency of propeller behind hull
η_H	$= R_T V/TV_A = (1 - t)/(1 - w)$, hull efficiency
η_O	$= T_O V_A/2\pi n Q_O$, open-water efficiency of propeller
η_R	$= \eta_B/\eta_O = Q_O T/Q T_O$, relative rotative efficiency of propeller
η_T	$= R_T V/2\pi n Q = \eta_O \eta_H \eta_R$, overall efficiency of propeller (often referred to as quasi-propulsive coefficient)

η_i	ideal propulsive efficiency of actuator disc
η_{max}	maximum efficiency
λ	$= K_T/J^2 = \pi C_T/8$
λ_j	$= V_j/V$
μ	dynamic viscosity of fluid
ρ; ρ_w	density of fluid; of water
σ	$= (p - p_v)/\frac{1}{2}\rho V_R^2$, cavitation index
σ_L	$= (p_r - p_v)/\frac{1}{2}\rho V_R^2$, local cavitation index
σ_N	$= (\bar{p} - p_v)/\frac{1}{2}\rho V_A^2$, nominal cavitation index
τ	$= T_p/T$ for ducted proepller
ϕ	angle of pitch
Ω	angular velocity of propeller
ω	angular velocity of particle at radius r

Superscript

$'$	refers to a model propeller geometrically similar to prototype (in Section 7.8)

Subscripts

M	refers to model
O	refers to open water
P	refers to prototype

Chapter 8

A	centre of curvature of circular path
AR'	$= 2AR$, effective aspect ratio
a	$= \frac{1}{2}\rho l(\partial C_Z/\partial\beta)_{\beta=0}$
b	span
b_H	spanwise distance of H from root of control surface
C	centre of mass
C_D	$= D/\frac{1}{2}\rho U^2 l^2$ or $D/\frac{1}{2}\rho SU^2$, drag coefficient
C_{D_C}	cross-flow drag coefficient
C_{D_0}	minimum drag coefficient (at $\alpha = 0$)
C_L	$= L/\frac{1}{2}\rho U^2 l^2$ or $L/\frac{1}{2}\rho SU^2$, lift coefficient
C_M	moment coefficient about quarter chord for all-movable control surface
C_{M_C}	$= M_C/\frac{1}{2}\rho V^2 l^3$, moment coefficient

C_T	total resistance coefficient for reference motion
C_X	$= X/\frac{1}{2}\rho V^2 l^2$, longitudinal force coefficient
C_Y	$= Y/\frac{1}{2}\rho V^2 l^2$, side force coefficient
C_Z	$= Z/\frac{1}{2}\rho V^2 l^2$, vertical force coefficient
c	chord length
D	drag force
F	fluid force
Fr	$= V/\sqrt{(gl)}$, Froude number
G_O	torque applied to control surface to maintain equilibrium
H	hydrodynamic centre for translational parasitic motion
h	height of centre of buoyancy above centre of gravity of submerged submarine
J	hydrodynamic centre for rotational parasitic motion
L	lift force
l	characteristic length
M_C	moment of fluid forces about axis through C
M_O	moment of fluid forces about axis of rotation of control surface
m	mass of vehicle
m'	$= m/\frac{1}{2}\rho l^3$
P	fluid force applied to control surface in direction of longitudinal axis Cx of vehicle
Q	fluid force applied to control surface transverse to longitudinal axis Cx of vehicle
Q'	$= Q/\frac{1}{2}\rho l^2 V^2$
R	Hydrodynamic centre of rudder
Re	$= \rho Vl/\mu$, Reynolds number
S	critical point determined by x_{crit} (see Section 8.5.2(b))
S	plan area
T	thrust of propulsor
$\bar{T}$	mean draught
t	maximum thickness of hydrofoil section
U	velocity of centre of mass or hinge of control surface
V_{ref}	reference velocity of vehicle
v	velocity of translation

X	fluid force in direction Cx (with prime; per unit span)
x_A	distance from C to Q_A (negative when aft of C)
x_F	distance from C to Q_F (positive when forward of C)
x_H	distance $\overline{CH}$ (positive when H forward of C)
x_J	distance $\overline{CJ}$ (positive when J forward of C)
x_R	distance $\overline{CR}$ (positive when R forward of C)
x_{crit}	see Section 8.5.2(b)
x'_H	$= x_H/l$
x'_J	$= x_J/l$
x'_R	$= x_R/l$
$\bar{x}$	distance from C to line of action of net force Q on hydroplanes (positive when Q forward of C)
Y	fluid force in direction Cy (with prime; per unit span)
Y_Ω	$= (\partial Y_J/\partial\Omega)_{\Omega=0}$
Z	fluid force in direction Cz
α	angle of incidence of control surface
β	angle of incidence of vehicle, or body in general
γ	angle between U and Cx axis of vehicle
θ	trim angle (inclination of Cx to horizontal)
Λ	sweep angle
λ	$= c_r/c_t$, taper ratio
ξ	angle of deflection of control surface
Ω	angular velocity of vehicle
Ω'	$= \Omega l/V$

Superscript

$\bar{\ }$	mean value

Subscripts

A	after
F	forward
H	located at H
J	located at J
R	rudder
r	root
t	tip

Axes

Where body axes $Cxyz$ are used, C is the centre of mass, Cx points forward, Cy points to starboard and Cz points downwards in the vehicle's intended attitude.

Chapter 9

This is a principal notation and excludes brief duplicated use of some parameters as dummy variables. Notation of the Appendices is also excluded.

A	area of material in hull cross section
$\mathbf{A}$	structural mass matrix
$\boldsymbol{\mathsf{A}}$	added mass matrix
a	radius of sphere; wave amplitude
$\mathbf{B}$	structural damping matrix
$\boldsymbol{\mathsf{B}}$	added damping matrix
b	damping constant; radius of cylinder; half beam of hull
C	centroid of cross section
$\mathbf{C}$	structural stiffness matrix
C_k	kth Fourier coefficient specifying effect of wake distribution
$C_{\mathrm{V}}, C_{\mathrm{H}}$	coefficients of added mass in symmetric and anti-symmetric hull vibration
C_{T}	coefficient of added moment of inertia of hull
$\boldsymbol{\mathsf{C}}$	added stiffness matrix
c	distance of C from shear centre
d	draught
E	Young's modulus (modulus of elasticity)
F_{H}	hydrodynamic force per unit length
$\mathbf{F}$	applied force matrix
F_y	bearing force in direction Oy
F	force applied by flowing fluid
f	applied force (excluding mean value)
$\mathbf{f}$	matrix of generalized forces
g_{r}	dimensionless force
I	second moment of area of section about neutral axis
I_{p}	polar second moment of area about centroidal axis
J	three-dimensional correction factor for C_{V} and C_{H}; concentrated moment of inertia

K	keel
K	torsional stiffness
K'	warping stiffness
$\mathbf{K}$	stiffness matrix
k	stiffness; wave number
L_n	see Fig. 9.3
l	length of beam segment
M	bending moment
$M^{W}(l/\Lambda)$	see Equation (9.79)
$\mathbf{M}$	mass matrix
m	mass
N	number of propeller blades
n	number of degrees of freedom; number of elements
P	point force
p	principal coordinate
Q	generalized force
q	applied force per unit length (see Fig. 9.16)
$\mathbf{q}$	matrix of generalized displacements
Re	real part
r	see Fig. 9.3
S	shear force
s	perimeter of wall
T	kinetic energy; twisting moment
T_f	fluid kinetic energy
t	time interval; wall thickness
U	velocity (see Fig. 9.2)
u	velocity (excluding mean value)
V	potential energy
v	beam deflection in direction Oy
W	work done by external forces
w	horizontal displacement in direction Oz of shear centre
X	displacement (see Fig. 9.2)
x	displacement; distance along axis of beam or hull
x_s	value of x at stern bearing of ship
α	coefficient of added mass; receptance
α_H	coefficient of added mass in horizontal motion
β	coefficient of added damping; local blade helix angle (see Fig. 9.3(a)); root of frequency equation

γ	coefficient of added stiffness; $(EI/m')^{1/2}$
ϵ	a small number
ζ	direct flexibility at tip slope of a cantilever; wave depression
η	cross flexibility between tip slope and tip deflection of a cantilever
θ	slope of beam ($\partial v/\partial x$ or $\partial w/\partial x$)
θ_n	angle between 1st and nth blades of propeller
Λ	wavelength
ξ	direct flexibility at tip deflection of a cantilever; dimensionless coordinate
ρ	density
ϕ	rotation of beam; characteristic mode shape
χ	flexibility in torsion
Ω	angular velocity of propeller
ω	frequency of excitation

Superscripts

$\bar{}$	amplitude of quantity; mean value
$'$	quantity augmented by added mass; transpose of matrix
$\hat{}$	coefficient

Chapter 10

A	arbitrarily selected origin of body axes
$A, B, C, E, F,$	dimensionless constants formed from slow motion derivatives (see Section 10.6.4)
$\mathbf{A}$	matrix of inertial constants
$a; b$	distance abaft C of hydrodynamic centre of rudder; skeg
$\mathbf{B}$	matrix of damping constants
C	centre of mass
$\mathbf{C}$	matrix of stiffness constants
$C_L; C_L$	lift coefficient of rudder; skeg
D	operator d/dt
Fr	Froude number
F	total externally applied force
F_h	hydrodynamic force applied to a control surface

F_r	rudder force
F_s	force transmitted to control surface by its stock
$\boldsymbol{G}$	total moment of external forces about C
G_h	moment of F_h about axis of stock
G_s	torque transmitted to control surface by its stock
G_y, G_z	moments about C of forces applied to a model by a PMM
h	height of centre of buoyancy of a submerged vehicle above C
$\boldsymbol{h}$	moment about C of absolute momentum
$\mathbf{h}$	matrix of moment about C of absolute momentum
h_x, h_y, h_z	components of $\boldsymbol{h}$ in directions $\hat{\imath}, \hat{\jmath}, \hat{k}$,
$\hat{I}, \hat{J}, \hat{K}$	unit vectors in directions OX, OY, OZ
$\mathbf{I}$	matrix whose elements are moments of inertia and (minus) products of inertia
$I_x, I_{xy} \ldots$	moments and products of inertia
$\hat{\imath}, \hat{\jmath}, \hat{k}$	unit vectors in directions Cx, Cy, Cz
K'	Nomoto steering index
K, M, N	components of $\boldsymbol{G}$ in directions $\hat{\imath}, \hat{\jmath}, \hat{k}$
L	length of vehicle
l_0	distance of C from point of attachment of PMM
m	mass of vehicle
$n_v(\tau), n_r(\tau), n_p(\tau)$	impulse response functions relating ΔN to anti-symmetric disturbances
P, Q, R	components of Ω in directions $\hat{\imath}, \hat{\jmath}, \hat{k}$ (i.e. angular velocities of roll, pitch and yaw)
PMM	abbreviation for 'planar motion mechanism'
p, q, r	small components of Ω in directions $\hat{\imath}, \hat{\jmath}, \hat{k}$
$\mathbf{Q}$	matrix of generalized forces
$\mathbf{q}$	matrix of generalized coordinates
q_0	$= \omega\theta_0$, amplitude of pitch velocity in sinusoidal motion
Re	Reynolds number
$\boldsymbol{R}$	position of general point in vehicle referred to axes OXYZ
R_C	radius of path of C
$\boldsymbol{R}_C$	position of C referred to axes OXYZ
$\boldsymbol{r}$	position of a point in vehicle referred to axes Cxyz
s	see Fig. 10.21
$\mathbf{T}$	orientation matrices defined in Section 10.3.1(a)

T'	Nomoto steering index
t	time interval
$\boldsymbol{U}$	velocity of C
U, V, W	components of $\boldsymbol{U}$ in directions $\hat{\imath}, \hat{\jmath}, \hat{k}$
$\boldsymbol{u}$	small departure from steady reference velocity
u, v, w	components of $\boldsymbol{u}$ in directions $\hat{\imath}, \hat{\jmath}, \hat{k}$
v_o	$= \omega y_o$, amplitude of sway velocity in sinusoidal motion
w_o	$= \omega z_o$, amplitude of heave velocity in sinusoidal motion
X, Y, Z	components of $\boldsymbol{F}$ in directions $\hat{\imath}, \hat{\jmath}, \hat{k}$ (note *usually* refers to fluid forces only)
$Y_v(\omega)$	$= Y_v^{\mathrm{Re}}(\omega) + \mathrm{i}Y_v^{\mathrm{Im}}(\omega)$, Fourier transform of $y_v(\tau)$
$y_v(\tau), y_r(\tau), y_\phi(\tau)$	impulse response functions relating ΔY to anti-symmetric disturbances
$Y_v(0)$	$= \lim_{\omega \to 0} [Y_v^{\mathrm{Re}}(\omega)]$
$Y_{\dot{v}}(0)$	$= \lim_{\omega \to 0} \left(\dfrac{Y_v^{\mathrm{Im}}(\omega)}{\omega} \right)$
$Z_w(\omega)$	$= Z_w^{\mathrm{Re}}(\omega) + \mathrm{i}Z_w^{\mathrm{Im}}(\omega)$, Fourier transform of $z_w(\tau)$
$z_w(\tau)$	impulse response function relating ΔZ to heave velocity disturbance
x, y, z	components of $\boldsymbol{r}$ in directions $\hat{\imath}, \hat{\jmath}, \hat{k}$; also $x = \int u\,\mathrm{d}t$, $y = \int v\,\mathrm{d}t$, $z = \int w\,\mathrm{d}t$
$Z_w(0)$	$= \lim_{\omega \to 0} [Z_w^{\mathrm{Re}}(\omega)]$
$Z_{\dot{w}}(0)$	$= \lim_{\omega \to 0} \left(\dfrac{Z_w^{\mathrm{Im}}(\omega)}{\omega} \right)$
α	angle of incidence of control surface
α, β	stability indices (see Section 10.7.1)
β	angle of incidence of hull
Δ	increment (e.g. ΔX) associated with small departure from reference motion
ϵ, λ	see Section 10.5.2(b)
η, ζ	control-surface deflections about axes in directions $\hat{\jmath}, \hat{k}$ (i.e. hydroplane and rudder deflections)
ζ_c	constant rudder deflection
ξ, η, ζ	coordinates used in Appendix
ξ_C	distance $\overline{\mathrm{AC}}$ (see Appendix)
ρ	see Fig. 10.35
τ	time

$\Psi\ \Theta\ \Phi$	angle of 'swing', 'tilt' and 'heel'
$\psi\ \theta\ \phi$	small angles of 'swing', 'tilt' and 'heel'
Ω	angular velocity of vehicle
ω	forcing frequency

Superscripts

$\dot{}$	time derivative, order signified by number of dots
$\hat{}$	unit vector
$\bar{}$	refers to steady reference motion
$\tilde{}$	oscillatory coefficient
*	relates to equilibrium axes; as a subscript refers to 'steady component'
′	non-dimensional

Subscripts

A	after
C	refers to centre of mass
F	forward
IN	denotes component of force in phase with oscillatory displacement
M	refers to model
o	amplitude
P	refers to prototype
QUAD	denotes component of force in quadrature with oscillatory displacement
R; S	as prefixes: contribution of rudder; skeg
x, y, z	refers to directions Cx, Cy, Cz, respectively

Axes

$A\xi\eta\zeta$	body axes introduced in Appendix
$Axyz$	body axes parallel to $Cxyz$
$Cxyz$	body axes fixed to vehicle as in Fig. 10.1
$C^*x^*y^*z^*$	equilibrium axes (i.e. body axes attached to a vehicle that only performs a reference motion)
$OXYZ$	Earth axes with plane OXY horizontal and OZ pointing downwards.

Index

Absorption of light, 27
Accelerometer, 173
Actuator disc, 353
  axial flow, 353
  ducted propeller, 358
  ideal efficiency, 355, 360, 361
  open propeller, 353
  in open water, 357
  rotational flow, 360
  thrust coefficient, 356
  in a wake, 357
Added damping, 469, 479, 487, 489
Added mass, 446, 471, 477, 489, 490
Added moment of inertia, 469, 487, 488
Added stiffness, 469
Aerodynamic supporting force, 307
Aeroelasticity, 440
Aeroplane (conventional) configuration, 267, 268, 290
Aerostatic supporting force, 102, 104, 298, 307
After cut-up (ACU), 90, 196
Aileron, 396
Air cushion vehicles (ACV), 57, 102, 298
  external loading, 129
  hovercraft, 102, 244, 298
  peripheral (annular) jet craft, 104, 298
  plenum chamber craft, 103, 298
  side wall, 298, 320
Air properties, 21
Airship, 185
Anhedral, 295
Angle of incidence (or attack), 271, 272, 400
  effective, 365
  nominal, 364, 365
Anticyclone, 35
Antisymmetric motion of uniform beam, 479
  added mass, 485
  cross receptance, 485
  free vibration, 479
  torsional stiffness, 481
  warping stiffness, 481
Aspect ratio
  effective, 435
  geometric, 226, 250, 278, 412, 435
Augment of resistance fraction, 367
Augmentation ratio, 308
Axial inflow factor, 353

Beam, 95, 162
Beaufort Scale, 41
Blade area ratio (BAR), 375, 387
Blasius equation (for laminar flow over flat plate), 225
Block coefficient, 98, 195
Bluff body, 208
Bonjean curves, 162
Bound vortex, 270
Boundary layer, 146, 189
  laminar, 191, 192
  Prandtl hypothesis, 189, 194
  separation, 192, 275
  thickness, 189
  turbulent, 191, 192
Buoyancy
  centre of, 63
  cross curves of, 71
  curve of, 73
  evolute of curve of, 74
  force, 58, 62, 185
  surface of, 68
Bulbous bow, 221

Canard configuration, 267, 268, 290
Cauchy number, 159
Cavitation, 158, 164, 171
  number, 159, 164, 282
  on hydrofoils, 282
  on propellers, 350, 387, 388
  supercavitation, 283
Cavitation on propeller, 380
  back cavitation, 382
  cavitation index, 380
  face cavitation, 381
  full (super) cavitation, 382, 389
  local cavitation index, 380
Centre of flotation, 65, 92
Centre of gravity, 60
Centre of pressure, 246
Centroid, 63
Chine line, 250
Circle manoeuvre, 417
Circulating water channel, 179

Circulation (about hydrofoil), 268
  control on propeller blades, 388
Clearance, 298
  daylight, 300
Climatic conditions, 42
Continental shelf, 11
  slope, 12
Control surface, 396, 406, 542
  derivatives, 546
  motion of, 543
Contouring, 287, 288, 323
Convection, 14
Conversion factor, 7, 135
Coordinates, 496
  imposed deflection, 496
  orientation, 498
  rigid body, 496, 497
Coriolis effect, 33
Correlation allowance, 211, 226
Corresponding speed, 163
Critical point (of submarine), 427
  speed, 431
Cross receptance, 474, 485, 491
Cushion, 298
Cushion-pressure coefficient, 305
Cyclone, 35, 38

Deadrise angle, 250
Deep-ocean circulation, 46
Deep-sea bottom, 12
Depth of frictional resistance, 46
Design, 1
Dicothermal layer, 24
Dihedral, 295
Dimension, 137
Dimensional analysis, 139
  dependent variable, 140
  independent variable, 140
  'Pi' theorem, 141
  Rayleigh's (indicial) method, 139
  recurring set, 141
Dimensional formula, 137
Dimensional homogeneity, 135, 139
Directional stability, 414
Dispersion of light, 26
Distorted model, 134
Docking, 90
Doldrums (Intertropical front or convergence zone), 34
Double-hull model, 195, 215
Downwash velocity, 278
Dracones, external loading, 129
Drag force, 186, 268, 400, 410
  calm water, 320
  coefficient, 280
  coefficient for control surface, 410, 437
  form, 297
  induced, 256, 278
  induced (drag) coefficient, 280, 318
  momentum, 318
  over-wave, 320
  profile (drag) coefficient, 280, 318
  section coefficient, 273
  wave-making, 298, 319
  wetting, 320
Draught, 91, 95, 162
Drift (sway), 498, 509
'Dry land' problem, 440, 448, 486, 489
Ducted propeller, 350
  Kort nozzle, 350
  pump jet, 350
Duhamel (convolution) integrals, 518
Dynamometer
  resistance, 167
  strain gauge, 167

Economic efficiency, 331
Effective power, 376
Ekman spiral, 44, 344
Elevator, 396
Equilibrium
  stable, 76, 77
  static, 76
  unstable, 76, 77
Equations of motion
  for parasitic motions, 510
  roll, pitch, yaw, 509
  surge, drift, heave, 508
Equilibrium vehicle, 525
Euler angles (modified), 499, 502
Evaporation, 14
External loading
  by hydronamic forces, 124
  by hydrostatic pressure, 126
  by inertia forces, 124
Extinction, 27

Fatigue, 129
Fineness coefficient, 95
Fineness ratio, 162
Finite element techniques, 130, 131, 253, 474
Flaps
  on hydrofoils, 290
  trim tab (or wedge), 252
Flettner rotor, 344
Flow in pipes
  Darcy's formula, 154
  friction factor, 154, 155
  head 'lost to friction', 154
  Lee's formula, 155
  Nikuradse relation, 156
  Rayleigh's relation, 155
  Reynolds' relation, 154
  Stanton and Pannell's experiments, 155
Flow pattern, 149, 195
Fluid hull, 314
Forces
  external, 107
  internal, 107

Form effect, 229
Form factor, 229
  for appendage, 236
Frames, 123
Free-running models, 173, 555
Froude number, 159, 401
  volume, 262
Fully planing régime, 253, 257, 266
Fully roused sea, 49

Gas turbine, 345
Generalized coordinates, 447
Geosims, 231
Geostrophic currents, 46
Gyre, 42

Hard angle, 250, 251
Halocline zone, 25
Hard chine, 'V'-bottom hull, 250
Heave, 498, 509
Heel, angle of 63
Helicopter, 57, 102, 105, 106
HMCS Bras D'Or, 286, 389, 391
HMS Greyhound, 232
HMS Penelope, 234
HMS Speedy, 291
Hogging, 116
Hollow (in resistance curve), 218
Homologous series (of models), 161
Horizontal motion (of interface vehicles), 527
Horse latitudes, 34
Horseshoe vortex, 276
Hughes' skin friction equation, 227
Hull efficiency, 371
Hump (in resistance curve), 218
  main (or primary), 219, 266, 296, 320
  prismatic, 219
Hurricane (typhoon), 38
Hydraulic jet propulsion, 345
  efficiency, 347
Hydrodynamic centre, 363, 400
  for control surface, 434, 437
  for rotation, 403, 405
  for translation, 400, 405
Hydrodynamic force, 245, 254
Hydrofoil, 267
Hydrofoil craft, 244, 267
  external loading, 129
Hydrofoil geometry
  camber, 273
  chord line, 273
  leading edge, 272, 273
  mean (camber) line, 273
  thickness, 273
  trailing edge, 272, 273
Hydrofoil section moment coefficient, 274
Hydroelasticity, 440
Hydroplane, 396, 421, 422, 434
  balance angle, 423
  no lift (inoperative) angle, 423
Hydrostatic force, 253, 254
Hydrostatic stability, 77, 78
  complete, 101
  curves of, 89
  effect of partially filled tanks on, 82, 101
  effect of small changes in geometry on, 95
  longitudinal, 81
  transverse, 81
  of uniform rectangular block, 96

Icebergs, 18
Ice breaking, 328
Impulse response function, 515, 518
Inclining experiment, 81
Inertia
  moment of, 505
  product of, 505
Interaction effects on resistance, 222
Inverse receptance, 521
Irrotational flow, 193, 268
Isopleths, 26
ITTC 1957 friction line, 227

Jet reaction force, 307
Jet stream, 33

Kirsten-Boeing propeller, 341, 342
Kites, 344
Kutta-Joukowski
  condition, 271
  Joukowski's hypothesis, 270
  law, 269

Lagrange's equations, 445
Lift force, 186, 268, 400, 410
  coefficient, 280, 410
  coefficient for control surface, 436
  depth effect, 282, 295
  section coefficient, 273
  total coefficient for hydrofoil craft, 290
  total for hovercraft, 317
Lifting-line theory, 277
Light transmission, variation with depth, 26
Loading
  buoyancy, 111
  gravity, 111
Loll, angle of, 85
Lucy Ashton, 232, 233

Mach number, 159, 160, 401
Magnitude, 135
  derived, 136
  dimensionless (non-dimensional), 138
  fundamental, 136
Main stream, flow in, 192
Manoeuvres, 555
  circle, 560
  pull out, 556
  spiral (Dieudonné), 557
  zig-zag (Kempf), 561
Manoeuvring, 527

Manoeuvring tank, 172
MCT, 93
Metacentre, 79
Metacentric height, 80
Models, 181
of expanded polystyrene, 182
of glass reinforced plastic, 182
of wax, 181
of wood, 181
Moment coefficient
for control surface, 437
for vehicle, 402
Momentum analysis
deeply submerged vehicle, 201
vehicle at interface, 204
Myklestad-Prohl method, 471

Neutral point, 426
Notation, 566

Occluded front, 35
Oceans, 10
Orifice, 133, 139, 142, 144
discharge coefficient, 134, 144
Ordinary algebra, 135
Oscillatory coefficients, 515, 517
for submarine in heave, 535
for submarine in pitch, 536
from model tests, 533

Panels, 122
Parallel sinkage (rise), 64
Parasitic motion, 397, 511
antisymmetric, 450
draft (sway), 398
heave, 398
pitch, 398, 422
symmetric, 450
yaw, 398
Pathline, 148
Perpendicular
aft, 92
fore, 91
length between (perpendiculars), 92
Physical algebra, 135
Pitch, 498, 509
Pitch angle, 365
Pitch (geometric), 365
nominal, 366
ratio, 375
Planar motion mechanism (PMM), 175, 518, 533, 538
comments on use of, 540
Planing craft, 244, 245
Platforming, 287, 288, 323
Plough in, 317
Polar easterlies, 34
Polynyas, 18
Porpoise motion, 261
Potential function (velocity potential), 193, 196
Power, 160
coefficient, 160, 234
Prandtl–Von Karman equation (for turbulent flow over flat plate), 225
Pressure coefficient, 194
Pressure hull, 127
Pressure, variation with depth, 22
in situ value, 23
potential value, 23
Prevailing westerlies, 35
Principal axes, 66
Prismatic coefficient, 212, 219
Pro-metacentre, 66
Propeller design, 386
lifting line theory, 386
lifting surface theory, 386
Propulsive power, 326
Propulsor, 338
Pycnocline zone, 26

Rafting, 18
Resistance, 160, 187, 199
aerodynamic, 236
flat plank, 209, 210
ice, 239
induced, 256
overall, 238
pressure, 199
residuary, 215, 223
skin friction, 199, 208, 214, 223
total, 199, 203, 207, 208, 214, 223
viscous, 200, 208
viscous pressure, 199, 200, 208, 209, 214, 256
wave-making, 196, 200, 214, 216, 217, 256
Resistance coefficient, 160
aerodynamic, 235, 236
appendage, 235, 236
attitude, 223, 235
form, 229
ice, 236, 239, 240
propeller-hull, 235, 236, 238
residuary, 216, 224
skin-friction, 208, 215, 224, 227, 259
total, 208, 215, 224
viscous pressure, 208, 215, 224
wave-making, 215, 224
Reynolds number, 159, 401
Ride quality, 326
Righting moments
cross curves of, 88
curves of, 84
Ring vortex, 306
Rocket motor, 338
Roll, 498, 509
Root vortex, 364
Rotating arm, 175
Rotational inflow factor, 361
Round-bottom (round bilge) hull, 250

Rudder, 396, 542
area coefficient, 432
balanced, 419, 432, 438
gnomen (skeg), 421
maximum deflection, 432
number, 432
position, 417, 551
size, 432
and skeg theory, 549
spade, 406, 410, 421, 434
speed of operation, 432
Run in point, 229

Sagging, 116
Sails, 342
Salinity, variation with depth, 25
Scale, 134
factor, 146, 152, 163
Scale effect, 161
Schoenherr (ATTC 1947) friction line, 226
Screw propeller, 349, 362
back of blade, 364
behind-the-hull efficiency, 370
cavitation on, 370
controllable pitch (CP), 387, 390
face of blade, 364
flow separation on, 370
open water efficiency, 370
overall efficiency (quasi-propulsive coefficient), 371
relative rotative efficiency, 370
vibration of, 370, 387

Sea ice, 17
fast, 18
floes, 18
flow (sheet), 18
frazil, 18
pack, 18
pancake, 18
slush, 18
Seakeeping, 322, 496
Sea mounts, 12
Sea water, properties, 16, 21
Section coefficient, 162
Self-propulsion point, 375
Shaft vibration (flexural), 490
Shaft vibration (longitudinal), 489
excitation, 489
natural frequencies, 490
principal modes, 490
systems, 489
Shaft vibration (torsional), 486
excitation, 487
forced, 488
natural frequencies, 488
principal modes, 488
system, 487
Shear stress, 189, 190, 192
Ship (hull) girder, 116, 470
Shore, 11
Similarity
dynamic, 150
geometric, 146
kinematic, 147, 150
physical, 145
Singing, 450
Skeg, 419
Skin friction
drag, 190
force, 190, 254
Skirts, 300, 315
bag, 314
fingers, 314
jupe, 315
Slamming, *frontispiece*, 173
Slenderness ratio, 212, 262
Slow motion derivatives, 515, 516
comments on measurements, 533
rotating arm measurements, 531
towing measurements, 530
Small-water-plane-area, twin-hull (SWATH) ship, 326, 330
Sofar, 30
Solar radiation, 13
Sonar, 28, 329
Sound channel, 30
Sound transmission, variation with depth, 27
Span, 400
Springing, 469
Squat, 235
SS Golar Nichu, 351
SS Great Britain, 349, 421
SS Koningin Elisabeth, 234
SS Meteor, 233
SS Reine Astrid, 234
Stabilizer, 396
Stagnation point, 193, 194, 246, 269, 272
Stagnation streamline, 245
Starting vortex, 270
Steady flow energy equation, 207
Steady motion, 185
Steering indices, 552, 553
Stepped hull, 252
Stiffened plates, 122
Stratification, 31
Streakline, 148
Streamline, 148
Streamlined body, 209, 212, 213
Strip theory, 130, 131, 469
Structural
deterministic analysis, 109
dynamics, 107
failure, 107
probabilistic (random) analysis, 109
statics, 107
Strut, 267
Surf, 49
Surface effect ship (SES), 320

Surface currents, 42
Surface roughness, 146, 155, 156, 211, 212
Surge, 498, 509
Symmetric motion of uniform beam, 454
application to ships, 466
cross receptance, 474
damping, 478
forced vibration, 459
free vibration, 455
'long' ship, 463
natural frequencies, 455
orthogonality of principal modes, 457
principal modes, 456
'Reed' ship, 463
resonant encounter, 466
ship-wave matching, 466
wave excitation, 461
wave excited bending moments, 465
Synoptic conditions, 42
System, 133
gravitational, 136
mathematical, 133
model, 133
prototype, 133
Sweepback, 281
Swell, 49

Tacking, 344
'Take-off' speed, 296
Taper, 281
Temperature, variation with depth, 23
Thermocline, 24
zone, 24
Thermohaline circulation, 46
Thrust, 58, 185, 254, 339
Thrust deduction fraction, 368
Tides, 51
apogee, 53
equilibrium, 52
neap, 54
perigee, 53
spring, 54
Time history (memory) effects, 518
Tip vortex, 223, 276, 350, 364
Tornado (twister), 39
Towing force, 187
Towing tank, 167
TPI, 64, 92
Trade winds, 34
Transfer matrix methods, 470
Transport efficiency, 331
Trench, 10, 12
Trim, 91
angle of, 63, 186, 253, 264, 290, 314
of submarine, 422, 423
Tropopause, 32
Troposphere, 32
Trough (of low pressure), 35
Tucumcari, 348
Turbulence, 190
intensity, 192

Unit, 134
Units, 7
Unit analysis, 110, 121, 130
Upwelling, 46
USS Albacore, 212
USS High Point, 291
USS Nautilus, 212
USS Plainview, 288

Vapour pressure, 380
Ventilation
on hydrofoils, 284
on propellers, 350
superventilation, 286
Vertical (hydro) dynamic force, 187, 249
coefficient, 249, 258
Vibration, 440
antisymmetric, 479
forced, 441, 448
free, 448
of hull, 450
linear, 442
nonlinear, 450
of propeller, 451, 470
random, 441
self-excited, 441, 449
symmetric, 454
transient, 441, 449, 490
Virtual mass, 454, 477
Voith-Schneider propeller, 341, 342
Volume displacement, 62, 185
Voyageur, 328

Wagner effect, 518
Wake, 189
fraction, 368, 369
traverse, 203
Wall-sided formula, 100
Water line length, 95, 214
Water molecule, 16
Water plane section, 63
second moment of area of, 66
Water tunnel, 171
Waves, 47
capillary, 47
deep water, 49
fetch, 47
frequency, 49
generated by vehicle, 196
gravity, 47
shallow water, 49
trochoidal, 50, 116
velocity of propagation, 48
Wave pattern, 195, 196
Weber number, 159, 401

Weight, 58
    deadweight, 59
    displacement, 62, 185
    distribution, 60
    gross (all-up), 59, 252

'Wet-sea' problem, 440, 450, 486, 490
Wind turbines, 344

Yaw, 498, 509

Zones of operation, 187